A Framework for Hyper-Heuristic Optimisation of Conceptual Aircraft Structural Designs

Thesis by

Jonathan George Allen

Submitted as partial consideration towards
the degree of Doctor of Philosophy

Computational Mechanics Group
School of Engineering and Computing Sciences
Durham University
United Kingdom

August 2014

Computational Mechanics Group
School of Engineering and Computing Sciences
Durham University
United Kingdom

Abstract

Conceptual aircraft structural design concerns the generation of an airframe that will provide sufficient strength under the loads encountered during the operation of the aircraft. In providing such strength, the airframe greatly contributes to the mass of the vehicle, where an excessively heavy design can penalise the performance and cost of the aircraft. Structural mass optimisation aims to minimise the airframe weight whilst maintaining adequate resistance to load. The traditional approach to such optimisation applies a single optimisation technique within a static process, which prevents adaptation of the optimisation process to react to changes in the problem. Hyper-heuristic optimisation is an evolving field of research wherein the optimisation process is evaluated and modified in an attempt to improve its performance, and thus the quality of solutions generated. Due to its relative infancy, hyper-heuristics have not been applied to the problem of aircraft structural design optimisation. It is the thesis of this research that hyper-heuristics can be employed within a framework to improve the quality of airframe designs generated without incurring additional computational cost.

A framework has been developed to perform hyper-heuristic structural optimisation of a conceptual aircraft design. Four aspects of hyper-heuristics are included within the framework to promote improved process performance and subsequent solution quality. These aspects select multiple optimisation techniques to apply to the problem, analyse the solution space neighbouring good designs and adapt the process based on its performance. The framework has been evaluated through its implementation as a purpose-built computational tool called AStrO. The results of this evaluation have shown that significantly lighter airframe designs can be generated using hyper-heuristics than are obtainable by traditional optimisation approaches. Moreover, this is possible without penalising airframe strength or necessarily increasing computational costs. Furthermore, improvements are possible over the existing aircraft designs currently in production and operation.

Declaration

The work in this document is based on research carried out in the Computational Mechanics Group of the School of Engineering and Computing Sciences at Durham University. No part of this document has been submitted for any other degree or qualification and the content represents the work of the author unless referenced to the contrary. The following publications were written by the author for presentation of this research to an audience of peers within the field of engineering design optimisation:

I. Allen, J. G., Coates, G., and Trevelyan, J., A Theoretical Framework for the Optimisation of the Structural Layout of an Aircraft using Deterministic and Stochastic Optimisation Techniques, *Proceedings of the 8th ASMO-UK/ISSMO Conference on Engineering Design Optimization Product and Process Improvement*, London, England, pp. 19–25, 2010;

II. Allen, J. G., Coates, G., and Trevelyan, J., Hyper-Heuristic Optimisation for Application to Aircraft Structural Design, *Proceedings of the 9th ASMO-UK/ISSMO Conference on Engineering Design Optimization Product and Process Improvement*, Cork, Republic of Ireland, pp. 1–6, 2012a;

III. Allen, J. G., Coates, G., and Trevelyan, J., Hyper-Heuristic Structural Optimisation of Conceptual Aircraft Designs, *14th AIAA/ISSMO Multidisciplinary Analysis and Optimization Conference*, Indianapolis, IN, USA, AIAA 2012-5527, 2012b;

IV. Allen, J. G., Coates, G., and Trevelyan, J., Approaches to Parameter Control for the Optimisation of Conceptual Aircraft Structural Designs, *Royal Aeronautical Society 3rd Aircraft Structural Design Conference*, Delft, The Netherlands, 2012c;

V. Allen, J. G., Coates, G., and Trevelyan, J., A Hyper-Heuristic Approach to Aircraft Structural Design Optimization, *Structural and Multidisciplinary Optimization*, 48(4), pp. 807–819, 2013;

VI. Allen, J. G., Coates, G., and Trevelyan, J., Dynamically-Controlled Variable-Fidelity Modelling for Aircraft Structural Design Optimisation, *Proceedings of the Institution of Mechanical Engineers, Part G: Journal of Aerospace Engineering*, 228(8), pp. 1434–1449, 2014.

Acknowledgements

The author would like to extend his sincere thanks to Dr Graham Coates and Prof Jon Trevelyan for their supervision and support throughout the duration of this research project. Their advice, experienced insight and enthusiasm for the project were invaluable in gaining an understanding of the research problem and for the progression of the initial problem to a viable and well-understood solution. The author thanks his colleagues at Durham University for their input during the project and the School of Engineering and Computing Sciences for financial support of the project.

The author would also like to thank the engineers at BAE Systems, Warton and (formerly) Chadderton, for their input and feedback throughout the project to better bridge the gap between academic research and industrial application of the framework. The depth of their knowledge was of great use in order to better understand and appreciate the theory and application of aircraft structural design within a leading aerospace design and manufacturing company. In addition, the author thanks the academics and industry experts who provided advice on the shaping of the project and framework during reviews of publications and discussions at conference events and other meetings.

Finally, extensive thanks is overdue from the author to his family for their unwavering guidance, encouragement and support not only during this project but also throughout the formative years. Their influence has been instrumental in promoting self-belief and a pursuit for greater knowledge, as well as installing a keen interest in aerospace engineering. Last but not least, the author thanks his newlywed wife for her patience during this project and uses these words to promise to finally take her on honeymoon!

Jonathan Allen
August 2014

Contents

List of Figures

List of Tables

Glossary

AM	all moves
AoA	angle-of-attack
AStrO	Aircraft Structural Optimiser
BP	breeder pool
BSA	bit-string affinity
BWB	blended-wing body
CAD	computer-aided design
CAE	computer-aided engineering
CFD	computational fluid dynamics
CoG	centre of gravity
CPU	central processing unit
CSV	comma-separated values
DE	differential evolution
DoE	design of experiments
DoF	degree of freedom
EA	evolutionary algorithm
EAS	equivalent airspeed
EMC	exponential Monte Carlo
EMCQ	exponential Monte Carlo with counter
EoM	equation of motion
FD	finite difference
FE	finite element
FEA	finite element analysis
FoS	factor of safety
GA	genetic algorithm
GR	greedy
GUI	graphical user interface
HC	hill climbing
HHA	hyper-heuristic approach
HPC	high-performance computing

ID	identification
IE	improving and equal
KQ	killer queen
LLH	low-level heuristic
LMC	linear Monte Carlo
LS	local search
MA	memetic algorithm
MC	Monte Carlo
MDO	multidisciplinary optimisation
MFC	Mircrosoft foundation class
MoI	measure of improvement
MPI	message-passing interface
OI	only improving
OOP	object-orientated programming
OpenGL	Open Graphics Library
PD	permutation descent
PE	permutation
PK	peckish
PSO	particle swarm optimisation
RC	radioactive contamination
RD	random descent
RI	random immigration
RW	roulette wheel
SA	simulated annealing
SD	steepest descent
SI	swarm intelligence
SQP	sequential quadratic programming
SR	simple random
TAS	true airspeed
TO	tournament selection
TS	tabu search
UAV	unmanned aerial vehicle
UML	unified modelling language
VB	Visual Basic
XCS	learning classifier system

Nomenclature

This nomenclature applies throughout the main body of this document and in Appendices C and D. The notations used in Appendices A and B are presented at the end of each appendix. Notation is defined on first usage within the text and takes the units listed below unless stated otherwise.

A	affinity, %
A	cross-sectional area, m^2
a	hyper-heuristic objective function normalising coefficient
b_r	spar root breadth, m
b_t	spar tip breadth, m
C1,..., 2	design constraint ID
c	chord length, m
c	design constraint value
c_1	design constraint on minimum FoS under yield
$c_{1,PSO}$	PSO cognitive parameter
c_2	design constraint on wingtip deflection, m
$c_{2,PSO}$	PSO social parameter
c_r	root chord length, m
c_t	tip chord length, m
d_e	engine nacelle diameter, m
d_r	spar root depth, m
d_t	spar tip depth, m
d_{wt}	wingtip deflection, m
d_x, d_y, d_z	displacement parallel to x, y, z-axis, m
E	elastic modulus, Pa
F	model fidelity level
F	solution fitness
F_{DE}	DE weight
f	unpenalised design objective value
f_1, f_2, f_3	first, second, third choice function components
f_x, f_y, f_z	force parallel to x, y, z-axis, N
G	shear modulus, Pa

g	value with respect to inequality design constraint
h	low-level heuristic
h	value with respect to equality design constraint
I_{yy}, I_{zz}	second moment of area about minor y, major z-axis, m^4
i	individual
J	torsion constant, m^4
j	design constraint
k	generation
k_b	Boltzmann's constant
L1,..., 11	load case ID
l	last instance of LLH selection
l	length, m
l_e	engine nacelle length, m
m	mass, kg
m	number of design constraints
m_e	engine mass, kg
m_{str}	structural mass, kg
N	generation of best solution discovery
N	node number
n	normal acceleration load factor
n	number of objects created by class
n_b	FoS against yield under beam bending stress
n_b	number of bits
n_c	number of crossover points
n_{DoF}	number of DoFs
n_E	FoS against critical Euler buckling stress
n_k	maximum number of generations
$n_{k,\lambda}$	adaptive penalty parameter generation period
n_{LLH}	number of LLHs
n_l	number of times LLH selected
n_{mem}	number of mission stages
$n_{\min}$	minimum FoS within structure
n_{PK}	number of LLHs for selection by PK hyper-heuristic
n_p	number of parameters
n_{sp}	number of slave processors
n_{TS}	tabu list length
n_{VM}	FoS against yield with respect to von Mises criterion
n_v	number of design variables

O1	design objective ID
P1,. . . , 18	dynamic parameter ID
p	probability
$p_{c,DE}$	DE crossover probability
$p_{c,GA}$	GA crossover probability
p_m	mutation probability
p_{neg}	negative move probability
Q_{ni}	consecutive generations without improvement
r	random number
$r_{1,PSO}$	PSO cognitive random number
$r_{2,PSO}$	PSO social random number
r_v	random variable
T	computation time, h
T_e	engine thrust, N
T_{SA}	SA temperature
t	thickness, m
V	airspeed, kts
V1,. . . , 50	design variable ID
V_A	manoeuvre speed, kts
V_B	maximum gust velocity speed, kts
V_C	cruise speed, kts
V_D	design diving speed, kts
v	design variable
X	population set
x	design variable value
x	position in x-direction, m
x_r	root position in spanwise x-direction, m
x_t	tip position in spanwise x-direction, m
$\{x\}$	position vector
$\{\dot{x}\}$	velocity vector
$\{\hat{x}\}$	best position vector
$\{\tilde{x}\}$	trial vector
y	position in y-direction, m
z	position in z-direction, m
z_{FS}	front spar position in longitudinal z-direction, m
z_{LE}	leading edge position in longitudinal z-direction, m
z_{RS}	rear spar position in longitudinal z-direction, m
α	first choice function component weighting

α	Newmark-β direct integration method constant
α	penalty parameter
α_1, α_2, α_3	first, second, third DE agent
α_{BP}	BP breeder pool intake
α_{RC}	RC contaminated population
α_{RI}	RI indigenous population
α_{SA}	SA cooling rate
β	feasible population, %
β	Newmark-β direct integration method constant
β	second choice function component weighting
β_1, β_2	adaptive penalty coefficient constants
γ	element member distribution factor
γ	modified choice function component weighting
Δc	feasibility difference with respect to design constraint
ΔF	model fidelity step size
Δk	hyper-heuristic evaluation period
ΔT	proportional difference in computation time
Δt	time step length, s
ΔV	design variable range
Δx	step size
Δx_{PA}	perturbation analysis step size
δ	convergence rate
δ	third choice function component weighting
δ_b	binary chromosome strand resolution
δ_F	model fidelity rate of change
ζ	damping ratio
η	success rate, %
θ_x, θ_y, θ_z	rotation about x, y, z-axis, rad
κ_{PSO}	PSO constriction constant
λ	penalty coefficient
μ	population size
μ_{BP}	BP breeder pool size
μ_{PA}	perturbation analysis population sample size
μ_{RC}	RC contaminated population size
μ_{RI}	RI indigenous population size
μ_{sub}	sub-population size

ρ	density, kg/m^3
τ	ranking
τ	time elapsed, s
Φ	design objective value
ϕ	hyper-heuristic objective value
$\hat{\phi}$	penalised hyper-heuristic objective value
ω_{PSO}	PSO inertia weight

"Engineering is the professional art of applying science to the optimum conversion of natural resources to the benefit of man."

Ralph J. Smith, 1962

Chapter 1

Introduction

The optimisation of an aircraft design is of increasing importance throughout the aerospace industry as competing airline operators look to reduce costs and militaries demand vehicles of superior performance on the battlefield. These demands are all the more important during difficult economic times and have led to the requirement for designs to maximise performance efficiency to ensure that the cost to the operator is at a minimum as well as the cost to the manufacturer in producing such aircraft. Therefore, there exists a necessity for effective tools to aid the engineer during the design process in developing near-optimal aircraft designs such that the resulting vehicles will be able to perform their required missions as efficiently as possible. The structural design of the aircraft is of critical importance in defining the strength of the airframe under load and contributes greatly to the mass of the aircraft. The latter in turn provides a key contribution to the vehicle manufacturing and operating costs through material costs, fuel consumption and subsequent performance such as reduced lift requirements and CO_2 emissions.

The process of aircraft design optimisation requires the consideration of numerous parameters due to the complicated nature of aircraft designs. Optimisation is performed using three types of design parameters: variables, constraints and objectives. Design variables are numerical representations of the properties of a design, e.g. the dimensions of the aircraft, the values of which uniquely define each individual design. These values are modified through optimisation in order to discover a combination of variables that produces a near-optimal solution to the presented design problem. Design constraints impose limits on the design, and thus the solution space, to ensure the final solution satisfies specific requirements such as those of aircraft performance, e.g. structural strength under load. Finally, design objectives represent the aims of the optimisation process, i.e. the measure of solution quality. A common objective of structural optimisation is an aircraft of minimal structural mass. Consequently, aircraft structural optimisation is conventionally performed by varying the design of the airframe for a solution of minimal mass whilst providing necessary resistance to loads likely to be encountered during operation, i.e. the aircraft mission.

Hyper-heuristic optimisation is a newly evolving field of research wherein the process of finding a solution to an optimisation problem is monitored and modified to further improve the quality of the solution and performance of the optimisation process. A hyper-heuristic approach (HHA) performs such monitoring and modification, typically through the selection and set up of the optimisation techniques employed and the analysis of the solution space surrounding sampled designs. This is contrary to the traditional static process where optimisation is performed with constant settings throughout its duration. The relative infancy of hyper-heuristics has resulted in limited application to aerospace design optimisation. Therefore, an opportunity exists to apply hyper-heuristics to the problem of aircraft structural design optimisation in order to improve the quality of solutions generated and the process by which this is accomplished.

A framework has been developed for the optimisation of the structural design of an aircraft at a conceptual level through the application of an HHA. The framework encourages the generation of near-optimal aircraft designs of various classes subject to the simulation of multiple loading conditions. Improved solution quality is promoted over traditional optimisation approaches through the use of the HHA, which discourages premature convergence and promotes learning of the solution space neighbouring good designs. This document describes the thesis for this framework, including a review of existing approaches, a description of the framework and its subsequent implementation, and an evaluation of the framework through a number of case studies. The framework is presented as a series of modules to perform the necessary tasks of aircraft design and hyper-heuristic optimisation. A software tool developed as a computational implementation of the framework called AStrO, an acronym of 'Aircraft Structural Optimiser', is described and employed for experimental evaluation of the framework. The results of the case studies indicate improved solution quality and feasibility over that obtainable by traditional methods, as well as indicating the influences of different load cases on specific areas of the airframe.

This chapter serves as an introduction to this research project and is structured as follows. A description of the aircraft and related terminology is provided in §1.1 followed by a description of the design process in §1.2 focussing on the conceptual design stage and optimisation during engineering design. The research aims and objectives are provided in §1.3, which includes a description of the thesis of this project. The methodology of this research project is then provided in §1.4 prior to a description of the structure of this document in §1.5.

1.1 The Aircraft

Within this document, an aircraft describes a fixed-wing heavier-than-air vehicle propelled through the atmosphere of Earth by mounted powerplant units with flight achieved through the generation of dynamic lift, i.e. an aerodyne. It can be assumed herein that an aircraft is piloted by a flight crew unless specified as an unmanned aerial vehicle (UAV). An example of a generic light civil aircraft is shown in Fig. 1.1.

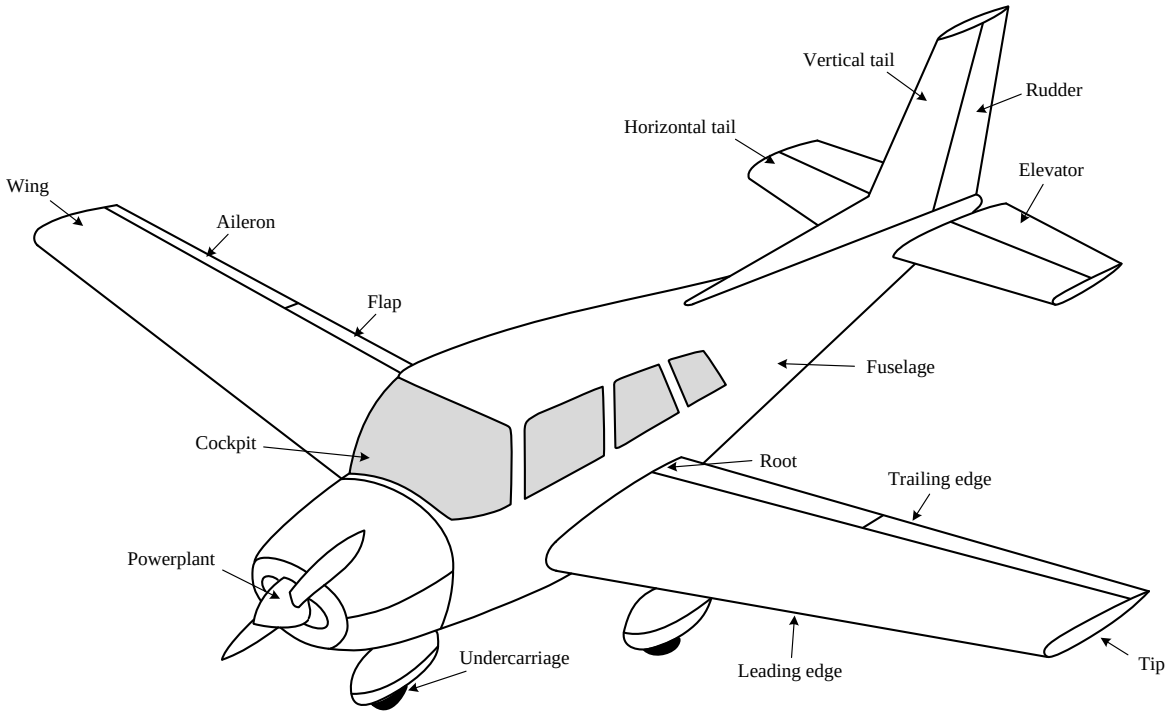

Figure 1.1: The aircraft

The conventional aircraft consists of three main sections: wing, empennage and fuselage. The wing is the main lifting surface of the aircraft with the primary requirement to generate sufficient lift to enable flight. Secondary purposes of the wing include carrying fuel and supporting the main undercarriage, powerplants and detachable ordnance such as external fuel tanks and stores, e.g. weapons. The wing typically includes flight controls such as the ailerons, to control roll about the aircraft longitudinal axis, and high-lift devices such as flaps to facilitate flight at a high angle-of-attack (AoA) without stall. High-lift devices are used principally during take-off and landing. The empennage is formed of the auxiliary lifting surfaces, i.e. horizontal and vertical tails, the designs of which are similar to that of the wing. These tails balance the aircraft to provide stability during flight as well as control of pitch about the lateral axis and yaw about the vertical axis by the elevators and rudder respectively. The fuselage is the main body of the aircraft containing the cockpit, main payload, nose undercarriage and additional fuel tanks and powerplants. The payload often refers to a mass of items or number of passengers to be transported. The undercarriage units, or landing gear, support the aircraft on the ground and provide manoeuvrability as well as absorbing landing loads. Powerplants, or engines, are usually installed within one or both of the fuselage and wing to provide the propulsion required to achieve flight and for manoeuvrability in the air and on the ground. Powerplants are internal combustion engines that function either as a propeller-driving piston engine or turbine, the latter of which includes turboprop and turbojet engines. Each lifting surface has a leading and trailing edge at the fore and aft-most points on the cross-section respectively. Similarly, the root and tip of each surface indicate respectively the positions closest to and furthest from the aircraft centreline along the lifting surface span.

The aircraft illustrated in Fig. 1.1 is typical of a light civil aircraft. The majority of past and present aircraft of different classes, e.g. large civil transport or military aircraft, possess similar sections within their design. The lack of significant innovation in this layout of an aircraft is most notable in the civil aviation market, where the success of a design is largely dependent on its acceptance by the passengers who are to fly in it. Nevertheless, future designs of aircraft have led to the proposal of novel configurations including twin-fuselage and blended-wing body (BWB) designs. The employment of remotely-piloted UAVs is increasing both in civil and military arenas. This significantly influences the requirements of the design by reducing dependencies on human responses and capabilities. Consequently, UAVs are designed based on operational demands, e.g. required endurance and manoeuvring capabilities, without the requirement to provide space and support for a human payload or flight crew, i.e. replacing a cockpit with remotely-operated flight equipment. Furthermore, this has created the possibility for autonomous aircraft no longer requiring any human input during operation, although many technological, legal and moral barriers currently prevent the operation of such a vehicle. Advances in material technologies have led to the increased use of composite materials within designs whilst manufacturing developments have created new possibilities in the production of aircraft components. Despite such advances creating excitement within the field for significant developments in aircraft design, there still exists a need to improve conventional designs. This is especially true given that the civil aircraft industry is dependent on its customers, i.e. the general public, who are notoriously cautious about flying in aircraft that appear to be drastically different from conventional designs.

1.1.1 Role of the Airframe

The design of an aircraft principally considers the following engineering disciplines:

- aerodynamics: design of external profile to provide appropriate airflow for flight manoeuvres;
- propulsion: design of engines with sufficient thrust for manoeuvrability in-flight and on the ground;
- systems: design of control, navigation, hydraulic, electrical and pneumatic systems;
- structures: design of the airframe to provide structural strength under load.

The aerodynamics of the aircraft are determined by the geometry of its external profile, leading to the determination of the amount of lift and drag generated by the aircraft and the geometric boundary within which the internal structural design is constrained. Propulsion determines the design of the engines, including the level of thrust available to the aircraft and the mass of the powerplant units. The design of the systems includes many different aspects of aircraft operation, most notably flying control surfaces such as ailerons, elevators, rudder, spoilers, flaps and other devices. The design of the structure, otherwise referred to as the airframe, provides the aircraft strength under applied loads such as those resulting from in-flight and ground manoeuvres. Additional loads include the effects of inertia, engine thrust and cabin pressurisation. There has been little fundamental change in the structural design of aircraft since the pioneering flying machines were developed at the start of the twentieth century. This is surprising given the substantial advances in engineering and technological capabilities over the period and the clear visible differences in leading designs across the age of flight, e.g. the Wright Flyer, Supermarine Spitfire, de Havilland Comet, Hawker Siddeley Harrier Jump Jet, Airbus A350 etc. In spite of this, upon inspection beyond the outer skin the structures of such aircraft are remarkably similar. Figure 1.2 shows the typical structures of a lifting surface and fuselage containing the following structural members:

- lifting surface:
  - ribs;
  - spars;
  - stringers;
- fuselage:
  - frames;
  - floor beams;
  - stringers.

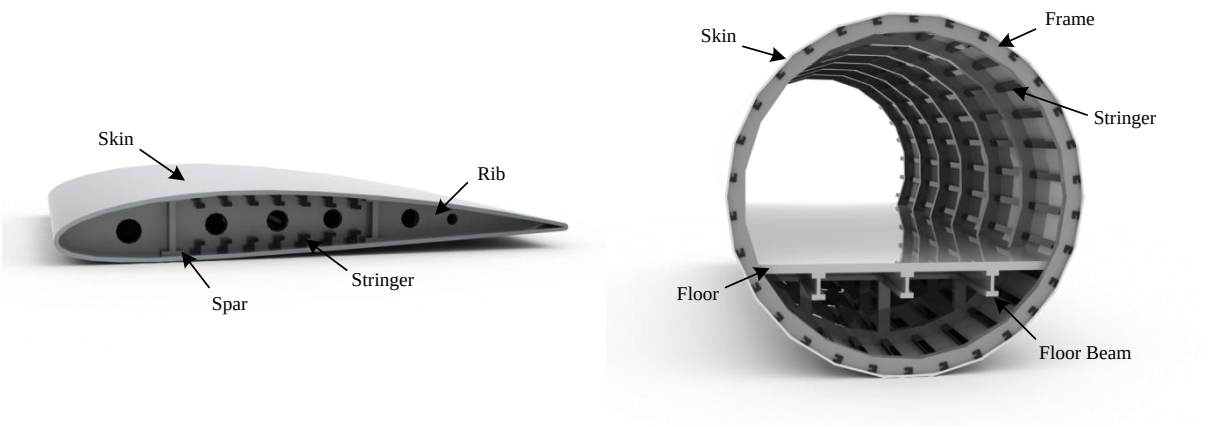

(a) Lifting surface (b) Fuselage

Figure 1.2: Typical airframe structure

Ribs are chordwise members that reinforce the skin to maintain the cross-sectional shape required to generate lift for flight. Ribs also provide resistance against shear and buckling, as well as transmitting local loads to the spars. Spars are spanwise members that withstand these transmitted local loads as well as bending and torsional loads. Spars are often shaped as I-sections through their formation of spar caps and webs. Stringers are similarly spanwise members that resist bending loads as well as axial loads. Stringers also divide the skin into smaller sections for improved resistance against buckling. Stringers are considerably smaller in cross-section than spars and are often shaped as C, T or Z-sections. The structural members within the fuselage perform similar functions to those within the lifting surfaces. Frames provide the equivalent support to the skin as ribs to maintain the cross-sectional shape of the fuselage and divide the skin into small panels for improved resistance against buckling, especially under pressure loads. Floor

beams provide support to the floor of the aircraft under load whilst stringers perform the same function as those within the lifting surfaces. Commonly longerons are included within the fuselage structure as larger members of the same nature as stringers. Due to the similarity in design, the terms longerons and stringers are often interchangeable within the fuselage. In addition to these members, skin over the aircraft exterior and the floor within the fuselage provide structural support to the airframe by acting in conjunction with the structural members to withstand bending, shear and torsion.

1.2 The Design Process

The design process aims to solve a given problem through the generation of new or improved designs to satisfy specific objectives. Blumrich (1970) states *"design establishes and defines solutions to and pertinent structures for problems not solved before, or new solutions to problems which have previously been solved in a different way"*. The problem concerned can take various forms depending on the disciplines involved and objectives to be satisfied. A good understanding of the problem is necessary such that an appropriate strategy is employed during the design process to increase the likelihood of satisfying the objectives. This includes the selection of achievable objectives and appropriate variables and constraints to represent the problem. The timescale over which the problem is to be solved also requires consideration, as greater problem complexity and detail can significantly lengthen the process.

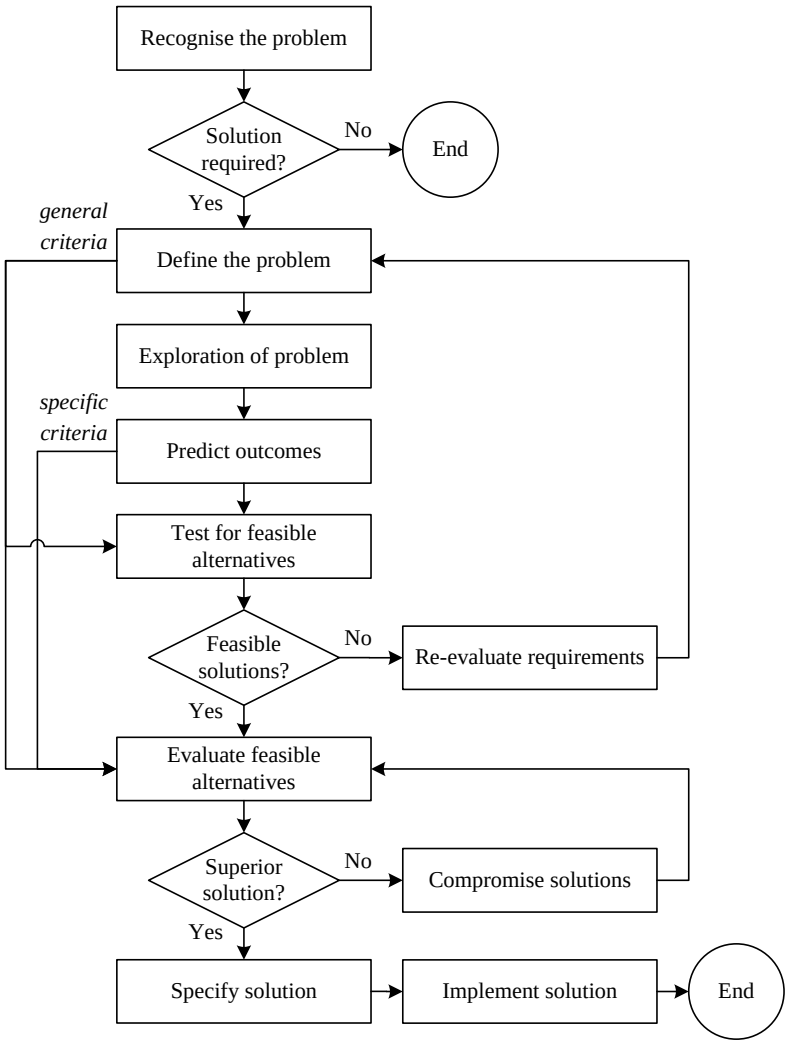

Figure 1.3: Design process flowchart (Lewis and Samuel, 1989, Fig. 1.6 p. 12)

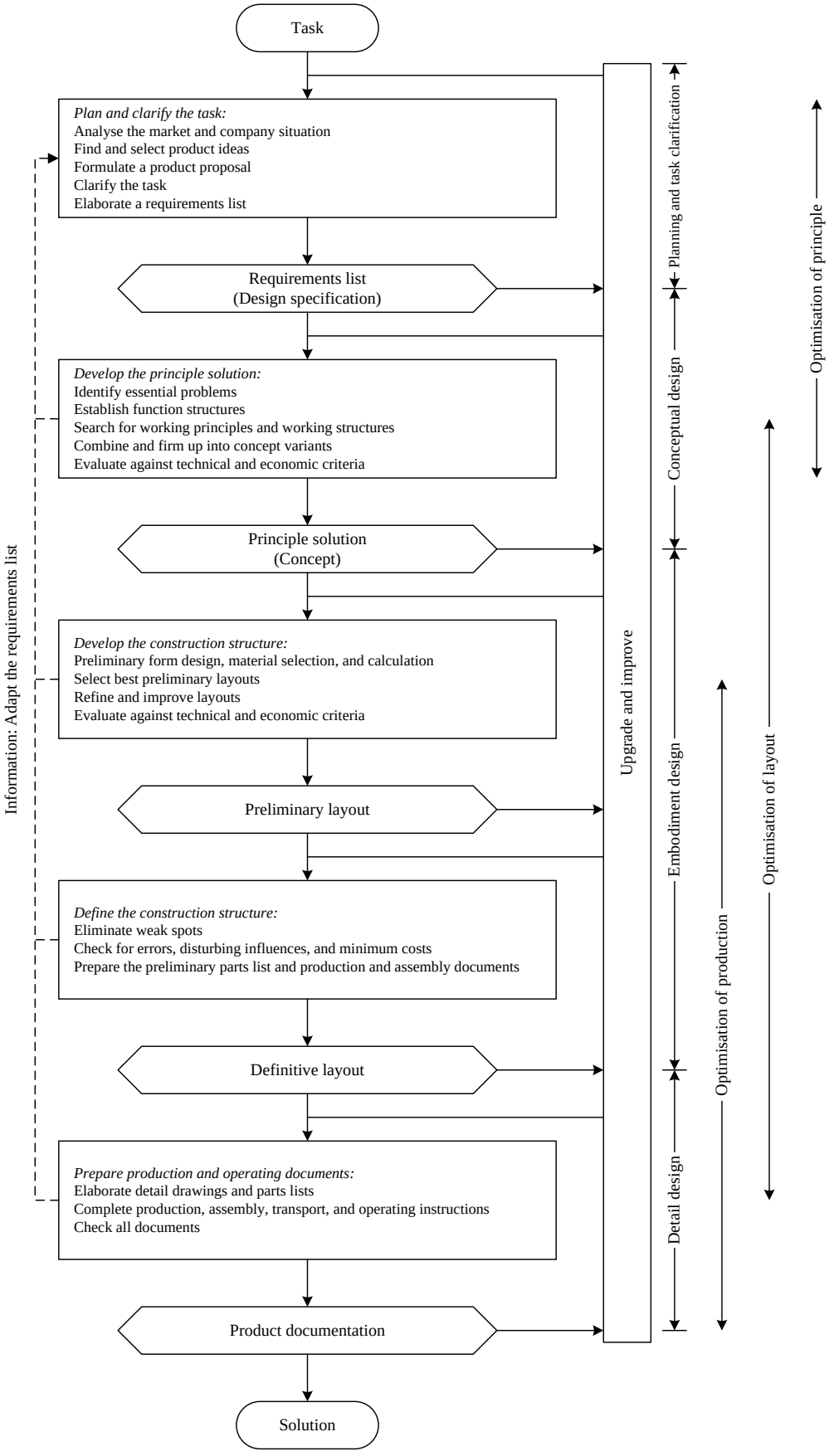

Figure 1.4: Planning and design process (Pahl et al., 2007, Fig. 4.3 p. 130)

Flowcharts, such as in Fig. 1.3 (Lewis and Samuel, 1989) and Fig. 1.4 (Pahl et al., 2007), illustrate the design process by showing the key tasks and decisions involved as well as the iterative nature of obtaining a solution. The stages of the design process shown in Fig. 1.3 may be grouped into the following stages:

1. problem recognition: the stimulus of engineering design is the identification of an engineering problem that requires addressing;
2. problem definition: a description of the problem, including the establishment of objectives, resources and constraints, such that quantitative information is possessed on the specifications of the problem;
3. problem exploration: a hypothesis of possible solutions and determination of a detailed strategy to be employed to solve the problem;
4. problem solution: investigation and development of possible solutions to the problem;
5. problem evaluation: analysis of the obtained solutions against the problem objectives to determine suitability of designs, specification of the solution and implementation of the design.

The alternative representation of the design process in Fig. 1.4 shows the flow of information between different process stages. This representation describes the tasks involved with greater precision and also indicates that the design process is conventionally divided into four phases: planning and task clarification, conceptual design, embodiment design and detail design.

1.2.1 Planning and Task Clarification

Planning and task clarification requires the design problem to be recognised and defined, leading to the collection of information to enable the proceeding stages of the process to be planned and executed appropriately. Such information includes the design requirements and the methods to be employed for design, manufacture and production. A hypothesis of the solution is also predicted and consequently a suitable design strategy created. The execution of the conceptual, embodiment and detail design stages are then based on this strategy. Continual updating of the plan and subsequent design requirements is performed throughout the design process as informed by experience gained during the process.

1.2.2 Conceptual Design

The conceptual phase of the design process begins following the completion of planning and task clarification. It is this phase of the design process that is the focus of this research project. The aim of conceptual design is to evaluate the requirements of the design before the later phases of the design process further explore and evaluate these potential design problem solutions. While several concepts may be taken forward to the next phase of the design process it is preferable to obtain a favoured concept that outperforms the other good concepts under consideration.

The generation of good concepts is critical to the design process, placing the greatest demands on a designer by providing the greatest opportunities for significant improvements to be made in the design. The knowledge required to make critical decisions is not always available at the start of the process; however, the flexibility for change of the design diminishes as such knowledge is obtained and applied due to increased commitment towards the developed design. Hence, it is important to evaluate the suitability of designs as early as possible during the design process such that informed decisions may be made in order to direct the development of suitable high-quality designs. This is illustrated in Fig. 1.5(a). Examples of such decisions during aircraft design concern the aircraft configuration, performance and size; thus defining the vehicle geometry, layout and attachment locations such as powerplant and undercarriage mountings. Other consequences of decisions made during the design process are the commitments of the cost of the design both at the current process phase and in the future, as indicated in Fig. 1.5(b).

The duration of conceptual design varies greatly depending on the design requirements, available resources and experience possessed. Computer-aided engineering (CAE) tools such as computer-aided design (CAD) are commonly employed during modern design, however such tools must be sufficiently

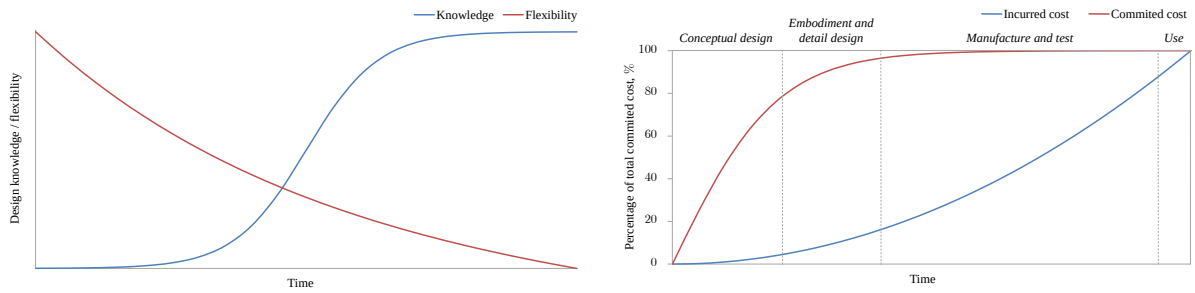

(a) Design knowledge and flexibility (b) Process cost allocation

Figure 1.5: Knowledge, flexibility and cost allocation during design process

fluid for use with rapidly evolving solutions. Therefore, these tools are often replaced by simpler methods such as stick or panel models to allow greater flexibility of design evolution whilst retaining the capacity for analysis at an appropriate level of detail. Detail levels during conceptual design are typically kept to a minimum to enable rapid modelling, analysis and evolution of numerous designs to permit the opportunity to explore a variety of problem solutions. Model fidelity describes the level of detail within a model and its subsequent precision with respect to reality. The level of model fidelity is typically increased during embodiment and detail design in order to obtain greater knowledge of the intricacies of a design. Figure 1.6 exemplifies increasing the fidelity used to model an I-beam with holes to enable greater precision in the analysis of the beam during the later phases of the design process.

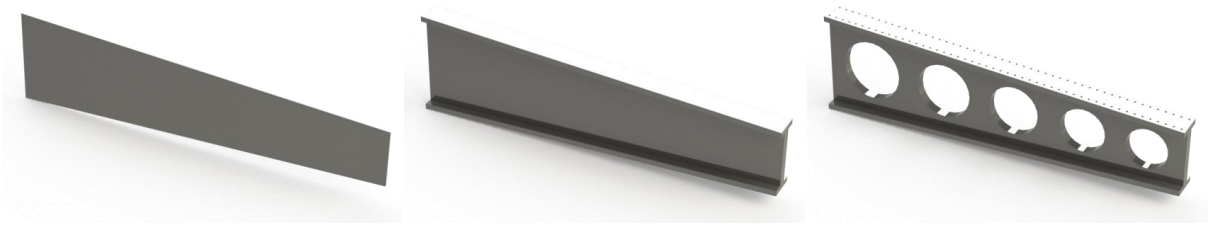

(a) Conceptual design (b) Embodiment design (c) Detail design

Figure 1.6: Level of detail during design process

1.2.3 Embodiment Design

Embodiment design, also referred to as preliminary design, begins after most major design decisions have been made and a concept has been selected. Embodiment design aims to mature this concept through its evolution into a design of higher definition by more detailed problem exploration and evaluation. This provides increased understanding of the design and increases the reliability on discipline-led design by offering greater control of specialist areas of the design to specific engineering departments, e.g. structures. The concept is subsequently developed into a design of higher definition and with greater understanding than was possible during the conceptual design phase.

1.2.4 Detail Design

The final phase of the design process concerns the detailed design of all aspects of the aircraft, including many intricate parts, to ensure the design will fulfill its potential and meet its requirements. During this phase, design is conducted at the highest degree of detail with respect to both computational models and manufactured prototypes. It is even possible for large manufacturers to develop flight simulators to evaluate the performance of aircraft designs. During the detailed design of an aircraft, it is common to consider each part of the aircraft independently, from the structural members in the airframe to the

fasteners attaching the skin. Much higher fidelity models are used than in the previous stages of the design process, resulting in a greatly increased demand on design time. It is for this reason that the preceding stages of the design process carry so much importance: to ensure the aircraft is designed suitably before attributing such a large quantity of resources upon the design of the details. Following the selection of a suitable solution to the problem, this design is specified for subsequent implementation through manufacture and operation.

1.2.5 Optimisation in Engineering Design

The optimisation of a solution to a problem is not a new area of study. Mathematicians in Ancient Greece were known to solve optimisation problems, such as Euclid (c. 300 BC) proving that a square provides the greatest area to be enclosed of all possible rectangles with same total length of sides. Another example is of Heron (c. 100 BC) finding that the shortest distance travelled by a path of light reflected by a mirror occurs when the angles of incidence and reflection are equal. In the subsequent ages, further problems were solved using optimisation and techniques were established for solving such problems. For example, Sir Issac Newton (1687 AD) determined that a symmetrical revolution provided the optimal body shape for minimal resistance to motion in a fluid, which led to the derivation of the resistance law of the body; a problem independently suggested earlier by Galileo Galilei (1638 AD). More recently, and with the advent of the computing age, many variations of optimisation techniques have been developed and applied to more complex problems. As the problems encountered during engineering became more complicated due to greater complexities and demands of design problems, the use of optimisation has become a critical aspect of the design process in many fields. This is indicated in Fig. 1.4 by the need to optimise the principle, layout and production of the design; hereby requiring an element of optimisation at all periods of the planning and design process.

Optimisation in engineering design aims to improve the quality of a solution to a problem through the modification of characteristics of the design. The quality of a design is measured with respect to a predetermined objective typically formed as a minimisation or maximisation function. A design is defined by the variables representing the design properties available for modification. Consequently, the best solution to a problem is found by the combination of design variable values that generates the minimum or maximum value as required to the corresponding objective function. The value of this objective function can include the consideration of the feasibility of a design with respect to imposed constraints. This consideration is often made through the use of a penalising strategy; as such, a solution that originally appears to be the best may not remain so should it violate a design constraint. The set-up of the optimisation process dictates the nature of the search for a suitable design solution. This process may be static, wherein the initial set-up remains constant throughout the search, or dynamic such that modifications can be made to the process to improve its performance and subsequent solution quality.

1.3 Research Aims and Objectives

The structural design of an aircraft drives the strength of the airframe under load and contributes greatly to its overall mass, which in turn influences the vehicle performance and cost. Given the importance of conceptual design in establishing suitable designs for further development, the generation of a high-quality, i.e. light, airframe concept is critical to the quality of the final aircraft design. Structural optimisation of the airframe for minimal mass provides the capability to generate such high-quality concepts. Furthermore, a dynamic optimisation process can lead to improved solution quality and process performance, e.g. computation speed, through the modification of the process during execution.

This research aims to develop a framework for the structural optimisation of an aircraft concept for minimal mass under load. An HHA is embedded within the framework to improve the operation of the optimisation process such that solution quality and computational expense can be improved and

reduced respectively. It is the thesis of this research that the use of hyper-heuristic optimisation within the framework can improve solution quality over that possible by traditional methods without incurring computational costs. The following objectives have been satisfied in conducting this research:

- a review of aircraft design optimisation to determine the requirements of the framework;
- a review of hyper-heuristic optimisation to encourage improved solution quality with the framework;
- the development and implementation of the framework for subsequent evaluation;
- evaluation of the framework against existing approaches to aircraft design optimisation.

The novelty of the framework lies principally in the application of hyper-heuristics to airframe design optimisation. This application aims to improve solution quality through the use of a dynamic optimisation process. Little research into the optimisation process was found in the review of literature concerning aircraft design optimisation, with no application of hyper-heuristics apparent to aircraft structural design. Hence, this framework is an original application of an HHA to aircraft structural design optimisation. The HHA modifies the optimisation process based on its performance as measured by an online learning mechanism. The HHA controls the optimisation process through four aspects: selection of optimisation techniques, distribution of solutions between multiple techniques, analysis of perturbations in the local solution space and modification of process parameters. Such a combination of four different aspects of hyper-heuristics within a single HHA was not discovered during the review of hyper-heuristic optimisation, where traditional approaches focus on a single aspect. Further capabilities of the framework that were not found in the majority of literary sources include a capability to consider various aircraft classes, the simulation of multiple load cases and the ability to generate a complete aircraft configuration rather than solely a single aircraft section, e.g. the wing.

1.4 Research Methodology

Figure 1.7 (Duffy and O'Donnell, 1998) illustrates the research methodology followed during this project. The design problem is identified through analysis of relevant literature and design practice. A hypothesis is formulated, from which the research problem is developed leading to the generation of a solution. This solution is then evaluated through common design practice. The problem and solution are subsequently documented such that the findings may themselves form part of the literature for future investigations.

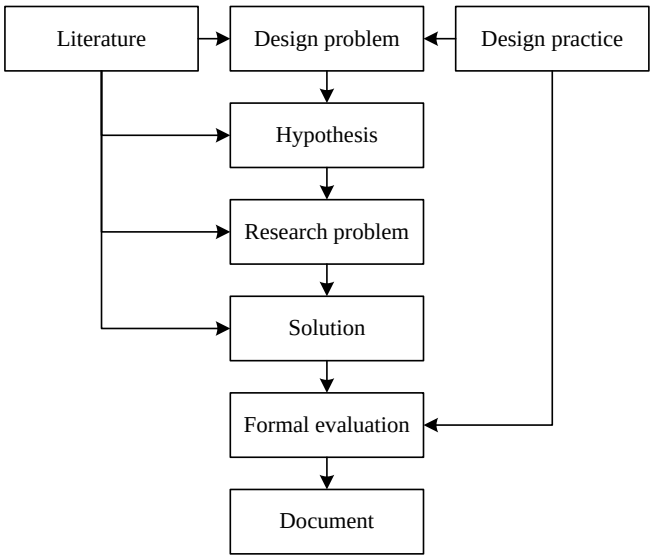

Figure 1.7: Research methodology (Duffy and O'Donnell, 1998, Fig. 7 p. 6)

1.5 Structure of Document

This document concerns the research, development and evaluation of the thesis described in §1.3. The work that is reported in this document is structured as follows:

Part I introduces the design problem, existing approaches to the problem and the research hypothesis:

Chapter 1 introduces the research including its motivation. This includes an overview of the design process and the use of optimisation in engineering followed by the aims, objectives and methodology of the research.

Chapter 2 reviews existing approaches to the aerospace design optimisation problem, principally focussing on the structural optimisation of conceptual aircraft designs. Common practices within this field are described and compared. This includes a detailed review of the existing approaches to aircraft design optimisation that are most pertinent to this project.

Chapter 3 provides an introduction to hyper-heuristic optimisation followed by a review of previous applications of hyper-heuristics. This includes a description of different aspects and techniques commonly included within an HHA.

Chapter 4 uses the findings of Chapters 2 and 3 to identify the requirements of a framework for aircraft structural design optimisation and research opportunities within this area, thus providing the research hypothesis. Key terminology is also defined for reference during Parts II and III of this document.

Part II describes the framework hypothesised as a solution to the research problem:

Chapter 5 describes the framework for hyper-heuristic aircraft structural optimisation created to investigate the hypothesis presented in Chapter 4. This framework is presented in three stages: aircraft design, structural analysis and airframe design optimisation. Aircraft design includes framework initialisation, mission definition, computation of load cases and generation of the aircraft design. Structural analysis concerns the generation and subsequent finite element analysis (FEA) of an airframe model followed by analysis of the stress field within the airframe. Airframe design optimisation includes the application of a penalising strategy, calculation of solution fitness and subsequent optimisation of the designs. This stage includes an embedded HHA that encourages improved solution quality and computational speed as well as improved feasibilities of designs and convergence on a high-quality solution.

Part III evaluates the framework as a solution to the research problem:

Chapter 6 introduces AStrO as a computational implementation of the framework. This tool is subsequently used to evaluate the framework through a series of investigations and case studies in Chapters 7 and 8 respectively.

Chapter 7 describes preliminary investigations into appropriate set-ups of AStrO for use during the case studies presented in Chapter 8. This includes FEA and optimisation verification followed by investigations into the optimisation process set-up, chiefly that of the HHA.

Chapter 8 presents the case studies used to evaluate the performance of the framework using AStrO for a selection of design problems. These studies investigate the effects of the HHA on the results of the optimisation process, as well as methods of controlling the optimisation process and the influences of different load cases on the aircraft design. Both novel and existing variants of a selection of civil and military aircraft are used for these studies.

Chapter 9 evaluates the framework against the requirements and opportunities in Chapter 4 through the discussion of the case study results presented in Chapter 8 and research thesis before providing suggestions for future work and concluding remarks concerning the thesis.

Four chapters are appended to this document as follows:

Appendix A provides the supporting theory for the aircraft design process within the framework.

Appendix B describes the theory behind FEA as employed by the framework for structural analysis.

Appendix C describes the numerical benchmark functions used during preliminary investigations.

Appendix D tabulates the set-ups and results of the preliminary investigations.

Chapter 2

Aircraft Design Optimisation

Many researchers have addressed the problem of aircraft structural optimisation in an attempt to obtain a solution of minimal mass whilst maintaining the necessary strength required under load. Such optimisation has often been combined with other disciplines, such as aerodynamics, leading to multi-disciplinary optimisation (MDO). Whilst the focus of this research is the structural optimisation of a conceptual aircraft design, consideration is made of previous research into other engineering disciplines and alternative stages of the design process. This chapter reviews such existing approaches to aircraft design optimisation through the following sections. An overview of different problems addressed within the domain of aircraft design optimisation is presented in §2.1. The traditional solution process is then described in §2.2 followed by popularly-applied optimisation techniques in §2.3. Methods of constraint handling are discussed in §2.4 due to the importance of obtaining a feasible airframe design that possesses sufficient structural integrity under load. A comparison of pertinent existing approaches to aircraft design optimisation is subsequently presented in §2.5 before the chapter is summarised in §2.6.

2.1 Optimisation of Aircraft Designs

The optimisation of an aircraft for structural performance, i.e. minimum mass whilst maintaining structural integrity under load, has been the subject of much research. Great variation exists in the classes of aircraft considered, where research has ranged from optimising the design of new or existing aircraft within the civil light, large or military classes as well as unmanned aerial vehicles (UAVs). Conventional aircraft, i.e. consisting of a fuselage, wing and empennage, are commonly subjected to optimisation, although recent studies increasingly explore novel designs such as a blended-wing body (BWB) aircraft (Lovell et al., 2004). The conceptual stage of the design process is an area of considerable interest as optimisation can present significant gains in solution quality at reduced cost due to the flexibility available in the design (Mavris and DeLaurentis, 2000). MDO is often performed within aerospace design due to the coupled properties between design disciplines (Cramer et al., 1994). This commonly, although not necessarily, results in optimisation of the structure for minimum mass in combination with optimisation of the aerodynamic profile for minimum drag, i.e. multi-objective optimisation (Sobieszczanski-Sobieski and Haftka, 1997). However, many studies consider a single design discipline such as the structure in order to focus on a specific design aspect or reduce interdisciplinary uncertainty during early stages of the design process (Daskilewicz et al., 2011; Ma and Ma, 2009). Often only a single section of the aircraft, commonly the wing, is considered rather than the entire aircraft. This permits greater design detail but fails to generate a complete configuration of the aircraft or take into account the interactions of different aircraft sections (Chacksfield, 1997; Sobieszczanski-Sobieski and Haftka, 1997).

Schuhmacher et al. (2002) investigated the MDO of the wingbox within a family of regional civil aircraft. The limitations of historical methods were investigated as well as obstacles to the use of MDO

compared to the traditional approach within an engineering company of individual design departments for each discipline. Finite element analysis (FEA) was employed to analyse the response of the wingbox to numerous loads leading to structural optimisation considering aeroelastic and structural constraints. A similar piece of research conducted was by Kesseler and Vankan (2006) into the optimisation of an aircraft wing to operate under loading conditions due to flight manoeuvres. The efficiency of the method was evaluated and the effects of the different flight conditions on the wing were described. The internal structure of the wing was optimised during this investigation, focussing mostly on component topology. Maute and Allen (2004) conducted similar research into the topology of the internal structure of the wing, where the structure was optimised for a given external profile through simulating the structural response. The results predicted a high dependency of the wing design on the aerodynamic loads experienced, and thus indicated a dependency between the aerodynamic and structural design for realistic application of flight loads to the airframe. The research of Mavris and DeLaurentis (2000) focused on the feasibility of the design of a supersonic transport aircraft, whilst Gantois and Morris (2004) investigated the optimisation for minimum weight, drag and cost of a large civil aircraft wing. In the latter, optimisation was performed during the preliminary design phase to find the design with the minimum direct operating costs through the minimisation of structural weight and drag. An MDO problem was also addressed by Çavuş (2009) for the optimisation of a UAV, a problem that was similarly tackled by Hu and Yu (2009) and Zhang et al. (2009), whilst Martins et al. (2002) performed aero-structural optimisation of a supersonic business jet for minimal drag and weight using variables controlling aircraft geometry and the thicknesses of structural members within the airframe. Ayele et al. (2013) applied MDO to two optimisation problems for a solar-powered UAV, with vehicle geometry and mission components optimised for minimal mass and maximal flight level in the first problem and maximal payload mass with minimal total vehicle mass in the second problem. Eves et al. (2009) similarly investigated the optimisation of a UAV concept. Topology optimisation was performed of the material distribution and member thickness of a BWB aircraft for a solution of minimal mass under deflection and buckling constraints.

The structural design of an aircraft wing was the subject of much research by Rao at various stages of a mission. This included the structural optimisation of the wing when subjected to loads resulting from landing (Rao, 1984), gusts (Rao, 1985) and taxi (Rao, 1987). A summary of the former two studies were also included in Rao (1986). The mathematics behind the structural optimisation problems were presented in these papers, as well as detailed reviews of previous work in the field. Another paper of Rao et al. (1979) researched minimising the weight of a wing structure whilst satisfying strength, stability and frequency requirements during more general flight conditions. Rinku et al. (2008) investigated the topology optimisation of three key structural components: a stub-wing spar, bracket for the nose undercarriage and wing attachment bulkhead, whilst Tong and Lin (2011) performed similar research. The former study was able to significantly reduce the mass of the components through optimisation whilst the latter obtained dramatic reductions in strain energy through similar optimisation of the component topology. Sofla et al. (2010) performed a review of recent activity in research into the morphing of the shape of a wing, including the use of smart materials and shape memory alloys. It was found that the use of such materials reduced the weight penalty of an actuation system through the ability of the structure to carry larger aerodynamic loads. Rothwell (1991) investigated the use of shell components for better distribution of stringer material within a wingbox, with optimisation performed for a design of minimum weight whilst maintaining adequate strength.

Arrieta and Striz (2005) performed structural mass optimisation of a military combat aircraft including damage tolerance analysis. The thicknesses of skin sections were optimised over the aircraft subject to stress and fatigue constraints. The optimisation of skin-stringer panels within the wingbox under compressive loads was investigated by Chintapalli et al. (2010). The results of the study indicated a significant saving in structural mass through the minimisation of member thickness whilst maintaining

structural integrity under the applied loads. Kaufmann et al. (2010) performed similar optimisation of skin-stringer panels under compressive loads to minimise the cost and mass of the structural members. The cost of members was approximated using empirical estimation models. Design variables included the thicknesses of composite skin plies as well as stringer pitch and geometry. A weight penalty was applied to high cost designs such that a single objective function was obtained; however, difficulty was encountered in incorporating this penalty into the optimisation problem due to uncertainty associated with defining the penalty to be applied. Pant and Fielding (1999) performed cost optimisation of a twin-turboprop short-haul commuter aircraft to minimise the generalised cost of travel including access cost, flight cost, time cost and airport cost. Wing geometry and position, component masses and flight configurations were optimised. This resulted in the generation of a solution that balanced reduced overall cost through an increase in passengers with greater required flight time and airport cost.

Sensmeier and Samareh (2004) examined the variations in the structural layouts of popular aircraft since World War II by studying cutaway drawings of the aircraft. The results of these findings were only approximate due to the inaccuracy of the drawings. Nevertheless, trends were able to be determined of how the layouts have changed over time. Limited variation was discovered in the design of the wings for commercial aircraft, but the spacing of the frames at the fore and aft-most ends the fuselage showed variations between the layouts adopted by different manufacturers. Also of interest was a large variation in the airframe designs of combat aircraft, most notably when comparing designs developed by different countries. Anhalt et al. (2003) considered a wing design with optimal aerodynamic efficiency during cruise to investigate the detrimental effects of wing structural deformation on performance. The research focused on the aeroelastic behaviour of the wing of a large civil aircraft, finding that both the lift and drag of the wing increased with tip deflection.

The optimisation of the use of composite materials within aircraft structures is a rapidly growing area of interest. Liu et al. (2011) investigated the optimisation of composite blending, including the effects of varying the stacking sequence of composite panels at predefined angles of orientation. Gasbarri et al. (2009) performed multi-level aeroelastic optimisation to firstly generate a high level design of an aircraft wing prior to further optimisation at a more detailed level. The objective of the optimisation was to maximise the flutter speed of the wing. The materials and thicknesses of the plies were optimised in the first level prior to the determination of the optimal ply orientations corresponding to these materials and thicknesses in the second level. Guo et al. (2003) researched methods of maximising the flutter speed and minimising the weight of a composite wing structure without penalising the strength of the structure. This was completed in two stages: the effects of bending and torsion on the flutter speed were firstly analysed before assessing the effects of the mass and strength of the laminates on the structure. Torsional rigidity was found to dominate the design whilst coupling rigidity significantly affected the flutter speed. Flutter speed was increased and mass reduced through the use of a thin-walled composite wingbox. Guo (2007) conducted further detailed research into flutter by focussing on the optimisation of a wing design for minimal weight whilst also investigating the subsequent effects on aeroelasticity. An investigation was conducted into methods of tailoring the wing of an aerobatic aircraft, whereby the wing was initially optimised for minimum weight before being tailored aeroelastically to achieve the maximum flutter speed. Significant mass savings and an increase in flutter speed were obtained through the optimisation of the fibre orientation of skin and spar web laminates.

Outside the domain of structural optimisation, Crawford and Simm (1999) investigated the MDO of a military fighter aircraft at the conceptual level of design with the aim of obtaining a design with a low infrared signature. In another study, Alonso et al. (2009) performed research in order to reduce the sonic boom of an aircraft travelling at supersonic speeds. Xia and Gao (2002) presented an MDO methodology for decomposition of a system, leading to a weighted objective function for aerodynamic and stealth optimisation of a wing design. The weights applied were adjusted depending on the rate of

improvement in the objective function. Koch et al. (1999) investigated MDO techniques when applied to a high-speed civil transport aircraft wing. It was found that increasing the problem size led to a large number of variables and necessary responses to be considered. This resulted in multiple objectives, uncertainty and a very computationally expensive process. Design of experiments (DoE) and statistical approximation techniques were applied to reduce the number of variables and responses and thus the computational expense. Li and Hu (2002) presented subspace approximation optimisation as a method of system decomposition for distributing the required computation in order to rapidly converge upon a robust optimum. Derivative-based optimisation methods were deemed to be too inaccurate and response surface methods too inefficient; thus leading to the development of a new method to optimise design objects within a system before passing the resulting objects into a parent system for further optimisation at the parent level. Different constraints were imposed at the differing system levels.

Ledermann et al. (2005) developed new methods to improve the accuracy, efficiency and flexibility of aircraft structure data prediction. This was performed using modular, knowledge-based computer-aided engineering (CAE) modules to permit easier modelling of complex aircraft structures so that FEA could be used to analyse the design. Decomposition was performed before organising the process into two sections: the organisational structure of components and the level of detail required. A new principle of using dynamic objects was applied to improve the optimisation methods. This involved objects being able to be varied through the design based on a predefined template, e.g. a series of frames defined by a pattern based upon a set template for a frame. The use of computer-aided design (CAD) software to model the design was found to be too time consuming to program as every possible event required programming, e.g. the addition and removal of a specific structural member. Therefore, an opportunity for a more efficient modelling tool was suggested to speed up the design process. Ledermann et al. (2006) performed further research into developing CAD models for use during preliminary design optimisation of a large civil aircraft without such expensive computational requirements. Aerodynamic optimisation was performed to establish the aircraft external profile prior to structural optimisation of the airframe. Improvements were made in the computational time but the program speed remained slow due to the complex requirements of the CAD system.

Amadori (2008) described a framework for the optimisation of conceptual aircraft designs. This framework performed MDO of an aircraft using existing software to subject each design to aerodynamic and structural analysis for a measure of feasibility against the design constraints. CAD was employed to perform parametric modelling of the airframe structural members within a BWB design. A framework for multi-level optimisation of a tiltrotor aircraft was presented by Kim et al. (2013). The upper layer of this multi-level framework optimised the mechanical properties of the aircraft wing before the lower level optimised the number and orientation of composite plies. This approach was deemed to be more appropriate to the aeroelastic requirements of a tiltrotor aircraft than a single-level framework. Raymer (2002) presented a tool to perform MDO of conceptual aircraft designs of various classes including a light civil aircraft, large civil transport aircraft, military fighter and UAV. The external aerodynamic profile of each aircraft was optimised for minimum cost for the military fighter and minimum mass for the other aircraft classes. The choice of optimisation technique was found to greatly affect the convergence rate of the process but not final solution quality.

2.2 Traditional Solution Process

The aircraft structural design process has been developed over many years, leading to the use of common methods and tools throughout the field (Pready, 2013). Consequently, a consistent process is followed within existing approaches to optimise the structural design of an aircraft (Amadori, 2008). Initialisation of the process is firstly performed, wherein input data are provided to define the requirements of the aircraft design and optimisation problem, i.e. specification of limiting values for design parameters

(Bartholomew, 1998). The aircraft mission is subsequently defined such that mass estimation may be performed to establish the aerodynamic requirements of the aircraft for flight (Raymer, 2006). Mass estimation is often empirical during conceptual design given lack of knowledge of the design, including contributions from items considered during later stages of the design process, e.g. fixtures, fittings, electronics and other systems (Allen, 2010b). The external profile of the aircraft is then generated using the accumulated data, empirical formulae and results of aerodynamic optimisation if performed (Kesseler and Vankan, 2006). The structural layout of the aircraft is subsequently modelled within the geometric boundary imposed by the external profile (Amadori et al., 2007a). This typically includes the number, position, size and topology of airframe structural members as defined by design variables (Schuhmacher et al., 2002). During structural optimisation, each individual design solution represents an independent airframe design defined by values of the design variables (Anhalt et al., 2003). The feasibility of each airframe design is determined through structural analysis of its performance under load with respect to the design constraints (Ledermann et al., 2006). Optimisation is performed of the airframe designs to search for an improved solution in terms of the design objective, typically minimum mass for structural optimisation (Sobieszczanski-Sobieski and Haftka, 1997). This process of generating designs for subsequent analysis and optimisation is repeated until a convergence criterion is satisfied, e.g. maximum number of optimisation generations or minimum population variance (Raymer, 2002).

A common strategy employed within existing approaches is to decompose the aircraft into smaller, simpler systems which in turn can be discretised further into smaller subsystems (Xia and Gao, 2002). This process is typically conducted until each individual component of the design is a separate entity (Ledermann et al., 2005). Consequently, this involves the aircraft being treated as a global system which is then decomposed into the wing, empennage and fuselage sections which can be considered much simpler than when combined as a complete aircraft configuration (Gantois and Morris, 2004). To study the internal structure of the aircraft, the aircraft sections are in turn decomposed into the individual structural members, e.g. ribs, spars and stringers, each of which is then considered as an independent entity and designed accordingly (Rinku et al., 2008). This lends itself to the use of patterns and parametric design when modelling similar components (Amadori et al., 2008). The interactions of entities within a system level, e.g. those between wing structural members under load, are then considered at the level above in the system hierarchy, in this case the wing section, when analysing the performance of this system (Amadori et al., 2007b). Such decomposition can be performed during the analysis or optimisation of the airframe, the latter of which is dependent on the problem design parameters. However, this can greatly increase the size of the optimisation problem and the effort required to find a high-quality solution.

2.2.1 Design Parameters

Design parameters constitute the variables, constraints and objectives of the optimisation process. Design variables are numerical representations of design properties, the values of which define the characteristics of the design. Design constraints impose limits on the solution space populated by the various design permutations created by different variable values. These limits require that the properties of a design satisfy the values of the constraints for the design to be deemed feasible. The design objective is the property of the design that is to be improved by searching the solution space for different design variants and measuring their quality as a function of this objective. Due to the conventional configuration of aircraft that has developed over time the parameters used by different researchers tend to be similar, although vary slightly depending on the purpose of the aircraft, i.e. aircraft class and mission.

Design variables within aircraft design optimisation typically define the aircraft geometry and occasionally its mission profile (MacMillin et al., 1997). Structural optimisation typically includes variables to define the numbers and positions of different structural member types (Ledermann et al., 2005). The size and shape of these members are also often considered as design variables (Eves et al., 2009), as is the material of the members (Ali and Behdinan, 2002). When a composite material is used within the

airframe, variables also include the number, order, thickness and orientation of the plies (Guo, 2007). MDO incorporating aerodynamic optimisation expands the problem and therefore the number and nature of variables used to define the aircraft (Raymer, 2002). This results in the aircraft external profile being defined by design variables (Amadori et al., 2007a). The wing is often the sole aircraft section considered during the optimisation process, therefore wing geometry is commonly defined by design variables (Koch et al., 1999). The fuselage, powerplant and, less frequently, empennage are optimised by design variables when the complete aircraft is considered (Raymer, 2002).

Design constraints are typically imposed to ensure satisfactory performance of the aircraft during operation, traditionally by calculating the response of the airframe to applied load cases when performing structural optimisation (Petersson et al., 2010). Structural analysis is consequently performed to determine the displacement and stress fields over the airframe for comparison against corresponding design constraints (Neufeld et al., 2010). These constraints are typically enforced as a maximum buckling, principal or von Mises stress, or alternatively as the minimum factor of safety (FoS) corresponding to these stresses (Schuhmacher et al., 2002). Wingtip deflection is also often used as a constraint to prevent excessive bending of the wing under load (Park et al., 2009). Additional constraints are imposed during MDO such as geometric limits on the aircraft size for feasible operation at a specific aerodrome (Raymer, 2002). Alternatively, powerplant and mission characteristics can form constraints (MacMillin et al., 1997), as can torsional rigidity and twist angle; although these are not considered herein.

The most common design objective of structural optimisation is minimum structural mass, resulting in an optimisation problem to generate a solution represented by design variables of minimal mass whilst satisfying the design constraints (Hu and Yu, 2009). Additional objectives are often included within MDO, such as minimal aerodynamic drag (Schuhmacher et al., 2002), minimal stealth profile (Crawford and Simm, 1999), minimal cost (Kaufmann et al., 2010), minimal emissions (Bower and Kroo, 2008) and minimal sonic boom (Alonso et al., 2009). Alternatively, MDO can be performed to consider multiple disciplines but with a single multi-objective function or through the isolation of the disciplines into independent single-objective problems (Hu and Yu, 2009). This approach can reduce the interdisciplinary dependencies and subsequent uncertainty in a multidisciplinary objective function as well as the computational requirements for modelling and analysis over multiple disciplines (Cramer et al., 1994).

2.2.2 Modelling and Analysis of the Aircraft

The aircraft is modelled such that analysis can be performed to determine the feasibility of each design solution with respect to the design constraints (Ali and Behdinan, 2002). The process of design optimisation is inherently iterative, requiring the generation of many aircraft models due to the large number of possible solutions resulting from variations in the design variables (Amadori et al., 2007b). Each design solution requires analysis by selected tools before repeating the process via optimisation to determine whether a better solution can be found within the solution space (Raymer, 2002). CAD is a popular tool for modelling the aircraft (Lovell et al., 2004), whilst computational fluid dynamics (CFD) is often used for aerodynamic analysis (Jameson and Ou, 2011) and FEA for structural analysis (Schuhmacher et al., 2002). FEA has been applied over many years for the analysis of various structural problems with great success (Toropov, 1989). Panel codes are alternatively employed for aerodynamic analysis, sacrificing precision for superior computational speed compared with CFD (Amadori et al., 2008). Established engineering software tools are often employed to perform these tasks such as CATIA for CAD (Ledermann et al., 2005) and Nastran for FEA (Hansen and Horst, 2008). MATLAB is commonly used as an orchestrating tool to link the various modules within the optimisation process (Ayele et al., 2013), whilst a user interface can be provided through software such as Microsoft Excel (Amadori, 2008). The optimisation task itself can be performed using existing software, e.g. OptiStruct (Eves et al., 2009) or Isight (Zhang et al., 2009). Alternatively, self-contained tools can be created to perform these tasks and thus remove any reliance on existing software and the computational penalties

inherent in linking packages (Azamatov et al., 2011).

The structural integrity of each airframe design is calculated in order to establish design feasibility. However, solving the analysis problem can become prohibitively expensive in terms of computation time when many solution evaluations are required (Amadori, 2010; Viana and Steffen Jr, 2009). As a result, attempts are often made to reduce the time required to perform such analysis (Koch et al., 1999). For example, structural members are commonly represented by simple shapes, with many members of the same type being approximated by bodies with similar features and idealised boundaries (Pready, 2013). Further, the size of an FEA problem can be reduced by using one or two-dimensional elements to model the airframe rather than three-dimensional elements (Arrieta and Striz, 2005). This reduces the number of model degrees of freedom (DoFs) and subsequent computational effort required to solve the problem, although at a cost to precision (González et al., 2004). Alternatively, a surrogate model can be employed in lieu of full analysis by approximating the performance of the aircraft based on a sample of analysis results (Hu and Yu, 2009). This reduces the computational expense of structural analysis by removing the need to perform FEA on every design solution (Shan and Wang, 2010). DoE is typically employed to suitably sample the solution space (Montgomery, 1997). This leads to the creation of a response surface of the approximation upon which optimisation is performed (Park et al., 2009). However, uncertainty and noise in a surrogate model approximation can penalise the reliability of results (Neufeld et al., 2010). Another approach is to reduce the model fidelity, i.e. modelling precision with respect to reality, to enable analysis with a reduced number of DoFs and thus smaller analysis problem size (Zadeh et al., 2009). A low-fidelity model possesses fewer DoFs than a more precise high-fidelity model, thus requires less computational effort to solve the problem (Viana and Steffen Jr, 2009), but once again can diminish the precision of analysis results (Martins et al., 2002). Problem detail can be varied during the optimisation process in an attempt to reduce the computational time taken without adversely penalising the search, typically through the refinement of the model approximation employed (Toropov, 2001). For example, an FEA problem can be approximated rapidly using a one or two-dimensional low-fidelity model prior to more detailed analysis of the solutions obtained using a three-dimensional high-fidelity model (Markine and Toropov, 2002). Such variable-fidelity modelling, also referred to as multi-fidelity modelling, employs multiple predefined levels of fidelity concurrently or at specific points during the optimisation process (Giunta, 1997). One approach is to employ a low-fidelity model for the majority of analysis with periodic use of a high-fidelity model to verify results (Alexandrov and Lewis, 2000). This approach requires additional computation to ensure correlation between the low and high-fidelity model results (Marduel et al., 2006). Alternatively, multiple model fidelity levels are specified to be employed over predetermined periods of the optimisation process, typically beginning with a low level of fidelity in order to rapidly obtain good design solutions prior to more detailed analysis at a higher level of fidelity towards the end of the process (Minisci et al., 2011). Variable-fidelity modelling has been combined with surrogate modelling such that a high-fidelity model is used to generate a reliable approximation for the surrogate model that is subsequently employed alongside analysis at low fidelity (Nguyen et al., 2013). Nevertheless, the use of such a high-fidelity model to obtain an accurate approximation can still be prohibitively expensive, especially with a large number of design variables (Zadeh and Toropov, 2002), therefore a low-fidelity model is often used to rapidly sample the solution space (Han et al., 2013). Different fidelity levels can be employed for the different design disciplines when performing MDO (MacMillin et al., 1997). Parallel programming can also be employed to reduce the computational cost of modelling and analysis (Alonso et al., 2004; Oktay et al., 2011). Each individual design solution within a population is independent of all others within the population and as such is modelled and analysed separately from the other individuals (Raymer, 2002). Parallel programming permits multiple individuals to be processed concurrently rather than sequential modelling and analysis of a population (Aguilar Maderia et al., 2005).

The loads applied to the model during analysis are of great importance as they drive the structural

integrity of the aircraft design. Structural analysis determines the feasibility of a design solution with respect to the design constraints when subjected to loads, which are typically applied as isolated load cases. Load cases incorporate a series of point and pressure loads along with corresponding boundary conditions (Laban, 2011). Pressure loads are commonly applied to low-fidelity models as point loads by considering the load distribution over the model (Venter and Sobieszczanski-Sobieski, 2004). Loads are typically taken from the extreme points within the flight envelope dictated by the airworthiness requirements, e.g. CS-23 and CS-25 for civil light and large aircraft respectively and Def.Stan.00-970 for military aircraft. Loads taken from such extreme points represent the greatest magnitude of loads the aircraft must withstand during operation. A $+2.5g$ symmetric pull-up manoeuvre is popularly applied to large civil aircraft (Kesseler and Vankan, 2006). The same manoeuvre is typically applied to aircraft of other classes but of differing magnitude, e.g. $+3.0g$ for a light civil aircraft (Amadori et al., 2008), $+3.5g$ for a UAV (Eves et al., 2009), $+1.5g$ for a micro air vehicle (Li and Hu, 2002) and $+9.0g$ for a military fighter (Arrieta and Striz, 2005). Multiple flight load cases are sometimes applied to include various symmetric and asymmetric manoeuvres (Schuhmacher et al., 2002). Alternatively, gust loads are used to simulate turbulence during flight (Petersson et al., 2010) and ground loads to simulate the loading of the airframe during landing and manoeuvres such as braking and taxiing (Rao, 1986). These loads are typically simulated as dynamic loads, thus requiring the calculation of the dynamic response of the aircraft to the loads over time, or pseudo-static loads (Howe, 2004). A mission simulation may include multiple load cases applied at specific periods during the defined mission, e.g. taxi, take-off, climb, cruise, descent and landing, although such analysis becomes computational expensive as analysis is required of numerous scenarios (Ledermann, 2010).

2.3 Optimisation Techniques

Many different methods of optimisation have been applied for aircraft design optimisation. These have included both stochastic and deterministic methods, of which both population-based and single-solution techniques have been employed. Stochastic optimisation techniques are inherently random, thus different solutions to a problem are likely to be obtained over a number of experiments even with the same initial conditions. Deterministic methods do not include randomness, hence produce identical results to a problem when given the same initial conditions. Population-based optimisation techniques consider a number of design solutions at any one time period. The 'population' refers to a set of 'individual' design solutions that populate the solution space explored by an optimisation technique. A single-solution technique only considers one solution at a time and is commonly a step-based approach to solution space exploration. The optimisation techniques discussed herein generate a solution which is then evaluated with respect to the design objective function and constraints. For each generation using a population-based technique, the best solution in the population is identified and stored as the current best solution if it provides an improvement in the objective function over the previous best solution. Similarly, with a single-solution technique the current solution is stored as the current best solution if it outperforms those generated during previous steps, otherwise the step is rejected.

2.3.1 Monte Carlo

Monte Carlo (MC) simulation is a stochastic population-based optimisation technique wherein a population contains randomly generated individuals from across the solution space. At each optimisation generation the population is created randomly, resulting in a diverse search across the solution space until a termination criterion is satisfied (Mavris and Bandte, 1997). The advantage of such a population-based optimisation technique is the ability to explore a larger proportion of the solution space than using a single-solution technique. However, a limitation is that it is unlikely that the global optimum, i.e. the best solution overall within the solution space, will be found due to the random nature of the search.

Furthermore, it is also unlikely that the scheme will converge at a local optimum, i.e. the best solution within a solution space neighbourhood, if the size of the population is too large (Raymer, 2002). These characteristics are true of all population-based techniques described herein. Moreover, the disadvantage of MC is that it lacks intuition in generating new populations, therefore the population does not evolve over generations and the chance of improving the best solution is random. Nevertheless, MC is often applied to large solution spaces containing many randomly-distributed solutions due its ability to maintain diversity throughout the search and thus avoid premature convergence of a population on a sub-optimal solution (Yang, 2010). The MC technique can be extended by allowing a sample of the previous population to be preserved for the next generation as the indigenous population. The remaining population is generated randomly, resulting in the technique being labelled random immigration (RI).

2.3.2 Evolutionary Algorithm

An evolutionary algorithm (EA) is a population-based optimisation technique that evolves a population of individual solutions over a period of generations in an attempt to improve their quality with respect to the objective function. Each generation involves the analysis of the population and calculation of their fitness, typically as a function of the design objective. The optimisation technique then evolves the population for another generation typically with bias towards the fittest individuals; thus employing Darwinian evolution for survival of the fittest (Julstrom, 1999).

The killer queen (KQ) is an EA that generates a new population through the mutation of the fittest individual within a population (Raymer, 2002). Mutation is performed by randomly altering the values of design variables, the method of which depends whether real or binary number representation of the solution is employed. Real number representation uses real numbers within a genome to represent the design within the optimisation problem. For example, a design can be represented by a genome

$$\mathrm{V1} \mid \mathrm{V2} \mid \ldots \mid \mathrm{V}n_v$$

where n_v denotes the number of design variables, V. Binary representation replaces the genome with a binary chromosome containing bits of value 0 or 1 to represent the real number values of the design variables. Each design variable is represented by a strand within the chromosome, the length and resolution of which determines the precision of the binary representation (Raymer, 2002).

Mutation within an EA is performed to stochastically modify randomly-selected design variables or bits. Typical mutation techniques include random, Gaussian and non-uniform for real numbers and bit-flip mutation for binary chromosomes (Deb, 2001). Random mutation generates a random value for a mutated variable. Gaussian mutation superimposes a Gaussian distribution over a variable to mutate its value using noise (Hinterding et al., 1996). Non-uniform mutation perturbs the value of a variable, the scale of which reduces over time to promote convergence (Michalewicz, 1996). Bit-flip mutation is performed to a variable strand bit by inverting its value (Gen and Cheng, 1997). The random nature of the mutation operator and selection of variable for mutation increase search diversity, with a mutation probability typically included to prevent excessive mutation resulting in a random search similar to MC. This probability can be static or dynamic, with the latter typically leading to a reducing probability over the search duration to promote convergence (Zhang et al., 2007). KQ requires a high mutation probability to prevent convergence on the current best solution as only this solution is used to generate the next population. KQ is deemed elitist as the number of individuals used to generate a new population is restricted to solely the fittest individual. This can saturate the search with an inappropriate mutation probability and lead to premature convergence upon a sub-optimal design (Raymer, 2002).

2.3.2.1 Differential Evolution

Differential evolution (DE) is an EA where population solutions evolve over generations based on the influences of other individuals, referred to as 'agents', within the population (Storn and Price, 1997). For

the evolution of a population individual, each design variable within the genome is subjected to mutation and crossover (Zaharie, 2002). For each individual, a 'trial vector' is constructed through the probabilistic crossover over the genome with a 'mutation vector'. The mutation vector is built using values obtained for each design variable through the combination of corresponding variable values from three randomly-selected agents within the population: α_1, α_2 and α_3. These agents cannot be the individual currently being evolved. For the ith individual within the population, the DE algorithm calculates the following value for the vth variable value of the trial vector for generation $k+1$ (Pedersen, 2010)

$$\tilde{x}_{i,v}^{k+1} = \begin{cases} x_{\alpha_1,v}^{k} + F_{DE}\left(x_{\alpha_2,v}^{k} - x_{\alpha_3,v}^{k}\right) & \text{if } r \in [0,1] < p_{c,DE} \text{ or } v = r_v \in [0, n_v] \\ x_{i,v}^{k} & \text{otherwise} \end{cases} \tag{2.1}$$

where F_{DE} differential weight
$p_{c,DE}$ crossover probability
r random number
$x_{i,v}^{k}$ value for vth variable of ith individual at kth generation
$\tilde{x}_{i,v}^{k+1}$ trial vector value for vth variable of ith individual for generation $k+1$

The first solution to Eqn. (2.1) represents the vth variable value of the mutation vector, formed using the corresponding variable values of the three agents. The mutation vector is guaranteed to be accepted for at least one randomly-selected variable, r_v, to prevent search stagnation (Storn and Price, 1997). The algorithm parameters are restricted to $0 \leq F_{DE} \leq 2$ and $0 \leq p_{c,DE} \leq 1$. The solution represented by the trial vector is analysed in the next generation, i.e. $k+1$ in Eqn. (2.1). If the objective value of this solution is an improvement over the original individual, the trial vector is accepted and replaces the original individual within the population for subsequent optimisation (Zaharie, 2002). Investigation of DE has found the technique to provide efficient exploration and convergence upon a high-quality solution with appropriately selected parameters (Pedersen, 2010).

2.3.2.2 Genetic Algorithm

A genetic algorithm (GA) is a class of EA wherein a population of design solutions is evolved over a number of generations through mating, also known as crossover (Goldberg, 1989a). A GA selects parent solutions from a population to crossover and generate offspring solutions to form the population of the next generation (Deb, 2001). Mutation can then be applied to the offspring for further population diversification; however, this is not always beneficial as a mutation can penalise the quality of the evolved solution (Ali and Behdinan, 2002). The ability of a GA to efficiently search the solution space through effective population evolution has made it a popular technique within aircraft design and other fields of optimisation (Raymer, 2010).

The individuals within a population represent designs within the solution space. The crossover of solutions results in the inheritance of their design characteristics by the offspring, leading to the evolution of the population (Davis, 1987). Consequently, a GA aims to select parents that will generate fitter offspring to improve the quality of the population, and thus the solutions to the problem, through the inheritance of good design characteristics and rejection of poor characteristics (Goldberg, 2002). GA operation is thus dependent on the method of selection employed to choose the parents and the crossover technique. Three selection methods that have been employed for aircraft design optimisation are: roulette wheel (RW), tournament selection (TO) and breeder pool (BP) (Raymer, 2002).

RW selection is based upon a roulette wheel within a casino, where a ball spins around the wheel and lands randomly in one of its sectors. Within a GA, each parent individual within a population is represented by a wheel sector, the size of which is calculated as the fitness of the individual as a proportion of the total population fitness (Xia and Gao, 2002). The sizes of individual sectors are calculated by

firstly determining the cumulative total fitness of the population. Individuals are then ranked in order of fitness and scaled using the cumulative population fitness, resulting in individuals of higher fitness possessing larger sectors than those of lower fitness such that fitter parent solutions are more likely to be selected. A random value is generated within the bounds of the wheel and the parent lying within the corresponding sector is selected (Raymer, 2002). An alternative approach to selection is TO, wherein candidate individuals compete to be the parents selected for crossover. The competition is formed by randomly selecting a minimum of two candidates from the population, the fittest of which wins the competition and becomes a parent. Therefore, four candidates are chosen from which two parents are selected (Michalewicz, 1996). All competitors are usually replaced back into the population following competition and crossover for future selection. BP selection is an elitist approach wherein only the fittest individuals within the population are permitted to be selected as parents for crossover. These individuals are placed within the breeder pool such that pairs of parents can be randomly selected from the pool (Guo et al., 2006). Replacement can be employed such that parents are returned to the pool following crossover and thus may be selected for future crossover. Alternatively, parents are not replaced to prevent repeated selection of the same parents which can lead to search stagnation (Raymer, 2002).

Crossover involves the combination of strands within the genomes, or chromosomes, of the parent solutions to generate a new offspring solution (Michalewicz, 1996). Typically methods of crossover include one-point, two-point and uniform crossover. One or two-point crossover results in parent genomes intersecting at the respective number of points randomly located along the length of the genome. For example, for one-point crossover the offspring inherits the design variables of one parent up to the crossover point from which it inherits those of the other parent (Goldberg, 1989a). The number of crossover points can alternatively be greater than two or be chosen randomly for each crossover event, i.e. random crossover. Uniform crossover randomly selects a parent for each design variable to pass its variable value to the offspring (Raymer, 2002). The function of a GA is based on 'building block theory' and thus typically uses a binary representation with crossover points occurring between the chromosome bits (Holland, 1975). Further, this enables crossover at points within the strand of each design variable, i.e. not restricted to the intersections between variables. Such crossover within a variable can be achieved with a real number representation using blend crossover to merge the variable values (Herrera et al., 2003). Alternatively, parameterwise crossover may be performed by choosing crossover points only at the intersections between design variables. Selection typically results in two parents being chosen for crossover, although a single parent can be chosen and subjected to mutation. Furthermore, one or two children can be generated depending on the method of crossover employed (Deb, 2001).

2.3.3 Particle Swarm Optimisation

Particle swarm optimisation (PSO) is an example of a swarm intelligence (SI) optimisation technique. SI methods are population-based and consider the knowledge passed between individuals of the population to direct the search within the solution space. Conventionally, the terms 'particle' and 'swarm' are used in place of 'individual' and 'population' when discussing PSO. Therefore, PSO encompasses a solution space search by a swarm of particles in an attempt to find global maximum or minimum corresponding to the objective function. The best solution discovered by all particle is stored and the swarm is made aware of this solution. The shared knowledge of good locations within the solution space reduces the likelihood of premature convergence upon a local sub-optimal solution and encourages global convergence upon the best solution found by the swarm (Hassan et al., 2005). The velocity and position of the ith particle at generation $k+1$ are given respectively by PSO as

$$\{\dot{x}\}_i^{k+1} = \omega_{PSO}\{\dot{x}\}_i^k + c_{1,PSO}r_{1,PSO}\left(\{\hat{x}\}_i^{1\to k} - \{x\}_i^k\right) + c_{2,PSO}r_{2,PSO}\left(\{\hat{x}\}_{1\to\mu}^{1\to k} - \{x\}_i^k\right) \tag{2.2a}$$

$$\{x\}_i^{k+1} = \{x\}_i^k + \{\dot{x}\}_i^{k+1} \tag{2.2b}$$

where
- $c_{1,PSO}$ cognitive parameter
- $c_{2,PSO}$ social parameter
- $r_{1,PSO}$ cognitive random number, $r_{1,PSO} \in [0,1]$
- $r_{2,PSO}$ social random number, $r_{2,PSO} \in [0,1]$
- $\{\hat{x}\}_i^{1\to k}$ best position of ith particle for generations 1 to k
- $\{\hat{x}\}_{1\to\mu}^{1\to k}$ best position of all μ particles for generations 1 to k
- μ population size
- ω_{PSO} inertia weight

The particle position represents its values of the design variables. The initial positions and velocities of particles are generated randomly (Venter and Sobieszczanski-Sobieski, 2004). The values of inertia weight and the cognitive and social parameters control the exploration and convergence tendencies of the swarm, i.e. high inertia weight promotes exploration, high cognitive bias promotes search around the particle best solution and high social bias promotes convergence on the swarm best solution (van den Bergh and Engelbrecht, 2006). A constriction constant can be used to apply velocity clamping to prevent excessively high swarm velocity resulting in an unstable algorithm, e.g. search explosion (Clerc and Kennedy, 2002). PSO is a popular optimisation technique and can provide a superior solution to EAs at reduced computational cost with the appropriate set-up of parameters (Hassan et al., 2005).

2.3.4 Local Search

Local search (LS) methods are single-solution techniques that explore the solution space in a series of steps. An LS technique evaluates the solution space surrounding its current position such that it may move to a nearby improved solution. These techniques can differ from each other in the method of stepping from the current solution space position or the acceptance criteria for a new position. The step definition can be random or based on the measurement of the surrounding solution space, whilst acceptance criteria control the permission or prevention of moves that return to previously-explored solution space regions or result in reduced solution quality, i.e. a negative move (Pant and Fielding, 1999). The step size of LS can be varied to encourage either more detailed local exploration, e.g. if nearing a turning point in the solution space, or increased global exploration, e.g. if deemed close to a plateau (Rohn, 1993). Step-based approaches are more likely than population-based techniques to converge upon the closest peak or trough as they to move towards local optima. However, this can lead to convergence on a local optimum of poorer quality than the global optimum, whereas population-based methods are less likely to do so through greater solution space exploration (Raymer, 2002).

2.3.4.1 Hill Climbing

Hill climbing (HC) represents the basic LS method wherein the optimisation process explores the solution space through a series of steps. Steps are determined as random vectors from the current solution, resulting in random solution space exploration; as such this approach is also referred to as a 'random walk' (Yang, 2010). A step is performed from the current position, leading to analysis of the solution at the new position. This new solution is accepted if it represents an improvement over the current solution. The next step is then made from this new position. Alternatively, the step is rejected if the new solution does not outperform the current position in terms of the objective function, in which case the next step is taken from the current position (Rao, 1996). The random nature of this technique decreases the likelihood of premature convergence on a local optimum rather than the global optimum through increased search diversification but reduces the probability that the search will converge on the best nearby solution (Raymer, 2002).

2.3.4.2 Steepest Descent

A more intuitive LS search method than a purely-random walk is the steepest descent (SD) method. This deterministic technique measures the gradient of the local solution space surrounding the current position and makes a step in the direction of greatest gradient (Polak, 1997). A step is accepted if the new position represents an improvement in solution quality over the current position. The step size is varied to encourage more detailed analysis close to a minimum as determined by the solution space gradient history (Rohn, 1993). SD assumes the search is performed against a minimisation objective function, e.g. minimal structural mass. This approach can alternatively be employed for a maximisation function and is then termed the 'steepest ascent' method (Raymer, 2002). Measurement of solution space gradients increases the probability of obtaining a good solution over HC, but can be computationally expensive for problems with large numbers of design variables due to the number of necessary gradient measurements (Guo, 2007). Moreover, the deterministic nature of the technique means the same solution will be obtained if the optimisation process is repeated under the same conditions (Polak, 1997).

2.3.4.3 Simulated Annealing

Simulated annealing (SA) develops the HC technique for stochastic solution space exploration but with the possibility of accepting a negative move, i.e. a move that does not offer an improvement on the current solution. This reduces the likelihood of the optimisation search becoming trapped in a solution space region and thus converging on a local optimum (Pant and Fielding, 1999). The method was inspired by the process of annealing metals, whereby the metal temperature during the cooling process is occasionally raised before being reduced once more to allow crystalline structures within the material to settle before solidification (Davis, 1987). In simulation of this procedure, SA probabilistically permits the acceptance of an optimisation step to a worse solution than the current solution, the probability of which is defined at the kth step as (Kirkpatrick et al., 1983)

$$p_{neg}^{k} = \frac{-\Delta\Phi^{k}}{k_b T_{SA}^{k}} \tag{2.3}$$

where k_b Boltzmann's constant
T_{SA}^{k} initial simulated annealing temperature at kth step
$\Delta\Phi^{k}$ change in objective value at kth step

The current SA temperature determines this probability of accepting a negative move. A cooling schedule reduces this temperature over time, i.e. the optimisation process duration, through quenching. This decreases the probability of accepting a negative move towards the end of the search, thus permitting early exploration of the solution space but encouraging convergence on the best solution towards the end of the process (van Laarhoven and Aarts, 1987). The cooling schedule of an SA technique is commonly exponential or linear, resulting in the following expression for the temperature at the kth step (Nourani and Andresen, 1998)

$$T_{SA}^{k} = \begin{cases} \alpha_{SA}^{k} T_{SA}^{0} & \text{for exponential cooling} \\ (1 - \alpha_{SA} k)\, T_{SA}^{0} & \text{for linear cooling} \end{cases} \tag{2.4}$$

where α_{SA} denotes the simulated annealing cooling rate. The cooling rate controls quenching of temperature and is typically set to reduce to zero by the end of the process, whilst the initial temperature is commonly set below one so that a negative move is never guaranteed (Nourani and Andresen, 1998).

2.3.4.4 Tabu Search

Tabu search (TS) is an LS method that possesses a short-term memory of the solution space regions previously explored (Glover and Laguna, 1997). This prevents repeated exploration of solution space regions that are known to contain worse solutions and can therefore prevent trapping of the optimisation search in a sub-optimal region. The short-term memory uses a tabu list to record recently explored solution space regions or steps, leading to a check at each step that the new position or step is not on the list, i.e. it is not tabu (Qiu and Zhang, 2010). The length of the tabu list defines the tabu memory such that entries are removed from the list after a predefined period to allow such moves later in the search, thus preventing saturation of the search (Glover and Laguna, 1997).

2.3.5 Hybrid Methods

Hybrid methods combine population-based and single-solution optimisation techniques such that the former stochastically explores the solution space to determine the most promising neighbourhood before allowing a step-based method, usually a deterministic technique, to locate the nearest local optimum (Bos, 1996). Typically a GA is employed to search the solution space and discover a promising region before a LS technique promotes convergence on the closest optimum (Sahab et al., 2005). Thus, a hybrid method aims to overcome the limitations of population-based and step-based techniques, i.e. lack of guaranteed convergence for the former and inadequate exploration leading to premature convergence for the latter (Qiu and Zhang, 2010). The principal limitation of a hybrid method is determining the point at which to change from the population-based technique to the single-solution technique and thus prevent excessive time spent on exploration whilst also ensuring the deterministic method starts from the most suitable region of the design space. Further, establishing an appropriate resolution of the deterministic method is also a challenge, i.e. the ranges of design variables and number of chromosome strand bits per variable if using a binary representation (Raymer, 2010). Typically, population convergence is measured over a period of generations such that the change from population-based to LS technique is made upon satisfactory convergence of the population (Hansen and Horst, 2008). An alternative method developed for use with binary chromosomes is bit-string affinity (BSA), where the similarity of population individuals is measured to enable termination of the search when the affinity exceeds a preset limit (Raymer, 2002). Affinity measures the difference between bits within a binary chromosome, with convergence recorded when the average affinity over all bits exceeds a threshold value.

2.3.6 Surrogate Modelling

Surrogate modelling has been applied during aircraft design optimisation in an attempt to reduce the number of solution evaluations by computationally expensive tools (Hu and Yu, 2009). A response surface is created through sampling of the solution space and performing analysis of the sample. DoE is commonly used to sample the solution space, within which a Latin hypercube is often used to select the sampling points (Toropov et al., 2005). The response surface is typically created using a series of second-order approximations (Park et al., 2009), leading to its evaluation by mathematical methods, e.g. finite difference (FD) or kriging (Forrester et al., 2007), or exploration using meta-heuristics, e.g. MC (Mavris and Bandte, 1997). As discussed in §2.2.2, the precision of the model, and thus the response surface, limits this method as the optimisation techniques are reliant on the quality of this approximation and the influence of noise (Raymer, 2002).

The mathematical methods used to solve the response surface problem have also been employed to solve optimisation problems themselves as a series of equations, e.g. FD (Rao et al., 1979) and sequential quadratic programming (SQP) (Rothwell, 1991). Such methods determine relationships between design parameters for the generation of system equations that are solved for the satisfaction of the objective function (Barthelemy and Haftka, 1993). These methods are not as popularly applied for modern optimi-

sation problems due to the increasing capabilities of computational tools and the increasing complexity, i.e. number and interaction of design parameters, of optimisation problems (Raymer, 2002). Therefore, such methods are now mostly coupled with surrogate modelling (Hu and Yu, 2009).

2.4 Constraint Handling

Solution feasibility is of critical concern during aircraft design optimisation to ensure the final design obtained is suitable for manufacture and operation. Feasibility is conventionally measured with respect to design constraints to create a constrained optimisation problem. Solutions that fail to satisfy a design constraint are infeasible and are said to violate the constraint. As a result, design constraints form the boundaries of the feasible and infeasible regions of the solution space. Design constraints are formed as

$$g_{i,j}(\mathrm{X}^k) \leq c_j \tag{2.5a}$$

$$h_{i,j}(\mathrm{X}^k) = c_j \tag{2.5b}$$

where c_j jth design constraint
$g_{i,j}(\mathrm{X}^k)$ value of ith individual with respect to jth inequality constraint at kth generation
$h_{i,j}(\mathrm{X}^k)$ value of ith individual with respect to jth equality constraint at kth generation
X population set of size μ individuals

Equation (2.5a) represents the required value for a feasible solution with respect to an inequality design constraint whilst Eqn. (2.5b) states the required value for an equality constraint. Note that the inequality constraint can alternatively be written to require a value greater than or equal to a specific value. Moreover, the symbols g and h are also often used to denote the magnitude of constraint violation, i.e. such that $g_{i,j}(\mathrm{X}^k) \leq 0$ indicates no violation of an inequality constraint whilst $g_{i,j}(\mathrm{X}^k) > 0$ expresses the magnitude by which the ith individual has violated the jth constraint. It is in this manner by which the symbols are used throughout the remainder of this document. During aircraft structural design optimisation, inequality constraints are most typically applied, e.g. to limit deflection or stress. Various strategies exist for dealing with constraint violations, three of which are (Gen and Cheng, 1997):

- rejection strategy;
- repairing strategy;
- penalising strategy.

2.4.1 Rejection Strategy

A rejection strategy discards all infeasible solutions regardless of the degree of constraint violation (Kramer, 2010). This strategy ensures a feasible solution will be obtained but can restrict the optimisation search by preventing the propagation of good design properties possessed by infeasible designs, most notably when applying an evolutionary optimisation technique (Michalewicz and Schoenauer, 1996). Further, such strategies perform poorly for highly constrained problems, are prone to premature convergence upon local optima for problems possessing multiple feasible regions of the solution space and do not consider the distance of infeasible solutions from the feasible regions (Yeniay, 2005). Moreover, the optimisation search requires a feasible initial population to prevent stagnation of the search, therefore rejection strategies are often used for convex optimisation problems where the feasible region constitutes a large proportion of the solution space (Coello Coello, 2002).

2.4.2 Repairing Strategy

A repairing strategy modifies the characteristics of an infeasible solution using a deterministic procedure to improve its feasibility (Kramer, 2010). Convergence within the infeasible solution space region is

typically discouraged by including no more than 15% of the repaired solutions in the next population (Michalewicz, 1996). The determination of the repair procedure can become difficult with a large number of variables and complicated dependencies, as well as being computationally expensive to assess. Further, repair operators can introduce strong search bias, penalising the effectiveness of evolutionary optimisation (Coello Coello, 2002). Finally, the repairing strategy is problem-dependent, thus requires considerable research to ensure a suitable procedure is followed (Gen and Cheng, 1997).

2.4.3 Penalising Strategy

A penalising strategy employs a penalty function to penalise the objective value of a solution based on its feasibility (Kramer, 2010). As a result, the constrained optimisation problem is replaced by a set of m unconstrained problems for m design constraints (Coello Coello, 2002). Penalty functions were originally presented in Courant (1943) and subsequently developed by Fiacco and McCormick (1968) leading to many types of functions. A penalty function results in a 'penalised' objective value which is obtained by combining the unpenalised objective value with the value of the penalty function. Most penalty functions are formed as one of the following:

- death penalty;
- interior penalty;
- exterior penalty.

2.4.3.1 Death Penalty

The death penalty applies an infinite penalty to an infeasible solution (Coello Coello, 2002). As such, this penalty function bears the same characteristics as the rejection strategy described in §2.4.1. For an inequality constraint, the resulting objective value of the ith individual within a population set X at the kth generation may be expressed as

$$\Phi_i(\mathrm{X}^k) = \begin{cases} \infty & \text{if } \sum_{j=1}^{m} g_{i,j}(\mathrm{X}^k) > 0 \\ f_i(\mathrm{X}^k) & \text{otherwise} \end{cases} \tag{2.6}$$

where $f_i(\mathrm{X}^k)$ unpenalised objective value of ith individual in population set X at kth generation
$\Phi_i(\mathrm{X}^k)$ penalised objective value of ith individual in population set X at kth generation

2.4.3.2 Interior Penalty

The interior penalty function penalises solutions as they approach a constraint boundary. Far from the constraint boundaries, the magnitude of penalty is small whereas the applied penalty tends to infinity at a boundary. As a result, a feasible solution is highly likely providing that the initial solution lies within the feasible region (Coello Coello, 2002). This requires an initial population to be entirely feasible to ensure a feasible solution. Furthermore, the interior penalty function cannot be used with equality constraints (Homaifar et al., 1994). The objective value resulting from an interior penalty function is expressed as

$$\Phi_i(\mathrm{X}^k) = f_i(\mathrm{X}^k) + \lambda \sum_{j=1}^{m} \frac{1}{|g_{i,j}(\mathrm{X}^k)|} \tag{2.7}$$

where λ represents a penalty coefficient to define the severity of penalisation. The magnitude of penalty applied considers only the distance between the solution and the constraint boundary and not whether the solution lies in the feasible or infeasible region (Rao, 1996). Consequently, the interior penalty function is often combined with the death penalty to form a barrier function to apply an infinite penalty to all infeasible solutions (Carroll, 1961; Nocedal and Wright, 1999).

2.4.3.3 Exterior Penalty

The exterior penalty function penalises only infeasible solutions by a magnitude proportional to the degree of constraint violation (Rao, 1996). Hence, unlike the interior penalty function exploration of the feasible solution space is possible without any penalisation. Solutions are penalised after crossing a boundary into an infeasible region of the solution space to promote feasible convergence (Coello Coello, 2002). An exterior penalty function for an inequality constraint generates the following objective value

$$\Phi_i(\mathrm{X}^k) = f_i(\mathrm{X}^k) + \lambda \sum_{j=1}^{m} \max\left[0, g_{i,j}(\mathrm{X}^k)\right]^{\alpha} \tag{2.8}$$

where α denotes the penalty parameter used to define the dimensionality of the penalty function, i.e. linear, quadratic etc. An alternative to this additive function is a multiplicative function (Yeniay, 2005)

$$\Phi_i(\mathrm{X}^k) = f_i(\mathrm{X}^k) \left\{ 1 + \lambda \sum_{j=1}^{m} \max\left[0, g_{i,j}(\mathrm{X}^k)\right]^{\alpha} \right\} \tag{2.9}$$

A study by Richardson et al. (1989) indicated that a penalty function that considers the degree of constraint violation would outperform one that only considers the number of violated constraints. Moreover, the latter would be unlikely to generate a feasible solution if the problem contains few constraints and feasible solutions. Consequently, the death penalty can be considered as the least suitable penalty function. Further, the exterior penalty function has been more generally applied than the interior function due to the removed requirement for a feasible starting point (Coello Coello, 2002).

2.4.3.4 Penalty Function Set-Up

A penalisation strategy is sensitive to the set-up of the penalty function employed due to the influence of its parameters on the severity of penalisation of solutions (Deb, 2000). The minimum penalty rule requires that the magnitude of penalty should be as small as possible so that infeasible solutions possess objective values marginally worse than those that are feasible (Coello Coello, 2002). Failure to follow this rule results in an ill-conditioned problem generating significantly worse objective values for penalised solutions, leading to a low probability that characteristics of these solutions will be included in the next generation. However, the penalty should be sufficiently great to promote convergence on a feasible solution. As a result, it can be difficult to ascertain the required magnitude of penalty to be applied for a problem with complex constraints (Coello Coello, 2002). The severity of penalty is controlled by the penalty coefficient and penalty parameter that encourage either informative preservation or selective pressure. Informative preservation attempts to ensure a sufficient number of infeasible solutions are considered to permit their beneficial characteristics to be preserved. Conversely, selective pressure encourages the rejection of infeasibility to promote a feasible solution. Additionally, the severity of penalty may be weighted to assign priority to feasibility with respect to specific constraints (Coello Coello, 2002).

The penalty parameter is typically maintained at a static value such that a simple penalty function is employed to ensure robust optimisation, with a quadratic function suggested as that of highest complexity (Beyer and Sendhoff, 2007). Furthermore, a quadratic function is often employed due to its early use with calculus-based optimisation techniques (Crossley and Williams, 1997). Alternatively, the penalty coefficient can be varied to create a dynamic function, commonly based on the generation number, i.e. time (Joines and Houck, 1994). This leads to lower penalties being applied to solutions during early generations to permit informative preservation prior to greater penalties towards the end of the search to apply selective pressure towards a feasible solution. However, such a generation-based function can lead to premature convergence due to the increasing restriction on the search (Michalewicz, 1996).

An alternative approach to the standard single-level penalty function was presented by Homaifar et al.

(1994), where multiple violation levels were defined such that the penalty parameter was greater for higher violation levels. However, this approach required $m\,(2l+1)$ parameters for l violation levels; thus needing a large number of parameters to define each problem (Yeniay, 2005). Gen and Cheng (1997) presented a different function that scaled the magnitude of penalty by the greatest violation within the current population. This encouraged population diversity to be maintained and resulted in the non-parameterisation of the design constraints. The exterior penalty function was given by

$$\Phi_i(\mathrm{X}^k) = f_i(\mathrm{X}^k)\left\{1+\lambda\sum_{j=1}^{m}\left\{\frac{\max\left[0, g_{i,j}(\mathrm{X}^k)\right]}{\max\left[\varepsilon, g_{\max,j}(\mathrm{X}^k)\right]}\right\}^{\alpha}\right\} \tag{2.10}$$

where ε is a small positive value to prevent division by zero. Bean and Hadj-Alouane (1992) developed an adaptive penalty function that modified the penalty coefficient depending on the feasibility of the best solution generated over the previous $n_{k,\lambda}$ generations

$$\lambda^k = \begin{cases} \dfrac{\lambda^{k-1}}{\beta_1} & \text{if best solution always feasible over previous } n_{k,\lambda} \text{ generations} \\ \lambda^{k-1}\beta_2 & \text{if best solution never feasible over previous } n_{k,\lambda} \text{ generations} \\ \lambda^{k-1} & \text{otherwise} \end{cases} \tag{2.11}$$

Constants $\beta_{1,2}$ determined the rate at which the penalty coefficient was increased or decreased as dictated by population feasibility, where $\beta_{1,2} > 1$, $\beta_1 > \beta_2$ and $\beta_1 \neq \beta_2$ to avoid cycling. The difficulty inherent with this function was the determination of a suitable value for $n_{k,\lambda}$ and the quantity of best solutions to be monitored (Coello Coello, 2002). Another adaptive penalty function was presented by Rasheed (1998) that monitored the individual solutions within the population set that corresponded to the least number of constraint violations and the maximum fitness. These individuals were compared after a predefined period of generations, leading to the increase of penalty parameter if they possessed different fitnesses. The penalty parameter was also reduced if the population was entirely feasible. The limitation of this function was the difficulty in selecting an initial penalty parameter and the period over which the individuals are monitored. Nanakorn and Messomklin (2001) developed a similar function that used a ratio between the average population fitness and that of the best infeasible solution to control the magnitude of penalty applied. This function was evaluated for the optimisation of three truss and frame structures with promising results that indicated high robustness of the function. However, the success of the method was also dependent on its initial set-up, i.e. the magnitude of scaling to be performed.

Crossley and Williams (1997) performed a study of different adaptive penalty functions coupled with a GA. The penalty parameter was adapted based on the standard deviation and variance of the population fitness and compared against a generation-based dynamic penalty function of varying gradient. TO and uniform crossover were employed with a crossover probability of 50% and with criteria for process termination after a maximum of 100 optimisation generations or a failure to improve the best solution over five successive generations. The problems solved included one and two-dimensional mathematical benchmark functions as well as the mass minimisation of a stiffened composite panel. The results indicated improved solutions with an adaptive or dynamic penalty function over a static function, with the generation-based control of the penalty parameter outperforming control by population fitness.

A self-adaptive penalty function was introduced by Coello Coello (2000) that considered the penalty as two independent parts: the number of constraints violated and the degrees of violation. This function was subsequently used for the coevolution of two populations, one of which was tasked with optimising the solutions to the problem whilst the second evolved the weights applied to the two penalty function parts. This function was found to be sensitive to the values of parameters input, leading to an extensive number of solution evaluations if not appropriately set up (Yeniay, 2005). An alternative approach was

presented by Deb (2000) that removed the penalty coefficient and parameter from the exterior penalty function. Instead the objective value of an infeasible solution was calculated as the sum of the worst feasible solution objective value and the constraint violations by the solution. This function assumed that any feasible solution was preferable over an infeasible solution. Although promising results were obtained, difficulty was observed in maintaining population diversity (Coello Coello, 2002).

2.4.4 Constraint Handling during Aircraft Design Optimisation

Aircraft design optimisation often requires a solution to be found close to the constraint boundary to avoid excessive cost in the design through unnecessarily high feasibility. Further, exploration beyond the constraint boundaries can be beneficial to allow good design characteristics of infeasible designs to propagate to those within the feasible solution space, thus improve the quality of feasible designs. As a result, penalty functions are typically employed for aircraft design optimisation. An interior penalty function was employed by Rao et al. (1979) and Rao (1984, 1985, 1986, 1987) to the problem of aircraft wing structural optimisation. This required the initial solution to be feasible and, as such, a feasible design was likely during optimisation. This research did not employ population-based optimisation, therefore the computational effort required to ensure a feasible initial solution was less than would have been necessary for an entirely feasible initial population of designs.

More recent investigations into aircraft design optimisation have applied an exterior penalty function, most notably when coupled with population-based optimisation. Furthermore, the lack of penalty applied to feasible solutions by an exterior penalty function permits greater opportunity for discovery of an optimum solution in close proximity to the constraint boundaries. For example, Rafique et al. (2011) employed an exterior penalty function using a penalty parameter $\alpha = 1$, whilst Amadori (2008) also used this penalty function with varying values of penalty parameter and coefficient. Raymer (2002) employed a dynamic exterior penalty function with a linear increase in the penalty parameter over time to encourage convergence on a feasible solution due to increasing penalty severity. This function was chosen having discovered limitations of applying a rejection strategy to the problem, i.e. too severe an environment was created for successful optimisation. Ali and Behdinan (2002) applied a scaled exterior penalty function to non-parameterise the function. The penalty parameter was increased during the optimisation process from $1 \leq \alpha \leq 3$ to similarly raise penalty severity over time.

Ponterosso and Fox (1999) employed an exterior penalty function with constraints on the maximum stress and displacement of each member within a two-dimensional truss structure. The degree of constraint violation was measured as the sum of the constraint violations of each structural member. Empirically-defined weights were also applied to the design constraints to differentiate between the importance of the two constraints. Pant and Fielding (1999) similarly weighted constraint violations by their importance on the design, as well as permitting constraints to be statically disabled prior to optimisation if deemed unnecessary for the current problem. Weighting was applied differently by Ölvander et al. (2009) to weight the different design objectives of the MDO problem. An exterior penalty function was employed, with constraint violations computed with respect to all design constraints across all disciplines. No weighting was applied to the resulting penalties, however the weighting applied to the objective function provided predetermined importance to each discipline. Qiu and Zhang (2010) used a fuzzy exterior penalty function to calculate the penalties to be applied to each design given the magnitude of constraint violations. This resulted in a set of static penalty values to be added to the objective value, the value of which was dependent on the magnitude of constraint violations.

Many publications within the field of aircraft design optimisation do not provide details of the nature of penalty function applied. For example, Reuther et al. (1999) described the use of a penalty function to avoid unreasonable design geometry, possibly suggesting the use of an interior penalty function to prevent the geometry from approaching the boundaries of a feasible solution. Similarly, a penalty function was employed by Majumder and Rao (2009) but not explicitly defined.

2.5 Comparison of Existing Approaches

Existing studies into aircraft design optimisation have varied in the focus of the research and the method employed to optimise a design. Despite this, similarities have been observed in the approaches employed to tackle this problem. Table 2.1 presents the results of the literature review into existing approaches to aircraft design optimisation. The results presented for each researcher include the publications of greatest significance to this research. These results are grouped into fields of research focus, aircraft class and section, static or variable model fidelity, load cases simulated during analysis, optimisation techniques and penalty functions employed, and design parameters considered. Table 2.1 provides the most frequently observed values within each field, with 'miscellaneous' capturing alternate or not clearly defined values.

The focusses of most of the approaches reviewed can be categorised by the descriptions given in the corresponding publications as either on the aerodynamics or structure of the aircraft. The former typically indicated an objective of minimal aerodynamic drag through the optimisation of the aircraft external profile whilst the latter led to optimisation of the airframe for minimal mass in most cases, as shown in Table 2.1. A selection of studies had an additional miscellaneous focal point, such as improving the computational efficiency of the optimisation process rather than focussing principally on improving the designs obtained. Alternatively, a miscellaneous focus can indicate a different aspect of engineering design under consideration, for example the research by Antoine et al. (2004) was focussed on improving the environmental impact of an aircraft. Nevertheless, the majority of the literature indicated research focussing on either the aircraft aerodynamics, structure or both. Within the specified area of focus, publications were concerned with either the development and evaluation of a framework for application to aircraft design optimisation or the improvement of aircraft designs using existing tools.

The class of aircraft most commonly studied in the literature was a large civil aircraft. The ability to consider a single class of aircraft, as was the case in most studies, limits the use of a framework or tool to that class alone. This prevents the use of a framework for other classes even though the design considerations are similar, and thus can be defined by similar design variables (Raymer, 2002), but with several key differences. These include the load cases to be applied to the aircraft, as these are dependent on aircraft class, as well as design variations, i.e. significant geometrical differences or mission-related features, e.g. payload. A similarly limiting factor included in many existing approaches was the consideration of only the aircraft wing. This permits greater detail in the design, modelling, analysis and optimisation of the wing without increasing the computational cost compared to modelling the entire aircraft. However, by considering only the wing it is not possible to generate a complete aircraft design for output to the next stage of the design process. The lack of a complete aircraft conceptual design is a disadvantage given the importance of generating a number of suitable concepts at the early stage of the design process for further detailed development into the final aircraft design, as was discussed in §1.2. In fact, such detailed design, modelling and optimisation of an aircraft section is better performed at later stages of the design process, i.e. embodiment or detail design, where the computational time required to perform such tasks is of less importance than the precision and quality of the design obtained (Raymer, 2006). For example, Chintapalli et al. (2010) investigated the optimisation of skin-stringer panels in the aircraft wingbox, but focussed their research on the embodiment stage of the design process.

Table 2.1 confirms that existing approaches predominantly employed static model fidelity. In approaches where variable-fidelity modelling was employed, this was typically achieved through surrogate modelling such as by Hu and Yu (2009). Variable-fidelity modelling is used in such cases to allow many analyses to be performed at low levels of fidelity before performing a small number of analyses high-fidelity models to account for the error in the low-fidelity models due to approximations. This introduces a reliability on the quality of approximation made of the solution space whereas variable-fidelity modelling without the use of a surrogate model, i.e. through simply changing the precision of computational model, removes this risk. Minisci et al. (2011) employed variable-fidelity modelling through discrete in-

creases in fidelity over the duration of the optimisation process. This permitted an approximation to be made of a good solution with a low-fidelity model prior to further improvement of the design at higher fidelity. However, this approach did not allow for a reduction in model fidelity if desired. For example, if a dramatic change was made in the best solution leading to relocation of the search to a new region of the solution space it may have been beneficial to explore this region with a low-fidelity model for rapid approximation of the solutions in the region. This was not possible with this variable-fidelity approach that only permitted increases in model fidelity.

A single load case was applied in the majority of studies, most commonly a symmetric pull-up manoeuvre of the greatest magnitude within the flight envelope. Rao et al. (1979, 1984, 1985, 1986 and 1987) included the optimisation of an aircraft wing for a variety of loading conditions including gust, landing and taxi loads. A single load case was applied during the experimentation of Kesseler and Vankan (2006), who acknowledged that all load cases required by the airworthiness requirements should be applied to the aircraft during the design process in order to certify the design. Raymer (2006) indicated that it can be acceptable to assess a design against a selection of critical load cases during the early stages of the design process, i.e. conceptual design. Nonetheless, applying a larger selection of load cases improves the likelihood that a realistic design solution will be obtained.

A number of different optimisation techniques have been employed for aircraft design optimisation. Most recently, GAs have found popularity within this domain, such as by Amadori et al. (2007a, 2007b, 2008), Ali and Behdinan (2002), Guo et al. (2006) and Raymer (2002), although other EAs and techniques such as MC, PSO and SA have also been applied. Surrogate modelling is a common method of reducing the effort required for analysis of a solution. Conversely, many frameworks within the literature preferred not to use surrogate modelling such that each design solution is analysed in similar conditions. An exterior penalty function is most often employed to encourage solution feasibility. As discussed in §2.4.4, this function is usually a static quadratic function, although deterministically-controlled dynamic functions were employed by Ali and Behdinan (2002) and Raymer (2002).

The similar requirements and configurations of aircraft designs over recent years have resulted in common design variables, constraints and objectives for existing approaches. Studies focussing on the aerodynamics of the aircraft tended to employ variables to define the geometry of the aircraft sections considered, i.e. wing, fuselage or empennage, as indicated in Table 2.1. The wing and empennage are commonly optimised using similar variables due to the similarity in their designs (Raymer, 2002). However, the wing is often optimised to greater detail with a larger number of variables than the empennage due to its importance as the primary lifting surface of a conventional fixed-wing aerodyne. These variables define the chordwise and spanwise profiles of a lifting surface, as well as its position and orientation relative to the fuselage. For example, typical design variables are those used by Venter and Sobieszczanski-Sobieski (2004) that included the chord length, thickness-to-chord ratio, surface area, aspect ratio, taper ratio and sweep angle. The fuselage is typically optimised through variation of its length and principal cross-section, as well as aspects of nose and tail geometry. The powerplant is occasionally optimised in coordination with the aircraft with respect to the number of engines and the vehicle thrust-to-weight ratio. Similarly, aircraft stability is employed as a design variable in the form of the static stability of the vehicle, although this factor is often used as a constraint instead. Alternatively, properties of the aircraft mission, e.g. cruise altitude and range, are included as design variables, commonly during the optimisation of the aircraft noise, emissions or cost performance.

Design variables concerning the structural layout of the airframe typically defined the number, position, size and material of airframe structural members. The number of members concerns the quantity of each type of member within each aircraft section, e.g. wing ribs. The positions of these members are defined either using formulae to determine their distribution within the aircraft section or through individual variables to set the positions of each member of the type. Similarly, the sizes of the structural

Table 2.1: Focus of aircraft design optimisation by other researchers

Researcher	Focus			Aircraft class					Aircraft section			Model fidelity		Load case				Optimisation technique				Penalty function		
	Aerodynamics	Structure	Miscellaneous	Civil light	Civil large	Military	UAV	Miscellaneous	Wing	Fuselage	Empennage	Static	Variable	Manoeuvre load	Gust load	Ground load	Miscellaneous	MC	EA	LS	Miscellaneous	Interior	Exterior	Dynamic
Ali and Behdinan (2002)	✓	✓			✓				✓	✓	✓								✓				✓	✓
Alonso et al. (2009)	✓	✓			✓				✓	✓	✓	✓		✓							✓			
Amadori et al. (2007a, 2007b, 2008)	✓	✓				✓		✓	✓	✓	✓	✓		✓					✓				✓	
Antoine et al. (2004)			✓		✓				✓	✓	✓								✓					
Arrieta and Striz (2005)	✓	✓				✓			✓			✓		✓							✓			
Ayele et al. (2013)	✓	✓					✓		✓	✓	✓								✓					
Bower and Kroo (2008)			✓		✓				✓	✓	✓								✓					
Çavuş (2009)		✓	✓		✓	✓		✓	✓	✓	✓		✓						✓		✓			
Chintapalli et al. (2010)		✓			✓				✓			✓					✓				✓			
Choi et al. (2008)	✓				✓				✓	✓	✓		✓								✓			
Crawford and Simm (1999)	✓	✓	✓			✓			✓	✓	✓										✓			
Eves et al. (2009)		✓				✓	✓	✓	✓			✓		✓							✓			
Gantois and Morris (2004)	✓	✓			✓				✓			✓		✓							✓			
González et al. (2004)	✓						✓		✓	✓	✓	✓							✓					
Guo et al. (2003, 2006, 2007)	✓	✓		✓				✓	✓			✓							✓	✓			✓	
Hansen and Horst (2008)		✓						✓	✓	✓		✓					✓		✓					
Hu and Yu (2009)	✓	✓					✓		✓			✓									✓			
Kaufmann et al. (2010)		✓			✓				✓			✓					✓			✓				
Kesseler and Vankan (2006)	✓	✓			✓				✓			✓		✓							✓			
Kim et al. (2013)		✓						✓	✓			✓					✓				✓			
Koch et al. (1999)	✓	✓	✓		✓				✓	✓	✓										✓			
Ledermann et al. (2005, 2006)		✓			✓				✓	✓		✓		✓					✓					

Table 2.1: Focus of aircraft design optimisation by other researchers (cont.)

Researcher	Focus			Design variable									Design constraint							Design objective			
	Aerodynamics	Structure	Miscellaneous	Mission	Powerplant	Cabin layout	Wing design	Fuselage design	Empennage design	Aircraft stability	Structural layout	Material	Mission	Powerplant	Wing design	Fuselage design	Airframe strength	Deflection	Miscellaneous	Minimum drag	Minimum mass	Minimum cost	Miscellaneous
Ali and Behdinan (2002)	✓	✓			✓	✓	✓		✓	✓		✓							✓		✓		
Alonso et al. (2009)	✓	✓		✓			✓			✓			✓	✓		✓							✓
Amadori et al. (2007a, 2007b, 2008)	✓	✓					✓		✓		✓				✓						✓		✓
Antoine et al. (2004)			✓	✓	✓		✓		✓			✓				✓			✓			✓	✓
Arrieta and Striz (2005)	✓	✓									✓						✓		✓		✓		
Ayele et al. (2013)	✓	✓		✓			✓												✓		✓		✓
Bower and Kroo (2008)			✓	✓	✓		✓			✓			✓		✓							✓	✓
Çavuş (2009)		✓	✓			✓		✓				✓		✓		✓			✓	✓	✓	✓	
Chintapalli et al. (2010)		✓									✓						✓				✓		
Choi et al. (2008)	✓					✓	✓	✓	✓				✓						✓				✓
Crawford and Simm (1999)	✓	✓	✓	✓			✓	✓					✓		✓	✓					✓		
Eves et al. (2009)		✓									✓						✓	✓			✓		
Gantois and Morris (2004)	✓	✓					✓				✓						✓	✓		✓	✓	✓	
González et al. (2004)	✓						✓	✓	✓				✓		✓					✓	✓		✓
Guo et al. (2003, 2006, 2007)	✓	✓					✓				✓	✓					✓						✓
Hansen and Horst (2008)		✓									✓						✓				✓		
Hu and Yu (2009)	✓	✓					✓				✓		✓				✓	✓		✓	✓		
Kaufmann et al. (2010)		✓									✓						✓		✓		✓	✓	
Kesseler and Vankan (2006)	✓	✓					✓				✓						✓						✓
Kim et al. (2013)		✓									✓	✓					✓						✓
Koch et al. (1999)	✓	✓	✓		✓		✓		✓				✓								✓	✓	✓
Ledermann et al. (2005, 2006)		✓									✓						✓	✓			✓		

Table 2.1: Focus of aircraft design optimisation by other researchers (cont.)

Researcher	Focus			Aircraft class					Aircraft section			Model fidelity		Load case				Optimisation technique				Penalty function		
	Aerodynamics	Structure	Miscellaneous	Civil light	Civil large	Military	UAV	Miscellaneous	Wing	Fuselage	Empennage	Static	Variable	Manoeuvre load	Gust load	Ground load	Miscellaneous	MC	EA	LS	Miscellaneous	Interior	Exterior	Dynamic
Li and Hu (2002)	✓							✓	✓				✓					✓	✓	✓		✓		
MacMillin et al. (1997)	✓	✓			✓				✓	✓	✓		✓								✓			
Majumder and Rao (2009)		✓						✓	✓			✓				✓						✓	✓	
Martins et al. (2002)	✓	✓		✓					✓	✓	✓	✓					✓			✓				
Maute and Allen (2004)	✓	✓			✓				✓			✓					✓				✓			
Mavris et al. (1997, 2000)			✓		✓				✓	✓	✓	✓		✓				✓			✓			
Minisci et al. (2011)	✓		✓					✓		✓			✓						✓		✓			
Nadir (2005)		✓						✓				✓		✓						✓				
Nguyen et al. (2013)			✓			✓	✓		✓				✓								✓			
Oktay et al. (2011)		✓						✓	✓			✓		✓						✓				
Pant and Fielding (1999)			✓	✓					✓	✓	✓									✓			✓	
Park et al. (2009)	✓	✓						✓	✓			✓		✓							✓			
Petersson et al. (2010)		✓			✓				✓			✓		✓	✓				✓					
Rafique et al. (2011)			✓					✓	✓	✓	✓	✓					✓		✓	✓	✓		✓	✓
Rao et al. (1979, 1984, 1985, 1986, 1987)		✓						✓	✓			✓			✓	✓					✓	✓		
Raymer (2002, 2006)	✓	✓		✓	✓	✓	✓		✓	✓	✓							✓	✓	✓			✓	✓
Ricci et al. (2012)	✓	✓			✓				✓				✓	✓						✓				
Rinku et al. (2008)		✓		✓					✓	✓		✓					✓				✓			
Rothwell (1991)		✓						✓	✓	✓		✓					✓				✓			
Schuhmacher et al. (2002)		✓		✓					✓			✓		✓							✓			
Venter and Sobieszczanski-Sobieski (2004)	✓	✓			✓				✓			✓		✓							✓			
Xia and Gao (2002)	✓		✓					✓	✓										✓					

Table 2.1: Focus of aircraft design optimisation by other researchers (cont.)

Researcher	Focus			Design variable									Design constraint							Design objective			
	Aerodynamics	Structure	Miscellaneous	Mission	Powerplant	Cabin layout	Wing design	Fuselage design	Empennage design	Aircraft stability	Structural layout	Material	Mission	Powerplant	Wing design	Fuselage design	Airframe strength	Deflection	Miscellaneous	Minimum drag	Minimum mass	Minimum cost	Miscellaneous
Li and Hu (2002)	✓			✓			✓													✓			
MacMillin et al. (1997)	✓	✓		✓	✓		✓	✓	✓				✓	✓	✓	✓					✓		✓
Majumder and Rao (2009)		✓			✓			✓			✓						✓				✓		✓
Martins et al. (2002)	✓	✓					✓	✓	✓		✓		✓				✓	✓		✓	✓		
Maute and Allen (2004)	✓	✓						✓			✓						✓		✓		✓		
Mavris et al. (1997, 2000)			✓	✓	✓		✓						✓	✓	✓						✓	✓	✓
Minisci et al. (2011)	✓		✓	✓				✓					✓										✓
Nadir (2005)		✓		✓							✓					✓					✓	✓	
Nguyen et al. (2013)			✓		✓		✓						✓						✓		✓		✓
Oktay et al. (2011)		✓									✓	✓							✓				
Pant and Fielding (1999)			✓	✓	✓		✓	✓					✓						✓			✓	
Park et al. (2009)	✓	✓					✓				✓				✓		✓				✓		
Petersson et al. (2010)		✓									✓						✓		✓		✓		
Rafique et al. (2011)			✓	✓	✓			✓					✓			✓					✓		
Rao et al. (1979, 1984, 1985, 1986, 1987)		✓					✓				✓						✓			✓	✓		
Raymer (2002, 2006)	✓	✓			✓	✓	✓	✓	✓	✓			✓	✓		✓	✓				✓	✓	
Ricci et al. (2012)	✓	✓									✓	✓					✓		✓		✓		
Rinku et al. (2008)		✓									✓						✓				✓		
Rothwell (1991)		✓									✓						✓				✓		
Schuhmacher et al. (2002)		✓									✓						✓				✓		
Venter and Sobieszczanski-Sobieski (2004)	✓	✓					✓				✓						✓				✓	✓	
Xia and Gao (2002)	✓		✓				✓								✓					✓			✓

members are typically determined by variables defining the cross-sectional shape of the member as well as its breadth and depth (Chintapalli et al., 2010). Materials can be varied either by using a database of common aerospace materials or through the optimisation of mechanical properties of the members. These variables are applied either for all structural members of a specific type within the airframe or for each member individually. The independent application of variables to individual members greatly increases the size of the optimisation problem, therefore is less commonly performed. Optimisation of the airframe using composite materials introduces new variables to define the number, orientation and thickness of plies of the composite materials (Kim et al., 2013). The inclusion of composites also leads to the requirement to consider new constraints on the design such as the joining of composite layers and manufacturing restrictions not inherent with metallic materials. Topology optimisation, such as that conducted by Oktay et al. (2011), is typically performed by discretising a member to permit the removal or addition of material from the member in order to optimise its design whilst maintaining satisfactory performance. Such optimisation is typically performed when considering isolated aircraft sections rather than the entire aircraft due to the level of detail employed during optimisation.

The design constraints can be grouped as either design or performance-based constraints. For example, design-based constraints restrict the geometry and design characteristics of the aircraft such as the wingspan, fuselage length and powerplant requirements (Raymer, 2002). These are typically used to ensure a reasonable aircraft design is obtained for manufacture and operation within existing aerodrome restrictions. Conversely, performance-based constraints determine the requirements of a design during its analysis, such as the structural integrity of the airframe as measured using FEA. Such structural integrity is typically established as using the minimum FoS under yield within the airframe structural members and the deflection of the structure under load. These constraints are defined by the airworthiness requirements or the aircraft geometry, e.g. constraining wingtip deflection against ground-strike based on the distance between the ground and tip at rest. Schuhmacher et al. (2002), however, included additional structural constraints including maximum values of stress components and buckling loads as well as step sizes in the geometry of adjacent members and a limiting flutter speed. Other common constraints include the twisting of lifting surfaces and the amount of lift required to be generated. Mission characteristics are also employed as constraints to ensure the design will be fit for operation, e.g. a minimum range of a large civil aircraft to ensure the vehicle can operate on a desired route. Generally, constraints on the structural integrity of the airframe are most common during structural optimisation and also most appropriate to ensure the optimisation process produces a reasonable design for manufacture and operation.

The most common design objective during structural optimisation was for an aircraft of minimal mass. This is to encourage improved operational performance of the aircraft leading to reduced fuel consumption, emissions, noise and cost as a result of the aircraft possessing a lighter airframe to propel through the air. Further, a lighter airframe can also lead to reduced manufacturing costs, although reducing mass through the use of new materials can conversely add cost to the design. The use of this objective function is typically coupled with variables to control the structural layout of the aircraft and, in some cases, the external geometry as well. Existing studies that include aerodynamic optimisation most commonly employ an objective function to minimise aerodynamic drag. Common alternative objective functions of existing approaches include minimal sonic boom (Alonso et al., 2009), emissions (Bower and Kroo, 2008) and cost (Kaufmann et al., 2010). These objectives are often used in combination with others for minimal mass, drag or both, typically through MDO.

The number of design parameters, i.e. variables, constraints and objectives, employed during studies differed greatly, typically numbering between four and 70 parameters. The consideration of a single section of the aircraft, such as the wing, provides the opportunity to reduce the number of parameters employed and, therefore, the size of the optimisation problem. Alternatively, the symmetry of the aircraft and similarity of external and internal geometry can enable a reduction in the number of variables by

geometric assumptions such as symmetric wing-mounted ordnance positions or identical cross-sectional geometry of airframe members of the same type, e.g. ribs. Increasing the number of variables greatly increases the number of design variations populating the solution space, therefore reducing the number of variables is beneficial to improve optimisation process convergence and prevent an excessively long solution process. Raymer (2002) listed the most critical design parameters during aircraft conceptual design optimisation, albeit without employing structural variables, and stated that five key variables were the minimum required for aircraft MDO assuming a fixed engine design: wing loading coefficient, aspect ratio, taper ratio, sweep and aerofoil thickness-to-chord ratio.

A common theme amongst existing approaches to the aircraft design optimisation problem is to employ a pre-determined solution process with limited ability to modify this process to improve its operation. The possibility of such adaptation would be beneficial in order to encourage improved search behaviour, e.g. solution space exploration to prevent premature convergence by an LS technique or convergence upon the neighbouring local optimum by a population-based optimisation technique. Such a dynamic optimisation problem would thus be more likely to generate a high-quality solution than a static pre-determined process. Furthermore, the majority of publications presented solely the process of finding solution to a particular problem of aircraft design optimisation. Notwithstanding this, a number of studies presented a framework for the optimisation of an aircraft. As a result, these studies provide the closest similarities to the aim of this research. Kesseler and Vankan (2006) presented a framework for the MDO of a wing design considering multiple performance objectives of minimum mass, maximum range and maximum fuel efficiency. This framework included the generation of aircraft geometry, engine sizing, load computation, aerodynamic and mission analysis, and structural optimisation. The framework only considered the design of the wing and applied a single isolated load case of a $+2.5g$ symmetric pull-up manoeuvre. This load case was selected to apply the greatest bending moments on the wing structure, with the software tool Nastran employed to perform FEA with a design constraint imposed on the maximum von Mises stress within the airframe. The design variables were not defined explicitly, i.e. it was stated that they control the sizes of structural members for mass optimisation whilst wing geometric properties were varied for the optimisation of range and fuel efficiency. The results of the investigation achieved significant improvements in the final design over the initial solution using the MDO framework. However, no comparison was performed of the designs against other approaches. Moreover, the results of the solution process were dependent on the geometry of the solution space resulting from the use of a Pareto frontier to measure the multiple design objectives.

Amadori (2008) presented a thesis that included a framework to connect analytical tools employed during the aircraft design optimisation process. This thesis was formed following a number of earlier publications (Amadori et al. 2007a, 2007b, 2008). The framework was designed to improve the efficiency of the MDO process using existing software tools. For example, Microsoft Excel was used for user input and subsequent process initialisation as well as aircraft sizing using Visual Basic (VB). CATIA was employed for modelling the aircraft and MATLAB used to simulate an aircraft mission, including the application of an isolated load case. This load case was a $+3.0g$ pull-up manoeuvre, which was chosen as the bounding load case to drive the aircraft size (Amadori, 2010). Aerodynamic analysis was performed using PANAIR, a panel code that was preferred over CFD due to the significant reduction in computational time required. OptiQuest was the tool employed to optimise the design solution. This tool included a library of optimisation techniques that were operated using the settings input in Microsoft Excel. The software tools were connected using the orchestrating tool Modelith. The design components were modelled using CAD, with parameterisation employed to establish a relationship between the design variables defining aircraft geometry and the subsequent CAD model. The use of CAD increased the flexibility of the optimisation through improved design precision compared to other methods. Nonetheless, the CAD model required a high degree of flexibility in order to robustly represent the wide variety of

design possibilities. A penalty on computational time also resulted from the use of such detailed modelling, leading to later development of the framework to employ simple beam models for more rapid modelling analysis if preferred over analysis precision (Amadori, 2010). A general structural element was used to model airframe members, with design variables controlling the number and positions of structural member types, e.g. ribs, frames etc., and the individual thickness of each member. Through scaling and design symmetry it was possible to reduce the number of variables, thus increasing process efficiency. For example, the number and positions of ribs in each wing were assumed to be the same given aircraft symmetry about the longitudinal axis, thus requiring half as many variables compared to an asymmetric design. It was also emphasised that over-constraining the solution could compromise the design process such that good attributes of infeasible designs are not considered.

Schuhmacher et al. (2002) introduced a framework for the MDO of a civil aircraft wingbox. The purpose of this publication was to demonstrate the benefits of a framework combining multiple groups of engineering design disciplines over the historic aircraft design process of individual design groups. The reasoning for this approach highlighted the interdependencies of the different disciplines, most notably aeroelastics and structures. Furthermore, more detailed modelling and analysis tools were included than common of the historic aircraft design process. For example, it was stated that a typical airframe model was constructed using beam elements to estimate the distribution of stiffness and mass over the airframe at a level appropriate for the detail required during conceptual design. The MDO framework replaced this model with a more detailed finite element (FE) model employing design variables to define the size of structural members. Nastran was employed to perform FEA whilst the Sol200 module of Nastran optimised the wingbox design. The use of this more detailed FE model with associated design variables resulted in a large number of variables to define each design. A total of 2,515 design variables were employed to define the design of the spars, stringers and skin, noting that the designs of the ribs were not considered. 805,402 design constraints imposed limits on the stresses in the airframe as well as limiting buckling criteria, geometric properties and the flutter speed when subjected to 96 different load cases. This level of detail was much greater than that usually employed during conceptual design, a result of the framework encompassing the entire aircraft design process.

Hansen and Horst (2008) presented a multi-level optimisation framework for application to aircraft structural design. This multi-level framework consisted of two tiers, the first of which concerned the optimisation of the airframe topology using an EA whilst the second employed a gradient-based LS optimisation technique to optimise the thicknesses and cross-sections of aircraft members. This framework was similar to a hybrid optimisation technique; however, the use of different variables within the two tiers created two variations of the optimisation problem and as such was not strictly a hybrid optimisation technique. The change from first to second framework tier was made based on the convergence of the population within the first tier. This enabled an approximation to be made of a suitable design in the first tier prior to more focussed deterministic optimisation of this design in the second tier. Structural analysis and optimisation were performed using Patran and Nastran Sol 200 respectively to search for a design of minimal mass. Two case studies were presented, the first of a cantilever truss structure under a tip load and the second the fuselage structure of a BWB under a pressurisation load. In the first problem, the design variables were nodal coordinates and element cross-sectional areas in the first and second tiers respectively. Two experiments were performed: optimisation with both tiers and optimisation with only the EA in the first tier. The objective value was lower using the two-tier framework than when using only the first tier, with fewer FEA evaluations required. The design variables of the second study were the topology and sizes of composite skin panels in the first and second tiers respectively. The mechanical properties of the materials remained constant throughout the optimisation, with constraints imposed on the buckling eigenvalues, von Mises stresses and failure indices in the structure. A total of 2,500 individual solutions were modelled and analysed in the first optimisation tier and a maximum of 35 steps

made in the second deterministic tier. Although a good design was obtained, no comparison was made in the second study between the presented framework and single-tier approaches. It was concluded that the computation time required was a limitation of the framework, with a consequential need for automated mesh generators. This indicated a reliability of the framework on the software tools employed and an inefficiency in the computation inherent with the framework.

Raymer (2002) performed MDO of conceptual aircraft designs of various classes including a civil light aircraft, a large civil transport aircraft, a military fighter and a UAV. The external aerodynamic profile of each aircraft was optimised for either minimum cost, in the case of the military fighter, or minimum mass, for the other aircraft classes. Various deterministic and stochastic optimisation techniques were employed, these included HC, SD, MC, GAs using RW, TO and BP selection, and KQ which was developed by the author. The results of experiments indicated that the GAs were able to rapidly identify a solution close to their final solution in a much shorter period of time than the considered LS techniques. The qualities of the solutions generated by all techniques were comparable, however the solutions obtained using LS techniques were the best. This was due to the ability of these techniques to locate the local minimum in their neighbouring solution space, although the time taken to solve the problem was much greater than for the population-based techniques due to poorer exploration capabilities. Ultimately, such improvement in solution quality was deemed not worth the additional required computational time.

Hu and Yu (2009) studied the MDO of a UAV flying wing for minimal aerodynamic drag and structural mass whilst constraining the aerodynamic and structural design requirements, payload internal volume and the radar cross-section to ensure a stealthy design. Surrogate modelling was employed to reduce the computational requirements of design analysis as well as disciplinary discretisation in order to perform independent analysis within each discipline. The highest system level performed MDO of global configuration variables over a number of generations. Below this level, a subsystem performed aerodynamic and stealth analysis of the aircraft external profile whilst a second subsystem performed similar analysis of the aircraft structure. These subsystems also included aerodynamic and structural optimisation of the aircraft by a GA. The subsystem solution spaces were sampled using Latin hypercubes to reduce the necessary analysis to those designs within each subsystem sample. FEA was conducted using Nastran on a low-fidelity model consisting of rods to model spars and web stiffeners and plates to model skin and the webs of spars, ribs and frames. Structural design variables controlled the areas and thicknesses of the spar caps, ribs and frames as well as the thickness of the wing skin and stiffener areas of webs. The constraints imposed on the structure were the maximum axial stress in rods, shear stress in plates and wingtip deflection. The results of subsystem analysis were used to form the response surface of the surrogate model at the highest system level. MDO was subsequently performed with six variables defining the aircraft external shape. Iterations of random sampling of the solution space were performed to validate the accuracy of the surrogate model through additional analysis. A cost of this approach was the need to double the subsystem sample size if the accuracy of the surrogate model was insufficient. Specifically, the initial Latin hypercube sample size was set at 100 points but was required to increase to 200 points if the surrogate model validation indicated inadequate precision. Also, a three-dimensional CAD model was built for the aerodynamic and stealth analysis in CATIA, which increased the computational cost of FEA, thus reducing the benefits of employing surrogate modelling.

Ali and Behdinan (2002) performed MDO of a large civil aircraft, the Boeing 717 aircraft, at a conceptual design level within a framework controlled by MATLAB. A binary GA was employed, with selection performed using either RW or TO by one-point, two-point or uniform crossover and bit-flip mutation. The population size was fixed at 80 individuals with the process terminated after 200 generations. Each experiment was performed five times to account for results variability. The 21 design variables defined the aircraft geometry, such as aspect and taper ratios, tail configurations, cabin layout and powerplant thrust. The scaled exterior penalty function of Eqn. (2.10) was employed with design constraints to

restrict the stability of the aircraft. The aircraft was optimised over a single cruise mission without the application of specific loading conditions typically encountered during flight, e.g. manoeuvre or gust loads. This approach to the optimisation problem was static with the exception of penalty function scaling based on the fitness of each population. The optimisation objective was for minimal aircraft mass; however, the design variables did not provide opportunities for optimisation of the airframe, nor did the design constraints consider the integrity of the airframe. The use of a single GA restricted the ability of the optimisation search to converge upon the local minimum closest to the best solution, with the authors stating a preference to obtain several near-optimal solutions that could be combined into a better solution. Poor convergence was observed by the GA, reducing the confidence that the solutions obtained were near-optimal. It was determined that RW selection led to the domination of elite designs until a late stage in the process by which point the population had mostly converged; this issue was not observed using TO selection. In spite of this, the best designs were generated using RW selection with uniform crossover. The static optimisation process employed prevented adaptation of the search to improve convergence having found promising design solutions. In fact, the authors posed the question of how to improve the set-up of the optimisation process to encourage better convergence, e.g. different population size as well as crossover and mutation rates.

2.6 Summary

Aircraft design optimisation has been the subject of much research in an attempt to improve the quality of aircraft designs output for manufacture and operation. The conceptual design stage of the design process has seen significant research given its importance in determining suitable concepts for further development into a final aircraft design. Structural mass optimisation is often performed during this stage in order to reduce the weight of the airframe whilst maintaining the required strength under load. The traditional existing approach involves a common process of initialisation, mission definition, mass estimation and external geometry definition prior to the design and optimisation of the airframe. The airworthiness requirements provide the loading conditions under which the aircraft must operate, typically leading to the simulation of the worst loads on the airframe during structural analysis. Such analysis is performed to determine the feasibility of an airframe design, leading to the optimisation of each design based on its objective value. Many different techniques have been employed for this optimisation with no indication of a dominant technique over all others. The optimisation process itself is not typically subject to much research, such that a static process is traditionally applied without the possibility to improve optimisation process performance and, as a result, further improve solution quality. This presents an opportunity for further research such that a dynamic optimisation process may be employed in an attempt to further improve the quality of aircraft designs generated and process by which this is achieved.

Chapter 3

Hyper-Heuristic Optimisation

Hyper-heuristic optimisation is an emerging area of research wherein the optimisation process followed to obtain a near-optimal solution to a problem is itself modified during execution in an attempt to improve its performance. A hyper-heuristic approach (HHA) is employed to promote such improvements in process performance in order to increase the likelihood that better problem solutions will be discovered. This is often coupled with the encouragement for improvements in other areas of process performance, e.g. computation time. The purpose of this chapter is to introduce and review the use of hyper-heuristic optimisation within the literature. The principles of hyper-heuristic optimisation are firstly introduced in §3.1 followed by descriptions of the four aspects of an HHA pertinent to this research in §3.2, §3.3, §3.4 and §3.5. Traditional applications of hyper-heuristics within the literature are subsequently presented in §3.6 before §3.7 summarises the chapter.

3.1 Principles of Hyper-Heuristic Optimisation

The optimisation of a solution to a problem is highly dependent on the process followed, including the choice and set-up of the optimisation technique employed (Özcan et al., 2008). This is notably true for a complex problem such as aerospace design where numerous design variables with contrasting influences on the solution require optimisation to satisfy a given objective function subject to strict constraints (Fukunaga et al., 1997). Wolpert and Macready (1997) stated a *"no free lunch theorem"* that one optimisation technique cannot be superior to all others across all classes of problems. Many state-of-the-art optimisation techniques are too problem-specific or knowledge-intensive for general application to a variety of problems (Burke et al., 2003a). Furthermore, the development and tuning of a high-quality technique for general application to different problems can be difficult and requires extensive investigation and validation, most notably when considering unpredictable domains with unknown solutions (Chakhlevitch and Cowling, 2008). Thus, optimisation techniques generally employed to solve a problem do so with an inherent penalty to performance and subsequent solution quality (Burke et al., 2003a).

Hyper-heuristic optimisation automates the design of optimisation processes for solving hard computational search problems (Burke et al., 2010b). The general aim of hyper-heuristic optimisation is to obtain a solution to a problem of comparable or better quality to those generated by traditional optimisation but at reduced cost (Kendall et al., 2002). It should be noted that within this document 'traditional optimisation' refers to optimisation performed without the use of hyper-heuristics. Hyper-heuristics raise the generality at which optimisation techniques can be applied, leading to the transformation of a problem by employing various techniques during the search (Burke et al., 2003a). The term 'hyper-heuristic' was coined by Denzinger et al. (1997) as a protocol for selecting and combining multiple methods of artificial intelligence. The term was subsequently independently introduced by Cowling et al. (2000) as *"an approach that operates at a higher level of abstraction than current meta-heuristic approaches"*. This

latter definition provides the basis for the application of hyper-heuristic optimisation across the two independent domains shown in Fig. 3.1: the problem and hyper-heuristic domains (Cowling et al., 2000).

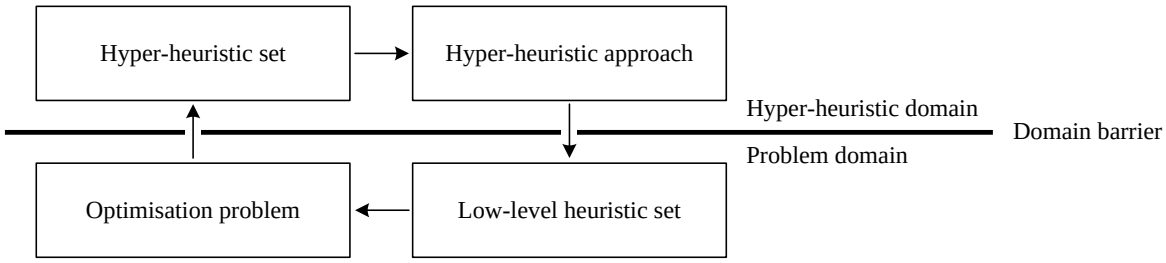

Figure 3.1: Domains of hyper-heuristic optimisation

Within the problem domain, a heuristic searches for a near-optimal solution to a given problem such as aircraft structural design optimisation. These heuristics are called low-level heuristics (LLHs), where it should be noted that the term 'heuristic' may refer to either a heuristic or meta-heuristic when discussing hyper-heuristic optimisation (Ross, 2004). Heuristics are techniques that attempt to solve an optimisation problem through the possession of problem knowledge whereas meta-heuristics similarly search for a problem solution but without such knowledge (Blum and Roli, 2003). Hyper-heuristics are applied in the higher-level domain to improve the performance of the optimisation process within the problem domain in order to satisfy a hyper-heuristic objective function, and thus encourage further solution improvement (Burke et al., 2010b). The hyper-heuristic objective function is similar in purpose to the optimisation problem objective function but is applied within the hyper-heuristic domain. A barrier restricts data flow between the domains to allow the passage of solely information that informs suitable actions of the hyper-heuristic (Chakhlevitch and Cowling, 2008). This information is independent of the problem to be solved, e.g. computation time or a change in objective value or fitness (Özcan et al., 2006).

Hyper-heuristic actions are dependent on the HHA employed, where each approach is defined by specific aspects in which the optimisation process is controlled and modified. These HHA aspects traditionally encompass the selection or generation of LLHs, distribution of a population between numerous LLHs, analysis of the solution space by perturbing individual solutions, and the control of optimisation process parameters (Burke et al., 2010b; Rafique et al., 2011). In essence, an HHA is formed of one or more of the following aspects:

- heuristic selection or generation;
- population distribution;
- perturbation analysis;
- parameter control.

An HHA employs a learning mechanism to gain knowledge of the optimisation process performance and inform the hyper-heuristic actions to be performed within each HHA aspect. This can increase the likelihood that such actions will be beneficial to the optimisation process (Özcan et al., 2010). Learning can be performed prior to the main optimisation process through a series of trials to determine the effects of changes in the process, i.e. offline learning, or during the execution of the process, i.e. online learning (Burke et al., 2009a). Reinforcement learning is popularly employed as online learning to assign a score to hyper-heuristic operations based on their effect on the optimisation process (Burke et al., 2010b). Positive reinforcement is most commonly used, wherein scores are based on the improvements made in the process, whereas negative reinforcement penalises operations that result in poorer performance (Kaelbling et al., 1996). Alternatively, learning may be excluded from the HHA such that random hyper-

heuristic operations are performed that do take into account the problem state or optimisation process performance. This increases the diversity of the hyper-heuristic search (Rafique et al., 2011).

3.2 Heuristic Selection

Heuristic selection is the aspect of hyper-heuristic optimisation that has been investigated to the greatest extent within the field (Burke et al., 2010b). Heuristic selection chooses the most appropriate LLH for application in the problem domain from a set of candidate heuristics, leading to an alternative description of hyper-heuristics as *"heuristics to choose heuristics"* (Burke et al., 2010b). LLHs may be constructive or perturbative, wherein the former creates a solution incrementally from an empty initial solution whilst the latter evolves a complete initial solution over a period of generations (Burke et al., 2010b). With constructive heuristics, an HHA is provided with a set of problem-specific LLHs for application to the problem with the aim of identifying the best LLH to be applied given a current problem state (Burke et al., 2009a). The process is performed until a solution is constructed having evaluated the finite number of LLH permutations, the quantity of which is defined by the size of the combinatorial problem (Burke et al., 2010b). Conversely, perturbative LLHs are selected to improve the quality of an initial solution over a period of generations. Perturbative heuristic selection is more popularly applied than constructive heuristic selection due to removal of the requirement to evaluate the potentially large number of LLH permutations (Burke et al., 2009b). Perturbative heuristic selection is performed by iteratively choosing an LLH to optimise solutions within the problem domain (Burke et al., 2010b). This process is two-fold: selection of a perturbative LLH by a hyper-heuristic followed by move acceptance to determine whether to approve or reject the use of the LLH within the problem domain (Özcan et al., 2008).

Heuristic generation is another aspect of hyper-heuristic optimisation similar to heuristic selection, although it is less popularly applied (Hyde, 2010). Heuristic generation aims to create a new LLH, rather than select an existing one from a heuristic set, for either a single application to a specific problem or for general use with similar problems (Burke et al., 2009a). The freedom to create a new optimisation technique results in a rich hyper-heuristic solution space, however implementation of heuristic generation is difficult due to the required decomposition of existing LLHs in order to generate a new LLH from their components (Burke et al., 2010b). Furthermore, implementation of heuristic generation requires additional computational effort over heuristic selection due to the need to evaluate numerous permutations of LLH components (Burke et al., 2010b).

3.2.1 Hyper-Heuristics

A heuristic selection hyper-heuristic employed by an HHA chooses a new LLH for application within the problem domain based on the rules embedded within the hyper-heuristic. The frequency of calling a hyper-heuristic to perform heuristic selection can be predetermined, i.e. each LLH is applied in the problem domain for a specific number of generations, or based on the success of an LLH in improving the problem solution. Cowling et al. (2000) introduced the simple random (SR), random descent (RD) and permutation descent (PD) hyper-heuristics. SR randomly selects an LLH to apply to the problem on each occasion the hyper-heuristic is called. RD similarly selects an LLH at random, but repeatedly applies the chosen technique to the problem until no further improvement is made in the solution, at which point another LLH is selected. PD is performed by initially generating a list of LLHs to establish the order in which they are to be applied to the problem. The order of this list is typically random. The hyper-heuristic selects the first LLH on the list and applies it repeatedly until no improvement is made. The next LLH on the list is then selected and the process repeated. The list is progressed through cyclically until termination of the optimisation process. The permutation (PE) hyper-heuristic is an alternative form of PD, wherein the operation is the same except each LLH is applied once before the next LLH from the list is selected (Bilgin et al., 2007). Cowling et al. (2000) also introduced the greedy

(GR) hyper-heuristic which applies the best-performing LLH to the problem. Initially all LLHs within the heuristic set are applied to the problem in order to establish which LLH yields the best solution. This LLH is subsequently employed over the following generations until no further improvement is made in solution quality, at which point all LLHs are re-evaluated for reselection. Peckish (PK) was introduced as a similar hyper-heuristic by Cowling and Chakhlevitch (2003) wherein an LLH is chosen from a candidate list of heuristics populated either randomly or by the best-performing LLHs. The latter consists of the LLHs that either generate the best solutions or provide the greatest improvement in solution quality. This hyper-heuristic has been found to be preferable over GR with a densely populated heuristic set by improving the likelihood of selecting an LLH that will improve a solution rather than allowing a small number of LLHs to dominate the process (Chakhlevitch and Cowling, 2008).

Alternatively, hyper-heuristics can be adapted from LLHs in the problem domain for use in the hyper-heuristic domain. For example, local search (LS) techniques have been employed as perturbative heuristics in the hyper-heuristic domain (Ross, 2004). Storer et al. (1995) employed a basic hill climbing (HC) technique to perturb the combinations of LLHs applied to a problem and indicated suitable alternatives such as genetic algorithm (GA) selection, simulated annealing (SA) and tabu search (TS). Cowling et al. (2000) used roulette wheel (RW) selection in a similar manner to within a GA to select an LLH based on past performance within the problem domain, whilst Drake et al. (2011) employed tournament selection (TO) for the same purpose. A TS hyper-heuristic was introduced by Burke and Soubeiga (2003) using reinforcement learning to assign a score to each LLH based on its performance. Scores are initialised at zero and updated after each use of an LLH. LLH scores are incremented if the LLH improves the solution and decremented otherwise. Subsequently, the LLH with the highest score is selected for application to the problem. In the event of multiple best LLHs, a random LLH is chosen from those concerned.

3.2.2 Move Acceptance

Perturbative hyper-heuristics employ move acceptance as rules to approve or reject the selection of an LLH. These rules are employed after employing an LLH within the problem domain to determine whether to continue to apply the current technique or to select a new LLH for application to the problem. Move acceptance rules are coupled with the rules of the hyper-heuristic employed for heuristic selection such that both the rules of the hyper-heuristic and move acceptance must be satisfied for the application of an LLH to continue (Özcan et al., 2008). Common rules of move acceptance include all moves (AM), only improving (OI), improving and equal (IE) and Monte Carlo (MC) methods (Özcan et al., 2008). AM permits heuristic selection regardless of performance. OI only permits selection of an LLH that improves the measured process performance, i.e. a positive move. IE permits the acceptance of a selected LLH if process performance is at least equal to previous performance, i.e. not a negative move. Simulated annealing (SA) can be used for move acceptance such that all positive moves are accepted as well as negative moves with decreasing probability over time (Bai and Kendall, 2005). MC methods were introduced by Ayob and Kendall (2003) to accept positive moves and randomly permit negative moves with linearly or exponentially decreasing probability. These rules were labelled linear Monte Carlo (LMC) and exponential Monte Carlo (EMC) respectively and are similar in formulation to the annealing schedule of SA. Exponential Monte Carlo with counter (EMCQ) move acceptance was also introduced to include a counter of iterations since last improvement within EMC to prevent convergence on local optima. The probability of accepting a negative move at the kth generation is defined as

$$p_{neg}^{k} = \begin{cases} M - \Delta F_{\max}(\mathrm{X})^{1\to k} & \text{for LMC} \\ \exp\left(-\Delta F_{\max}(\mathrm{X})^{1\to k}\right) & \text{for EMC} \\ \exp\left(-\left(\dfrac{k}{vQ_{ni}}\right)\Delta F_{\max}(\mathrm{X})^{1\to k}\right) & \text{for EMCQ} \end{cases} \tag{3.1}$$

where $\Delta F_{\max}(\mathrm{X})^{1\to k} = F_{\max}(\mathrm{X})^{1\to k} - F_{\max}(\mathrm{X})^{k}$
$F_{\max}(\mathrm{X})^{1\to k}$ maximum fitness in population set X for generations 1 to k
Q_{ni} counter of consecutive generations without improvement

Ayob and Kendall (2003) found by experiment that the best values of constants M and v were $M = 5$ and $v = 1$from possible ranges of $0 \leq M \leq 100$ and $0 \leq v \leq 1$. A positive reinforcement learning mechanism is popularly employed to assign a score to the different LLHs based on their ability to generate a positive move (Özcan et al., 2010). This score is then used by the hyper-heuristic within heuristic selection when choosing the next LLH for application in the problem domain (Burke and Soubeiga, 2003). Alternatively, a learning mechanism may not include a scoring system and may simply rank LLHs based on the measure of process performance used to define a positive move (Chakhlevitch and Cowling, 2008). This measure of improvement (MoI) in process performance is often the problem objective function, i.e. a positive move results when an LLH discovers an improved solution to the optimisation problem (Özcan et al., 2008). When employed in this manner, the MoI is equivalent to the hyper-heuristic objective function. This MoI was assumed during the descriptions of hyper-heuristics in §3.2.1 as this is the typical measure employed; however, a different MoI criterion can be employed. Cowling et al. (2000) defined an alternative MoI criterion called a 'choice function', comprised of three components of performance for each LLH within the heuristic set:

- recent effectiveness of the LLH;
- recent effectiveness of consecutive pairs of LLHs;
- time since the LLH was selected.

The first component measures, at the kth generation, the change in problem objective value made by the hth LLH respective of the time taken for the n_l previous instances for which the heuristic was employed

$$f_{1,h}^{k} = \sum_{l=1}^{n_{l,h}} \alpha^{l-1} \frac{\Delta\Phi_{h}^{l}}{T_{h}^{l}} \tag{3.2}$$

where T_h^l time taken lth previous time hth LLH was selected
α first choice function component weighting
$\Delta\Phi_h^l$ change in objective value lth previous time hth LLH was selected

This component encourages repeated selection of an LLH if it performed well recently. The second component measures dependencies between pairs of LLHs when the h_2th heuristic immediately follows the h_1th heuristic

$$f_{2,h_1,h_2}^{k} = \sum_{l=1}^{n_{l,h}} \beta^{l-1} \frac{\Delta\Phi_{h_1,h_2}^{l}}{T_{h_1,h_2}^{l}} \tag{3.3}$$

where T_{h_1,h_2}^l time taken lth previous time h_1th LLH followed h_2th LLH
β second choice function component weighting
$\Delta\Phi_{h_1,h_2}^l$ change in objective value lth previous time h_1th LLH followed h_2th LLH

The second component biases selection following the application of the h_1th heuristic towards the h_2th heuristic if this combination performed well recently. The third component measures the time since the last use of the LLH, where τ_h denotes the time elapsed since the hth LLH was last selected

$$f_{3,h}^{k} = \tau_h \tag{3.4}$$

While the first two components intensify the search by choosing LLHs that have performed well, the third component provides diversification by encouraging the selection of LLHs that have not been used

recently. The choice function is formed at the kth generation using these three components as

$$\phi_h^k = \max\left(\hat{\phi}_h^k, Q\rho^{-\hat{\phi}_h^k}\right) \tag{3.5}$$

where $\hat{\phi}_h^k = -\alpha f_{1,h}^k - \beta f_{2,h_1.h_2}^k + \delta f_{3,h}^k$

$$Q = \frac{1}{10n_{LLH}} \sum_{h=1}^{n_{LLH}} \max\left(0, \hat{\phi}_h^k + \varepsilon\right)$$

The component weights are set to prioritise different function components, where $0 \leq \alpha, \beta, \delta \leq 1$. Constants ε and ρ increase heuristic selection diversification by ensuring LLHs that result in negative moves maintain a small non-zero probability of selection, with values of $\varepsilon = 1$ and $\rho = 1.5$ used by Cowling et al. (2000). The parameter Q is used to prevent search stagnation by promoting diversification if the recently-used LLHs have failed to improve the solution. The choice function was subsequently employed to measure process performance coupled with GR, PK and RW hyper-heuristics. Drake et al. (2012) modified the choice function to include additional component weighting

$$\phi_h^k = \gamma_h^l f_{1,h}^k + \gamma_h^l f_{2,h_1,h_2}^k + \delta_h^l f_{3,h}^k \tag{3.6}$$

In this function, l denotes the number of times since the hth heuristic last made an improvement in the solution. The weights γ and δ are updated by magnitudes determined by whether an improvement is made in the objective value or not. This results in increased search intensification and reduced diversification whenever an improvement is made in order to exploit a well-performing LLH, whilst promoting the opposite if the search fails to improve the solution, thus removing the need for parameter Q in Eqn. (3.5)

$$\gamma_h^l = \begin{cases} 0.99 & \text{if an improvement is made} \\ \max\left(\gamma_h^{l-1} - 0.01, 0.01\right) & \text{if no improvement is made} \end{cases} \tag{3.7a}$$

$$\delta_h^l = 1 - \gamma_h^l \tag{3.7b}$$

3.3 Population Distribution

Population distribution divides a set of solutions between multiple LLHs for each generation of the optimisation process. This can be seen as an extension of heuristic selection as the operation of both HHA aspects encompass the choosing of LLHs to be applied to the problem. With population distribution, each selected LLH possesses a sub-population of individuals such that the LLH optimises solely the solutions within its sub-population. When a single-solution LLH is selected, each sub-population individual is optimised independently one step per population generation. Population distribution is either performed equally, randomly or based on the performances of the LLHs. The latter leads to the distribution of a greater number of individuals, i.e. larger sub-population sizes, to better-performing LLHs.

Population distribution aims to overcome limitations of individual heuristics through the availability of alternatives (Rafique et al., 2011). Sub-populations must be adequately sized to allow sufficient opportunity for improvement by each LLH. A dynamic population size can enable sub-populations to be resized such that improvement opportunities exist whilst avoiding an excessively-large population. For example, Arabas et al. (1994) presented a method for a dynamic population size where individuals are assigned a lifetime to permit the rejection of individuals at the end of their life. This lifetime is calculated using the fitness of the individuals such that poor solutions possess shorter lifetimes. As a result, fitter individuals remain in the population for a greater number of generations, thus promoting improvement of

solution quality whilst rejecting poorer solutions. However, this approach is more elitist than a dynamic population where individuals are rejected randomly through the bias towards fitter solutions. Sahab et al. (2005) introduced another method wherein the population size is reduced as the population converges by removing all-but-one of individuals possessing identical fitnesses. A lower limit is imposed on the population set size to prevent eliminating too many individuals, and thus hindering the search.

3.4 Perturbation Analysis

Perturbation analysis encourages learning of the local solution space surrounding an individual using a memetic algorithm (MA) (Moscato and Cotta, 2003). An MA performs population-based optimisation coupled with local searches of the solution space neighbouring individuals. The analysis of the local solution space is performed through the perturbation, and subsequent analysis, of a sample of individuals using an LS technique (Ong et al., 2006). As such, MAs are often viewed as hybrid GAs (Krasnogor and Smith, 2000). The criteria for operating an MA include (Krasnogor and Smith, 2005):

- when to perform perturbation analysis;
- how to sample the population;
- the duration of perturbation analysis;
- which LS optimisation technique to employ;
- which evolutionary principle to employ.

The frequency of performing perturbation analysis is commonly either at each optimisation generation or on each occasion at which an improvement is made in the best solution (Krasnogor and Smith, 2005). Higher frequencies of perturbation analysis require greater numbers of solution evaluations, which can lead to greater computational costs. The sample size is typically a proportion of the population, sampled either randomly or selected from the best population individuals (Hart, 1994). Perturbation analysis is then performed either for a predefined number of iterations or until no further improvement is made in the quality of each sampled solution (Nguyen et al., 2009). Hill climbing (HC), simulated annealing (SA) and tabu search (TS) are commonly employed as LLHs to perturb and subsequently optimise the sampled individuals using a selected evolutionary principle (Krasnogor and Smith, 2000). This evolutionary principle is either Lamarckian or Baldwinian evolution. The theory of Lamarckian evolution was presented by Lamarck (1809), stating that the characteristics acquired by a parent during its lifetime may be inherited by its offspring. Alternatively, the Baldwin effect was proposed by Baldwin (1896) as a mechanism of the evolutionary learning of offspring based on the knowledge obtained by their parents during earlier generations. Perturbation analysis using Lamarckian evolution results in the design variable values of a perturbed solution being stored within the individual for use during the generation of the next population of solutions, i.e. the perturbed individual replaces the unperturbed solution within the population. Baldwinian evolution during perturbation analysis results in solely the objective value of an individual being stored, i.e. the unperturbed individual remains in the population but is assigned the objective value of the corresponding perturbed solution. Thus, evolutionary optimisation without perturbation analysis is based on Darwinian evolution (Julstrom, 1999). Adaptive MAs can be employed to adapt these criteria based on the effectiveness of perturbation analysis (Krasnogor, 2002). For example, heuristic selection can be performed to choose the LS technique employed (Burke et al., 2010b). Perturbation analysis is similar to the hybrid optimisation techniques discussed in §2.3.5, however differs by not restricting the use of the LS to after a specified point during the optimisation process or to a single solution.

3.5 Parameter Control

The values of parameters used during optimisation are critical to the success of the process. These values determine the behaviour of the search for a solution to a problem. Parameter tuning may be performed

pre-optimisation through a series of trials in order to establish appropriate values of parameters for use in solving a problem. Such tuning for specific problems can be difficult, especially in unpredictable and large domains without known solutions. This tuning problem can be exacerbated by numerous permutations of values for independent parameters. As such, an extensive period of investigation and validation may be required to ensure that the resulting process set-up is appropriate to the problem and possesses sufficient robustness to account for any problem variation during the solution process (Eiben et al., 2007).

Parameter control modifies the values of parameters during the optimisation process. This reduces the need for parameter tuning pre-optimisation by providing the capability for real-time adjustment of the optimisation process based on the state of the problem (Eiben et al., 2007). Such changes may be made either through perturbation of existing values or selection of the better-performing settings; the latter is referred to as operator selection (Maturana et al., 2010). An evaluation period is included to allow changes to parameters to take effect. Investigation of mechanisms for such automated control of process parameters has seen been subject to limited research, in part due to the highly nonlinear interactions between parameters of the process (Coello Coello, 2009). Approaches to parameter control employed to aid the process of solving an optimisation problem possess three principal characteristics to describe their operation (Smith and Fogarty, 1997):

- what parameter is being changed;
- the scope of the parameter change;
- the basis for the change of a parameter.

The first characteristic concerns the choice of process parameters to be controlled. This is important to ensure that control of the parameters will enable effective changes in the process. Such parameters include operators, e.g. GA crossover and mutation probability, as well as the representation of the problem, e.g. the number of variables of the problem or length of genomes of solutions. The scope of change can be defined at three levels: population, individual and component. Population-level changes are applied to all individuals within the population set. At an individual-level, values are updated for each member of the population independently. Component-level changes are applied to each component of a solution individually. It should be noted that population-level and individual-level control are equivalent when employing a single-solution optimisation technique. Finally, the basis for change defines the reason for and method of parameter modification. Reasons are usually based on the position in time of the process, i.e. optimisation generation, or process performance, e.g. solution quality or population diversity, as informed by a feedback loop. Empirical rules classically dictate changes made to values (Smith and Fogarty, 1997). These three characteristics are defined by the parameter control approach applied within the optimisation process. Four such approaches are: deterministic, adaptive, self-adaptive and hyper-heuristic parameter control. These approaches contrast with static optimisation wherein the set-up of the optimisation process is not modified during optimisation, i.e. the initial values of parameters remain constant.

3.5.1 Deterministic Control

Deterministic parameter control uses predetermined rules to modify the optimisation process. These modifications are typically made using time-based rules, therefore process performance does not affect modification (Eiben et al., 2007). Examples include the annealing schedule of SA and decaying mutation probability of an evolutionary algorithm (EA) to promote convergence towards the end of the process (van Laarhoven and Aarts, 1987; Zhang et al., 2007). The scope of the changes is usually on a population-level as rules do not usually consider differences between individuals or components.

3.5.2 Adaptive Control

An adaptive approach employs a feedback loop to inform a learning mechanism of the current performance of the optimisation process. Changes are then made to parameters based on performance data us-

ing empirical rules with predetermined performance limits included to trigger such changes (Eiben et al., 2007). An example of such adaptive optimisation is the population-level adaptive penalty parameter of Eqn. (2.11) introduced by Bean and Hadj-Alouane (1992). Other examples are the individual-level adaptive GA crossover and mutation probabilities defined by Srinivas and Patnaik (1994), which encourage the crossover and mutation of poorer individuals whilst maintaining the best solutions, and the adaptive range GA proposed by Arakawa and Hagiwara (1998), which directs a population towards promising regions of the solution space by continuously updating its boundaries. Adaptation may be performed at any level of scope depending on the parameter under control (Smith and Fogarty, 1997).

3.5.3 Self-Adaptive Control

Self-adaptive parameter control is so named because the optimisation technique applied to solve the problem also controls the adjustment of values of parameters that it itself uses. This is accomplished through the encoding of the parameters within the genome of solutions subjected to optimisation, leading to the coevolution of the parameters of the process and solutions to the problem (Meyer-Nieberg and Beyer, 2007). For example, considering the following design genome containing n_v design variables

$$\mathrm{V1} \mid \mathrm{V2} \mid \ldots \mid \mathrm{V}n_v$$

n_p process parameters are appended to the genome as

$$\mathrm{V1} \mid \mathrm{V2} \mid \ldots \mid \mathrm{V}n_v \mid \mathrm{P1} \mid \mathrm{P2} \mid \ldots \mid \mathrm{P}n_p$$

The scope of control is at an individual-level, where each population member possesses a personal value of each controlled process parameter (Eiben et al., 2007). For each optimisation generation, the values of parameters of an individual solution are stored and used to optimise the individual. As these parameters are within the genome of the individual, their values are also included within the optimisation operations, e.g. crossover and mutation. Thus, the values that generate the better solutions within the population propagate through the process, leading to the convergence of the population not only on a near-optimal solution, but also upon near-optimal values of parameters (Meyer-Nieberg and Beyer, 2007).

3.5.4 Hyper-Heuristic Control

Hyper-heuristic control is similar to adaptive control except that a hyper-heuristic is employed to perturb parameters or select new values from those that previously performed well (Burke et al., 2010b). Popular hyper-heuristics include local search (LS), simulated annealing (SA) and tabu search (TS) to perturb parameters and simple random (SR), greedy (GR), peckish (PK) and GA selection techniques to select parameter values (Burke et al., 2010b; Chakhlevitch and Cowling, 2008). These hyper-heuristics operate as described in §3.2.1 for heuristic selection, albeit by considering process parameters as variables instead of LLHs. Reinforcement learning is popularly employed to reward beneficial changes to the optimisation process or penalise detrimental changes (Burke et al., 2010b). Process parameters may be controlled at any level of scope by the hyper-heuristic.

3.6 Applications of Hyper-Heuristic Optimisation

Heuristic selection has been subject to the greatest amount of research within the field of hyper-heuristic optimisation and has historically been employed to solve problems such as timetabling, scheduling, bin-packing and vehicle routing; as well as for comparative studies of different hyper-heuristics, move acceptance rules and HHAs in solving mathematical benchmark functions (Burke et al., 2010b). Bilgin et al. (2007) conducted a comparative study of hyper-heuristics for heuristic selection. The hyper-heuristics evaluated included permutation (PE), permutation descent (PD), random descent (RD), SR, GR and TS as well as the choice function as a selection method wherein the best LLH measured by the function was selected. All moves (AM), only improving (OI), improving and equal (IE) and Monte Carlo (MC)

were amongst the rules of move acceptance considered. Different hyper-heuristics performed well on different benchmark functions, most notably the choice function, whilst IE outperformed the other move acceptance rules. These approaches to heuristic selection were then evaluated for an exam timetabling problem, where the choice function combined with MC move acceptance performed better than all other set-ups. Another study was performed by Özcan et al. (2008) for the same hyper-heuristics and similar benchmark functions, finding that IE and exponential Monte Carlo with counter (EMCQ) move acceptance performed well. SR also performed well, as did optimisation using the choice function to measure process performance. A set of four frameworks were also presented that employed different combinations of population-based and LS techniques to the problem. The study indicated that the best framework included perturbation analysis after each generation.

Ross et al. (2002) performed heuristic selection of problem-specific LLHs for bin-packing problems using a learning classifier system (XCS) mechanism. An XCS measures process performance against an expected payoff such that the optimisation process learns a set of rules associated with different problem-specific states (Wilson, 1995). The bin-packing problem was tackled by considering different problem state instances and searching for a rule to define the most appropriate LLH for each instance. The XCS subsequently evolved these rules based on the performance of each LLH application to a problem state. As a result, chromosomes of problem states and corresponding LLHs were generated for crossover and mutation in order to find the optimal combination of problem instances and LLHs. These problem states and LLHs were represented by identification numbers within chromosomes. The XCS learning mechanism required numerous iterations of the problem for satisfactory learning in order to evolve these rules and find a solution. This problem was similarly investigated by Ross et al. (2003) using a GA hyper-heuristic to evolve a sequence in which to apply the different LLHs. The HHA aimed to learn which LLHs were best to apply to the problem given its current state. Results of these studies indicated that the HHA generated substantially better solutions than any of the LLHs when applied in isolation for traditional optimisation. Similarly promising results were obtained during the investigations of Schulenburg et al. (2002), Marín-Blázquez and Schulenburg (2007) and Terashima-Marín et al. (2010) that extended the XCS mechanism for application to the bin-packing problem.

Ross et al. (2004) and Ross and Marín-Blázquez (2005) applied the GA hyper-heuristic of Ross et al. (2003) to the timetabling problem, whilst Ochoa et al. (2009) also applied a GA hyper-heuristic to this problem. The latter research included an analysis of the hyper-heuristic solution space to study the nature of the domain. The study indicated a globally convex solution space, albeit with a large number of local optima and plateaux. Moreover, bias towards the LLHs employed during initial optimisation generations indicated a critical influence of these techniques on solution quality. The performance of EA hyper-heuristics at tackling the examination timetabling problem was investigated by Pillay (2009) following an earlier study by Pillay and Banzhaf (2007). The earlier study employed the EA to evolve an LLH sequence from five problem-specific heuristics. The later study investigated different representations of lists of LLHs, i.e. LLH chromosomes. These representations differed in the chromosome structure, namely using static, deterministic and adaptive chromosome lengths to represent the LLH lists. The static length was found to perform worst whilst the performance of the remaining structures was problem-dependent.

A GA hyper-heuristic was proposed by Garrido and Riff (2007) to solve packing problems through the evolution of the application sequence of four LLHs. A variable length sequence was considered, with the results of the study using the HHA outperforming those of problem-specific techniques when applied to the packing problem and a set of benchmark functions. Crossover of LLHs chromosomes during heuristic selection was investigated by Drake et al. (2011) for a knapsack problem using the best hyper-heuristic framework presented by Özcan et al. (2008). One-point, two-point and uniform crossover of the LLHs chromosomes was performed by selecting an LLH by tournament selection (TO) from a list populated either randomly or by the best LLHs. This selection was performed for both the hyper-heuristic and

problem domain, i.e. for selection of hyper-heuristics as well as LLHs. Results indicated that move acceptance had a greater influence on hyper-heuristic performance than the selection mechanism.

An HHA was developed by Burke et al. (2007) to solve the timetabling problem using a TS hyper-heuristic to improve the order of application of five problem-specific LLHs through heuristic selection. Every LLH sequence generated by the hyper-heuristic was evaluated through the construction and analysis of a timetable, leading to online learning of process performance in an attempt to improve this performance. This work was extended by Qu and Burke (2009) to include a comparison of the application of different hyper-heuristics to the problem including LS and variable neighbourhood search. The investigations indicated that these techniques were more effective for exploring the hyper-heuristic solution space than the original TS hyper-heuristic. The solution space was therefore hypothesised to be smooth with large plateaux such that solutions of similar quality would be generated from similar LLH sequences. Combination of this HHA with problem domain perturbation analysis was found to further improve the process to a similar quality to state-of-the-art approaches.

Vázquez-Rodríguez et al. (2007) optimised the application order of dispatching rules for production scheduling using a GA hyper-heuristic. The study showed that the HHA was superior to the employment of a single dispatching rule for the entire scheduling process due to the ability of the former to learn effective combinations of rules. The generality of the HHA was proven through experimentation with various objective functions. A multi-objective job shop scheduling problem was subsequently addressed by Vázquez-Rodríguez and Petrovic (2010) using a development of this HHA which outperformed the original HHA and the traditional application of a GA to the problem. Ochoa et al. (2009) analysed the hyper-heuristic solution space for dispatching scheduling problems whilst Ochoa et al. (2009) performed similar analysis for timetabling problems. The findings indicated that the hyper-heuristics investigated were equally suitable for application to timetabling or scheduling problems. A GA hyper-heuristic was employed by Hart and Ross (1998) and Hart et al. (1998) to evolve a sequence of application of LLHs to a scheduling problem. This problem was also the subject of investigations by Crowston et al. (1963), Dorndorf and Pesch (1995), Fisher and Thompson (1963) and Storer et al. (1995) prior to the definition of a hyper-heuristic. The principles underpinning hyper-heuristic optimisation can be traced back to the hypotheses of Crowston et al. (1963) and Fisher and Thompson (1963) for combining job shop production scheduling rules. These investigations employed a stochastic LS to schedule rule sequences, finding that an unbiased random combination of rules determined in this manner was superior to the independent use of the individual rules. Storer et al. (1995) stated the problem of designing a suitable combination of problem-specific optimisation techniques to satisfactorily solve an optimisation problem and proposed the perturbation of LLH combinations by an LS technique. These hypotheses led to the development of heuristic selection and generation methods (Burke et al., 2010b).

Cowling et al. (2000) tackled the scheduling problem using a hyper-heuristic to perform heuristic selection of ten problem-specific LLHs. The choice function was found to yield better solutions with roulette wheel (RW) selection than other approaches, including GR, SR, RD and PE hyper-heuristics. Cowling et al. (2001) further investigated this problem with the added capability of parameter control. Similar results were found to the previous study, notably that AM move acceptance outperformed OI. This HHA was further applied by Cowling et al. (2002b) to the nurse rostering problem and by Cowling et al. (2002c) to a scheduling problem. The latter included a comparison against a new choice function consisting of objective function-dependent components; however, the original choice function was found to be superior. Timetabling of a training schedule was addressed by Cowling et al. (2002a) using a GA hyper-heuristic to evolve the order of application of the problem-specific LLHs. These LLHs were concerned with adding or removing tasks from the schedule, such that the chromosomes of the hyper-heuristic contained integers to identity each LLH. Two measures of hyper-heuristic objective value were employed: the problem objective value and objective value over central processing unit (CPU) time. These functions

were coupled with adaptive crossover and mutation probabilities, leading to four different hyper-heuristic objective functions. The adaptive parameter control prevented premature convergence but better solutions were obtained with static parameter values tuned to the problem. This work was extended by Han et al. (2002) to enable adaptation of the chromosome length and by Han and Kendall (2003) to include a tabu tenure to prevent the selection of poorly-performing LLHs for a number of iterations. This tenure value assigned a negative score to an LLH if it did not improve the hyper-heuristic objective function. The tenure value denoted the number of subsequent heuristic selection events for which the LLH could not be selected to prevent the technique from hindering the optimisation process. The adaptive chromosome length penalised long chromosomes due to the extended computation time required to solve the problem with a greater number of LLHs, thus promoting a rapid optimisation process employing the minimum number of LLHs. These adaptive approaches were found to be superior to those presented by Cowling et al. (2002a) and Cowling et al. (2002c). Drake et al. (2012) applied a modified choice function to a variety of problems including bin-packing and personnel scheduling, including a comparison against eight different hyper-heuristics. The results of the investigation found improved performance over the original choice function of Cowling et al. (2000); nevertheless, better results still were obtained using a selection of hyper-heuristics without the choice function. Kendall et al. (2002) tackled the personnel scheduling problem to compare the use of an SR hyper-heuristic against the choice function selecting the best-performing LLH from the heuristic set. AM and OI move acceptance were used with both hyper-heuristics. The investigation showed that the choice function outperformed SR and was also superior to a modified SR hyper-heuristic that incorporated the choice function to rank LLHs in order to calculate the probabilities of selecting each LLH. The choice function was found to be powerful in tailoring the probabilities of selecting a suitable well-performing LLH.

MC-based move acceptance criteria were used during heuristic selection by Ayob and Kendall (2003) to optimise the component placement sequence during the manufacture of printed circuit boards. The optimisation problem was to minimise assembly time through the minimisation of the distance travelled by the robotic device employed to place components. Six problem-specific LLHs were developed to swap the pickup sequence, placement sequence, pickup nozzle, placement nozzle, circuit board point and tour order of the robot arm. The new move acceptance rules were compared against AM and OI with and without the use of the choice function. The choice function performed poorly in combination with the SR hyper-heuristic due to this unrepresentative performance of LLHs in pairs when using the purely random hyper-heuristic. Conversely, linear Monte Carlo (LMC), exponential Monte Carlo (EMC) and EMCQ performed well, the latter of which was found to provide speed and robustness to the heuristic selection procedure. Heuristic selection was similarly performed by Cobos et al. (2011) to choose the best LLHs for the clustering of web documents. SR and RW heuristic selection was performed for a heuristic set including a GA and particle swarm optimisation (PSO). The HHA produced promising results, however no comparison was given between the different methods of heuristic selection. A simulated annealing (SA)-based hyper-heuristic was employed by Downsland et al. (2007) for the optimisation of shipping container sizes by incorporating an annealing schedule into the TS hyper-heuristic developed by Burke et al. (2003b). Experiments were performed using different numbers of LLHs within the heuristic set with no significant difference being found in the convergence time. Moreover, the solutions obtained were of lower quality than data provided by a retail company, although good solutions were generated at a reasonable cost in computation time.

An SA hyper-heuristic was employed by Bai and Kendall (2005) to optimise the assignment of shelf space within a retail store. The objective was to maximise the overall profit by ensuring stock was appropriately distributed over the available shelf space, i.e. a multi-knapsack problem. SA was employed for heuristic selection and subsequent move acceptance. The LLHs within the heuristic set added, deleted, swapped or interchanged items from the shelves. The SA hyper-heuristic was compared against GR and

SR hyper-heuristics with AM and OI move acceptance and was found to generate solutions of higher quality than using other hyper-heuristics or the traditional application of SA. This hyper-heuristic was subsequently included within a framework in Bai et al. (2007) and applied with similar success to nurse rostering, university course timetabling and bin-packing problems. The LLHs within the heuristic set typically performed swap operations between two candidate nurses based on their availability within the roster. Burke et al. (2008) analysed the results of Bai et al. (2007) and Özcan et al. (2008) to find that SA move acceptance outperformed EMCQ for exam scheduling and, subsequently, that SR selection without any learning yielded even better results. The nurse rostering problem was also tackled by Burke and Soubeiga (2003) using a TS hyper-heuristic and Bilgin et al. (2010) using SR heuristic selection and SA move acceptance. In the latter, a GR shuffle hyper-heuristic was also employed to further improve solution quality by swapping sections of different solutions.

Burke et al. (2010a) presented an HHA to perform heuristic selection of LLHs for a selection of problems: one-dimensional bin-packing, job timetabling and personnel scheduling. Crossover, mutational and LS LLHs were among those included within the heuristic set and selected using either SR or TS with reinforcement learning. This HHA was compared against an iterated LS method wherein all LLHs were applied to each solution in a predetermined order. The HHA performed worse than iterated LS, indicating a need to improve the HHA for these problems. An investigation was performed by Özcan and Kheiri (2012) into applying a multi-stage HHA to the same problems as Burke et al. (2010a). This HHA firstly applied a GR hyper-heuristic to evaluate all LLHs and generate a list of available LLHs for application to the problem. This stage can be viewed as the opposite to TS by creating a list of permitted moves rather than a list of prohibited moves. The second stage then employed RD to apply an LLH from the list until no further improvement was made. Experimental results indicated that this HHA was more generally applicable than the methods of Burke et al. (2010a) and provided improved solution quality.

Grobler et al. (2010) performed heuristic selection from a set of perturbative LLHs including variations of a GA, particle swarm optimisation (PSO) and differential evolution (DE). Real number representations of design variables were employed rather than binary representations to facilitate the use of these LLHs, with heuristic selection performed every 25 generations using an SR, RW or TS hyper-heuristic with AM or SA move acceptance rules. LLH parameter values were controlled deterministically such that each parameter varied linearly between preset initial and final values. The HHA was evaluated over a series of benchmark functions to find that RW and TS heuristic selection performed best whilst SA move acceptance outperformed AM, although it was concluded that AM could provide faster convergence for simpler problems. A TS hyper-heuristic was employed for heuristic selection by Domingos and Platt (2013) during the optimisation of the design of a nuclear reactor core. The LLH set included differential evolution (DE), PSO, SA and hill climbing (HC), with the hyper-heuristic obtaining comparable results to the traditional application of GAs, DE and PSO in minimising the average power peak factor in reduced computation time, in fact outperforming the latter two techniques.

An HC hyper-heuristic was employed by Garrido and Castro (2009) to solve the vehicle routing problem. Constructive and perturbative LLHs were employed in pairs to solve the problem. An investigation of the HHA performance against well-established methods generated good quality results for a series of benchmark problems. Garrido and Riff (2010) extended this work through the addition of noisy LLHs to the heuristic set. A dynamic vehicle routing problem was solved during this study, with high-quality results indicating that the HHA was apt at adapting to the dynamic nature of the problem. Variable and value ordering of the constraint satisfaction problem was addressed by Bittle and Fox (2009), requiring the determination of all possible permutations of design variables that satisfy all design constraints. The problem was solved by firstly choosing a variable for instantiation prior to the selection of a value for the variable from a set of possible values. Constraints were then checked to ensure solution feasibility. Hyper-heuristics are employed to solve map colouring and job shop scheduling problems by choosing

LLHs that select variables based on the variable characteristics, e.g. number of linked constraints. Cognitive architecture underpinned the learning mechanism such that the order in which variables and their values were selected was improved. This problem was similarly addressed by Ortiz-Bayliss et al. (2011), leading to the generation of hyper-heuristics of comparable quality to the LLHs traditionally employed. Terashima-Marín et al. (2008) similarly considered the use of hyper-heuristics to solve the variable ordering problem. A training period was conducted for learning of the problem prior to the solving the optimisation problem. Promising results were obtained against multiple benchmark functions.

A memetic approach to the nurse rostering problem was investigated by Burke et al. (2001), wherein TO-based GA optimisation of a population was performed followed by perturbation analysis using TS until no improvement was made in the solution over two consecutive iterations. The better-performing individuals subsequently possessed a higher probability of selection by the GA. Greatly improved solution quality was observed using this HHA over a traditional TS algorithm, however this was at the expense of an increase in computation time due to the steepest descent (SD)-based stepping employed by TS. A memetic algorithm (MA) was similarly presented by Özcan and Başaran (2009) for application to the knapsack problem. Random and gradient-based LS methods were applied with Lamarckian evolution to improve the solutions generated by a GA with success, although without any indication of possible computation time effects of employing the MA. Krasnogor and Smith (2000) applied an MA for perturbation analysis during the optimisation of the travelling salesman problem. The study found that the SA-based MA coupled with a GA outperformed traditional use of the GA. Ong et al. (2006) employed static, adaptive and self-adaptive MAs to numerical benchmark problems at both the problem and hyper-heuristic level, where the latter performed perturbation analysis of heuristic selection using SR, RW and TS hyper-heuristics. The adaptive MA performed best during this study, whilst perturbation analysis at a hyper-heuristic level was able to appropriately control the frequency and duration of perturbation analysis through the use of a suitably-designed hyper-heuristic objective function as the MoI. Noman and Iba (2008) performed perturbation analysis with a similarly adaptive MA coupled with DE to numerical benchmark functions, finding improved solution quality and convergence with such analysis over algorithms in the literature.

Julstrom (1999) performed a comparative study of Darwinian, Lamarckian and Baldwinian evolution during the perturbation analysis of a population of solutions generated by a GA. Perturbation analysis using Lamarckian evolution performed considerably better than the other approaches, although Darwinian evolution was also effective at solving the problem. The use of Baldwinian evolution was found to deteriorate the performance of the GA, resulting in the worst solutions. Lamarckian evolution was also found to generate the best solutions with an MA by Özcan et al. (2008). Conversely, Kheng et al. (2010) found that Baldwinian evolution outperformed Lamarckian evolution when used to solve noisy mathematical benchmark functions, although the study did indicate that Lamarckian evolution was better at solving such problems without the presence of noise. A study by Whitley et al. (1994) obtained similar results; however Baldwinian evolution required a longer search duration in order to converge on a better solution than using Lamarckian evolution.

Parameter control was investigated by Brest et al. (2006) during DE optimisation of numerical benchmark functions. Self-adaptive control was performed of the technique operators, leading to comparable or better solutions than with a static tuned DE algorithm. A further investigation by Brest et al. (2007) compared the performance of a DE algorithm with adaptive and self-adaptive parameter control. The results of this study indicated better results using self-adaptive control through the coevolution of a solution and suitable algorithm parameter values. Deterministic, adaptive and self-adaptive control of a GA were investigated by Fernandez-Prieto et al. (2012) for optimising computer network traffic patterns. The dynamic optimisation processes generated better results than a static process with the exception of individual-level adaptive control which performed poorly. This indicated the importance of appropriate design of parameter control rules. Srinivas and Patnaik (1994) presented a GA with individual-level

adaptive crossover and mutation probabilities to prevent premature convergence on local optima and improve search diversity. The use of such an adaptive optimisation process enabled fitter individuals to be maintained within the population whilst poorer solutions were rejected in favour of exploration. An adaptive penalty function was presented by Bean and Hadj-Alouane (1992) wherein the penalty parameter was adapted to encourage a feasible solution whilst discouraging search far from the constraint boundaries. Nanakorn and Messomklin (2001) similarly introduced an adaptive penalty function to a structural design optimisation problem, finding improved robustness using this function and a lack of dependency of solution quality on predetermined values of function parameters. Both of these adaptive penalty functions were applied with a scope of population-level adaptation.

Hyper-heuristic optimisation has seen limited application within the domain of aerospace design. Fukunaga et al. (1997) investigated the automation of the optimisation process in spacecraft design. This research was conducted prior to the definition of a hyper-heuristic, therefore the method was not described as employing hyper-heuristic optimisation. Nevertheless, optimisation techniques were selected from a set of LLHs including a GA and SA to solve particular instances of the problem based on past performance. A multi-objective MA was employed by Song (2009) to minimise the drag of an aerofoil at four different flight conditions. The LS technique optimised the solutions on the Pareto front formed by the multi-objective function following population optimisation by a GA. Although a comparison was not performed with existing methods, the approach was found to be robust in generating solutions of high quality. Hyper-heuristic optimisation was also performed for aerospace design by Rafique et al. (2011), where population distribution was conducted between three LLHs during the multidisciplinary optimisation (MDO) of a satellite launch vehicle for minimum gross launch mass. The disciplines addressed during optimisation included the vehicle configuration, propulsion unit, aerodynamics and mission. Population distribution was performed randomly using a non-learning function between a GA, PSO and SA LLHs. Parameter control was also performed using an SR hyper-heuristic, therefore no learning was included within the HHA. The HHA was applied within an outer loop whilst optimisation of the solutions was performed within an inner loop. The inner loop was executed over 120 generations for each outer loop iteration, itself limited to 50 iterations. Therefore, population distribution and parameter control was performed for each outer loop generation, i.e. at a frequency of 120 optimisation generations. The process was limited to 100,000 function evaluations. The HHA was found to outperform the individual LLHs when applied to a set of benchmark functions. Moreover, the satellite launch vehicle optimisation problem was solved with greater success using the HHA than by traditional optimisation using each LLH independently.

3.7 Summary

Hyper-heuristic optimisation is an emerging area of research wherein the optimisation process is modified during execution to promote further improvement in its performance, most commonly measured by solution quality. As a result, optimisation is performed across two domains: the hyper-heuristic and problem domain. Hyper-heuristics select LLHs for application in the problem domain and control the values of optimisation process parameters. Furthermore, multiple LLHs may be employed through population distribution and local solution space learning may be encouraged through perturbation analysis. Consequently, hyper-heuristic optimisation provides opportunities to improve the optimisation process performance and quality of solutions generated over that possible by traditional optimisation. However, this can result in a computational cost due to additional analysis of solutions or to allow opportunities for changes in the process to take effect. Although hyper-heuristic optimisation has seen considerable research in its relatively short life, little research has been performed within the domain of aerospace design. Most notably, hyper-heuristic optimisation has not yet been applied within the field of aircraft structural design optimisation. This presents the opportunity to apply an HHA within this domain in an attempt to improve the process followed during the optimisation of an airframe design.

Chapter 4

Requirements and Opportunities

Reviews conducted of existing approaches to aircraft design optimisation and hyper-heuristic optimisation have been presented in Chapters 2 and 3. These reviews identified a number of traditional requirements of a framework in order to generate, analyse and optimise a conceptual aircraft design and employ hyper-heuristics to improve a problem solution. This chapter expands on the requirements in §4.1 to define the bounds within which the framework proposed by this research must be developed. These literature reviews have also led to the identification of a number of research opportunities for improvement of the traditional aircraft design optimisation solution process and the traditional use of a hyper-heuristic approach (HHA). These opportunities are discussed in §4.2 in order to present the ways in which the framework may be designed to provide an improvement over existing approaches to the aircraft design optimisation problem. This chapter also includes a section, in §4.3, to define key terminology used in describing the framework in subsequent chapters. The chapter is summarised in §4.4.

4.1 Traditional Requirements

The reviews of aircraft design optimisation and hyper-heuristic optimisation identified a number of traditional requirements for the optimisation of an aircraft design and employment of an HHA. The framework proposed by this research must incorporate these requirements in order to facilitate the generation and optimisation of an airframe design using an HHA and thus satisfy the research aim in §1.3.

4.1.1 Aircraft Design Optimisation

The review of aircraft design optimisation in Chapter 2 discovered a common procedure that is followed in order to solve the presented optimisation problem. This procedure, described in §2.2, is inherently iterative given the traditional evolution of an initial baseline design into a near-optimal solution. In order to follow this procedure, the framework requires the following stages within the solution process:

- initialisation of the optimisation problem and process;
- definition of an aircraft mission;
- estimation of aircraft mass;
- generation of the external profile;
- iterative generation, analysis and optimisation of the airframe;
- termination of the process.

The solution process begins with its initialisation, including the input of design and process requirements. It is essential that these data are provided otherwise the optimisation problem will not be defined nor process set up to enable a solution to be found. The aircraft mission is then defined, using data input during initialisation, including the selection of load cases to be applied to the aircraft during analysis.

Most approaches discussed in §2.1 and §2.5 applied isolated load cases to the aircraft, however the inclusion of a mission is preferred in order to simulate realistic loading conditions likely to be encountered by the aircraft during operation. Moreover, a mission is necessary in order to perform the next tasks of the process. Empirical mass estimation is performed during conceptual design optimisation to establish the necessary size of the aircraft for flight based on its mission, i.e. lifting surfaces geometry required to generate sufficient lift to sustain flight given the estimated vehicle mass. Empirical formulae can be used as a result of the similarities in previous and current aircraft designs. Further, mass has to be estimated rather than calculated precisely due to the lack of information about the design at this stage of the process. Having established the geometric requirements for flight, the aircraft external profile is determined using either data input during initialisation, empirical relationships or both. It is necessary to perform this task such that the geometric boundary within which the airframe is to exist is defined. During conceptual design, use of such empirical formulae for aircraft profile generation is appropriate a given lack of design knowledge and the reduced precision typically used during this design process phase.

Structural optimisation is performed within the boundary of the external profile through the iterative generation, analysis and optimisation of airframe design solutions. This is conducted using either a single or population of design variants depending on the optimisation technique employed. As stated in §2.3, no one specific optimisation technique is employed consistently throughout the existing approaches, however evolutionary algorithms (EAs) are the most popular during recent studies. This indicates a lack of consensus as to the best techniques to be applied to the problem. Dominant optimisation design variables include the quantity, position, size and material of structural members commonly employed, whilst the minimum factor of safety (FoS) and wingtip deflection under load are typical design constraints. Structural analysis is performed of airframe designs under the selected load cases and at a defined model fidelity level, leading to the employment of a penalty function to calculate a penalisation value due to design infeasibility with respect to the design constraints. The value of the design objective function, typically minimum structural mass, is subsequently calculated and penalised where appropriate by the penalty function. The exterior penalty function, as described in §2.4, is the most popular penalty function as it permits the consideration with decreasing probability of infeasibilities. Use of such a function is necessary to promote feasibility in the solution, otherwise the resulting design may be of little value for manufacture and operation. The optimisation technique is applied to generate a new population of designs for analysis and subsequent optimisation. The optimisation process continues until a termination criterion is satisfied, at which point a design solution is output. The set-up of structural analysis, commonly performed using finite element analysis (FEA), determines the precision and computational effort of assessing the feasibility of design solutions. Similarly, the settings of optimisation process dictate process behaviour and thus influence the quality of solution generated.

Variation from this traditional solution process is not appropriate for the framework in order to investigate the application of hyper-heuristics to the problem. A research objective stated in §1.3 was to evaluate the framework developed by this research against existing approaches to aircraft design optimisation in order to assess the thesis. Consequently, the principal variation between existing approaches and the framework is required to be the inclusion of an HHA to improve the optimisation process, and thus solution quality. Therefore, it is appropriate that the framework follows the traditional solution process of aircraft design optimisation, except in the inclusion of an HHA.

4.1.2 Hyper-Heuristic Optimisation

The review of hyper-heuristic optimisation in Chapter 3 introduced an HHA as an approach employed to improve the value of a hyper-heuristic objective function, which in turn encourages improvement in the performance of the optimisation process. The requirements of an HHA are:

- the aspects of the optimisation process to be controlled;

- a hyper-heuristic objective function;
- a learning mechanism;
- the hyper-heuristic optimisation set-up.

An HHA can control the optimisation process through a number of aspects, the selection of which is required in order to apply the HHA. The most commonly-applied aspects were described in §3.2, §3.3, §3.4 and §3.5. Within these HHA aspects, a hyper-heuristic objective function is required in order to measure the performance of the optimisation process. This function is similar to the objective function of the optimisation problem but focuses on improving process performance rather than the quality of solutions generated to the optimisation problem. Notwithstanding this, solution quality may be used as a component of the hyper-heuristic objective function to measure process performance if desired. This objective function should be carefully designed to ensure the most appropriate process characteristics are considered and weighted appropriately to encourage the desired behaviour at suitable points during the process. Measures of performance used within existing studies include improvements in the problem objective value and the computation time taken. A learning mechanism is then required to monitor such process performance and instruct the HHA of actions to perform in an attempt to improve the hyper-heuristic objective value. As discussed in §3.1, independence must be maintained between the problem domain and hyper-heuristic domain by ensuring that any data passed across the domain barrier are problem independent. The hyper-heuristic objective function and learning mechanism must be implemented in such a way that domain independence is maintained. Hence, the hyper-heuristic objective function is traditionally based on the dimensionless fitness of solutions, whilst reinforcement learning is commonly used to assign a score to the performance of the process that does not use problem-specific data. The set-up of the HHA includes the selection of hyper-heuristics for application within the hyper-heuristic domain. Similarly, a low-level heuristic (LLH) set requires populating when employing heuristic selection or population distribution to define which optimisation techniques may be employed within the problem domain. Many different hyper-heuristics and LLHs have been employed for hyper-heuristic optimisation, as discussed in §3.6, with no consensus on the best techniques for specific problems, and few applications of such optimisation to aerospace design.

The framework is required to include an HHA in order to apply hyper-heuristic optimisation to the problem of conceptual aircraft structural design and hence investigate the thesis of this research. This HHA must be designed within the traditional bounds in order to show the effect of applying hyper-heuristics to the problem and thus satisfy the research aim. The inclusion of various HHA aspects within the framework may enable a detailed comparison to be performed of conceptual aircraft structural design using traditional optimisation and different methods of hyper-heuristic optimisation.

4.2 Research Opportunities

To satisfy the aim of this research presented in §1.3, the framework must incorporate the traditional requirements of airframe design optimisation as well as those of hyper-heuristic optimisation identified in §4.1. As hyper-heuristic optimisation has not been performed within the field of aircraft structural design, this presents an opportunity to investigate the effects of an HHA on such problems. Further opportunities have been identified during the reviews in Chapters 2 and 3 to improve the aircraft design optimisation process and the traditional implementation of an HHA. The identified research opportunities are:

- apply hyper-heuristics to aircraft structural optimisation;
- develop a novel HHA for the aircraft design optimisation problem;
- include multiple hyper-heuristic aspects within the HHA;
- create a versatile framework for a variety of aircraft structural optimisation problems.

The principal research opportunity is to apply hyper-heuristic optimisation to the problem of conceptual aircraft structural design optimisation within the framework. The review of existing hyper-heuristic applications identified three applications of an HHA in the domain of aerospace engineering:

- Fukunaga et al. (1997): spacecraft design optimisation with heuristic selection;
- Song (2009): aerofoil profile optimisation with perturbation analysis;
- Rafique et al. (2011): satellite launch vehicle optimisation with population distribution and parameter control.

None of these problems considered optimisation of the vehicle structure, presenting the opportunity to investigate the application of an HHA to aircraft structural design optimisation. The application of hyper-heuristics to this problem can be beneficial by improving the quality of solutions generated as well as the performance of the optimisation process, e.g. time taken to find a high-quality solution. Hyper-heuristic optimisation is well-suited to aircraft design optimisation due to the complexity of the problem. More specifically, an arbitrary optimisation technique can experience difficulty in reliably locating a near-optimal solution to a problem when there are a large number of design variables or when the solution space is unpredictable. Furthermore, the tuning of such techniques to improve its performance for a particular problem can be prohibitively expensive and may only be appropriate to one instance of the problem. In contrast, hyper-heuristics enable optimisation techniques to solve a problem through more general application without requiring extensive tuning for the problem instance. The lack of consensus regarding a dominant optimisation technique and set-up that was discovered during the aircraft design optimisation review in Chapter 2 implies that the use of hyper-heuristics to control the selection and set up of the techniques applied to the problem would be desirable.

Given the lack of application of hyper-heuristic optimisation to the aircraft structural design problem, an opportunity exists to develop a novel HHA to provide benefits specifically to the process of solving this problem. For example, existing uses of heuristic selection have often included problem-specific LLHs whereas more general optimisation techniques are employed for aerospace design optimisation. Therefore, the HHA can be designed to perform heuristic selection of general LLHs including both population-based and single-solution techniques. The optimisation of an aircraft design is typically performed through the iterative evolution of a baseline design. This requires the generation and subsequent optimisation of many aircraft designs due to the large number of possible solutions resulting from variations in the design variables. As a result, the problem is more suited to perturbative hyper-heuristics than constructive heuristics as the former evolves a baseline solution whereas the latter constructs a solution from an empty initial solution given the problem state and a set of appropriate rules. Moreover, the optimisation techniques historically employed for aerospace design optimisation are, by this classification, perturbative. The use of heuristic selection is further supported by variety of different optimisation techniques used for aircraft design optimisation without a clear indication of a dominant technique. Furthermore, by including population distribution in the HHA it is possible to simultaneously employ multiple LLHs to evolve a population of solutions. This can provide greater opportunities for solution space exploration by not limiting the search to the capabilities of a single technique in current use. This search can be further enhanced through the inclusion of perturbation analysis to provide opportunities to learn the nature of the solution space which is often complex and unknown before the search has begun. Additionally, by employing a dynamic optimisation process through parameter control it is possible for the process to be modified online to improve the optimisation search process as well as solution quality. For example, a dynamic process can vary the step size of local search (LS) technique to avoid premature convergence or the crossover and mutation rates of a genetic algorithm (GA) to encourage population convergence on a good solution. Further, parameter control can be applied to other aspects of the optimisation process such as penalty function severity to promote the discovery of a feasible airframe design solution. Finally,

the hyper-heuristic parameter control of variable-fidelity modelling during structural analysis can be investigated in an attempt to encourage appropriate analysis precision and computational speed during the optimisation process.

The reviews of different HHAs presented in §3.6 indicated that a single aspect of hyper-heuristic optimisation is traditionally applied to each problem, i.e. most applications of hyper-heuristics involved performing only heuristic selection for a problem without population distribution, perturbation analysis or parameter control. A selection of studies did include a second aspect of hyper-heuristic optimisation, i.e. either heuristic selection coupled with perturbation analysis or parameter control, but none were identified that incorporated the four hyper-heuristic aspects of heuristic selection, population distribution, perturbation analysis and parameter control. Consequently, a research opportunity exists to investigate the concurrent application to a problem of these aspects of hyper-heuristic optimisation within a single HHA. This can provide further improvement in solution quality and process performance due to the similar aims of the HHA aspects, e.g. heuristic selection in combination with population distribution to provide performance-based selection of multiple LLHs.

An additional research opportunity is for the framework to be sufficiently flexible to consider a variety of aircraft classes and designs as well as numerous loading conditions of varying nature. It was identified in §2.5 that the majority of existing approaches considered a single aircraft class or design, thus limiting the potential use of the corresponding frameworks to solely that aircraft class or design. Similarly, many studies applied a single isolated load case to the aircraft during analysis. This approach leads to an unrealistic assessment of the structure by neglecting to consider the effects of different load cases that may drive the strength of the airframe in particular regions. For example, the maximum positive flight manoeuvre was identified as being most popularly applied in existing approaches, however a landing load case may be more severe at the local attachment points of the undercarriage to the airframe structure. By developing a framework that possesses sufficient versatility to consider different loading conditions and aircraft classes, opportunities are presented to perform studies of the effects of different load cases on an aircraft design as well as the effects of applying an HHA to the optimisation of various aircraft designs. Furthermore, by ensuring the entire aircraft design can be modelled and analysed rather than solely a single section, the framework will provide greater value to the conceptual design process through the output of a complete aircraft configuration.

4.3 Terminology

Various terminology is defined in this section prior to description of the framework in Chapter 5 for clarification of misleading or similar terms used within the different fields pertinent to this research, i.e. aircraft design, structural analysis and hyper-heuristic optimisation. This is principally required to maintain consistency during the description of the framework in light of variations in the conventional terms used to describe different optimisation techniques. Furthermore, key equations are introduced here for reference during the description of the framework. This is to promote the understanding of the objectives of using the framework for hyper-heuristic aircraft design optimisation.

The framework is described as being employed to solve a single optimisation problem for a near-optimal airframe design. References to the ‘engineer’ concern the individual or team implementing the framework for this purpose. Optimisation is described for a population set of individual solutions, i.e. aircraft structural designs, over a number of generations. This terminology is used throughout the framework description for ease of comparison of different optimisation techniques. The terms ‘individual’ and ‘population’ respectively replace the more commonly used terms ‘particle’ and ‘swarm’ for particle swarm optimisation (PSO) due to their commonality when describing other population-based techniques. Similarly, the term ‘generation’ is used in place of ‘step’ or ‘iteration’ when describing LS techniques for consistency whilst ‘individual’ replaces ‘agent’ in describing differential evolution (DE).

The framework optimises the design of an airframe over n_k generations in an attempt to satisfy the following objective function for a solution of minimum structural mass

$$\min\left(\Phi(\mathrm{X}^k)\right) \text{ for } k = 1, 2, \ldots, n_k \tag{4.1}$$

The feasibility of an individual design solution is determined by comparing the results of structural analysis against two hard design constraints. The limiting values for these constraints are input during initialisation such that a feasible solution satisfies the following expression

$$g_{i,1}(\mathrm{X}^k) \geq c_1 \tag{4.2a}$$

$$\left|g_{i,2}(\mathrm{X}^k)\right| \leq |c_2| \tag{4.2b}$$

where c_1 design constraint on minimum FoS under yield
c_2 design constraint on maximum magnitude of wingtip deflection, m

An HHA within the framework aims to improve the optimisation process performance by satisfying a hyper-heuristic objective function measuring process performance

$$\max\left(\phi^k\right) \text{ for } k = 1, 2, \ldots, n_k \tag{4.3}$$

These expressions are explained further in Chapter 5 during the description of the framework, including the definitions of the components of the hyper-heuristic objective function that measure the performance of the optimisation process.

4.4 Summary

The review of existing approaches to aircraft design optimisation and hyper-heuristic optimisation identified that the framework presented by this research must incorporate a number of traditional requirements to perform its function. Additionally, a number of research opportunities have been identified for exploitation in order to improve the process by which the optimisation problem is solved and by which an HHA is employed. The principal opportunity identified is the chance to apply hyper-heuristic optimisation to aircraft structural design through the development of a framework with an embedded HHA. Additional opportunities include the possibility to develop a novel HHA for airframe optimisation, employ four hyper-heuristic aspects in the HHA and develop a versatile framework for a variety of aircraft structural design optimisation problems. This has led to the development of a framework to perform such hyper-heuristic optimisation of a conceptual aircraft design in order to obtain a solution of minimal mass under load.

Chapter 5

Framework for Hyper-Heuristic Aircraft Structural Optimisation

A framework is presented for the hyper-heuristic structural optimisation of a conceptual aircraft design. The framework defines the process by which an airframe design is optimised to minimise its structural mass in accordance with the requirements and opportunities identified in Chapter 4. This framework differs from existing approaches to aircraft design optimisation through the inclusion of a hyper-heuristic approach (HHA) to improve solution quality and the performance of the optimisation process. The HHA includes heuristic selection, population distribution, perturbation analysis and parameter control. The framework may be used for aircraft of various classes, layouts and missions through the simulation of multiple static or dynamic load cases. Furthermore, the aircraft designs generated by the framework are complete configurations, i.e. not solely a single aircraft section such as the wing, fuselage or empennage. The feasibility of designs is measured using finite element analysis (FEA) with respect to specified design constraints. This chapter provides an overview of the framework followed by its description in detail. The framework is formed of three principal stages:

1. aircraft design procedure: input of design requirements and aircraft design generation;
2. structural analysis: airframe modelling, evaluation of its response to loads and stress analysis;
3. airframe design optimisation: mass optimisation of the airframe using the HHA.

The framework stages are constructed using the modules listed in Table 5.1. Each module is comprised of a number of tasks to be performed. This results in a framework hierarchy in descending order of stages, modules and tasks. The framework is formed through the connection of modules as illustrated in Fig. 5.1, where the labelling of modules corresponds to that within Table 5.1. All tasks are performed within the framework modules without the need for external modules, e.g. for FEA or optimisation, to eliminate any reliance on such independent sources.

Table 5.1: Framework modules

Aircraft design procedure	Structural analysis	Airframe design optimisation
1.1 Initialisation	2.1 Sectional properties	3.1 Population feasibility
1.2 Mission definition	2.2 Structural mass	3.2 Population fitness
1.3 Mass estimation	2.3 Airframe model	3.3 Termination criteria
1.4 Aircraft profile generation	2.4 Finite element analysis	3.4 Hyper-heuristic approach
1.5 Aircraft loads	2.5 Stress analysis	3.5 Design optimisation
1.6 Structural layout generation		3.6 Data output

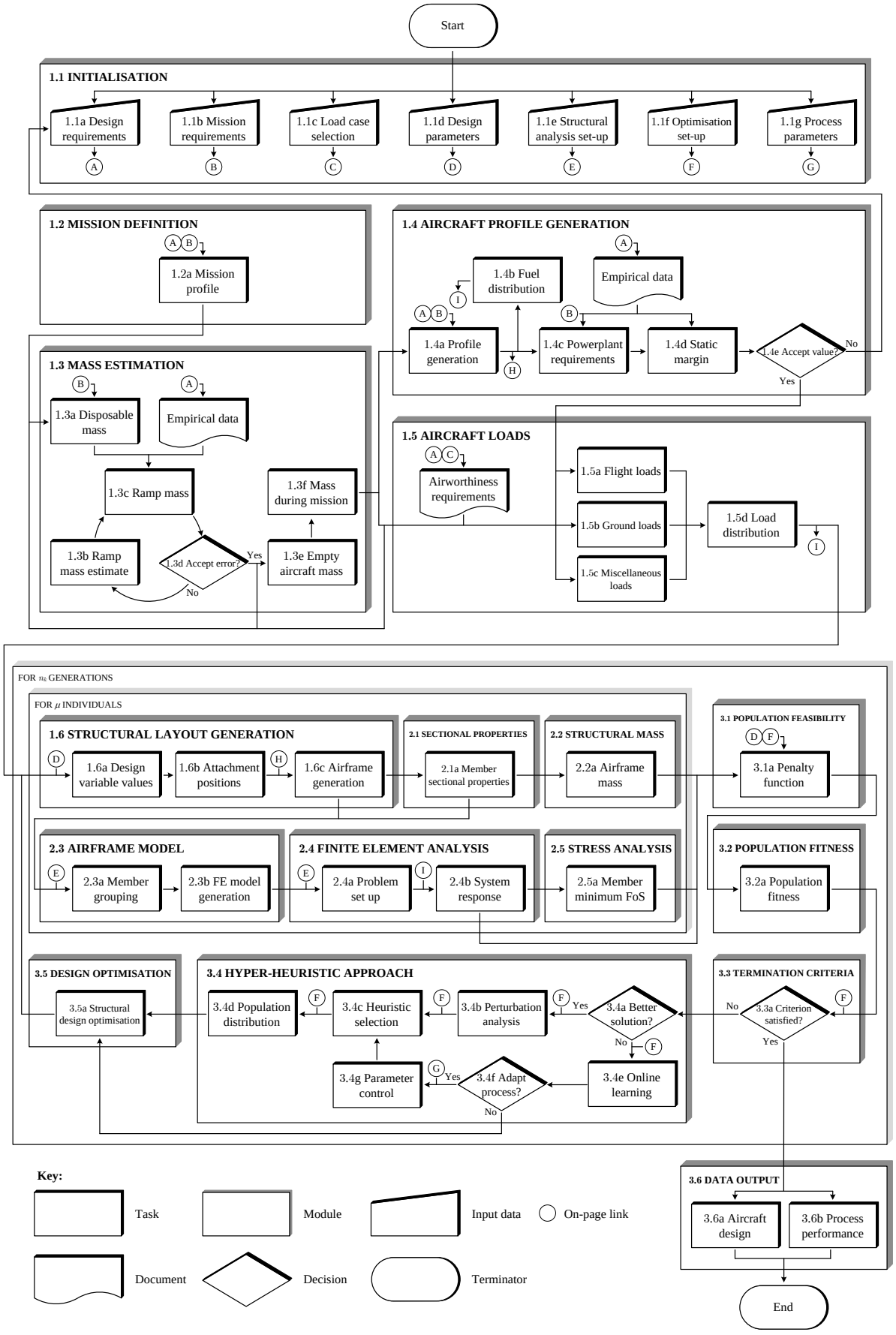

Figure 5.1: Framework for hyper-heuristic optimisation of conceptual aircraft structural designs

The key tasks performed within each module are shown in Fig. 5.1, e.g. the first task within the 'Initialisation' module is the 'Design requirements' task. The description of the framework that follows is consistent with this labelling of framework stages, modules and tasks. The identification numbers of modules and tasks are included in this description in parentheses to correspond with Table 5.1 and Fig. 5.1.

This chapter describes the methodology of the framework as follows. The aircraft design procedure stage is described in §5.1. This includes descriptions of the modules that perform the initialisation of the framework in §5.1.1, definition of an aircraft mission in §5.1.2, empirical mass estimation in §5.1.3 and generation of the aircraft external profile in §5.1.4. The calculation of load cases is discussed in §5.1.5 before the description of the generation of an airframe design based on the values of the design variables in §5.1.6. The structural analysis stage is then described in §5.2. This section details modules performing the calculation of structural member sectional properties in §5.2.1 and airframe structural mass in §5.2.2. The procedure followed to model the airframe is then described in §5.2.3 prior to the process of analysing this model by FEA in §5.2.4 and subsequent stress analysis using the results of FEA in §5.2.5. The airframe design optimisation stage is then described in §5.3. The modules within this stage are described, beginning with the calculation of solution feasibility in §5.3.1 and fitness in §5.3.2. The definitions of the termination criteria are then provided in §5.3.3 followed by a description of the HHA embedded within the framework in §5.3.4. The optimisation techniques employed to optimise the airframe are then described in §5.3.5 before discussion of the data output from the framework to record results in §5.3.6. Finally, a summary of the chapter is provided in §5.4.

5.1 Aircraft Design Procedure

The aircraft design procedure is the first stage of the framework. This encompasses the modules and tasks required to generate an aircraft design given input requirements. This involves the initialisation of the framework, definition of an aircraft mission, estimation of vehicle mass, generation of the aircraft external profile, calculation of load cases and the generation of the airframe as defined by design variables. All modules within this stage are performed once within the framework, except structural layout generation which is performed once for each individual design solution during optimisation. Additional information, supporting theory and relevant airworthiness requirements are provided in Appendix A.

5.1.1 Initialisation

The initialisation module, a process requirement identified in §4.1.1, encompasses the input of the optimisation problem and process set-up. These include the requirements of the aircraft design (task 1.1a in Fig. 5.1 denoted by '[1.1a]' herein) and mission [1.1b], selection of load cases [1.1c], input of design parameters [1.1d], set up of structural analysis [1.1e] and the optimisation process [1.1f], and input of process parameters [1.1g]. Table 5.2 lists these tasks, including references to the uses of the input data within the framework and tables listing the input parameters in more detail within Appendix A.1.

Initialisation of the design requirements includes the decision to concentrate on the structural optimisation of either an existing aircraft design variant or a novel concept. The tasks within the mass estimation and aircraft profile generation modules are reduced if an existing aircraft design variant is to be generated. The aircraft class is also selected during the input of design requirements from the following:

- civil light:
  - normal;
  - aerobatic;
  - utility;
  - commuter;
- civil large;
- military:
  - trainer;
  - interceptor;
  - ground attack;
  - bomber;
  - transport.

Table 5.2: Initialisation of design process

Task	Description	Relevant section	Listing
1.1a Design requirements	Aircraft geometry, materials Powerplants, undercarriage, ordnance Alternative selection of existing aircraft	§5.1.2, §5.1.3, §5.1.4	Table A.1
1.1b Mission requirements	Class, stall speed, payload, aerodromes Specification of mission stages	§5.1.2, §5.1.3, §5.1.4	Table A.2
1.1c Load case selection	Selection of load cases to apply	§5.1.5	Table A.3
1.1d Design parameters	Design variables and constraints ranges	§5.1.6	Table 5.3
1.1e Structural analysis	Model fidelity level Dynamic load solution method Direct integration scheme and set-up	§5.2.3, §5.2.4	Table A.4
1.1f Optimisation set-up	Static optimisation parameters Termination criteria	§5.3.4, §5.3.5	Table A.5
1.1g Process parameters	Dynamic parameters ranges	§5.3.4	Table 5.4
	Selection of LLHs and hyper-heuristics	§5.3.4, §5.3.5	Table A.6

These aircraft classes are those commonly used within airworthiness requirements and literature such as Howe (2004). Properties of the aircraft mission are input for use during mission definition. The load cases for application during structural analysis are selected and the permitted ranges of design variables and constraints input. The parameters of the structural analysis and airframe design optimisation are also input and are discussed further during the descriptions of these stages §5.2 and §5.3 respectively.

Table 5.3 lists the design parameters, i.e. design variables, constraints and objective, employed within the framework. These design parameters correspond with those commonly employed within the existing approaches reviewed in Chapter 2. The optimisation process aims to improve the value of the design objective, O1, through modification of the values of the design variables, V1 to V50, whilst satisfying the design constraints, C1 and C2. The number and geometry of structural members define the airframe size, thus driving the mass of the structure, where the quantities of member types are defined by variables V1 to V11. Member positions are defined by the spacing and distribution of members, V12 to V18, to define the distribution of structural strength about the aircraft. The member cross-sections, V21 to V25, determine the strength of individual members to loads in various orientations. Variables V19, V20 and V26 to V47 control member geometry by defining the breadth and depth of either the member sections, i.e. flanges and webs, or the entire member, the choice of which is dependent on the member cross-sectional profile. The materials of members performing the similar structural roles described in §1.1.1 are defined by variables V48 to V50. The minimum factor of safety (FoS) under yield, C1, is a critical design constraint in establishing whether the structural members within each design solution will fail under the applied load cases. The maximum wingtip deflection, C2, is also an important constraint to prevent excessive bending or wing ground-strike. Finally, the design objective of minimum structural mass, O1, promotes the generation of a structural design of minimum mass, thus intending to provide improved aircraft performance and potentially reduced manufacturing and operating costs.

Parameter control within the HHA encourages the adaptation of specific process parameters for the improvement of a hyper-heuristic objective function. The initialisation of the optimisation process includes the input of the ranges permitted for these dynamic process parameters. The controlled parameters included within the framework are listed in Table 5.4. Model fidelity, P1, controls the precision of the finite element (FE) model and subsequent computation time required to perform structural analysis of each design solution. The penalty coefficient, P2, determines the severity of penalisation made by the penalty function. The binary chromosome strand length, P3, enables the adaptation of variable strand lengths to encourage the optimisation process to focus on variables failing to converge. The remaining

parameters, P4 to P18, determine the behaviour of low-level heuristics (LLHs) when employed within the problem domain, variations of which promote solution space exploration or population convergence. The use and control of these parameters are discussed further where appropriate in §5.1.6, §5.2 and §5.3.

Table 5.3: Structural design parameters

Design variable			
V1	Number of fuselage frames	V26	Fuselage frames breadth
V2	Number of fuselage stringers	V27	Fuselage frames depth
V3	Number of horizontal tail ribs	V28	Fuselage frames thickness
V4	Number of horizontal tail spars	V29	Fuselage floor beams flange breadth
V5	Number of horizontal tail stringers	V30	Fuselage floor beams flange depth
V6	Number of vertical tail ribs	V31	Fuselage floor beams web breadth
V7	Number of vertical tail spars	V32	Fuselage floor beams web depth
V8	Number of vertical tail stringers	V33	Fuselage stringers breadth
V9	Number of wing ribs	V34	Fuselage stringers depth
V10	Number of wing spars	V35	Fuselage stringers thickness
V11	Number of wing stringers	V36	Lifting surface ribs flange breadth
V12	Horizontal tail rib spacing exponent	V37	Lifting surface ribs flange depth
V13	Vertical tail rib spacing exponent	V38	Lifting surface ribs web breadth
V14	Wing rib spacing exponent	V39	Lifting surface spars flange breadth
V15	Distribution of frames to nose	V40	Lifting surface spars flange depth
V16	Distribution of frames to wingbox	V41	Lifting surface spars web breadth
V17	Distribution of frames to tail	V42	Lifting surface spars cap thickness
V18	Front wing spar chordwise root position	V43	Lifting surface stringers breadth
V19	Spar root breadth scaling factor	V44	Lifting surface stringers depth
V20	Spar root depth scaling factor	V45	Lifting surface stringers thickness
V21	Fuselage frames section	V46	Skin thickness
V22	Fuselage stringers section	V47	Floor thickness
V23	Horizontal tail stringers section	V48	Frames, floor beams, ribs and floor material
V24	Vertical tail stringers section	V49	Spars material
V25	Wing stringers section	V50	Stringers and skin material
Design constraint		Design objective	
C1	Factor of safety under yield, Eqn. (4.2a)	O1	Minimum structural mass, Eqn. (4.1)
C2	Wingtip deflection, Eqn. (4.2b)		

Table 5.4: Controlled dynamic process parameters

Dynamic parameter			
P1	FE model fidelity	P10	BP breeder pool intake
P2	Penalty coefficient	P11	RC contaminated population
P3	Strand length	P12	PSO inertia weight
P4	RI indigenous population	P13	PSO cognitive parameter
P5	DE crossover probability	P14	PSO social parameter
P6	DE differential weight	P15	PSO constriction constant
P7	GA crossover points	P16	LS step size
P8	GA crossover probability	P17	SA cooling rate
P9	GA mutation probability	P18	TS tabu list length

5.1.2 Mission Definition

The aircraft mission profile is defined using the mission requirements that were input during initialisation [1.2a]. Definition of an appropriate mission is critical to ensuring the design generated is suitable to the

requirements of an operator, and was identified as a framework requirement in §4.1.1. To achieve this, the following information is input during initialisation:

- airspeeds: suitable stall, manoeuvring, cruise and diving airspeeds;
- payload: including cargo, passengers, ordnance, and other disposable items;
- field length: distance during take-off and landing to clear aerodrome screen;
- range: distance of travel required by aircraft;
- cruising altitude: desired flight level during mission cruise.

Requirements and experience inform the aircraft design speeds, payload and aerodromes input during initialisation. The field lengths of the latter dictates the necessary powerplant performance. The mission profile is subsequently generated using input ranges, airspeeds and altitudes for a series of mission stages. This profile describes the manoeuvres to be performed by the aircraft during operation. Depending on the aircraft class, these mission stages may include take-off, climb, cruise, aerobatics, combat, payload drop, descent, loiter and landing. Figure 5.2 shows a sample of typical mission profiles.

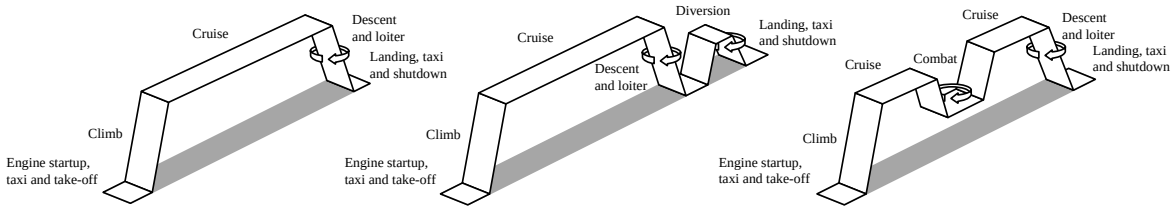

(a) Single cruise (b) Cruise with diversion (c) Military combat

Figure 5.2: Sample of mission profiles

The mission shown in Fig. 5.2(a) is typical of a large civil aircraft. After startup, taxi and take-off, the aircraft climbs to cruise for a given range before descending to land at the destination aerodrome followed by taxi to the ramp and shutdown. A loiter of set duration can be included to allow for the aircraft being held in the aerodrome holding pattern prior to landing. This profile may be extended to a mission with multiple cruises including transitions between flight levels via climbing or descending stages. For example, Fig. 5.2(b) demonstrates a mission with a diversion to an alternative aerodrome as may be required after an aborted landing. An example of a military combat mission is shown in Fig. 5.2(c) with a combat period midway through the cruise. Combat can represent air-to-air combat, a high or low-level strike, surveillance, humanitarian drop, air-to-air refuelling or an aerobatic display. This stage lasts for a predetermined duration rather than a range due to the unpredictable nature of military operations.

5.1.3 Mass Estimation

The aircraft mass is estimated using empirical data developed by Roskam (1986) and Raymer (2006) to establish the mass of the vehicle over the mission. It is necessary to use empirical data due to the lack of information about the aircraft prior to its conceptual design. These empirical methods consider the aircraft mass as the sum of the following components:

- disposable mass;
- fuel mass;
- trapped fuel and oil mass;
- empty aircraft mass.

Disposable mass encompasses items that are removed from the aircraft between missions, e.g. the mission payload input during initialisation [1.3a]. An estimate of the aircraft ramp mass is made based on the

aircraft class and mission using empirical data [1.3b]. The empirical methods developed by Roskam (1986) and Raymer (2006) are employed to iteratively estimate a more precise value of ramp mass as described in Appendix A.2 [1.3c]. This iterative process is performed until the error between the input and output masses reduces to less than 1×10^{-6} [1.3d]. The mass of the empty aircraft is subsequently found [1.3e] and thus the aircraft mass during each mission stage is calculated [1.3f].

The need to perform empirical mass estimation is discussed in §2.2 and §4.1.1. The method of Roskam (1986) is more established within the field of aircraft design but the method of Raymer (2006) is more recent, thus taking into account newer aircraft designs and materials. Both methods are used by the framework such that the more-established formulae of Roskam (1986) are employed to estimate mission fuel mass whilst the more recent data of Raymer (2006) are used to estimate ramp mass to take account of newer data. Therefore, the framework exploits the reliability of the former well-established method and the more recent data employed by the latter method. Empirical data are unavailable for mission stages such as combat and aerobatic manoeuvres. Therefore, the estimation of these stages are substituted for periods of loiter as they are defined over a duration of time and are fuel intensive. The module outputs the aircraft mass during each mission stage, as required to generate the aircraft external profile and calculate mass-dependent load cases, i.e. those during specific mission stages.

5.1.4 Aircraft Profile Generation

The aircraft external profile establishes the geometric boundary within which the airframe structure is designed, analysed and optimised. As discussed in §4.1.1, the aircraft profile requires definition to establish the boundary within which the structure is designed. Geometric and empirical formulae determine the aircraft size required for flight [1.4a] and carry the mission fuel [1.4b] as well as the powerplant specifications required for take-off and landing [1.4c] and establish the aircraft stability [1.4d]. Appendix A.3 lists the principle formulae used within this module. These tasks are not performed for existing aircraft design variants as such aircraft geometry and properties are input during initialisation. The external design of the aircraft is checked by the engineer to ensure the baseline solution is suitable before commencing the design, analysis and optimisation of the airframe within this external profile [1.4e].

The wing external profile is firstly designed to ensure sufficient main lifting surface area to generate lift for flight. Aircraft flight mass is at its greatest during take-off; thus requires the maximum lift loading coefficient, i.e. force applied to the wing per unit area, to achieve flight. Consequently, the take-off mass output from mass estimation is used to calculate the wing loading coefficient, from which the wing profile is generated. The geometry of this profile is constrained by values input during initialisation as listed in Table A.1 within Appendix A.1. The selected aerofoil provides the coordinates to define the wing cross-section and the coefficients of lift and drag. The internal volume available to contain the mission fuel is found by approximating the wing cross-sectional area at a series of spanwise location using the trapezium rule and aerofoil coordinates as shown in Fig. 5.3 (Maltbaek, 1961).

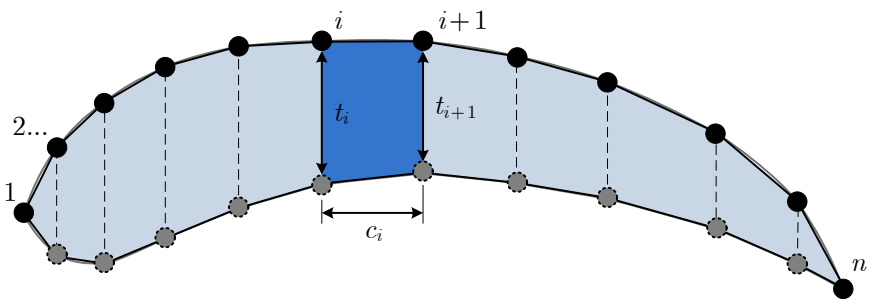

Figure 5.3: Surface area of aerofoil

$$A = \frac{1}{2} \sum_{i=1}^{n-1} \frac{c_i \left(t_i + t_{i+1} \right)}{2} \tag{5.1}$$

where A aerofoil cross-sectional area
c_i ith segment chord length
t_i ith segment thickness

The necessary fuel tank volume within the wing is estimated empirically given the fuel mass output from mass estimation and fuel density specified during initialisation. If the wing tank is of insufficient volume to hold the fuel, the wingspan is increased and loading coefficient recalculated. Sizing of the empennage follows a similar procedure to the wing due to the similarity in external profiles and operations, albeit without the need to carry mission fuel. The fuselage size is dominated by the accommodation of the nose, flight deck, cabin or payload compartment, and tapered tail. The tail design assumes equal tapering of the fuselage sides, as is common of most aircraft, and tapering of the fuselage base to avoid ground-strike with the runway on take-off rotation.

The powerplant properties of a new concept design are estimated empirically such that the aircraft possess sufficient thrust to satisfy the balanced field length of the aerodromes selected during mission definition for take-off and landing. Engine thrust is determined through the calculation of the required aircraft thrust-to-weight ratio given the estimated masses during take-off and landing. Solution of the balanced field length is a well-established iterative process that determines the powerplant thrust necessary to satisfy three field length cases for an engine-out take-off, emergency stop on take-off and landing. The latter is not considered for aircraft without reverse thrust as the powerplants are assumed to be idling throughout the landing. The aircraft decision speed during take-off is estimated iteratively, from which the other airspeeds during the take-off runs are found by the airworthiness requirements (CS-23, CS-25, Def.Stan.00-970), until the error in the field length calculated for the three cases is reduced to less than 1×10^{-6}. This solution process is described in Appendix A.3.1. The engine maximum thrust is then found given the estimated take-off mass and thrust-to-weight ratio required to satisfy the balanced field length. The powerplant properties of an engine possessing such peak thrust are estimated using data compiled for existing powerplant designs (Jackson, 2009; Meier, 2005). For example, the mass and geometry of a turbofan powerplant for a large civil transport aircraft are found using Fig. 5.4.

The positions of attachments, i.e. undercarriage, powerplant and ordnance, input during initialisation are updated if the external profile contradicts the input values, e.g. if the spanwise position of a wing-mounted ordnance unit exceeds the wingspan then the unit is positioned at the wingtip. The longitudinal stability of the aircraft is found by calculating the static margin given the external profile and powerplant characteristics. Empirical formulae are used to estimate the centre of gravity (CoG) positions of the aircraft sections and their subsequent moments about the aircraft CoG. The aircraft CoG position is then estimated, from which the position of neutral stability is calculated. The static margin is calculated as the difference between these positions, where positive longitudinal stability is indicated by a CoG forward of the neutral point. The empirical formulae used to calculate the CoG positions and static margin are provided in Appendix A.3.2.

The aircraft external design, powerplant properties and static margin are output to the engineer to check that a suitable, stable aircraft design has been generated. If this is not the case, the design requirements are modified by repeating the previous framework modules, i.e. initialisation, mission definition, mass estimation and aircraft profile generation, until a suitable external design has been created. This is the only interaction the engineer has with the framework after initialisation. Following acceptance of the design, the aircraft external profile is fixed for the remainder of framework operation as the design, analysis and structural optimisation of the airframe do not provide any inputs to this module. Consequently, structural optimisation is performed within the constraints of the external profile.

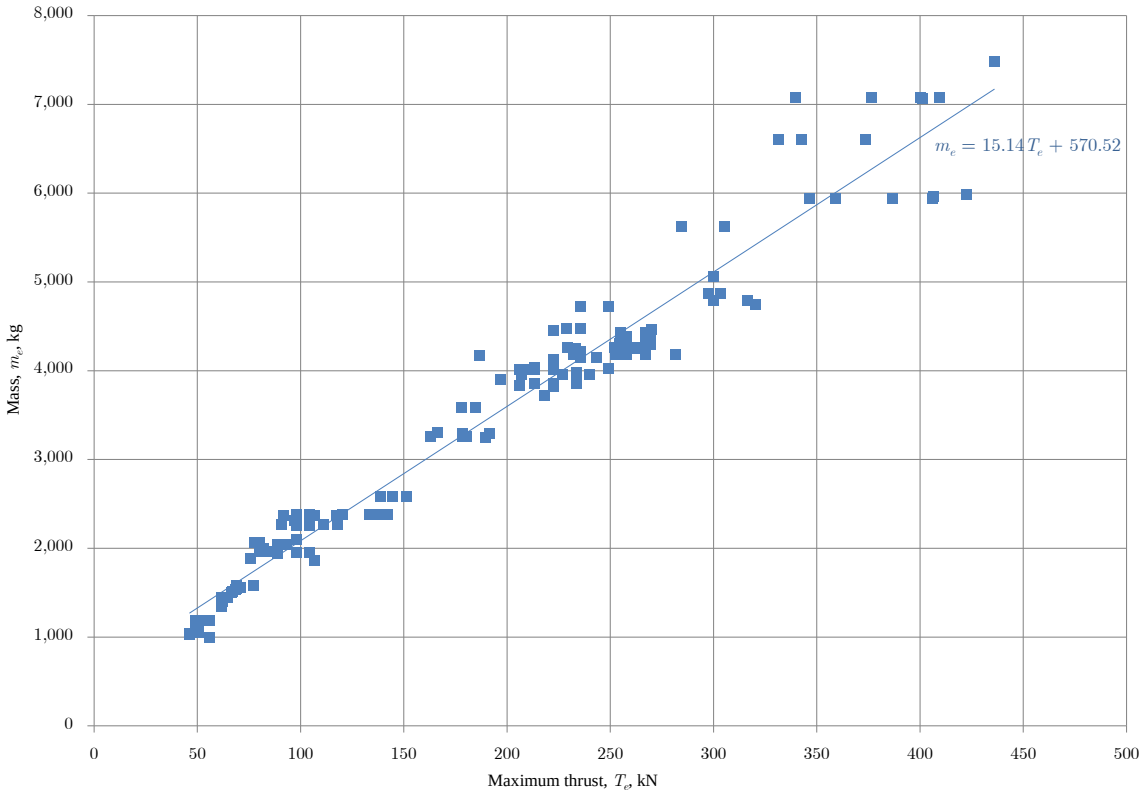

(a) Powerplant unit mass

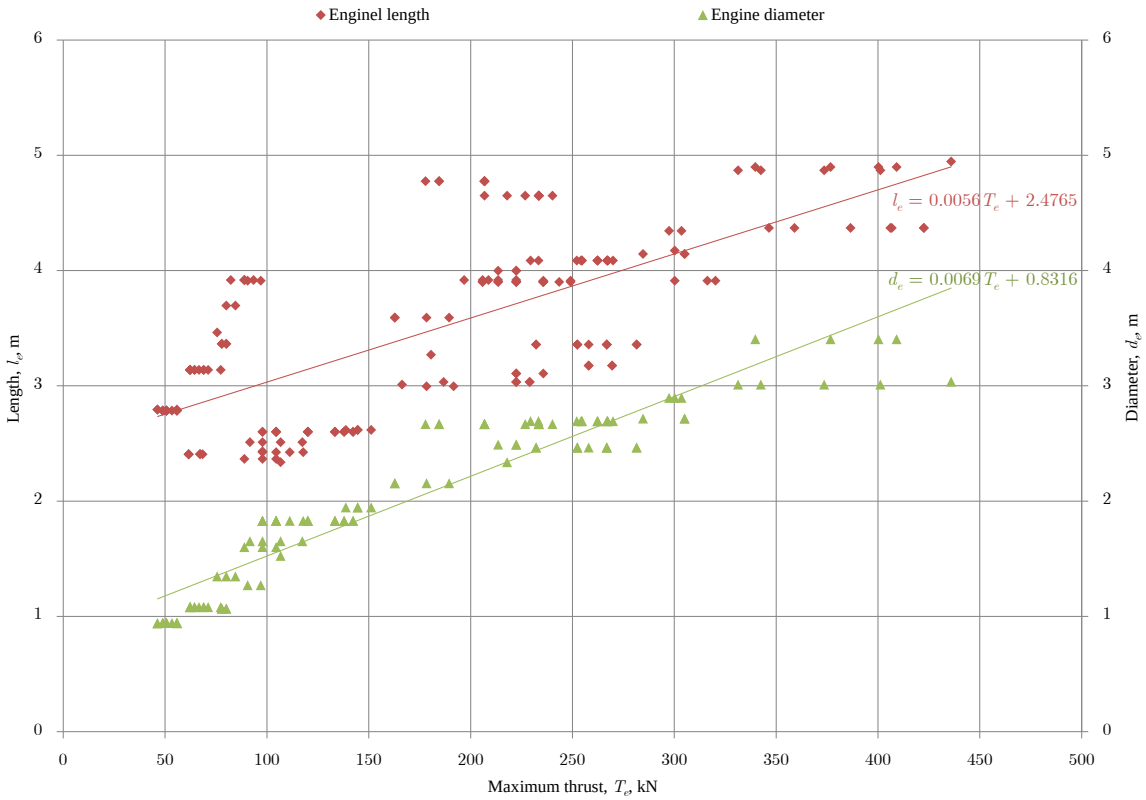

(b) Nacelle length and diameter

Figure 5.4: Historical data for large civil aircraft turbofan powerplants (Jackson, 2009; Meier, 2005)

5.1.5 Aircraft Loads

Loads to be applied to the airframe during structural analysis are selected during initialisation from the database in Table A.3 within Appendix A.1. The magnitudes of these loads are computed prior to starting the optimisation process such that the loads can then be applied at precise locations to each airframe design. The loads within the database are categorised as flight loads due to airborne manoeuvres and gust conditions [1.5a], ground loads resulting from operations during landing and taxiing [1.5b] and miscellaneous loads [1.5c]. The distribution of load over the aircraft exterior is also established given the design output from the previous module [1.5d]. Load cases are calculated with reference to the airworthiness requirements for European civil aircraft and military aircraft of the United Kingdom:

- civil light aircraft: CS-23;
- civil large aircraft: CS-25;
- military aircraft: Def.Stan.00-970.

The calculation of the loads as defined by the airworthiness requirements is described in Appendix A.4. More specifically, the load case calculations are presented as follows based on their classification:

- flight loads: Appendix A.4.1;
- ground loads: Appendix A.4.2;
- miscellaneous loads: Appendix A.4.3.

The flight loads are computed through the consideration of the flight envelope, which is formed through the superposition of the manoeuvre and gust envelopes. The constructions of the manoeuvre and gust envelopes are described in Appendices A.4.1.1 and A.4.1.2 respectively. Figure 5.5 illustrates the flight envelope with the annotated positions of the flight loads contained within the framework load case database. Manoeuvre loads include the maximum positive and negative manoeuvre loads, denoted by L1 and L2 respectively as in Table A.3, as these represent the extreme load factors within the manoeuvre envelope and are therefore the greatest manoeuvre loads the aircraft is required to withstand. Discrete gusting conditions are applied at the maximum gust velocity and during the mission cruise, L3 and L4 respectively. Manoeuvre loads are static loads whilst gust loads require dynamic analysis of the aircraft as it travels through the gust. The magnitudes of these loads are determined by the aircraft class as defined in the corresponding airworthiness requirements.

Ground loads include loads during landing and ground manoeuvre operations, the calculations of which are provided in Appendices A.4.2.1 and A.4.2.2 respectively. Landing loads are typically of greater magnitude than flight loads but are less frequently encountered by the aircraft during a mission, i.e. only during taxi, take-off and landing. These loads are applied to localised areas of the airframe as transmitted through the undercarriage units. These include the nose undercarriage mounted in the fuselage nose and the main undercarriage units mounted in the wing or fuselage. The main units are assumed to be symmetrical about the fuselage centreline. Such undercarriage configurations are typical through the field of aircraft design (Howe, 2004). The positions of the undercarriage units are output from the airframe profile generation module, the landing loads on which consider the following configurations:

- two-point landing, L5: initial touchdown on main units shortly followed by nose unit touchdown;
- three-point landing, L6: simultaneous touchdown on all three units.

These are the most likely landing configurations required for consideration by the airworthiness requirements. Ground loads due to surface unevenness and dynamic braking, L7 and L8 respectively, are calculated for take-off and taxi, with the greater magnitude applied to the airframe. These loads ensure the undercarriage supporting structure can withstand sudden loads during ground operations.

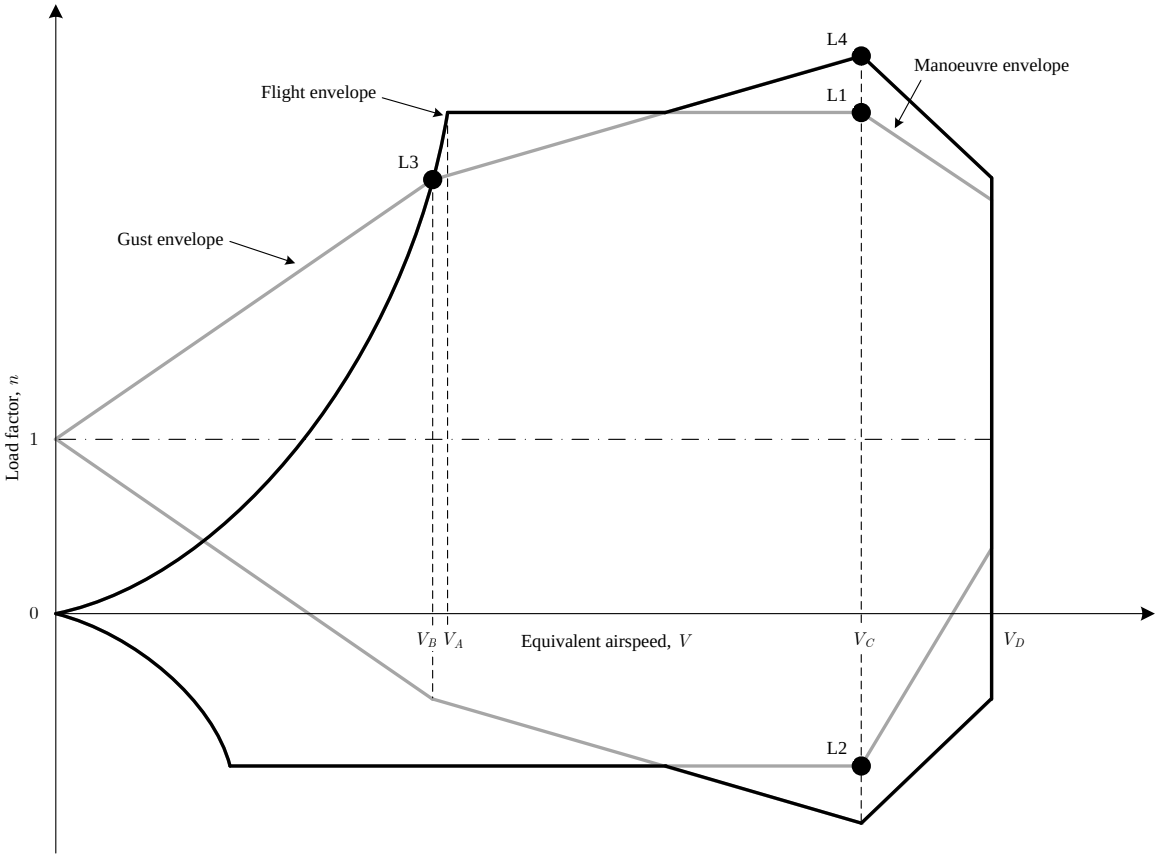

Figure 5.5: Load cases within the flight envelope

Miscellaneous loads include cabin pressurisation, powerplant thrust and gravity, as denoted by L9, L10 and L11 respectively. The greatest pressure differential as a result of fuselage cabin pressurisation is determined given the mission altitudes to ensure sufficient airframe strength under pressurisation. Loads on the airframe as a result of powerplant thrust are also considered to similarly ensure sufficient structural integrity. The magnitudes of the cabin pressurisation and powerplant thrust loads vary depending on the mission stage given their respective dependency on altitude and engine thrust setting. Aircraft self-weight is also applied to ensure the aircraft can withstand the loads imposed on itself by its design. This encompasses the calculation of the weight of aircraft attachments, e.g. powerplants and ordnance, which are added to the masses of individual structural members following the generation of aircraft structural designs during the optimisation process. The miscellaneous loads are applied concurrently with the flight or ground load as the aircraft is always subjected to such loads.

Appropriate distribution of pressure loads over the lifting surfaces is necessary to ensure the realistic application of loads, and thus reliable structural analysis results, given the effects of an aerofoil on the surrounding airflow. The lift generation by an aerofoil-shaped lifting surface considers:

- chordwise distribution: effects of the aerofoil cross-section;
- spanwise distribution: effects of the aerofoil across the lifting surface finite span.

The chordwise distribution is defined by the geometry and angle-of-attack (AoA) of the aerofoil at specific spanwise positions, dictating the torque of the lifting surface and local shear and bending within ribs. The spanwise distribution is determined by the lifting surface planform geometry and dictates the global shear and bending moments across the span of the surface. Figure 5.6 illustrates the theoretical pressure distributions in the chordwise and spanwise directions over an aircraft lifting surface. In reality, the amount of lift reduces close to the root due to the interference of the fuselage with the airflow.

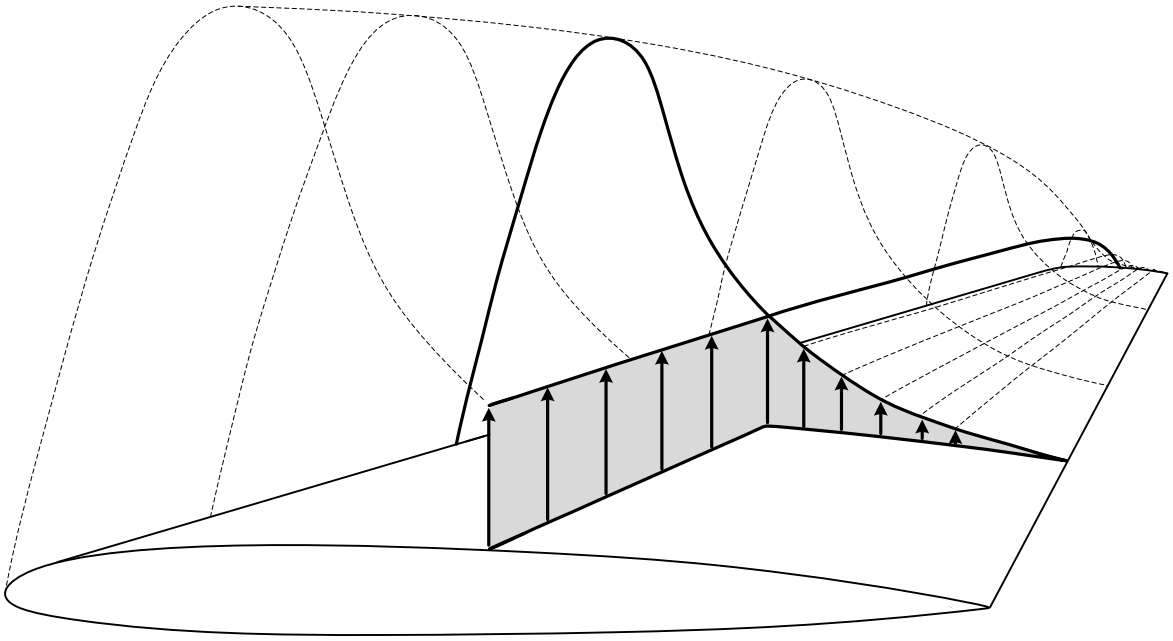

Figure 5.6: Lift distribution over lifting surface

The flight loads within the database in Table A.3 are distributed between the wing and horizontal tail proportionally based on the surface areas of the lifting surfaces. These loads are distributed over each lifting surface by initially calculating the pressure load distribution over lifting surface span before then calculating the chordwise distribution at spanwise locations. The pressure distributions are independent of the structural design, i.e. are based on the lifting surface profiles, hence are computed prior to beginning the optimisation process and stored for subsequent application to the airframe during structural analysis. The spanwise pressure distribution is determined using the Schrenk approximation (Schrenk, 1940) whilst the chordwise pressure distribution is determined using a two-dimensional vortex panel code. These methods are based on lifting line theory, the theory of which is provided in Appendix A.4.4. The theory of the Schrenk approximation is similarly presented in Appendix A.4.5 and for the vortex panel method in Appendix A.4.6. Joints between panels in the latter are defined by the coordinates of the lifting surface aerofoil selected during initialisation. Alternative approaches of calculating the lifting surface pressure distribution include thin aerofoil theory, three-dimensional panel codes and computational fluid dynamics (CFD). However, the precision of thin aerofoil theory is restricted to aerofoils with a thickness-to-chord ratio of no greater than 12% at small AoAs whilst three-dimensional panel codes or CFD are more complicated and computationally-intensive, as such not suitable for repeated use during conceptual design optimisation (Anderson Jr, 1991). Ground loads are applied as concentrated loads to the undercarriage units for transmission to the supporting structure. Powerplant thrust loads are also applied as point loads at their attachment positions whilst cabin pressurisation is applied as a pressure load to the fuselage skin and floor. The self-weight of each structural member is applied to the member, as well as appropriate point load masses for attachments and pressure loads due to fuel and payload weight.

5.1.6 Structural Layout Generation

Optimisation of the airframe is performed through the generation of a population of structural designs within the previously established external profile. This is a requirement of the solution process, as identified in §4.1.1. Optimisation is performed over n_k generations for a population set containing μ individual

airframe design solutions. Each design solution is independent of the remainder of the population, as a result structural layout generation and subsequent analysis is performed separately for each population individual, as indicated in Fig. 5.1. Consequently, the following descriptions of structural layout generation and analysis concern the generation of a single airframe design.

The generation of an individual airframe design solution is based on the values of the design variables within Table 5.3 [1.6a]. The positions of airframe attachments, i.e. undercarriage, powerplant and ordnance, are then considered to ensure structural members are positioned appropriately to support these attachment units [1.6b]. The airframe represented by this design solution is subsequently created for structural analysis [1.6c] under the loads calculated in the previous module.

The values of design variables listed in Table 5.3 principally determine the structural design represented by an individual. The variables determine the number, position, geometry and material of airframe structural members. These variables have been selected in accordance with those commonly employed within the literature to define the airframe, as discussed in §2.2.1 and §2.5. The values of variables for each individual solution in the initial population are either generated randomly or seeded during initialisation as specific values to provide greater control over the optimisation problem initial conditions. Design variable values of individuals in subsequent populations are generated by the LLH during optimisation. This is discussed further in §5.3. The number of fuselage frames is determined by design variable V1. Frames are firstly positioned at the following critical locations:

- forward-most fuselage location;
- nose undercarriage connection;
- main undercarriage connections (if fuselage-mounted);
- powerplant connections (if fuselage-mounted);
- wing spar root connections;
- empennage spar root connections;
- nose-flight deck intersection;
- flight deck-cabin intersection;
- cabin-tail taper intersection;
- aft-most fuselage location.

Variables V15, V16 and V17 define the number of remaining frames distributed within the fuselage nose, wingbox and tail respectively to provide additional support against transmitted lifting surface and undercarriage loads. The nose is defined as forward of the cabin, the wingbox as between the front and rear wing spars, and the tail as aft of the forward-most empennage spar. Frames are distributed evenly within each of these sections, as are the remaining frames throughout the rest of the fuselage. The quantity of fuselage floor beams is defined by the number of frames within the cabin. One horizontal floor beams lies across the fuselage width at each cabin frame position. Three vertical beams connect the floor to a cabin frame at the fuselage centreline and at half the floor width on either side. Three longitudinal floor beams support the floor along the length of the cabin at the same lateral positions as the vertical beams. Design variable V2 determines the number of stringers within the fuselage. These members are distributed at equal intervals around the fuselage circumference.

The aircraft is assumed to be symmetrical along the fuselage centreline, therefore design variables are used to define the layout of a single lifting surface which is then mirrored to create the second surface, i.e. port and starboard wings and tails. Variables V3, V6 and V9 define the number of ribs in each horizontal tail, vertical tail and wing lifting surface respectively. The spanwise position of the ith rib is defined by these variables and V12, V13 and V14 for the horizontal tail, vertical tail and wing respectively

$$x_i = \frac{i^{\alpha_R}}{n_R^{\alpha_R}} (x_t - x_r) + x_r \tag{5.2}$$

where n_R V3, V6, V9 as required
α_R V12, V13, V14 as required
x_r lifting surface root spanwise position
x_t lifting surface tip spanwise position

These variables permit increased concentration of ribs towards the lifting surface root for additional support against bending loads. A rib is fixed at the root and tip of each lifting surface, as well as two wing ribs at the corresponding floor beam lateral locations within the fuselage, i.e. fuselage centreline and half floor width. Further, ribs are positioned at locations of wing-mounted attachments. Ribs are aligned parallel to the aircraft longitudinal axis, i.e. flight direction.

Variables V4, V7 and V10 determine the number of spars in the horizontal tail, vertical tail and wing respectively. Variable V18 defines the chordwise root position of the front wing spar to control the structural response to torsion resulting from the applied flight loads. The rear wing spar and empennage spar root positions are defined empirically based on the data in Sensmeier and Samareh (2004)

$$z_{FS} = \begin{cases} K_{FS,r} c_r + z_{LE,r} & \text{at root} \\ K_{FS,t} c_t + z_{LE,r} & \text{at tip} \end{cases} \tag{5.3a}$$

$$z_{RS} = \begin{cases} K_{RS} c_r + z_{FS,r} & \text{at root} \\ K_{RS} c_t + z_{FS,t} & \text{at tip} \end{cases} \tag{5.3b}$$

where $K_{FS,r} = \begin{cases} \text{V18} & \text{for wing} \\ 0.25 & \text{for horizontal, vertical tail} \end{cases}$

$K_{FS,t} = \begin{cases} 1.15\,\text{V18} & \text{for wing} \\ 0.3 & \text{for horizontal, vertical tail} \end{cases}$

$K_{RS} = \begin{cases} 3.2 - 1.1 \left\{ \dfrac{\text{V18} - \text{V18}_{\min}}{\Delta\text{V18}} \right\} & \text{for wing} \\ 0.4 & \text{for horizontal tail} \\ 0.45 & \text{for vertical tail} \end{cases}$

$z_{LE,r}$ leading edge root position, m

Intermediate spars are distributed evenly between the front and rear spars. Variables V19 and V20 define linear scaling of spar breadth and depth at the root relative to the tip to provide greater resistance to bending and shear at the fuselage connection

$$b_r = \text{V19} b_t \tag{5.4a}$$

$$d_r = \text{V20} d_t \tag{5.4b}$$

where $b_{r,t}$ root, tip spar breadth, m

$d_{r,t}$ root, tip spar depth, m

The numbers of stringers on each of the upper and lower surfaces of the horizontal tail, vertical tail and wing are defined by variables V5, V8 and V11 respectively. Stringers are distributed evenly across the lifting surface chord between the front and rear spars.

Design variables V21 to V25 define the cross-section of frames and stringers whilst variables V26 to V45 determine the cross-sectional geometry of the airframe structural members. Frames and stringers may be either C, I, T or Z-sections, whilst floor beams, ribs and spars are always I-sections - these cross-sections are used as they are common for these member types (Howe, 2004). Design variable V21 defines the cross-section and V26 to V28 the cross-sectional geometry of fuselage frames. Variables V29 to V32 determine the geometry of the floor beams. The cross-sections of fuselage stringers are defined by variable V22 and the geometry by variables V33 to V35. The geometry of ribs is defined by variables

V36 to V38 whilst variables V39 to V42 define the geometry of spars. Design variables V23, V24 and V25 determine the cross-sections of horizontal tail, vertical tail and wing stringers respectively, whilst variables V43 to V45 determine their breadth, depth and thickness. The geometric control of structural member cross-sections is illustrated in Fig. 5.7. Spar caps provide additional reinforcement to the spars as shown in Fig. 5.7(b) by dashed lines. Variable V42 defines the breadth of the spar caps, from which the spar cap depth is calculated given the web thickness such that the spar caps are square across the member cross-section. The depths of ribs and spars are dictated by the chordwise and spanwise position of the member within the lifting surface.

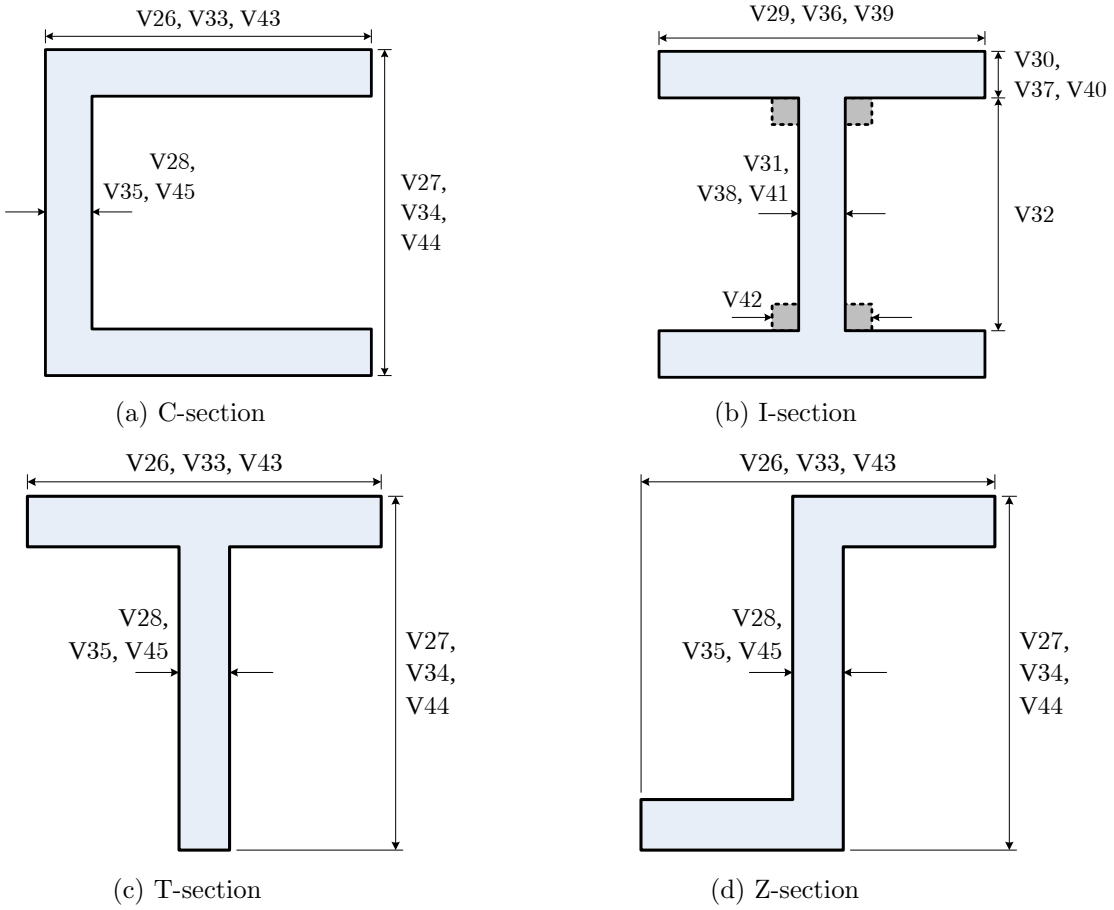

(a) C-section (b) I-section

(c) T-section (d) Z-section

Figure 5.7: Airframe member structural geometry

Skin thickness over the aircraft is defined by variable V46 whilst cabin floor thickness is determined by V47. Skin thickness is not normally constant across the entire aircraft, but is assumed so in this instance. This is acceptable given the early stage of the design process and obviates unnecessarily increasing the number of design variables. Design variables V48 to V50 define the materials from which the airframe member types are constructed. Variable V48 determines the material of ribs, frames, floor beams and floor, V49 defines spar material and V50 specifies the material of stringers and skin. Frames and ribs perform similar roles to strengthen the airframe whilst floor beams reinforce the floor and react pressurisation loads in conjunction with frames. Spars are typically formed of stronger material, i.e. of greater yield stress, due to their critical role in reacting applied loads, therefore their material is determined independently of other member types. Stringers reinforce the skin hence are formed of the same material. The grouping of member types by material reduces the number of design variables and thus the size of the optimisation problem. Similarly, members of the same type possess identical cross-sectional geometry to reduce the size of the optimisation problem. Such approximations are appropriate, and common, during

the conceptual design phase (Pready, 2013; Raymer, 2006). Traditional airframe metallic materials, e.g. grades of aluminium, are considered rather than composite materials to reduce the number of design variables required, i.e. not requiring optimisation of the ply numbers, orientations and orders.

5.2 Structural Analysis

The structural analysis stage determines the feasibility of each airframe design generated in §5.1.6 with respect to the design constraints stated in Table 5.3 of minimum FoS under yield and maximum wingtip deflection. As stated in §4.1.1, this is critical to promote the generation of a feasible design during optimisation that does not violate either of the design constraints and thus will be suitable for further design and subsequent manufacture and operation. It is also useful to perform structural analysis for an understanding of the influences of different loads on the airframe strength. The description that follows of the structural analysis module is formed with respect to the analysis of a single airframe design solution. Supporting theory for this stage is provided in Appendices A and B.

5.2.1 Sectional Properties

The cross-sectional properties of each airframe structural member are calculated based on their cross-sectional profile shape and geometry as defined by the design variables V21 to V45 [2.1a]. These properties are required in order to calculate the mass of the airframe and define the mechanical properties of the FE model. The sectional properties defined at this stage include the cross-sectional surface area, centroid location, second moments of area and torsion constant. The formulae used to calculate these properties are provided in Appendix A.5.

5.2.2 Structural Mass

The mass of the airframe is calculated as the sum of the masses of individual structural members within the airframe [2.2a]. The aircraft structural mass represents the unpenalised objective value of the design solution of the optimisation problem. The masses of structural members also determine the self-weight load of the member to be applied for load case L11. The airframe structural mass is calculated as the cumulative mass of the n_{mem} airframe members as follows

$$m_{str} = \sum_{s=1}^{n_{mem}} m_s \tag{5.5}$$

where $m_s = \rho_s A_s l_s$

- ρ_s sth structural member material density, kg/m^3
- A_s sth structural member cross-sectional area, m^2
- l_s sth structural member length, m

The mass of the sth member with constant cross-section, i.e. fuselage members and stringers, is calculated as given in Eqn. (5.5) for m_s. The masses of members without constant cross-section are approximated based on the cross-sectional variation of the members over their length. Specifically, spar mass is approximated by the mean surface area of the linearly tapered members whereas rib mass is found as the sum of the flange and web masses over the breadth of the member using formulae presented by Maltbaek (1961). Floor mass is calculated as the cumulative mass of sections between floor beam positions and skin mass is similarly found as the cumulative mass of sections between stringers. The approximation of the airframe mass in this manner does not consider details of the design such as lightening holes and fittings. However, such design details are not considered during the early design process phase of conceptual design (Allen, 2010a), therefore Eqn. (5.5) provides a reasonable approximation of the aircraft structural mass.

5.2.3 Airframe Model

The airframe design is represented by an FE model such that FEA may be performed to establish the response of the structure to the applied load cases. This model approximates the airframe as a finite number of interconnecting elements of defined geometry, sectional properties and material joined by nodes at nodal points. The computation time required for solution analysis is of great concern during conceptual design optimisation when considering numerous design solutions. This computational expense is dependent on the sizes of the global FEA matrices, which are defined by the number of system degrees of freedom (DoFs). The DoFs define the system mechanics and indicate the configurations in which a system may be excited or displaced. The number of DoFs is determined by the FE model precision and influences the accuracy of the FEA approximation. Model fidelity defines the accuracy of the model in representing reality, with a balance required between model, and thus analysis, precision and computational expense.

Model precision is dependent on the dimensionality, type and number of elements used. One-dimensional linear beam elements model the aircraft with two nodes per element and up to six DoFs per node. This reduces the number of DoFs compared to other types of elements, e.g. quadratic beam elements or elements of higher dimensionality, thus reducing the computational effort required to form the problem, i.e. generate the model and system matrices, and conduct analysis of the model. However, such elements provide sufficient precision for analysis during an early stage of the design process provided that an adequate number of elements are used and are positioned appropriately (Amadori, 2010). The shape of a linear beam element, with nodes N_1 and N_2, and its DoFs for displacement, d, and rotation, θ, are illustrated in Fig. 5.8 in the element local xyz Cartesian coordinate system used herein.

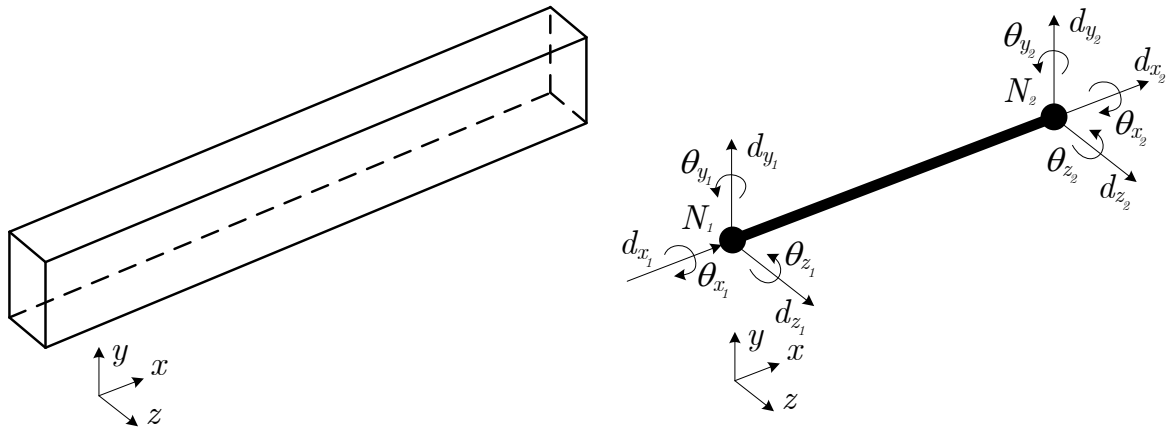

(a) Element shape (b) Element degrees of freedom

Figure 5.8: Linear beam element shape and DoFs

The following types of beam elements are used to model the airframe structural members:

- pin-jointed truss: three DoFs per node for translational but not rotational freedom in all axes;
- fix-ended space frame: six DoFs per node for translational and rotational freedom in all axes.

With the exception of ribs, all structural members are modelled as space frame elements to permit displacement and rotation in all DoFs. Truss elements possess no rotation stiffness; hence are used to model the ribs to prevent their loading with bending moments that could be unrealistic in the event of exaggerated twisting of the lifting surface. Such excessive twisting is possible as a result of the approximation of the load distribution described in §5.1.5 creating an unrealistic load imbalance over the lifting surface. More precise calculation of the load distribution, e.g. using CFD, could reduce the likelihood of this occurring; however, this would incur a significant penalty in terms of the time required

to perform these calculations.

The generation of the FE model contains two principal tasks. Firstly, the airframe structural members are grouped by type to reduce the number of DoFs within the model, and thus the computational effort required to model and solve the FEA problem [2.3a]. The degree of this grouping is defined by the model fidelity level. Secondly, the FE model is constructed based on the number of elements required following the completion of member grouping [2.3b].

5.2.3.1 Structural Member Grouping

Similar structural members, e.g. wing ribs, are grouped together within elements to reduce the number of system DoFs and computational effort required to solve the FEA problem. Critical members are exempt from such grouping, e.g. lifting surface spars and members with attachments, due to the importance of local loads on these members in defining airframe integrity under load. Additionally, skin is lumped within stringers and floor within floor beams due to the purpose of these members to stiffen the skin and floor respectively against applied loads. Lifting surface stringers are in turn lumped within spars as both provide resistance against bending. Member grouping is performed using the following criteria:

1. geometry;
2. sectional properties;
3. material properties.

An example of member grouping is shown in Fig. 5.9 where six structural members are grouped within two FE model elements. The element centroid is positioned at the location corresponding to that of the central member within the element when grouping an odd number of members or at the mean of the two central members if an even number of members are grouped, i.e. in Fig. 5.9 the element centroids are at the centroids of members 2 and 5.

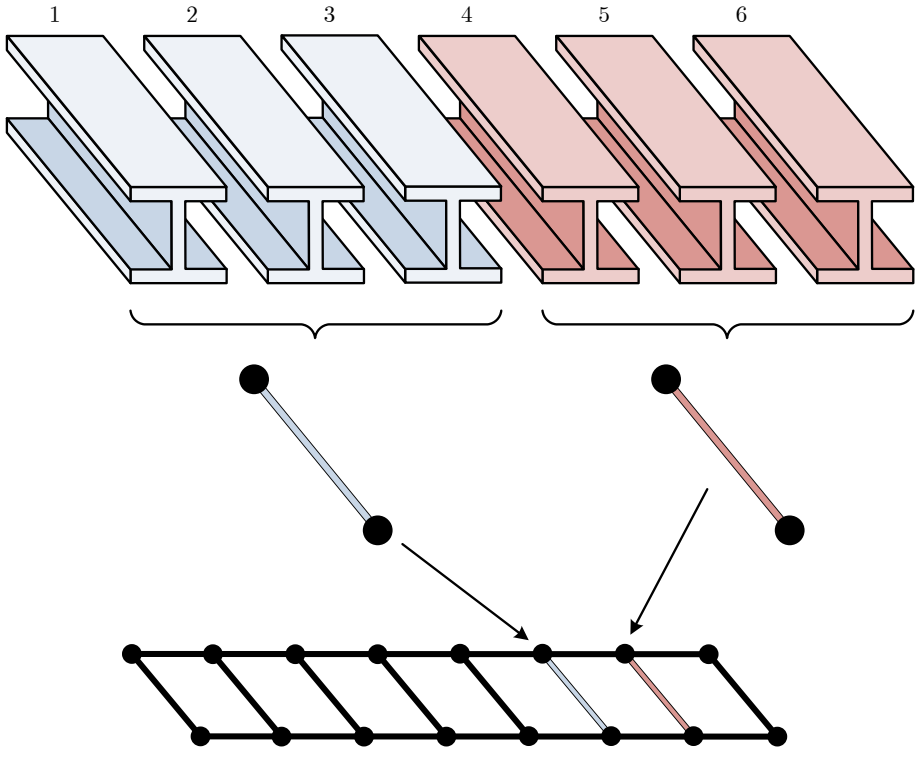

Figure 5.9: Example of member grouping within FE model

Rectangular beam elements idealise the geometry of members of different cross-section, i.e. C, I, T and Z-sections, to permit members of varying cross-sections to be grouped together. The cross-sectional area of the eth element is calculated as the cumulative area of the n^e_{mem} structural members within the element

$$A_e = \sum_{i=1}^{n^e_{mem}} A_i \tag{5.6}$$

The expressions described in Appendix A.5 for the sectional properties of a structural member are employed to calculate the corresponding element properties. Specifically, Eqns. (A.80a), (A.80b) and (A.80c) are used to determine the element breadth and depth given the centroid location and cross-sectional area. The parallel axis theorem, Eqn. (A.81), calculates the second moment of area of each member relative to the element centroid. The rotations of structural members relative to the element are accounted for by Eqn. (A.84). The second moment of area of an element is calculated as the sum of the second moments of area of the element members. The element product second moment of area and polar second moment of area are determined respectively using Eqns. (A.79c) and (A.83) whilst the torsion constant is found for the rectangular element by Eqn. (A.82). The length of an element is calculated as the difference between the element nodal point coordinates.

Members of the same type are grouped together given that they are constructed of the same material, as defined by design variables V48, V49 and V50, and thus possess consistent material properties, e.g. elastic section modulus, Poisson's ratio, density and yield strength. Specifically, multiple ribs are grouped into a smaller number of rib elements. Similarly, multiple fuselage frames, floor beams and stringers are grouped respectively into fewer frame, floor beam and stringer elements. Lifting surface stringers are grouped within the nearest spar element, however these member types may be constructed of dissimilar materials given they are defined by different variables, i.e. V49 and V50. The material properties of spar-stringer elements are subsequently approximated as the surface area-weighted average of the member properties, e.g. for the eth element elastic section modulus

$$E_e = \frac{\sum_{i=1}^{n^e_{mem}} E_i A_i}{\sum_{i=1}^{n^e_{mem}} A_i} \tag{5.7}$$

Model fidelity determines the precision of the FE model by defining the extent to which grouping is performed, and thus the level of smearing of element properties due to such grouping. The fidelity level takes a value between $0.1 \leq F \leq 1.0$ to denote the approximate number of elements per member type. For example, a design with 100 members modelled at $F = 1.0$ would model each member explicitly, whereas modelling at $F = 0.1$ would model one in ten members as elements. In the latter, each model element would nominally include the grouping of the nine members closest to the element. The fidelity level of the grouping shown in Fig. 5.9 is $F = 0.33$. Powerplant, undercarriage and ordnance attachments to the airframe are made at the corresponding nodal points of frames or rib-spar junctions. Therefore, the corresponding members are modelled in isolation due to their critical role in supporting these attachments. Elements are always positioned at lifting surface roots and tips as well as the fuselage ends and intermediate transition points between the nose, flight deck, cabin and tail taper to bound the FE model.

5.2.3.2 Finite Element Model Generation

Linear beam elements are used to construct the FE model of an airframe design solution following the grouping of similar structural members. Each group of frames is modelled as a series of circumferential elements joining at nodal points defined by the positions of floor beam and stringer nodes. Grouped floor beams are constructed using horizontal, vertical and longitudinal elements, with the floor lumped within

these members. Longitudinal stringer elements connect the frame and floor beam nodes along the length of the fuselage and include the lumped skin properties. Chordwise rib elements are constructed within lifting surfaces and subsequently connected by spanwise elements representing spars with grouped stringers and lumped skin. The sizes of members are assumed to be the same throughout the aircraft to reduce the size of the optimisation problem by eliminating the need to represent each member within the conceptual design with an individual set of design variables. Furthermore, this eliminates the need to consider members close to the lifting surface roots as independent of the remaining fuselage members. However, the typical size of these members is inadequate to withstand the large lifting surface loads transmitted to the fuselage. As a result, the nodes between fuselage and lifting surface members are independently connected to the respective section elements, thus lifting surface loads are not transmitted into the fuselage. This approximation of the joints between the fuselage and lifting surfaces is representative of the carrythrough structure within most existing large civil or military aircraft (Raymer, 2006). This structure also enables the wingbox to continue through the fuselage width such that the two sides of the lifting surface are not independent, i.e. spars continue from the starboard to port lifting surface tips. The use of fixings to connect the lifting surfaces and fuselage will lead to the transmission of loads between these aircraft sections. However, these details are beyond the scope of conceptual design and thus require consideration during later design phases, i.e. embodiment or detail design.

Figure 5.10(a) shows the model of an arbitrary aircraft design to indicate the layout of the structural members within the airframe. The corresponding FE model of the aircraft is illustrated in Fig. 5.10(b) including the model global coordinate system used during FEA within the framework. The global xyz Cartesian coordinate system used for airframe modelling and analysis is shown in Fig. 5.10(b) such that the x, y and z-axes are parallel with the aircraft spanwise, vertical and longitudinal axes respectively. Grouping of multiple airframe members within elements can be seen in Fig. 5.10(b) by the reduced number of elements to represent the structure. For example, the two lifting surfaces spars and stringers in Fig. 5.10(a) are modelled in combination as pairs of spanwise elements in Fig. 5.10(b) consisting of each spar and the stringers closest to the spar.

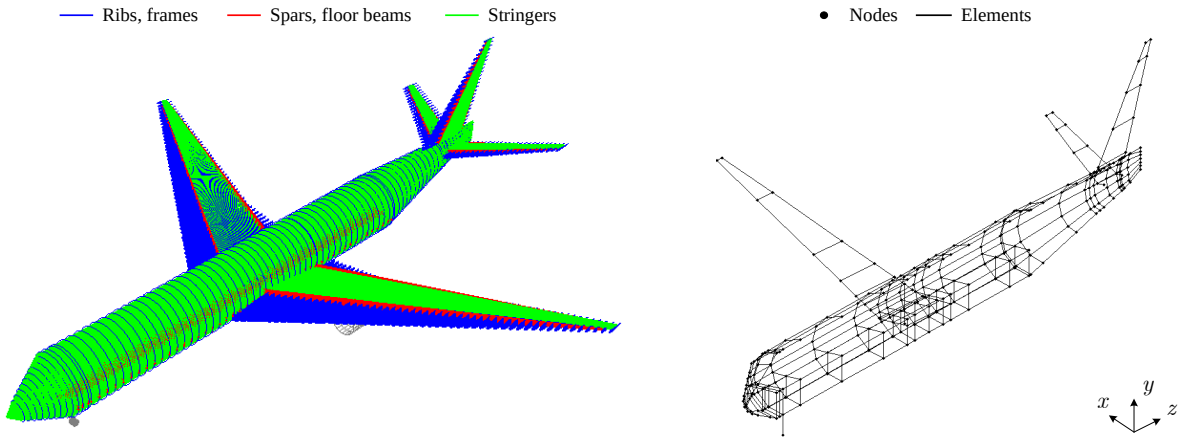

(a) Airframe model (b) FE model

Figure 5.10: Example of aircraft FE model

The nodal point locations within the FE model depend on the structural layout of the aircraft and the element positions resulting from member grouping. Nodes are assigned global numbers that determine the location of the element properties within the global FEA matrices, as is discussed further in §5.2.4. The FE model is created by progressing from the fuselage nose to tail, and then for each lifting surface from root to tip. Nodes are numbered in ascending order as elements are created such that interconnecting

elements possess nodal numbers within similar ranges. This numbering order maintains a low bandwidth of the FEA matrices to assist in reducing the computation time required for analysis. Figure 5.11 illustrates the node numbering order within the fuselage and for a lifting surface with three spars.

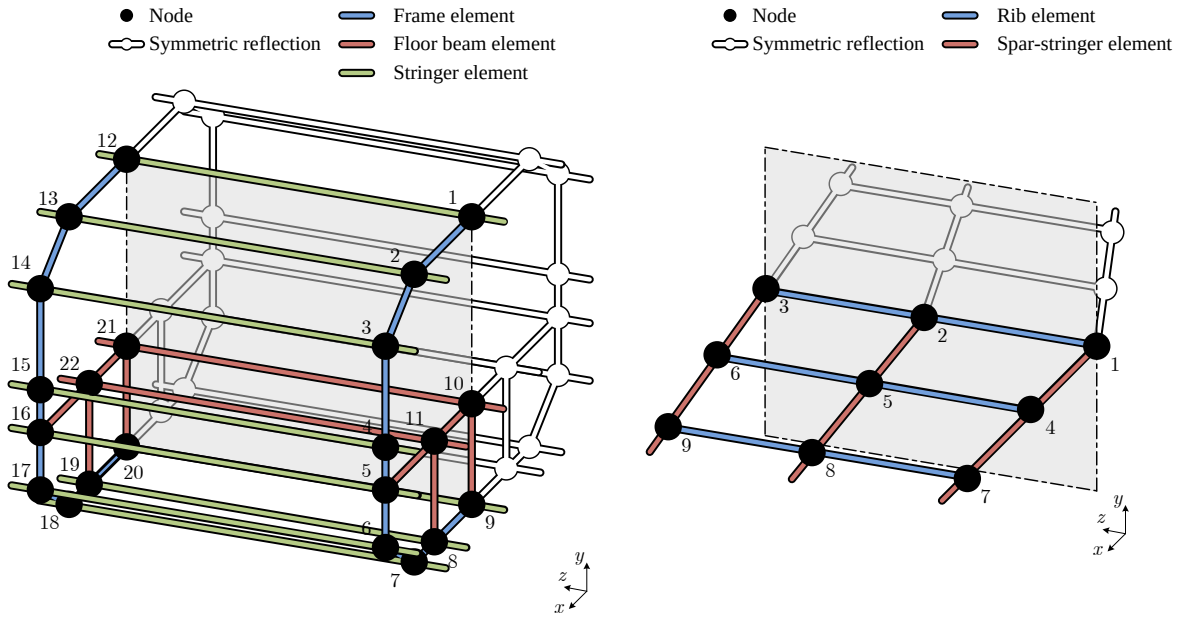

(a) Fuselage (b) Lifting surface

Figure 5.11: Node numbering order

The FE model is created as a half-model, as shown in Figs. 5.10(b) and 5.11, to exploit the possibility to reduce model size given that all applied load cases are symmetric about the fuselage centreline. This reduction in model size reduces the number of nodes and elements within the FE model, and thus the sizes of the FEA matrices and corresponding computational effort required to perform FEA. The response of the aircraft port side is established by mirroring the response of the modelled starboard side in the global yz-plane of symmetry, thus the response of the entire aircraft is obtained.

5.2.4 Finite Element Analysis

FEA is performed of an airframe FE model to establish the displacement and rotational response of the structure when subjected to the selected load cases. This is achieved through firstly forming the problem through approximation of the airframe mechanics, boundary conditions and excitation, i.e. applied load cases, [2.4a] followed by the calculation of the problem solution in the displacement field [2.4b].

The theory underpinning FEA as performed within the framework is described in Appendix B. FEA approximates the airframe response to the selected load cases through substitution of the structure as a matrix system formed using the properties of the FE model. The versatility of FEA permits the consideration of arbitrary geometry, constraints and loads to rapidly find a reasonable approximate solution to a complicated problem given appropriate modelling and loading. FEA is performed as follows:

- formulation of the problem using the FE model properties;
- application of boundary conditions and the selected load cases;
- determination of the system response in the displacement field.

The FEA problem is formed through the creation of the global system matrices using the properties of the FE model. These matrices describe the stiffness, mass and damping properties of the system. The stiffness and mass matrices are determined by firstly calculating the corresponding matrices for

each individual element. This results in pairs of matrices within the local coordinate systems of the corresponding elements. These matrices are transformed into the global coordinate system of the FE model and positioned within the global stiffness and mass matrices. The damping matrix is approximated for the global system using Rayleigh damping, which includes the requirement to solve the eigenvalue problem to find the Rayleigh damping coefficients. The theory supporting the creation of these system matrices is provided in Appendix B.1.

Boundary conditions are applied to the model by fixing the lifting surface spar roots in all DoFs, the theory behind which is contained in Appendix B.2. The nodes of floor beam elements connected to lifting surface spars are fixed to prevent the transmission of lifting surface loads into fuselage not strengthened to withstand such loads. These boundary conditions simulate the carrythrough structure of the lifting surfaces discussed in §5.2.3.2. Symmetric boundary conditions are applied to all nodes on the plane of symmetry to implement the symmetry of the half-model representation of the aircraft.

The magnitude, direction and distribution of the applied excitation is defined by the load cases selected during initialisation. Loads are simulated as either static, pseudo-static or linear transient dynamic loads as chosen during initialisation. Point loads are applied directly to the nodal DoFs, as described in Appendix B.3, whereas the nodal load resulting from a pressure load is established through consideration of the surface area surrounding the node at which the pressure is applied, as illustrated in Fig. 5.12. The coverage area of each node is calculated by considering the area surrounding the node, the size of which is determined by the connecting elements. For example, in Fig. 5.12 the pressure load applied to the central node is sum of the loads in each of the four quadrants surrounding the node, $A_{i,1...4}$. The load on each element is distributed between the two element nodes, hence the quadrants are sized such that they extend along half of the length of each element, i.e. $0.5l_{i,j}$ where i is the node number and j the connected element number. Consequently, the load on the central node comprises of the pressure loads within the four surrounding quadrants. A similar process is followed in determining the distribution of self-weight across the aircraft, wherein the mass of the element is distributed equally between its two nodes. The directions of loads are determined through consideration of the load origin. For example, flight manoeuvre loads are applied perpendicularly to the lifting surface chord line whereas cabin pressurisation loads are applied normal to the fuselage skin. Ground loads are applied in the global coordinate system as the load components defined in the airworthiness requirements, as discussed in Appendix A.4.

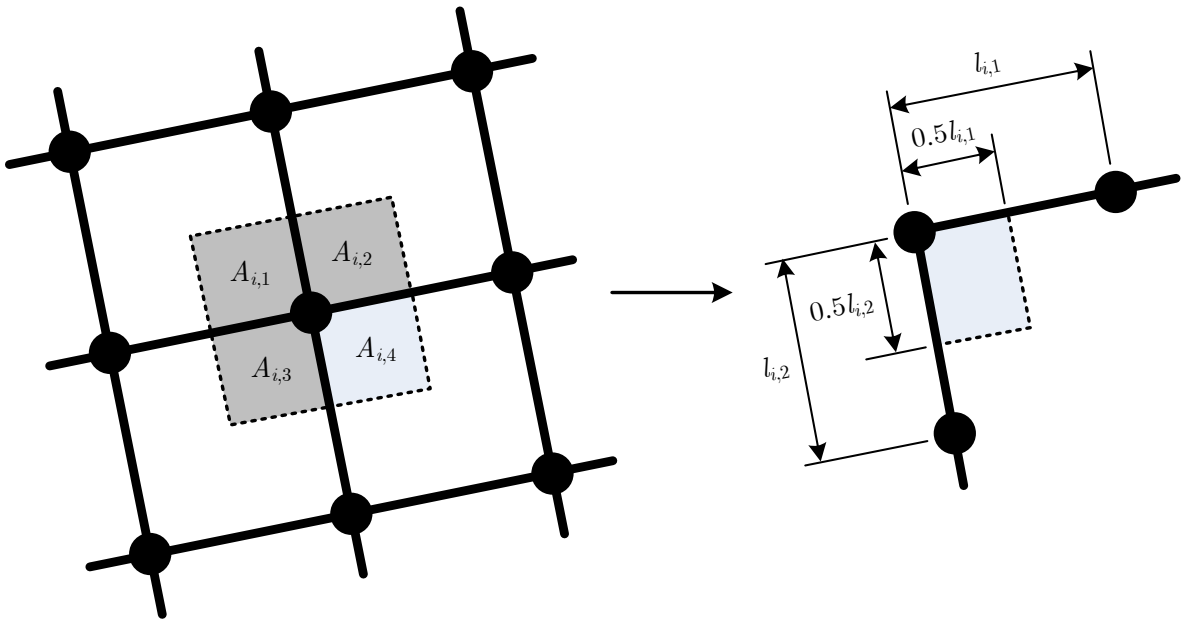

Figure 5.12: Concentration of pressure load at a point

The solution procedure for determining the system response in the displacement field to an applied static, pseudo-static or dynamic load is described in Appendix B.4. The system response to a static load is found using Gaussian elimination with back-substitution to avoid the computationally-intensive task of inverting the stiffness matrix. The transient response to a dynamic load case is approximated over the number of time steps input during initialisation using direct numerical integration by either the central difference, Houbolt, Wilson-θ or Newmark-β method; the choice of which is made during initialisation. The critical time step for finding the dynamic response is calculated during problem formulation, as such the time step size input during initialisation may be reduced if required for stability. The displacements of nodes at the wingtip are stored such that the greatest vertical displacement may be compared against the design constraint for maximum wingtip deflection, C2, as a measure of design feasibility. The responses of individual elements are extrapolated from the global system response through the discretisation of the global system vectors into element vectors. The forces and moments within each element are then calculated using the corresponding equation of motion (EoM). These values are used as inputs to the stress analysis module to establish the minimum FoS within each structural member for comparison against design constraint C1.

5.2.5 Stress Analysis

Analysis of the airframe stress field is performed given the forces and moments output from FEA to find the minimum FoS of each airframe structural member [2.5a]. The minimum FoS is calculated through consideration of the von Mises stress, Euler buckling load and maximum bending stress within a structural member. Prior to this calculation, the forces and moments within each member are recovered from the corresponding values for the FE model elements following the lumping of members within elements during model generation. Established theory supporting this stress analysis is provided in Appendix A.6.

5.2.5.1 Recovery of Member Response

The generation of the FE model in §5.2.3 grouped structural members together within elements leading to smeared mechanical properties. Therefore, the forces and moments within each member lumped within an element must be recovered from the element results prior to stress analysis of the members. This is accomplished individually for each DoF of the member excitation whilst assuming equal behaviours of grouped members. Specifically, the axial force of members grouped within an element is recovered by assuming equal extension of all members in the element. Similarly, the bending moments are recovered by assuming equal slope, the shear forces by assuming equal angles of shear, and torsion by assuming equal twist of all element members. Consequently, the force in the jth DoF of the ith member within the eth element is determined as

$$f_j^i = \frac{f_j^e}{\sum_{k=1}^{n_{mem}^e} \frac{\gamma_j^i}{\gamma_j^k}} \tag{5.8}$$

where γ_j^i denotes the ith element member distribution factor in the jth DoF. The element member distribution factor represents assumptions made of the proportional response of members within an element. These factors are derived by considering the mechanics of the assumptions made by the coupled responses of element members in terms of displacement and rotation within each DoF (Young et al., 2012). For example, the axial force of the element equates to the cumulative axial force of all members grouped within the element

$$f_x^e = \sum_{k=1}^{n_{mem}^e} f_x^k \tag{5.9}$$

Given Hooke's law and by assuming equal axial extension, d_x^e, of all members contained within the

element, the axial force in the element can be written as

$$f_x^e = \sum_{k=1}^{n_{mem}^e} \frac{E^k A^k}{l^k} d_x^e \tag{5.10}$$

where $d_x^e = d_x^k$ for $k = 1, 2, \ldots, n_{mem}^e$

The member distribution factor is substituted into Eqns. (5.9) and (5.10) to lead to the following expression for the first element member, i.e. $i = 1$, by denoting this DoF as $j = 1$

$$f_x^e = \left\{ 1 + \frac{\gamma_1^1}{\gamma_1^2} + \frac{\gamma_1^1}{\gamma_1^3} + \cdots + \frac{\gamma_1^1}{\gamma_1^{n_{mem}^e}} \right\} f_x^1 \tag{5.11}$$

where $\gamma_1^k = \dfrac{l^k}{E^k A^k}$ for $k = 2, 3, \ldots, n_{mem}^e$

Equation (5.8) is subsequently obtained by simplifying and rearranging Eqn. (5.11). Similar expressions are derived for shear, torsion and bending to permit the forces and moments within a structural member to be recovered from the corresponding values for an element, i.e. for the ith element member

$$\gamma_j^i = \begin{cases} \dfrac{l^i}{E^i A^i} & \text{for axial force, } f_x \ (j = 1), \text{ assuming equal extension} \\ \dfrac{l^i}{G^i A^i} & \text{for shear force, } f_y \ (j = 2), \text{ assuming equal shear angle} \\ \dfrac{l^i}{G^i A^i} & \text{for shear force, } f_z \ (j = 3), \text{ assuming equal shear angle} \\ \dfrac{l^i}{G^i J^i} & \text{for torsional moment, } m_x \ (j = 4), \text{ assuming equal twist} \\ \dfrac{l^i}{E^i I_{yy}^i} & \text{for bending moment, } m_y \ (j = 5), \text{ assuming equal slope} \\ \dfrac{l^i}{E^i I_{zz}^i} & \text{for bending moment, } m_z \ (j = 6), \text{ assuming equal slope} \end{cases} \tag{5.12}$$

5.2.5.2 Factor of Safety

Stress analysis establishes the stress field in each airframe structural member given the forces and moments recovered during the previous task. This leads to the calculation of the minimum FoS against three potential causes of failure commonly considered during airframe design (Howe, 2004):

- violation of the von Mises yield criterion;
- exceeding critical Euler buckling stress;
- yield of slender members due to bending.

Violation of the von Mises criterion is considered by calculating the principal stresses within a member, as found using the stress tensor. This is performed at the various points on the member cross-section that generate the greatest values of the stress components. For example, the evaluation points on an I-section member are shown in Fig. 5.13 as these generate the greatest normal and shear stresses in the local x, y and z-directions. The normal tensile or compressive stress is constant across the cross-section, whilst bending stresses are greatest at the extreme fibres of the section. The torsional shear stress is dependent on the enclosed section area at the evaluation point, whilst the transverse shear stresses are greatest at the section neutral axes. The calculation of these stresses is performed using well-established formulae, as described in Appendix A.6.1. Analysis is performed of the stress tensor against the von Mises yield criterion to determine the point on the cross-section at which the lowest FoS against yield exists.

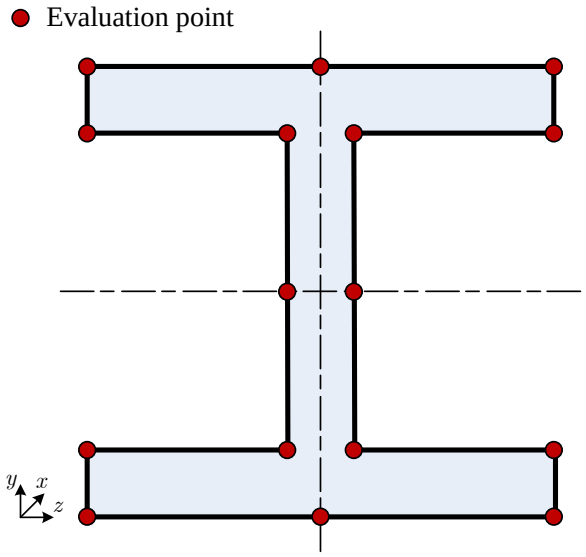

Figure 5.13: I-section stress analysis evaluation points

The second failure cause considered is the buckling of thin members under applied or transmitted compressive loads. Stringers, frames and floor beams, including horizontal, vertical and longitudinal beams, are scrutinised due to their roles in supporting the skin or floor against such failure under pressure loads. This failure cause is analysed by comparing the compressive loads within each member against the critical Euler buckling load at the onset of the first buckling mode. The established theory behind this calculation is provided in Appendix A.6.2. The Euler buckling load is determined by considering the member as a simply-supported pin-ended strut constrained against lateral translation under compression. This is a pessimistic assumption as these members possess freedom for translation, but is required for such analysis. The critical buckling load and stress are subsequently calculated, leading to the determination of the member FoS against buckling through consideration of the axial compressive load on the member. It should be noted that the Euler buckling formula is only applicable to struts with high slenderness ratios, i.e. members with lengths much greater than their cross-sections. Stringers, frames and floor beams possess such slenderness, hence the formula is applicable; however, each member is assessed between its intersections with other members, e.g. stringers crossing ribs, where in reality there will be attachments. As a consequence, the assumption of a pinned joint at these intersections may not be realistic, but it is an appropriate idealisation given that such attachments are not always completely rigid and assuming a pin-ended joint rather than a fixed joint is conservative. Spars do not principally provide resistance against buckling, therefore are not subjected to such scrutiny. Ribs are not suitable for such analysis due to their non-uniform cross-section; however, compression of these members is included during consideration of the first failure cause. Further, buckling of the skin is not considered in isolation; although the analysis of the stringers does include the lumped skin properties within the members.

The final failure cause that is assessed is the potential for stringers and floor beams to fail under bending. This is scrutinise the roles of these slender members in supporting the skin and floor against pressure loads. The maximum normal stress due to bending is calculated by representing members as simply-supported beams under pressure loads applied due to flight loads, cabin pressurisation and payload mass. This end condition is appropriate as it permits longitudinal translation and rotation of the member ends, whilst transverse translation is not considered during this analysis. The maximum bending stress for the simply-supported beam is then compared against the member material yield stress and the resulting FoS calculated, as is described in Appendix A.6.3.

The stress analysis module outputs the minimum FoS within each structural member, and the airframe as a whole, in order to record the most onerous loads on the structure and calculate the feasibility of the design solution. This value is calculated as the minimum value of FoS from the three considered potential causes of structural member failure

$$n_{\min} = \min\left(n_{VM}, n_E, n_b\right) \tag{5.13}$$

where n_b FoS against yield under beam bending stress, $n_b = \infty$ if rib, spar or frame
n_E FoS against critical Euler buckling stress, $n_E = \infty$ if rib or spar
n_{VM} FoS against yield with respect to von Mises criterion

5.3 Airframe Design Optimisation

The aircraft structural designs are optimised for a solution of minimal structural mass. This is performed subject to the design constraints to ensure adequate structural performance. Each design is optimised using an LLH chosen from the heuristic set by the embedded HHA. The HHA performs heuristic selection and population distribution to increase the likelihood that well-performing LLHs are employed to optimise solutions. Perturbation analysis is additionally performed by the HHA to evaluate the solution space surrounding improved designs. Parameter control is also incorporated within the HHA to control the set-up of the optimisation process and model fidelity, such that solution quality, optimisation process performance, and computation speed may be improved. Termination criteria are included to enable cessation of the optimisation process and the output of data for post-processing outside of the framework.

5.3.1 Population Feasibility

A penalty function is employed to discourage convergence on a design that lies outside the feasible region of the solution space by penalising the objective values of infeasible solutions in proportion to the degree of constraint violation [3.1a]. A penalising strategy is chosen over a rejection or repairing strategy due to the former not considering potentially beneficial characteristics of infeasible solutions and the latter relying on an appropriately designed repair procedure, as discussed in §2.4. The feasibility of each individual structural design solution is determined by comparing the minimum FoS within the airframe and maximum wingtip deflection calculated during structural analysis against the corresponding design constraints. Recalling the optimisation problem objective function in Eqn. (4.1)

$$\min\left(\Phi(\mathrm{X}^k)\right) \text{ for } k = 1, 2, \ldots, n_k$$

This objective value is initially calculated for the ith structural design as the unpenalised objective value of the aircraft structural mass, as recalled from Eqn. (5.5)

$$f_i(\mathrm{X}^k) = m_{i,str} = \sum_{s=1}^{n_{i,mem}} m_s$$

The penalised objective value is obtained by applying a penalty function to the unpenalised objective function. Specifically, the penalised objective value is calculated as follows by recalling Eqn. (2.9)

$$\Phi_i(\mathrm{X}^k) = f_i(\mathrm{X}^k)\left\{1 + \lambda \sum_{j=1}^{m} \max\left[0, g_{i,j}(\mathrm{X}^k)\right]^{\alpha}\right\}$$

The magnitude of penalty is dependent on the feasibility of each design as measured against the design constraints, as was discussed in §2.4. The feasibility of an airframe design is determined by calculating

the magnitudes of the violations of constraint C1 by all structural members within the design, in addition to the magnitude of violation of C2 as a result of the wingtip deflection under load. The feasibility of the ith individual with respect to the jth design constraint is calculated as follows, where $n_{s,\min}$ denotes the minimum FoS within the sth structural member and $d_{i,y_{\max,wt}}$ represents the maximum wingtip vertical deflection by the ith individual design

$$g_{i,j}(\mathrm{X}^k) = \begin{cases} \sum_{s=1}^{n_{i,mem}} n_{s,\min} - c_j & \text{for the minimum FoS within the airframe members, } j = 1 \\ \left|d_{i,y_{\max,wt}}\right| - |c_j| & \text{for the maximum magnitude of wingtip deflection, } j = 2 \end{cases} \tag{5.14}$$

The framework employs either the death, interior or exterior penalty function as selected and set up during initialisation, i.e. Eqns. (2.6), (2.7) or (2.9) respectively. These penalty functions are selected as they are commonly applied to similar optimisation problems, as reported in §2.4.4. Additionally, the penalty function chosen may be employed as a scaled penalty function, i.e. as in Eqn. (2.10), or as an adaptive penalty function, i.e. as given by Eqn. (2.11), to vary the penalty coefficient over time, i.e. as λ^k. However, the adaptive function within the framework is a development of that of Bean and Hadj-Alouane (1992) by placing greater consideration on population feasibility rather than the feasibility of solely the best solution. This encourages the convergence on a highly-feasible population of design solutions through relaxation of the penalty for such populations, thus permitting greater exploration within the feasible solution space, but discourages highly-infeasible populations though applying pressure to such populations to reject infeasible solutions. The adaptive penalty coefficient is given as follows, where $\beta(\mathrm{X}^k)$ denotes feasible percentage of the population set at kth generation

$$\lambda^k = \begin{cases} \dfrac{\lambda^{k-1}}{\beta_1} & \text{if } \beta(\mathrm{X}^{k-1}) > 80\% \\ \beta_2 \lambda^{k-1} & \text{if } \beta(\mathrm{X}^{k-1}) < 20\% \\ \lambda^{k-1} & \text{otherwise} \end{cases} \tag{5.15}$$

The thresholds for changing the penalty coefficient of 20% and 80% are selected such that the penalty coefficient is most likely to remain constant during early generations prior to convergence. Thus, the adaptive penalty coefficient is only intended to affect the search during convergence if the population is highly feasible or infeasible. This avoids excessive interference with the optimisation search, but provides incentives towards exploration closer to the constraint boundaries if the population is converging to be highly-feasible or within the feasible solution space if the population is highly-infeasible.

5.3.2 Population Fitness

The fitness of structural design solutions is calculated for use by genetic algorithms (GAs) if selected for employment as LLHs within the problem domain [3.2a]. Fitness is commonly measured by ranking the population in order of objective value before assigning a fitness value to each rank (Fan et al., 2004; Sadjadi, 2004). The population set is sorted in descending order of objective value before calculating the proportional rank of each individual solution. Thus, high ranks are assigned to better solutions, i.e. the individual of lowest mass is assigned the first rank whereas the individual of highest mass is assigned the rank μ. Thus, the ith individual fitness is calculated as follows, where $\tau(\Phi_i(\mathrm{X}^k))$ represents the objective value ranking of the ith individual at kth generation

$$F_i(\mathrm{X}^k) = \frac{\mu - \tau(\Phi_i(\mathrm{X}^k)) + 1}{\sum_{j=1}^{\mu} \tau(\Phi_j(\mathrm{X}^k))} \tag{5.16}$$

$$\text{where} \quad F_i(\mathrm{X}^k) \quad = \begin{cases} \dfrac{\mu}{\sum_{j=1}^{\mu} \tau(\Phi_j(\mathrm{X}^k))} & \text{for best solution in population set X} \\ \dfrac{1}{\sum_{j=1}^{\mu} \tau(\Phi_j(\mathrm{X}^k))} & \text{for worst solution in population set X} \end{cases}$$

This rank-based fitness function is chosen as it is problem-independent, and thus does not unduly influence the characteristics of the optimisation search. This latter decision was made to ensure the HHA possesses control of the optimisation process. Furthermore, search diversity is maintained by using the rank of individuals rather than objective function value.

5.3.3 Termination Criteria

Termination criteria are checked prior to optimisation to permit the cessation of the optimisation process if a further improvement in the best solution is unlikely [3.3a]. These criteria are defined during initialisation and consist of the following:

- maximum number of generations;
- maximum number of consecutive generations without improvement of the best solution;
- maximum population affinity.

The limit on the maximum number of optimisation generations, n_k, prevents the process from running indefinitely. This value is input during initialisation by considering the population size, to ensure an adequate number of individual solutions are considered, and the time available to solve the optimisation problem. Termination as a result of exceeding the maximum number of successive generations without improvement in the best solution prevents the search from continuing excessively when it is unlikely a better solution will be found, i.e. following search stagnation. The maximum limit on population affinity enables the process to terminate if the population has converged. Termination at this point is beneficial to save computational effort as the converged population is unlikely to improve the solution. Population affinity is based on bit-string affinity (BSA) presented in Raymer (2002), as described in §2.3.5, and is measured as the mean affinity of design variables across the population

$$A(\mathrm{X})^k = \frac{1}{n_v} \sum_{v=1}^{n_v} A_v(\mathrm{X})^k \tag{5.17}$$

where $A_v(\mathrm{X})^k$ denotes the affinity, as a percentage, of the vth variable over population set at the kth generation. The affinity of each design variable is calculated by comparing the value of the variable possessed by one individual within the population set against the corresponding values of all other individuals within the population. The total number of matching values is then recorded for the individual. For a discrete variable, a match is recorded if the values for the two individuals are identical. For a continuous variable, a match is identified if the variable values possessed by the two individuals are within 2% of the variable range, $\Delta\mathrm{V}$. This value is selected in accordance with the design of BSA in Raymer (2002), wherein a population of binary chromosomes was deemed to have converged if the population affinity exceeded 98%. The affinity of the vth variable at the kth generation is expressed as

$$A_v(\mathrm{X})^k = \sum_{i=1}^{\mu-1} \frac{1}{\mu - i} \sum_{j=i+1}^{\mu} A_{v,i,j} \tag{5.18}$$

$$\text{where} \quad A_{v,i,j} = \begin{cases} 1 & \text{if } x_{i,v} = x_{j,v} \text{ and } v\text{th variable discrete} \\ 1 & \text{if } \dfrac{|x_{i,v} - x_{j,v}|}{\Delta \mathrm{V}_v} < 2\% \text{ and } v\text{th variable continuous} \\ 0 & \text{otherwise} \end{cases}$$

The affinity of categorical variables, i.e. V21 to V25 and V48 to V50 defining member cross-sections and materials, is measured by assigning each discrete possible value of the variable a numeric value. For example, the variables representing structural member cross-sections are assigned the following values:

1. C-section;
2. I-section;
3. T-section;
4. Z-section.

Materials are similarly assigned a discrete numeric value, the values of which depend on the number of materials input to the materials database during initialisation. This permits the affinities of the variables to be measured and thus contribute to the overall population affinity. If no termination criterion is satisfied, the optimisation process continues for another generation.

5.3.4 Hyper-Heuristic Approach

A hyper-heuristic approach (HHA) is embedded within the framework to encourage improved solution quality and process performance over traditional optimisation. The HHA includes the following four aspects of hyper-heuristic optimisation:

1. heuristic selection: employment of appropriate LLH for use in the problem domain;
2. population distribution: allocation of population individuals to multiple LLHs;
3. perturbation analysis: local solution space learning around a sample of design solutions;
4. parameter control: adaptation of process parameters to promote improved optimisation.

The HHA operates for each optimisation generation as follows. Improvements in the quality of the current best solution are identified [3.4a] leading to perturbation analysis through the sampling of the solution space [3.4b]. Heuristic selection chooses the local search (LS) hyper-heuristics to perturb the sampled solutions [3.4c] before the sampled population is distributed between the chosen heuristics [3.4d]. This leads to optimisation and repeated analysis of the perturbed solutions. When no improvement is made in solution quality or perturbation analysis has been completed, the performance of the optimisation process is measured using an online reinforcement learning mechanism [3.4e]. A decision is subsequently made whether to adapt the optimisation process based on the output of this learning mechanism [3.4f], with parameter control performed if it is deemed necessary to adapt the process [3.4g]. Heuristic selection and population distribution are then performed to select and assign the LLHs for optimisation of the population during the next generation, i.e. [3.4c] and [3.4d] once more. The decision made by the learning mechanism as to whether to modify the optimisation process is based on the rules of the hyper-heuristics employed and the evaluation period set during initialisation to allow sufficient generations for changes in the optimisation process to take effect within the problem domain.

Heuristic generation is not included within the HHA because, as discussed in §3.2, this aspect consists of the creation of a new LLH for application to a specific problem or for general use with similar problems. The new LLH is formed of components of existing LLHs, requiring the decomposition and evaluation of the different LLH components. This is computationally expensive, whilst the appropriate decomposition and generation of LLHs can be difficult when needing to be applied to various configurations of complex optimisation problems such as aerospace design. Furthermore, heuristic selection includes only perturbative heuristics, and not constructive heuristics, as these are representative of the optimisation

techniques traditionally employed for aerospace design optimisation. Such heuristics evolve an initial solution through the perturbation of variables towards a final solution. Conversely, constructive heuristics create a solution from an empty initial solution by applying problem-specific LLHs to the problem to evaluate the best technique for different problem states. Such problem-specific LLHs were not employed within the existing approaches discussed in §2.3. Moreover, an objective of using the framework for this research project is to evaluate whether employing hyper-heuristics can improve solution quality compared to traditional optimisation. Therefore, it is appropriate to use the same LLHs within the framework as those employed traditionally, thus rendering the use of heuristic generation and constructive heuristics within the HHA as inappropriate for such an evaluation.

As operation of the HHA precedes optimisation of the population, references are made to the LLHs before they are described. These descriptions of individual LLHs are presented in §5.3.5, including the introduction of a novel GA selection method within the framework: radioactive contamination (RC). Furthermore, the descriptions of heuristic selection and population distribution are presented prior to perturbation analysis, although they follow this HHA aspect within Fig. 5.1, as these aspects are used during perturbation analysis to select the memetic algorithms (MAs) for application.

5.3.4.1 Heuristic Selection

Heuristic selection enables the different LLHs, listed in Table A.6, to be employed during the optimisation process to reduce the likelihood that limitations of individual techniques will hinder the search for a near-optimal solution. For example, a convergence-encouraging LLH such as an LS technique could promote convergence prematurely during the search, but would be desired to encourage such convergence towards the end of the process. A hyper-heuristic is employed to select an LLH from the heuristic set. Heuristic selection is performed whenever perturbation analysis is conducted to choose the hyper-heuristic to optimise the sampled population. Heuristic selection is also performed every Δk generations during the optimisation process, where Δk denotes the period over which attempted improvements in optimisation process performance are monitored by the learning mechanism. This period is referred to as the hyper-heuristic evaluation period. The heuristic selection hyper-heuristics listed in Table A.6 include:

- simple random (SR): random LLH selection;
- random descent (RD): SR selection with LLH application until no further improvement made;
- permutation (PE): selection of LLH from randomly-ordered list;
- permutation descent (PD): PE selection with LLH application until no further improvement made;
- greedy (GR): selection of best-performing LLH;
- peckish (PK): random LLH selection from best n_{PK} LLHs;
- roulette wheel (RW): selection of LLH using a roulette wheel;
- tournament selection (TO): selection of LLH following a competition of fitness.

The operation of these hyper-heuristics is described in §3.2.1. The LLH selected by the hyper-heuristic optimises the population over the hyper-heuristic evaluation period of generations. Move acceptance rules are applied mid-way through this period to determine whether the LLH should continue for the rest of the period or be rejected. Rejection leads to repeated heuristic selection for a replacement LLH. Move acceptance is performed using one of the following rules:

- all moves (AM): permit positive and negative moves;
- improving and equal (IE): permit non-negative moves only;
- simulated annealing (SA): permit positive moves and probabilistically permit negative moves;
- exponential Monte Carlo with counter (EMCQ): permit positive and probabilistically permit negative moves.

These rules of move acceptance are selected in accordance with the results of studies into the performances of the rules by Bilgin et al. (2007), Cowling et al. (2001), Drake et al. (2012) and Özcan et al. (2008) discussed in §3.6. Descriptions of these move acceptance rules are provided in §3.2.2, where the HHA uses the same values for the EMCQ constants as those evaluated as providing best performance during the experimental studies of Ayob and Kendall (2003).

The learning mechanism determines whether an improvement has been made using a newly-selected LLH through the measure of improvement (MoI) criterion. The MoI criterion employed by the HHA within the framework is the hyper-heuristic objective function given by Eqn. (4.3). Each LLH possess an individual value of the hyper-heuristic objective function, the value of which determines the likelihood of selection by the hyper-heuristic. Consequently, the hyper-heuristic objective function in Eqn. (4.3) may be rewritten as follows for the hth LLH

$$\max\left(\phi_h^k\right) \text{ for } k = 1, 2, \ldots, n_k \tag{5.19}$$

The value of this function is defined in §5.3.4.4 with reference to the manner in which this function encourages such process behaviour during parameter control. A tabu tenure may be incorporated within heuristic selection to prevent the reselection of a poorly-performing LLH. The tabu tenure, based on that developed by Han and Kendall (2003), counts the number of successive generations over which a selected LLH fails to improve the MoI criterion compared to the criterion value at the generation preceding the selection of the LLH. The tenure is reset to zero whenever the LLH generates an improvement in the criterion. This enables the HHA to learn as to which techniques are improving the process and further reduce the likelihood that a poorly-performing LLH will be selected. The tabu tenure approach is employed using one of the following methods chosen during initialisation:

- tabu list assistance;
- MoI penalisation.

Tabu list assistance prevents the selection of an LLH for a pre-determined number of heuristic selection occurrences if it fails to improve the MoI criterion, i.e the LLH is added to a tabu list, as was performed by Han and Kendall (2003). MoI penalisation uses the tabu tenure to apply a penalty to the MoI in a similar manner to an exterior penalty function within the problem domain. Consequently, the penalised hyper-heuristic objective value associated with the hth LLH is calculated as

$$\hat{\phi_h^k} = \frac{\phi_h^k}{Q_{h,ni}} \tag{5.20}$$

The tabu tenure, $Q_{h,ni}$ for the hth LLH, is decremented over each generation for which the LLH is not employed to discourage immediate use of poorly-performing LLHs but permit the techniques to be employed at later generations once the tabu tenure has reduced to zero. In the event that all LLHs in the heuristic set possess a non-zero tabu tenure, i.e. no techniques improved the MoI criterion when last applied, the tenures of all heuristics are decremented until at least one LLH possess no tabu tenure.

When using the GR, PK, RW or TO hyper-heuristics, all LLHs are applied during early generations such that a measure of performance may been obtained for each before beginning MoI-based selection. Heuristic selection is also employed in conjunction with population distribution and perturbation analysis. The former involves the selection of numerous LLHs to be employed during each generation, whilst the latter encompasses the selection of an LS hyper-heuristic to perturb individual solutions.

5.3.4.2 Population Distribution

Population distribution permits multiple LLHs to be employed concurrently during the optimisation of the population in order to overcome the limitations of individual techniques and better explore the

solution space. During a given generation, each LLH optimises the solutions contained within the LLH sub-population. A sub-population is optimised in isolation from all other sub-populations, leading to the independent search by LLHs in the periods between population distribution. This period between distributions is the same as that for heuristic selection described in §5.3.4.1, i.e. Δk. When a single-solution LLH is employed, i.e. an LS technique, sub-population individuals are optimised independently of all others to maintain the characteristic of the technique. The distribution of a population may be performed using one of two methods, the choice of which is made during initialisation:

- even: the population set is distributed evenly between all LLHs;
- heuristic: heuristic selection is used to choose an LLH to optimise each individual.

Even distribution ensures all LLHs are allocated the same number of individuals to permit each LLH an equal opportunity to improve the population. If the population size is not divisible by the number of LLHs, each remaining individual is allocated to a random LLH with the condition that each LLH may only receive one additional individual. This ensures the population is distributed as evenly as possible. Heuristic distribution couples population distribution with heuristic selection, resulting in the selection of an individual LLH for each population individual. The individuals assigned with the same LLH form the sub-population for that LLH. This increases the probability that better-performing LLHs receive a larger proportion of the population for sub-population optimisation, thus increasing the likelihood of an improvement in the current solution. Such heuristic population distribution reduces to a random distribution if the SR hyper-heuristic is employed. The initial population is always evenly-distributed between the available LLHs unless the SR hyper-heuristic is employed. Sub-population sizes are adjusted if required to ensure that a sufficient number of individuals are present for the LLH to function

$$\mu_{sub} \geq \begin{cases} 4 & \text{for TO: four candidates for tournament} \\ 4 & \text{for DE: three agents plus evolving individual} \\ \dfrac{2}{\alpha_{BP}} & \text{for BP: two parents from breeder pool for crossover} \\ 2 & \text{for RW, RC: two parents for crossover} \\ \dfrac{1}{\alpha_{RI}} & \text{for RI: one individual from indigenous population} \\ 1 & \text{otherwise} \end{cases} \tag{5.21}$$

The maximum number of different LLHs to be employed during each generation is set during initialisation to prevent too many LLHs being employed with inadequately small sub-populations for effective optimisation. A dynamic population size, similar to that of Arabas et al. (1994), can be chosen during initialisation such that the sizes of sub-populations are limited to prevent LLH domination. Within the framework, sub-populations exceeding this limit are reduced through the random rejection of individuals. If population distribution then leads to all sub-population sizes falling below the limit, randomly-generated individuals are injected into the population until either all sub-populations or the total population set reaches their respective maximum limits. Random rejection and insertion of individuals preserves population diversity and prevents search bias, e.g. if the poorest solutions were rejected and good solutions replicated for insertion.

5.3.4.3 Perturbation Analysis

Perturbation analysis is performed to encourage learning of the solution space neighbouring a sample of individuals, thus encouraging the optimisation search to be better directed towards promising regions. An LS technique perturbs selected individuals in an attempt to make further improvements in their objective value. This occurs at every generation at which a better design is obtained in the population set than the current best solution, i.e. the best design found during preceding generations. This analysis frequency

is chosen over analysis after each generation to avoid substantially increasing the computational cost of such analysis. Avoidance of incurring such computational costs through the use of hyper-heuristics is key to supporting the thesis discussed in §1.3. The population set is sampled either randomly or based on fitness, the method and sample size of which is chosen during initialisation. Each individual selected for perturbation analysis has a random number of variables perturbed by the LS hyper-heuristic, leading to the structural analysis of the perturbed solution. Acceptance or rejection of the perturbed solution is based on the rules of the hyper-heuristic employed. Hill climbing (HC), simulated annealing (SA) and tabu search (TS) are the hyper-heuristics used to perform the MA local search, the selection of which is made by heuristic selection and population distribution over the sampled population. As is described in §3.4, perturbation analysis includes the following criteria which are defined during initialisation:

- evolution: Lamarckian or Baldwinian;
- sample size, μ_{PA}: single solution or proportion of population set;
- perturbation scale, $\Delta x_{v,PA}$: size of step made by hyper-heuristic.

Acceptance of a perturbed solution through Lamarckian evolution leads to the replacement of the unperturbed individual with the perturbed design, whereas Baldwinian evolution keeps the unperturbed solution but replaces its objective value with that of the perturbed individual. Population individuals are either sampled randomly or from the best μ_{PA} individuals within the population set. A larger sample size increases the probability of improving the population through perturbation analysis. However, this also increases the number of individuals requiring structural analysis, which will lead to an increase in computation time. The perturbation scale determines the size of step taken in the solution space when perturbing an individual. This step size should be smaller than that used by the LS techniques as LLHs during principal design optimisation to maintain the nature of this analysis as only perturbing solutions, not exploring larger areas of the solution space. No set-up of perturbation analysis was discovered during the review presented in §3.6 that outperformed all others, hence flexibility is permitted in the settings of perturbation analysis within the framework. The perturbation analysis of each individual continues through repeated perturbations until no further improvement is made in the solution quality.

5.3.4.4 Parameter Control

Parameter control modifies the values of the process parameters to encourage specific behaviour within the optimisation search. Such behaviour includes:

- solution space exploration to prevent premature convergence on local optima;
- improved convergence on the best solution obtained;
- avoidance of convergence on an infeasible solution;
- focus on critical variables failing to converge;
- reduction of computation expense.

Table 5.4 lists the parameters controlled by the HHA to encourage such process behaviour. Parameter P1 defines the level of FE model fidelity employed during structural analysis. This parameter is controlled to promote the use of a low-fidelity model during early optimisation generations prior to a higher-fidelity model towards the end of the process. This enables early designs to be analysed rapidly before more detailed analysis of designs neighbouring the best solution obtained. Early generations of optimisation prior to population convergence are more likely to include greater population diversity. This is likely to lead to designs possessing many structural members, and thus many DoFs, as the population will not have converged on a solution of low mass, i.e. one likely to possess fewer members. The required computational time for FEA of such designs is reduced by using a low-fidelity model. More detailed analysis is then encouraged of lighter designs, i.e. those likely to possess fewer DoFs, as the search converges upon the best solution. This can lead to further design improvements and the output of more detailed FEA results for

post-processing. Parameter P2 is the penalty function coefficient which is modified by the HHA as defined in Eqn. (5.15). This increases the penalty applied to populations possessing many infeasible solutions and relaxes the penalisation of populations that are highly-feasible, i.e. containing many feasible solutions. This control of parameter P2 is different from that of all other dynamically-controlled parameters due to the existence of this specific rule to control the parameter, i.e. Eqn. (5.15).

Parameters P3 to P18 are operators of the LLHs within the heuristic set that are defined to encourage either solution space exploration or convergence upon the current best solution. The effects of this control are established through consideration of the design of these optimisation techniques, as described in §2.3 and §5.3.5. Binary chromosome strand length, P3, is defined independently for each design variable to enable the shortening of converged variable strands and lengthening of variables failing to converge. The RI indigenous population size, P4, is reduced to encourage exploration by increasing the population diversity or increased to encourage convergence through the reduction of such diversity. The DE crossover probability and differential weight, P5 and P6 respectively, are increased to provide greater influences of agents on individuals, and thus encourage exploration, or reduced to promote the opposite. The number of GA points and GA crossover and mutation probabilities, P7, P8 and P9 respectively, are increased for greater population diversity and subsequent exploration or reduced to promote convergence. The BP intake, P10, is increased for greater exploration by considering more parent candidates or, conversely, reduced for convergence. Similarly, the RC contaminated population, P11, is increased or greater population diversity and subsequent exploration by encouraging mutation of the population, but is reduced for population convergence through reduced mutation. This novel LLH is described in detail in §5.3.5.3. The PSO parameters, P12 to P15, are modified to encourage exploration by increasing the inertia weight and cognitive parameter and decreasing the social parameter and constriction constant. Convergence is encouraged by adapting these parameters in the opposite manner. Parameter P16 defines the step size made by LS LLHs, where increases in its value leads to larger steps to prevent search stagnation due to plateaux or by being restricted to a small area of the solution space. Conversely, the parameter is reduced for smaller steps to promote convergence. A high value of P17, the SA cooling rate, reduces the probability of accepting a negative move and thus promotes convergence, whereas a low value encourages the opposite. Finally, the tabu list length, P18, is extended to promote convergence by limiting moves away from the local solution space, whilst the reverse is performed for exploration.

All parameters except P3, the binary chromosome strand length of design variables, are optimised by the hyper-heuristic without bias in the step direction. The direction of the step made in parameter P3 for each variable is determined based on the affinity of the variable. This parameter enables the HHA to refine the resolution at which each design variable may be optimised. This encourages the strand lengths to be increased for variables failing to converge, thus permitting greater resolution in the optimisation of these variables, and reduced for variables that are converging to allow the optimisation process to focus on the variables yet to converge. The step direction of P3 is biased to encourage this behaviour based on the affinity of the variable measured across the population set using Eqn. (5.18). The hyper-heuristic makes a step to shorten the strand length of converging variables with affinities greater than the population affinity measured in Eqn. (5.17), i.e. the mean for all variables, whilst making a step to lengthen the strand length of variables with affinities less than average. Reducing the strand length of converging variables can prevent optimisation at greater resolution of these variables, which in turn could prevent improvements being made through these variables. However, such improvements are likely to be small given that the variables have almost converged based on their high affinities. The strand lengths of the eight categorical variables, i.e. V21 to V25 and V48 to V50 defining member cross-sections and materials, remain constant throughout the process and are not affected by P3. This is because increments or decrements in the values of these variables can cause dramatic changes in solution quality through their effect on the design mechanical properties, e.g. abrupt changes in material grades. Consequently, there

are $n_v - 8$ values of P3 to define the strand lengths of the $n_v - 8$ controlled numerical design variables.

The perturbed values of parameters are accepted if an improvement is measured by a hyper-heuristic objective function or if the hyper-heuristic employed permits a negative move, e.g. when using the SA hyper-heuristic. The hyper-heuristic objective function considers the five following criteria:

1. objective value of best solution;
2. mean objective value;
3. mean population affinity;
4. mean convergence rate;
5. computation time.

These criteria are selected to encourage process behaviour that is likely to result in a higher quality solution without incurring computational cost, i.e. as hypothesised in §1.3. The first two components aim to improve the quality of the best solution and the average quality of the population. The next two components aim to prevent premature convergence by encouraging early solution space exploration prior to the opposite towards the end of the process. The final component aims to minimise the computation time required by the process. These criteria are selected such that the hyper-heuristic objective function is similarly-designed to the choice function of Drake et al. (2012), given in Eqn. (3.6), which was found to perform well during the studies reviewed in §3.6. However, the hyper-heuristic objective function presented herein gives greater consideration to aspects of process performance other than solution quality and computation time. Moreover, this function is employed for parameter control as well as heuristic selection, whereas the choice function was employed solely for heuristic selection. The choice function of Drake et al. (2012) was chosen over the original function of Cowling et al. (2000) as the basis for this function herein given that the former was found outperform the latter within the literature. Furthermore, the modified choice function employs component weights that adapt dynamically during the search based on the performance of the HHA rather that static weights that require tuning pre-optimisation.

The hyper-heuristic objective function utilises positive reinforcement learning to reward changes to the process that improve its performance as measured by the five criteria of the function. The objective values are measured using Eqn. (4.1), leading to the determination of the best solution objective value and the mean value across the population. Population affinity is measured using Eqn. (5.17). The population convergence rate represents the magnitude of change in objective value, i.e. without distinguishing between a gain or lack of improvement in solution quality, to determine whether the search is stagnating

$$\delta(\mathrm{X})^k = \left|\Phi(\mathrm{X})^k - \Phi(\mathrm{X})^{k-1}\right| \tag{5.22}$$

The hyper-heuristic objective function is defined at the kth generation by recalling Eqn. (4.3)

$$\max\left(\phi^k\right) \text{ for } k = 1, 2, \ldots, n_k$$

The value of this hyper-heuristic objective function is defined at the kth generation as

$$\phi^k = \sum_{f=1}^{5} a_f^k \phi_f^k \tag{5.23}$$

where a_f^k fth normalising coefficient at the kth generation
ϕ_f^k fth hyper-heuristic objective function component at the kth generation

The five aforementioned criteria of optimisation process performance are measured using the five components of the hyper-heuristic objective function, as follows at the kth generation

$$\phi_1^k = \frac{1}{\min \Phi(\mathrm{X})^{\Delta k}} \tag{5.24a}$$

$$\phi_2^k = \frac{1}{\overline{\Phi(\mathrm{X})^{\Delta k}}} \tag{5.24b}$$

$$\phi_3^k = k\overline{A(\mathrm{X})^{\Delta k}} \tag{5.24c}$$

$$\phi_4^k = k\overline{\delta(\mathrm{X})^{\Delta k}} \tag{5.24d}$$

$$\phi_5^k = \left(1 - \frac{k}{n_k}\right)\tau^{\Delta k} \tag{5.24e}$$

where $\tau^{\Delta k}$ denotes the computation time taken over the HHA evaluation period of Δk generations. Components ϕ_1^k and ϕ_2^k promote improvement in the quality of the best solution and population throughout the process. Components ϕ_3^k and ϕ_4^k are weighted to discourage affinity, i.e. population similarity, and convergence during early generations for solution space exploration before promoting these characteristics during later generations. This weighting is based on the position in time, i.e. generation, of the optimisation process to distinguish between early and later generations. Finally, component ϕ_5^k promotes rapid optimisation during early generations by attempting to reduce the computation time taken before encouraging more thorough analysis during later generations. This final component is included principally to control the level of FE model fidelity employed to avoid spending too much time assessing potentially poor solutions at high-fidelity whilst allowing high-fidelity analysis of the better solutions as the population converges on the final solution. The other components are included to principally control the optimisation process parameters. However, due to domain independence, changes in the process parameters are able to influence the other function components in an attempt to improve the overall value of Eqn. (5.23), i.e. changes in optimisation parameters that improve the final component or changes in model fidelity that improve the other four components.

No weighting is applied to the function components other than the generation-based weighting of components ϕ_3^k, ϕ_4^k and ϕ_5^k. This is to provide equal importance of all process characteristics considered within the hyper-heuristic objective function. However, a normalising coefficient, a_f^k, is calculated for the fth component of Eqn. (5.23) at the kth generation to restrict its value to the range

$$0 \leq a_f^k \phi_f^k \leq \frac{1}{5} \tag{5.25}$$

where $\quad a_f^k = \dfrac{1}{5 \max\left(\phi_f^k, \phi_f^{k-\Delta k}\right)}$

The use of such normalisation coefficients enables the values of Eqn. (5.23) to be similarly bound for successive evaluation periods, i.e. ending at generations k and $k - \Delta k$, and thus ensure homogeneity between the hyper-heuristic objective values

$$0 \leq \phi^k, \phi^{k-\Delta k} \leq 1 \tag{5.26}$$

This permits the values of the hyper-heuristic objective function over successive evaluation periods to be compared in order to determine whether an improvement has been made in the process performance, i.e.

if $\phi^k > \phi^{k-\Delta k}$. The new parameter values are accepted if such an improvement is recorded. The previous values of parameters are restored if an improvement is not made by rejecting the modified values, unless the hyper-heuristic used permits a negative move, e.g. SA.

5.3.5 Design Optimisation

Optimisation of each generation of the population set within the problem domain is performed by the selected LLHs to improve the performance of solutions with respect to the objective function of Eqn. (4.1) [3.5a]. This is accomplished through the modification of the values of design variables of individuals within the population set. These individuals are represented by the design genome in either real or binary form as selected during initialisation. The latter employs a binary chromosome to represent each individual solution, which is divided such that each strand of the chromosome represents a design variable. The number of bits in each strand, n_b, is controlled dynamically by the HHA as an individual value of parameter P3 for the variable. The resolution between each strand bit for the vth variable is calculated as follows by considering the number of permutations available within the variable range

$$\delta_{b,v} = \frac{\Delta \mathrm{V}_v}{2^{n_{b,v}} - 1} \tag{5.27}$$

Subsequently, the real number value of the vth design variable represented by the strand is

$$x_v = \mathrm{V}_{v,\min} + \delta_{b,v} \sum_{b=1}^{n_{b,v}} \left\lfloor 2^{n_{b,v}-b} \right\rceil B_b \tag{5.28}$$

where B_b denotes the binary chromosome value for bth bit, i.e. 0 or 1. Discrete variables have a finite number of permutations; therefore, if the number of bit permutations available for the vth variable exceeds than the number of discrete variable permutations, the strand length is reduced to the minimum required to represent all discrete permutations

$$n_{b,v} = \left\lceil \frac{\log \Delta \mathrm{V}_v}{\log 2} \right\rceil \tag{5.29}$$

The optimisation techniques are selected from the LLH set listed in Table A.6 by the HHA. Multiple techniques may be selected for population distribution, in which case each LLH optimises a sub-population of individuals, whilst the values of the LLH operators are determined by the parameter control HHA aspect. The optimisation techniques employed by the framework as LLHs are those commonly employed within the field of aerospace design, as identified in §2.3, and may be categorised as follows:

- random generation;
- evolutionary algorithm (EA);
- genetic algorithm (GA);
- swarm intelligence (SI);
- local search (LS).

The following discussion of optimisation by the different LLHs is formed as if a single technique is being applied to a population for ease of understanding. These descriptions are equally applicable when population distribution is performed; however, the LLH is applied to a sub-population only, thus discussion of the 'population' strictly refers only to the corresponding 'sub-population' in this situation.

5.3.5.1 Random Generation

These techniques randomly generate new values for design variables; consequently, individual solutions do not evolve over optimisation generations. Such techniques enable diversity to be maintained within the population set but are less likely to converge on good solutions. The random search does not consider the quality of previous solutions, therefore it is less likely that a high-quality solution will be obtained

than when employing the other categories of LLHs. The random techniques within the heuristic set are Monte Carlo (MC) and random immigration (RI), and are described in §2.3.1. For RI, parameter P4 defines the indigenous population proportion, α_{RI}, such that the size of the indigenous population is

$$\mu_{RI} = \alpha_{RI}\mu \tag{5.30}$$

5.3.5.2 Evolutionary Algorithm

An EA operates by evolving individuals within the population set over the generations of the optimisation process. This involves the use of the existing individual solutions to determine the values of design variables for the next generation of solutions. Hence, the optimisation process is better guided than for random generation. The EAs included within the heuristic set are killer queen (KQ) and differential evolution (DE), which are described in §2.3.2. For KQ, a mutation probability is used to enable preservation of a sample of individuals and thus increase the likelihood of convergence, i.e. unlike when introduced in Raymer (2002) when mutation was a certainty. For DE, the probability of crossover and differential weight are controlled by parameters P5 and P6 respectively for dynamic operation of the LLH.

5.3.5.3 Genetic Algorithm

A GA performs similar evolution of the population set as by an EA, however parents are selected from the current population and mated through crossover to generate an offspring solution. Mutation can then be applied as appropriate. GAs were introduced in §2.3.2.2, including descriptions of the roulette wheel (RW), tournament selection (TO) and breeder pool (BP) selection methods. GAs are included within the heuristic set using each of these selection methods, as such these LLHs are referred to as RW, TO and BP herein. Within BP, parameter P10 defines the proportion of the population within the breeder pool, α_{BP}, such the breeder pool size is given by

$$\mu_{BP} = \alpha_{BP}\mu \tag{5.31}$$

In addition to the three aforementioned well-established GAs, a novel algorithm that has been developed as part of this research is included within the heuristic set: radioactive contamination (RC). This selection method considers the population as two groups: uncontaminated and contaminated individuals. The idea behind this GA selection method is that in the event of a radioactive outbreak, the fittest individuals are most likely to escape contamination. These individuals are therefore less likely to be mutated than those that are contaminated. The contaminated proportion of the population set is defined by parameter P11, α_{RC}, such that the size of the contaminated population is calculated as

$$\mu_{RC} = \alpha_{RC}\mu \tag{5.32}$$

Two parents are randomly selected from the entire population set for crossover. Mutation is then applied with the following probability for the ith offspring individual at the kth generation

$$p^k_{m,i} = \begin{cases} p^k_m & \text{if both parents contaminated} \\ \dfrac{p^k_m}{2} & \text{if one parent contaminated} \\ 0 & \text{otherwise} \end{cases} \tag{5.33}$$

Therefore, the offspring of weak, contaminated parents are more likely to be mutated to enable solution space exploration whilst the offspring of strong, uncontaminated parents evolve without mutation. This preserves the characteristics of good individuals in the population whilst allowing poorer individuals to explore the solution space. The RC selection method does not introduce bias into the selection of parents,

as with RW and TO, nor permit only a sample of individuals to be parents, as with BP, thus maintaining search diversity. An LLH formed as a GA with RC selection is referred to simply as RC herein.

The crossover techniques used by the GAs are selected during initialisation from uniform, point and blend, where the latter is performed only if a real representation is used. These techniques are described in §2.3.2.2. The probability of crossover is defined by parameter P8 whilst the number of crossover points during point crossover is defined by parameter P7. Offspring mutation is applied following crossover, the probability of which is defined by dynamic process parameter P9. Elitist selection, where a sample of individuals from the parent population are retained within the next population without crossover or mutation, is not permitted in order to maintain population diversity and allow the parameter control aspect of the HHA to control the generation of populations.

5.3.5.4 Swarm Intelligence

SI techniques explore the solution space over a period of generations based on the feedback of information from the population individuals during their independent exploration of the solutions space. Consequently, solution space learning is shared amongst the population set. This leads to coordinated searching of the solution space for good designs before convergence upon the best solution. Such shared learning reduces the likelihood of premature convergence on local optima whilst improving the global convergence on the minimum closest to the best solution. Particle swarm optimisation (PSO), as described in §2.3.3, is included in the LLH set as an SI technique. The search behaviour of the population individuals is dependent on the values of technique parameters which are initialised randomly between limits set during initialisation for parameters P12 to P15. The initial velocities of individuals for each variable are also initialised randomly. The velocity clamping of Clerc and Kennedy (2002) is applied by the constriction constant, P15, to reduce the likelihood of explosion and thus improve the stability of the LLH. This results in the modification of Eqn. (2.2) as

$$\{\dot{x}\}_i^{k+1} = \chi\left\{\omega_{PSO}\{\dot{x}\}_i^k + c_{1,PSO}r_{1,PSO}\left(\{\hat{x}\}_i^{1\to k} - \{x\}_i^k\right) + c_{2,PSO}r_{2,PSO}\left(\{\hat{x}\}_{1\to\mu,v}^{1\to k} - \{x\}_i^k\right)\right\} \tag{5.34a}$$

$$\{x\}_i^{k+1} = \{x\}_i^k + \{\dot{x}\}_i^{k+1} \tag{5.34b}$$

$$\text{where} \quad \chi = \begin{cases} \sqrt{\dfrac{2\kappa_{PSO}}{\rho - 2 + \sqrt{\rho^2 - 4\rho}}} & \text{if } \rho > 4 \\ \sqrt{\kappa_{PSO}} & \text{otherwise} \end{cases}$$

$$\rho = c_{1,PSO}r_{1,PSO} + c_{2,PSO}r_{2,PSO}$$

The constriction constant is constrained between $0 \leq \kappa_{PSO} \leq 1$. Setting the constriction constant to its maximum bound restricts the velocities of individuals as they search the solution space, thus allowing greater exploration of neighbouring regions and reducing search instability. Conversely, setting the parameter to zero reduces Eqn. (5.34) to the original form of the PSO algorithm given in Eqn. (2.2), i.e. unconstricted search without any velocity clamping. By permitting the HHA to control the value of the constriction constant as P15, the degree of velocity clamping may vary during the process to encourage, or discourage, search constriction.

5.3.5.5 Local Search

LS techniques optimise a single individual design solution rather than a population of individuals. Therefore, individuals within the population set are optimised independently when an LS LLH is selected by the HHA. Such single-solution techniques perform trajectory-based optimisation to make steps across the solution space to explore new designs, but are prone to premature convergence on local optima. However, such convergence tendencies increase the likelihood that the local optimum is found closest to a known

good solution, which overcomes the corresponding limitation with population-based techniques. Hill climbing (HC), simulated annealing (SA) and tabu search (TS) are LS methods included in the LLH set. These optimisation techniques are described in more detail in §2.3.4. Given that the framework considers 50 design variables, the steepest descent (SD) LS technique is not included due to the large number of gradient evaluations required with many design variables in order to identify the path of steepest descent.

The LS techniques step in a random direction across the solution space. The sizes of these steps are defined by dynamic process parameter P16. SA is performed using either linear or exponential cooling, as input during initialisation, with a cooling rate defined by parameter P17. The initial temperature is also input during initialisation. Finally, parameter P18 defines the tabu list length used by the TS technique, thus determining the memory of forbidden moves.

5.3.6 Data Output

The history of the best aircraft design solution is output following termination of the optimisation process [3.6a]. The history of optimisation process performance is also output [3.6b]. It is therefore possible to analyse these data and determine any further action, e.g. continuation to embodiment design or repetition of framework operation with updated input data. The data output by the framework include:

- best aircraft structural design solution;
- history of best design solution during process;
- FEA report for running best solution;
- history of optimisation process performance, including changes made by HHA.

The history of the running best design solution includes the values of design variables, worst values with respect to the design constraints and design objective value for the running best solution after each optimisation generation. FEA reports corresponding to the analysis of these designs are also output. These reports describe the FE model of the airframe design, the model response to each applied load case, including the boundary conditions applied, and the subsequent results of stress analysis. These data are included such that the solutions may be analysed using a post-processing tool. These reports may be output for all airframe designs if requested during initialisation. A history of population feasibility and affinity is also output as an indication of optimisation process performance. As a result, these data may be analysed for use in determining the next stage of the design process, or used to repeat the process with an updated set-up for analysis of a different aircraft design variation.

5.4 Summary

The framework presented in this chapter performs structural optimisation of an aircraft structural design subject to feasibility under load as measured using FEA. An HHA is embedded within the framework to further improve solution quality and the performance of the optimisation process as measured by a hyper-heuristic objective function. This framework includes three stages within the solution process: aircraft design procedure, structural analysis and airframe design optimisation.

The aircraft design procedure generates the external profile of the aircraft using the data input during initialisation and outputs of mission definition and mass estimation. Structural designs are generated within this profile given the values of design variables. The loads to be applied to each airframe design during structural analysis are also computed. This procedure avoids repeated computation of these tasks for each individual structural design, with the exception of structural layout generation.

Structural analysis determines the objective value and feasibility of each aircraft design, the latter of which is performed using FEA having generated an FE model of the airframe with multiple structural members grouped within elements for improved computation speed. The response of the structure to the selected load cases is computed for either static or dynamic loads. This response is measured in

the displacement field, leading to the calculation of the wingtip deflection for comparison against the corresponding design constraint. The forces and moments within the airframe members are subsequently obtained, permitting analysis of the stress field within each member. Consequently, the minimum FoS under yield of each member is calculated for comparison against the corresponding design constraint.

Airframe designs are optimised to minimise structural mass following the application of a penalty function to encourage feasibility. Population fitness is calculated using the ranks of individuals. Each structural design is optimised using an LLH chosen from the heuristic set by heuristic selection within the HHA. This can be coupled with population distribution for concurrent employment of multiple LLHs. Perturbation analysis is performed to further improve the quality of a sample of solutions, whilst parameter control is conducted in an attempt to improve process performance as measured by a hyper-heuristic objective function. Termination criteria are checked at the end of each generation to determine if the process should cease or continue for another generation. Data are output upon termination to enable post-processing such that embodiment and detail design of the aircraft may be performed.

This framework differs from those currently employed for conceptual aircraft structural design optimisation through the inclusion of the HHA for improved process performance and solution quality. Furthermore, the novel HHA varies from those traditionally employed for hyper-heuristic optimisation by including four HHA aspects: heuristic selection, population distribution, perturbation analysis and parameter control. Additionally, the framework is sufficiently versatile to be able to consider a variety of new and existing aircraft design variants of various classes, whilst possessing the ability to apply a number of load cases to the airframe. These characteristics are not common amongst frameworks currently employed within the field of aerospace design optimisation.

Chapter 6

AStrO

The framework described in Chapter 5 has been implemented as a computational tool called AStrO, an acronym of 'Aircraft Structural Optimiser', for its evaluation in Chapters 7 and 8. AStrO is a purpose-built stand-alone software tool for use on multiple operating systems. It includes a graphical user interface (GUI) for interaction with the engineer and implements parallel programming through the message-passing interface (MPI) library. This chapter introduces AStrO by providing an overview of its design and operation. The implementation of the framework is discussed in §6.1, including the GUI, use of parallel programming and post-processing procedure. A summary to the chapter is provided in §6.2.

6.1 Implementation of Optimisation Framework

The implementation of the framework as the computational tool AStrO is consistent with the modular description provided in Table 5.1. These modules are linked through a central orchestrating module to control the execution of tasks within the framework indicated in Fig. 5.1. Within the framework stages, all module tasks are performed explicitly within AStrO, i.e. without the use of any external software tools. Therefore, AStrO contains the necessary empirical formulae to generate an aircraft design, purpose-built structural analysis modules including finite element (FE) model generation and finite element analysis (FEA), and a programmed implementation of the embedded hyper-heuristic approach (HHA) to improve process performance and solution quality. Libraries store key mathematical functions, unit conversion tables and databases of existing aircraft, powerplants, ordnance, materials and aerodromes. Further, numerical recipes are employed to perform common operations such as the matrix computations required for FEA. The use of these libraries and recipes improves the computational efficiency of the tool and provides accessible data for use during initialisation, e.g. lists of common aerospace materials.

AStrO is programmed in C++ due to the support offered by the language for object-orientated programming (OOP). In OOP, a program is represented as a set of intellectual objects, i.e. classes, that pass data between each other to execute the program. The fundamental features of OOP include:

- abstraction: represent data by semantics without specific details;
- encapsulation: creation of self-contained, isolated classes;
- inheritance: passing of data structures through hierarchy;
- polymorphism: consider an object in multiple forms.

Abstraction standardises the code by reducing the dependency on complicated data, and thus permits the substitution of similar objects through polymorphism. Encapsulation enables different classes to function independently without requiring any knowledge of program operations outside the class. For example, the calculation of member sectional properties is performed independently for all structural members without relying on any information other than input data and coded formulae. Class structures are

inherited through a hierarchy leading to the generation of sub-classes, e.g. the class defining the airframe passes information to a set of sub-classes that each define member positions and sizes, the properties of which are dependent on design variable values and encoded formulae.

An example of the class structure used throughout AStrO is shown in Fig. 6.1 using unified modelling language (UML) notation (Miles and Hamilton, 2006). This diagram illustrates the hierarchy of classes that perform the airframe generation task within the structural layout generation module, i.e. task 1.6c in Fig. 5.1. The aircraft generation task comprises of a class that polymorphically creates n structural member objects from another class based on the values of the design variables. The profile and material of each member is defined by sub-classes using common operations, thus maintaining abstraction. The member position is inherited following its calculation in another class based on the pre-determined aircraft external profile and attachment positions read in to the main class of the airframe generation task.

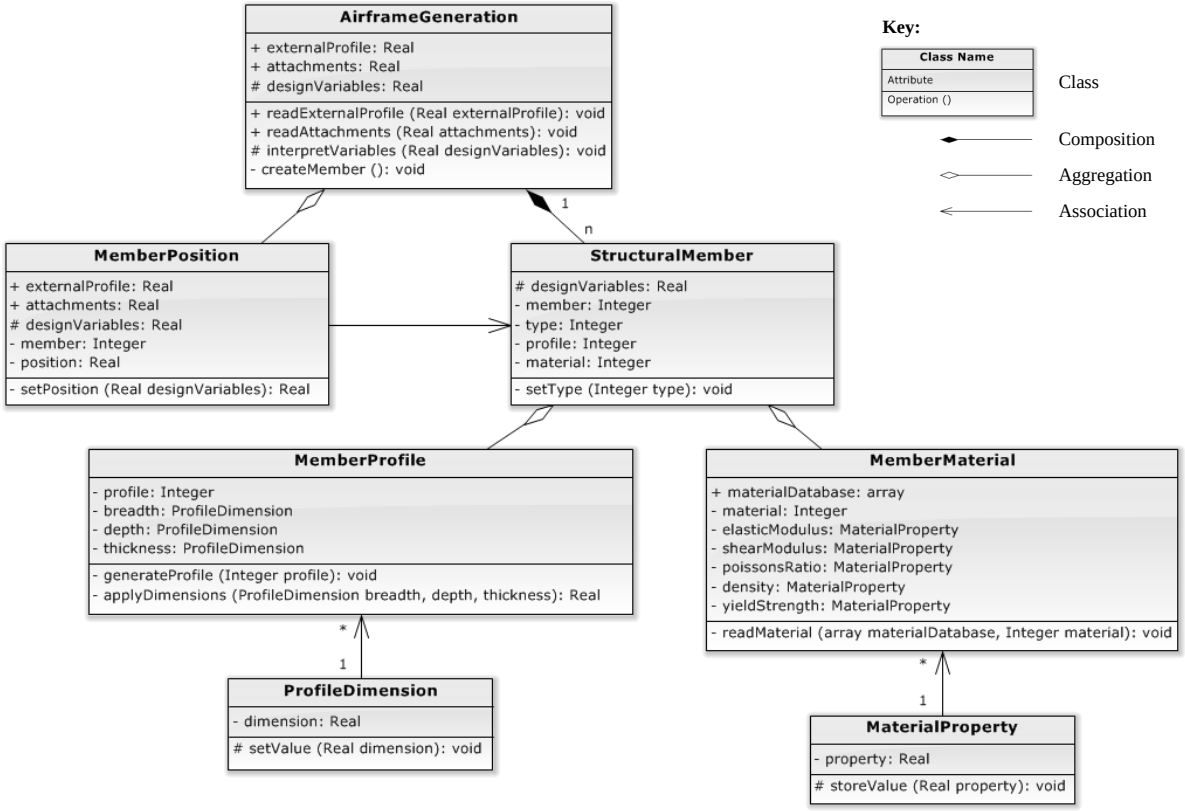

Figure 6.1: Example of AStrO class structure using UML notation

Ease of programming and maintenance are important advantages of C++ with respect to the creation of AStrO by ensuring efficient implementation of the framework, thus improving the reliability of experimental results, as well as the vast quantity of resources for programming in C++. Microsoft Visual Studio 2005 is used for programming AStrO, including the use of Mircrosoft foundation class (MFC) libraries. These libraries enable the design of familiarly-structured GUI for ease of operation. Additionally, the message-passing capabilities of MFC programming are beneficial for the rapid modification and subsequent update of data within the program following the input of data. This improves the real-time behaviour of AStrO, such as for updates of the GUI during execution. The portability of C++ increases the versatility of AStrO by removing restrictions of operating systems. AStrO is designed for use on three operating systems: Microsoft Windows, Linux and Unix. The GUI is programmed to be employed on Microsoft Windows due to the popular worldwide use of this operating system. Operating of AStrO from the Linux and Unix-based systems requires the use of a command line version of AStrO due to

incompatibility of the GUI. However, these operating systems are chosen principally such that AStrO may be used on high-performance computing (HPC) resources to enable more rapid execution, for which a GUI is not necessary when supplied with appropriate comma-separated values (CSV) input files.

6.1.1 Graphical User Interface

When run on a Microsoft Windows operating system, AStrO is controlled through a GUI to input data, monitor execution and perform post-processing. The GUI includes three principal windows:

- main: control the program and launch the following GUI windows;
- input data: implement the initialisation module of the framework;
- run program: execute and monitor the optimisation process.

Figure 6.2 shows the toolbar of the main program window. This toolbar is used to create, open, save or close a project file, edit the view settings for the current aircraft model, launch the input data or run program windows, or output results for analysis in the form of spreadsheets. The buttons corresponding to the latter three tasks are labelled in Fig. 6.2.

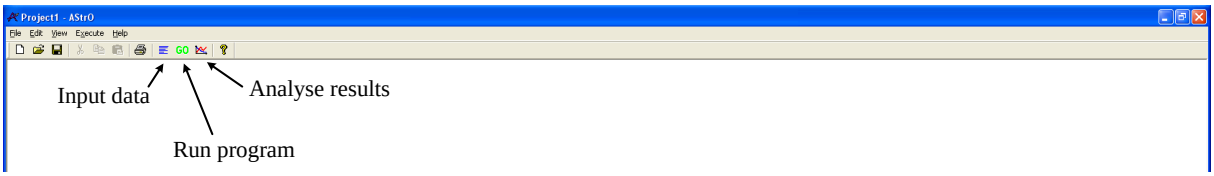

Figure 6.2: AStrO main user interface toolbar

The input data window in Fig. 6.3 is launched upon selecting 'Input data' from the main window. Radio buttons select the category for which data are to be input. Figure 6.3 shows the input data for the

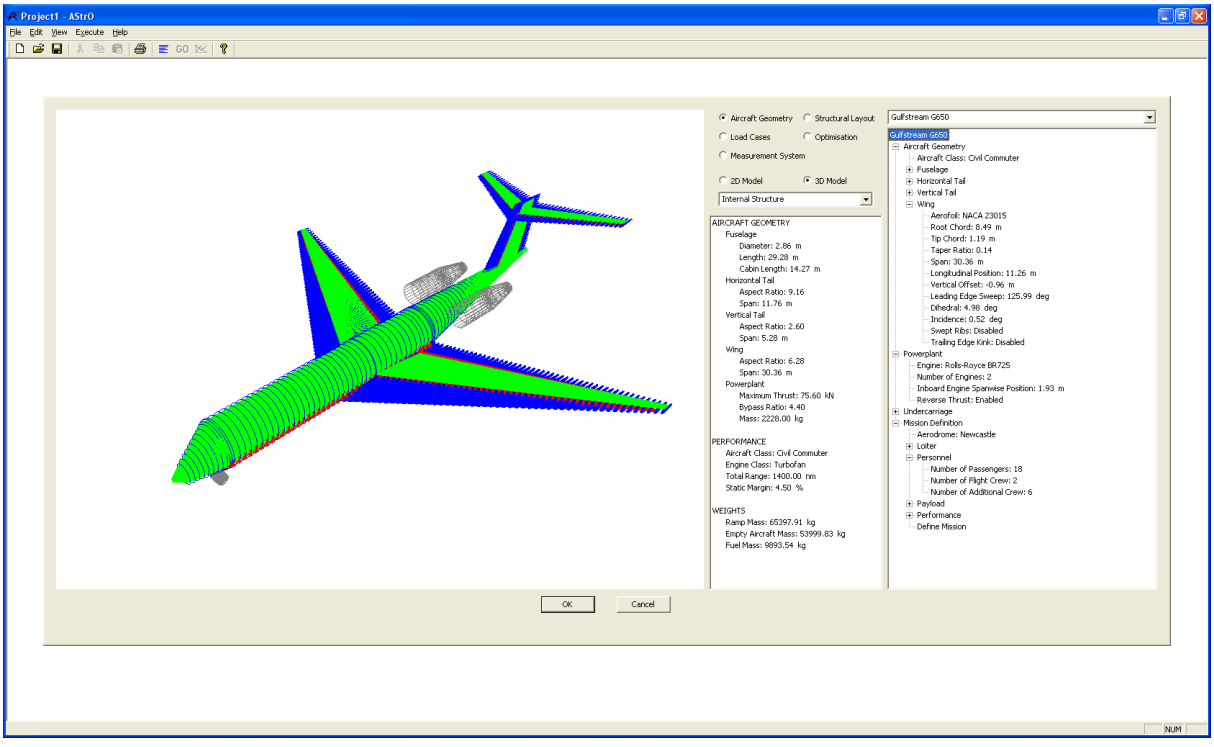

Figure 6.3: AStrO input data user interface

'Aircraft geometry' category to define properties of the aircraft external profile, powerplants and mission. A summary of the aircraft design represented by the input data is included alongside an image of the external or internal design in either two or three-dimensions using the Open Graphics Library (OpenGL).

Figure 6.4 shows the AStrO window during the execution of the optimisation process to inform the engineer of process progress. This window is launched upon commencing execution of the framework by selecting 'Run Program' from the main toolbar. An image of the current best design solution is shown alongside the history of the running best solution and process in tabular and graphical form.

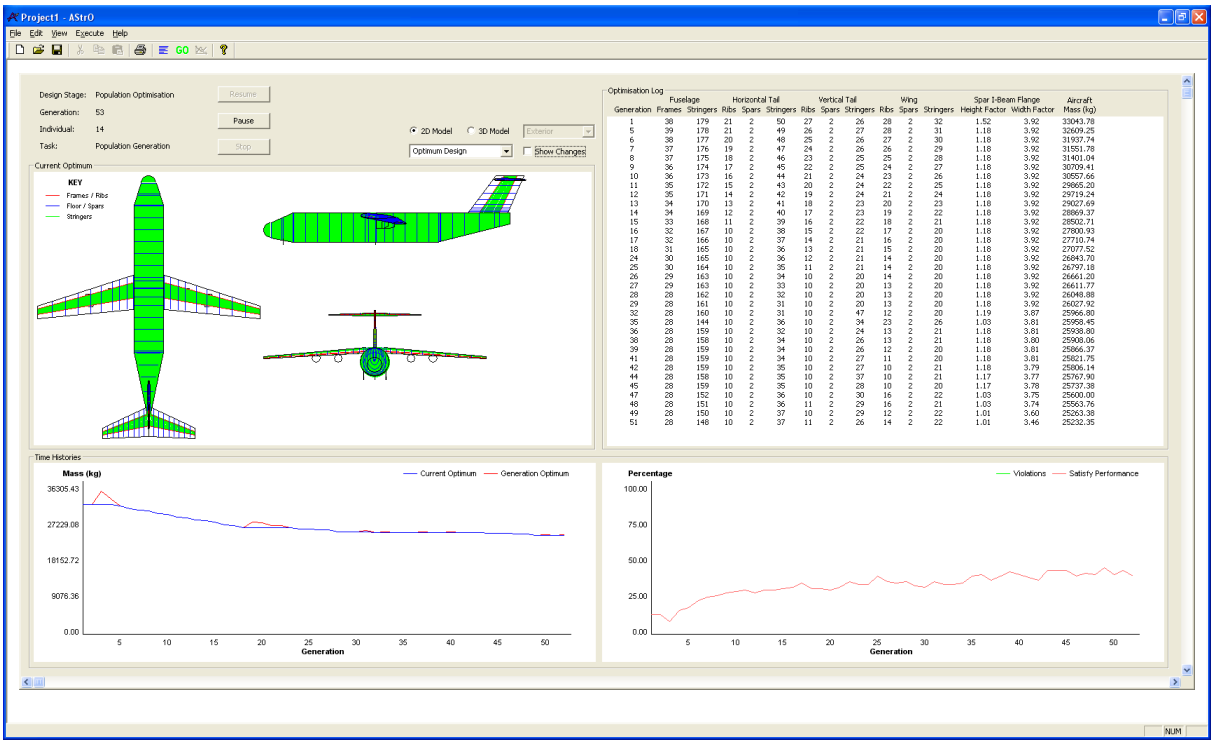

Figure 6.4: AStrO run program user interface

The image of the current best solution shows the corresponding airframe design in a view selected by the engineer. This view can show either:

- all structural members, i.e. as in Fig. 6.4;
- only structural members that have changed compared to the previous best solution;
- the minimum factor of safety (FoS) within each member;
- the critical load case for each member.

The latter concerns the load case resulting in the lowest FoS within each member, thus providing the ability to assess the airframe integrity to determine which loads are most onerous for different structural members. The GUI buttons permit the process to be paused or terminated if necessary. This may occur if the engineer is not satisfied with the search direction, e.g. the design solution is unsuitable, or if the problem is to be redefined. The optimisation log tabulates the running best solutions during the process, including their design variable values, limiting values with respect to the design constraints and objective value. These instances of improvements in the best solution are also illustrated by a plot of solution history at the bottom-left of the window in Fig. 6.4, alongside a plot of process performance in the bottom-right. The keys within the two plots shown in Fig. 6.4 indicate:

- 'Current Optimum': objective value of the best solution found thus far;
- 'Generation Optimum': objective value of the best solution in each generation;

- 'Violations': percentage of structural members in best solution violating a constraint;
- 'Satisfy Performance': feasible percentage of population at current generation.

The post-processing of results is performed upon selection of 'Analyse Data' following the termination of the optimisation process, i.e. after the end of the process described by the framework in Fig. 5.1. As this process is outside the scope of the framework, an external software tool is used to perform this data analysis task, further discussion of which is included in §6.1.3.

6.1.2 Parallel Programming

All modules of the aircraft design procedure except structural layout generation, i.e. modules 1.1 to 1.5 in Table 5.1 and Fig. 5.1, are employed once for each execution of AStrO. Similarly, the airframe design optimisation modules, i.e. modules 3.1 to 3.6, are employed once for each generation of the optimisation process during program execution. Conversely, structural layout generation and structural analysis, i.e. modules 1.6 and 2.1 to 2.5, are executed once for each individual airframe design solution within a population generation due to the requirement to perform analysis of each airframe design solution. Assuming a constant population size, these modules are executed μn_k times for a population set of size μ individuals over n_k generations. This generates the greatest computational demands on the solution process, in part due to the computational costs inherent of performing FEA discussed in §2.2.2.

The tasks within the structural layout generation and analysis modules are identical for each individual solution and do not depend on any information concerning other individuals within the population set. Therefore, parallel programming is incorporated within AStrO to execute modules 1.6 to 2.5 simultaneously for batches of population set individuals. This is achieved using the MPI library to pass messages between a master processor and a number of slave processors such that each processor performs these module tasks in isolation. This avoids the need for serial population analysis on a single processor, thus significantly reducing the computation time required for the solution process. MPI possesses the following properties that are beneficial to this application:

- high performance in handling tasks and operating numerous processors;
- versatility for use on various computer processors with fast or slow connections;
- explicit definition of message passing for ease of debugging;
- suitability for parallel execution of tasks of potentially imbalanced durations.

This final property is critical as concurrent analysis of multiple individuals is unlikely to take the same length of time for each individual, i.e. the durations of FE modelling and analysis are dependent on the number of degrees of freedom (DoFs) within each individual model. Parallel tasks are performed by firstly broadcasting the set-up of each optimisation generation from the master processor to the slaves to ensure all processors possess the current settings. Each processor is then assigned an individual from the population set by sending the design variable values of the individual from the master processor to the slave. Isolated structural analysis of the individual is then performed, the results of which are passed back from the slave processor to the master before the next batch of individuals is analysed. When all individuals within the population have been assessed, the master processor optimises the population before the next generation is analysed in parallel by repeating the process. Consequently, the structural layout generation module and structural analysis stage of the framework shown in Fig. 5.1 may be rearranged as shown within Fig. 6.5 to indicate the parallel analysis of a batch of population set individuals rather than serial analysis of the entire population.

Parallel structural analysis is performed over $n_{sp} + 1$ processors, i.e. n_{sp} slave processors and one master processor. Hence, the population is analysed in batches of $n_{sp} + 1$ individuals, i.e. one individual per processor, repeatedly until the entire population set has been modelled and analysed. The final batch of each generation is limited to the number of solutions yet to be assessed if this number is less than the

number of processors. The master processor performs the serial tasks of the aircraft design procedure, i.e. modules 1.1 to 1.5, and airframe design optimisation, i.e. modules 3.1 to 3.6. Perturbation analysis similarly exploits parallel programming to analyse the sampled population individuals and thus reduce the additional computational expense of this aspect of the HHA.

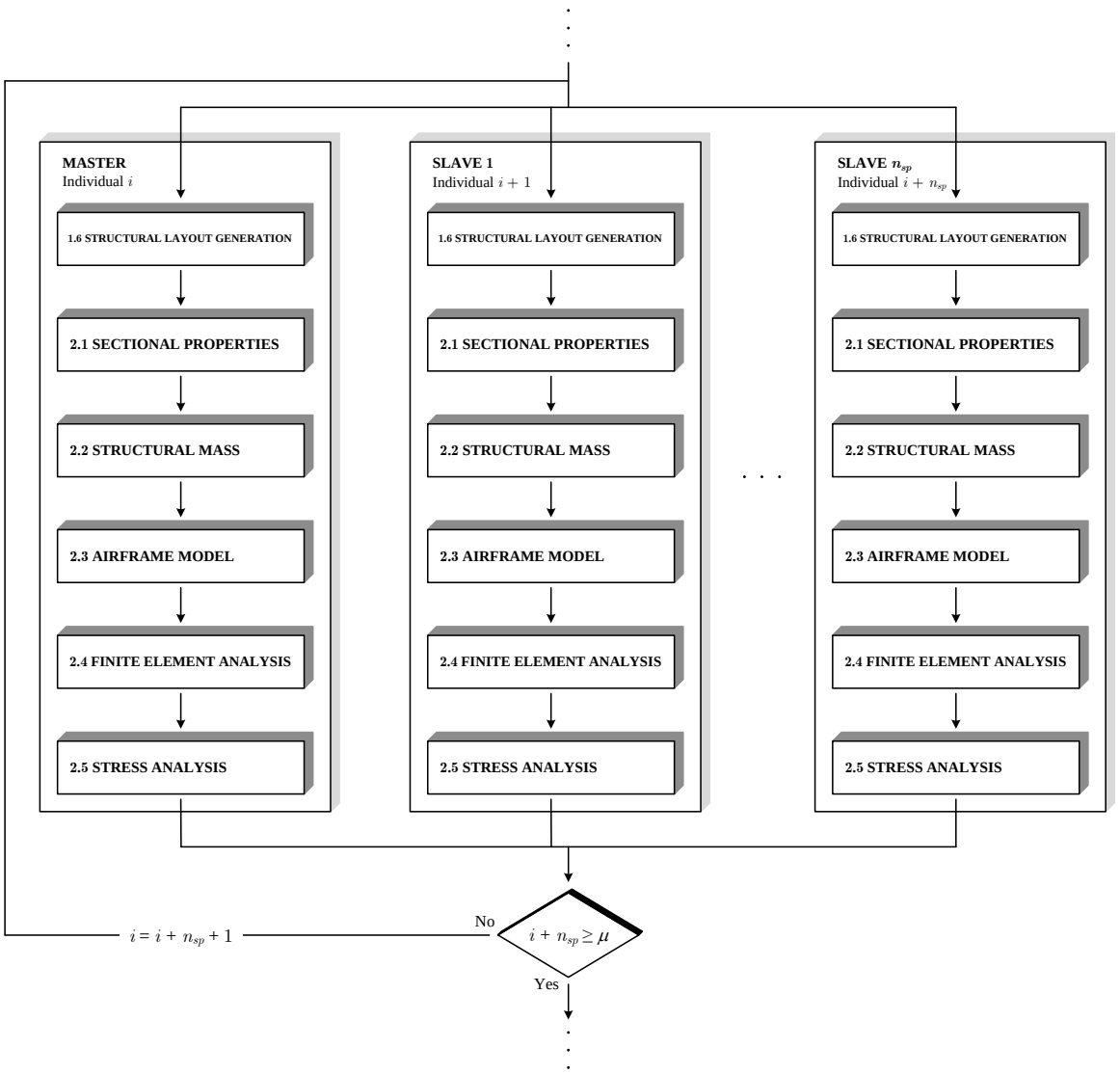

Figure 6.5: Parallel structural analysis of population set within framework

6.1.3 Post-Processing

The post-processing of results is performed externally from AStrO following selection of 'Data Analysis' from the main window of AStrO shown in Fig. 6.2. AStrO generates a number of CSV files to capture the data listed in §5.3.6. These files provide input data to Microsoft Excel for the post-processing of the results. Upon selection of 'Data Analysis' within AStrO, a Microsoft Excel workbook template is launched and a Visual Basic (VB) script within this workbook is executed automatically to import the data within the CSV files into the workbook. Consequently, a series of tables and figures are plotted to provide a visual representation of the optimisation process results. A sample of these figures as displayed in Microsoft Excel is shown in Fig. 6.6 to show the variation in objective value and a selection of design variables over the duration of an arbitrary experiment performed using AStrO. Similar plots are generated for all design variables to illustrate the variation in their values for the best aircraft design. This provides

a clear description of the histories of the best aircraft design and the optimisation process and simplifies the data analysis task such that the interpretation and manipulation of the output CSV data is avoided.

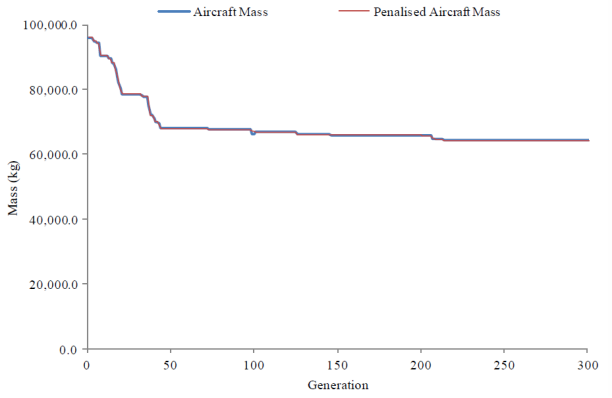

(a) Objective value

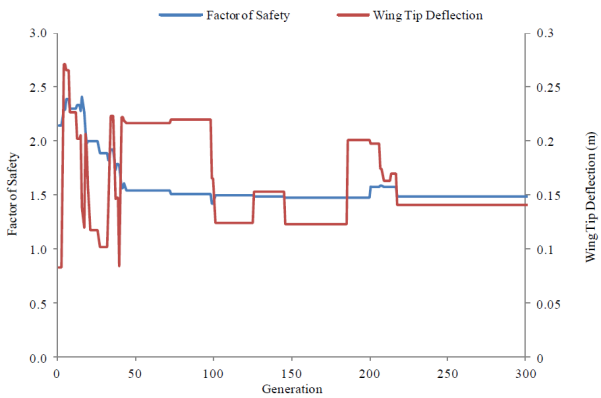

(b) Limiting values with respect to constraints

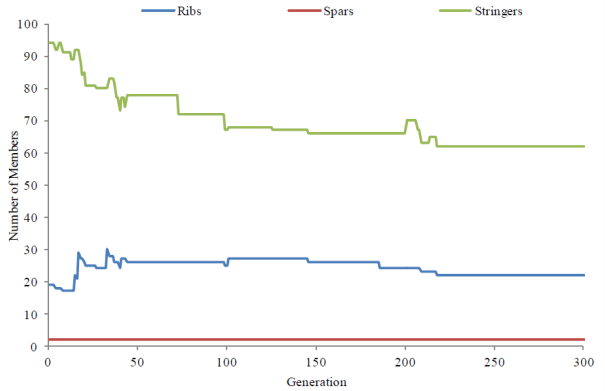

(c) Number of wing members, V9 to V11

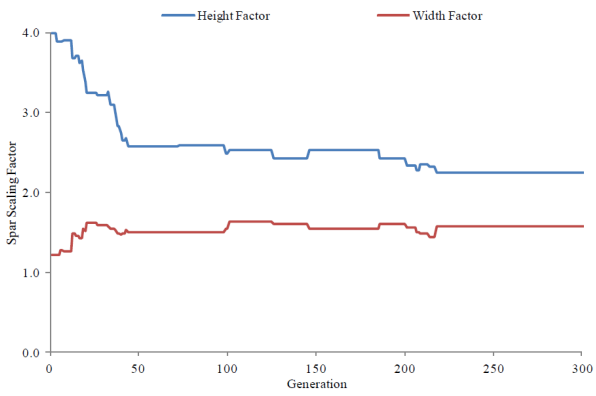

(d) Spar root scaling factors, V19 and V20

Figure 6.6: Sample of results as displayed in Microsoft Excel following output from AStrO

The output of structural analysis reports for all design solutions can be requested during initialisation. Alternatively, the output of such reports can be restricted to designs that improve upon the currently-stored best solution, and therefore reduce the storage space required for results files. A structural analysis report permits the assessment of the response of an airframe design to each load case and, therefore, compare the variations in responses of good and poor solutions. Such analysis enables a better understanding of the qualities of a good solution, and correspondingly the weaknesses of a poor solution. Furthermore, the influences of different load cases on a design can be assessed, thus permitting the determination of the most onerous loading condition for each structural member within different airframe designs.

6.2 Summary

AStrO is a computational implementation of the framework described in Chapter 5. The tool is programmed using C++ for operation on multiple systems, with a GUI provided when using a Microsoft Windows system. Alternatively, HPC resources can be employed to improve computational efficiency for large problems when using a Linux or Unix systems. The engineer interacts with AStrO to set up and execute the program, monitor and potentially interrupt the optimisation process, and enable post-processing of results in the form of spreadsheets. Parallel programming has been implemented to enable concurrent assessment of multiple airframe design solutions using the structural analysis module, thus improving the computational efficiency of the tool. The development of AStrO permits evaluation of the framework to establish its performance and thus assess the hypothesis of this research project.

Chapter 7

Preliminary Investigations

The framework presented in Chapter 5 is evaluated in its implementation as AStrO through a series of case studies in Chapter 8. Preliminary investigations are conducted prior to these case studies to verify the results generated by the framework and also gain a better understanding of how to set up the framework to suitably bound an optimisation problem. These investigations, as well as the case studies that follow, are performed using high-performance computing (HPC) resources to execute AStrO on a Unix environment, as described in Chapter 6. These resources offer quicker execution than is available on typical desktop computers, thus permitting a greater number of experiments to be performed.

This chapter describes the set-ups and results of the preliminary investigations shown in Fig. 7.1. These preliminary investigations are not intended to serve as a detailed evaluation of the framework but rather establish appropriate set-ups of the framework for the case studies; as such this chapter presents only a summary of the investigations. Two investigations into the structural analysis module are firstly presented in §7.1. The first investigation verifies the finite element analysis (FEA) module against existing software to validate the results output for use during optimisation. The second investigation examines the effects of varying finite element (FE) model fidelity on the feasibility measured for an airframe design. A preliminary investigation to verify the results of the optimisation process follows in §7.2 for a set of known problems posed by mathematical benchmark functions. The set-up of the optimisation process for the problem of aircraft structural design optimisation is then investigated in §7.3. This includes investigation of the effects of different parameter values and penalty functions, as well as the performance of optimisation techniques with different set-ups. The set-up of the hyper-heuristic approach (HHA) is then investigated in §7.4 to compare process performance with varying set-ups of heuristic selection, population distribution, perturbation analysis and parameter control. The chapter is summarised in §7.5.

7.1 Structural Analysis

Investigations of the structural analysis framework stage are performed to verify the results of FEA and investigate the effects of varying model fidelity on the feasibility calculated for a solution. FEA verification is performed in §7.1.1 by comparing the results obtained for a series of problems against existing software. Model fidelity is then investigated in §7.1.2 by varying the fidelity used to model and analyse a number of airframe designs, thus leading to the determination of the effects of such variation on design feasibility.

7.1.1 Finite Element Analysis

Verification is performed of the FEA module against existing software to ensure reliable results are output for subsequent use within the optimisation process. The results of FEA inform the optimisation process as to the feasibility of different airframe design solutions. Therefore, reliability in these results is required to avoid misguiding the optimisation process with regard to solution quality, i.e. the solution objective value following possible penalisation based on the measured design feasibility. In this investigation a set of

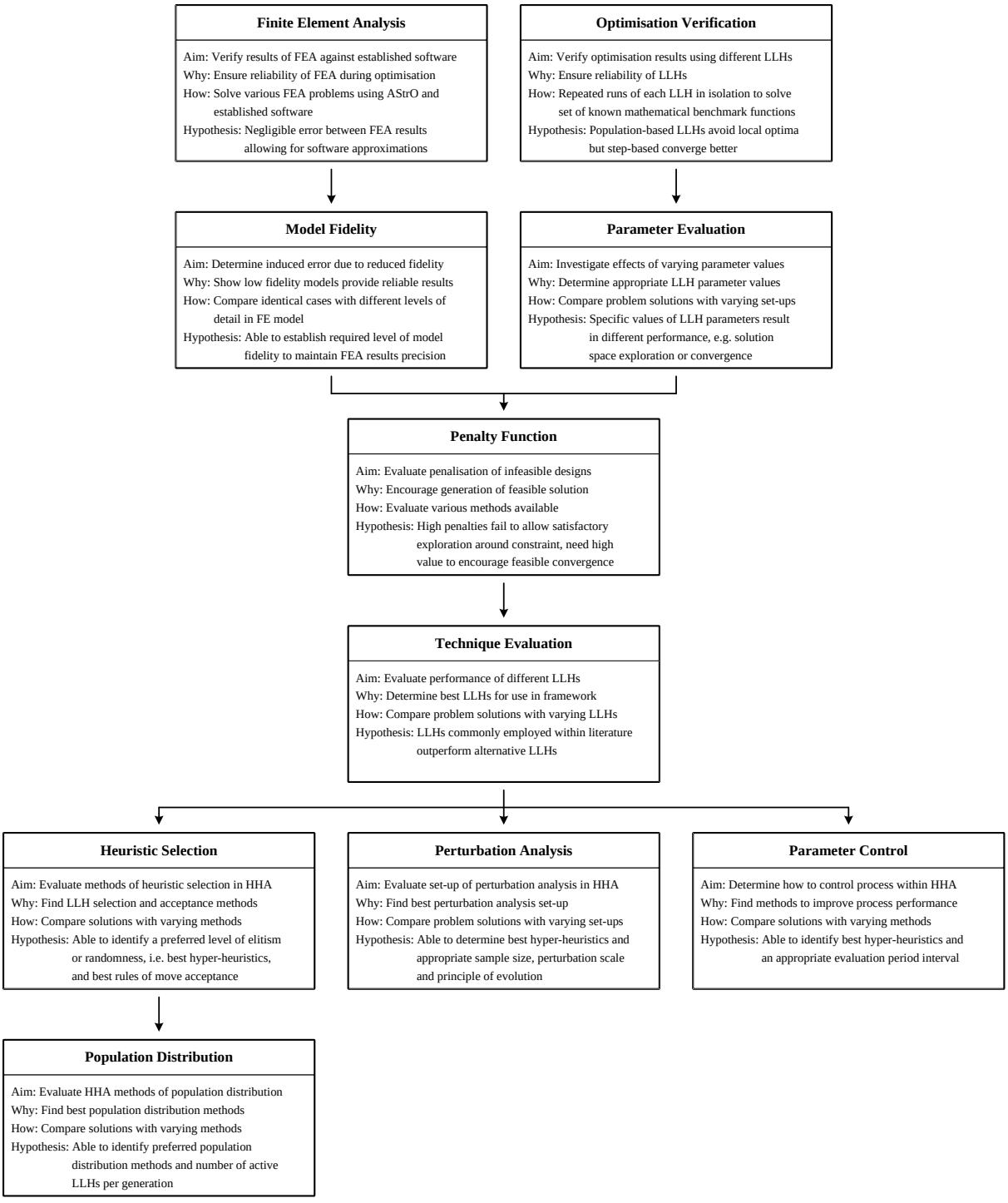

Figure 7.1: Plan of preliminary investigations

problems are solved by the framework FEA module, described in §5.2.4 and implemented within AStrO, as well as by two established commercial FEA software packages: Strand7 (Strand7, 2005) and VisualFEA (VisualFEA, 2011). These packages are selected as they provide detailed outputs of the input data and calculated results. The following problems are investigated:

- simple cantilever beam;
- detailed cantilever beam;

- tapered cantilever beam;
- airframe design.

These problems are all three-dimensional and are modelled using one-dimensional beam elements as described in §5.2.3. The simple cantilever beam problem is included for a rapid verification of the problem formulation and static solution results. The detailed cantilever beam extends this problem with a greater number of degrees of freedom (DoFs) for the evaluation of a more complex model with larger global system matrices. This problem also includes verification of both static and dynamic response results. These two problems are modelled as shown in Fig. 7.2, indicating the nodal and element numbers used in black or blue and red respectively. Consistent node and element numbering of the structure is maintained between the software tools to permit clear verification. The cantilever beams analysed in these problems possess identical geometry, differing only in the level of fidelity employed to model the beam, i.e. the quantity of beam elements within the model as illustrated in Fig. 7.2. The model in Fig. 7.2(a) is constructed by elements at the extremes of the cantilever whereas the model in Fig. 7.2(b) is created by evenly discretising the cantilever over its breadth, width and length. The tapered cantilever beam problem is similar to these problems however includes elements at angles not orthogonal to the global coordinate system, hence enabling verification of the rotation matrix and subsequent FEA results with arbitrary element angles. This is necessary given that the orientations of structural members within the airframe are not always orthogonal to the global coordinate system. Finally, verification of the results of FEA for an airframe design is performed to ensure appropriate modelling and analysis of an airframe.

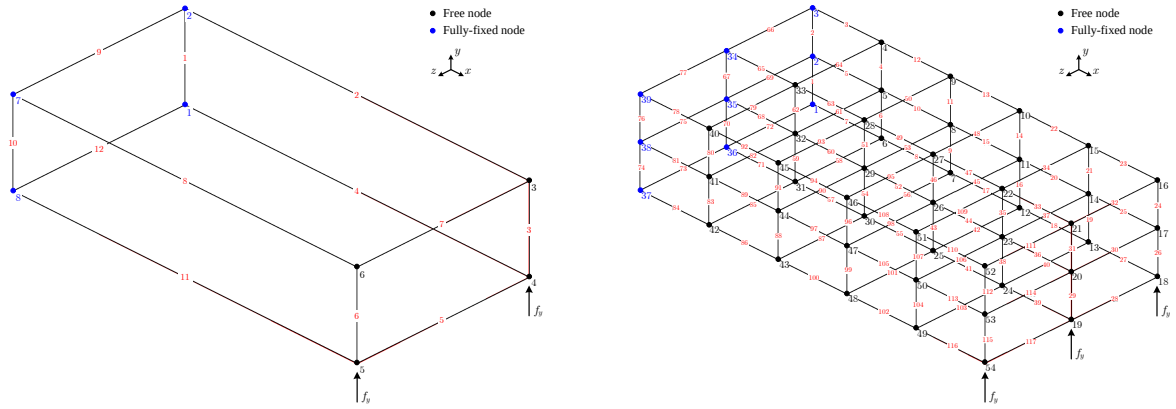

(a) Simple cantilever beam (b) Detailed cantilever beam

Figure 7.2: FE models of simple and detailed cantilever beams during FEA verification

The properties of the simple cantilever problem system are listed in Table 7.1, where the point load is applied to the beam at nodes 4 and 5 in Fig. 7.2(a). The sectional properties of the beam elements are calculated as discussed in §5.2.1 and §5.2.3.1 such that they possess the equivalent properties of the cantilever beam. Verification is firstly performed of the formulation of the system matrices and application of boundary conditions within AStrO compared to the two existing pieces of software to ensure appropriate problem set up. The problem is subsequently solved independently by the three FEA tools for the static system response. The percentage differences in the nodal responses between the software tools measures the variation in results between the different packages.

The verification of problem set up indicated negligible differences in the system matrices and application of boundary conditions between the software tools. This provided confirmation that the system matrices were correctly calculated and boundary conditions were appropriately applied within the framework. The greatest percentage difference in the responses of similar nodes calculated using AStrO and

Table 7.1: Cantilever beam preliminary investigation set-up

Property	Value
Beam depth	0.5 m
width	1.0 m
length	2.0 m
Element depth	0.1 m
width	0.1 m
Material density	7850 kg/m^3
Poisson's ratio	0.25
elastic modulus	200 GPa
shear modulus	80 GPa
Load case	5 kN vertical point load

Strand7 was 1.79% whilst the corresponding value with respect to VisualFEA was 0.008%. These differences were due to rounding errors within the software, where the result for Strand7 was misleadingly high due to the reduced precision provided in the output of results. The response of the system, albeit small, as calculated by AStrO is shown in red in Fig. 7.2(a).

The detailed cantilever problem extends the simple problem to a model of greater detail under two isolated load cases: a point load of 5 MN applied to tip nodes 18, 19 and 54 in Fig. 7.2(b) as either a static or dynamic load. The latter load case enables verification of the response calculated using the central difference, Wilson-θ and Newmark-β direct integration methods against those calculated in VisualFEA. Strand7 does not include the central difference method as an integration scheme, therefore verification against Strand7 is limited to the responses calculated by the implicit Wilson-θ and Newmark-β methods. Verification of the Houbolt method in this manner is not possible as neither VisualFEA nor Strand7 includes these schemes. The dynamic response is determined over 1,000 time steps of $\Delta t = 0.05$ ms with $\zeta = 0.05$, $\alpha = 0.25$, $\beta = 0.5$ and $\theta = 1.4$ for stable analysis (Rao, 2004). The mechanical properties of the cantilever beam are the same as listed in Table 7.1. The greatest percentage difference between the static nodal responses obtained using AStrO and Strand7 was 0.95% whilst the corresponding value for VisualFEA was 0.03%. These differences were again due to software rounding errors and output precision. Similar variations were observed in the dynamic responses using the different integration methods. For example, the significant displacements and rotation of node 54 calculated by the FEA tools using the Newmark-β method are shown in Fig. 7.3, indicating similar transient results having accounted for rounding errors and output precision.

The cantilever problem is extended further by introducing a 30° taper of the beam along its span such that the local coordinate systems of elements are not always orthogonal to the global coordinate system. This enables verification of the transformation matrix formulation to ensure the correct transformation of elements at arbitrary orientations. The system properties and loading conditions are as described in Table 7.1. The greatest percentage difference recorded in the static responses of AStrO and Strand7 was 9.81%. Although this value was greater than for the previous two problems, the difference was once more due to the reduced output precision of Strand7 compared to AStrO. In contrast, the largest percentage difference between AStrO and VisualFEA was 0.04%, i.e. of similar magnitude to the previous problems. Recovery of element response by AStrO was similarly verified for this problem, with the greatest difference between the forces and moments calculated for an element by AStrO and those measured by Strand7 and VisualFEA of 0.01% and 0.04% respectively. The difference between AStrO and Strand7 was noticeably lower for the element response than for the global system response. This was due to the forces and moments being of larger magnitudes than the displacements and rotations, thus reducing the rounding errors inherent with the output precision of Strand7.

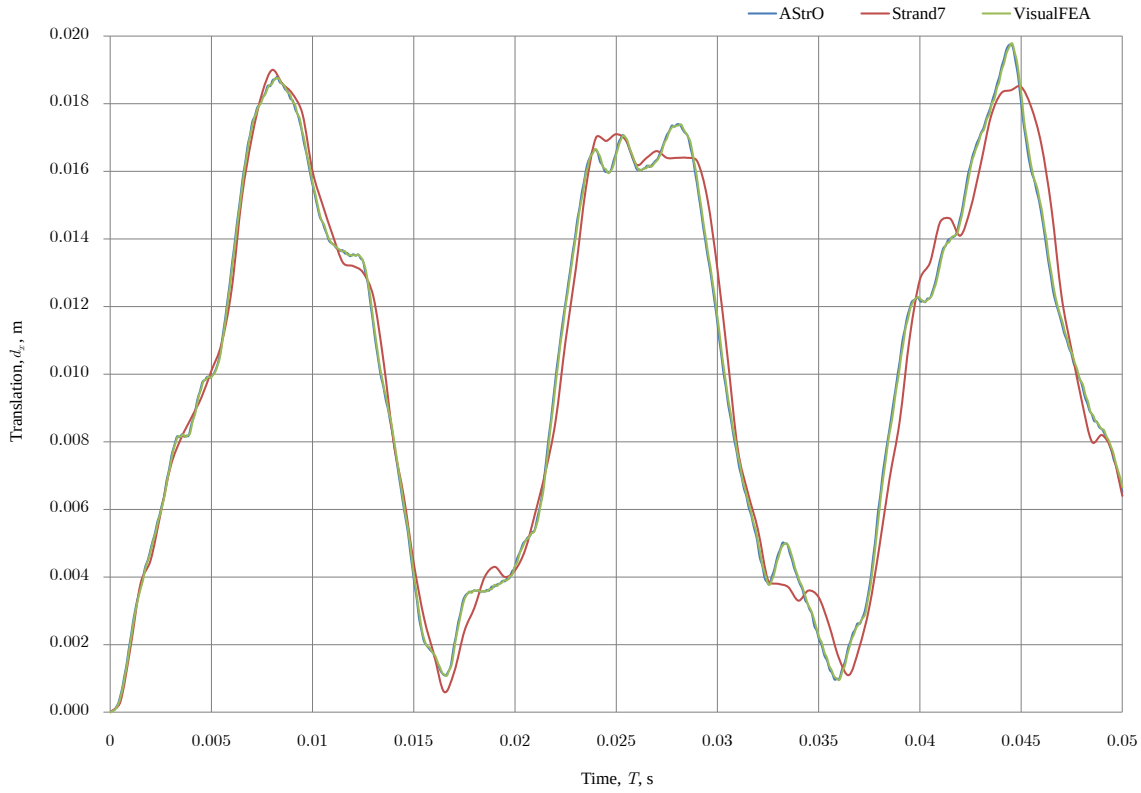

(a) Node 54 translation in x-direction

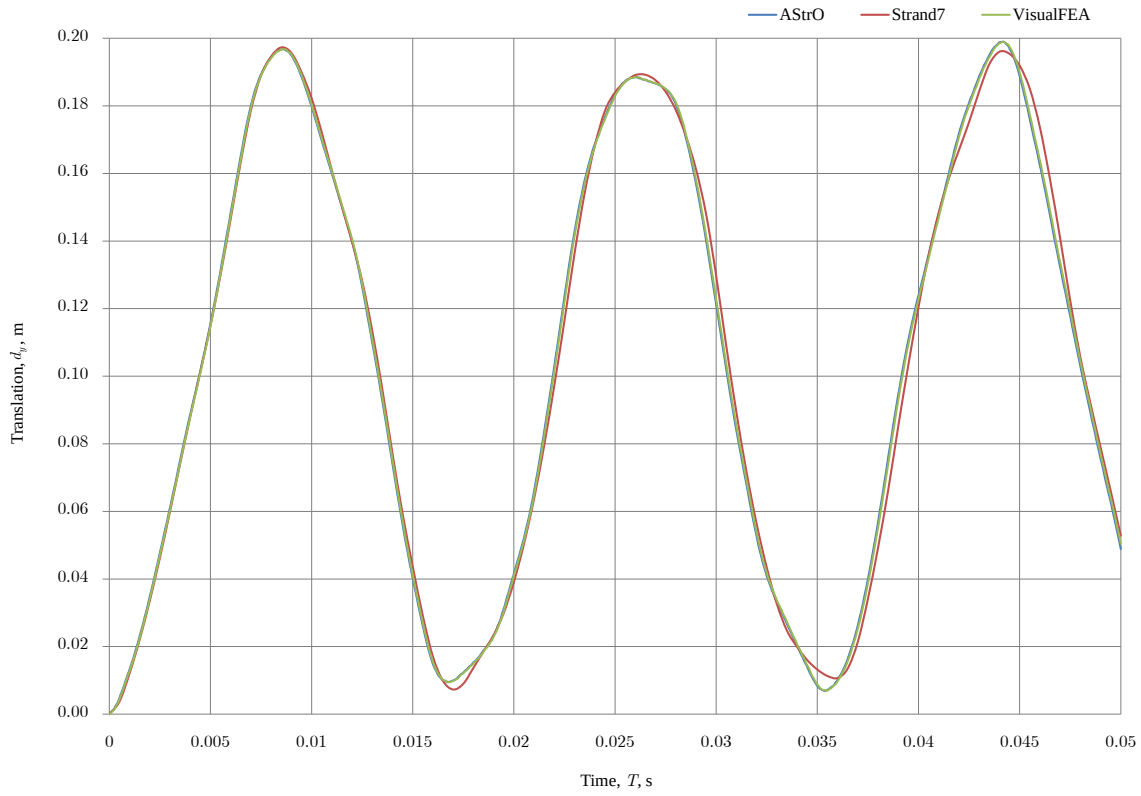

(b) Node 54 translation in y-direction

Figure 7.3: Dynamic response of cantilever tip

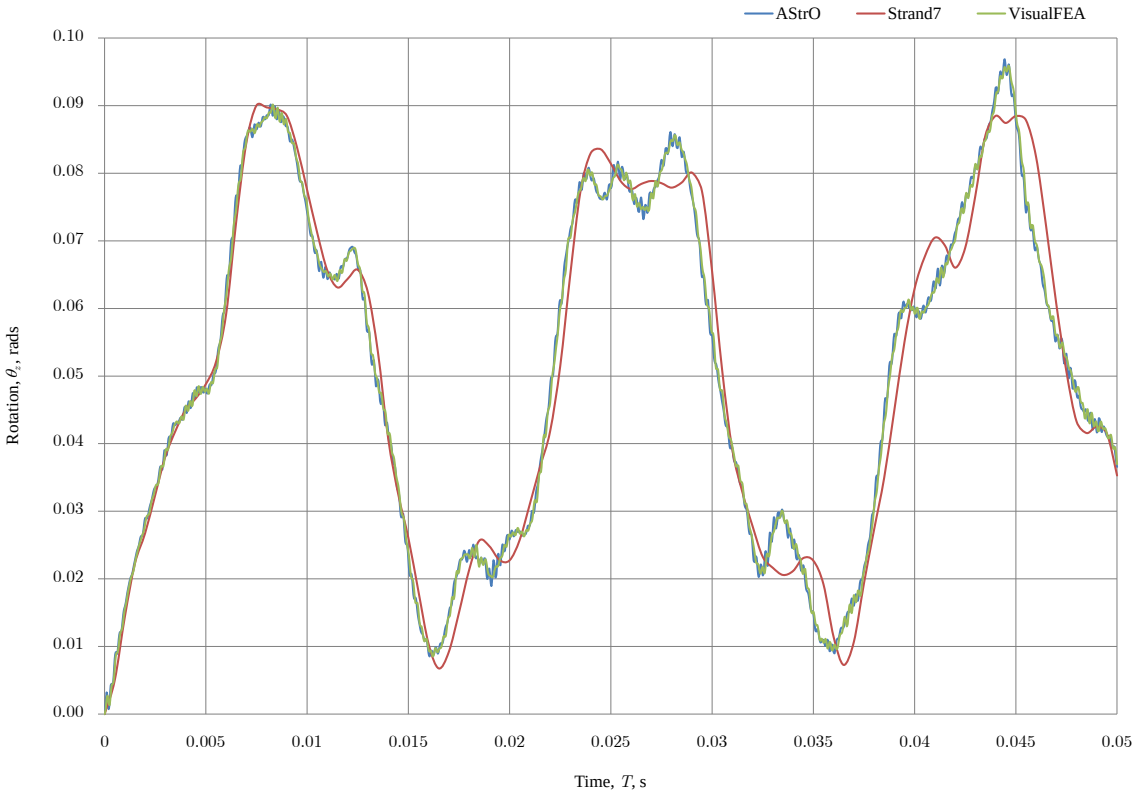

(c) Node 54 rotation about z-axis

Figure 7.3: Dynamic response of cantilever tip (cont.)

FEA of an aircraft design is performed using AStrO and Strand7 to verify the response calculated to loads within the load case database. VisualFEA is not employed for this problem due to modelling restrictions. This verification also provides a means to test all modules within the aircraft design procedure and structural analysis framework stages. All load cases within Table A.3 are applied in isolation to the arbitrary aircraft design shown in Fig. 7.4. The greatest difference in the response calculated by AStrO with respect to Strand7 was 0.01%. This difference was principally due to the output precision of Strand7.

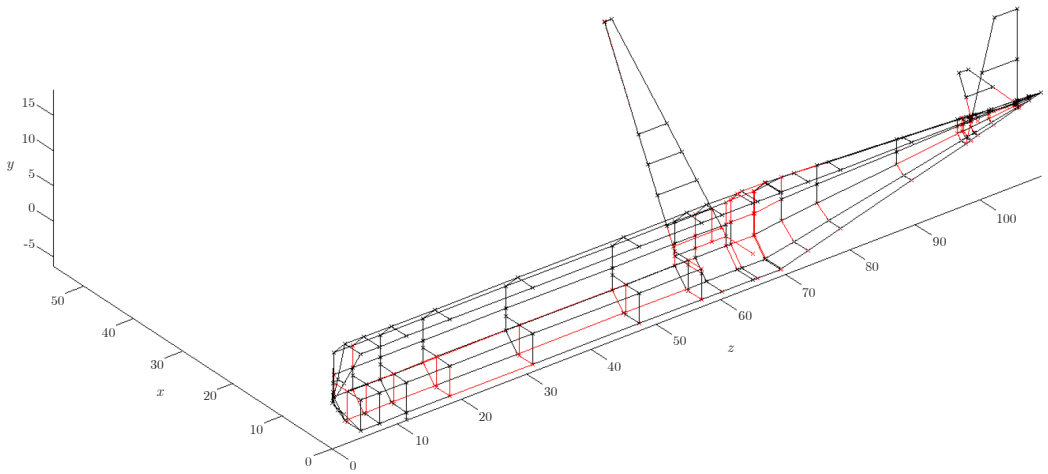

Figure 7.4: FE model of arbitrary airframe design during FEA verification

This preliminary investigation indicates negligible differences between the results of FEA carried out using AStrO and two existing software tools. This provides the confidence that the formulation and solution of a structural analysis problem are correctly executed within the framework. As a result, the modules are fit for purpose to generate and evaluate the structural designs of aircraft during optimisation.

7.1.2 Model Fidelity

An investigation is conducted into the effects of varying model fidelity on the measured feasibility of a design solution. Model fidelity affects FEA accuracy through the determination of the number of DoFs within the model and degree of structural member grouping. Inaccuracies in the results of FEA can misguide the optimisation process by providing misleading feasibility information. Hence, it is necessary to ensure that similar feasibility results are obtained for a design at varying levels of fidelity.

A selection of different airframe designs are subjected to FEA at varying levels of model fidelity to determine the differences in measured feasibility with varying fidelity. Constant test conditions are maintained by using an identical aircraft external profile and load case throughout. The chosen aircraft is the Embraer E-195 as it represents a recent design of civil large aircraft, therefore an appropriate existing design for structural optimisation. A selection of properties of the aircraft are listed in Table 7.2 (Embraer SA, 2011; Jackson, 2009). The maximum positive flight manoeuvre, i.e. load case L1, is applied during cruise as this case represents the greatest load on the aircraft during flight, i.e. a $+2.5g$ symmetric pull-up manoeuvre. A flight load is selected rather than a ground load as the latter applies loads to only a small number of nodes, i.e. undercarriage ground contact points, whereas the former applies loads over a larger region of the aircraft. Cabin pressurisation, engine thrust and gravity, i.e. miscellaneous load cases L9, L10 and L11, are superimposed on L1 as such loads are also present during cruise.

Table 7.2: Selected properties of Embraer-195 aircraft

Property	Value
Wing span	28.72 m
sweep	27.0°
Tail span	12.09 m
height	10.57 m
Fuselage length	38.67 m
width	3.35 m
Undercarriage track	5.94 m
wheelbase	14.64 m
Powerplant	2x General Electric CF34-10E
Mass operating empty	28,700 kg
maximum take-off	48,790 kg
Cruise altitude	35,000 ft
range	1,400 nmi
speed	0.8 M
Number of flight crew	2
passengers	118
Aircraft class	Civil large
Load case	$+2.5g$ pull-up manoeuvre

FEA is performed of 20 arbitrary structural designs that differ by the values they possess for the design variables. Each design is analysed at 10 equally-spaced levels of fidelity between $0.1 \leq F \leq 1.0$. The minimum limit is chosen to ensure a sufficient number of nodes to construct a model of the aircraft whilst the maximum limit represents the greatest possible precision, i.e. without any of the member grouping discussed in §5.2.3.1. Table 7.3 lists the levels of model fidelity used to model each design alongside

the results of the investigation. These results include the mean number of DoFs of the 20 designs at each fidelity level, $\overline{n_{DoF}}$, mean computation time for modelling and analysis, $\overline{T}$, and mean differences in measured feasibility with respect to design constraints C1 and C2 at the fidelity level compared to at the highest fidelity level of $F = 1.0$, $\overline{\Delta c_{1,2}}$.

Table 7.3: Variation in number of DoFs and design constraint values with model fidelity

F	$\overline{n_{DoF}}$	$\overline{T}$, s	$\overline{\Delta c_1}$	$\overline{\Delta c_2}$, m
0.1	1,566	1.83	0.9712	0.0108
0.2	2,420	11.16	0.7419	0.0107
0.3	3,718	65.67	0.2593	0.0051
0.4	5,193	155.44	0.0000	0.0061
0.5	7,113	474.86	0.0000	0.0090
0.6	8,983	1,100.42	0.0000	0.0091
0.7	10,563	1,825.44	0.0000	0.0084
0.8	11,125	1,784.60	0.0000	0.0049
0.9	12,767	2,480.84	0.0000	0.0017
1.0	15,671	4,084.63	0.0000	0.0000

Small differences were observed in Table 7.3 in the values measured with respect to the design constraints at different levels of fidelity compared to the variation in number of DoFs. Greater differences were measured in C1 than C2. This was due to model fidelity determining the mechanical properties of the airframe model that are used to calculate the stress fields of structural members, which in turn drives design feasibility with respect to C1. Therefore, this feasibility is dependent on approximations made during both the grouping of members and recovery of the member stress field. In contrast, feasibility with respect to C2 is dependent solely on the deflection of the wingtip; therefore, does not rely on the member stress field recovery, thus reducing the effects of approximations made due to model fidelity. Furthermore, this indicates that the approximations made during member grouping do not introduce inaccuracies in the resulting model mechanical properties as the dependent nodal deflection did not vary greatly from the case without any grouping at maximum fidelity. At $F \geq 0.4$, negligible difference was observed in Δc_1, whilst at $F < 0.4$ Δc_1 increased with decreasing fidelity due to the reduced model precision. Critically, analysis at $F < 0.4$ did not lead to any design being assessed as feasible or infeasible in contrast to that at $F \geq 0.4$, thus FEA at such low fidelity is acceptable for optimisation purposes.

The variations in the number of DoFs and the mean computation time taken for structural modelling and analysis are plotted in Fig. 7.5 against model fidelity. The time taken for modelling and analysis was greatly reduced at lower model fidelity due to the reduced number of DoFs, with a mean time taken at $F = 0.1$ of 0.04% of that required at $F = 1.0$. This indicates a beneficial reduction in computational expense when such modelling and analysis is employed during lengthy optimisation problems. This is especially true given the small differences measured in feasibility between the different fidelity levels. A discrepancy in the general increase in computation time with model fidelity was apparent between $F = 0.7$ and $F = 0.8$ even though an increase in the number of DoFs was recorded. This was most likely due to reduced bandwidth of the FEA matrices at $F = 0.8$ over $F = 0.7$ as a result of variations in the FE models. FE models of one of the airframe designs generated are illustrated in Fig. 7.6 at a sample of fidelity levels. Only the starboard side of the aircraft was modelled given that the applied load case was symmetric along the vehicle longitudinal axis. A clear increase can be seen in the number of elements and nodes, thus DoFs, with increasing model fidelity. This leads to reduced grouping and smearing and thus superior precision but increased computational expense. The limited variation in the feasibility measured at different levels of fidelity provides confidence that reducing model fidelity will not result in misleading design feasibility information whilst providing benefits in computational speed.

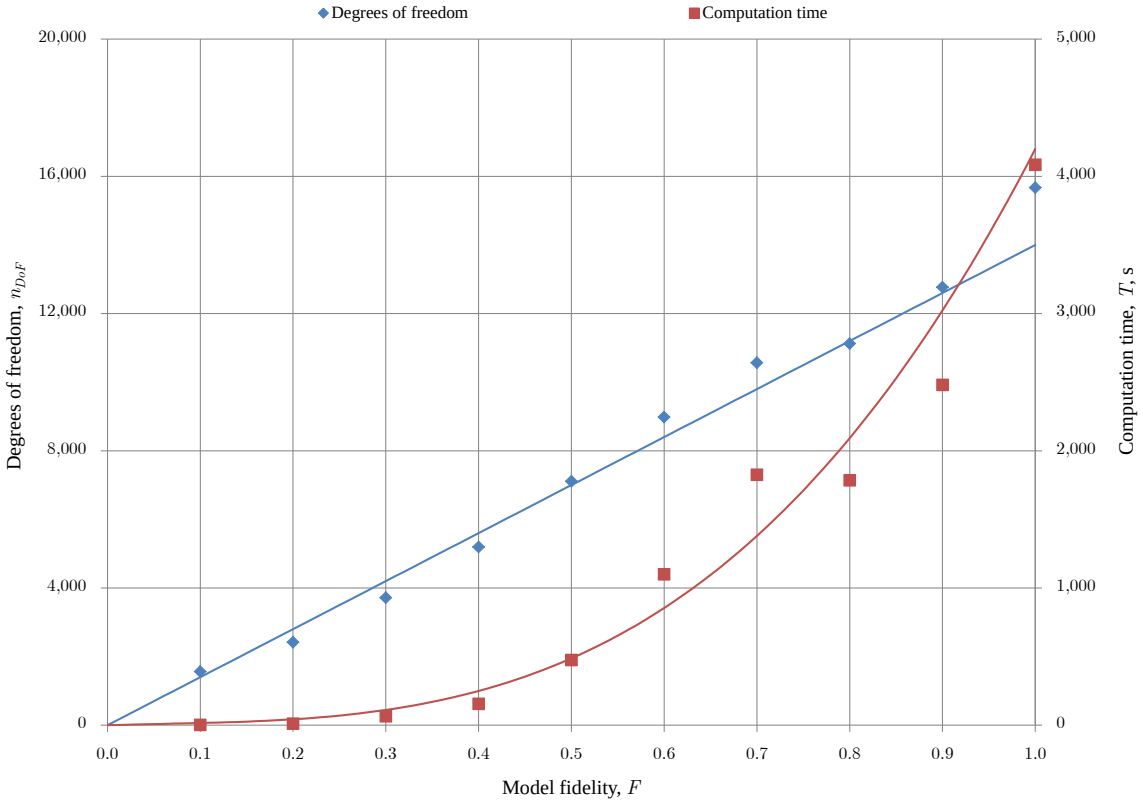

Figure 7.5: Variations in number of DoFs and computation time with increasing model fidelity

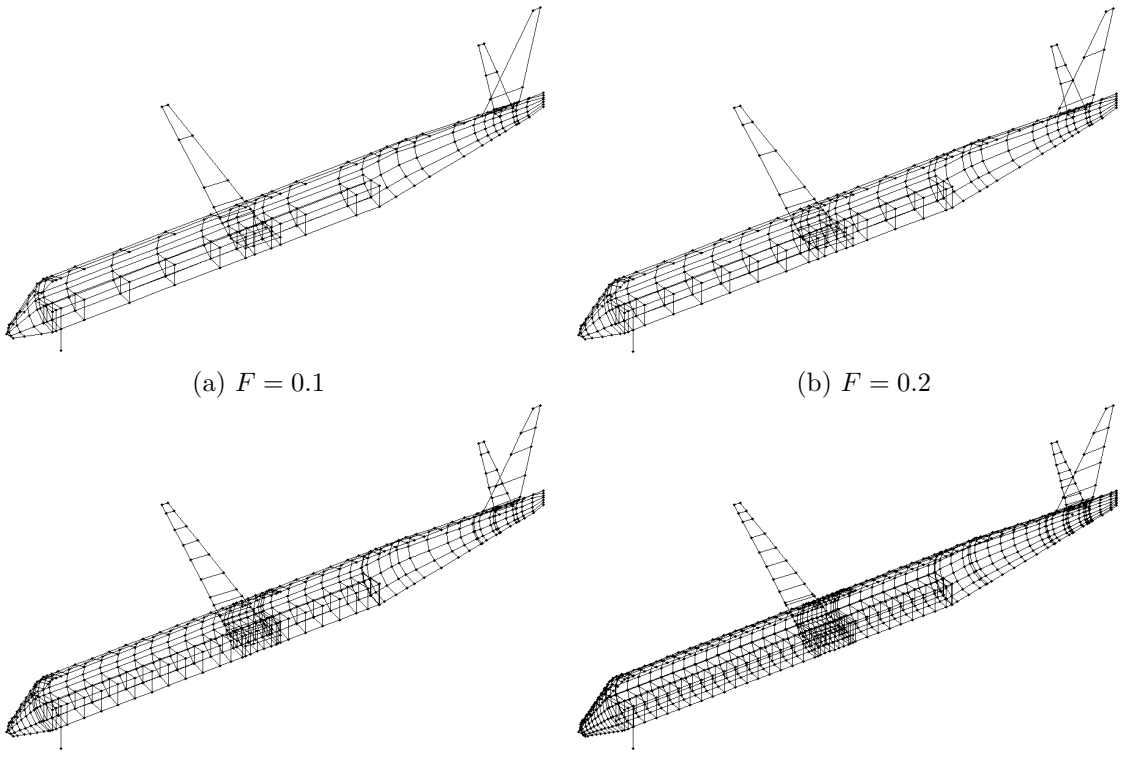

(a) $F = 0.1$

(b) $F = 0.2$

(c) $F = 0.4$

(d) $F = 0.6$

Figure 7.6: FE models of an Embraer E-195 design at a sample of model fidelity levels

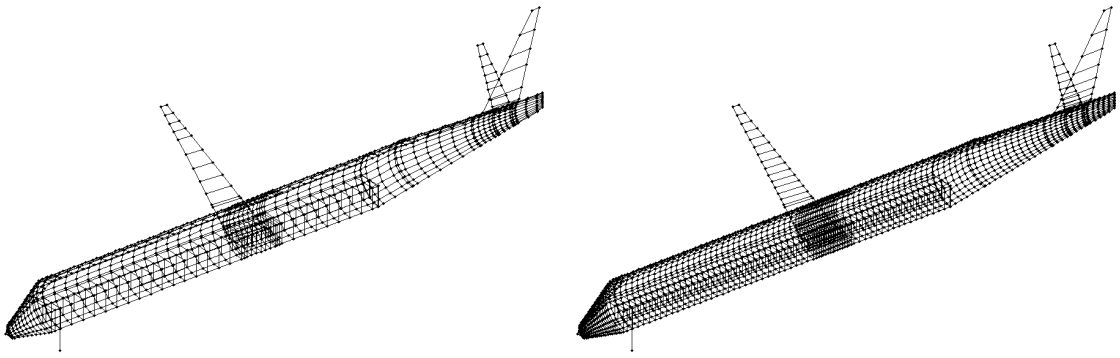

(e) $F = 0.8$ (f) $F = 1.0$

Figure 7.6: FE models of an Embraer E-195 design at a sample of model fidelity levels (cont.)

Finally, it should be noted that the computation times taken during this investigation are dependent on the solver used during FEA. Gaussian elimination with back substitution is performed within AStrO using a basic form of solver that requires the computation of all zero and non-zero stiffness matrix indices. This can lead to an excessive number of operations, i.e. $\mathcal{O}(n^3)$ for a system with n equations, in order to evaluate the sparse matrices that usually represent such FE models. The use of a more efficient solver could significantly reduce the computational time required to solve each static analysis problem, thus decreasing the time benefit of using a low-fidelity model.

7.2 Optimisation Verification

Verification of the optimisation process is required to ensure the optimisation techniques can solve problems with known solutions before being applied to find an unknown solution to a more complicated problem, i.e. aircraft structural design optimisation. This verification is performed by employing the different low-level heuristics (LLHs) to solve a set of mathematical benchmark functions by traditional optimisation, i.e. without the use of the HHA. The benchmark functions used during this investigation are taken from Molga and Smutnicki (2005), Özcan et al. (2008), Rafique et al. (2011) and Yang (2010) and are described in Appendix C. The differing nature of the functions provide various challenges for optimisation techniques, e.g. presenting a high probability of convergence on a local, but not global, optimum. The dimensionality of each problem solution space is determined by the number of variables included within the problem, the values of which are taken from the aforementioned literary sources. Table 7.4 lists functions investigated alongside the number of variables used for each function. Where applicable, Table 7.4 also states the number of function variables and optimisation techniques employed during similar investigations by Özcan et al. (2008) and Rafique et al. (2011). Molga and Smutnicki (2005) and Yang (2010) only presented sets of benchmark functions, i.e. they did not perform any investigations.

The HHA is not used during this investigation as the aim is to assess the capabilities of independent LLHs at solving the optimisation problems without the assistance of hyper-heuristics. Each benchmark function is solved 100 times by each LLH starting from a random initial population or solution. Population-based techniques use a population set of 100 individuals with a maximum number of 1,000 generations forming the sole termination criterion to prevent premature termination of the search. The corresponding criterion for local search (LS) techniques is a maximum number of 100,000 iterations, thus both population-based and step-based LLHs evaluate the same number of design solutions. The LLHs are set up using common parameter values from within the literature (Clerc and Kennedy, 2002; Grefenstette, 1986; Pedersen, 2010; Raymer, 2002; van Laarhoven and Aarts, 1987) as listed in Table 7.5. Parameters P1 and P2 are inactive as there is no structural analysis feasibility measurement during this investigation. A real representation is employed, therefore parameter P3 is also inactive.

Table 7.4: Benchmark functions during preliminary investigation

			Özcan et al.			
		AStrO	(2008, Table 3 p. 11)		Rafique et al. (2011, p. 153)	
Function	Appendix	n_v	n_v	Methods	n_v	Methods
De Jong sphere	C.1	30	10	GA, HHA	30	GA, PSO, SA, HHA
Axis-parallel hyper-ellipsoid	C.2	10				
Schwefel double sum	C.3	10	10	GA, HHA		
Rastrigin	C.4	20	10	GA, HHA	20	GA, PSO, SA, HHA
Griewank	C.5	10	10	GA, HHA	10	GA, PSO, SA, HHA
Schwefel	C.6	10	10	GA, HHA	2	GA, PSO, SA, HHA
Six-hump camel back	C.7	2			2	GA, PSO, SA, HHA
Rosenbrock valley	C.8	20	10	GA, HHA	20	GA, PSO, SA, HHA
Branin	C.9	30				
Easom	C.10	6	6	GA, HHA		
Ackley path	C.11	10	10	GA, HHA	10	GA, PSO, SA, HHA
Drop wave	C.12	30				
Step	C.13	10	10	GA, HHA		
Goldberg	C.14	30	30	GA, HHA		
Whitley	C.15	6	6	GA, HHA		

Table 7.5: Benchmark functions preliminary investigation optimisation set-up

Process parameter		LLH	Value
P4	Indigenous population	RI	$\alpha_{RI} = 0.10$
P5	Crossover probability	DE	$p_{c,DE} = 0.50$
P6	Differential weight	DE	$F_{DE} = 0.90$
P7	Crossover points	RW, TO, BP, RC	$n_c = 1$
P8	Crossover probability	RW, TO, BP, RC	$p_{c,GA} = 1.00$
P9	Mutation probability	RW, TO, BP, RC	$p_m = 0.01$
P10	Breeder pool intake	BP	$\alpha_{BP} = 0.20$
P11	Contaminated population	RC	$\alpha_{RC} = 0.30$
P12	Inertia weight	PSO	$\omega_{PSO} = 0.729$
P13	Cognitive parameter	PSO	$c_{1,PSO} = 1.80$
P14	Social parameter	PSO	$c_{2,PSO} = 1.30$
P15	Constriction constant	PSO	$\kappa_{PSO} = 1.00$
P16	Step size	HC, SA, TS	$\Delta x_v = 0.1\Delta \mathrm{V}_v$
P17	Cooling rate	SA	$\alpha_{SA} = 0.95$
P18	Length of tabu list	TS	$n_{TS} = 100$

The results of this investigation are listed in Table D.1 within Appendix D.1. These include the mean and standard deviation of final objective value as well as the success rate of each method, where a success indicates an optimisation technique obtaining a solution within 4×10^{-4} of the global minimum (Rafique et al., 2011). The results indicated that particle swarm optimisation (PSO) and genetic algorithms (GAs) using roulette wheel (RW), tournament selection (TO), breeder pool (BP) or radioactive contamination (RC) selection performed best across all benchmark functions. The killer queen (KQ) and differential evolution (DE) evolutionary algorithms (EAs) also performed well, however were less likely to find the global minimum when it covered a small region of the solution space, i.e. the Easom and Ackley path functions. The random nature of Monte Carlo (MC) limited its success through a lack of evolution of good solutions; however, random immigration (RI) maintained good solutions within the population which led to greater success. The LS techniques, i.e. hill climbing (HC), simulated annealing (SA) and tabu search (TS), suffered from premature convergence upon local optima within multimodal solution spaces but performed much better in unimodal solution spaces, although not always finding the global minimum due to the static step size employed. The performances of RW, PSO and SA were similar to

that in Rafique et al. (2011), providing further confidence in the LLH operation. These results are compared in Table 7.6. Notably, the success rates of RW and PSO were often greater than in the literature, although the performance of SA was worse. The nature of the results presented in Özcan et al. (2008) prevents a similar comparison. The results of this investigation provide confidence that the LLHs within the heuristic set can locate a global minimum of a known function with reasonable success, most notably the GAs and PSO. Further, the performance of LS techniques in unimodal solution spaces indicates that perturbation analysis could provide further solution improvements if performed near a local optimum.

Table 7.6: Comparison of benchmark function preliminary investigation success rate

	AStrO results Success rate, %			Rafique et al. (2011, Table 2 p. 154) Success rate, %		
LLH	RW	PSO	SA	RW	PSO	SA
De Jong sphere	97	100	98	95	90	92
Rastrigin	85	83	78	88	81	84
Griewank	84	82	79	88	80	82
Schwefel	96	96	86	96	95	97
Six-hump camel back	100	100	90	90	86	93
Rosenbrock valley	89	95	81	97	91	94
Ackley path	92	88	80	89	85	80

7.3 Optimisation Set-Up

The set-up of the optimisation process is investigated in order to determine appropriate values of parameters for use in the case studies in Chapter 8. Investigations are performed into the effects of varying values of optimisation process parameters in §7.3.1 and the influences of different penalty functions on solution quality and feasibility in §7.3.2. The LLHs are then evaluated with varying set-ups in §7.3.3. The results of different investigations should not, however, be compared due to ongoing developments made to AStrO throughout the period of these investigations and variations in the initial conditions of different investigations, i.e. seeded population and optimisation process set-up.

Table 7.7: Selected properties of Boeing 777-200 aircraft

Property	Value
Wing span	60.93 m
sweep	34.0°
Tail span	21.53 m
height	18.50 m
Fuselage length	62.94 m
width	6.20 m
Undercarriage track	10.97 m
wheelbase	25.88 m
Powerplant	2x Rolls-Royce Trent 884-17
Mass operating empty	135,600 kg
maximum take-off	247,200 kg
Cruise altitude	35,000 ft
range	1,400 nmi
speed	0.8 M
Number of flight crew	2
passengers	375
Aircraft class	Civil large
Load case	$+2.5g$ pull-up manoeuvre

The Boeing 777-200 civil large transport aircraft is selected for optimisation throughout these preliminary investigations, a selection of properties of which is presented in Table 7.7 (Boeing Commerical Airplanes, 2011; Jackson, 2009). Optimisation of the aircraft is conducted considering a single cruise mission between two aerodromes with the application of the maximum positive flight manoeuvre load, i.e. load case L1, in combination with cabin pressurisation, engine thrust and gravitational loads, i.e. L9, L10 and L11. All load cases are simulated as static loads to minimise the computational time required for this investigation. Table 7.8 lists the design variables used during these investigations. Only these variables are used to avoid creating an excessively-large problem for such a preliminary investigation. The constraints imposed on the remaining variables are based on the design properties as listed in Table 7.9. Note, the heights of ribs and spars vary depending on the member spanwise and chordwise position. The values in Tables 7.8 and 7.9 are typical of civil light aircraft structural designs, e.g. each lifting surface is set to contain two spars (Howe, 2004; Raymer, 2006; Sensmeier and Samareh, 2004).

Table 7.8: Optimisation set-up preliminary investigations design variables

Design variable		Minimum	Maximum
V1	Number of fuselage frames	20	160
V2	Number of fuselage stringers	30	180
V3	Number of horizontal tail ribs	10	40
V5	Number of horizontal tail stringers	10	80
V6	Number of vertical tail ribs	10	40
V8	Number of vertical tail stringers	10	80
V9	Number of wing ribs	10	100
V11	Number of wing stringers	20	120
V12	Horizontal tail rib spacing exponent	1.0	3.0
V13	Vertical tail rib spacing exponent	1.0	3.0
V14	Wing rib spacing exponent	1.0	3.0
V15	Distribution of frames to nose, %	5.0	15.0
V16	Distribution of frames to wingbox, %	5.0	20.0
V17	Distribution of frames to tail, %	5.0	15.0
V18	Front wing spar chordwise root position, c_r	0.2	0.35
V19	Spar root breadth scaling factor	1.0	4.0
V20	Spar root depth scaling factor	1.0	4.0

Table 7.9: Optimisation set-up preliminary investigations constraints on inactive design variables

Structural member	Material	Profile	Thickness, mm	Depth, mm	Breadth, mm
Lifting surface rib	Al 7075-T6	I	5.0 (web) 10.0 (flange)	Varies	10.0
spar	Al 7178-T6	I	4.0 (web) 20.0 (flange)	Varies	30.0
stringer	Al 2014-T6	Z	5.0	20.0	20.0
Fuselage frame	Al 7075-T6	T	10.0	80.0	80.0
stringer	Al 2014-T6	Z	5.0	20.0	20.0
floor beam	Al 7075-T6	I	20.0 (web) 20 (flange)	80.0	40.0
Skin	Al 2014-T6	-	3.0	-	-
Floor	Al 7075-T6	-	20.0	-	-

The termination criteria are set as a maximum population affinity of 98%, no more than 250 consecutive generations without solution improvement and a maximum number of optimisation generations of

$100,000/\mu$, where μ denotes the population set size. The investigations are set up based on design of experiments (DoE) methodology such that an adequate sample of conditions are investigated without creating an excessively large number of experiments within each investigation (Montgomery, 1997). Five runs are performed of each investigation experiment to obtain a measure of the variability in the results. The set-ups and results of the investigations are presented in Appendix D, where results include those of the run generating the best solution for each experiment, i.e. that with the minimum objective value, as well as the average results over the five runs. For conciseness, this section presents only a summary of the set-ups and key results observed during the experiments performed for these preliminary investigations.

7.3.1 Parameter Evaluation

The values of the parameters that control the LLH drive the behaviour of these optimisation techniques in their attempts to improve the value of the objective function. Hence, it is necessary to perform an evaluation of the effects of these parameters on the optimisation search in order to establish suitable values for LLHs during the case studies, as well as predict the effects parameter control may have on the search by modifying these parameters.

The investigation is performed by solving the same optimisation problem using different LLHs with varying set-ups. These set-ups are defined by the values of process parameters, leading to an investigation of 130 different set-ups of the problem. These set-ups are listed in Table D.2 within Appendix D.2. The ranges imposed on the parameters are defined by values used during investigations within the literature (Clerc and Kennedy, 2002; Deb, 2001; Goldberg, 1989a; Grefenstette, 1986; Pedersen, 2010; Raymer, 2002; Trela, 2003; van Laarhoven and Aarts, 1987). The first 30 experiments investigate different solution representations and population sizes when employing a selection of LLHs. These experiments are labelled PE1 to PE30 in Table D.2. GA representation, strand length and the methods and probabilities of crossover and mutation are then investigated in PE31 to PE65. The mutation probability with KQ is investigated in PE66 to PE71 before the influence of the RI indigenous population size is examined in PE72 to PE77. The influences of breeder pool intake and contaminated population size are investigated in PE78 to PE83 and PE84 to PE89 respectively, followed by investigations of DE and PSO parameters in PE90 to PE95 and PE96 to PE103 respectively. Finally, the effects of varying values of LS step size, SA annealing and the TS tabu list length are investigated in PE104 to PE113, PE114 to PE123 and PE124 to PE130 respectively.

Table D.3 in Appendix D.2 presents the results of each experiment corresponding to the run that generated the best solution of minimum objective value. The average results for each experiment over all five runs are similarly presented in Table D.4, also within Appendix D.2. No specific population size and corresponding number of generations provided a clear advantage in solution quality during experiments PE1 to PE30 due to the fact that all of these experiments evaluated the same number of design solutions overall. However, the experiments performed with a population size of 100 to 200 individuals resulted in shorter durations of the optimisation process than with larger populations without a significant penalty on solution quality. For example, Table D.4 shows that the average time taken for PE14 with the RW LLH and $\mu = 200$ was 1.40 h compared to 3.72 h for PE18 with $\mu = 544$, i.e. $4n_v n_b$ where $n_v = 17$ and $n_b = 8$, at an increase of less than 1% in the best solution quality. Moreover, a real number representation generated improved solutions for RW as shown by a comparison of experiments PE7 to PE12 against PE13 to PE18, as well as PE31 to PE44 against PE45 to PE49. Parameterwise crossover performed well during PE31 to PE44, which also indicated the benefits of crossover between design variables, i.e. the conventional method of crossover with a real number representation. Uniform crossover generated good solutions in all representations. A higher crossover probability during experiments PE50 to PE53 promoted greater search diversity and led to improved final solutions whilst Gaussian mutation with a low mutation probability provided the best solutions in PE54 to PE65 by permitting diversity without excessive randomness. A low mutation rate with KQ in PE66 to PE71 improved solution quality by

similarly preventing the search becoming overly-driven by randomness. A smaller indigenous population during PE72 to PE77 and breeder pool intake during PE78 to PE83 resulted in increased solution space exploration, thus generated better solutions. During experiments PE84 to PE89, a smaller contaminated population improved solution quality with binary RC; however, a larger contaminated population provided the best solutions with a real representation. Less conclusive results were found for variations in the DE parameters during PE90 to PE95. The solutions of minimal mass were found with a low differential weight and crossover probability but higher values of these parameters generated the best solutions on average. The evaluation of PSO parameters during PE96 to PE103 indicated a critical requirement for swarm constriction, i.e. setting the constriction constant to zero in PE102 resulted in search explosion and thus an inability to improve the initial solution. A larger step size with HC in experiments PE104 to PE113 enabled greater solution space exploration by avoiding premature convergence and therefore the discovery of a better final solution, with the real representation greatly outperforming a binary representation. Exponential SA cooling with a higher cooling rate marginally outperformed linear cooling or lower cooling rates during PE114 to PE123. Similar solutions were obtained with varying initial annealing temperatures, although a higher temperature was seen to encourage solution space exploration during early steps. A longer tabu list length in experiments PE124 to PE130 was found to be beneficial in exploring the solution space without premature convergence. Nevertheless, a shorter list tended to result in a better final solution over a greater number of steps.

The results of this investigation indicated that an intermediate population size, i.e. $\mu = 100$ to 200, reduced the computational time required to generate a good solution, whilst a real number solution representations outperformed a binary representation with most LLHs. Uniform crossover and Gaussian mutation with low probabilities, i.e. $p_m = 0.005$ to 0.01, generated the best solutions with a GA. A moderate KQ mutation probability, i.e. $p_m = 0.5$, was most appropriate, whilst the best solutions were generated using low values for the RI indigenous population and BP breeder pool intake but a large value for the RC contaminated population, i.e. $\alpha_{RI} = 0.1$, $\alpha_{BP} = 0.1$ and $\alpha_{RC} = 0.5$. Constriction of PSO exploration was critical to prevent search explosion. A large LS step size, i.e. $\Delta x_v \geq 0.5\Delta \mathrm{V}_v$, and SA exponential cooling schedule also promoted the generation of solutions of higher quality, although the former was due to excessive solution space exploration not typical of the philosophy of a local search.

7.3.2 Penalty Function

The penalty function employed during optimisation determines the treatment of solutions with respect to their feasibility measured during FEA. This directly affects the fitness of solutions, which in turn affects the direction of the optimisation search by determining the influence a solution has on the next generation. Hence, it is essential to ensure an appropriate penalty function is employed for the optimisation problem in hand to encourage the generation of a high-quality and feasible airframe design.

This investigation compares the quality and feasibility of airframe design solutions generated whilst employing a selection of penalty functions commonly applied within the field of aerospace design optimisation. 56 different experiments are performed, i.e. PF1 to PF56, that vary in the penalty function employed, value of penalty parameter, population size and adaptation interval for adaptive functions. Appendix D.3 lists these experiments in Table D.5. Experiments PF1 to PF3 firstly perform optimisation without any penalty function to indicate the effects of disregarding feasibility on solution quality. Subsequent experiments employ the death penalty, PF4 to PF6, interior function with and without a barrier on the constraints, PF7 to PF12 and PF13 to PF18 respectively, and the exterior function as both a static and dynamic function, PF19 to PF30 and PF31 to PF36 respectively. The static exterior function is also employed as the scaled function of Eqn. (2.10) in experiments PF25 to PF30, whilst static and dynamic variants of the adaptive penalty function of Bean and Hadj-Alouane (1992) are employed during experiments PF37 to PF46 and PF47 to PF56 respectively. These adaptive functions are formed using the standard static or dynamic function whilst providing control of the penalty coefficient

as described in Eqn. (2.11) by Bean and Hadj-Alouane (1992). The HHA is disabled throughout this investigation. The LLH employed through this investigation is RW with binary representation, a strand length of 8-bits, uniform crossover of 0.9 probability and no mutation. This set-up is chosen to maintain static test conditions throughout the investigation and thus reduce the effects of the LLH on the variation measured in investigation results.

The best solutions over the five runs of each experiment are presented in Table D.6 and the average results are listed in Table D.7. Optimisation without a penalty function in PF1 to PF3 generated the lightest airframe designs; however, these designs were highly infeasible. The death penalty function, PF4 to PF6, prevented the propagation of beneficial characteristics possessed by infeasible solutions due to the rejection of these designs, thus leading to poorer final solutions than those obtained with other penalty functions. The interior penalty function without a barrier in PF7 to PF12 performed similarly to optimisation without a penalty function by encouraging the generation of a solution far from the constraint barrier leading to a highly-infeasible solution. The inclusion of a barrier within the interior penalty function in PF13 to PF18 led to similar performance as with the death penalty by applying severe pressure to keep the search within the feasible solution space. The exterior penalty function outperformed the previous functions in terms of combined solution objective value and feasibility. Further, the penalty function encouraged convergence upon final populations of higher feasibility. The static penalty function provided the best solutions in PF19 to PF30, however solution feasibility was low when using the scaled static exterior penalty function in PF25 to PF30. The dynamic penalty function encouraged increased feasibility towards the end of the optimisation process, therefore PF31 to PF36 provided improved final population feasibility at a cost to the quality of the best solution due to this restriction of the search. This behaviour indicated the benefits of a dynamic penalty function in improving population feasibility when presented with a highly-infeasible population. However, the function required the ability to relax the penalty applied following the improvement to population feasibility to avoid excessive search restriction. This would have then enabled further solution improvement through exploration close to the constraint boundaries. The adaptive penalty function of Bean and Hadj-Alouane (1992) employed in PF37 to PF56 did not, however, provide these improvements in solution quality and population feasibility. This indicated an opportunity to investigate other methods of controlling an adaptive penalty function such as through the use of parameter control within the HHA.

7.3.3 Technique Evaluation

The optimisation techniques employed as LLHs within the problem domain are investigated in order to establish the ability of each technique in solving the aircraft structural design optimisation problem. This investigation is an extension of the parameter evaluation investigation presented in §7.3.1 by solving the same problem with varying set-ups of LLHs. In contrast to the previous investigation, this study aims to determine which LLHs are most suitable for use within the framework rather than evaluate variations in LLH parameter values. Further, the set-ups of these experiments are informed by the results of the previous investigation.

The optimisation techniques are evaluated over the 116 experiments listed in Table D.8 of Appendix D.4 to determine the best-performing LLHs for aircraft structural design optimisation. The performance of MC with different solution representations is investigated during experiments TE1 to TE4. The effects of representation and indigenous population size on the performance of RI is investigated in TE5 to TE10. Similarly, the effects of representation and mutation probability on the quality of solutions generated by KQ are investigated in TE11 to TE16. The effects of representation and GA crossover are investigated at a probability of 0.9 for RW, TO, BP and RC in TE17 to TE26, TE27 to TE36, TE37 to TE56 and TE57 to TE76 respectively, including the influences of breeder pool intake and contaminated population size for the latter two respectively. Different set-ups of DE and PSO are investigated in experiments TE77 to TE81 and TE82 to TE93 respectively. Finally, different set-ups

of the LS techniques HC, SA and TS are evaluated in TE94 to TE98, TE99 to TE107 and TE108 to TE116 respectively. The values of parameters used are taken from those that performed well during the investigation presented in §7.3.1. The static exterior penalty function is employed throughout following good performance during the investigation presented in §7.3.2.

The results of this investigation are presented in Tables D.9 and D.10, respectively listing the results for the experiment run that generated the best solutions and the average results of all five runs of each set-up. The best solutions overall were generated using RW, TO and BP selection within a GA, with PSO also providing good solutions when using a high constriction constant to prevent search explosion. RC did not perform well due to excessive selection of parents from the contaminated population. This was due to a lack of bias towards the selection of fitter individuals. All LS techniques produced solutions of similar quality to the EAs, GAs and PSO, indicating that these techniques were able to perform better in the solution space of aircraft structural optimisation than in those investigated during the optimisation verification presented in §7.2. Furthermore, this indicated that the solution space consisted of reduced noise than those corresponding to the Rastrigin, Griewank, Ackley path and drop wave benchmark functions. The results of this investigation found that MC, RI, RC and DE did not perform as well as the other LLHs, indicating that these techniques are not as suitable to solving the problem of aircraft structural design optimisation as the other LLHs.

7.4 Hyper-Heuristic Approach

Preliminary investigations of the HHA are performed in order to understand its effects on the optimisation process and resulting solution quality. These investigations enable the identification of appropriate HHA set-ups for use during the case studies in Chapter 8. The heuristic selection aspect of the HHA is firstly investigated in §7.4.1 to establish the methods of heuristic selection and move acceptance that result in airframe designs of lowest mass. Population distribution is subsequently investigated in §7.4.2 and perturbation analysis in §7.4.3 to obtain similar information. Finally, parameter control within the HHA is investigated in §7.4.4 to evaluate the effects of varying process parameters on solution quality, feasibility and population exploration and convergence. The Boeing 777-200 is the aircraft subjected to structural optimisation as in §7.3 with the same test conditions applied and the static exterior penalty function employed throughout. Only the HHA aspect at the focus of each investigation is active during the corresponding investigation. Experiments are performed over five runs, with the set-ups and results of these experiments presented in Appendix D. This section presents a summary of the set-ups and key results observations made during the experiments performed for conciseness.

7.4.1 Heuristic Selection

The investigation of heuristic selection examines the effects of different hyper-heuristics, measure of improvement (MoI) criteria and move acceptance rules on solution quality. This investigation is intended to establish the most appropriate heuristic selection set-ups to be employed during the case studies. The hyper-heuristic objective function of Eqn. (4.3) employed as an MoI criterion is compared against two alternative criteria: the problem objective value in Eqn. (4.1) and the choice function of Drake et al. (2012) given in Eqn. (3.6) upon which the hyper-heuristic objective function is based. These criteria are chosen given that they are commonly employed in existing HHAs whereas the hyper-heuristic objective function is novel function within the framework.

The different set-ups of heuristic selection are investigated over the 132 experiments listed in Table D.11 within Appendix D.5. Experiments HS1 to HS4 employ the simple random (SR) hyper-heuristic with different methods of move acceptance, namely all moves (AM), improving and equal (IE), exponential Monte Carlo with counter (EMCQ) and SA. Random descent (RD) heuristic selection is investigated for the same move acceptance rules in HS5 to HS8. These hyper-heuristics are random, therefore do not

consider an MoI criteria to measure the performance of LLHs applied in the problem domain. The experiments of HS9 to HS24 employ the permutation (PE) hyper-heuristic with different MoI criteria and move acceptance rules. Similar experimental set-ups are employed in HS25 to HS40 for permutation descent (PD), HS41 to HS52 for greedy (GR), HS53 to HS64 for peckish (PK), HS65 to HS76 for RW, HS77 to HS88 for TO and HS89 to HS100 for the TS hyper-heuristics. The experiments of HS101 to HS132 then investigate employing tabu-assisted and MoI-penalised hyper-heuristics coupled with the best-performing MoI criteria and move acceptance rules from HS41 to HS100. The heuristic set is populated with all LLHs within Table A.6 during all experiments. An evaluation period of one generation is used, as was found to be most common within existing approaches in the literature.

Tables D.12 and D.13 present the results of this investigation. The SR and RD hyper-heuristics in HS1 to HS4 and HS5 to HS8 respectively generated poorer solutions than most other hyper-heuristics due to the lack of an MoI criterion to measure the performance of different LLHs. The use of the choice function of Drake et al. (2012) or hyper-heuristic objective function as the MoI criterion generally resulted in the generation of the better designs than using the problem objective value by considering aspects of process performance other than solution quality, thus increasing search diversity. The GR, PK, RW and TO hyper-heuristics performed well with a variety of set-ups. No move acceptance rule clearly outperformed the others, although it was noted that IE move acceptance performed worse than the other three rules. Nevertheless, the average solution quality was often better using EMCQ move acceptance, most notably when coupled with the choice function or hyper-heuristic objective function as the MoI criterion. The inclusion of tabu penalisation of the MoI criterion resulted in improved solution quality, most notably when the RW hyper-heuristic was employed. This penalisation reduced the likelihood of selecting poorly-performing LLHs, thus encouraging the selection of LLHs that previously improved the solution. Tabu assistance, wherein LLHs are stored on a tabu list if performing poorly, did not perform as well as tabu penalisation. This was due to the increased diversity of heuristic selection when employing tabu penalisation which prevented dominance by a small number of LLHs, the latter of which was observed when using tabu assistance.

This investigation provide an indication of the hyper-heuristics, move acceptance rules and MoI criteria that may the greatest provide improvements in solution quality during the case studies. Specifically, the GR, PK, RW and TO hyper-heuristics and EMCQ move acceptance rules provided the greatest interest in terms of high solution quality. The hyper-heuristic objective function provided a better MoI criterion than the problem objective function, and competed with the choice function of Drake et al. (2012) in terms of solution quality. Tabu penalisation provided further improvements in solution quality, although tabu assistance was less effective in improving the best design solution generated.

7.4.2 Population Distribution

The population distribution investigation examines the effects of employing multiple LLHs during an optimisation generation on the quality of the final solution and time taken by the process. The employment of multiple optimisation techniques during a generation reduces the opportunities for each LLH to find an improved solution within its sub-population over the sole use of the technique for the entire population set. However, employing multiple techniques during a generation reduces the detrimental effects imposed on the search due to the limitations of a single LLH. Therefore, this investigation is required in order to determine an appropriate method of distributing a population between a number of LLHs. A further area of interest is the effect of coupling of heuristic selection and population distribution through combined operation within the HHA due to their similar aim of improving the use of LLHs.

The investigation is performed over 96 experiments, listed within Appendix D.6 in Table D.14, that vary in the methods of population distribution and heuristic selection, as well as the heuristic set size, population set size and the distribution interval. The heuristic set varies between containing three and all 12 LLHs. When fewer than 12 LLHs are included within the heuristic set, those that performed

best during the technique evaluation investigation in §7.3.3 are used. Furthermore, a balance of different classes of optimisation techniques, i.e. swarm intelligence (SI), EA or LS, is maintained where possible. Therefore, a heuristic set of size three is populated by the RW, PSO and SA LLHs. KQ is also included for a heuristic set of four LLHs whilst TO and TS are added for a heuristic set of six LLHs. An even population distribution over a varying number of LLHs with different population sizes is investigated in experiments PD1 to PD20. Varying the population size determines the number of opportunities for an LLH to improve its sub-population but also greatly affects the process time. The remaining experiments employ a hyper-heuristic to select the LLHs from the heuristic set whilst varying the size of the population. The SR hyper-heuristic is used for PD21 to PD32 resulting in random distribution of the population between LLHs before the best set-ups of heuristic selection from the investigation presented in §7.4.1 are employed for experiments PD33 to PD56. The best-performing set-ups of heuristic set and population size from HS1 to HS32 are used during these experiments. Finally, the best set-ups from PD33 to PD56 are employed during PD57 to PD96 with varying distribution intervals to investigate the effects of changing the duration over which a population is optimised prior to redistribution.

The results of this investigation are presented in Tables D.15 and D.16. The investigation into an even distribution of individuals in PD1 to PD20 indicated that the best solutions were obtained with an intermediately-sized heuristic set and a sub-population size of 100 individuals per LLH, e.g. PD13 with six LLHs and a total population size of 600 individuals. Such a heuristic set size prevented prohibitively small sub-populations from not allowing sufficient opportunities for solution improvement by each LLH, a factor that was also assisted through the increase in population size. However, this increased the computation time required by the optimisation process. The coupling of population distribution with a performance-based heuristic selection hyper-heuristic improved the quality of solutions generated in PD33 to PD56. This was most notable when employing an MoI-penalised RW hyper-heuristic with three or four LLHs within the heuristic set and a population size of 100 to 300 individuals. In these cases, the computational penalty of employing multiple LLHs was reduced or even eliminated by enabling bias of the population towards better-performing LLHs. The best set-ups of experiments PD33 to PD56 were subsequently employed during PD57 to PD96 to investigate the effects of varying the distribution interval. The results of these experiments suggested that an interval of 40 to 60 generations between population distributions performed best, especially when using a GA-based heuristic selection hyper-heuristic.

The results of this investigation indicated that coupling heuristic selection and population distribution provided opportunities to improve the quality of the solution generated if heuristic selection was performed by a hyper-heuristic with an appropriate MoI criterion and move acceptance rule. Distribution between three or four LLHs generated the best solutions with population sizes of 100 to 300 individuals. Consequently, the population size could be reduced such that each LLH required fewer individuals within its sub-population than was generally required when operating alone. This presented the possibility to obtain improvements in solution quality without prohibitively increasing the computation time.

7.4.3 Perturbation Analysis

An investigation is performed into the use of perturbation analysis to further improve the quality of design solutions. This investigation is necessary in order to identify the features of this HHA aspect that promote the greatest improvement in solution quality without incurring excessive computational cost due to additional solution analysis required. Consequently, this investigation aims to establish suitable set-ups of perturbation analysis for use during the case studies.

Perturbation analysis is investigated over the 74 experiments listed in Table D.17 within Appendix D.7. These experiments vary in the hyper-heuristic used, the evolutionary principle employed for solution space learning, the method and size of population sampling and the perturbation scale. PA1 to PA18 employ the HC hyper-heuristic with Lamarckian or Baldwinian evolution and varying population sampling methods and sizes. Experiment set-ups PA19 to PA36 and PA37 to PA54 perform similar investigations using

the SA and TS hyper-heuristics respectively. The effects of varying the perturbation scale are then investigated in experiments PA55 to PA74 using the best-performing set-ups from PA1 to PA54. The settings of the optimisation process are constant throughout all experiments to limit their influences on the optimisation process. More specifically, the LLH employed within the problem domain is RW with real number representation and one-point crossover at a probability of 0.9 without mutation following good performance during the investigations in §7.3.

Table D.18 presents the results of this investigation corresponding to the run that generated the best solution for each experiment. The average results over all five runs are given in Table D.19 and show similar final solution quality over experiments PA1 to PA54, although with greater variation using the TS hyper-heuristic than with HC or SA. The best solutions were obtained using the SA or TS hyper-heuristics coupled with Lamarckian evolution and small samples of the best population individuals, i.e. $\mu_{PA} \leq 0.1\mu$. Noticeably, the increase in computation time was not significantly greater when taking a large sample of the population as this resulted in a greater number of solution improvements leading to individuals with fewer DoFs, i.e. smaller airframes, during FEA in subsequent generations. However, this did not lead to the discovery of better solutions than with small samples of the best individuals within the population. The smallest perturbation scale during experiments PA55 to PA74 generated the solutions of minimal mass, although these solutions were not lighter than the best obtained in the corresponding experiments during PA1 to PA54. The use of perturbation analysis in many experiments led to high convergence, however on a highly-infeasible populations close to the constraint boundaries. This indicated that including control of the penalising strategy could allow convergence to occur near the constraint boundaries but within the feasible region. The results of this investigation indicated that SA and TS were the better perturbation analysis hyper-heuristics, with Lamarckian evolution and small perturbation scales leading to the best solutions of minimal mass.

7.4.4 Parameter Control

Parameter control is the subject of the final preliminary investigation to establish appropriate set-ups of this HHA aspect for use during the case studies. Parameter control promotes improvement in solution quality through appropriately-timed solution space exploration or convergence whilst also attempting to reduce the computational time required for optimisation. This is achieved by satisfying the hyper-heuristic objective function given by Eqn. (4.3). This investigation is therefore required to ensure that parameter control may perform as well as possible during the case studies in order to provide the greatest possible improvements in the optimisation process.

The investigation is focussed on the different hyper-heuristics employed for parameter control within the HHA and the period over which the hyper-heuristic objective function is evaluated between the modification of parameters. 114 experiments are investigated with varying hyper-heuristics used to control the different parameters given in Table 5.4. The ranges imposed on parameters are determined by the results of the earlier investigations in §7.1 and §7.3. The parameters are investigated in groups to maintain a manageable quantity of experiments through consideration of the LLHs employing the parameters. Consequently, the LLH employed during each experiment is the technique that uses the parameters investigated. Appendix D.8 lists the set-ups of the experiments in Table D.20. Experiments PC1 to PC9 investigate the effects of controlling FE model fidelity, P1, whilst PC10 to PC18 perform a similar investigation of the effects of varying the penalty function coefficient, P2. The RW LLH is employed for experiments PC1 to PC18 since these experiments do not investigate parameters associated with a specific LLH. The RI indigenous population size, P4, is controlled in PC19 to PC27 whereas the DE crossover probability and differential weight, P5 and P6 respectively, are controlled during PC28 to PC36. GA strand length, crossover technique and probabilities of crossover and mutation, P3, P7, P8 and P9 respectively, are investigated during PC37 to PC45. The breeder pool intake and contaminated population, P10 and P11 respectively, are investigated during experiments PC46 to PC54 and PC55 to

PC63 respectively. The control of PSO parameters, P12 to P15, are investigated in PC64 to PC72 whilst the LS step size, P16, SA cooling rate, P17, and tabu list length, P18, are investigated in PC73 to PC81, PC82 to PC90 and PC91 to PC99 respectively.

The investigation results are presented in Tables D.21 and D.22. Similar results were obtained using the different hyper-heuristics, although SA and TS generated mostly better solutions than HC. Hyper-heuristic control of model fidelity in PC1 to PC9 resulted in infeasible solutions of low mass, with the average final population feasibility higher using SA and TS rather than HC. However, the infeasibility of the solutions indicated that coordinated control of FE model fidelity and the penalty function coefficient may be required. The SA hyper-heuristic provided the best mean final population feasibility when controlling the penalty coefficient in PC10 to PC18 by generating populations of higher feasibility than when using TS or HC. Moreover, similar objective values were obtained as in all other experiments within this investigation. This indicated improved control of the penalty coefficient over that obtained using the adaptive penalty function in §7.3.2 where poor solutions were generated. The TS hyper-heuristic provided best control of the RI indigenous population in PC19 to PC27, whilst all hyper-heuristics generated solutions of similar quality when controlling the DE operators in PC28 to PC36, GA parameters in PC37 to PC45 and breeder pool intake in PC46 to PC54. Great variation was observed in solution quality when controlling RC contaminated population in PC55 to PC63, with much poorer solutions generated than using the other LLHs. The performance of PSO relative to other LLHs was better during PC64 to PC72 than has been observed during the investigation of §7.3.3, indicating benefits in possessing dynamic control of the LLH operators. Hyper-heuristic control of the LS parameters in PC73 to PC99 did not greatly improve the performance of the LLHs relative to the population-based LLHs compared to optimisation with static operators in §7.3.3. A longer evaluation period, i.e. 50 generations, generally resulted in the best final solution quality by permitting changes to parameters to take effect and attempt to improve the value of the hyper-heuristic objective function before making further changes to the parameter values.

7.5 Summary

A series of preliminary investigations have been performed to verify the implementation of the framework and determine appropriate settings for use during case studies presented in Chapter 8. The verification of the structural analysis and optimisation processes provide confidence that reliable results can be obtained using the framework. Furthermore, the effects of varying the set-up of the optimisation process, including the HHA, have been evaluated such that the experiments performed during the case studies can be set up with appropriate values of problem and hyper-heuristic domain process parameters, as well as using the better-performing LLHs and hyper-heuristics. As a result, case studies can be performed to assess the performance of the framework in solving aircraft structural design optimisation problems with the process set up in accordance with the findings of these investigations.

Chapter 8

Case Studies

Four case studies are performed to evaluate the framework described in Chapter 5 through its implementation as AStrO. These studies investigate different aspects of the framework to enable a thorough evaluation. The set-up of the framework during these studies is based on the results of the preliminary investigations as presented in Chapter 7. The results of these case studies are discussed further in Chapter 9 to complete the evaluation of the framework. This chapter describes the set-ups and the results of the case studies. The first study in §8.1 aims to establish the effects of the hyper-heuristic approach (HHA) on the optimisation process in comparison to traditional optimisation using a single low-level heuristic (LLH). The second case study presented in §8.2 expands this assessment of the HHA for a novel aircraft concept under numerous load cases. A further study in §8.3 examines the effects of different methods of parameter control, including hyper-heuristic control, on solution quality and computational expense. Finally, the study presented in §8.4 examines the effects of different load cases on the structural integrity of the airframe. The chapter is summarised in §8.5.

8.1 Airbus A340-300

The first case study evaluates the HHA embedded within the framework by comparing its performance against traditional methods of optimisation, i.e. the application of a single static optimisation technique. This comparison is made with respect to the quality of the best solutions generated using different set-ups of the HHA and traditional LLHs. Furthermore, considerations are made of solution feasibility and the behaviour of the optimisation process in exploring the solution space and converging on a good solution. The aim of this study is to determine the benefits and limitations of the HHA with respect to traditional optimisation. The results presented in §7.4 are used as a foundation for the study. The case study is performed using an existing aircraft, the Airbus A340-300 large civil aircraft, as the external profile within which the airframe is designed and optimised. Selected properties of this aircraft are presented in Table 8.1 (Airbus SAS, 2012; Jackson, 2009), including the single cruise mission simulated during the investigation and the two applied load cases of the maximum positive flight manoeuvre and a two-point landing, L1 and L5 respectively. These load cases are selected as they represent two of the most onerous cases within the load case database and are applied as static loads in combination with the miscellaneous loads of cabin pressurisation, engine thrust and gravity, i.e. L9, L10 and L11 respectively.

The Airbus A340-300 is a similar aircraft in class, design and purpose to the Boeing 777-200 used during the investigations in §7.3 and §7.4. For this reason, the same active design variables and corresponding ranges are used for this case study as stated in Table 7.8. Similarly, the constraints imposed on inactive variables are the same as during the preliminary investigations as given in Table 7.9. The number of active variables is limited in this manner as the focus of the study is on a comparison of optimisation methods rather than the details of different designs.

Table 8.1: Selected properties of Airbus A340-300 aircraft

Property	Value
Wing span	60.30 m
sweep	30.0°
Tail span	19.40 m
height	16.99 m
Fuselage length	63.69 m
width	5.64 m
Undercarriage track	10.69 m
wheelbase	25.37 m
Powerplant	4x CFM International 56-5C4
Mass operating empty	130,200 kg
maximum take-off	276,500 kg
Cruise altitude	35,000 ft
range	5,000 nmi
speed	0.82 M
Number of flight crew	2
passengers	335
Aircraft class	Civil large
Load case in-flight	$+2.5g$ pull-up manoeuvre
on ground	Two-point landing

The dynamic process parameters are varied by parameter control within the ranges specified in Table 8.2. The selection of these values is based on the results of the preliminary investigations presented in §7.3 and §7.4.4. An evaluation period of 50 generations is used as a consequence of the preliminary investigations results given in §7.4.4. Initial values of these process parameters are generated using the simple random (SR) hyper-heuristic. Static model fidelity, P1, at $F = 0.1$ is employed to allow this study to focus on the optimisation aspects of the process, i.e. without the influences of varying the set-up of structural analysis on solution quality. As a result, the final component of Eqn. (4.3) measuring computation time is disabled since this component is included chiefly to influence the level of fidelity employed.

Table 8.2: Airbus A340-300 aircraft case study dynamic process parameters

Process parameter		LLH	Minimum	Maximum
P2	Penalty coefficient	-	0.25	2.00
P3	Strand length	-	4-bits	16-bits
P4	Indigenous population	RI	0.10	0.40
P5	Crossover probability	DE	0.00	1.00
P6	Differential weight	DE	0.00	2.00
P7	Crossover points	RW, TO, BP	1	Random
P8	Crossover probability	RW, TO, BP	0.50	1.00
P9	Mutation probability	RW, TO, BP	0.00	0.01
P10	Breeder pool intake	BP	0.10	0.30
P12	Inertia weight	PSO	0.55	0.75
P13	Cognitive parameter	PSO	1.40	2.10
P14	Social parameter	PSO	0.90	1.80
P15	Constriction constant	PSO	0.50	0.50
P16	Step size	HC, SA, TS	$0.001\Delta V_v$	$0.01\Delta V_v$
P17	Cooling rate	SA	0.00	0.95
P18	Tabu list length	TS	0	100

Eight experiments varying in the set-up of the HHA or traditional optimisation process are performed. Table 8.3 describes these experiments, with ticks indicating active aspects of the HHA during each experiment. Experiment 1 employs the Monte Carlo (MC) LLH to perform a random search for a solution and thus provide a baseline for the comparison of all other experiments. Experiment 2 employs the roulette wheel (RW) LLH for traditional optimisation by a genetic algorithm (GA). The HHA is then employed in experiments 3 to 8. Solely perturbation analysis and parameter control are applied in experiments 3 and 4 respectively to study the effects of these aspects in isolation. The perturbation analysis sample size is the best 10% of the population during the previous generation in accordance with the findings in §7.4.3. Experiment 5 applies only the heuristic selection aspect using the greedy (GR) hyper-heuristic whilst experiment 6 applies heuristic selection by RW selection and population distribution. These hyper-heuristics are selected following good performance during the preliminary investigations in §7.4.1 and §7.4.2. Experiments 7 and 8 employ the complete HHA. All LLHs within Table A.6 populate the heuristic set except radioactive contamination (RC) since this is a novel technique and its inclusion would not be appropriate for a comparison against traditional optimisation methods. A maximum of three LLHs per generation are permitted during population distribution in experiments 6 and 7, as suggested by the results presented in §7.4.2. A dynamic population size, as described in §5.3.4.2, is used during experiment 8 with a sub-population size limit of 100 individuals, i.e. a maximum size of 1,100 individuals for distribution between all 11 LLHs within the heuristic set. All experiments are seeded within an identical initial population, with the exterior penalty function, uniform crossover and exponential Monte Carlo with counter (EMCQ) move acceptance. The termination criteria are set as a limit of 1,000 generations, maximum population affinity of 98% and 250 successive generations without improvement. This final criterion is increased to 350 generations when using parameter control to allow changes in parameters to take effect. The design constraints are set at $c_1 \geq 1.5$ and $|c_2| \leq 7.5$ m.

Table 8.3: Airbus A340-300 aircraft case study set-up of experiments

	Experiment							
Aspect	1	2	3	4	5	6	7	8
Population size	100	100	100	100	100	300	300	$\leq$ 1,100
Heuristic selection					✓	✓	✓	✓
Population distribution						✓	✓	✓
Perturbation analysis			✓				✓	✓
Parameter control				✓			✓	✓
Low-level heuristic	MC	RW	RW	RW	Experiments 5-8: All except RC			
Hyper-heuristic:								
Heuristic selection					GR	RW	RW	RW
Perturbation analysis			SA				TS	TS
Parameter control				SA			SA	SA

10 runs are conducted of each experiment to account for the variability in the results due to the stochastic nature of the heuristics employed. For each experiment, Table 8.4 presents the results of the run generating the best solution as well as the average results over all runs. This includes the objective value for the best solution generated during the experiment, $\Phi_{\min}$, and the percentage difference between this solution and the best design generated over all experiments, $\Delta\Phi_{\min}$. The worst values with respect to the design constraints, $c_{1,2}$, and feasible proportion of structural members, η, are also provided for the best solution from the experiment. The feasibility, $\beta(\mathrm{X}^{n_k})$, and affinity, $A(\mathrm{X}^{n_k})$, of the final population, i.e. at generation n_k, are also given as well as the computation time taken as a proportion of that required for the experiment that generated the overall best solution, ΔT. This latter value is presented rather than the computation time, T, because a varying number of high-performance computing (HPC) processors

are required to complete each experiment within a hardware time constraint of 72 h due to the different population sizes. The average results include the maximum, mean, and standard deviation of the best objective values across all runs, $\Phi_{\max}$, $\overline{\Phi}$, and $\sigma(\Phi)$ respectively.

Table 8.4: Airbus A340-300 case study solution of minimal mass and average results

	Experiment							
Result	1	2	3	4	5	6	7	8
$\Phi_{\min}$, kg	57,922	50,234	50,609	50,465	47,069	47,659	46,228	45,323
$\Delta\Phi_{\min}$, %	24.41	10.28	11.02	10.74	3.78	5.02	1.98	0.00
c_1	1.63	1.52	1.58	1.51	1.58	1.46	1.51	1.59
c_2, m	-0.46	-0.23	-0.54	-0.27	-0.28	-0.23	-0.23	-0.24
η, %	100.00	100.00	100.00	100.00	100.00	96.06	100.00	100.00
$\beta(\mathrm{X}^{n_k})$, %	9.00	85.00	72.00	97.00	11.00	98.78	29.27	12.50
$A(\mathrm{X}^{n_k})$, %	56.27	96.56	90.16	91.10	57.03	96.01	73.73	61.92
n_k	489	691	386	1,000	994	938	1,000	1,000
ΔT	0.08	0.04	0.04	0.04	0.06	0.19	0.22	1.00
$\Phi_{\max}$, kg	63,021	64,150	60,418	60,344	50,940	50,829	48,266	46,644
$\overline{\Phi}$, kg	60,744	56,583	53,880	53,604	48,466	48,763	47,028	45,931
$\sigma(\Phi)$, kg	1,661	5,673	3,053	4,068	1,151	1,042	669	480

Experiments 1 and 2 provided useful benchmarks of optimisation using a random search and a traditional GA for comparison against the HHA in experiments 3 to 8. Experiment 1 generated the worst solution with poor convergence and population feasibility due to the random nature of the search. Solution quality, population feasibility and population affinity were greatly improved using the GA in experiment 2. Figure 8.1 shows the variations in the objective value of the best solution during each experiment presented in Table 8.4. The evolution of the best solution in experiment 2 can be seen whereas experiment 1 indicates more discrete solution improvements due to the purely random nature of the search. Both experiments converged prematurely on poorer solutions than those of experiments 3, 5, 6, 7 and 8.

Perturbation analysis in experiment 3 provided instances of significant improvement in the solution. This is illustrated in Fig. 8.2(a) to show the objective value of the running best solution, i.e. as in Fig. 8.1, alongside the affinity and feasibility of the population for experiments 3 and 4. Improvements in the objective function of at least 10% following perturbation analysis are labelled 'PA'. Experiment 3 suffered premature convergence after the discovery of a local minimum after 136 generations. The improvement in the objective value of the best solution during experiment 4 initially followed a similar trend to that of experiment 3. However, periods of deteriorating population feasibility led to the application of parameter control to promote feasibility by increasing the penalty coefficient. Four instances of such control are labelled 'PC' in Fig. 8.2(a), showing decreasing feasibility over generations preceding increases in the penalty coefficient and subsequently population feasibility. This adaptation improved solution quality, population feasibility, and increased population affinity. Ultimately, the solution obtained during experiment 4 was poorer than that for experiment 2. However, final population feasibility was improved and a solution closer to the constraint boundaries found, as seen by the margin between the limiting values of the design constraints and the constraints themselves in Table 8.4.

The use of heuristic selection during experiments 5 to 8 improved the quality of the final airframe design solution over experiments 1 to 4. The elitist nature of the GR hyper-heuristic in experiment 5 produced a better solution than the RW hyper-heuristic in experiment 6 due to the possibility of selecting poorer performing LLHs using RW. However, this elitist behaviour resulted in the dominance of exploration-encouraging LLHs, such as MC and differential evolution (DE), leading to poor convergence and population feasibility as indicated in Table 8.4. Figure 8.2(b) is annotated to indicate the selection

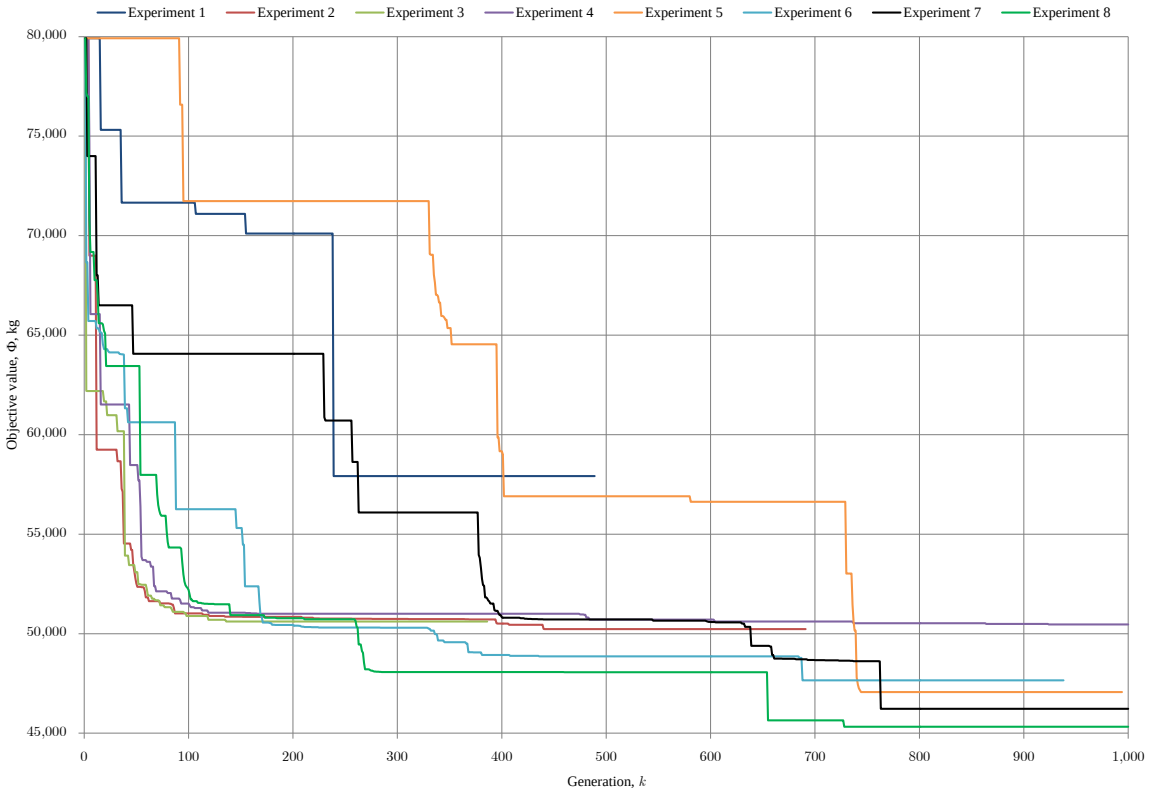

Figure 8.1: History of best solution objective value during Airbus A340-300 case study

of LLHs during experiment 5. Influences of different heuristics on population diversity can be seen by the patterns in affinities and feasibility. Similar trends were observed during experiment 6; however, population distribution reduced such LLH dominance, resulting in greater population feasibility and affinity over that obtained during experiment 5 through the use of all LLHs multiple times.

Perturbation analysis during experiment 7 improved the final solution compared to experiment 6. However, parameter control did not provide any benefits in population feasibility and convergence due to sub-populations converging independently. This poor convergence led to large variations in population feasibility, as shown in Fig. 8.2(c) alongside the objective values of experiments 7 and 8. Figure 8.2(c) is annotated by 'HS' to indicate generations at which heuristic selection was performed. Additional annotations indicate perturbation analysis, 'PA', and generations at which parameter control was applied with notable effects, 'PC', as for Fig. 8.2(a). Poor convergence was also apparent during experiment 8, with a large increase in computation time due to a maximum population size of up to 1,100 individuals. The dynamic population size reduced the population to 848 individuals through the elimination of individuals from sub-populations that violated the limit of 100 individuals per sub-population. However, this failed to encourage convergence on a small number of LLHs to reduce the population set size, leading to six LLHs possessing full sub-populations of 100 individuals at the end of the search. These LLHs were MC, RW, DE, random immigration (RI), tournament selection (TO) and breeder pool (BP). Consequently, the resulting population size for experiment 8 was still much larger than during all other experiments, therefore it was more likely to find a better solution to the problem. Nevertheless, the computational time required to do so was much greater than for traditional optimisation, as stated in Table 8.4, which greatly penalised the benefits of employing this set-up of the HHA. Notwithstanding this, inclusion of the final component of Eqn. (4.3) during the study would have promoted the reduction of this cost.

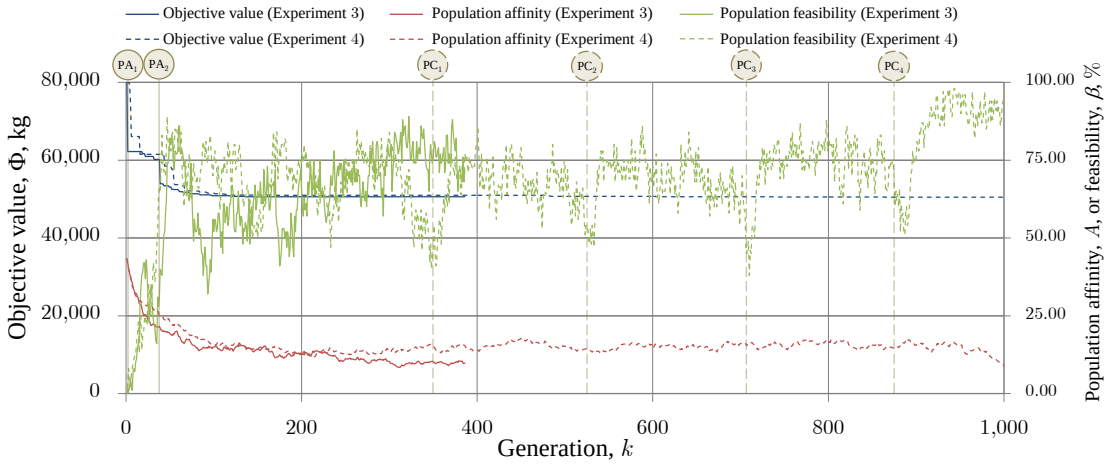

(a) Running best solution objective value, population feasibility and affinity during experiments 3 and 4

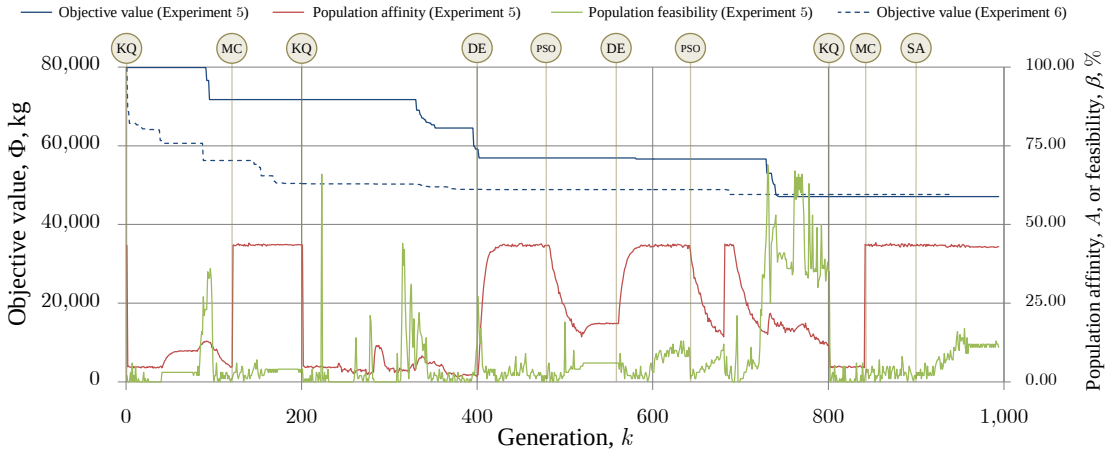

(b) Running best solution objective value, population feasibility and affinity during experiments 5 and 6

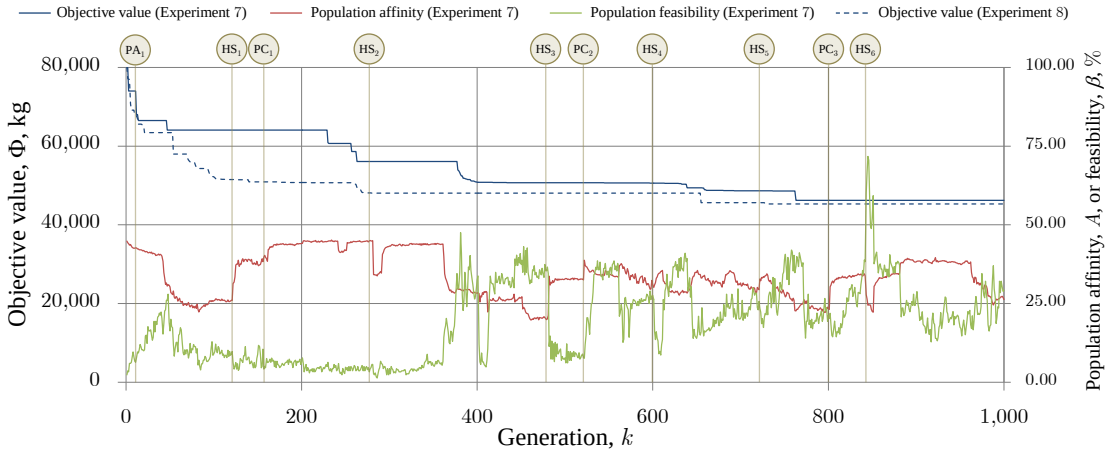

(c) Running best solution objective value, population feasibility and affinity during experiments 7 and 8

Figure 8.2: History of best solution and population during Airbus A340-300 case study

Experiments with parameter control terminated upon reaching the limiting number of optimisation generations whilst all others terminated due to successive generations without improvement. The number of

solution evaluations ranged from 38,600 evaluations for experiment 3 to 857,272 evaluations for experiment 8. These values are comparable to those of similar studies in Raymer (2002), where the number of solution evaluations for successful experiments ranged from 2,514 to 42,562, and in Rafique et al. (2011) and Özcan et al. (2008), where the average number of evaluations for different functions ranged from 2,953 to a maximum of 100,000 evaluations (Rafique et al., 2011) and from approximately 1,000,000 to 100,000,000 evaluations (Özcan et al., 2008).

The evolution of the solution during experiment 8 is shown in Fig. 8.3. The numbers of frames and ribs, V1, V3, V6 and V9, noticeably decreased over the generations and there was also a noticeable variation in the distributions of both member types, V12 to V17, throughout the aircraft. A regular increase in spar thickness at the root was seen throughout, V19 and V20, leading to the strengthening of the wing at the root to react the bending loads imposed by the load cases. The number of fuselage stringers, V2, was driven by cabin pressurisation and bending due to the landing load.

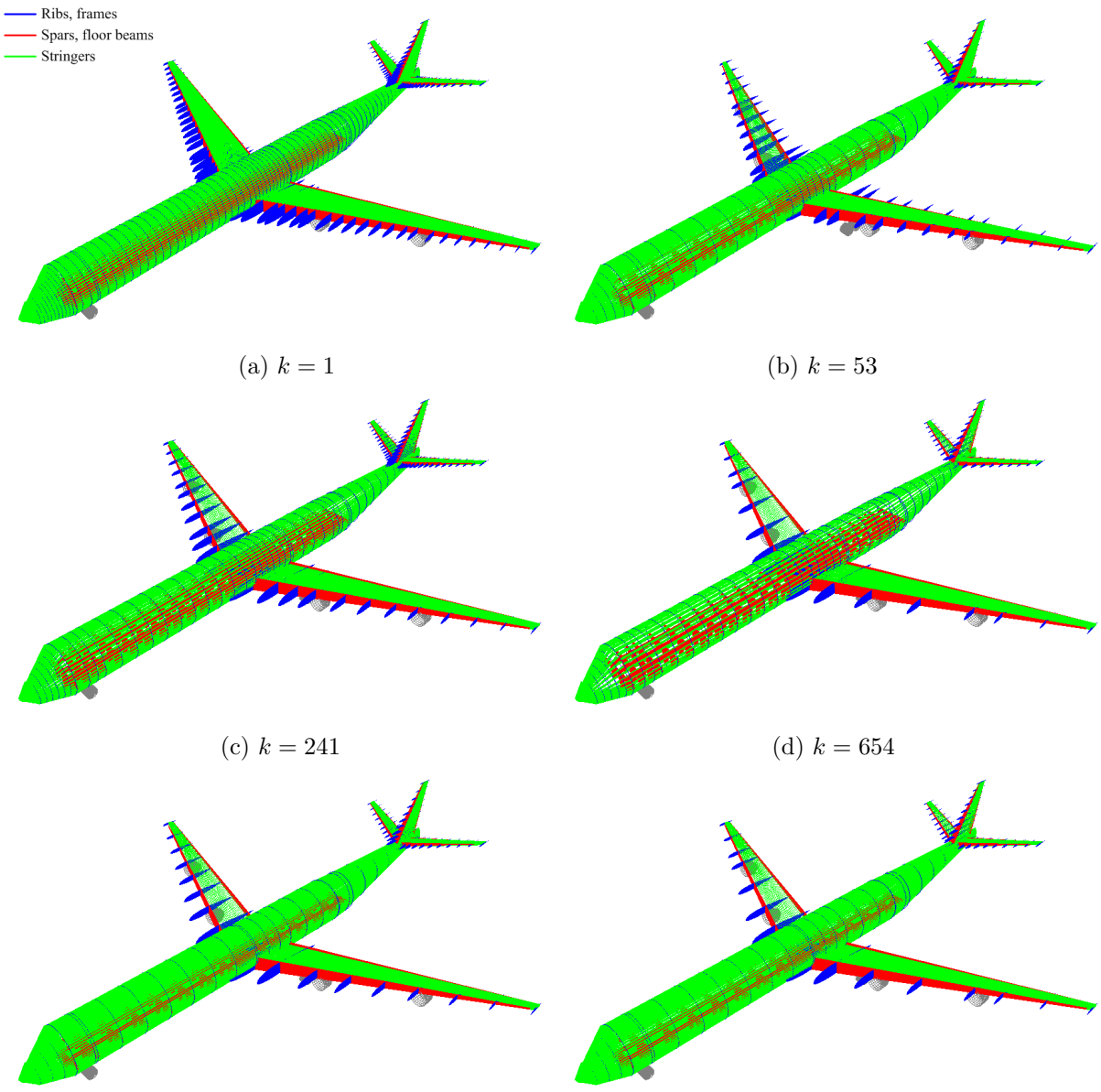

(a) $k = 1$ (b) $k = 53$

(c) $k = 241$ (d) $k = 654$

(e) $k = 727$ (f) $k = 1,000$

Figure 8.3: Evolution of overall best solution for Airbus A340-300 airframe design

The behaviours of experiments were consistent across all runs although there was variability in final solution quality for each experiment. The mean objective values of the best solutions during experiments 5 to 8 were lower than for experiment 2, the best-performing traditional method, with analysis indicating statistically significant differences under t-tests for means with assumed unequal variance: $p < 0.001$. However, no statistically significant difference existed between experiment 2 and experiments 3 and 4 due to the prevailing influence of the same GA employed as the LLH during these runs: $p \approx 0.1$. The lowest means and standard deviations in solution quality were generated during experiments 7 and 8, indicating the greatest repeatability of high-quality solutions when using the complete HHA.

Noticeable differences exist between the best design generated overall and the existing design of the Airbus A340-300. The front wing spar was positioned at $0.34c_r$ rather than approximately $0.22c_r$ for the existing Airbus A340-300 design (Sensmeier and Samareh, 2004). This position is closer to that of the larger and heavier Airbus A380 and reduced the sweep of the spars leading to lower shear load due to the angle between the applied load and member. A greater concentration of ribs and increased spar thickness strengthened the wing root and led to the airframe containing fewer than 30% of the number of wing ribs than within the existing aircraft design (Sensmeier and Samareh, 2004). The Airbus A340-300 operating empty mass is 130,200 kg (Jackson, 2009), a value that includes the masses of non-structural aspects of the design such as systems and powerplants. The airframe structural mass can be estimated empirically for a long-haul jet as approximately 40% of the operating empty mass (Torenbeek, 1982, p. 266). Thus, an empirical estimate of the airframe structural mass of the airframe is 52,293 kg, which provides a better value for comparison with the results of the study. Hence, the best solutions of experiments 1 to 8 were between approximately 87% and 111% of the estimated structural mass of the existing Airbus A340-300 aircraft design. However, it should be noted that this mass for the Airbus A340-300 is an estimate based on the final aircraft designed to a greater level of detail than would be used during conceptual design. Furthermore, this study only considered two loading conditions, whereas the complete design process would apply a greater selection of load cases which would further increase the structural mass in order to obtain a design with satisfactory strength under load. Nevertheless, all experiments using the HHA, except the prematurely-converged experiment 3, indicated improved conceptual airframe designs with respect to the structural mass.

8.2 AStrO-1

The second case study extends the framework evaluation through its use to generate a novel concept of a military training aircraft, named AStrO-1, with a greater selection of load cases and the consideration of all design parameters, i.e. variables, constraints and the objective, within Table 5.3. Optimisation of a novel concept, rather than an existing design variant, requires all tasks of the aircraft design procedure stage to generate the aircraft external profile for subsequent structural optimisation within. Table 8.5 lists a selection of the properties of the external profile as input during initialisation, i.e. those parameters listed in Table A.1, as well as data generated by the aircraft design procedure stage of the framework. These include the powerplant designs generated empirically in order to satisfy the balanced field length of RAF Leeming aerodrome, selected through its current role as a military training base, as well as the mission requirements of AStrO-1. The mission and loads are selected to simulate a training mission encompassing a cruise to a combat zone including demanding manoeuvres, L1 and L2, and gusting conditions, L4. Both two-point and three-point landings, L5 and L6 respectively, are included to simulate a missed approach and subsequent reattempted landing in a different landing configuration. Dynamic braking, L8, is included to simulate an interrupted taxi. The miscellaneous loads of low differential cabin pressurisation, L9, engine thrust, L10, and gravity, L11, are superimposed on these loading conditions, which are applied as pseudo-static loads to reduce computation time.

Table 8.5: Selected properties of AStrO-1 aircraft

Property	Value
Wing span	9.04 m
sweep	1.0°
Tail span	3.07 m
height	1.99 m
Fuselage length	7.77 m
width	1.10 m
Undercarriage track	1.84 m
wheelbase	1.90 m
Powerplant power	507.10 kW
mass	149.25 kg
Cruise altitude	15,000 ft
range	500 nmi
Combat altitude	10,000 ft
duration	2 h
Number of flight crew	2
Ordnance	2x 72 L external fuel tanks
Aircraft class	Military trainer
Load cases in-flight	$+7.0g$ pull-up manoeuvre
	$-1.1g$ push-down manoeuvre
	20.0 m/s gust during cruise
on ground	Two-point landing
	Three-point landing
	Dynamic braking

The ranges imposed on dynamic process parameters during the parameter control aspect of the HHA are given in Table 8.6, chosen following the preliminary investigations in §7.3 and §7.4.4. In contrast to the previous study in §8.1, variable model fidelity is considered. Variable-fidelity modelling is set up in accordance with the results presented in §7.1.2 that indicated insignificant benefits in finite element

Table 8.6: AStrO-1 aircraft case study dynamic process parameters

Process parameter		LLH	Minimum	Maximum
P1	FE model fidelity	-	0.10	0.40
P2	Penalty coefficient	-	1.00	5.00
P3	Strand length	-	0-bits	16-bits
P4	Indigenous population	RI	0.10	0.30
P5	Crossover probability	DE	0.00	1.00
P6	Differential weight	DE	0.90	2.00
P7	Crossover points	RW, TO, BP, RC	1	Random
P8	Crossover probability	RW, TO, BP, RC	0.10	0.90
P9	Mutation probability	RW, TO, BP, RC	0.00	0.05
P10	Breeder pool intake	BP	0.10	0.30
P11	Contaminated population	RC	0.10	0.30
P12	Inertia weight	PSO	0.55	0.75
P13	Cognitive parameter	PSO	1.40	2.10
P14	Social parameter	PSO	0.90	1.80
P15	Constriction constant	PSO	0.75	1.00
P16	Step size	HC, SA, TS	$0.001\Delta V_v$	$0.02\Delta V_v$
P17	Cooling rate	SA	0.00	0.95
P18	Tabu list length	TS	0	100

analysis (FEA) precision at $F > 0.4$ compared to the increased computational cost. Additionally, the strand length, P3, is permitted to be reduced to 0-bits in order to disable converged variables and thus focus on variables yet to converge, as described in §5.3.4.4.

All design variables within Table 5.3 are active during this case study within the ranges presented in Table 8.7, the values of which are selected to envelope those typical of a military trainer aircraft (Howe, 2004; Raymer, 2006; Sensmeier and Samareh, 2004). This leads to variables V4, V7 and V10 being active during the study to enable optimisation of the number of lifting surface spars. This is appropriate given that military aircraft often possess more than two spars per lifting surface (Sensmeier and Samareh, 2004). Variables V21 to V50 are similarly active for this study within ranges set to permit modification above and below the values listed in Table 7.9 during previous experiments. Variables V21 to V25 represent the member type sections from either C, I, T or Z-sections whilst variables V48 to V50 define the materials of different member types. The possible materials to be used for the design are different grades of aluminium: Al 2014-T4, Al 2014-T6, Al 2024-T3, Al 2024-T4, Al 2024-T351, Al 2219-T87, Al 6061-T6, Al 7075-T76, Al 7075-T73, Al 7178-T6. Aluminium is chosen as it is a common metallic material used in the designs of aircraft structures (Howe, 2004). The design constraints limit the minimum factor of safety (FoS) to 1.5, C1, and the wingtip deflection to 1.0 m, C2; the latter values is selected to avoid ground-strike following inspection of the aircraft external profile as generated by the framework.

Table 8.7: AStrO-1 case study design variables

Design variable		Min.	Max.	Design variable		Min.	Max.
V1	Number of fuselage frames	20	160	V27	Fuselage frames depth, mm	100.0	300.0
V2	Number of fuselage stringers	30	180	V28	Fuselage frames thickness, mm	5.0	20.0
V3	Number of horizontal tail ribs	10	40	V29	Floor beams flange breadth, mm	100.0	600.0
V4	Number of horizontal tail spars	2	4	V30	Floor beams flange depth, mm	5.0	100.0
V5	Number of horizontal tail stringers	10	80	V31	Floor beams web breadth, mm	5.0	100.0
V6	Number of vertical tail ribs	10	40	V32	Floor beams web depth, mm	100.0	600.0
V7	Number of vertical tail spars	2	4	V33	Fuselage stringers breadth, mm	50.0	500.0
V8	Number of vertical tail stringers	10	80	V34	Fuselage stringers depth, mm	50.0	500.0
V9	Number of wing ribs	10	100	V35	Fuselage stringers thickness, mm	1.0	20.0
V10	Number of wing spars	2	4	V36	Ribs flange breadth, mm	50.0	400.0
V11	Number of wing stringers	10	120	V37	Ribs flange depth, mm	5.0	50.0
V12	Horizontal tail rib spacing exponent	1.0	3.0	V38	Ribs web breadth, mm	5.0	50.0
V13	Vertical tail rib spacing exponent	1.0	3.0	V39	Spars flange breadth, mm	50.0	400.0
V14	Wing rib spacing exponent	1.0	3.0	V40	Spars flange depth, mm	20.0	200.0
V15	Nose frames distribution, %	5.0	15.0	V41	Spars web breadth, mm	2.0	40.0
V16	Wingbox frames distribution, %	5.0	20.0	V42	Spars cap thickness, mm	20.0	200.0
V17	Tail frames distribution, %	5.0	15.0	V43	Lifting surface stringers breadth, mm	30.0	120.0
V18	Front wing spar root position, c_r	0.20	0.35	V44	Lifting surface stringers depth, mm	30.0	120.0
V19	Spar root breadth scaling factor	1.0	4.0	V45	Lifting surface stringers thickness, mm	1.0	10.0
V20	Spar root depth scaling factor	1.0	4.0	V46	Skin thickness, mm	1.0	10.0
V26	Fuselage frames breadth, mm	100.0	300.0	V47	Floor thickness, mm	5.0	50.0

Seven experiments are performed, the first four of which employ traditional methods of optimisation whilst the latter three apply the HHA. The set-ups of these experiments are presented in Table 8.8. This study extends the investigation performed during the study in §8.1 to a different aircraft, whilst focussing on improving the computational cost of employing the HHA for the control of FE model fidelity. Therefore, all five aspects of the hyper-heuristic objective function, Eqn. (4.3), are active during this study. Increasing the population size during the study in §8.1 led to improved solutions but required greater computation time. Therefore, the HHA is employed in experiments 5 to 7 with varying population sizes to investigate ways to reduce this cost. Experiment 5 has a population of 100 individuals for direct

comparison with experiments 1 to 3 whereas experiments 6 and 7 employ larger populations of up to 300 and 600 individuals respectively to investigate the distribution of the larger populations. Sub-populations are limited to 100 individuals to promote improved convergence towards the end of the process with fewer well-performing LLHs over that experienced by experiment 8 in §8.1 that employed a dynamic population size. Furthermore, dynamic control of the population size is not included in this study as its performance during the previous study failed to indicate significant benefits to the optimisation process.

Table 8.8: AStrO-1 aircraft case study set-up of experiments

	Experiment						
Aspect	1	2	3	4	5	6	7
Population size	100	100	100	1	100	300	600
Heuristic selection					✓	✓	✓
Population distribution					✓	✓	✓
Perturbation analysis					✓	✓	✓
Parameter control					✓	✓	✓
Low-level heuristic	MC	RW	PSO	SA	Experiments 5-7: All in Table A.6		
Hyper-heuristic:							
Heuristic selection					RW	RW	RW
Perturbation analysis					SA, TS	SA, TS	SA, TS
Parameter control					SA	SA	SA

A maximum number of 1,000 generations, or 100,000 steps for simulated annealing (SA) in experiment 4, is the sole termination criteria such that each experiment considers the same number of design solutions. The exterior penalty function is employed whilst the EMCQ move acceptance rule and measure of improvement (MoI) penalisation are applied for heuristic selection following promising performances reported in §7.3.2, §7.4.1 and §7.4.2. The HHA learning mechanism measurement period is set at 50 generations in accordance with the findings in §7.4.2 and §7.4.4 to permit numerous opportunities to encourage an improvement in the hyper-heuristic objective function used for heuristic selection and parameter control. This also provides an adequate number of generations to allow such improvements to take effect within the problem domain without premature interference from the HHA. To enable control of the chromosome strand length, P3, a binary representation is employed with bit-flip mutation for the GAs. Design variables are disabled if their affinities exceed a threshold of 90% over the hyper-heuristic measurement period. Heuristic selection and population distribution are also performed for the hyper-heuristic used for perturbation analysis. The perturbation analysis sample size is set as 10% of the population set in accordance with the best results presented in §7.4.3.

Table 8.9 shows the results for the run that generated the best solution for that experiment over the five runs performed. The data included are the same as was presented in Table 8.4 for the case study in §8.1 with the addition of $\overline{\Delta T}$ to show the mean time taken for each experiment over all runs. Table 8.9 shows that the best solution was generated using the HHA during experiment 7. This solution was 28.48% lighter than the best generated by traditional optimisation, i.e. that given by experiment 2 using a GA with RW selection. All experiments using the HHA outperformed those using traditional optimisation in terms of final solution quality. Experiment 7 also generated the lowest mean and standard deviation in final solution quality. This indicated that the larger population size is beneficial for improved solution quality, albeit at a penalty to computation time due to the increased number of FEA tasks. This was also observed in the previous case study presented in §8.1; however, inclusion of the computation time term within the hyper-heuristic objective function reduced the comparative cost. This can be seen by comparing the differences in ΔT between experiments 1 to 4 and experiment 7 within Table 8.9 and those between experiments 1 and 2 and experiment 8 in Table 8.4. Notably, experiment 5 used an identically-

sized population set to the population-based methods of traditional optimisation, i.e. experiments 1 to 3, and produced a better solution in less time. This was an improvement over the performance of the HHA during the previous study in §8.1 where improvements in solution quality using the HHA came at a cost to computation time. Further, the mean time taken to reach the final solution was lower for experiment 5 than experiments 1 to 4. Thus, experiment 5 indicated that an improved solution could be found using the HHA under similar test conditions to traditional optimisation without incurring computational costs.

Table 8.9: AStrO-1 case study solution of minimal mass and average results

	Experiment						
Result	1	2	3	4	5	6	7
$\Phi_{\min}$, kg	3,285	2,122	2,170	5,368	1,750	1,631	1,518
$\Delta\Phi_{\min}$, %	73.59	33.21	35.39	111.83	14.21	7.23	0.00
c_1	1.96	1.57	1.50	1.37	1.50	1.50	1.50
c_2, m	0.00	0.00	0.00	0.00	-0.01	0.00	0.00
η, %	100.00	100.00	100.00	99.79	100.00	100.00	100.00
$\beta(\mathrm{X}^{n_k})$, %	18.00	0.00	1.00	100.00	92.00	88.33	94.83
$A(\mathrm{X}^{n_k})$, %	5.14	94.39	91.46	-	86.24	88.39	88.90
n_k	1,000	1,000	1,000	100,000	1,000	1,000	1,000
ΔT	0.21	0.13	0.15	0.37	0.11	0.40	1.00
$\Phi_{\max}$, kg	4,928	3,076	2,372	6,038	2,273	2,046	1,639
$\overline{\Phi}$, kg	4,395	2,541	2,269	5,633	1,922	1,881	1,600
$\sigma(\Phi)$, kg	684	371	82	319	218	186	50
$\overline{\Delta T}$	0.19	0.15	0.17	0.37	0.12	0.45	1.00

Figure 8.4 shows the objective value of the running best solution during the experiment run presented in Table 8.9. Experiment 4, traditional optimisation by SA, was performed over 100,000 steps rather than 1,000 generations; therefore, the data for experiment 4 are scaled along the x-axis by 0.01 such that all experimental results may be presented on the same axis. This experiment performed the worst of all, with SA struggling in the solution space of high dimensionality formed by the 50 design variables. The random search of MC performed better in experiment 1 than SA, but the running best solution objective value was still noticeably poorer than for all other experiments. Traditional optimisation by RW and particle swarm optimisation (PSO), experiments 2 and 3 respectively, resulted in similar plots of running best solution mass. The GA in experiment 2 identified its best solution after 269 generations but was then unable to improve the solution further during the remaining 731 generations. PSO in experiment 3 took longer to locate its best solution, finding a local optimum after 592 generations and failing to improve this solution further. In both of these experiments, the populations converged rapidly upon local optima due to the static process settings, thus eliminating the possibility of further solution improvements.

Experiments 5 to 7 generated better solutions using the HHA than experiments 1 to 4 did by traditional optimisation. This was largely due to the continued improvement of solutions throughout the optimisation process rather than the limited improvements experienced in experiments 1 and 4, or premature convergence as was experienced in experiments 2 and 3. The objective value of the best solution for experiment 2 was the minimum of all experiments up to generation 20 due to the HHA employing all LLHs randomly at first, thus requiring a greater number of generations to evolve good solutions within smaller sub-populations. From this point onwards, the HHA improved solution quality by a great degree, as can be seen in Fig. 8.4 most noticeably in experiments 6 and 7, leading to continued improvement in the solution. In contrast, the preferred LLHs between generations 50 and 149 of experiment 5 were BP, killer queen (KQ) and tabu search (TS), i.e. techniques that are not as biased towards exploration as much as others such as MC. During these generations the HHA attempted to improve the hyper-

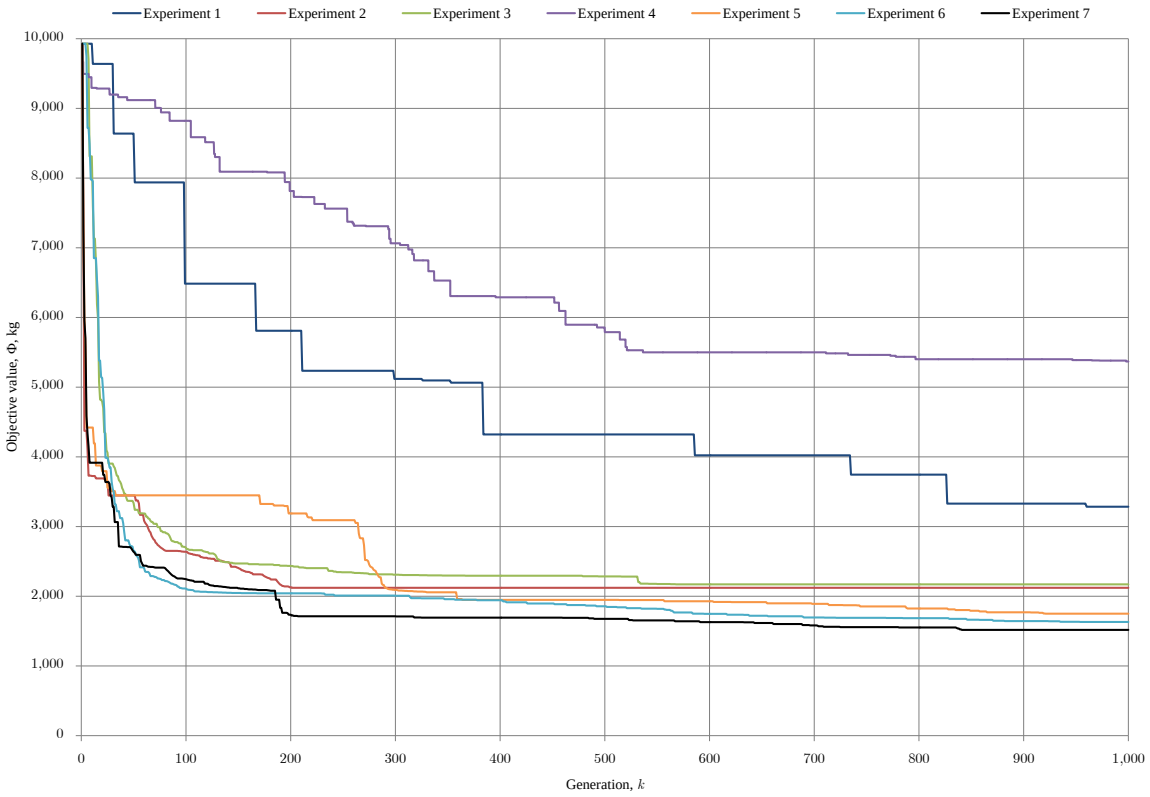

Figure 8.4: History of best solution objective value during AStrO-1 case study

heuristic objective value, and thus solution quality as one of its components, through perturbation of process parameters and redistribution of the population. However, the random perturbations by the SA hyper-heuristic did not offer lead to any improvements over these generations, i.e. most parameter perturbations failed to sufficiently encourage solution space exploration. Eventually, at generation 150, the HHA selected DE and PSO as LLHs with parameters set to encourage exploration, i.e. high values of DE crossover probability, P5, DE differential weight, P6, PSO inertia weight, P12, and PSO social parameter, P14. As a result, the solution space was better explored and the solution was improved.

All experiments except experiment 4 generated feasible solutions, however the HHA in experiments 5 to 7 and PSO in experiment 3, were able to identify a solution on the constraint boundary for C1. Constraint C2 had little effect on solution feasibility during this study due to the dominance of C1 in determining feasibility. The feasibility of the final population was greater using the HHA through the control of the penalty function coefficient, P2, to increase the penalty on infeasible solutions towards the end of the process. Encouragement of rapid exploration during early periods of the optimisation process was performed by setting high values of P2, P3, P5 to P14, and P16 whilst using low values for the other parameters. Towards the end of the process, convergence was promoted by performing the opposite operations to these parameters, as desired in order to improve the hyper-heuristic objective value. Selection of different LLHs during the process enabled exploration-encouraging techniques to assist in avoiding premature convergence during the process prior to convergence on the best solution prior to termination. For example, experiment 7 employed different GAs with high crossover and mutation probabilities in early generations as well as MC and PSO in order to explore the solution space. However, towards the end of the process SA and BP, with a low pool intake, were employed to promote convergence and thus improve the value of the hyper-heuristic objective function. In spite of this, it was not possible to

identify whether one HHA aspect, i.e. coupled heuristic selection and population distribution or parameter control, was more responsible than the others for promoting such search characteristics. FE model fidelity, P1, was maintained at a low level throughout despite frequent attempts to increase fidelity. These attempts were rejected in favour of low fidelity due to the penalties on computational time for FE modelling and analysis. However, the fidelity levels did generally increase towards the end of the process following the reduction of design variables V1 to V11, i.e. the numbers of members, to low quantities.

Perturbation analysis of the solution space neighbouring good solutions facilitated additional solution improvements during experiments 5 to 7. Perturbation analysis was more costly during this case study than the previous study in §8.1 due to the greater number of load cases for the airframe to be assessed against following each individual perturbation. Parameter control of the variable strand length, P3, enabled the strands of converged variables to be reduced such that the optimisation process focussed on improving the solution based on the values of other variables without penalising the problem size. Figure 8.5 shows the mean lengths of design variable during experiment 7, i.e. the experiment that produced the best aircraft design. For clarity, strands as grouped by the nature of the variable with respect to the airframe design, i.e. member number, position, size, section or material. The maximum strand lengths of discrete numerical variables were limited by the variable ranges. The strand lengths of categorical discrete variables, i.e. section profiles and materials, were kept constant throughout the process as discussed in §5.3.4.4. The strand lengths of variables defining the quantity and positions of members were reduced over the process as the search converged on an airframe with fewer members at set positions. Conversely, the strand lengths of the continuous variables defining member sizes increased to provide greater resolution in these variables in order to better refine the member geometry. This enabled the optimisation process to obtain improvements in the objective value compared to traditional optimisation through refinement of these variables whilst not focussing on the variables already converged.

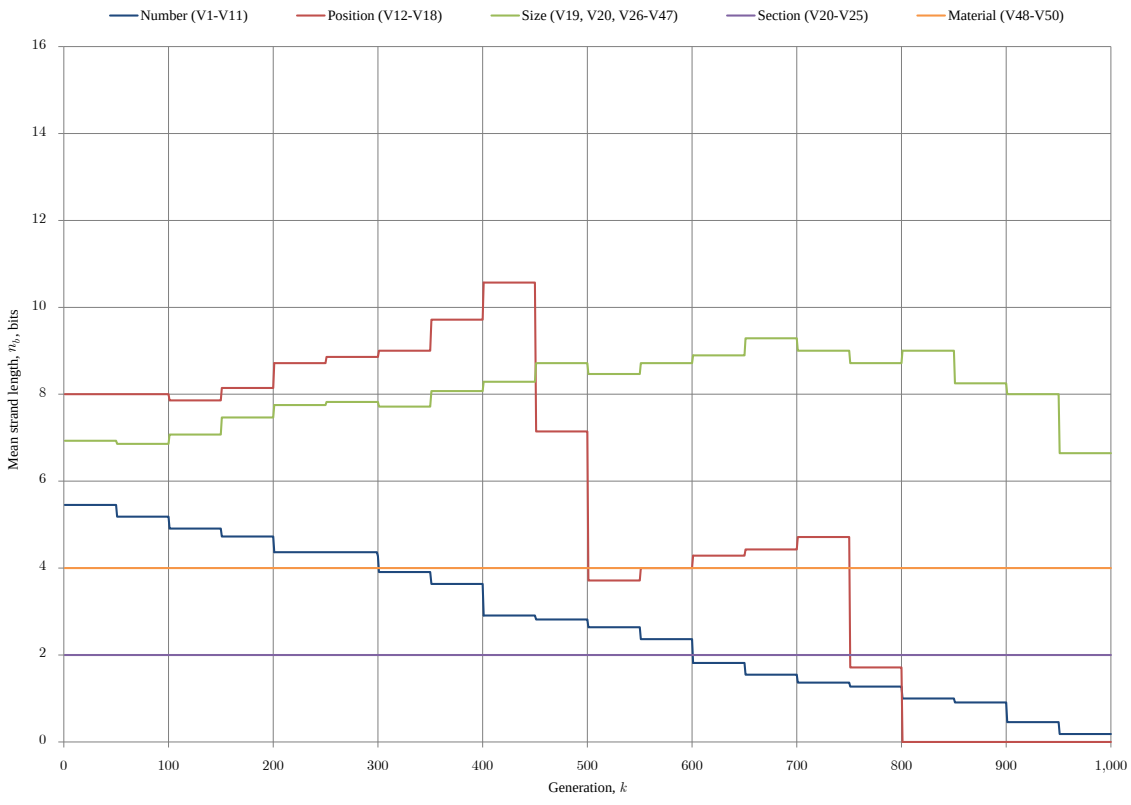

Figure 8.5: History of variable strand lengths during AStrO-1 case study experiment 7

The use of only one termination criterion, i.e. maximum number of generations, ensured that all experiments considered the same number of design solutions. This resulted in stagnation of the searches by RW and PSO in experiments 2 and 3 once they had converged close to a local optimum. Conversely, removal of the termination criteria for stopping the search if no improvement is made over successive generations resulted in experiments 1 and 4 continuing to find improvements in the solution throughout the process, albeit with numerous periods without any improvement. The final affinities of all experiments except the random MC-driven experiment 1 and single-solution SA-driven experiment 4 were greater than 85%, indicating good convergence of these experiments. The values for experiments 5 to 7 using the HHA were below 90% due to the use of population distribution preventing as well focussed convergence as by the GA or PSO alone. A test of significance compared the mean objective values of the best solutions in experiments 5 to 7 that employed the HHA against experiment 2, i.e. the traditional method that performed best. Statistically significant differences were observed in these results under t-tests for means with assumed unequal variance: $p < 0.01$ for experiments 5 and 6, and $p < 0.005$ for experiment 7.

Table 8.10 lists the design variable values for the best solution generated in each experiments, as described in Table 8.9. Most experiments, apart from the stochastic MC-driven experiment 1, generated the best solutions with low numbers of structural members close to or upon the lower bound defined in Table 8.7, V1 to V11. This was most obvious for the larger structural members, i.e. frames, ribs and spars. However, the numbers of empennage members, i.e. V3, V4, V6 and V7, in experiments 3 and 4 were driven above their lower bounds due to the load cases being more severe for the wing structure. Consequently, the optimisation process focussed on improving the design of the wing over the empennage. Variations existed in the frame distribution in the nose, wingbox and tail, V15, V16 and V17 respectively, most notably for experiments 1 and 4 which generated the poorest solutions. Similarly, experiments 1 and 4, as well as experiment 3, produced a design with a front wing spar position, V18, further forward than the better solutions of experiments 2, 5, 6 and 7. Furthermore, the spar scaling factors, V19 and V20, for the better-performing experiments 2, 3, 5, 6 and 7 were close to one, i.e. constant spanwise spar size, whereas the poorer solutions possessed increased thickness over the lifting surface span.

The size of the frames, V26 to V28, was reduced to a greater degree in experiments 2, 5, 6 and 7 than in experiments 1, 3 and 4. However, sufficient strength was maintained under the applied ground loads when transmitted through the nose undercarriage. The loads on the aircraft did not include significant internal fuselage loads. Consequently, the sizes of the floor beams and floor, V29 to V32 and V47 respectively, were able to be reduced towards their lower bounds during optimisation without significantly compromising structural integrity. This occurred during experiments 2, 3, 5, 6, and 7 which generated the best solutions. Similar patterns could be seen for the sizes of fuselage stringers, V33 to V35, as well as the lifting surface ribs, V36 to V38, spars, V39 to V42, and stringers, V43 to V45. The variables defining the thicknesses of stringers, V35 and V45, and spar webs, V41, were driven to their lower bounds in most experiments in order to reduce the member mass. This was also evident for the skin thicknesses, V46, due to a sufficient quantity of stringers ensuring the necessary coordinated strength for resistance of the applied loads.

Significant variations were evident in the optimal section profiles for the members types, V21 to V25, although T and Z-sections were preferred over C-sections in all experiments except experiment 1. Similarly, the materials chosen for variables V48 to V50 varied across all experiments. The best solution overall, generated during experiment 7, was comprised of materials with greater yield strength, but such materials also possessed greater density. However, this permitted the optimisation process to reduce the sizes of structural members compared to other experiments in order to reduce the mass of the airframe whilst maintaining sufficient strength under load. Conversely, traditional optimisation in experiments 1 to 4 chose weaker, less dense materials for most members and thus required a greater quantity or size of members. The large variations in these variables across the experiments were increased by their discrete nature, i.e. variable perturbations resulted in abrupt changes in the mechanical properties of the airframe.

Table 8.10: Best designs generated during AStrO-1 case study

	Experiment						
Parameter	1	2	3	4	5	6	7
V1	26	20	20	21	20	20	20
V2	46	37	46	66	30	30	32
V3	40	10	10	25	10	10	10
V4	4	2	2	3	2	2	2
V5	33	34	49	43	57	50	42
V6	20	13	10	24	10	10	10
V7	2	2	4	3	2	2	2
V8	49	42	54	45	40	40	38
V9	16	10	10	15	20	20	20
V10	2	2	2	2	2	2	2
V11	36	31	62	51	40	39	40
V12	1.59	1.67	1.09	2.21	1.00	1.00	1.35
V13	2.61	1.36	1.40	1.93	1.09	1.00	1.00
V14	2.04	1.01	1.00	2.30	1.00	1.00	1.00
V15, %	9.93	14.83	13.05	11.11	13.79	13.28	14.92
V16, %	16.48	8.82	6.29	14.79	5.00	8.71	5.11
V17, %	14.86	12.31	14.74	9.93	11.63	10.84	7.53
V18, c_r	0.24	0.34	0.27	0.27	0.35	0.35	0.35
V19	1.48	1.04	1.00	1.54	1.00	1.00	1.00
V20	2.10	1.07	1.01	1.42	1.00	1.00	1.00
V21	C-Section	T-Section	T-Section	T-Section	Z-Section	T-Section	Z-Section
V22	C-Section	Z-Section	Z-Section	T-Section	C-Section	Z-Section	Z-Section
V23	T-Section	Z-Section	Z-Section	T-Section	Z-Section	T-Section	Z-Section
V24	T-Section	C-Section	Z-Section	C-Section	Z-Section	T-Section	C-Section
V25	C-Section	Z-Section	T-Section	T-Section	T-Section	T-Section	Z-Section
V26, mm	233.28	102.12	200.00	210.67	100.00	100.00	101.21
V27, mm	137.52	101.16	200.00	141.06	100.00	100.00	100.13
V28, mm	7.08	5.00	5.00	10.12	5.00	5.00	5.04
V29, mm	126.04	100.05	100.03	113.39	100.00	100.00	100.15
V30, mm	100.00	100.00	100.00	100.00	100.00	100.00	100.00
V31, mm	18.12	5.07	5.01	22.42	5.00	5.00	5.00
V32, mm	275.10	106.96	100.40	186.54	126.56	100.00	102.91
V33, mm	141.60	50.71	51.42	188.98	50.00	51.84	50.18
V34, mm	130.70	190.68	124.53	199.13	131.04	183.23	155.99
V35, mm	9.97	1.03	1.00	1.55	1.00	1.00	1.02
V36, mm	92.74	50.39	50.09	58.07	50.00	50.00	50.04
V37, mm	50.00	50.00	50.00	50.00	50.00	50.00	50.00
V38, mm	36.72	49.75	49.94	27.41	50.00	50.00	49.99
V39, mm	77.10	50.06	50.07	75.65	50.00	50.00	50.18
V40, mm	102.42	41.25	40.30	74.60	40.00	40.00	41.08
V41, mm	37.46	2.66	2.04	21.64	2.00	2.00	2.00
V42, mm	41.21	40.22	40.33	74.71	40.00	40.00	40.01
V43, mm	34.21	31.18	30.02	57.25	30.38	30.00	30.41
V44, mm	70.51	30.24	30.20	69.05	50.25	45.85	52.70
V45, mm	5.86	1.00	1.00	3.00	1.00	1.00	1.03
V46, mm	8.52	1.00	1.01	4.74	1.00	1.00	1.00
V47, mm	13.07	5.03	5.03	21.53	5.00	5.00	5.68
V48	Al 7075-T6	Al 2219-T87	Al 6061-T6	Al 6061-T6	Al 2219-T87	Al 2219-T87	Al 2219-T87
V49	Al 2219-T87	Al 6061-T6	Al 7075-T6	Al 2024-T4	Al 2024-T4	Al 7075-T6	Al 7178-T6
V50	Al 2024-T3	Al 2014-T6	Al 2014-T4	Al 2219-T87	Al 7178-T6	Al 2014-T6	Al 7075-T73
Φ_{min}, kg	3,285	2,122	2,170	5,368	1,750	1,631	1,518
c_1	1.96	1.57	1.50	1.37	1.50	1.50	1.50
c_2, m	0.00	0.00	0.00	0.00	-0.01	0.00	0.00
η, %	100.00	100.00	100.00	99.79	100.00	100.00	100.00

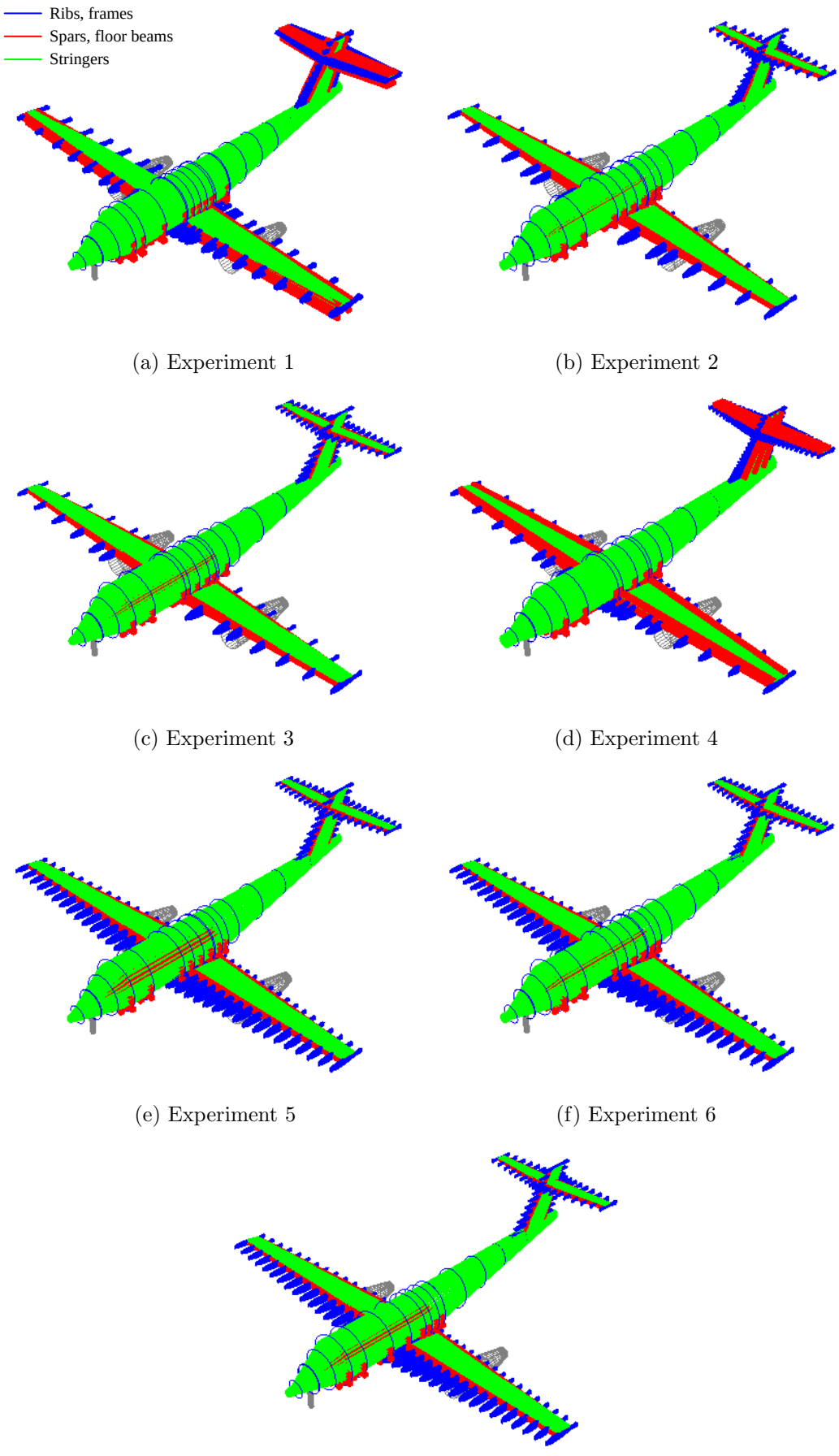

(a) Experiment 1

(b) Experiment 2

(c) Experiment 3

(d) Experiment 4

(e) Experiment 5

(f) Experiment 6

(g) Experiment 7

Figure 8.6: Best solutions of each experiment during AStrO-1 case study

The best designs generated by each experiment, i.e. the designs listed in Table 8.10, are illustrated in Fig. 8.6. These images show the larger number of members in the lifting surfaces for experiments 5 to 7 compared to experiment 1 to 4. This was due to the members within the solutions of experiments 5 to 7 being of smaller size than those of experiments 1 to 4, thus requiring a greater number to provide structural integrity. Consequently, the greater number of ribs provided more strength over the lifting surface span than in the solutions with fewer ribs, leading to the ability to reduce the size of these members, and thus mass, whilst maintaining sufficient resistance to load. Additionally, the best solutions of experiments 1 to 4 possessed larger lifting surface spars than in the other experiments, which led to poorer quality solutions. Note, these illustrations of the aircraft are limited by the AStrO graphical user interface (GUI) imaging, e.g. lack of visible propellers and floor beams protruding out of the fuselage.

A direct comparison of the structural mass of AStrO-1 against existing military trainer aircraft is inappropriate given that AStrO-1 is a novel concept and as such there is no corresponding existing design. However, the aircraft is similar in class and purpose to the Aermacchi SF-260 and Embraer EMB-314 Super Tucano. The empirical data used to perform a comparison of structural mass in §8.1 are not available for this aircraft class, however the empty aircraft masses of these aircraft are 779 kg and 2,420 kg respectively (Jackson, 2009). Therefore, the mass of the best solutions in this case study, 1,518 kg, appears to be reasonable given the empty masses of similar aircraft. Nevertheless, the many differences in the designs of the aircrafts, e.g. aircraft size, powerplant design and mass calculation, prevent any significant conclusions to be made from these comparisons.

8.3 Embraer E-195

The preliminary investigation presented in §7.1.2 found that modelling with reduced levels of model fidelity could reduce the computational expense of structural analysis without critically hindering the measurement of design feasibility. This case study is performed to evaluate the ability of the HHA to control the level of model fidelity compared to traditional methods of parameter control. This is achieved through the control of dynamic process parameter P1 during the optimisation process to enable variable-fidelity modelling. The results of the study in §8.2 provide additional motivation to study the control of this parameter as poor control of model fidelity was apparent during this study. Only parameter P1 is varied during this study to prevent variations in other dynamic process parameters P2 to P18 from affecting the results. The traditional methods of parameter control used for comparison are deterministic and self-adaptive controls of model fidelity. Deterministic control of model fidelity is performed using the following rule at the kth optimisation generation

$$F^k = F_{\min} + \frac{\left\{{}^{k}/_{n_k}\left(F_{\max} - F_{\min}\right)\right\}^{\delta_F}}{\left(F_{\max} - F_{\min}\right)^{\delta_F - 1}} \tag{8.1}$$

where δ_F represents the model fidelity rate of change. This rule is designed to encourage rapid low-fidelity analysis at the start of the optimisation process prior to more detailed analysis at higher fidelity during later generations of the better solutions. The rate of increase in fidelity is controlled by δ_F. Self-adaptive parameter control is performed by appending model fidelity to the end of solution genomes, i.e. V51 = P1. Optimisation is also performed with static model fidelity to provide a benchmark for comparison against the results with dynamic fidelity. Adaptive control is not included as no such rule for controlling model fidelity was discovered during the literature reviews in Chapters 2 and 3. The LLH employed is RW with a real representation, one-point crossover at 90% probability and Gaussian mutation at 1% probability. A static exterior penalty function is applied to penalise infeasible solutions within a population set of 100 individuals optimised over up to 1,000 generations. This set-up is chosen based on the results of the preliminary investigations in §7.3.

The Embraer E-195 large civil aircraft is the baseline design for this study, the properties of which are

listed in Table 7.2 alongside the static load applied. The case is study is performed over 17 experiments that vary in the control of model fidelity listed in Table 8.11. Each experiment is performed over five runs to account for variability in the results. Experiments 1 to 4 employ static model fidelity at different levels, the bounds of which are set as $0.1 \leq F \leq 0.4$ in accordance with the results of the preliminary investigation presented in §7.1.2 indicating negligible difference in measured fidelity at $F \geq 0.4$. Deterministic control of model fidelity is performed in experiments 5 to 11 at various rates of change in fidelity. The minimum and maximum values of δ_F are selected as the reciprocals of each other, i.e. ¼ and 4, to suitably bound the investigation. Experiments 12 to 15 investigate hyper-heuristic control with various limits on variable-fidelity modelling. In this study, the underlying deterministic rule of Eqn. (8.1) is employed with hyper-heuristic control of the rate of fidelity change, i.e. P1 $= \delta_F$. This is a modification of the control employed during the preliminary investigation in §7.4.4 and case study of §8.2 due to unsatisfactory solution feasibility in the former and computational expense in the latter when controlling the model fidelity level itself. The hyper-heuristic objective function is employed using only the first and fifth components of Eqn. (4.3), i.e. best solution objective value and computation time, to focus the learning mechanism on improving solution quality and computation speed through the control of model fidelity. The effects on average population quality, affinity and convergence are not as important during this study and thus not included in the hyper-heuristic objective function. Experiment 16 applies self-adaptive control of fidelity by encoding the fidelity level as an additional design variable. Experiment 17 performs variable-fidelity modelling representative of that employed within the literature by Minisci et al. (2011) for a comparison against an existing approach of model fidelity control. This experiment varies model fidelity in discrete steps of $\Delta F = 0.06$ every 180 generations for five equal deterministic increases of fidelity during the optimisation process from $F = 0.1$ to $F = 0.4$. The design constraints are set at $c_1 \geq 1.5$ and $|c_2| \leq 3.4$ m.

Table 8.11: Embraer E-195 case study parameter control set-up

Experiment	Parameter control	Model fidelity
1	Static	$F = 0.1$
2	Static	$F = 0.2$
3	Static	$F = 0.3$
4	Static	$F = 0.4$
5	Deterministic	$\delta_F = 0.25$
6	Deterministic	$\delta_F = 0.5$
7	Deterministic	$\delta_F = 0.75$
8	Deterministic	$\delta_F = 1.0$
9	Deterministic	$\delta_F = 2.0$
10	Deterministic	$\delta_F = 3.0$
11	Deterministic	$\delta_F = 4.0$
12	Hyper-heuristic	$0.1 \leq$ P1 ≤ 1.0
13	Hyper-heuristic	$0.1 \leq$ P1 ≤ 2.0
14	Hyper-heuristic	$1.0 \leq$ P1 ≤ 3.0
15	Hyper-heuristic	$1.0 \leq$ P1 ≤ 5.0
16	Self-adaptive	$F =$ V51
17	Discrete	$\Delta F = 0.06$

Table 8.12 lists the ranges of design variables for this case study. The numbers of lifting surface spars, V4, V7 and V10, are set at two, i.e. the common value for a large civil aircraft (Howe, 2004; Raymer, 2006; Sensmeier and Samareh, 2004). The variables controlling airframe member geometry and material properties, i.e. V19 to V50, are not varied as model fidelity principally determines the number and position of FE model elements; therefore these variables will not significantly affect the performances of

the different parameter control methods. The values listed in Table 8.13 are used for these variables, whilst spar thickness is kept constant along the span, i.e. variables V19 and V20 are set equal to one. The same design constraints are applied as for the previous study in §8.2.

Table 8.12: Embraer E-195 case study design variables

Design variable		Minimum	Maximum
V1	Number of fuselage frames	8	100
V2	Number of fuselage stringers	8	120
V3	Number of horizontal tail ribs	2	50
V5	Number of horizontal tail stringers	2	100
V6	Number of vertical tail ribs	2	50
V8	Number of vertical tail stringers	2	100
V9	Number of wing ribs	2	100
V11	Number of wing stringers	2	120
V12	Horizontal tail rib spacing exponent	1.0	3.0
V13	Vertical tail rib spacing exponent	1.0	3.0
V14	Wing rib spacing exponent	1.0	3.0
V15	Distribution of frames to nose, %	5.0	15.0
V16	Distribution of frames to wingbox, %	5.0	15.0
V17	Distribution of frames to tail, %	5.0	15.0
V18	Front wing spar chordwise root position, c_r	0.2	0.35

Table 8.13: Embraer E-195 case study constraints on inactive design variables

Structural member	Material	Profile	Thickness, mm	Depth, mm	Breadth, mm
Lifting surface rib	Al 7075-T6	I	5.0 (web) 5.0 (flange)	Varies	8.0
spar	Al 7178-T6	I	4.0 (web) 30.0 (flange)	Varies	60.0
stringer	Al 2014-T6	Z	2.0	20.0	20.0
Fuselage frame	Al 7075-T6	T	5.0	80.0	80.0
stringer	Al 2014-T6	Z	2.0	20.0	20.0
floor beam	Al 7075-T6	I	15.0 (web) 20.0 (flange)	100.0	50.0
Skin	Al 2014-T6	-	2.0	-	-
Floor	Al 7075-T6	-	20.0	-	-

Table 8.14 presents the best designs generated in all five runs performed for each experiment. The results in Table 8.14 concerning experiments 1 to 4, i.e. with static levels of model fidelity, show an improvement in the solution with greater model detail. The best design at lowest fidelity during experiment 1 was 12.39% heavier than that at highest fidelity in experiment 4, principally due to the increase in V1 which determined the number of frames and, subsequently, the number of floor beams in the cabin. However, the computational time required for experiment 4 was 4.1 times of that for experiment 1 due to the greater number of degrees of freedom (DoFs) during the modelling and analysis of design solutions at higher fidelity. Improvements were made in solution quality with variable-fidelity modelling during experiments 5, 6, 8, 10, 12, 13, 14 and 15 compared to experiment 4, i.e. the best solution with static fidelity. Furthermore, decreased computation time was required for these experiments compared to experiment 4 without a loss in design quality due to fewer generations at high levels of fidelity.

Early discoveries of promising design characteristics at low fidelity were observed for experiments 5, 6 and 12 prior to further improvements at higher fidelity. In these experiments, small rates of change

in model fidelity led to the final design being obtained in fewer generations than in other experiments. For example, the best design overall, obtained in experiment 5, was found during generation 341 of the experiment after 3.1 h of computation, whereas the best design with static fidelity, i.e. from experiment 4, was found during generation 974 of the experiment after 14.2 h. Further, the quickest discovery of a best design with static fidelity was found after 3.4 h at generation 977 in experiment 1. More specifically, this best design in experiment 5 was 1.36% lighter than the best with static fidelity in experiment 4 and was found in 57.55% of the time. Experiments 7, 9, 11 and 16 generated worse designs than experiment 4, although only marginally for experiments 7 and 16. The loss of quality was caused by too many generations performed at low fidelity due to the higher values of the model fidelity rate of change lower bound. However, discrete changes in model fidelity during experiment 17 generated a considerably heavier design than for all other experiments except experiment 1. Hyper-heuristic control of the model fidelity rate of change improved solution feasibility over that obtained when controlling the fidelity level during the preliminary investigation in §7.4.4, as well as reducing the computational cost to the optimisation process observed in §8.2. This indicated a better method of control of FE model fidelity.

Table 8.14: Best designs generated during Embraer E-195 case study

	Experiment																
Param.	1	2	3	4	5	6	7	8	9	10	11	12	13	14	15	16	17
V1	51	33	33	34	32	32	33	33	35	33	34	32	34	33	32	35	49
V2	22	70	49	36	46	46	46	46	40	46	42	46	49	49	46	43	27
V3	3	3	3	9	3	3	3	3	3	3	3	3	3	3	3	3	3
V5	30	32	32	30	32	32	28	32	29	26	38	34	27	35	27	32	36
V6	3	3	3	3	3	3	3	3	3	3	3	3	3	3	3	3	3
V8	34	35	35	35	35	35	32	36	39	32	42	35	34	35	33	35	37
V9	6	7	7	7	7	7	8	7	7	7	7	7	8	7	7	7	7
V11	20	21	21	20	21	20	19	20	23	18	25	22	19	21	20	21	23
V12	1.59	1.00	1.00	1.00	1.00	1.00	1.00	1.00	1.00	1.00	1.00	1.00	1.11	1.00	1.00	1.00	1.00
V13	1.00	1.00	1.14	1.00	1.00	1.00	1.00	1.00	1.00	1.00	1.00	1.00	1.00	1.00	1.00	1.00	1.00
V14	1.79	1.33	1.00	1.62	1.00	1.00	1.00	1.00	1.00	1.00	1.00	1.00	1.00	1.00	1.38	1.17	1.00
V15, %	10.69	15.00	13.15	12.09	13.19	14.51	14.34	14.34	10.54	15.00	15.00	13.52	14.19	15.00	13.36	15.00	12.73
V16, %	15.00	5.00	6.80	5.60	5.00	5.00	5.00	5.72	6.85	8.86	8.76	5.00	6.00	5.00	5.00	6.17	9.86
V17, %	10.55	11.21	13.75	9.72	13.03	14.06	9.03	13.29	15.00	9.58	8.21	14.11	15.00	12.77	13.45	13.34	12.84
V18, c_r	0.35	0.25	0.30	0.31	0.32	0.31	0.33	0.25	0.31	0.25	0.21	0.33	0.23	0.25	0.31	0.27	0.35
Φ, kg	10,864	9,787	9,673	9,666	9,535	9,536	9,671	9,583	9,756	9,613	9,818	9,543	9,665	9,612	9,562	9,669	9,956
c_1	1.50	1.50	1.50	1.49	1.50	1.50	1.50	1.50	1.50	1.50	1.51	1.49	1.49	1.47	1.49	1.50	1.50
c_2, m	-0.06	0.12	0.19	0.11	0.20	0.20	0.11	0.16	0.19	0.18	0.14	0.20	0.08	0.16	0.15	0.14	0.23
η, %	100.0	99.18	99.14	99.41	99.12	99.11	99.70	99.12	100.0	100.0	100.0	99.13	98.79	99.14	98.77	98.84	98.47
T, h	3.49	6.11	8.73	14.44	8.31	7.38	8.19	10.92	13.04	8.28	10.46	9.56	13.32	10.69	8.73	13.08	8.80

Figures 8.7 and 8.8 show the variations in model fidelity and running optimum objective value for the run of each experiment that produced the best solution for that experiment, i.e. the solution listed in Table 8.14. The general increase in fidelity with hyper-heuristic control is clear for experiments 12 to 15 due to the use of the deterministic rule. Additional perturbations of the fidelity rate of change, P1, are evident by the non-uniform fluctuations in fidelity. The fidelity of the running optimum during self-adaptive control of experiment 16 indicates early selection of a high-fidelity model, leading to a high computational cost as stated in Table 8.14. The discrete changes to fidelity made during experiment 17 every 180 generations are similarly shown. The early increases in fidelity during experiments 5, 6 and 12 that led to quicker discovery of the best designs are also visible in Fig. 8.7. This showed that model fidelity should begin at a low value for a short period of generations prior to a steep increase in order to minimise the computational time required to generate a high-quality design, i.e. $\delta_F \leq 1.0$.

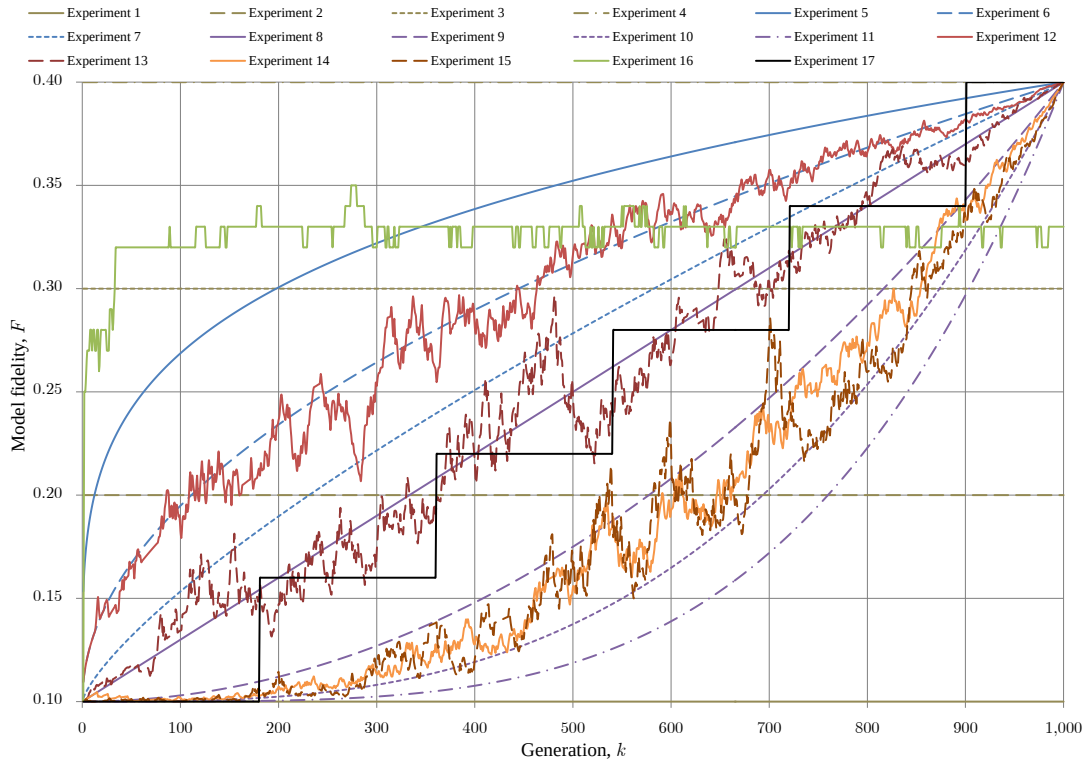

Figure 8.7: History of model fidelity during the Embraer E-195 case study

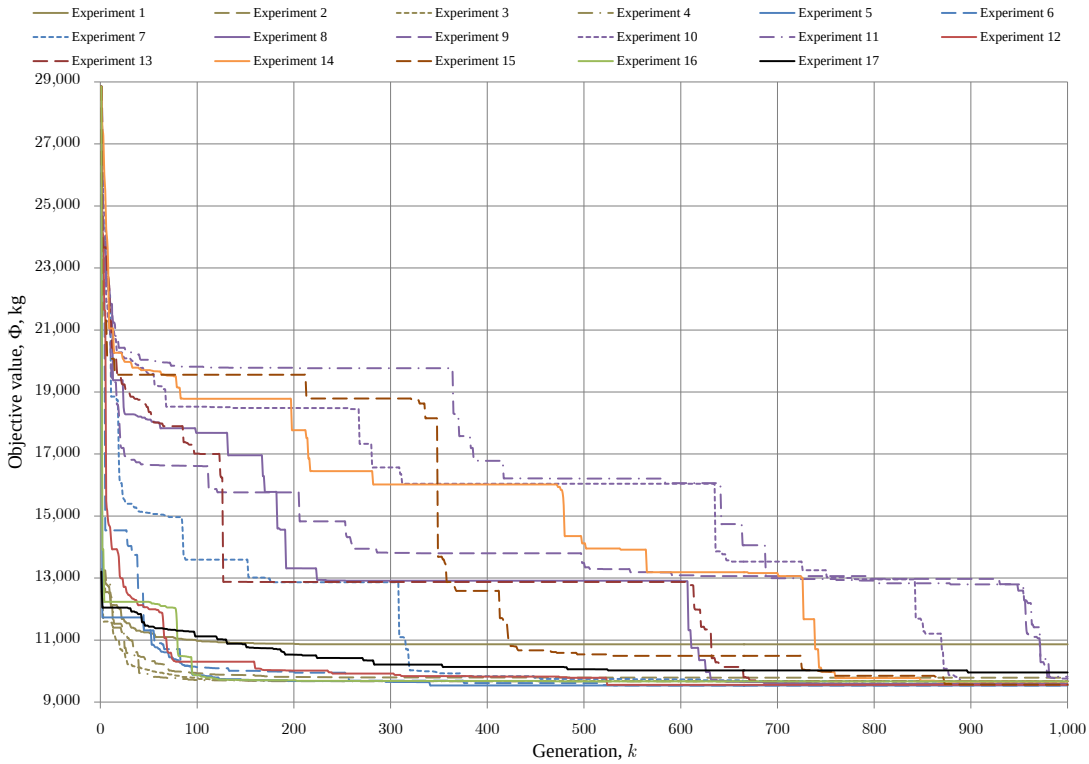

Figure 8.8: History of structural mass during the Embraer E-195 case study

Figure 8.8 shows that experiments 2, 3 and 4 quickly discovered low mass solutions within the first 100 generations but failed to improve these solutions over the subsequent generations. This also occurred during experiment 5, 6 and 12, resulting in the propagation throughout the population of designs with few structural members, leading to reduced model size and computation time. This was evident for experiment 16 with self-adaptive control but without such gains in computation time. This was due to the time taken to analyse, in parallel, each batch of individual designs being dependent on the highest level of fidelity possessed by the individuals. Therefore, the inclusion of high levels of fidelity within the population greatly increased the solution process runtime.

The best solutions generated from each experiment of the study were subjected to further FEA with $F = 1.0$ to verify the differences in measured feasibility at the corresponding fidelity levels. The differences in values measured with respect to the design constraints are presented in Table 8.15 containing similar values to those listed in Table 7.3 during the preliminary investigation into the effects of fidelity on FEA. These results indicate that varying model fidelity during optimisation did not lead to inaccurate measurements of design feasibility with respect to structural analysis at greatest fidelity.

Table 8.15: Variation in worst values with respect to the design constraints with model fidelity

Experiment	F	Δc_1	Δc_2, m
1	0.10	0.0000	0.0000
2	0.20	0.6197	0.0006
3	0.30	0.2478	0.0007
4	0.40	0.0015	0.0001
5	0.33	0.2208	0.0003
6	0.33	0.2253	0.0002
7	0.33	0.1387	0.0018
8	0.33	0.1385	0.0002
9	0.40	0.0028	0.0005
10	0.33	0.2015	0.0001
11	0.38	0.0764	0.0002
12	0.32	0.2101	0.0002
13	0.33	0.1202	0.0060
14	0.32	0.1543	0.0002
15	0.33	0.1978	0.0003
16	0.33	0.0100	0.0000
17	0.34	0.2181	0.0086

The mean mass and computation time over all runs of each experiment are shown in Fig. 8.9. Two thresholds are plotted in Fig. 8.9 for the lowest values of mean mass and computation time with static fidelity, i.e. during experiments 4 and 1 respectively. The mean mass was lower during experiments 5, 6, 12, 15 and 16 than experiment 4. However, no experiment with variable-fidelity modelling provided quicker computation than with the minimum static level of fidelity in experiment 1 due to the higher levels of fidelity, and thus model DoFs, used over periods of experiments 5 to 17. Nevertheless, the mean times for all experiments using variable-fidelity modelling were lower than that for experiment 4, i.e. the best design with static fidelity, except for experiment 16 due to the independent level of fidelity possessed by population individuals resulting in lengthy structural analysis for each generation. These findings indicate that optimisation with variable-fidelity modelling was capable of obtaining comparable, and sometimes better, solutions than the highest level of static fidelity whilst reducing the computation time required to do so. The approach representative of Minisci et al. (2011) during experiment 17 generated the worst mean mass of all experiments using variable-fidelity modelling, with only experiment 1 generating a solution of worse quality but in a considerably shorter period of time.

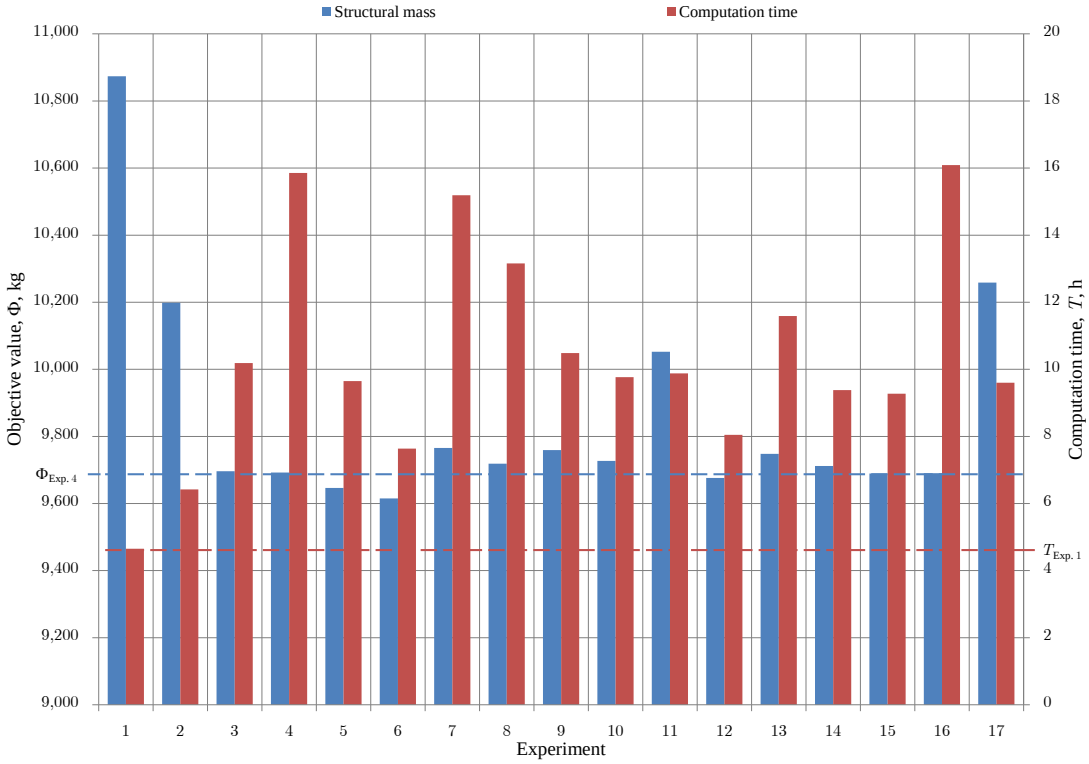

Figure 8.9: Mean structural mass and computation time during the Embraer E-195 case study

The operating empty mass of the Embraer E-195 is 28,700 kg (Embraer SA, 2011); therefore, using the empirical estimation described in §8.1, the structural mass of the existing design is approximately 11,954 kg (Torenbeek, 1982, p. 266). Thus, all designs in this study were lighter than the existing aircraft: the best herein weighed approximately 80% of the mass of the existing design, experiment 5, and the worst about 91%, experiment 1. However, as for the Airbus A340-300 in §8.1, the mass of the existing Embraer E-195 is an estimation based on the final aircraft design which will have been designed to a greater level of detail than herein. Further, only a single load case was considered whereas the final design will have been analysed under numerous loads; this would have increased the structural mass to maintain integrity. The evolution of the best design obtained in this study is shown in Fig. 8.10. A lack of data in the public domain prevents analysis of differences between the existing design and the solutions herein.

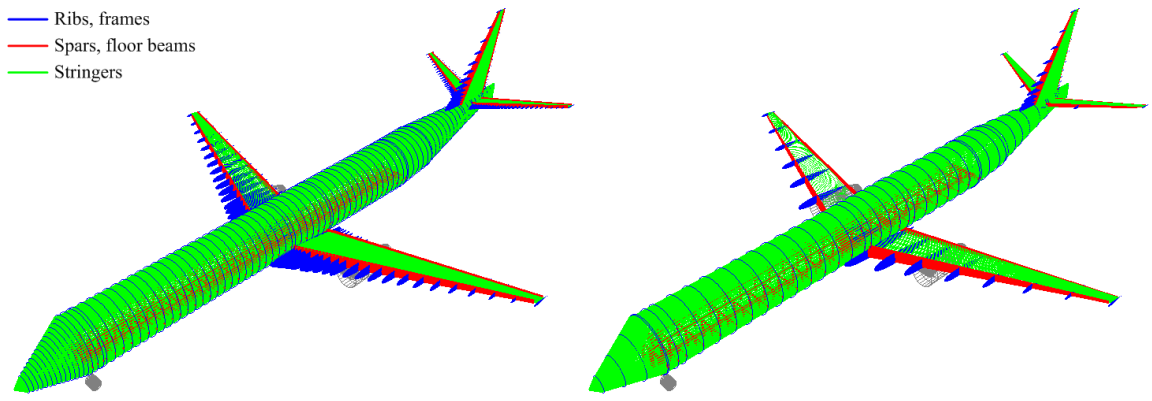

(a) $k = 1$ (b) $k = 45$

Figure 8.10: Evolution of overall best solution for Embraer E-195 airframe design

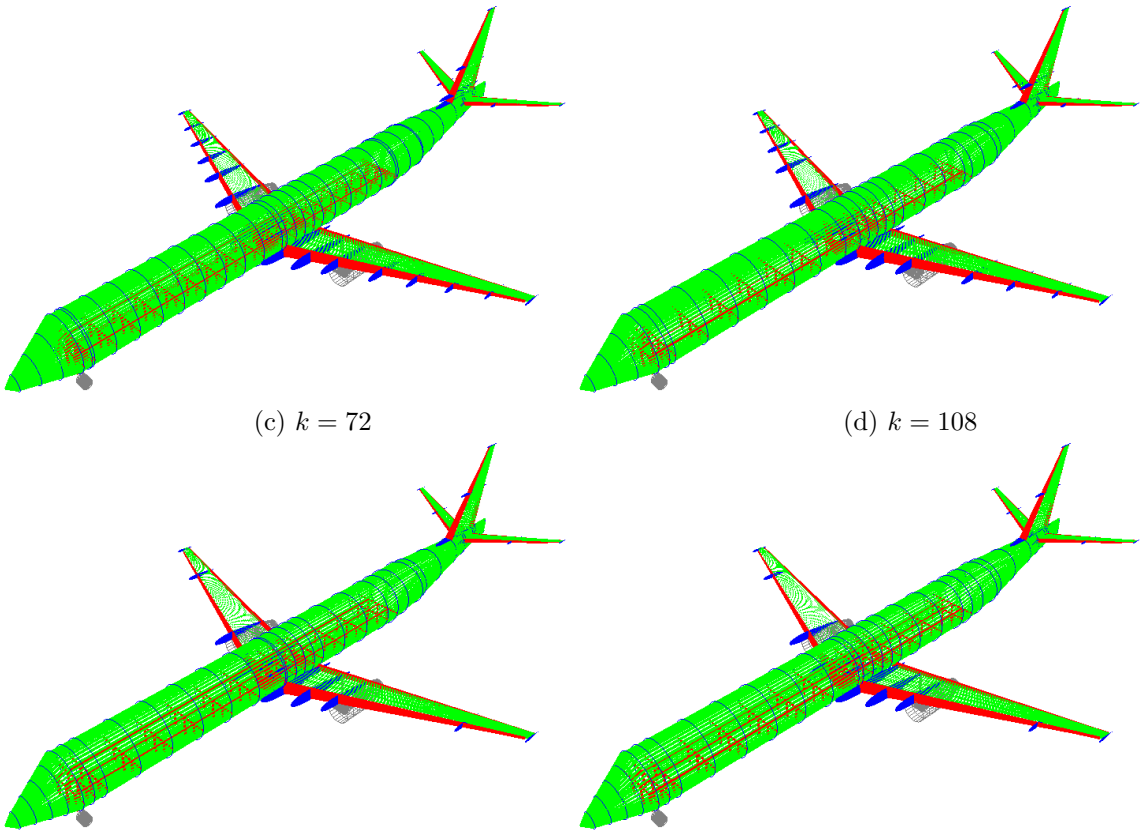

(c) $k = 72$ (d) $k = 108$

(e) $k = 194$ (f) $k = 341$

Figure 8.10: Evolution of overall best solution for Embraer E-195 airframe design (cont.)

8.4 Boeing C-17A Globemaster III

The final case study investigates the effects of different load cases on the quality of airframe design solutions generated through optimisation. The aim of this study is to identify the load cases that drive the airframe design solution, and thus establish which loads should be applied during optimisation in order to obtain a suitable airframe design solution. This is desirable given that most studies reviewed in the literature employed a single load case believed to be the most onerous, however it is not accepted that this will necessarily be the case for all areas of the aircraft. This study performs structural optimisation of the Boeing C-17A Globemaster III existing aircraft design. This military transport aircraft is employed by leading military forces to move large volumes of cargo and troops between various arenas. The properties of the aircraft are presented in Table 8.16 (Jackson, 2009). The aircraft mission includes a payload drop of 13,600 kg, typical of an airdrop performed by the aircraft, midway through the mission.

This case study is formed of 12 experiments, each performed over five runs to account for results variability. These experiments differ only in the load cases applied to the airframe during structural analysis as described by Table 8.17. Experiment 1 applies all load cases from the database listed in Table A.3 to the aircraft as pseudo-static loads whilst experiment 2 applies the maximum positive flight manoeuvre, L1, and three-point landing, L6, loads. Experiments 3 to 10 then apply the nine different loading conditions in isolation as pseudo-static loads to determine the differences in the airframe design generated. Load cases L1 and L6 are then applied as dynamic loads in experiments 11 and 12 respectively to evaluate any differences in the designs due to the nature of response calculated. Cockpit pressurisation, engine thrust and gravity are included within all experiments. The Newmark-β direct integration method is employed for experiments 11 and 12 with constants $\alpha = 0.25$ and $\beta = 0.5$, a Rayleigh damping ratio of $\zeta = 0.03$ and a step size of $\Delta t = 0.001$ s for a stable response calculation during FEA (Rao, 2004).

Table 8.16: Selected properties of Boeing C-17A Globemaster III aircraft

Property	Value
Wing span	51.74 m
sweep	25.0°
Tail span	19.81 m
height	16.79 m
Fuselage length	48.49 m
width	6.86 m
Undercarriage track	10.26 m
wheelbase	20.06 m
Powerplant	4x Pratt and Whitney F117-100
Mass operating empty	125,645 kg
maximum take-off	265,350 kg
Cruise altitude	28,000 ft
range	2,400 nmi
speed	0.74 M
Number of flight crew	3
Cargo mass	13,600 kg
Aircraft class	Military transport
Load case	See Table 8.17

The number of time steps is limited to 100 to prevent an excessively long simulation. Model fidelity is maintained at $F = 0.1$ throughout all experiments to prevent variable-fidelity modelling from affecting the results and allow rapid analysis of multiple pseudo-static and dynamic load cases. The maximum positive and negative flight manoeuvres, i.e. L1 and L2, are $+2.5g$ pull-down and $-0.9g$ push-down manoeuvres respectively as defined in the airworthiness requirements for the aircraft class in Table A.11.

Table 8.17: Boeing C-17A Globemaster III case study applied load cases

	Load case											Response	
Experiment	L1	L2	L3	L4	L5	L6	L7	L8	L9	L10	L11	Static	Dynamic
1	✓	✓	✓	✓	✓	✓	✓	✓	✓	✓	✓	✓	
2	✓					✓			✓	✓	✓	✓	
3	✓								✓	✓	✓	✓	
4		✓							✓	✓	✓	✓	
5			✓						✓	✓	✓	✓	
6				✓					✓	✓	✓	✓	
7					✓				✓	✓	✓	✓	
8						✓			✓	✓	✓	✓	
9							✓		✓	✓	✓	✓	
10								✓	✓	✓	✓	✓	
11	✓								✓	✓	✓		✓
12						✓			✓	✓	✓		✓

Optimisation is performed using the same set-up of the HHA for all experiments of this study. This includes RW heuristic selection with EMCQ move acceptance from a heuristic set limited to three LLHs: RW, PSO and SA. These LLHs are selected as they are of differing natures, i.e. a GA, swarm intelligence (SI) and local search (LS) technique respectively, and also performed well during the preliminary investigations and earlier case studies. The population set contains 100 design individuals, with population distribution between the LLHs enabled without a limit on the maximum sub-population size. Perturbation analysis of a newly-discovered best solution is performed using SA. Parameter control is also

performed using the SA hyper-heuristic, but is restricted to the penalty coefficient and operators of the LLHs within the heuristic set, i.e. P2, P7 to P9 and P12 to P17, within the ranges given in Table 8.2. The evaluation period used by the HHA between operation is 50 generations in accordance with the preliminary investigations reported in §7.4.2 and §7.4.4. Table 8.18 lists the permitted ranges of design variables during this case study (Howe, 2004; Raymer, 2006; Sensmeier and Samareh, 2004). These include all design variables from Table 5.3 that define the number and positions of structural members. Inactive design variables are defined as in Table 7.9 for a similarly large transport aircraft. Design constraints of $c_1 \geq 1.5$ and $|c_2| \leq 4.2$ m are applied, the latter calculated to prevent ground-strike.

Table 8.18: Boeing C-17A Globemaster III case study design variables

Design variable		Minimum	Maximum
V1	Number of fuselage frames	30	160
V2	Number of fuselage stringers	30	180
V3	Number of horizontal tail ribs	10	40
V4	Number of horizontal tail spars	2	4
V5	Number of horizontal tail stringers	10	80
V6	Number of vertical tail ribs	10	40
V7	Number of vertical tail spars	2	4
V8	Number of vertical tail stringers	10	80
V9	Number of wing ribs	10	100
V10	Number of wing spars	2	4
V11	Number of wing stringers	20	120
V12	Horizontal tail rib spacing exponent	1.0	3.0
V13	Vertical tail rib spacing exponent	1.0	3.0
V14	Wing rib spacing exponent	1.0	3.0
V15	Distribution of frames to nose, %	5.0	15.0
V16	Distribution of frames to wingbox, %	5.0	15.0
V17	Distribution of frames to tail, %	5.0	15.0
V18	Front wing spar chordwise root position, c_r	0.2	0.35
V19	Spar root breadth scaling factor	1.0	4.0
V20	Spar root depth scaling factor	1.0	4.0

The best designs generated by each experiment are presented in Table 8.19 and Fig. 8.11. There are noticeable variations in the airframe designs generated under different applied loads. These are most noticeable in the number and distribution of fuselage frames, V1 and V15 to V17 respectively, as well as the number of horizontal tail ribs, V3, and distribution of wing ribs, V14. For example, experiments 3 to 6 generated results possessing the minimum number of frames during the application of flight loads only whereas the application of landing loads in experiments 7 to 10 led to the requirement for a greater number of frames. Similar lifting surface designs were generated with different load cases in experiments 3 to 6. In these experiments, the quantities of all structural members except vertical tail stringers were reduced to their minimum constraints. This implies that the constant member sizes defined in Table 7.9 were excessively large, as such feasible structures were obtainable with low numbers of members.

All experiments generated a feasible solution due to the dynamic penalty coefficient increasing the penalties applied to infeasible populations towards the end of optimisation. Experiment 1 generated the heaviest solution due to the larger selection of loads applied to the airframe requiring greater global strength to satisfy the design constraints. Dynamic structural analysis in experiments 11 and 12 produced lighter designs than in the experiments 3 and 8 that applied the same load cases as pseudo-static loads. The static response is an approximation of the final response of a structure having come to rest following an applied excitation. Therefore, the dynamic response provides greater accuracy but is also subject to approximations through the direct integration method employed and step size used. Nevertheless, during

Table 8.19: Best designs generated during Boeing C-17A Globemaster III case study

	Experiment											
Parameter	1	2	3	4	5	6	7	8	9	10	11	12
V1	125	56	30	30	30	30	68	48	31	65	30	31
V2	30	30	30	30	30	30	30	30	30	30	31	30
V3	24	14	10	10	10	10	13	23	10	13	10	10
V4	2	2	2	2	2	2	2	2	2	2	2	2
V5	10	10	10	10	10	11	10	10	10	13	10	10
V6	14	13	10	10	10	10	14	23	10	10	10	10
V7	2	2	2	2	2	2	2	2	2	2	2	2
V8	29	25	27	24	26	27	25	22	27	29	26	27
V9	10	10	10	10	10	10	11	10	10	10	10	10
V10	2	3	2	2	2	2	3	4	2	2	2	2
V11	20	20	20	20	20	20	20	20	20	20	20	20
V12	1.00	1.02	1.00	1.00	1.00	1.00	1.00	1.25	1.00	1.77	1.00	1.00
V13	1.35	1.38	1.00	1.15	1.04	1.00	1.31	1.04	1.00	1.27	1.00	1.00
V14	1.72	1.73	1.82	1.78	1.77	1.85	2.25	1.80	1.00	1.73	1.00	1.00
V15, %	12.32	14.25	14.88	12.69	11.20	13.35	14.76	14.53	12.85	14.98	11.83	14.83
V16, %	5.08	5.35	9.29	8.24	7.35	7.41	5.00	5.03	8.87	5.23	8.08	8.58
V17, %	14.90	13.43	14.53	12.06	13.82	12.22	14.76	7.86	14.49	13.12	11.28	14.68
V18, c_r	0.27	0.25	0.34	0.35	0.35	0.35	0.24	0.33	0.35	0.29	0.35	0.27
V19	1.04	1.00	1.00	1.10	1.00	1.00	1.01	1.41	1.00	1.75	1.00	1.00
V20	1.46	1.48	1.49	1.40	1.48	1.48	1.48	1.08	1.00	1.00	1.00	1.00
Φ, kg	22,227	20,429	18,938	18,993	18,994	18,945	20,863	21,093	17,665	20,398	17,680	17,615
c_1	1.50	1.50	1.50	1.50	1.50	1.50	1.50	1.51	1.50	1.52	1.50	1.50
c_2, m	-0.04	-0.07	0.04	-0.08	-0.03	-0.04	-0.07	-0.09	-0.02	-0.04	-0.02	-0.02

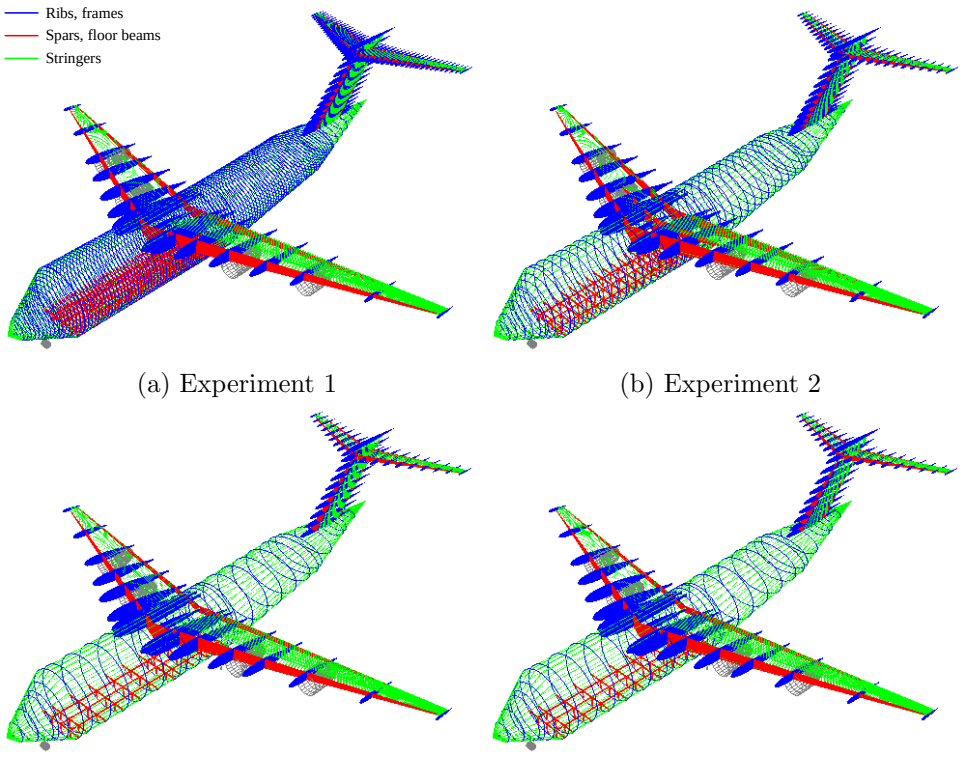

(a) Experiment 1 (b) Experiment 2

(c) Experiment 3 (d) Experiment 4

Figure 8.11: Best solutions of each experiment during Boeing C-17A Globemaster III case study

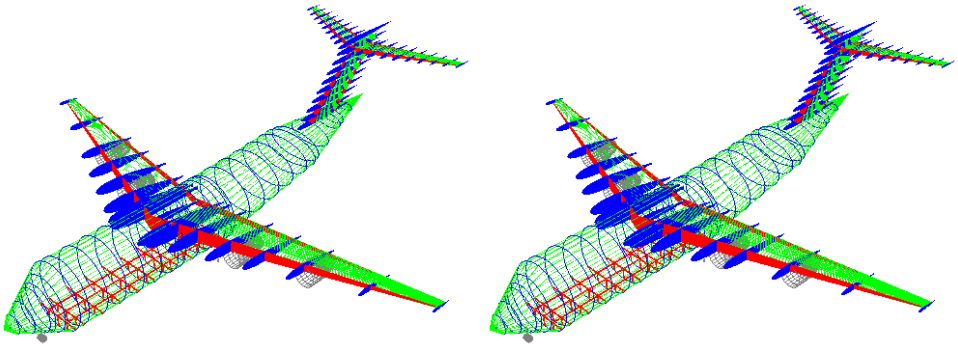

(e) Experiment 5 (f) Experiment 6

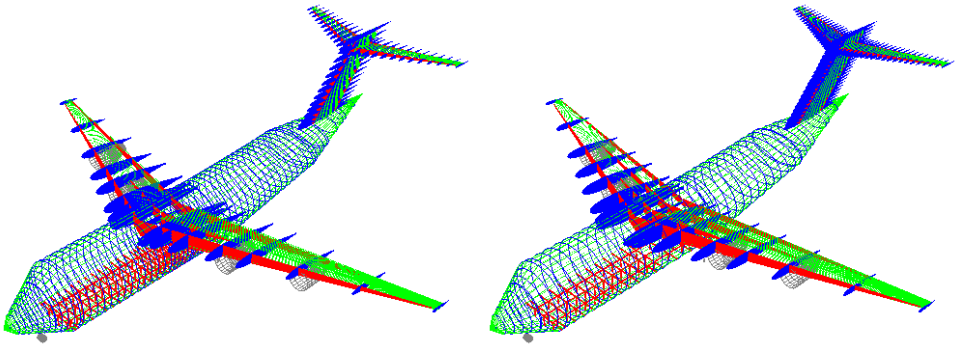

(g) Experiment 7 (h) Experiment 8

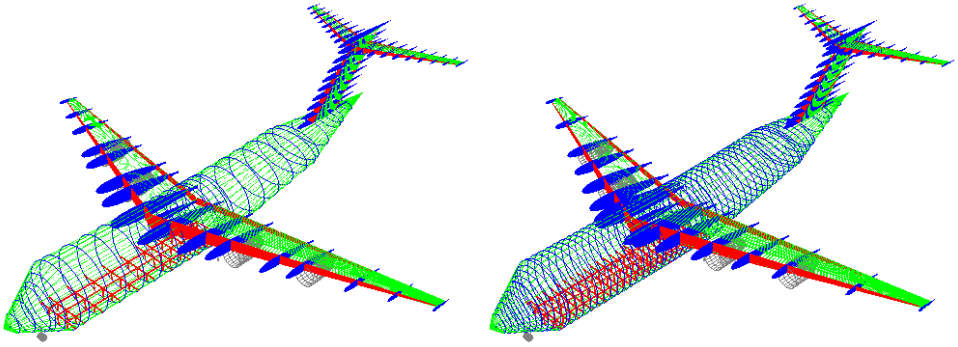

(i) Experiment 9 (j) Experiment 10

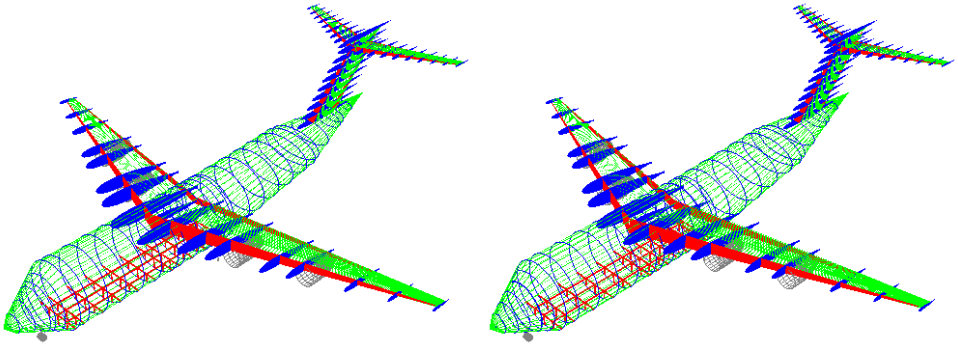

(k) Experiment 11 (l) Experiment 12

Figure 8.11: Best solutions of each experiment during Boeing C-17A Globemaster III case study (cont.)

dynamic analysis the minimum FoS within each structural member calculated over the transient is stored for comparison against the design constraints during optimisation. Therefore, these analyses used the most conservative values for each member, despite the lowest values not necessarily occurring at the same time step for different members, but were still able to direct the optimisation towards a lighter solution

than by static analysis. This may be due to the duration of the transient being too short to simulate the time step associated with the most onerous loading condition, i.e. the analyses had terminated prior to generating as high stresses in the airframe as during static analysis.

The results of this case study indicate that the search for an optimal aircraft design is highly dependent on the load cases applied to the airframe due to their effects on the structural integrity of the airframe at different locations over the aircraft. Therefore, application of a small number of load cases may not provide a near-optimal solution that is representative of the required solution for later stages of design, manufacture, certification and subsequent operation. Although the final aircraft generated in experiment 1 was heavier than the solutions of all other experiments, it is this design that provides the greatest amount of information regarding the airframe response to load. Figure 8.12 shows the critical load cases for each structural member within the best airframe design generated during experiment 1. The critical load case is defined as that which results in the lowest FoS within a member during structural analysis. The four load cases labelled in Fig. 8.12 were the most onerous for members of the airframe. The flight manoeuvre loads determined the integrity of the structure of the horizontal lifting surfaces. The maximum positive flight manoeuvre, L1, drove the strength of spars and lower surface stringers, whereas the maximum negative flight manoeuvre, L2, was dominant for ribs outboard of the fuselage and upper surface stringers. Load case L1 was also the critical load for the vertical tail root rib, spars and stringers, and fuselage floor and lower surface stringers. Cabin pressurisation at flight altitude applied a greater load to the fuselage floor and stringers than the ground loads, resulting in this flight load driving the integrity of these members. The two-point landing load, L5, was the critical load for the frames forward of the wingbox and at the empennage connection as well as the fuselage stringers not on the lower surface. Dynamic braking, L8, was most onerous for the fuselage frames aft of the wingbox but forward of the

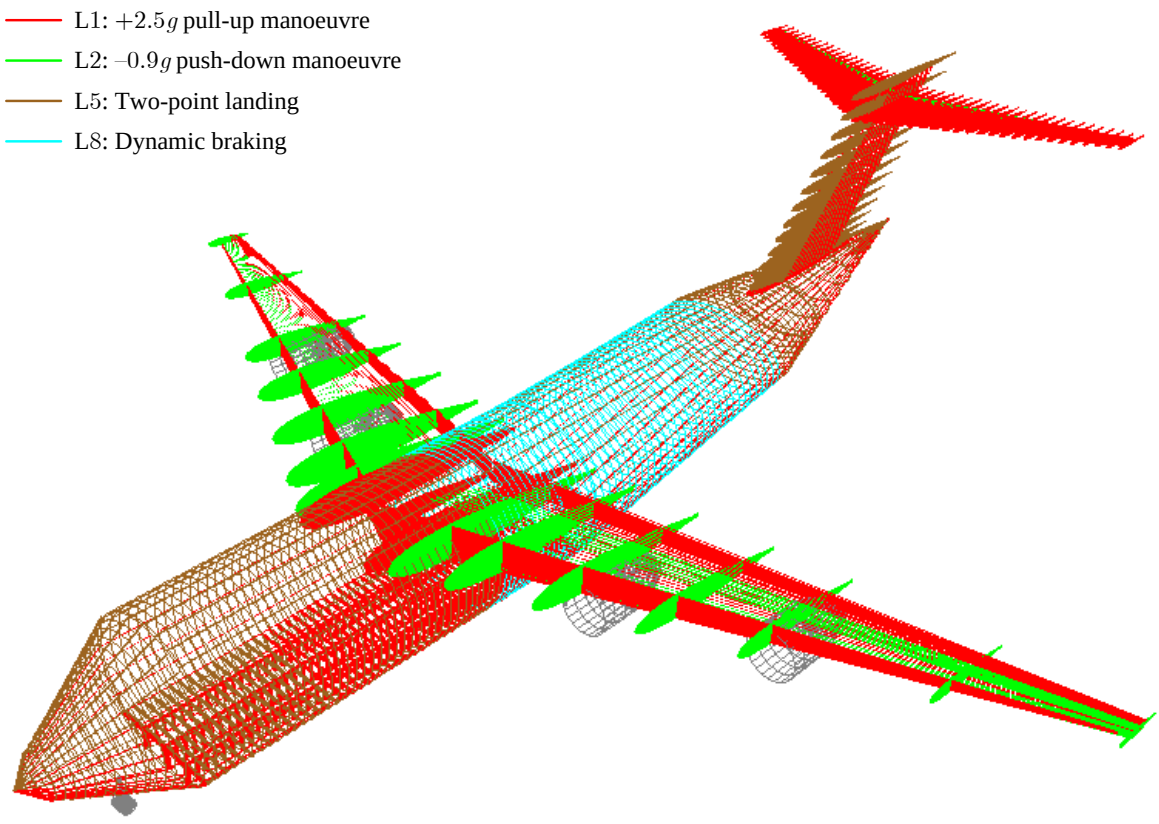

Figure 8.12: Critical loads cases for Boeing C-17A Globemaster III airframe during experiment 1

empennage. The variation in critical load in the fuselage was due to the different bending responses of the structure under landing and braking loads. Further, transmission of ground loads from the fuselage into the vertical tail proved to be more significant than flight loads. The fact that the maximum manoeuvre envelope and two-point landing case were amongst those most onerous to the airframe supports the basis as to why these loads alone are most often applied within the literature. However, the results in Table 8.19 show that a more useful aircraft design solution for subsequent embodiment design, detail design and future operation is obtained when considering a greater selection of load cases.

The operating empty weight of the Boeing C-17A Globemaster III is 125,645 kg (Jackson, 2009). No empirical formula for the structural mass of a turbofan-powered military transport aircraft is available, however an estimate can be obtained by substituting the aircraft with a turboprop-powered long-haul freighter. Subsequently, the airframe mass is approximately 43% of the operating empty mass (Torenbeek, 1982, p. 266), giving the structural mass of the existing design as 54,583 kg. The best solution generated in experiment 1, i.e. with all load cases applied, was approximately 41% of the structural mass of the existing design. This indicates a remarkable improvement in the structural mass, but it should be noted that the level of detail employed in developing the final design of the existing aircraft will have been greater than that used herein, as was the case for the studies in §8.1 and §8.3. Furthermore, even though a larger selection of load cases was applied during this case study than for the earlier studies, the existing design will have been subjected to a wider selection of loads. Moreover, localised loads will have been applied to areas of the structure requiring additional reinforcement to enable the aircraft to perform its mission of heavy lift, e.g. strengthened floor and attachment points for carrying heavy vehicles, cargo and weapons. Finally, the empirical estimate of airframe mass will be less accurate given the substitution performed of the aircraft class in order to perform this comparison.

8.5 Summary

Four case studies have been performed to evaluate the performance of the framework presented in Chapter 5. These studies have included the structural optimisation of two existing large civil aircraft, one existing military transport aircraft and one novel military trainer aircraft. The HHA was found to provide significant improvements in solution quality over traditional optimisation methods. In the first study, experimentation with the four individual aspects of the HHA indicated that heuristic selection provided the greatest improvements by ensuring better-performing LLHs were applied to the problem. Application of the complete HHA in this study led to a large penalty in computation time, although this was partly due to the computation time component of the hyper-heuristic objective function not being employed. The second study did employ this component, resulting in significant improvements in the computational cost using the HHA. Critically, improved solutions were found using the HHA over those obtained by traditional optimisation under similar conditions at a reduction in computation time. This provided the evidence that the HHA can improve solution quality without inherently incurring a computation cost. Explicit control of model fidelity as a parameter of the HHA did not provide conclusive results during this case study; as such a further case study was performed to focus on variable-fidelity modelling. The results of this third study indicated that the HHA could provide beneficial control of fidelity when coupled with a deterministic rule to encourage a general fidelity increase over time. The final case study examined the effects of load case selection on solution quality. The most onerous load cases to the lifting surfaces and fuselage were identified, confirming why these loads are most commonly applied during aircraft design optimisation. Nevertheless, this study showed that selection of appropriate load cases is critical to ensure the solution that is generated will be useful for further design, certification, manufacture and operation. These case studies have thus provided the means to perform an evaluation of both the framework and the thesis underpinning this research project.

Chapter 9

Discussion and Conclusions

This document presents a framework for the structural optimisation of aircraft conceptual designs through the use of a hyper-heuristic approach (HHA). This framework has been developed to investigate the thesis that hyper-heuristics can provide improved conceptual aircraft structural designs over those obtained by traditional optimisation without incurring computational costs. The framework, which is described in Chapter 5, has been evaluated through its implementation as AStrO over a number of case studies, the results of which are presented in Chapter 8. These case studies were set up following preliminary investigations into the effects of varying the framework set-up, presented in Chapter 7, that also provided insights into framework performance. A summary of the contributions made by this research to the field of aircraft structural design optimisation is shown in Fig. 9.1. These include the principal contribution of the framework for hyper-heuristic structural optimisation of a conceptual aircraft design as well as additional contributions through the reviews of the literature and the evaluation of the framework through its implementation as AStrO.

This chapter discusses the key findings of this evaluation, with consideration made of the requirements and research opportunities identified in Chapter 4, and provides a conclusion to this document. The results of the investigations into structural analysis are discussed in §9.1 followed by similar discussion of the investigations into the different optimisation techniques in §9.2. The evaluation of the HHA is discussed in §9.3 before the aircraft designs generated during the case studies are discussed in §9.4. The thesis presented by this research project is evaluated in §9.5 through discussion of the research aims and objectives. Suggestions for future research are made in §9.6 prior to concluding remarks in §9.7.

9.1 Structural Analysis

The framework structural analysis stage assesses the integrity of each airframe design when subjected to selected load cases. This determines design feasibility, which is a key requirement during the optimisation of an aircraft as identified in §4.1. Preliminary investigations presented in §7.1 verified the results of the finite element analysis (FEA) module and examined the effects of varying model fidelity. Further, the case study presented in §8.3 investigated different methods of controlling variable-fidelity modelling whilst the investigation presented in §7.3.2 evaluated the suitability of penalty functions for constraint handling.

9.1.1 Finite Element Analysis

The FEA module was verified against two commercial FEA tools in §7.1.1: Strand7 and VisualFEA. Four problems of varying complexity were solved to obtain the static or dynamic responses of the corresponding systems. The comparison of results for static and dynamic responses provided negligible difference in the results of AStrO and VisualFEA, i.e. $\leq 0.03\%$. Discrepancies between Strand7 and the other packages existed due to rounding errors within Strand7. The successful verification of the AStrO FEA module enabled its use within the framework during the solution of optimisation problems. This removed the

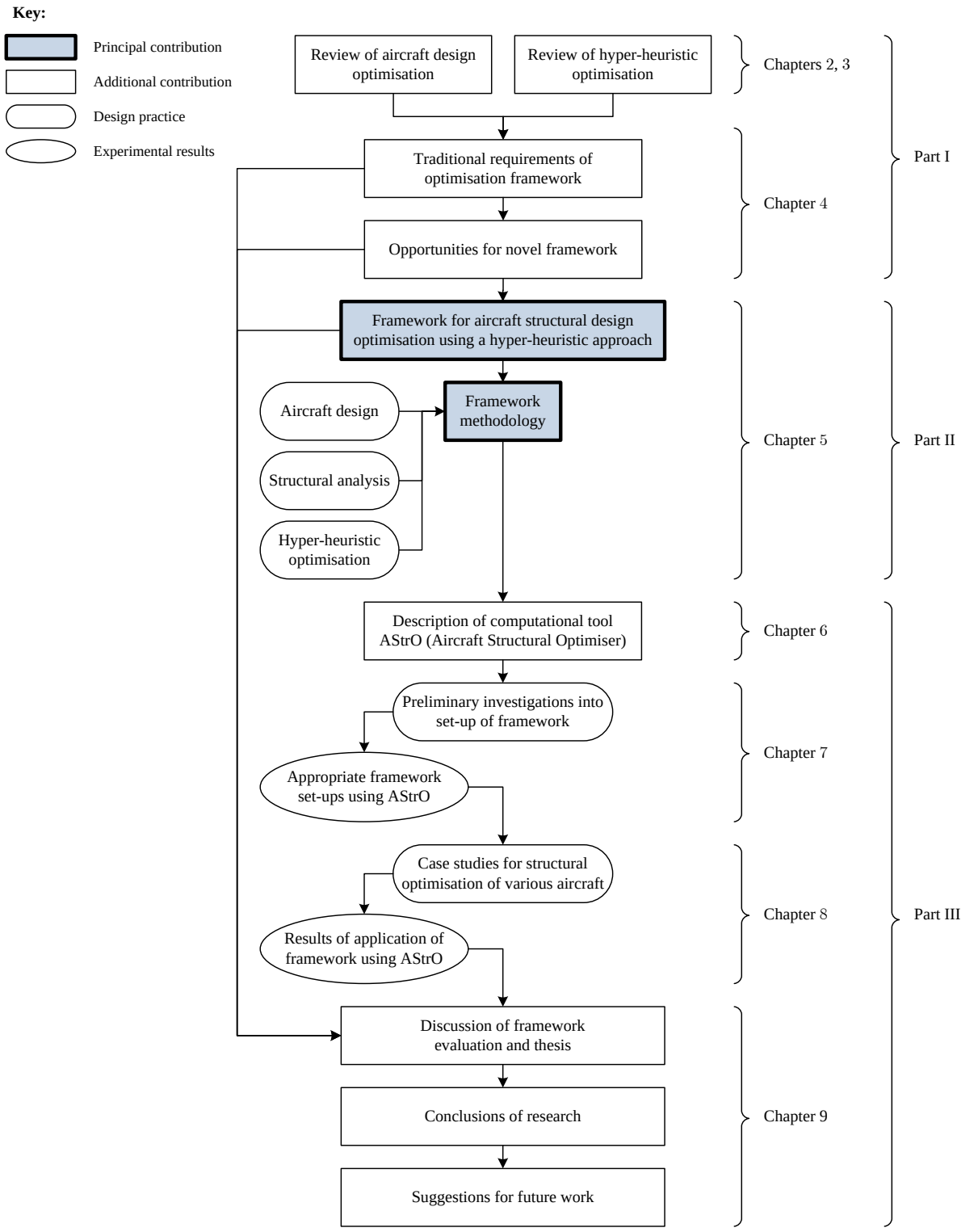

Figure 9.1: Summary of research contributions

need to generate output files for an external FEA package and subsequently read input files produced by the package to inform optimisation. By avoiding the need to perform these tasks, potential errors during the input or output of data were removed, as was the computational effort required to do so - a valuable asset during lengthy optimisation problems.

9.1.2 Model Fidelity

The model fidelity investigation presented in §7.1.2 established the degree of inaccuracy in solution feasibility that was inherent with using reduced levels of fidelity. This was compared to the benefits in terms of the computational time required to set up and solve the FEA problem. The solutions to 20 FEA problems were obtained at evenly-spaced levels of model fidelity. When compared against the model of highest fidelity, the accumulated error in feasibility was greater with reducing levels of fidelity. However, the computational time required for modelling and analysis was substantially less with reduced fidelity. It was established that $F = 0.4$ provided a threshold fidelity level, wherein the accumulated error in feasibility with respect to the driving design constraint, C1, was negligible above this value. No such trend was observed in the error in calculating the value corresponding to constraint C2. This investigation showed that the gains in computational cost were great using a low-fidelity model, i.e. the mean time taken at $F = 0.1$ was 0.04% of that at $F = 1.0$, whilst negligible errors in feasibility were recorded when performing FEA at $F = 0.4$. Consequently, the case studies were set up with variable-fidelity modelling at $0.1 \leq F \leq 0.4$ in order to exploit the opportunity to reduce computational cost at $F = 0.1$ whilst allowing the possibility of greater analysis precision at $F = 0.4$.

The case study in §8.3 examined the effects of different methods of parameter control for variable-fidelity modelling on final solution quality and computation time. Hyper-heuristic control of model fidelity was identified as a research opportunity in §4.2; as such, the parameter control aspect of the HHA was investigated alongside more traditional methods of deterministic and self-adaptive parameter control. The rate of change of model fidelity was controlled by the HHA rather than the fidelity level itself following poor control of the fidelity level during the case study in §8.2. The results of the study showed that optimisation at a static high level of fidelity led to an improved design over that at low fidelity but at an increase in computation time, i.e. the best solution at $F = 0.1$ was 12.39% heavier than that at $F = 0.4$ but the latter took 4.1 times as long to find. This corresponded with the results for the analysis of individual airframe designs during the preliminary investigation in §7.1.2. Moreover, the aircraft designs generated using variable-fidelity modelling were of higher quality than the best obtained using static fidelity by up to 1.36%. Furthermore, the corresponding design provided a reduction of 42.45% in the computation time taken. Utilising a low-fidelity model for a small number of generations at the start of optimisation, i.e. $F \leq 0.2$ for the first 100 generations, before increasing fidelity often led to the early discovery of the best design. The computation time taken with variable-fidelity modelling was greater than at the lowest level of static fidelity $F = 0.1$; however, solution quality was sacrificed when using such a low static fidelity level compared to all other experiments. This evaluation indicated the benefits of employing variable levels of model fidelity over static fidelity modelling.

9.1.3 Design Feasibility

The preliminary investigation into constraint handling presented in §7.3.2 found that the exterior penalty function outperformed the alternative penalty functions: the death penalty and interior penalty function. This was due to the exterior function permitting the inclusion of infeasible designs within the next population but discouraging convergence outside the feasible solution space. This enabled populations to evolve whilst considering design traits that caused light, but infeasible, designs whilst the penalty function attempted to remove such infeasibilities. The margin of feasibility of a high quality airframe design was small such that the design did not possess excessive weight for structural strength under load. Therefore, the exterior penalty function was well-suited to enable the optimisation search to focus on the regions of the solution space close to the constraint boundaries. The adaptive penalty function of Bean and Hadj-Alouane (1992) performed poorly, which was likely to be due to its reliance on its set-up. Therefore, this presented the opportunity to include adaptation of the penalty function by the parameter control aspect of the HHA within the investigation in §7.4.4 and the case studies of Chapter 8. Hyper-

heuristic control of the penalty parameter during these experiments was seen to encourage the generation of feasible solutions close to the constraint boundaries, i.e. solutions were found on the constraint boundary of the driving design constraint, C1. This led to solutions of lower mass than those with greater margins to this constraint boundary due to the excessive mass required. Further investigation of such penalty coefficient control would be beneficial, such as varying the adaptation thresholds defined in Eqn. (5.15) to tune the adaptive rule and provide greater control of population feasibility.

9.2 Optimisation Techniques

Optimisation techniques are employed by the framework as low-level heuristics (LLHs) within the problem domain to solve the aircraft structural design optimisation problem. The qualities of solutions generated by the optimisation process are highly dependent on the performance of these techniques. A research opportunity was identified in §4.2 for an HHA within the framework to adapt these techniques for improved process performance and subsequent solution quality. Firstly, the optimisation process within the framework was verified using a set of benchmark functions in §7.2 to ensure appropriate LLH operation. The investigations presented in §7.3 then examined the effects of varying the set-ups of the LLHs on the solutions generated to the aircraft structural design optimisation problem.

9.2.1 Optimisation Verification

The optimisation process was verified in §7.2 by employing the LLH optimisation techniques within the heuristic set to solve a set of numerical benchmark functions. This verification was critical to ensure the optimisation techniques could solve a series of known problems before being applied to an unknown problem. The results of these experiments were compared against data from the literature, which showed that the LLHs were equally successful as those used within the literature, with the genetic algorithms (GAs) and particle swarm optimisation (PSO) providing the best performances with mean success rates over all functions of 92.77% and 93.87% respectively. These results provided the confidence that the optimisation techniques operated correctly. Although the population-based techniques performed notably better than the local search (LS) techniques for non-convex multimodal problems, the latter were able to locate a solution closer to the global optimum of a unimodal problem, most notably simulated annealing (SA) and tabu search (TS). This supported the incentive to employ such techniques during perturbation analysis to further improve the quality of a solution by searching the local solution space.

9.2.2 Optimisation Set-Up

Investigations into appropriate set-ups of the optimisation process for use during the case studies were reported in §7.3.1 and §7.3.3. These investigations observed trends in results that were consistent with the findings reported in the literary sources reviewed in Chapter 2. A GA with roulette wheel (RW), tournament selection (TO) or breeder pool (BP) selection generated the best solutions, however PSO also performed well with appropriate constriction. Explosion of the PSO search was problematic without the use of a high constriction constant; however, too great a value, i.e. $\kappa_{PSO} \approx 1.0$, limited exploration.

The LS techniques performed better when applied to the aircraft design problem than the benchmark functions in §7.2. This indicated that the solution space was not as noisy as those of the benchmark functions over which the step-based LLHs struggled to locate the global optimum. This was likely to be due to different dependencies between design variables when considering the benchmark functions or the aircraft structural design problem. For example, the continuous variables of the aircraft structural design problem defining the cross-section of a structural member type, V26 to V47, were linked in their effects on the objective value, i.e. increasing these values increases the objective value of structural mass. The influences of the quantities and positions of members, V1 to V20, on the objective function are similarly connected. As such a smoother solution space landscape existed compared to that of the multimodal benchmark functions. Variables such as member section profile and material, V21 to V25 and V48 to

V50 respectively, were not as well connected given that discrete changes to these variables were more likely to result in abrupt changes in the solution space landscape.

Radioactive contamination (RC), the GA selection method pioneered by this research, did not perform well due to poor selection of parents from the parent population. A proposed method of improving this technique would be to couple the mutation operator of RC with another GA crossover selection mechanism, e.g. RW, TO or BP, or revise the mutation probabilities in Eqn. (5.33). Noticeably, a real number representation outperformed a binary representation of a GA due to the increased resolution possible in the genomes of design solutions.

The performances of the optimisation techniques when applied to the aircraft structural design problem indicated that different techniques may be more suitable to solving different problem states. For example, a random technique, e.g. Monte Carlo (MC) or random immigration (RI), or PSO with bias towards cognitive search rather than social interaction, i.e. $c_{1,PSO} >> c_{2,PSO}$, encouraged exploration and avoidance of search stagnation. Conversely, convergence was promoted using an elitist set-up of an evolutionary algorithm (EA), e.g. low mutation probability. This supported the incentive to use heuristic selection and population distribution within the HHA to vary the LLHs employed and parameter control to modify the LLH operators in order to encourage such behaviour during optimisation.

9.3 Hyper-Heuristic Approach

The framework includes an HHA to improve solution quality and optimisation process performance in order to exploit the principal research opportunity described in §4.2. The use of the HHA during the case studies provided significantly better design solutions than when using traditional optimisation. Premature convergence was not experienced with the complete HHA to the same degree as that by traditional optimisation. Greater freedom for variation in the penalty function coefficient led to improved population feasibility. Better solutions were reported in §8.1 using the entire HHA than with only one aspect of the HHA in isolation, i.e. heuristic selection, population distribution, perturbation analysis or parameter control. Moreover, the case study in §8.2 used the HHA to generate an improved solution in a shorter time than by traditional optimisation under similar test conditions.

9.3.1 Heuristic Selection

Heuristic selection is included in the HHA to promote the use of better-performing LLHs during the optimisation process, whilst also permitting the probabilistic selection of poorer performing techniques for added search diversity. This HHA aspect improves the quality of solutions generated by the optimisation process by removing the reliance on the benefits and limitations of a single optimisation technique. The preliminary investigations into heuristic selection presented in §7.4.1 indicated that the greedy (GR), peckish (PK), RW and TO hyper-heuristics performed well with a variety of set-ups, whilst exponential Monte Carlo with counter (EMCQ) performed the best out of the move acceptance rules, most notably when coupled with either the choice function or hyper-heuristic objective function measure of improvement (MoI) criterion. The hyper-heuristic objective function performed as well as the choice function as an MoI criterion, indicating its suitability for use within the HHA. The case study in §8.1 applied different aspects of the HHA, the results of which showed that heuristic selection provided greater improvements in solution quality than the other HHA aspects in isolation, i.e. the best solution found using only heuristic selection in experiment 5 was lighter than those obtained using only perturbation analysis or parameter control by 6.99% or 6.73% respectively. The GR hyper-heuristic in experiment 5 outperformed the RW hyper-heuristic in experiment 6 by 1.24% when comparing the quality of the best solution from each experiment, but by only 0.61% when comparing the average solution qualities. However, the elitist GR hyper-heuristic permitted the dominance of exploration-encouraging LLHs, e.g. MC, that led to poor population convergence. Conversely, the RW hyper-heuristic coupled with population distribu-

tion outperformed GR during early optimisation and population convergence. Specifically, for the run that produced the best solution, the final population affinities were 57.03% with GR compared to 96.01% with RW heuristic selection. Furthermore, the best solutions overall were obtained in experiments 7 and 8 of this case study when the entire HHA was applied with RW heuristic selection.

9.3.2 Population Distribution

The HHA includes population distribution to permit multiple LLHs to be employed during a generation. This prevents the optimisation search from being restricted to a limited area of the solution space due to the characteristics of a single technique. The set-up of population distribution was investigated in §7.4.2 and the HHA aspect was employed during the case studies of Chapter 8. These experiments found that applying multiple optimisation techniques prevented the search from being directed by a single LLH, which could lead to poor exploration or premature convergence due to the limitations inherent to the LLH. Coupling population distribution with heuristic selection provided further improvements in solution quality by increasing the likelihood that well-performing LLHs are selected. An interval of 40 to 60 generations between redistributions of the population provided time for each LLH to optimise its sub-population. However, careful consideration was required in the number of LLHs over which the population was distributed and the sizes of each sub-population, and thus the total population. An excessive number of LLHs led to each technique being applied to a small sub-population without sufficient opportunities to evolve the solutions, thus penalising the search. This was evident during experiment 6 of the case study in §8.1, where the best solution was 1.24% heavier than that found during experiment 5 without population distribution. Conversely, too large a population led to significant increases in the computation time required to solve the optimisation problem. This was also noticeable in the case study presented in §8.1, where the time taken by traditional GA optimisation in experiment 2 was 96.09% less than that using population distribution with a population set up to 11 times larger in experiment 8. Furthermore, this use of population distribution led to a poor value final population affinity of 61.92% due to the independent optimisation of sub-populations. The case study in §8.2 also employed the HHA with population distribution in experiments 5, 6 and 7 with total population set sizes of 100, 300 and 600 individuals respectively. In this study, the time taken by experiments 5 and 6 were 11.17% and 39.75% of that required by experiment 7 respectively.

9.3.3 Perturbation Analysis

Perturbation analysis using a memetic algorithm (MA) is included within the HHA to offer opportunities for learning of promising solution space regions within the problem domain. This was intended to improve solution quality with little additional computational cost by perturbing a small number of individuals and recording any improvements found. The preliminary investigations presented in §7.4.3 indicated better performance of the SA and TS hyper-heuristics over hill climbing (HC), especially when coupled with Lamarckian evolution and small samples of the best population individuals, i.e. $\mu_{PA} \leq 0.1\mu$. Analysing the entire population did not increase the computation time as it resulted in greater improvements of the population as a whole, leading to airframes possessing fewer degrees of freedom (DoFs) and, thus, decreasing the time required for FEA. A small perturbation scale, i.e. $\Delta x_{v,PA} \leq 0.01\Delta \mathrm{V}_v$ generally provided better solutions and lower computation costs by restricting the analysis to a highly localised search. Perturbation analysis provided good solutions during the case studies, although premature convergence of the search was an issue in §8.1 when the termination criteria included the maximum population affinity and maximum number of successive generations without improvement. In essence, the search converged on a local optimum much quicker in this case study than would have occurred without perturbation analysis. In contrast with the preliminary investigation, there was a computational penalty when using perturbation analysis during the case studies, i.e. in §8.1 the same time was taken by the traditional GA in experiment 2 as for experiment 3 using perturbation analysis even through the GA continued for

1.79 times as many optimisation generations. This penalty was exacerbated further when considering numerous load cases due to increasing the demand on FEA of each design solution as in the subsequent study in §8.2. Nevertheless, the improvements in solution quality offered using the HHA during this study often led to the recovery of the computational cost.

9.3.4 Parameter Control

Parameter control is the final aspect of the HHA in order to improve the performance of the optimisation process through the dynamic modification of values of key process parameters. These parameters include the level of detail employed during FEA, the severity of penalty applied to infeasibility and the values of operators used by the LLHs. The preliminary investigations presented in §7.4.4 into parameter control indicated that, as for perturbation analysis, the SA and TS hyper-heuristics performed better than HC. This was due to the latter representing a purely random step-based search whereas the two former heuristics probabilistically permitted negative changes in parameters which could enable new exploration in the hyper-heuristic search. The SA and TS hyper-heuristics performed similarly throughout the investigation, without a clear indication as to which technique was best for control of all parameters. An evaluation period of 50 generations provided an appropriate balance between the time allowed for parameters to take effect, and thus have an opportunity to improve hyper-heuristic objective value, and the number of opportunities for parameter modification during the optimisation search, i.e. nominally 20 opportunities over 1,000 optimisation generations. The case study of §8.2 included control of the variable strand lengths to permit increased resolution of continuous variables during convergence prior to disabling converged variables for improved refinement of other variables yet to converge. This enabled the optimisation process to focus on variables failing to converge, and thus the experiments that employed the HHA provided better solutions than those using traditional optimisation by up to 53.79%. Further, the control of LLH operators during this case study led to modifications of the LLH set-ups in order to encourage exploration during early generations or during search stagnation and convergence towards the end of the process. For example, the crossover and mutation probabilities of the LLHs were increased to their upper bounds in Table 8.6 within the first 100 generations to increase solution space exploration.

The case study presented in §8.3 regarding control of model fidelity showed that hyper-heuristic parameter control provided a balance between solution quality and computational expense, as was discussed in §9.1.2. Deterministic and hyper-heuristic parameter control generated the lightest aircraft designs at lowest computational cost, i.e. minimum objective values of 9,535 kg in 8.31 h and 9,543 kg in 9.56 h respectively. This was most noticeable with small values of $\delta_F \leq 1.0$ to encourage early discovery of promising design traits. Self-adaptive control generated a mean solution of similar quality, 9,669 kg, however at a much higher computational cost of 13.08 h due to the individual levels of model fidelity possessed by each population. Hence, coevolution of fidelity with the structural design failed to generate an improved parameter value over those defined by deterministic and hyper-heuristic parameter. The discrete method of parameter control representative of that employed in Minisci et al. (2011) produced the worst mean solution quality in a time greater than many cases employing variable-fidelity modelling through deterministic, self-adaptive or hyper-heuristic parameter control, i.e. 9,956 kg in 8.80 h. This study showed that hyper-heuristic control of the rate of change of fidelity coupled with an underlying deterministic rule instead of direct control of the fidelity level improved the HHA performance in terms of solution feasibility and computation time compared to the results presented in §7.1.2 and §8.2 respectively. Control of the rate of fidelity change rather than the fidelity level itself forced the optimisation process to increase model precision during the process but enabled perturbation of the parameter such that periods of reduced or increased fidelity were included. This enabled periods of rapid low-fidelity analysis or more detailed high-fidelity analysis as demanded by the process, whilst maintaining a general increase in fidelity for detailed assessment of later designs during convergence.

9.3.5 Computational Expense

A principal claim of the thesis described in §1.3 was that hyper-heuristic optimisation could be performed for aircraft design optimisation without incurring computational costs. This was to ensure that using the framework would not increase the already lengthy period of conceptual design. The results of the case study presented in §8.1 indicated that using the complete HHA required up to 96.09% more computation time to complete the optimisation process. However, this study was focussed on examining the affects of the different HHA aspects on the optimisation process, therefore the computation cost component of the hyper-heuristic objective function of Eqn. (4.3) was not included. Moreover, this component was designed to principally control the level of finite element (FE) model fidelity employed, whereas variable-fidelity modelling was not performed during this study. However, the second case study in §8.2 did include this term in the hyper-heuristic objective function whilst also including variable-fidelity modelling. In this study, the computation time required using the HHA was reduced by 15.38% compared to that required by traditional optimisation when using the same size of population set. Moreover, the quality of solution obtained was 17.53% lighter when comparing these experiments. This supported the thesis that hyper-heuristic optimisation could be employed to improve solution quality without increasing the computational cost. Nevertheless, the computational expense of employing the HHA was the principal limitation during the case studies, requiring appropriate set up of the framework to avoid such a penalty. For example, the study presented in §8.3 showed the importance of selecting an appropriate rule for variable-fidelity modelling on the subsequent computation time required for optimisation. Therefore, computational expense remains a key concern when using the HHA. Notwithstanding this, it is important to acknowledge that the computation times of all simulations were greatly affected by the efficiency of the solvers implemented within AStrO. Thus, using more efficient solvers could reduce the differences in computation times between different simulations, thus further diminish any computational costs associated with employing the HHA.

9.4 Aircraft Designs

The objective of the framework is to generate near-optimal airframe solutions for an aircraft under load. The airframe designs generated during the case studies in Chapter 8 were compared with the existing designs of the aircraft. Such direct comparison was not possible for the study presented in §8.2 as the aircraft design being optimised was a novel concept. Hence, a comparison was performed between this design and the designs of aircraft of similar class and intent.

The best Airbus A340-300 design generated in the study of §8.1 weighed approximately 87% of the estimated structural mass of the existing design. Similarly, the best solution of the case study in §8.3 weighed approximately 80% of the estimated structural mass of the existing Embraer E-195 aircraft design. Notwithstanding this, these improvements in airframe mass cannot be read as direct indications of better designs due to the fact that the existing aircraft designs will have been designed to a greater level of detail than those presented herein. The structural mass is calculated in the framework using Eqn. (5.5) as the sum of the approximated mass of the airframe structural members; thus, includes a margin of error in the approximation used and does not take into account fasteners and other detailed components that contribute to the structural mass. Furthermore, the final existing designs will have been subjected to a larger set of load cases for certification than those simulated during these studies. The principal Boeing C-17A Globemaster III design solution reported in §8.4 weighed 41% of the structural mass of the existing design. This aircraft was subjected to all load cases in the framework database, however this is still significantly fewer loads than the existing aircraft will have been certified against. Furthermore, the loads were applied on a global scale to the entire airframe, whereas such a long-haul military freighter would be subjected to more detailed local loading of the supporting structure and attachment points to provide reinforcement of the design. As a result, it is accepted that the improvements in objective value

of the best solutions over the existing aircraft designs may be exaggerated. Nonetheless, the solutions obtained indicate the possibility to improve the existing designs by using the framework.

The best structural design of the novel AStrO-1 aircraft presented in §8.2 was compared against two similar military trainer aircraft which indicated that a design of similar quality was obtained. The principal differences between generating a novel concept or an existing design variant using the framework are the tasks required by the aircraft design procedure module. The AStrO-1 designs output from the aircraft design procedure module during this study were reasonable given the designs of these existing aircraft. This provided the evidence that these modules are appropriate in generating a suitable aircraft external profile to serve as a geometric boundary within which structural optimisation is performed. Furthermore, this proved that the framework can optimise the structural designs of both existing and novel aircraft of various classes. Additionally, such optimisation includes the entire aeroplane rather than only a single section, e.g. the wing.

Variations were identified in the structural layout of the existing design of the Airbus A340-300 and the best solution generated in the corresponding case study reported in §8.1. These were most notably in the position of the front wing spar and distribution of ribs over the wingspan. Similar comparisons could not be performed for the results of the studies of the Embraer E-195 and Boeing C-17A Globemaster III given in §8.3 and §8.4 respectively due to a lack of public domain data concerning the structural designs of these aircraft. Such variations in the Airbus A340-300 design are likely to be due to the differing levels of detail to which the designs have been subjected and the reduced number of loads applied to the designs during the case study. The influences of load cases on the airframe was investigated by the case study presented in §8.4. These results clearly showed the areas of the Boeing C-17A Globemaster III aircraft driven by flight or ground loads, with flight manoeuvres, two-point landing and dynamic braking load cases proving most onerous. This design was heavier than all other solutions for this study as a result of the greater required structural strength. However, this design would be most suitable for further development during embodiment design due to the greater variety of loads applied. This study serves to prove the importance of load case selection during optimisation and the need to consider not only the most severe loads to the global system in order to generate a useful design concept.

9.5 Research Aims and Objectives

The research aim in §1.3 is for the development of a framework to perform structural optimisation of an aircraft concept for a design of minimal mass under load. This framework includes an HHA to improve the operation of the optimisation process and consequently provide better solutions to the optimisation problem without increasing computational expense. It is the thesis of this research that hyper-heuristic optimisation within this framework can improve the quality of solutions generated over those obtained by traditional approaches to the problem without increasing the computational cost. The research objectives stated in §1.3 have been satisfied in order to investigate this thesis.

The first two research objectives were to perform reviews of existing approaches to aircraft design optimisation and hyper-heuristic optimisation. These objectives have been satisfied through literature reviews in these two areas, presented in Chapters 2 and 3 respectively, followed by the identification of framework requirements and research opportunities in Chapter 4. The review of existing approaches to aircraft design optimisation revealed a traditional process for solving the problem with limited investigation into its improvement. Such improvement could be of great use to further improve the quality of solutions generated through appropriate online process adaptation. Moreover, optimisation techniques are applied without significant dynamic control of their operation. A single load case is usually applied to the airframe to determine design feasibility rather than exposing the structure to the variety of loads likely to be encountered during operation. Typically, a single class of aircraft is considered and many studies focussed on one section of the aircraft alone, e.g. the wing. The review of hyper-heuristic

optimisation discovered four common aspects of an HHA: heuristic selection, population distribution, perturbation analysis and parameter control. The former two aim to improve the choice of LLH applied to the problem whilst the latter two respectively encourage learning of the solution space and process modification to promote beneficial search behaviour. An HHA requires a suitably-designed objective function, a learning mechanism and domain independence. Only three literary sources were discovered that applied hyper-heuristic optimisation within the domain of aerospace design optimisation, with none considering structural design optimisation. The findings of these reviews presented the opportunity to use hyper-heuristics to improve the aircraft structural design optimisation solution process. Furthermore, opportunities were identified to develop a novel HHA to encourage improvement in multiple aspects of the optimisation process. Additionally, it was identified that the usefulness of the framework could be improved by permitting design, analysis and optimisation of different aircraft classes, entire aircraft configurations and the simulation of multiple load cases.

The third research objective described in §1.3 was to develop and implement a framework for subsequent evaluation. Chapter 5 presented the framework developed by this research, which is formed of three stages: aircraft design procedure, structural analysis and airframe design optimisation. The aircraft design procedure initialises the framework, defines the aircraft mission, estimates the vehicle mass, generates its external profile and calculates the loading conditions. The structural layout of the aircraft is then designed within the established external profile. This layout is defined by the values of the optimisation problem design variables. Numerous variants of the aircraft structure are generated in this manner for structural analysis using FEA followed by optimisation of the airframe in order to minimise its mass. The feasibility of designs is established by structural analysis by measuring their response to the applied load cases with respect to two design constraints concerning structural strength and deflection. The aircraft model is idealised by grouping similar structural members to reduce the computational cost of FEA. The HHA is employed during optimisation to improve the performance of the optimisation process employed to minimise the structural mass of designs. This HHA includes the four aspects identified during the literature review within a single approach. This encourages solution quality to be improved without increasing the computational cost of implementing the framework.

The final research objective stated in §1.3 was to evaluate the framework against existing approaches to aircraft design optimisation. This evaluation was conducted using a purpose-built computational implementation of the framework called AStrO, which is described in Chapter 6. Chapters 7 and 8 presented and discussed the variety of optimisation problems that were solved to evaluate the framework. The solutions that were output using the HHA outperformed those obtained by traditional methods. These improvements in solution quality were found to be statistically significant. All four aspects of the HHA assisted the optimisation process in achieving these gains. Heuristic selection provided the capability to vary the LLH applied to the problem and thus not be restricted by the characteristics of a single technique. Of the four HHA aspects, it was heuristic selection that provided the greatest improvements in solution quality over traditional optimisation. Population distribution provided similar advantages for each generation and thus discourage search stagnation. Perturbation analysis encouraged additional improvements to be made in solution quality by exploring the solution space neighbouring good designs. Finally, parameter control promoted exploration, convergence, feasibility and speed through the adaptation of a selection of key process parameters to satisfy the corresponding hyper-heuristic objective function. This led to additional improvements in terms of feasibility, avoidance of premature convergence and structural analysis precision by using the HHA.

The computational time taken to solve the optimisation problem was greater in most experiments when using the HHA compared to when performing traditional optimisation. Computation time was increased using the HHA during the first case study within §8.1. This was due to the larger population sizes required to perform population distribution over multiple LLHs whilst maintaining sufficient op-

portunities for improvement within a sub-population. Subsequently, a greater number of FEA runs were required and convergence occurred later due to each sub-population converging independently. Further, the additional FEA required for perturbation analysis also lengthened the optimisation process. However, the contrasting effect of perturbation analysis was improved solution quality, and the increased computational cost was minimised by suitable sampling of the population set. Furthermore, the preliminary investigation in §7.4.3 showed that the computational penalty was minimal with larger sample sizes due to the greater number of improvements made to the population resulting in smaller FE models with fewer DoFs, thus requiring less time for structural analysis. It was this time taken by the structural analysis module that drove the overall computation time required to solve each optimisation problem. The computational cost of the HHA in the second case study within §8.2 was reduced compared to the first study through the inclusion of computation time within the hyper-heuristic objective function. In fact, the computation time was shorter using the HHA than by traditional optimisation when the same population set size was used for both methods. Consequently, it was proven during the evaluation that such an increase in computation time could be reduced, and even eliminated. However, attempts to increase model fidelity during the process, and thus the number of DoFs of models during structural analysis, were found to be unsuccessful when controlling the model fidelity level explicitly. Control of the model fidelity rate of change solved this issue in the third case study within §8.3, leading to reduced computational cost compared to optimisation at the static levels of fidelity required to generate solutions of similar quality. This reduced the computational cost of applying the HHA; in fact providing improvements against high-fidelity modelling. Nevertheless, greater computational cost was required over the optimisation at the lowest level of fidelity. This suggested an area for improvement to reduce the computational demands of the framework. Response surface modelling, such as through the use of a surrogate model, would be an appropriate tool to minimise the computation required for by FEA during structural analysis, and thus reduce the driving computational cost of the framework. This would provide benefits to both traditional and hyper-heuristic optimisation within the framework; however, the HHA would profit more due to the inclusion of computation time within the hyper-heuristic objective function, i.e. the corresponding fifth function term would not dominate HHA operation and thus permit greater focus on the terms controlling solution quality, feasibility and exploration or convergence. Notwithstanding this, even on the occasions when the computational time did increase during this evaluation, the benefits made in solution quality were significant, and thus could justify the additional cost with the current framework design.

The framework presented by this research is an original and significant contribution to the field of aircraft structural design. The principal originality of the framework is provided by the embedded HHA to improve the performance of the optimisation process, and thus obtain better designs than are possible by traditional approaches. The significance of this contribution lies with the ability of the framework to obtain better aircraft designs without increasing computational cost. As discussed in Chapter 1, conceptual design provides the greatest opportunities during the design process to improve solution quality but also requires considerable time. The novel HHA within this framework has been shown to generate better solutions without necessarily increasing the time required for conceptual design; thus supporting the thesis of this research and providing an original and significant contribution to the field.

9.6 Future Research

The research presented in this document represents the first use of an HHA within the domain of conceptual aircraft structural design optimisation. Consequently, there are a number of potential avenues for future work, the most obvious of which would encompass further investigation and improvement of the HHA and the enhancement of the framework as a whole for more varied application. Although the HHA significantly improved solution quality, the computational cost of employing the approach was large if the optimisation process was not appropriately set up. Therefore, the principal area for future

work is to investigate methods of improving the use of the HHA to reduce this cost. Possible areas for improvement are the hyper-heuristic objective function, LLHs applied to the problem, hyper-heuristics applied to the process and the method of performing structural analysis. The latter is most likely to provide the greatest reductions in the computational cost of implementing the hyper-heuristic framework. Surrogate modelling, rather than exclusively FEA, would be a suitable method to reduce the burden of structural analysis. Given that perturbation analysis has been shown to efficiently explore the solution space neighbouring good solutions, a similar approach could be applied to find near-optimal locations on a response surface formed by a surrogate model. This would require substantial development of the framework to design the surrogate model but would significantly improve its operation. Alternatively, refinement of the hyper-heuristic objective function or techniques within the heuristic sets would require less framework development whilst offering improved HHA operation. For example, the design of the hyper-heuristic objective function could be subject to further research to investigate the use of different aspects of process performance as its components or the application of different weighting factors to these components, i.e. not purely generation-based. However, it is likely that the computational cost of the framework would still be heavily dependent on its set-up. Development of the FEA solvers is an alternative avenue of investigation with regards to reducing computational cost, which could obviate the need to improve the computational efficiency of the HHA if able to sufficiently improve the structural analysis stage such that computational cost becomes negligible.

The framework was developed to tackle the conceptual aircraft structural design optimisation problem using an HHA. The level of detail included within the modelling and analysis tools could be refined to enable the framework to be used during the embodiment and detail design phases of the design process. However, this would require a greater number of design variables in order to optimise the design at a greater level of detail. Furthermore, it would be appropriate to include a larger selection of load cases and failure modes, leading to the need to consider more design constraints. The optimisation problem could also be expanded to enable multidisciplinary optimisation (MDO) by including properties of the external geometry of the aircraft as design variables, e.g. wingspan, fuselage fineness ratio. This would require small adaptations of the framework to include the aircraft profile generation and aircraft loads modules within the optimisation stage of Fig. 5.1. However, this would increase the computational cost of the framework by performing the tasks of these two modules for every individual design solution. In spite of this, such costs would not be affected greatly by the use of the HHA, i.e. they would be inherent of the framework operation by either traditional or hyper-heuristic optimisation. Inclusion of aerodynamic, emissions or cost optimisation modules would provide the facility for multi-objective optimisation, albeit requiring significant development of the framework to include the facilities necessary to assess designs with respect to these objectives and corresponding constraints. This would be beneficial if the framework were to be enhanced for use in later stages of the design process, potentially leading to the extension of the framework to encompass the entire process of aircraft design.

9.7 Concluding Remarks

Hyper-heuristics provide the facility to obtain solutions of higher quality to a problem than is generally possible through traditional optimisation. This research has showed that an HHA can be applied to the problem of conceptual aircraft structural design optimisation to exploit these benefits. The framework developed during this research has been successfully implemented using an HHA to generate near-optimal solutions of various aircraft under numerous loading conditions. The use of the HHA has enabled lighter airframe designs to be found than by traditional optimisation, including structural analysis using variable-fidelity modelling to balance precision with computational effort. As a result, the thesis has been proven that hyper-heuristic optimisation can be employed within the conceptual aircraft structural design process to improve the quality of the obtained design solutions without incurring computational costs.

References

Ackley, D. H., An Empirical Study of Bit Vector Function Optimization, *Proceedings of Genetic Algorithms and Simulated Annealing*, pp. 170–215, 1987.

Aguilar Maderia, J. F., Rodrigues, H., and Pina, H., Multi-Objective Optimization of Structures Topology by Genetic Algorithms, *Advances in Engineering Software*, 36, pp. 21–28, 2005.

Airbus SAS, *Airbus A340-200/-300 Airplane Characteristics for Airport Planning*, 2012.

Alexandrov, N. M., and Lewis, R. M., Optimization with Variable-Fidelity Models Applied to Wing Design, *Proceedings of the 38th Aerospace Sciences Meeting and Exhibit*, Reno, NV, USA, 2000.

Ali, N., and Behdinan, K., Conceptual Aircraft Design - A Genetic Search and Optimization Approach, *23rd Congress of the International Council of the Aeronautical Sciences*, Toronto, Canada, 2002.

Allen, J. G., Minutes of Meeting held at BAE Systems, Chadderton on 10 November, 2010a.

Allen, J. G., Minutes of Meeting held at BAE Systems, Warton on 10 November, 2010b.

Allen, J. G., Minutes of Meeting held at BAE Systems, Warton on 12 January, 2012.

Allen, J. G., Coates, G., and Trevelyan, J., A Theoretical Framework for the Optimisation of the Structural Layout of an Aircraft using Deterministic and Stochastic Optimisation Techniques, *Proceedings of the 8th ASMO-UK/ISSMO Conference on Engineering Design Optimization Product and Process Improvement*, London, England, pp. 19–25, 2010.

Allen, J. G., Coates, G., and Trevelyan, J., Hyper-Heuristic Optimisation for Application to Aircraft Structural Design, *Proceedings of the 9th ASMO-UK/ISSMO Conference on Engineering Design Optimization Product and Process Improvement*, Cork, Republic of Ireland, pp. 1–6, 2012a.

Allen, J. G., Coates, G., and Trevelyan, J., Hyper-Heuristic Structural Optimisation of Conceptual Aircraft Designs, *14th AIAA/ISSMO Multidisciplinary Analysis and Optimization Conference*, Indianapolis, IN, USA, AIAA 2012-5527, 2012b.

Allen, J. G., Coates, G., and Trevelyan, J., Approaches to Parameter Control for the Optimisation of Conceptual Aircraft Structural Designs, *Royal Aeronautical Society 3rd Aircraft Structural Design Conference*, Delft, The Netherlands, 2012c.

Allen, J. G., Coates, G., and Trevelyan, J., A Hyper-Heuristic Approach to Aircraft Structural Design Optimization, *Structural and Multidisciplinary Optimization*, 48(4), pp. 807–819, 2013.

Allen, J. G., Coates, G., and Trevelyan, J., Dynamically-Controlled Variable-Fidelity Modelling for Aircraft Structural Design Optimisation, *Proceedings of the Institution of Mechanical Engineers, Part G: Journal of Aerospace Engineering*, 228(8), pp. 1434–1449, 2014.

Alonso, J. J., LeGresley, P., van der Weide, E., et al., pyMDO: A Framework for High-Fidelity Multi-Disciplinary Optimization, *Proceedings of the 10th AIAA/ISSMO Multidisciplinary Analysis and Optimization Conference*, Albany, NY, USA, 2004.

Alonso, J. J., LeGresley, P., and Pereyra, V., Aircraft Design Optimization, *Mathematics and Computers in Simulation*, 79, pp. 1948–1958, 2009.

Amadori, K., *On Aircraft Conceptual Design - A Framework for Knowledge Based Engineering and Design Optimization*, Ph.D. Thesis, Linköping University, Linköping, Sweden, 2008.

Amadori, K., Personal Communication, 2010.

Amadori, K., Johansson, B., and Krus, P., Using CAD Tools and Aerodynamic Codes in a Distributed Conceptual Design Framework, *45th AIAA Aerospace Sciences Meeting and Exhibit*, Reno, NV, USA, 2007a.

Amadori, K., Jouannet, C., and Krus, P., A Framework for Aerodynamic and Structural Optimization in Conceptual Design, *25th AIAA Applied Aerodynamics Confernece*, Miami, FL, USA, 2007b.

Amadori, K., Jouannet, C., and Krus, P., Aircraft Conceptual Design Optimization, *46th AIAA Aerospace Meeting and Exhibit*, Reno, NV, USA, 2008.

Anderson Jr, J. D., *Fundamentals of Aerodynamics*, 2nd Ed., McGraw-Hill, 1991.

Anhalt, C., Monner, H. P., and Breitback, E., *Interdisciplinary Wing Design - Structural Aspects*, Technical Report 03WAC-29, German Aerospace Centre (DLR), 2003.

Antoine, N., Kroo, I., Willcox, K., et al., A Framework for Aircraft Conceptual Design and Environmental Performance Studies, *Proceedings of the 10th AIAA/ISSMO Multidisciplinary Analysis and Optimization Conference*, Albany, NY, USA, 2004.

Arabas, J., Michalewicz, Z., and Mulawka, J., GAVaPS - a Genetic Algorithm with Varying Population Size, *Proceedings of the 1st IEEE Conference on Evolutionary Computation*, pp. 73–78, 1994.

Arakawa, M., and Hagiwara, I., Development of Adaptive Real Range (ARRange) Genetic Algorithms, *JSME International Journal Series C: Mechanical Systems, Machine Elements and Manufacturing*, 41(4), pp. 969–977, 1998.

Arrieta, A. J., and Striz, A. G., Optimal Design of Aircraft Structures with Damage Tolerance Requirements, *Structural and Multidisciplinary Optimization*, 30(2), pp. 155–163, 2005.

Ayele, A., Gur, O., and Rosen, A., Conceptual Multidisciplinary Design Optimization (MDO) of Solar Powered UAV, *Proceedings of the 53rd Israel Annual Conference on Aerospace Sciences*, Tel-Aviv and Haifa, Israel, 2013.

Ayob, M., and Kendall, G., A Monte Carlo Hyper-Heuristic To Optimise Component Placement Sequencing For Multi Head Placement Machine, *2003 International Conference on Intelligent Technologies*, pp. 132–141, 2003.

Azamatov, A., Lee, J. W., and Byun, Y. H., Comprehensive Aircraft Configuration Design Tool for Integrated Product and Process Development, *Advances in Engineering Software*, 42(1-2), pp. 35–49, 2011.

Bai, R., and Kendall, G., An Investigation of Automated Planograms Using a Simulated Annealing Based Hyper-Heuristic, *Metaheuristics: Progress as Real Problem Solvers*, Springer, Vol. 32 of *Operations Research/Computer Science Interfaces*, pp. 87–108, 2005.

Bai, R., Blazewicz, J., Burke, E. K., et al., *A Simulated Annealing Hyper-Heuristic Methodology for Flexible Decision Support*, Technical Report NOTTCS-TR-2007-8, University of Nottingham, Nottingham, UK, 2007.

Baldwin, J. M., A New Factor in Evolution, *The American Naturalist*, 30(354), pp. 441–451, 1896.

Barnard, R. H., and Philpott, D. R., *Aircraft Flight: A Description of the Physical Principles of Aircraft Flight*, Longman Singapore Publishers, 1993.

Barthelemy, J. F. M., and Haftka, R. T., Approximation Concepts for Optimum Structural Design - a Review, *Structural Optimization*, 5(3), pp. 129–144, 1993.

Bartholomew, P., The Role of MDO within Aerospace Design and Progress Towards an MDO Capability, 98-4705, pp. 1–9, 1998.

Bean, J. C., and Hadj-Alouane, A. B., *A Dual Genetic Algorithm for Bounded Integer Programs*, Technical Report 92-53, Department of Industrial and Operations Engineering, University of Michigan, Ann Arbor, MI, USA, 1992.

Benham, P. P., Crawford, R. J., and Armstrong, C. G., *Mechanics of Engineering Materials*, 2nd Ed., Addison-Wesley, Harlow, England, 1996.

Beyer, H. G., and Sendhoff, B., Robust Optimization - A Comprehensive Survey, *Computing Methods in Applied Mechanics and Engineering*, 196, pp. 3190–3218, 2007.

Bilgin, B., Özcan, E., and E.Korkmaz, E., An Experimental Study on Hyper-heuristics and Exam Timetabling, *Practice and Theory of Automated Timetabling VI*, Springer, Vol. 3867 of *Lecture Notes in Computer Science*, pp. 394–412, 2007.

Bilgin, B., Demeester, P., Misir, M., et al., A Hyper-Heuristic Combined with a Greedy Shuffle Approach to the Nurse Rostering Competition, *The 8th International Conference on the Practice and Theory of Automated Timetabling (PATAT '10) - the Nurse Rostering Competition*, Belfast, Northern Ireland, 2010.

Bittle, S. A., and Fox, M. S., Learning and Using Hyper-Heuristics for Variable and Value Ordering in Constraint Satisfaction Problems, *Proceedings of the 11th Annual Conference Companion on Genetic and Evolutionary Computation Conference: Late Breaking Papers*, New York, NY, USA, pp. 2209–2212, 2009.

Blum, C., and Roli, A., Metaheuristics in Combinatorial Optimization: Overview and Conceptual Comparison, *ACM Computing Surveys*, 35(3), pp. 268–308, 2003.

Blumrich, J. F., Design, *Science*, 168(3939), pp. 1551–1554, 1970.

Boeing Commerical Airplanes, *Boeing 777-200/200ER/300 Airplane Characteristics for Airport Planning*, 2011.

Bos, A. H. W., *Multidisciplinary Design Optimization of a Second-Generation Supersonic Transport Aircraft using a Hybrid Genetic/Gradient-Guided Algorithm*, Ph.D. Thesis, Delft University of Technology, Delft, The Netherlands, 1996.

Bower, G. C., and Kroo, I. M., Multi-Objective Aircraft Optimization for Minimum Cost and Emissions over Specific Route Networks, *26th International Congress of the Aeronautical Sciences*, 2008.

Branin, F. K., A Widely Convergent Method for Finding Multiple Solutions of Simultaneous Nonlinear Equations, *IBM Journal of Research and Development*, pp. 504–522, 1972.

Brest, J., Greiner, S., Bošković, B., et al., Self-Adapting Control Parameters in Differential Evolution: a Comparative Study on Numerical Benchmark Problems, *IEEE Transactions on Evolutionary Computation*, 10(6), pp. 646–657, 2006.

Brest, J., Bošković, B., Greiner, S., et al., Performance Comparison of Self-Adaptive and Adaptive Differential Evolution Algorithms, *Soft Computing*, 11, pp. 617–629, 2007.

Burke, E., and Soubeiga, E., Scheduling Nurses Using a Tabu-Search Hyperheuristic, *Proceedings of the 1st Multidisciplinary International Conference on Scheduling: Theory and Applications*, Nottingham, UK, pp. 197–210, 2003.

Burke, E., Cowling, P., De Causmaecker, P., et al., A Memetic Approach to the Nurse Rostering Problem, *Applied Intelligence*, 15(3), pp. 199–214, 2001.

Burke, E., Hart, E., Kendall, G., et al., Hyper-Heuristics: An Emerging Direction in Modern Search Technology, *Handbook of Meta-Heuristics*, Kluwer Academic Publishers, pp. 457–474, 2003a.

Burke, E. K., Kendall, G., and Soubeiga, E., A Tabu-Search Hyperheuristic for Timetabling and Rostering, *Journal of Heuristics*, 9(6), pp. 451–470, 2003b.

Burke, E. K., McCollum, B., Meisels, A., et al., A Graph-Based Hyper-Heuristic for Educational Timetabling Problems, *European Journal of Operational Research*, 176, pp. 177–192, 2007.

Burke, E. K., Kendall, G., Misir, M., et al., A Study of Simulated Annealing Hyperheuristics, *Proceedings of the 7th International Conference on the Practice and Theory of Automated Timetabling*, pp. 18–22, 2008.

Burke, E. K., Hyde, M., Kendall, G., et al., A Classification of Hyper-Heuristic Approaches, *Handbook of Metaheuristics*, pp. 1–21, 2009a.

Burke, E. K., Hyde, M. R., Kendall, G., et al., Exploring Hyper-heuristic Methodologies with Genetic Programming, *Computational Intelligence: Collaboration, Fusion and Emergence*, pp. 177–201, 2009b.

Burke, E. K., Curtois, T., Hyde, M. R., et al., Iterated Local Search vs Hyper-Heuristics: Towards General-Purpose Search Algorithms, *IEEE Congress on Evolutionary Computation*, pp. 1–8, 2010a.

Burke, E. K., Hyde, M., Kendall, G., et al., *Hyper-Heuristics: a Survey of the State of the Art*, Technical Report NOTTCS-TR-SUB-0906241418-2747, University of Nottingham, Nottingham, UK, 2010b.

Carroll, C. W., The Created Response Surface Techniques for Optimizing Nonlinear, Restrained Systems, *Operations Research*, 9(2), pp. 169–185, 1961.

Case, J., Chilver, A. H., and Ross, C. T. F., *Strength of Materials and Structures*, 4th Ed., Arnold Publishing, London, England, 1999.

Çavuş, N., *Multidisciplinary and Multiobjective Design Optimization of an Unmanned Combat Aerial Vehicle (UCAV)*, Master's Thesis, Middle East Technical University, 2009.

Chacksfield, J. E., Multivariate Optimisation Techniques and their Impact on the Aircraft Design Process, *Progress in Aerospace Sciences*, 33, pp. 731–757, 1997.

Chakhlevitch, K., and Cowling, P., Hyperheuristics: Recent Developments, *Adaptive and Multilevel Metaheuristics*, Springer-Verlag, pp. 3–29, 2008.

Chintapalli, S., Elsayed, M. S. A., Sedaghati, R., et al., The Development of a Preliminary Structural Design Optimization Method of an Aircraft Wing-Box Skin-Stringer Panels, *Aerospace Science and Technology*, 14, pp. 188–198, 2010.

Choi, S., Alonso, J. J., Kroo, I. M., et al., Multifidelity Design Optimization of Low-Boom Supersonic Jets, *Journal of Aircraft*, 45(1), pp. 106–118, 2008.

Clerc, M., and Kennedy, J., The Particle Swarm - Explosion, Stability, and Convergence in a Multidimensional Complex Space, *IEEE Transactions on Evolutionary Computation*, 6(1), pp. 58–73, 2002.

Coates, R. C., Coutie, M. G., and Kong, F. K., *Structural Analysis*, 3rd Ed., Van Nostrand Reinhold, Wokingham, England, 1988.

Cobos, C., Mendoza, M., and León, E., A Hyper-Heuristic Approach to Design and Tuning Heuristic Methods for Web Document Clustering, *IEEE Congress on Evolutionary Computation*, New Orleans, LA, USA, 2011.

Coello Coello, C. A., Use of a Self-Adaptive Penalty Approach for Engineering Optimization Problems, *Computers in Industry*, 41(2), pp. 113–127, 2000.

Coello Coello, C. A., Theoretical and Numerical Constraint-Handling Techniques used with Evolutionary Algorithms: a Survey of the State of the Art, *Computer Methods in Applied Mechanics and Engineering*, 191(11-12), pp. 1245–1287, 2002.

Coello Coello, C. A., Evolutionary Multi-Objective Optimization: Some Current Research Trends and Topics that Remain to be Explored, *Frontiers of Computer Science in China*, 3(1), pp. 18–30, 2009.

Cook, R. D., *Finite Element Modeling for Stress Analysis*, John Wiley & Sons, New York, NY, USA, 1995.

Corke, T. C., *Design of Aircraft*, Pearson Education, Upper Saddle River, NJ, USA, 2003.

Courant, R., Variational Methods for the Solution of Problems of Equilibrium and Vibrations, *Bulletin of the American Mathematical Society*, 49, pp. 1–23, 1943.

Cowling, P., and Chakhlevitch, K., Hyperheuristics for Managing a Large Collection of Low Level Heuristics to Schedule Personnel, *IEEE Conference on Evolutionary Computation*, Canberra, Australia, pp. 1214–1221, 2003.

Cowling, P., Kendall, G., and Soubeiga, E., A Hyperheuristic Approach to Scheduling a Sales Summit, *Practice and Theory of Automated Timetabling III*, Springer-Verlag, Vol. 2079 of *Lecture Notes in Computer Science*, pp. 176–190, 2000.

Cowling, P., Kendall, G., and Soubeiga, E., A Parameter-Free Hyperheuristic for Scheduling a Sales Summit, *Proceedings of the 4th Metaheuristic International Conference*, 2001.

Cowling, P., Kendal, G., and Han, L., An Investigation of a Hyperheuristic Genetic Algorithm Applied to a Trainer Scheduling Problem, *Proceedings of the Congress on Evolutionary Computation*, Honolulu, HI, USA, pp. 1185–1190, 2002a.

Cowling, P., Kendall, G., and Soubeiga, E., Hyperheuristics: a Robust Optimisation Method Applied to Nurse Scheduling, *Parallel Problem Solving from Nature VII*, Springer-Verlag, Vol. 2439 of *Lecture Notes in Computer Science*, pp. 851–860, 2002b.

Cowling, P., Kendall, G., and Soubeiga, E., Hyperheuristics: A Tool for Rapid Prototyping in Scheduling and Optimisation, *Applications of Evolutionary Computing: Proceedings of Evo Workshops 2002*, Kinsale, Republic of Ireland, Vol. 2279 of *Lecture Notes in Computer Science*, pp. 269–287, 2002c.

Craig, R. R., and Kurdila, A. J., *Fundamentals of Structural Dynamics*, John Wiley & Sons, New York, NY, USA, 2011.

Cramer, E. J., Denis Jr, J. E., Frank, P. D., et al., Problem Formulation for Multidisciplinary Optimization, *SIAM Journal on Optimization*, 4, pp. 754–776, 1994.

Crawford, C., and Simm, S., Conceptual Design and Optimisation of Modern Combat Aircraft, *NATA RTO Symposium*, Ottawa, Canada, 1999.

Cross, N., *Engineering Design Methods: Strategies for Product Design*, 2nd Ed., John Wiley & Sons, Chichester, England, 1994.

Crossley, W. A., and Williams, E. A., *A Study of Penalty Functions for Constrained Genetic Algorithm-Based Optimization*, Technical Report AIAA Paper 97-0083, AIAA, 1997.

Crowston, W. B., Glover, F., Thompson, G. L., et al., *Probabilistic and Parametric Learning Combinations of Local Job Shop Scheduling Rules*, ONR Research Memorandum 117, Carnegie Mellon University, United States Office of Naval Research, 1963.

Cutler, J., *Understanding Aircraft Structures*, 2nd Ed., Blackwell Scientific Publications, Oxford, England, 1993.

Daskilewicz, M. J., German, B. J., Takahashi, T. T., et al., Effects of Disciplinary Uncertainty on Multi-Objective Optimization in Aircraft Conceptual Design, *Structural and Multidisciplinary Optimization*, 44(6), pp. 831–846, 2011.

Davis, L., (Ed.) *Genetic Algorithms and Simulated Annealing*, Pitman Publishing, London, England, 1987.

Davis, L., Bit-Climbing, Representational Bias, and Test Suite Design, *Proceedings of the 4th International Conference on Genetic Algorithms*, Morgan Kauffman, San Mateo, CA, USA, 1991.

De Jong, K., *An Analysis of the Behaviour of a Class of Genetic Adaptive Systems*, Phd thesis, University of Michigan, Michigan, MI, USA, 1975.

Deb, K., An Efficient Constraint Handling Method for Genetic Algorithms, *Computer Methods in Applied Mechanics and Engineering*, 186, pp. 311–338, 2000.

Deb, K., *Multi-Objective Optimization using Evolutionary Algorithms*, John Wiley & Sons, Chichester, England, 2001.

Denzinger, J., Fuchs, M., and Fuchs, M., High Performance ATP Systems by Combining Several AI Methods, *Proceedings of the 15th International Joint Conference on Artificial Intelligence*, pp. 102–107, 1997.

Dieter, G. E., and Schmidt, L. C., *Engineering Design*, 4th Ed., McGraw-Hill, New York, NY, USA, 2009.

Dixon, L. C. W., and Szego, G. P., The Optimization Problem: An Introduction, *Towards Global Optimization II*, North Holland, NY, USA, 1978.

Domingos, R. P., and Platt, G. M., Hyper-Heuristic Applied to Nuclear Reactor Core Design, *Journal of Physics: Conference Series*, 410, 2013.

Dorndorf, U., and Pesch, E., Evolution Based Learning in a Job Shop Scheduling Environment, *Computers and Operations Research*, 22(1), pp. 25–40, 1995.

Downsland, K. A., Soubeiga, E., and Burke, E., A Simulated Annealing Based Hyperheuristic for Determining Shipper Sizes for Storage and Transportation, *European Journal of Operational Research*, 179, pp. 759–774, 2007.

Drake, J. H., Özcan, E., and Burke, E. K., *Controlling Crossover in a Selection Hyper-Heuristic Framework*, Technical Report NOTTCS-TR-SUB-1104181638-4244, University of Nottingham, Nottingham, UK, 2011.

Drake, J. H., Özcan, E., and Burke, E. K., An Improved Choice Function Heuristic Selection for Cross Domain Heuristic Search, *Parallel Problem Solving from Nature XII*, Springer, Vol. 7492 of *Lecture Notes in Computer Science*, pp. 307–316, 2012.

Duffy, A. H. B., and O'Donnell, F. J., A Design Research Approach, *5th International Conference on Artificial Intelligence in Design: Workshop on Research Methods in AI Design*, Lisbon, Portugal, pp. 20–27, 1998.

Easom, E. E., *A Survey of Global Optimization Techniques*, Meng thesis, University of Louisville, Louisville, KY, USA, 1990.

Eiben, A. E., Michalewicz, Z., Schoenauer, M., et al., Parameter Control in Evolutionary Algorithms, *Parameter Setting in Evolutionary Algorithms*, Springer-Verlag, Berlin, Germany, pp. 19–46, 2007.

Embraer SA, *Embraer 195 Airport Planning Manual*, 2011.

Erickson, L. L., *Panel Methods - An Introduction*, Technical Report 2995, NASA, 1990.

European Aviation Safety Agency, *Certification Specifications for Normal, Utility, Aerobatic, and Commuter Category Aeroplanes, CS-23*, Ammendment 3, EASA, 2012a.

European Aviation Safety Agency, *Certification Specifications for Large Aeroplanes, CS-25*, Ammendment 12, EASA, 2012b.

Eves, J., Toropov, V. V., Thompson, H. M., et al., Topology Optimization of Aircraft with Non-Conventional Configurations, *8th World Congress on Structural and Multidisciplinary Optimization*, Lisbon, Portugal, pp. 1–9, 2009.

Fan, W., Fox, E. A., Pathak, P., et al., The Effects of Fitness Functions on Genetic Programming-Based Ranking Discovery for Web Search, *Journal of the American Society for Information Science and Technology*, 55(7), pp. 628–636, 2004.

Fenner, R. T., *Finite Element Methods for Engineers*, Imperial College Press, London, England, 1996.

Fernandez-Prieto, J. A., Canada-Bago, J., Gadeo-Martos, M. A., et al., Optimisation of Control Parameters for Genetic Algorithms to Test Computer Networks under Realistic Traffic Loads, *Applied Soft Computing*, 12, pp. 1875–1883, 2012.

Fiacco, A. V., and McCormick, G. P., *Nonlinear Programming: Sequential Unconstrained Minimization Techniques*, John Wiley & Sons, New York, NY, USA, 1968.

Fisher, H., and Thompson, G. L., Probabilistic Learning Combinations of Local Job-Shop Scheduling Rules, *Industrial Scheduling*, Prentice Hall, New York, NY, USA, pp. 225–251, 1963.

Fletcher, R., *Practical Methods of Optimization*, John Wiley & Sons, New York, NY, USA, 1987.

Fletcher, R., and Powell, M. J. D., A Rapidly Convergent Descent Method for Minimization, *Computer Journal*, 6(2), pp. 163–168, 1963.

Forrester, A. J., Sóbester, A. S., and Keane, A. J., Multi-Fidelity Optimization via Surrogate Modelling, *Proceedings of the Royal Society A*, 463(2088), pp. 3251–3269, 2007.

Fox, R. L., *Optimization Methods for Engineering Design*, Addison-Wesley, Reading, MA, USA, 1971.

French, M. J., *Conceptual Design for Engineers*, 2nd Ed., Springer-Verlag, Berlin, Germany, 1985.

Fukunaga, A. S., Chien, S., and Mutz, D., Automating the Process of Optimization in Spacecraft Design, *Proceedings of the IEEE Aerospace Conference*, Snowmass, CO, USA, 1997.

Gallagher, R. H., and Zienkiewicz, O. C., (Eds.) *Optimum Structural Design*, John Wiley & Sons, Chichester, England, 1973.

Gantois, K., and Morris, A. J., The Multi-Disciplinary Design of a Large-Scale Civil Aircraft Wing Taking Account of Manufacturing Costs, *Structural and Multidisciplinary Optimization*, 28(1), pp. 31–46, 2004.

Garrido, P., and Castro, C., Stable Solving of CVRPS using Hyperheuristics, *Proceedings of the 11th Annual Conference on Genetic and Evolutionary Computation*, pp. 255–262, 2009.

Garrido, P., and Riff, M. C., An Evolutionary Hyperheuristic to Solve Strip-Packing Problems, *Proceedings of the 8th International Confernece on Intelligent Data Engineering and Automated Learning*, Springer, Vol. 4881 of *Lecture Notes in Computer Science*, pp. 406–415, 2007.

Garrido, P., and Riff, M. C., DVRP: A Hard Dynamic Combinatorial Optimisation Problem Tackled by an Evolutionary Hyper-Heuristic, *Journal of Heuristics*, 16(6), pp. 795–834, 2010.

Gasbarri, P., Chiwiacowsky, L. D., and de Campos Velho, H. F., A Hybrid Multilevel Approach for Aeroelastic Optimization of Composite Wing-Box, *Structural and Multidisciplinary Optimization*, 39(6), pp. 607–624, 2009.

Gen, M., and Cheng, R., *Genetic Algorithms and Engineering Design*, John Wiley & Sons, New York, NY, USA, 1997.

Ginsberg, J. H., *Engineering Dynamics*, Vol. 10, Cambridge University Press, Cambridge, England, 2008.

Giunta, A., *Aircraft Multidisciplinary Design Optimization using Design of Experiments Theory and Response Surface Modeling Methods*, Ph.D. Thesis, Virginia Polytechnic Institute and State University, Blacksburg, VI. USA, 1997.

Glauert, H., *The Elements of Aerofoil and Airscrew Theory*, 2nd Ed., Cambridge University Press, Cambridge, England, 1948.

Glover, F., and Laguna, M., *Tabu Search*, Kluwer Academic Publishers, Dordrecht, The Netherlands, 1997.

Goldberg, D. E., *Genetic Algorithms in Search, Optimization, and Machine Learning*, Addison-Wesley, 1989a.

Goldberg, D. E., Genetic Algorithms and Walsh Functions: Part I, A Gentle Introduction, *Complex Systems*, 3, pp. 129–152, 1989b.

Goldberg, D. E., Genetic Algorithms and Walsh Functions: Part II, Deception and its Analysis, *Complex Systems*, 3, pp. 153–171, 1989c.

Goldberg, D. E., *The Design of Innovation: Lessons from and for Competent Genetic Algorithms*, Kluwer Academic Publishers, 2002.

Golub, G. H., and van Loan, C. F., *Matrix Computations*, 3rd Ed., The John Hopkins University Press, Baltimore, MD, USA, 1996.

González, L. F., Whitney, E. J., Srinivas, K., et al., Multidisciplinary Aircraft Design and Optimisation using a Robust Evolutionary Technique with Variable Fidelity Models, pp. 1–42, 2004.

Grefenstette, J. J., Optimization of Control Parameters for Genetic Algorithms, *IEEE Transactions on Systems, Man and Cybernetics*, 16(1), pp. 122–128, 1986.

Griewank, A. O., Generalized Descent for Global Optimization, *Journal of Optimization Theory and Applications*, 34(1), pp. 11–39, 1981.

Grobler, J., Engelbrecht, A. P., Kendall, G., et al., Alternative Hyper-Heuristic Strategies for Multi-Method Global Optimization, *Proceedings of the 2010 IEEE Congress on Evolutionary Computation*, 2010.

Gropp, W., Lusk, E., and Skjellum, A., *Using MPI - Portable Parallel Programming with the Message-Passing Interface*, 2nd Ed., The MIT Press, Cambridge, MA, USA, 1999.

Guo, S., Aeroelastic Optimization of an Aerobatic Aircraft Wing Structure, *Aerospace Science and Technology*, 11, pp. 396–404, 2007.

Guo, S., Cheng, W., and Cui, D., Aeroelastic Tailoring of Composite Wing Structures by Laminate Layup Optimization, *AIAA Journal*, 44(12), pp. 3146–3149, 2006.

Guo, S. J., Banerjee, J. R., and Cheung, C. W., The Effect of Laminate Lay-Up on the Flutter Speed of Composite Wings, *Proceedings of the Institution of Mechanical Engineers, Part G: Journal of Aerospace Engineering*, 217, pp. 115–122, 2003.

Han, L., and Kendall, G., An Investigation of a Tabu Assisted Hyper-Heuristic Genetic Algorithm, *The 2003 Congress on Evolutionary Computation*, Vol. 3, pp. 2230–2237, 2003.

Han, L., Kendall, G., and Cowling, P., An Adaptive Length Chromosome Hyperheuristic Genetic Algorithm for a Trainer Scheduling Problem, *Proceedings of the 4th Asia-Pacific Conference on Simulated Evolution and Learning*, Orchid Country Club, Singapore, pp. 267–271, 2002.

Han, Z. H., Görtz, S., and Zimmermann, R., Improving Variable-Fidelity Surrogate Modeling via Gradient-Enhanced Kriging and a Generalized Hybrid Bridge Function, *Aerospace Science and Technology*, 25(1), pp. 177–189, 2013.

Hansen, L. U., and Horst, P., Multilevel Optimization in Aircraft Structural Design Evaluation, *Computers and Structures*, 86, pp. 104–118, 2008.

Hart, E., and Ross, P. M., A Heuristic Combination Method for Solving Job-Shop Scheduling Problems, *Parallel Problem Solving from Nature V*, Springer-Verlag, Vol. 1498 of *Lecture Notes in Computer Science*, pp. 845–854, 1998.

Hart, E., Ross, P. M., and Nelson, J. A. D., Solving a Real-World Problem using an Evolving Heuristically Driven Schedule Builder, *Evolutionary Computing*, 6(1), pp. 61–80, 1998.

Hart, W. E., *Adaptive Global Optimization with Local Search*, Ph.D. Thesis, University of California, San Diego, CA, USA, 1994.

Hassan, R., Cohanim, B., De Weck, O., et al., A Comparison of Particle Swarm Optimization and the Genetic Algorithm, *46th AIAA/ASME/ASCE/AHS/ASC Structures, Structural Dynamics and Materials Conference*, Austin, TX, USA, 2005.

Herrera, F., Lozano, M., and Sánchez, A. M., A Taxonomy for the Crossover Operator for Real-Coded Genetic Algorithms: an Experimental Study, *International Journal of Intelligent Systems*, 18, pp. 309–338, 2003.

Hinterding, R., Michalewicz, Z., and Peachey, T. C., Self-Adaptive Genetic Algorithm for Numeric Functions, *Parallel Problem Solving from Nature IV*, Springer-Verlag, Vol. 1141 of *Lecture Notes in Computer Science*, pp. 420–429, 1996.

Hoblit, F. M., *Gust Loads on Aircraft: Concepts and Applications*, AIAA Education Series, Washington, DC, USA, 1988.

Holland, J. H., *Adaptation in Natural and Artificial Systems*, University of Michigan Press, Ann Arbor, MI, USA, 1975.

Homaifar, A., Qi, C. X., and Lai, S. H., Constrained Optimization Via Genetic Algorithms, *Simulation*, 62(4), pp. 242–254, 1994.

Howe, D., *Aircraft Loading and Structural Layout*, Professional Engineering Publishing, Bury St. Edmunds, England, 2004.

Hu, T., and Yu, X., Aerodynamic/Stealthy/Structural Multidisciplinary Design Optimization of Unmanned Combat Air Vehicle, *Chinese Journal of Aeronautics*, 22, pp. 380–386, 2009.

Hyde, M., *A Genetic Programming Hyper-Heuristic Approach to Automated Packing*, Ph.D. Thesis, University of Nottingham, 2010.

Jackson, P., (Ed.) *Jane's All the World's Aircraft 2009-2010*, Jane's Information Group, Coulsdon, England, 2009.

Jameson, A., and Ou, K., 50 Years of Transonic Aircraft Design, *Progress in Aerospace Sciences*, 47(5), pp. 308–318, 2011.

Jenkinson, L. R., Simpkin, P., and Rhodes, D., *Civil Jet Aircraft Design*, Arnold Publishing, London, England, 1999.

Joines, J. A., and Houck, C. R., On the Use of Non-Stationary Penalty Functions to Solve Nonlinear Constrained Optimization Problems with GA's, *Proceedings of the 1st IEEE Conference on Evolutionary Computation*, IEEE Press, Orlando, FL, USA, pp. 579–584, 1994.

Julstrom, B. A., Comparing Darwinian, Baldwinian, and Lamarckian Search in Genetic Algorithm for the 4-Cycle Problem, *Late Breaking Papers at the 1999 Genetic and Evolutionary Computation Conference*, 1999.

Kaelbling, L. P., Littman, M. L., and Moore, A. W., Reinforcement Learning: a Survey, *Journal of Artificial Intelligence Research*, 4, pp. 237–285, 1996.

Karamcheti, K., *Principles of Ideal Fluid Aerodynamics*, John Wiley & Sons, New York, NY, USA, 1966.

Kaufmann, M., Zenkert, D., and Wennhage, P., Integrated Cost/Weight Optimization of Aircraft Structures, *Structural and Multidisciplinary Optimization*, 41(2), pp. 325–334, 2010.

Kendall, G., Soubeiga, E., and Cowling, P., Choice Function and Random Hyperheuristics, *Proceedings of the 4th Asia-Pacific Conference on Simulated Evolution and Learning*, pp. 667–671, 2002.

Kesseler, E., and Vankan, W. J., Multidisciplinary Design Analysis and Multi-Objective Optimisation Applied to Aircraft Wing, *WSEAS Transactions on Systems and Control*, 1(2), pp. 221–227, 2006.

Kheng, C. W., Lim, M. H., and Chong, S. Y., A Study on Lamarckian and Baldwinian Learning on Noisy and Noiseless Landscapes, *Proceedings of the 24th European Conference on Modelling and Simulation: Simulation Meets Global Challenges*, Kuala Lumpar, Malaysia, 2010.

Kim, T., Lim, J., Shin, S., et al., Structural Design Optimization of a Tiltrotor Aircraft Composite Wing to Enhance Whirl Flutter Stability, *Composite Structures*, 95, pp. 283–294, 2013.

Kirkpatrick, S., Gelatt Jr, C. D., and Vecchi, M. P., Optimization by Simulated Annealing, *Science*, 220(4598), pp. 671–680, 1983.

Koch, P. N., Simpson, T. W., Allen, J. K., et al., Statistical Approximations for Multidisciplinary Design Optimization: The Problem of Size, *Journal of Aircraft*, 36(1), pp. 275–286, 1999.

Kramer, O., A Review of Constraint-Handling Techniques for Evolution Strategies, *Applied Computational Intelligence and Soft Computing*, pp. 1–11, 2010.

Krasnogor, N., *Studies on the Theory and Design Space of Memetic Algorithms*, Ph.D. Thesis, University of the West of England, Bristol, England, 2002.

Krasnogor, N., and Smith, J., A Memetic Algorithm With Self-Adaptive Local Search - TSP as a Case Study, *Proceedings of the Genetic and Evolutionary Computation Conference*, 2000.

Krasnogor, N., and Smith, J., A Tutorial for Competent Memetic Algorithms: Model, Taxonomy, and Design Issues, *IEEE Transactions on Evolutionary Computation*, 9(5), pp. 474–488, 2005.

Laban, M., Personal Communication, 2011.

Lamarck, J. B. P. A., *Philosophie Zoologique: ou Exposition des Considérations Relatives à l'Histoire Naturelle des Animaux*, Technical report, Oxford, England, 1809.

Ledermann, C., Personal Communication, 2010.

Ledermann, C., Hanske, C., Wenzel, J., et al., Associative Parametric CAE Methods in the Aircraft Pre-Design, *Aerospace Science and Technology*, 9, pp. 641–651, 2005.

Ledermann, C., Ermanni, P., and Kelm, R., Dynamic CAD Objects for Structural Optimization in Preliminary Aircraft Design, *Aerospace Science and Technology*, 10, pp. 601–610, 2006.

Lewis, W. P., and Samuel, A. E., *Fundamentals of Engineering Design*, Prentice Hall, Sydney, Australia, 1989.

Li, W., and Hu, Y., A New Effective Multidisciplinary Design Optimization Algorithm, *23rd Congress of the International Council of the Aeronautical Sciences*, Toronto, Canada, 2002.

Liu, D., Toropov, V. V., Querin, O. M., et al., Bilevel Optimization of Blended Composite Wing Panels, *Journal of Aircraft*, 48(1), pp. 107–118, 2011.

Lovell, D. A., Crawford, C. A., and Restrick, K. W., Recent Advances in Air-Vehicle Design Synthesis and Optimisation, *24th International Congress of the Aeronautical Sciences*, 2004.

Ma, T. L., and Ma, D. L., Multidisciplinary Design-Optimization Methods for Aircrafts using Large-Scale System Theory, *Systems Engineering - Theory and Practise*, 29(9), pp. 186–192, 2009.

MacMillin, P. E., Golovidov, O., Mason, W. H., et al., *An MDO Investigation of the Impact of Practical Constraints on an HSCT Configuration*, Technical Report 1997-0098, AIAA, 1997.

Majumder, L., and Rao, S. S., Interval-Based Optimization of Aircraft Wings under Landing Loads, *Computers and Structures*, 87(3-4), pp. 225–235, 2009.

Maltbaek, J. C., Moments of Area of Aerofoil Sections, *Aircraft Engineering and Aerospace Technology*, 33(12), pp. 351–353, 1961.

Marduel, X., Tribes, C., and Trépanier, J. Y., Variable-Fidelity Optimization: Efficiency and Robustness, *Optimization and Engineering*, 7(4), pp. 479–500, 2006.

Marín-Blázquez, J. G., and Schulenburg, S., A Hyper-Heuristic Framework with XCS: Learning to Create Novel Problem-Solving Algorithms Constructed from Simpler Algorithmic Ingredients, *Learning Classifier Systems*, Springer, Vol. 4399 of *Lecture Notes in Computer Science*, pp. 193–218, 2007.

Markine, V. L., and Toropov, V. V., Use of High- and Low-Fidelity Models In Approximations for Design Optimization, *9th AIAA/ISSMO Symposium on Multidisciplinary Analysis and Optimization*, Atlanta, GA, USA, AIAA 2002-5651, 2002.

Martins, J. R. R. A., Alonso, J. J., and Reuther, J. J., High-Fidelity Aero-Structural Design Optimization of a Supersonic Business Jet, *Proceedings of the 43rd AIAA/ASME/ASCE/AHS/ASC Structures, Structural Dynamics, and Materials Conference*, Denver, CO, USA, AIAA 2002-1483, 2002.

Maturana, J., Lardeux, F., and Saubion, F., Autonomous Operator Management for Evolutionary Algorithms, *Journal of Heuristics*, 16, pp. 881–909, 2010.

Maute, K., and Allen, M., Conceptual Design of Aeroelastic Structures by Topology Optimization, *Structural and Multidisciplinary Optimization*, 27, pp. 27–42, 2004.

Mavris, D. N., and Bandte, O., A Probabilistic Approach to Multivariate Constrained Robust Design Simulation, *SAE World Aviation Congress and Exposition*, Anaheim, CA, USA, AIAA Paper 1997-5508, 1997.

Mavris, D. N., and DeLaurentis, D. A., A Probabilistic Approach for Examining Aircraft Concept Feasibility and Viability, *Aircraft Design*, 3(2), pp. 79–101, 2000.

McGuire, W., Gallagher, R. H., and Ziemian, R. D., *Matrix Structural Analysis*, 2nd Ed., John Wiley & Sons, New York, NY, USA, 1999.

Megson, T. H. G., *Aircraft Structures for Engineering Students*, 3rd Ed., Arnold Publishing, London, England, 1999.

Meier, N., *Jet Engine Specification Database*, 2005, URL http://www.jet-engine.net, Accessed: November 2010.

Meyer-Nieberg, S., and Beyer, H. G., Self-Adaptation in Evolutionary Algorithms, *Parameter Setting in Evolutionary Algorithms*, Springer-Verlag, Berlin, Germany, pp. 47–76, 2007.

Michalewicz, Z., *Genetic Algorithms + Data Structures = Evolution Programs*, 2nd Ed., Springer-Verlag, Berlin, Germany, 1996.

Michalewicz, Z., and Schoenauer, M., Evolutionary Algorithms for Constrained Parameter Optimization Problems, *Evolutionary Computation*, 4(1), pp. 1–32, 1996.

Miles, R., and Hamilton, K., *Learning UML 2.0*, O'Reilly Media, Sebastopol, CA, USA, 2006.

Minisci, E., Vasile, M., and Liqiang, H., Robust Multi-Fidelity Design of a Micro Re-Entry Unmanned Space Vehicle, *Proceedings of the Institution of Mechanical Engineers, Part G: Journal of Aerospace Engineering*, 225, pp. 1195–1209, 2011.

Ministry of Defence, *Design and Airworthiness Requirements for Service Aircraft, Part 1 - Fixed Wing, Def.Stan.00-970*, Issue 6, MoD, 2010.

Molga, M., and Smutnicki, C., *Test Functions for Optimization Needs*, Technical report, 2005.

Montgomery, D. C., *Design and Analysis of Experiments*, 4th Ed., John Wiley & Sons, New York, NY, USA, 1997.

Moscato, P., and Cotta, C., A Gentle Introduction to Memetic Algorithms, *Handbook of Metaheuristics*, Kluwer Academic Publishers, Vol. 57, pp. 105–144, 2003.

Nadir, W. D., *Multidisciplinary Structural Design and Optimization for Performance, Cost, and Flexibility*, Master's Thesis, Massachusetts Institute of Technology, Boston, MA, USA, 2005.

Nanakorn, P., and Messomklin, K., An Adaptive Penalty Function in Genetic Algorithms for Structural Design Optimization, *Computers and Structures*, 79(29-30), pp. 2527–2539, 2001.

Neufeld, D., Chung, J., and Behdinan, K., An Approach to Multi-Objective Aircraft Design, *Future Application and Middleware Technology on e-Science*, Springer Science+Business Media, New York, NY, USA, pp. 103–112, 2010.

Nguyen, N. V., Choi, S. M., Kim, W. S., et al., Multidisciplinary Unmanned Combat Air Vehicle System Design using Multi-Fidelity Model, *Aerospace Science and Technology*, 26(1), pp. 200–210, 2013.

Nguyen, Q. H., Ong, Y. S., and Lim, M. H., A Probabilistic Memetic Framework, *IEEE Transactions on Evolutionary Computation*, 13(3), pp. 604–623, 2009.

Niu, M. Y. C., *Airframe Structural Design*, Conmilit Press, Hong Kong, 1988.

Niu, M. Y. C., *Airframe Stress Analysis and Sizing*, 2nd Ed., Conmilit Press, Hong Kong, 1999.

Nocedal, J., and Wright, S., *Numerical Optimization*, Springer, New York, NY, USA, 1999.

Noman, N., and Iba, H., Accelerating Differential Evolution using an Adaptive Local Search, *IEEE Transactions on Evolutionary Computation*, 12(1), pp. 107–125, 2008.

Nourani, Y., and Andresen, B., A Comparison of Simulated Annealing Cooling Strategies, *Journal of Physics A: Mathematical and General*, 31(41), pp. 8373–8385, 1998.

Ochoa, G., Vázquez-Rodríguez, J. A., Petrovic, S., et al., Dispatching Rules for Production Scheduling: a Hyper-Heuristic Landscape Analysis, *Proceedings of the IEEE Congress on Evolutionary Computation*, pp. 1873–1880, 2009.

Oktay, E., Akay, H. U., and Merttopcuoglu, O., Parallelized Structural Topology Optimization and CFD Coupling for Design of Aircraft Wing Structures, *Computers and Fluids*, 49(1), pp. 141–145, 2011.

Ölvander, J., Lundén, B., and Gavel, H., A Computerized Optimization Framework for the Morphological Matrix Applied to Aircraft Conceptual Design, *Computer-Aided Design*, 41(3), pp. 187–196, 2009.

Ong, Y. S., Lim, M. H., Zhu, N., et al., Classification of Adaptive Memetic Algorithms: a Comparative Study, *IEEE Transactions on Systems, Science and Cybernetics*, 36(1), pp. 141–152, 2006.

Ortiz-Bayliss, J. C., Terashima-Marín, H., Özcan, E., et al., Variable and Value Ordering Decision Matrix Hyper-Heuristics: A Local Improvement Approach, *Advances in Artificial Intelligence*, Springer, Vol. 7094 of *Lecture Notes in Computer Science*, pp. 125–136, 2011.

Özcan, E., and Başaran, C., A Case Study of Memetic Algorithms for Constraint Optimization, *Soft Computing*, 13(8-9), pp. 871–882, 2009.

Özcan, E., and Kheiri, A., A Hyper-Heuristic based on Random Gradient, Greedy and Dominance, *Computer and Information Sciences II*, Springer-Verlag, London, England, pp. 557–563, 2012.

Özcan, E., Bilgin, B., and Korkmaz, E. E., Hill Climbers and Mutational Heuristics in Hyperheuristics, *Proceedings of the 9th International Conference on Parallel Problem Solving from Nature*, Reykjavik, Iceland, pp. 202–211, 2006.

Özcan, E., Bilgin, B., and Korkmaz, E. E., A Comprehensive Analysis of Hyper-heuristics, *Intelligent Data Analysis*, 12(1), pp. 3–23, 2008.

Özcan, E., Misir, M., Ochoa, G., et al., A Reinforcement Learning - Great-Deluge Hyper-Heuristic for Examination Timetabling, *Applied Metaheuristic Computing*, 1(1), pp. 39–59, 2010.

Pahl, G., Beitz, W., Feldhusen, J., et al., *Engineering Design: A Systematic Approach*, 3rd Ed., Springer-Verlag, London, England, 2007.

Pant, R., and Fielding, J., Aircraft Configuration and Flight Profile Optimization using Simulated Annealing, *Aircraft Design*, 2(4), pp. 239–255, 1999.

Park, C., Joh, C. Y., and Kim, Y. S., Multidisciplinary Design Optimization of a Structurally Nonlinear Aircraft Wing via Parametric Modeling, *International Journal of Precision Engineering and Manufacturing*, 10(2), pp. 87–96, 2009.

Pedersen, M. E. H., *Good Parameters for Differential Evolution*, Tech. Report HL1002, Hvass Laboratories, 2010.

Petersson, O., Stroscher, F., and Baier, H., Multidisciplinary Optimisation of Aircraft Wings Including Gust Loads, *Royal Aeronautical Society 2nd Aircraft Structural Design Conference*, London, England, 2010.

Pillay, N., Evolving Hyper-Heuristics for the Uncapacitated Examination Timetabling Problem, *Proceedings of the 4th Multidisciplinary International Conference on Scheduling: Theory and Applications*, Dublin, Republic of Ireland, pp. 447–457, 2009.

Pillay, N., and Banzhaf, W., A Genetic Programming Approach to the Generation of Hyper-Heuristics for the Uncapacitated Examination Timetabling Problem, *Progress in Artificial Intelligence - Proceedings of the 13th Portuguese Conference on Aritficial Intelligence,*, Springer, Vol. 4874 of *Lecture Notes in Computer Science*, pp. 223–234, 2007.

Polak, E., *Optimization - Algorithms and Consistent Approximations*, Springer, New York, NY, USA, 1997.

Ponterosso, P., and Fox, D. S. J., Heuristically Seeded Genetic Algorithms Applied to Truss Optimisation, *Engineering with Computers*, 15, pp. 345–355, 1999.

Prandtl, L., and Tietjens, O. G., *Applied Hydro- and Aeromechanics*, United Engineering Trustees, 1934.

Pready, N., Evolving Aerospace - Taking Inspiration from NASA to the Mass Market, *Aerospace*, 40(12), pp. 14–17, 2013.

Press, W. H., Teukolsky, S. A., Vetterling, W. T., et al., *Numerical Recipes in C++*, 2nd Ed., Cambridge University Press, Cambridge, England, 2002.

Qiu, Z., and Zhang, Y., Parametric Optimization Design of Aircraft Based on Hybrid Parallel Multiobjective Tabu Search Algorithm, *Chinese Journal of Aeronautics*, 23(4), pp. 430–437, 2010.

Qu, R., and Burke, E. K., Hybridisations within a Graph Based Hyper-Heuristic Framework for University Timetabling Problems, *Journal of the Operational Research Society*, 60, pp. 1273–1285, 2009.

Rafique, A. F., He, L., Kamran, A., et al., Hyper Heuristic Approach for Design and Optimization of Satellite Launch Vehicle, *Chinese Journal of Aeronautics*, 24(2), pp. 150–163, 2011.

Rao, S. S., Optimization of Airplane Wing Structures Under Landing Loads, *Computers and Structures*, 19(5-6), pp. 849–863, 1984.

Rao, S. S., Optimization of Airplane Wing Structures Under Gust Loads, *Computers and Structures*, 21(4), pp. 741–749, 1985.

Rao, S. S., Automated Optimum Design of Wing Structures: A Probabilistic Approach, *Computers and Structures*, 24(5), pp. 799–808, 1986.

Rao, S. S., Optimization of Airplane Wing Structures Under Taxiing Loads, *Computers and Structures*, 26(3), pp. 469–479, 1987.

Rao, S. S., *The Finite Element Method in Engineering*, 2nd Ed., Pergamon Press, Oxford, England, 1989.

Rao, S. S., *Engineering Optimization: Theory and Practice*, John Wiley & Sons, 1996.

Rao, S. S., *Mechanical Vibrations*, 4th Ed., Pearson Education, Upper Saddle River, NJ, USA, 2004.

Rao, V. R., Iyengar, N. G. R., and Rao, S. S., Optimization of Wing Structures to Satisfy Strength and Frequency Requirements, *Computers and Structures*, 10, pp. 669–674, 1979.

Rasheed, K. M., *GADO: A Genetic Algorithm for Continuous Design Optimization*, Phd thesis, The State University of New Jersey, New Jersey, NJ, USA, 1998.

Rastrigin, L. A., Extremal Control Systems, *Theoretical Foundations of Engineering Cybernetics Series*, Moscow, USSR, 1974.

Raymer, D. P., *Enhancing Aircraft Conceptual Design Using Multidisciplinary Optimization*, Phd thesis, Kungliga Tekniska Högskolan, Stockholm, Sweden, 2002.

Raymer, D. P., *Aircraft Design: A Conceptual Approach*, 4th Ed., AIAA Education Series, Reston, VI, USA, 2006.

Raymer, D. P., Personal Communication, 2010.

Reuther, J. J., Alonso, J. J., Martins, J. R. R. A., et al., A Coupled Aero-Structural Optimization Method For Complete Aircraft Configurations, AIAA Paper 1999-0187, 1999.

Ricci, S., Castellani, M., and Romanelli, G., Multi-Fidelity Design of Aeroelastic Wing Tip Devices, *Proceedings of the Institution of Mechanical Engineers, Part G: Journal of Aerospace Engineering*, 2012.

Richardson, J. T., Palmer, M. R., Liepins, G. E., et al., Some Guidelines for Genetic Algorithms with Penalty Functions, *Proceedings of the Third International Conference on Genetic Algorithms*, Morgan Kaufmann, Reading, MA, USA, pp. 191–197, 1989.

Rinku, A., Prashanth, R., and Kumar, R. O. N., *Structural Optimization of Typical Light Transport Aircraft Components*, Technical Report HTC08, 2008.

Rohn, J., A Step Size Rule for Unconstrained Optimization, *Computing*, 49, pp. 373–376, 1993.

Rosenbrock, H. H., An Automated Method for Finding the Greatest or Least Value of a Function, *Computer Journal*, 3, pp. 175–184, 1960.

Roskam, J., Rapid Sizing Method for Airplanes, *Journal of Aircraft*, 23(7), pp. 554–560, 1986.

Roskam, J., *Airplane Design*, Vol. 1-8, Design, Analysis and Research Corporation, Ottawa, KS, USA, 2000.

Ross, P., Hyper-Heuristics, *Introductory Tutorials in Optimisation, Decision Support and Search Methodology*, Kluwer Academic Publishers, pp. 529–556, 2004.

Ross, P., and Marín-Blázquez, J. G., Constructive Hyper-Heuristics in Class Timetabling, *Proceedings of the IEEE Congress on Evolutionary Computation*, Vol. 2, pp. 1493–1500, 2005.

Ross, P., Schulenburg, S., Marín-Blázquez, J. G., et al., Hyper-Heuristics: Learning to Combine Simple heuristics in Bin-Packing Problems, *Genetic and Evolutionary Computation Conference (GECCO 2002)*, New York, NY, USA, pp. 942–948, 2002.

Ross, P., Marín-Blázquez, J. G., Schulenburg, S., et al., Learning a Procedure that Can Solve Hard Bin-Packing Problems: a New GA-Based Approach to Hyper-heuristics, *Genetic and Evolutionary Computation - GECCO 2003*, Springer, Vol. 2724 of *Lecture Notes in Computer Science*, pp. 1295–1306, 2003.

Ross, P., Marín-Blázquez, J. G., and Hart, E., Hyper-Heuristics Applied to Class and Exam Timetabling Problems, *Proceedings of the IEEE Congress on Evolutionary Computation*, Portland, OR, USA, Vol. 2, pp. 1691–1698, 2004.

Rothwell, A., Multi-Level Optimization of Aircraft Shell Structures, *Thin-Walled Structures*, 11, pp. 85–103, 1991.

Ruijgrok, G. J. J., *Elements of Airplane Performance*, VSSD, Delft, The Netherlands, 2009.

Sadjadi, F. A., Optical Information Systems II, *Proceedings of SPIE*, Vol. 5557, pp. 356–364, 2004.

Sahab, M. G., Ashour, A. F., and Toropov, V. V., A Hybrid Genetic Algorithm for Reinforced Concrete Flat Slab Buildings, *Computers and Structures*, 83, pp. 551–559, 2005.

Schrenk, O., *A Simple Approximation Method for Obtaining the Spanwise Lift Distribution*, Technical Report TM-948, National Advisory Commitee for Aeronautics, 1940.

Schuhmacher, G., Murra, I., Wang, L., et al., Multidisciplinary Design Optimization of a Regional Aircraft Wing Box, *9th AIAA/ISSMO Symposium on Multidisciplinary Analysis and Optimization*, Atlanta, GA, USA, AIAA Paper 2002-5406, 2002.

Schulenburg, S., Ross, P., Marín-Blázquez, J. G., et al., A Hyper-Heuristic Approach to Single and Multiple Step Environments in Bin-Packing Problems, *Proceedings of the 5th International Workshop on Learning Classifier Systems*, 2002.

Schwefel, H. P., *Numerical Optimization of Computer Models*, John Wiley & Sons, 1981.

Sensmeier, M. D., and Samareh, J. A., A Study of Vehicle Structural Layouts in Post-WWII Aircraft, *45th AIAA/ASME/ASCE/AHS/ASC Structures, Structural Dynamics and Materials Conference*, Palm Springs, CA, USA, AIAA Paper 2004-1624, 2004.

Sforza, P. M., *Commerical Airplane Design Handbook*, Gainesville, FL, USA, 2008.

Shan, S., and Wang, G. G., Survey of Modeling and Optimization Strategies to Solve High-Dimensional Design Problems with Computationally-Expensive Black-Box Functions, *Structural and Multidisciplinary Optimization*, 41, pp. 219–241, 2010.

Smith, I. M., and Griffiths, D. V., *Programming the Finite Element Method*, 4th Ed., John Wiley & Sons, Chichester, England, 2004.

Smith, J. E., and Fogarty, T. C., Operator and Parameter Adaptation in Genetic Algorithms, *Soft Computing*, 1(2), pp. 81–87, 1997.

Sobieszczanski-Sobieski, J., and Haftka, R. T., Multidisciplinary Aerospace Design Optimization: Survey of Recent Developments, *Structural Optimization*, 14, pp. 1–23, 1997.

Sofla, A. Y. N., Meguid, S. A., Tan, K. T., et al., Shape Morphing of Aircraft Wing: Status and Challenges, *Materials and Design*, 31(3), pp. 1284–1292, 2010.

Song, W., Multiobjective Memetic Algorithm and its Application in Robust Airfoil Shape Optimization, *Multi-Objective Memetic Algorithms*, Springer, Vol. 171 of *Studies in Computational Intelligence*, pp. 389–402, 2009.

Srinivas, M., and Patnaik, L. M., Adaptive Probabilities of Crossover and Mutation in Genetic Algorithms, *IEEE Transactions on Systems, Man and Cybernetics*, 24(4), pp. 656–667, 1994.

Stinton, D., *The Design of the Aeroplane*, Collins Professional and Technical Books, London, England, 1983.

Storer, R. H., Wu, S. D., and Vaccari, R., Problem and Heuristic Space Search Strategies for Job Shop Scheduling, *ORSA Journal of Computing*, 7(4), pp. 453–467, 1995.

Storn, R., and Price, K., Differential Evolution - a Simple and Efficient Heuristic for Global Optimization over Continuous Spaces, *Journal of Global Optimization*, 11, pp. 341–359, 1997.

Strand7, Release 2.3.8, Software, Strand7 Pty Ltd, 2005.

Süli, E., and Mayer, D. F., *An Introduction to Numerical Analysis*, Cambridge University Press, Cambridge, England, 2003.

Sutton, R. S., and Barto, A. G., *Reinforcement Learning: An Introduction*, The MIT Press, Cambridge, MA, USA, 1998.

Terashima-Marín, H., Ortiz-Bayliss, J. C., Ross, P., et al., Hyper-Heuristics for the Dynamic Variable Ordering in Constraint Satisfaction Problems, *Proceedings of the 10th Annual Conference on Genetic and Evolutionary Computation*, Atlanta, GA, USA, pp. 571–578, 2008.

Terashima-Marín, H., Ross, P., Farias-Zarate, C. J., et al., Generalized Hyper-Heuristics for Solving 2D Regular and Irregular Bin Packing Problems, *Annals of Operations Research*, 179(1), pp. 369–392, 2010.

Thom, T., *The Air Pilot's Manual: The Aeroplane - Technical*, 2nd Ed., Airlife Publishing, Shrewsbury, England, 1988.

Timoshenko, S. P., Young, D., and Weaver, W., *Vibration Problems in Engineering*, 4th Ed., John Wiley & Sons, Chichester, England, 1974.

Tong, L., and Lin, J., Structural Topology Optimization with Implicit Design Variable - Optimality and Algorithm, *Finite Elements in Analysis and Design*, 47(8), pp. 922–932, 2011.

Torenbeek, E., *Synthesis of Subsonic Airplane Design*, Delft University Press, Delft, The Netherlands, 1982.

Toropov, V. V., Simulation Approach to Structural Optimization, *Structural Optimization*, 1, pp. 37–46, 1989.

Toropov, V. V., Modelling and Approximation Strategies in Optimization-Global and Mid-Range Metamodels, Response Surface Methods, Genetic Programming, and Low/High Fidelity Models, *Emerging Methods for Multidisciplinary Optimization*, Springer, Berlin, Germany, pp. 202–256, 2001.

Toropov, V. V., Schramm, U., Sahai, A., et al., Design Optimization and Stochastic Analysis based on the Moving Least Squares Method, *6th World Congress of Structural and Multidisciplinary Optimization*, Rio de Janeiro, Brazil, 2005.

Trela, I. C., The Particle Swarm Optimization Algorithm: Convergence Analysis and Parameter Selection, *Information Processing Letters*, 85(6), pp. 317–325, 2003.

van den Bergh, F., and Engelbrecht, A. P., A Study of Particle Swarm Optimization Particle Trajectories, *Information Sciences*, 176(8), pp. 937–971, 2006.

van Laarhoven, P. J. M., and Aarts, E. H. L., *Simulated Annealing: Theory and Applications*, Kluwer Academic Publishers, Dordrecht, The Netherlands, 1987.

Vázquez-Rodríguez, J. A., and Petrovic, S., A New Dispatching Rule based Genetic Algorithm for the Multi-Objective Job Shop Problem, *Journal of Heuristics*, 16(6), pp. 771–793, 2010.

Vázquez-Rodríguez, J. A., Petrovic, S., and Salhi, A., A Combined Meta-Heuristic with Hyper-Heuristic Approach to the Scheduling of the Hybrid Flow Shop with Sequence Dependent Setup Times and Uniform Machines, *Proceedings of the 3rd Multidisciplinary International Scheduling Conference: Theory and Applications*, 2007.

Venter, G., and Sobieszczanski-Sobieski, J., Multidisciplinary optimization of a transport aircraft wing using particle swarm optimization, *Structural and Multidisciplinary Optimization*, 26, pp. 121–131, 2004.

Viana, F. A. C., and Steffen Jr, V., Optimization of Aircraft Structural Components by using Nature-Inspired Algorithms and Multi-Fidelity Approximations, *Journal of Global Optimization*, 45(3), pp. 427–449, 2009.

VisualFEA, Version 5.06, Software, Intuition Software, 2011.

Weissinger, J., *The Lift Distribution of Swept-Back Wings*, Technical Report 1120, National Advisory Commitee for Aeronautics, 1947.

Whitley, D., Fundamental Principles of Deception in Genetic Search, *Foundations of Genetic Algorithms*, Morgan Kaufmann, San Mateo, CA, USA, 1991.

Whitley, D., Scott Gordon, V., and Mathias, K., Lamarckian Evolution, The Baldwin Effect and Function Optimization, *Parallel Problem Solving in Nature - PPSN III*, Springer, Vol. 866 of *Lecture Notes in Computer Science*, pp. 5–15, 1994.

Wilson, S. W., Classifier Systems Based on Accuracy, *Evolutionary Computation*, 3(2), pp. 149–175, 1995.

Wolpert, D. H., and Macready, W. G., No Free Lunch Theorems for Optimization, *IEEE Transactions on Evolutionary Computation*, 1(1), pp. 67–82, 1997.

Xia, L., and Gao, Z., The Investigation of Multi-Disciplinary and Multi-Objective Optimization Method for the Aircraft Configuration Design, *23rd Congress of the International Council of the Aeronautical Sciences*, Toronto, Canada, 2002.

Yang, X. S., Test Problems in Optimization, *Engineering Optimization: An Introduction with Metaheuristic Applications*, John Wiley & Sons, 2010.

Yang, Y. B., Yau, J. D., and Wu, Y. S., *Vehicle-Bridge Interaction Dynamics: with Applications to High-Speed Railways*, World Scientific, London, England, 2004.

Yeniay, O., Penalty Function Methods for Constrained Optimization with Genetic Algorithms, *Mathematical and Computational Applications*, 10(1), pp. 45–56, 2005.

Young, W. C., Budynas, R. G., and Sadegh, A. M., *Roark's Formulas for Stress and Strain*, 8th Ed., McGraw-Hill, New York, NY, USA, 2012.

Zadeh, P. M., and Toropov, V. V., Multi-Fidelity Multidisciplinary Design Optimization based on Collaborative Optimization Framework, *9th AIAA/ISSMO Symposium on Multidisciplinary Analysis and Optimization*, Atlanta, GA, USA, AIAA 2002-5504, 2002.

Zadeh, P. M., Toropov, V. V., and Wood, A. S., Metamodel-Based Collaborative Optimization Framework, *Structural and Multidisciplinary Optimization*, 38(2), pp. 103–115, 2009.

Zaharie, D., Critical Values for the Control Parameters of Differential Evolution Algorithms, *Proceedings of the 8th International Mendel Conference on Soft Computing*, Brno, Czech Republic, pp. 62–67, 2002.

Zhang, J., Chung, H. S. H., and Lo, W. L., Clustering-Based Adaptive Crossover and Mutation Probabilities for Genetic Algorithms, *IEEE Transactions on Evolutionary Computation*, 11(3), pp. 326–335, 2007.

Zhang, Z., Yu, X., and Hu, T., Two-Level Optimization on Structural Layout and Component Size of Flying Wing Aircraft, *Computer Aided Engineering*, 1, pp. 27–30, 2009.

Zienkiewicz, O. C., and Morgan, K., *Finite Elements and Approximation*, John Wiley & Sons, New York, NY, USA, 1983.

Zienkiewicz, O. C., Taylor, R. L., and Zhu, J. Z., *The Finite Element Method: Its Basis and Fundamentals*, 6th Ed., Butterworth-Heinemann, Oxford, England, 2005.

Appendix A

Aircraft Design Theory

This appendix contains additional information, established theory and the airworthiness requirements relevant to the procedure followed by the framework during the generation of an aircraft design. The principal resources that support this theory include Anderson Jr (1991), Howe (2004), Megson (1999), Niu (1988), Raymer (2006), Roskam (2000), Torenbeek (1982) and Young et al. (2012). The nomenclature used to describe this theory is listed at the end of this appendix.

A.1 Initialisation

Table A.1 contains the parameters input during initialisation to define the aircraft design.

Table A.1: Aircraft design input data

Aircraft section	Parameter
Fuselage	*two of* diameter, length *and* fineness ratio
	Nose radius *and* vertical position
	Tail side *and* base taper angles
	Flight deck length *and* floor vertical position
	Cabin enabled *or* disabled
	if enabled: number of seats, number per row, width *and* pitch
	number of aisles *and* width
Horizontal tail	Aerofoil profile *from database of NACA aerofoils*
	two of root chord, tip chord *and* taper ratio
	Span *or* aspect ratio
	Tail arm *and* vertical position
	Dihedral, incidence *and* leading edge sweep angles
Vertical tail	Aerofoil profile *from database of NACA aerofoils*
	two of root chord, tip chord *and* taper ratio
	Span *or* aspect ratio
	Tail arm
	Cant, incidence *and* leading edge sweep angles
	Twin tail enabled *or* disabled
	if enabled: twin tail spacing
Wing	Aerofoil profile *from database of NACA aerofoils*
	two of root chord, tip chord *and* taper ratio
	Span *or* aspect ratio
	Longitudinal *and* vertical position
	Dihedral, incidence *and* leading edge sweep angles
	Trailing edge kink enabled *or* disabled

Table A.1: Aircraft design input data (cont.)

Aircraft section	Parameter
Powerplant	Class *can be* propeller-driving *or* turbofan *or* turbojet
	if propeller-driving: maximum power
	else: maximum thrust *and* bypass ratio
	Number of units
	for each unit: attachment position
	Nacelle diameter, length *and* mass *if existing powerplant unit*
	Reverse thrust enabled *or* disabled
Undercarriage	Attachment position
	Number of wheels *including* tyre diameter *and* width
	Number of struts *including* diameter *and* length
	Material *from database of metallic materials*
Ordnance	Number of units
	for each unit: attachment position, mass, length, diameter *and* range *or* volume
Materials	*from database of metallic materials*
Fuel	*including* density

Table A.2 contains the properties of the aircraft mission to be input during initialisation.

Table A.2: Aircraft mission input data

Parameter	Note
Aircraft class	*including* civil *or* military
Stall speed	
Payload	*including* flight crew, cabin crew, passengers, luggage *and* cargo
Origin and destination aerodromes	New *or* existing *including* elevation *and* runway length
Mission profile stages	Type, altitude, range *and* airspeed *for each stage*
Loiter	Duration, altitude *and* airspeed

Table A.3 contains the database of load cases to be selected from during initialisation.

Table A.3: Load case database

Flight load		Ground load		Miscellaneous	
L1	Maximum positive flight manoeuvre	L5	Two-point landing	L9	Cabin pressurisation
L2	Maximum negative flight manoeuvre	L6	Three-point landing	L10	Engine thrust
L3	Maximum strength gust	L7	Surface unevenness	L11	Gravity
L4	Gust during cruise	L8	Dynamic braking		

Table A.4 contains the parameters of structural analysis to be input during initialisation.

Table A.4: Structural analysis settings

Parameter	Note
Model fidelity	Static *or* dynamic
if static: fidelity level	$0.1 \leq F \leq 1.0$
else: fidelity limits	$F_{\min} \leq F \leq F_{\max}$
fidelity rate of change	

Table A.4: Structural analysis settings (cont.)

Parameter	Note
Dynamic load case solver	Pseudo-static *or* linear transient dynamic
if linear transient dynamic:	
Time step	Size *and* quantity
Damping ratio	
Direct integration method	Central difference, Houbolt, Wilson-θ *or* Newmark-β
if Wilson-θ: constant	$\theta \geq 1.37$ for unconditional stability
if Newmark-β: constants	$\alpha \geq 0.25\,(\beta + 0.5)^2$, $\beta \geq 0.5$ for unconditional stability

Table A.5 contains the optimisation process parameters to be input during initialisation.

Table A.5: Optimisation process settings

Parameter	Note
Population size	*including* seeded initial population individuals
Representation	Binary *or* real
Penalty function	None, death, interior *or* exterior
Termination criteria:	
Number of generations	
Generations without improvement	
Maximum population affinity	
Genetic algorithm (GA):	
Crossover technique	One, two, random-point, uniform *or* blend
Parameterwise crossover	Enabled *or* disabled
Mutation	Enabled *or* disabled
if enabled: technique	Bit-flip, Gaussian, non-uniform *or* random
Simulated annealing (SA) cooling schedule	Linear *or* exponential *including* initial temperature
Hyper-heuristic approach (HHA):	
Heuristic set size	
Measure of improvement (MoI)	Evaluation period *and* tabu tenure method
Move acceptance rule	All moves (AM), only improving (OI), exponential Monte Carlo with counter (EMCQ) *or* simulated annealing (SA)
Maximum sub-population size	
Perturbation analysis sampling	Solution quality *or* random *including* sample size
Evolutionary principle	Lamarckian *or* Baldwinian
Maximum variable affinity	

Table A.6 contains the database of heuristics to be selected from during initialisation.

Table A.6: Heuristic sets database

Classification	Heuristic
Low-level heuristic (LLH):	
Random generation	Monte Carlo (MC)
	Random immigration (RI)
Evolutionary algorithm (EA)	Killer queen (KQ)
	Differential evolution (DE)
Genetic algorithm (GA)	Roulette wheel (RW)
	Tournament selection (TO)

Table A.6: Heuristic sets database (cont.)

Classification	Heuristic
	Breeder pool (BP)
	Radioactive contamination (RC)
Swarm intelligence (SI)	Particle swarm optimisation (PSO)
Local search (LS)	Hill climbing (HC)
	Simulated annealing (SA)
	Tabu search (TS)
Heuristic selection	Simple random (SR) *or* random descent (RD)
	Permutation (PE) *or* permutation descent (PD)
	Greedy (GR)
	Peckish (PK)
	Roulette wheel (RW)
	Tournament selection (TO)
Perturbation analysis	Hill climbing (HC)
and parameter control	Simulated annealing (SA)
	Tabu search (TS)

A.2 Mass Estimation

An empirical method of mass estimation presented in Roskam (1986) is well-established for obtaining an initial estimate of the mass of different aircraft components. This method defines the aircraft ramp mass, i.e. mass before any mission operation, as

$$m_0 = m_D + m_{TFO} + m_F + m_E \tag{A.1}$$

where m_D disposable mass, kg
m_E empty aircraft mass, kg
m_F fuel mass, kg
m_{TFO} trapped fuel and oil mass, kg

Each ith mass component is estimated as a mass or alternatively as a fraction of the ramp mass

$$M_i = \frac{m_i}{m_0} \tag{A.2}$$

Disposable mass constitutes all removable non-fuel mission-specific mass such as the mission payload, i.e. passengers and luggage for civil aircraft or ordnance for military. Human mass is defined by the airworthiness requirements as 77 kg for civil normal, commuter and large aircraft, 86 kg for civil acrobatic and utility aircraft and 120.5 kg for military aircraft (CS-23.25, CS-25.562, Def.Stan.00-970.Vol. 1 Leaflet 105/3). Trapped fuel and oil consists of the masses of these substances that cannot be removed from the aircraft systems. An estimate of the trapped fuel and oil mass fraction is $M_{TFO} = 0.005$.

Mission fuel mass is estimated based on the aircraft class and mission profile. Table A.7 gives the mass fraction of fuel consumed over non-fuel intensive mission stages. The aircraft classes in Roskam (1986) are different from those used in the framework, as such are substituted through consideration of the aircraft design intent and powerplant. Civil light normal and aerobatic aircraft are substituted with single or twin-engine propeller aircraft, utility with agricultural, and commuter with either single or twin-engine propeller, regional turboprop or business jet aircraft. Civil large aircraft are substituted with transport jets. Military trainers and bombers require no substitution, whilst interceptors and ground attack aircraft are substituted with fighters and transport aircraft with military cargo aircraft.

Table A.7: Mission stage fuel mass fractions (Roskam, 1986, Table 3 p. 557)

Aircraft class	Engine startup	Taxi	Take-off	Climb	Descent	Landing, taxi and shutdown
Civil:						
Single-engine propeller	0.995	0.997	0.998	0.992	0.993	0.993
Twin-engine propeller	0.992	0.996	0.996	0.990	0.992	0.992
Agricultural	0.996	0.995	0.996	0.998	0.999	0.998
Regional turboprop	0.990	0.995	0.995	0.985	0.985	0.995
Business jet	0.990	0.995	0.995	0.980	0.990	0.992
Transport jet	0.990	0.990	0.995	0.980	0.990	0.992
Military:						
Trainer	0.990	0.990	0.990	0.980	0.990	0.995
Fighter	0.990	0.990	0.990	0.90-0.96	0.990	0.995
Cargo, bomber	0.990	0.990	0.995	0.980	0.990	0.992

The mass fractions for fuel intensive mission stages, i.e. cruise and loiter, are estimated using the Breguet equations for the kth stage, the coefficients of which are listed in Table A.8

$$\frac{M_k}{M_{k-1}} = \begin{cases} \exp\left\{\dfrac{-R_k C_j}{V_k (L/D)}\right\} & \text{for jet-powered aircraft during cruise} \\ \exp\left\{\dfrac{-R_k C_p}{550 \eta_p (L/D)}\right\} & \text{for propeller-driven aircraft during cruise} \end{cases} \tag{A.3a}$$

$$\frac{M_k}{M_{k-1}} = \begin{cases} \exp\left\{\dfrac{-T_k C_j}{(L/D)}\right\} & \text{for jet-powered aircraft during loiter} \\ \exp\left\{\dfrac{-T_k V_k C_p}{550 \eta_p (L/D)}\right\} & \text{for propeller-driven aircraft during loiter} \end{cases} \tag{A.3b}$$

where
- C_j jet engine specific fuel consumption, mg/Ns
- C_p propeller engine specific fuel consumption, mg/J
- (L/D) lift-to-drag ratio
- R_k range of kth stage, m
- T_k duration of kth loiter, s
- V_k true airspeed (TAS), i.e. airspeed relative to surrounding air, in kth stage, m/s
- η_p propeller efficiency

Table A.8: Breguet equation coefficients (Roskam, 1986, Table 4 p. 557)

	Cruise				Loiter			
Aircraft class	(L/D)	C_j	C_p	η_p	(L/D)	C_j	C_p	η_p
Civil:								
Single-engine propeller	8-10		0.5-0.7	0.8	10-12		0.5-0.7	0.7
Twin-engine propeller	8-10		0.5-0.7	0.82	9-11		0.5-0.7	0.72
Agricultural	5-7		0.5-0.7	0.82	8-10		0.5-0.7	0.72
Regional turboprop	11-13		0.4-0.6	0.85	14-16		0.5-0.7	0.77
Business jet	10-12	0.5-0.9			12-14	0.4-0.6		
Transport jet	13-15	0.5-0.9			14-18	0.4-0.6		
Military:								
Trainer	8-10	0.5-1.0	0.4-0.6	0.82	10-14	0.4-0.6	0.5-0.7	0.77
Fighter	4-7	0.6-1.4	0.5-0.7	0.82	6-9	0.6-0.8	0.5-0.7	0.77
Cargo, bomber	13-15	0.5-0.9	0.4-0.7	0.82	14-18	0.4-0.6	0.5-0.7	0.77

The mass fraction of mission fuel over n_m mission stages is subsequently calculated as

$$M_F = 1 - \prod_{k=1}^{n_m} \frac{M_k}{M_{k-1}} \tag{A.4}$$

The empty aircraft mass represents the ramp mass minus all removable mission-specific components. This mass component is obtained iteratively given the known components of disposable, trapped fuel and oil, and fuel mass. This procedure firstly estimates the ramp mass before calculating the empty aircraft mass given the other known mass components. Two methods of calculating the empty aircraft mass are typically employed, those of Roskam (1986) and Raymer (2006). The former is more well-established whilst the latter takes account of more recent materials and designs. The resulting expressions are as follows, where the regression coefficients A and B are given in Table A.9

$$\log m_E = \frac{\log m_0 - A}{B} \qquad \text{(Roskam, 1986)} \tag{A.5a}$$

$$M_E = A m_0^B K_{vs} \qquad \text{(Raymer, 2006)} \tag{A.5b}$$

$$\text{where} \quad K_{vs} = \begin{cases} 1.04 & \text{for variable sweep wings} \\ 1.00 & \text{otherwise} \end{cases}$$

Table A.9: Empty mass coefficients (Roskam, 1986, Table 2 p. 555; Raymer, 2006, Table 3.1 p. 18)

	Roskam (1986, Table 2 p. 555)		Raymer (2006, Table 3.1 p. 18)	
Aircraft class	A	B	A	B
Civil:				
Single-engine propeller	-0.1440	1.1162	2.05	-0.18
Twin-engine propeller	0.0966	1.0298	1.40	-0.10
Agricultural	-0.4398	1.1946	0.72	-0.03
Regional turboprop	0.3774	0.9647	0.92	-0.05
Business jet	0.2678	0.9979		
Transport jet	0.0833	1.0383	0.97	-0.06
Military:				
Trainer	0.6632	0.8640	1.47	-0.10
Fighter	0.1362	1.0116	2.11	-0.13
Cargo, bomber	-0.2009	1.1037	0.88	-0.07

The mass components are then input into a rearranged form of Eqn. (A.1) to obtain the ramp mass

$$m_0 = \begin{cases} \dfrac{m_E + m_D}{1 - M_{TFO} - M_F} & \text{given } m_E \\ \dfrac{m_D}{1 - M_E - M_{TFO} - M_F} & \text{given } M_E \end{cases} \tag{A.6}$$

The ramp mass output from Eqn. (A.6) is then compared against the value input into Eqn. (A.5) and the process is repeated iteratively until the error satisfies

$$\frac{|\tilde{m}_0 - m_0|}{m_0} \leq 1 \times 10^{-6} \tag{A.7}$$

where $\tilde{m}_0$ and m_0 denote the ramp masses in Eqns. (A.5) and (A.6) respectively.

A.3 Aircraft Profile Generation

The aircraft external profile is generated using empirical and geometric formulae. The maximum wing loading coefficient is calculated given the aerofoil maximum lift coefficient and stall speed as

$$(W/S) = \frac{1}{2}\rho_0 C_{L,\max} V_s^2 \tag{A.8}$$

where $C_{L,\max}$ maximum lift coefficient
V_s stall speed, m/s
ρ_0 sea level air density, kg/m^3

The reference surface area necessary to provide the required loading coefficient on take-off, i.e. at mass m_{TO}, is given by

$$S = \frac{m_{TO}}{(W/S)} \tag{A.9}$$

The lifting surface taper ratio given the root and tip chord lengths is defined by

$$\lambda = \frac{c_t}{c_r} \tag{A.10}$$

where c_r root chord length, m
c_t tip chord length, m

The mean aerodynamic chord of the lifting surface is subsequently computed as

$$\bar{c} = c_r \frac{2\left(1+\lambda+\lambda^2\right)}{3+(1+\lambda)} \tag{A.11}$$

The lifting surface span is calculated as

$$b = \frac{S}{c_r + c_t} \tag{A.12}$$

Subsequently, the aspect ratio is determined by

$$\mathcal{AR} = \frac{b^2}{S} \tag{A.13}$$

The quarter-chord sweep angle is calculated given the leading edge sweep, Λ_{LE}, as

$$\Lambda_{c/4} = \Lambda_{LE} - \frac{1-\lambda}{\mathcal{AR}\,(1+\lambda)} \tag{A.14}$$

As a result, the lift coefficient per angle of incidence is found

$$C_{L,\alpha} = \begin{cases} \dfrac{4}{\sqrt{M_C^2-1}} & \text{for supersonic flight at } M_C > \dfrac{1}{\cos\Lambda_{LE}} \\ \dfrac{2\pi\mathcal{AR}}{2+\sqrt{4+\left\{\dfrac{4\pi^2\mathcal{AR}^2\sqrt{1-M_C^2}}{C_{l,\alpha}}\left(1+\dfrac{\tan\Lambda_{c/4}{}^2}{1-M_C^2}\right)\right\}}} & \text{otherwise} \end{cases} \tag{A.15}$$

where $C_{l,\alpha}$ lift curve slope
M_C cruise Mach number

The wing drag-due-to-lift is determined using the Oswald efficiency number, e

$$k = \frac{1}{\pi\mathcal{AR}e} \tag{A.16}$$

where $e = \begin{cases} 1.78\left(1 - 0.045\mathcal{AR}^{0.68}\right) - 0.64 & \text{if } \Lambda_{LE} \leq 120° \\ 4.61\left(1 - 0.045\mathcal{AR}^{0.68}\right)\left(\cos\left(\Lambda_{LE} - 90\right)^{0.15} - 3.1\right) & \text{otherwise} \end{cases}$

The volume of the wing fuel tanks is estimated empirically as follows given the root and tip cross-sectional areas, A_r and A_t respectively

$$v_{ft} = \frac{b}{4}\left(A_r + A_t + \sqrt{A_r A_t}\right) \tag{A.17}$$

The downwash derivative on the horizontal tail is calculated given the wing lift coefficient per angle of incidence and aspect ratio

$$\frac{\partial \varepsilon}{\partial \alpha} = \frac{2}{\pi}\left(\frac{C_{L,\alpha}}{\mathcal{AR}}\right)_w \tag{A.18}$$

The fuselage fineness ratio is found given the fuselage length and diameter as

$$(l/d) = \frac{l_f}{d_f} \tag{A.19}$$

where d_f fuselage diameter, m
l_f fuselage length, m

The flight deck length is estimated empirically

$$l_{fd} = \begin{cases} 3.80 \text{ m} & \text{for civil large transport aircraft} \\ 1.78 \text{ m} & \text{otherwise} \end{cases} \tag{A.20}$$

The cabin length is estimated empirically

$$l_c = \max\left\{p_s\left\lceil\frac{n_s}{n_{s,r}}\right\rceil, 20\left\{\frac{n_s p_s}{16.8 n_{s,r}}\right\}^{1.052}\right\} \tag{A.21}$$

where n_s number of seats
$n_{s,r}$ number of seats per row
p_s seat pitch, m

The positions along the fuselage at which taper of the base and side begin are found respectively as

$$z_{\theta_b} = l_f - \frac{d_f}{\tan\theta_b} \tag{A.22a}$$

$$z_{\theta_s} = l_f - \frac{d_f}{2\tan\theta_s} \tag{A.22b}$$

where θ_b fuselage tail base taper, rad
θ_s fuselage tail side taper, rad

The fuselage volume is estimated as

$$v_f = \frac{1}{4}\pi d_f^2\left(l_c + l_{fd}\right) \tag{A.23}$$

The fuselage wetted surface area is similarly approximated as

$$S_f = \pi l_f d_f\left\{1 + \frac{1}{(l/d)^2}\right\}\left\{1 - \frac{2}{(l/d)}\right\}^{0.667} \tag{A.24}$$

A.3.1 Balanced Field Length

The field length on take-off is the distance required for the aircraft to accelerate from rest, suffer an engine failure at a prescribed decision point, and the greater of either coming to a complete stop after aborting the run or clearing the aerodrome screen at a prescribed climb angle. The field length on landing is the distance required for the aircraft to approach at a given angle, touchdown and come to a stop. The take-off balanced field length is found by satisfying the following cases, as illustrated in Fig. A.1:

Case 1: normal take-off;

Case 2: take-off with engine failure at decision point;

Case 3: aborted take-off after engine failure at decision point.

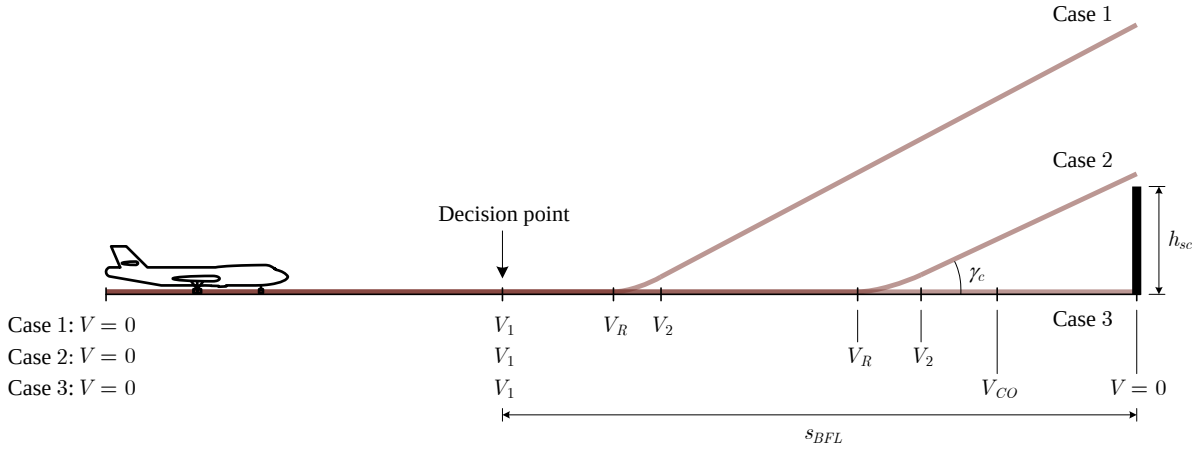

Figure A.1: Balanced field length

Airworthiness requirements define the airspeeds in Fig. A.1 (CS-23.51, CS-25.107, Def.Stan.00-970.2.4.20):

- decision speed, V_1: airspeed at which decision is made to continue or abort take-off run;
- rotation speed, V_R: airspeed at which pilot applies control input for lift-off from ground;
- take-off speed, V_2: airspeed required for climb-out at angle γ_c from lift-off location to clear screen;
- cut-off speed, V_{CO}: airspeed at which engine reverse thrust is cut-off during emergency stop.

Case 1 is ignored as greater thrust is available during a normal take-off than following an engine failure. Hence, the balanced field length is found by satisfying Cases 2 and 3. Case 2 consists of three phases:

1. ground roll: the period over which the aircraft accelerates from rest through V_1 to V_R;
2. transition: period during which the aircraft rotates to leave the ground and accelerates to V_2;
3. climb: steady climb period at angle γ_c for the aircraft to clear the screen of height h_{sc}.

The distance required for the ground roll on take-off is defined by the integral

$$s_{g,TO} = \frac{1}{2}\int_0^{V_R} \frac{dV^2}{a} \tag{A.25}$$

This calculation is solved in two parts given unequal acceleration, a, following the engine failure at V_1:

1. the period of acceleration from rest to V_1 with all n_e engines functional;
2. further acceleration period to V_R with reduced thrust due to the loss of one engine.

The ground roll is approximated by the aircraft thrust and aerodynamics and rolling friction coefficient as defined by the airworthiness requirements (CS-25.109)

$$s_{g,TO} = a_{BFL} \ln \left\{ \left(\frac{K_T + K_A V_1^2}{K_T} \right) \left(\frac{\kappa_e K_T + K_A V_R^2}{\kappa_e K_T + K_A V_1^2} \right) \right\} \tag{A.26}$$

where $a_{BFL} = \dfrac{1}{2gK_A}$

$K_A = \dfrac{\rho_a}{2(W/S)} \left(\mu_f C_{L,\max} - C_{D,0} - k C_{L,\max}^2 \right)$

$K_T = (\overline{T}/W) - \mu_f$

$\kappa_e = 1 - \dfrac{1}{n_e}$

$C_{D,0}$ zero-lift drag coefficient

$(\overline{T}/W)$ mean thrust-to-weight ratio

μ_f rolling friction coefficient

ρ_a aerodrome altitude air density, kg/m^3

The aircraft rotates during the transition stage to create a circular arc tangential to the vectors of ground roll and climb. The radius of this rotation is calculated as

$$r = \frac{5}{g} \left\{ \frac{V_R + V_2}{2} \right\}^2 \tag{A.27}$$

Given the radius of rotation and the climb-out angle set by the airworthiness requirements (CS-23.67, CS-25.121), the altitude of the aircraft at the end of the transition stage is determined

$$h_{tr} = r \left(1 - \cos \gamma_c \right) \tag{A.28}$$

Thus, the respective distances travelled across the ground during the transition and climbing phases are

$$s_{tr} = \begin{cases} r \sin \gamma_c & \text{if } h_{tr} < h_{sc} \\ \sqrt{r^2 - (r - h_{tr})^2} & \text{otherwise} \end{cases} \tag{A.29}$$

$$s_c = \begin{cases} \dfrac{h_{sc} - h_{tr}}{\tan \gamma_c} & \text{if } h_{tr} < h_{sc} \\ 0 & \text{otherwise} \end{cases} \tag{A.30}$$

The field length required by Case 2 is calculated as the sum of Eqns. (A.26), (A.29) and (A.30). For the aborted take-off of Case 3, it is assumed that the ground roll progresses as for Case 2 up to the decision point when an emergency stop is performed by applying the aircraft brakes following a pilot reaction time. Engine reverse thrust is also applied if available, otherwise the engines are at idle. If reverse thrust is applied, constant deceleration is assumed until the cut-off speed, at which point the engines are idled and the braking force alone decelerates the aircraft. The total corresponding ground run is calculated as follows assuming the availability of reverse thrust above a cut-off speed V_{CO}

$$s_{g,ATO} = a_{BFL} \ln \left\{ \left(\frac{K_T + K_A V_1^2}{K_T} \right) \left(\frac{K_A V_1^2 - \kappa_e K_T}{K_A V_{CO}^2 - \kappa_e K_T} \right) \left(\frac{\mu_f - K_A V_{CO}^2}{\mu_f} \right) \right\} + V_1 T_{pr} \tag{A.31}$$

where T_{pr} is the pilot reaction time. If reverse thrust is not available, the middle product term is ignored and V_{CO} is replaced with V_1 in the final product term. A similar procedure is followed to analyse the landing process given a corresponding screen height upon approach and the required stopping distance. Similar expression to Eqns. (A.30), (A.29) and (A.31) are obtained for the distance of approach, s_a, flare before touchdown, s_{fl}, and ground run stop to rest, $s_{g,L}$, respectively. Consequently, the balanced field length is expressed as

$$s_{BFL} = \begin{cases} s_{g,TO} + s_{tr} + s_c & \text{for engine-out take-off} \\ s_{g,ATO} & \text{for aborted take-off} \\ s_{g,L} + s_{fl} + s_a & \text{for landing} \end{cases} \tag{A.32}$$

The balanced field length is determined by solving Eqn. (A.32) for the three cases. The maximum value of average thrust-to-weight ratio can therefore be established during take-off by rearranging Eqn. (A.26) for $(\overline{T}/W)$. The peak thrust-to-weight ratio is then determined as

$$(\hat{T}/W) \approx \sqrt{2}(\overline{T}/W) \tag{A.33}$$

For propeller-driven aircraft, the power-to-weight ratio is found by assuming peak thrust upon rotation

$$(\hat{P}/W) = \frac{V_R(\hat{T}/W)}{\eta_p} \tag{A.34}$$

A.3.2 Aircraft Stability

Aircraft longitudinal stability is determined by calculating the static margin between the centre of gravity (CoG) and neutral stability positions. Empirical formulae estimate the masses of aircraft sections and the subsequent moments about the CoG. Conventional aircraft symmetry results in the lateral CoG position lying on the fuselage centreline. The vertical and longitudinal CoG positions are found by calculating the moments of the aircraft sections about datum positions. The masses of the wing, horizontal tail, vertical tail, fuselage, main undercarriage, nose undercarriage and engine section masses for a civil light aircraft are estimated respectively using imperial units as

$$m_w = 0.036 S_w^{0.758} \lambda_w^{0.04} \left\{ \frac{\text{Æ}_w}{\cos^2 \Lambda_{c/4,w}} \right\}^{0.6} \left\{ \frac{100(t/c)_w}{\cos \Lambda_{c/4,w}} \right\}^{-0.3} (m_{TO} n_1)^{0.49} m_F^{0.0035} (\rho_C V_C)^{0.006} \tag{A.35a}$$

$$m_{ht} = 0.016 S_{ht}^{0.896} \lambda_{ht}^{-0.02} \left\{ \frac{\text{Æ}_{ht}}{\cos^2 \Lambda_{c/4,ht}} \right\}^{0.043} \left\{ \frac{100(t/c)_{ht}}{\cos \Lambda_{c/4,ht}} \right\}^{-0.12} (m_{TO} n_1)^{0.414} (\rho_C V_C)^{0.168} \tag{A.35b}$$

$$m_{vt} = 0.073 (1 + 0.2 K_{Tt}) S_{vt}^{0.873} \lambda_{vt}^{0.039} \left\{ \frac{\text{Æ}_{vt}}{\cos^2 \Lambda_{c/4,vt}} \right\}^{0.357} \left\{ \frac{100(t/c)_{vt}}{\cos \Lambda_{c/4,vt}} \right\}^{-0.49} (m_{TO} n_1)^{0.376} (\rho_C V_C)^{0.122} \tag{A.35c}$$

$$m_f = 0.052 S_f^{1.086} l_{ht}^{-0.051} (m_{TO} n_1)^{0.177} (\rho_C V_C)^{0.241} (L/D)^{-0.072} + 11.9 (v_f \Delta P)^{0.271} \tag{A.35d}$$

$$m_{mu} = 0.095 \left\{ \frac{l_{mu}}{12} \right\}^{0.409} (m_L n_L)^{0.768} \tag{A.35e}$$

$$m_{nu} = 0.125 \left\{ \frac{l_{nu}}{12} \right\}^{0.845} (m_L n_L)^{0.566} \tag{A.35f}$$

$$m_e = 2.575 n_e m_e^{0.922} \tag{A.35g}$$

where $K_{Tt} = \begin{cases} 1.0 & \text{for T-tail} \\ 0.0 & \text{otherwise} \end{cases}$

l_{ht} horizontal tail arm, ft

l_{mu} main undercarriage unit length, ft

l_{nu} nose undercarriage unit length, ft

m_e engine mass, lb
m_L landing mass, lb
n_1 maximum flight envelope load factor
n_L maximum landing load factor
(t/c) thickness-to-chord ratio
V_C cruise speed, ft/s^2
ΔP cabin differential pressure, lb/ft^2
ρ_C cruise altitude air density, lb/ft^3

The estimated masses of civil large and military bomber or transport aircraft sections are

$$m_w = 0.0051 S_w^{0.649} \left(1+\lambda_w\right)^{0.1} \mathcal{R}_w^{0.5} \cos\Lambda_{c/4,w}{}^{-1.0} (t/c)_w^{-0.4} \left(m_{TO} n_1\right)^{0.557} \tag{A.36a}$$

$$m_{ht} = 0.0162 S_{ht}^{0.75} \mathcal{R}_{ht}^{0.166} \cos\Lambda_{c/4,ht}{}^{-1.0} \left\{1+\frac{w_{f,ht}}{b_{ht}}\right\}^{-0.25} l_{ht}^{-0.296} m_{TO}^{0.639} n_1^{0.1} \tag{A.36b}$$

$$m_{vt} = 0.0026 \left(1+K_{Tt}\right)^{0.225} S_{vt}^{0.5} \mathcal{R}_{vt}^{0.35} \cos\Lambda_{c/4,vt}{}^{-1.0} (t/c)_{vt}^{-0.5} l_{vt}^{0.375} m_{TO}^{0.556} n_1^{0.536} \tag{A.36c}$$

$$m_f = 0.328 \left(1+K_{ws}\right)^{0.04} S_f^{0.302} \left(l_f - r_n\right)^{0.25} \left(m_{TO} n_1\right)^{0.5} (L/D)^{0.1} \tag{A.36d}$$

$$m_{mu} = 0.0106 l_{mu}^{0.4} n_{w,mu}^{0.321} n_{ss,mu}^{-0.5} m_L^{0.888} n_L^{0.25} V_s^{0.1} \tag{A.36e}$$

$$m_{nu} = 0.032 l_{nu}^{0.5} n_{w,nu}^{0.45} m_L^{0.646} n_L^{0.2} \tag{A.36f}$$

$$m_e = 1.128 K_{ng} S_e^{0.224} n_1^{0.119} d_e^{0.294} l_e^{0.1} m_e^{1.512} n_e^{0.984} \left(K_p K_{rt}\right)^{0.611} \tag{A.36g}$$

where
$$K_{ng} = \begin{cases} 1.017 & \text{for pylon-mounted nacelle} \\ 1.0 & \text{otherwise} \end{cases}$$
$$K_p = \begin{cases} 1.4 & \text{for propeller-powered engine} \\ 1.0 & \text{otherwise} \end{cases}$$
$$K_{rt} = \begin{cases} 1.18 & \text{for engine with reverse thrust} \\ 1.0 & \text{otherwise} \end{cases}$$
$$K_{ws} = 0.75 b_w \left\{\frac{1+2\lambda_w}{1+\lambda_w}\right\} \left\{\frac{\tan\Lambda_{c/4,w}}{l_f}\right\}$$

d_e engine nacelle diameter, ft
l_e engine nacelle length, ft
l_{vt} vertical tail arm, ft
n_{ss} number of shock struts
n_w number of wheels
r_n nose radius, ft
$w_{f,ht}$ fuselage width at horizontal tail, ft

Estimated military trainer, interceptor and ground attack aircraft section masses are

$$m_w = 0.0103 K_{dw} K_{vs} S_w^{0.622} \left(1+\lambda_w\right)^{0.05} \mathcal{R}_w^{0.785} \cos\Lambda_{c/4,w}{}^{-1.0} (t/c)_w^{-0.4} \left(m_{TO} n_1\right)^{0.5} \tag{A.37a}$$

$$m_{ht} = 3.316 S_{ht}^{0.806} \left\{1+\frac{w_{f,ht}}{b_{ht}}\right\}^{-2.0} \left\{\frac{m_{TO} n_1}{1000}\right\}^{0.26} \tag{A.37b}$$

$$m_{vt} = 0.452\,(1+K_{Tt})^{0.5}\,S_{vt}^{0.718}\,(1+\lambda_{vt})^{0.25}\,A\!R_{vt}^{0.223}\cos\Lambda_{c/4,vt}{}^{-0.323}\,(m_{TO}n_1)^{0.488}\,M_C^{0.341}\,l_{vt}^{-1.0} \tag{A.37c}$$

$$m_f = 0.499 K_{dwf} d_f^{1.534} l_f^{0.5} m_{TO}^{0.35} n_1^{0.25} \tag{A.37d}$$

$$m_{mu} = l_{mu}^{0.973}\,(m_L n_1)^{0.25} \tag{A.37e}$$

$$m_{nu} = l_{nu}^{0.5} n_{w,nu}^{0.525}\,(m_L n_1)^{0.29} \tag{A.37f}$$

$$m_e = 0.01 n_e m_e^{0.717} n_1 + 0.013 n_e^{0.795} T_e^{0.579} n_1 \tag{A.37g}$$

where $K_{dw} = \begin{cases} 0.768 & \text{for delta wing} \\ 1.0 & \text{otherwise} \end{cases}$

$K_{dwf} = \begin{cases} 0.774 & \text{for delta wing} \\ 1.0 & \text{otherwise} \end{cases}$

$K_{vs} = \begin{cases} 1.19 & \text{for variable sweep wings} \\ 1.0 & \text{otherwise} \end{cases}$

T_e engine thrust, lb

The vertical and longitudinal origins employed are the undercarriage ground contact point and fuselage nose tip respectively. The distances from these points of origin to the CoGs of the aircraft sections are estimated empirically using the expressions within Table A.10. The vertical and longitudinal distances from the origin to the ith section approximate aerodynamic centre are denoted by y_i and z_i respectively.

Table A.10: Aircraft section positions with respect to origins

i	Aircraft section	Vertical distance, Δy	Longitudinal distance, Δz
1	Wing	$0.5d_f + l_{mu} + y_w$	$0.15\overline{c_w} + z_w$
2	Horizontal tail	$0.5d_f + l_{mu} + y_{ht}$	$0.15\overline{c_{ht}} + l_{ht} + z_w$
3	Vertical tail	$d_f + l_{mu} + 0.25b_{vt}$	$0.4\overline{c_{vt}} + 0.75\overline{c_{ht}} + l_{ht} + z_w - c_{r,vt}$
4	Fuselage	$0.5d_f + l_{mu}$	$0.5d_f$
5	Main undercarriage	0.0	$0.5\overline{c_w} + z_w$
6	Nose undercarriage	0.0	$r_n + 0.1l_f$
7	Powerplant and ordnance	$0.5d_f + l_{mu} + y_w - 0.5d_e$	$0.5\overline{c_w} + z_w$

As a result, the CoG position is found, e.g. in the longitudinal axis

$$z_{CoG} = \frac{\sum_{i=1}^{7} m_i \Delta z_i}{\sum_{i=1}^{7} m_i} \tag{A.38}$$

where m_i represents the mass of the ith aircraft section listed in Table A.10. The longitudinal position of neutral stability is subsequently calculated as

$$z_{NS} = \frac{C_{L,\alpha,w}\frac{\Delta z_w}{\overline{c_w}} - \frac{K_f d_f^2 l_f}{\overline{c_w} S_w} + \eta_{ht} C_{L,\alpha,ht} \frac{S_{ht}}{S_w}\left\{1 - \frac{\partial\varepsilon}{\partial\alpha}\right\}\frac{\Delta z_{ht}}{\overline{c_w}} + \frac{\Delta z_e}{\overline{c_w}}}{C_{L,\alpha,w} + \eta_{ht} C_{L,\alpha,ht}\frac{S_{ht}}{S_w}\left\{1 - \frac{\partial\varepsilon}{\partial\alpha}\right\}} \tag{A.39}$$

where $K_f = 0.003 \exp\left\{\frac{4.6042 z_w}{l_f}\right\}$

η_{ht} horizontal tail relative dynamic pressure

The static margin is calculated as the difference between the neutral stability and CoG positions.

A.4 Aircraft Loads

Aircraft loads are classified as either flight, ground or miscellaneous loads. These loads are calculated as defined by the airworthiness requirements applicable to the aircraft class.

A.4.1 Flight Loads

Flight loads concern loads resulting from airborne manoeuvres and gusting conditions during flight. These loads respectively define the manoeuvre and gust envelopes, which in turn define the flight envelope to indicate the load factors that the aircraft must withstand in-flight.

A.4.1.1 Manoeuvre Envelope

The manoeuvre envelope indicates the greatest loads to be withstood by the aircraft as a result of performing airborne manoeuvres in pitch, roll and yaw. Loads are determined at an equivalent airspeed (EAS), i.e. airspeed at sea level at which dynamic pressure equals that at the aircraft flight altitude:

- manoeuvre speed, V_A: the minimum airspeed at which the aircraft may manoeuvre;
- cruise speed, V_C: the cruising airspeed of the aircraft;
- design diving speed, V_D: the maximum airspeed of the aircraft to be obtained during a dive.

The greatest load factors at these airspeeds are defined by the airworthiness requirements (CS-23.337, CS-25.337, Def.Stan.00-970.3.3.3). These values are listed in Table A.11, leading to the generation of the manoeuvre envelope as in Fig. A.2. For a selection of civil aircraft classes $n_{1,4}$ is defined as follows, with limits of $n_{1,4} < 3.8$ for civil normal aircraft and $2.5 < n_{1,4} < 3.8$ for civil large aircraft

$$n_{1,4} = 2.1 + \frac{24,000}{m_{TO} + 10,000} \quad \text{with } m_{TO} \text{ in pounds, lb} \tag{A.40}$$

Table A.11: Manoeuvring load factor limits

Aircraft class	n_1	n_2	n_3	n_4
Civil:				
Normal *or* commuter	Eqn. (A.40)	0	$-0.4n_1$	Eqn. (A.40)
Aerobatic	6.0	-3.0	-3.0	6.0
Utility	4.4	-1.0	-1.76	4.4
Large	Eqn. (A.40)	0	-1.0	Eqn. (A.40)
Military:				
Trainer	7.0	-1.1	-3.6	7.0
Interceptor	6.0	-0.8	-3.0	6.0
Ground attack	8.0	-1.4	-4.2	8.0
Bomber	5.0	-0.5	-2.4	5.0
Transport	2.5	0.25	-0.9	2.5

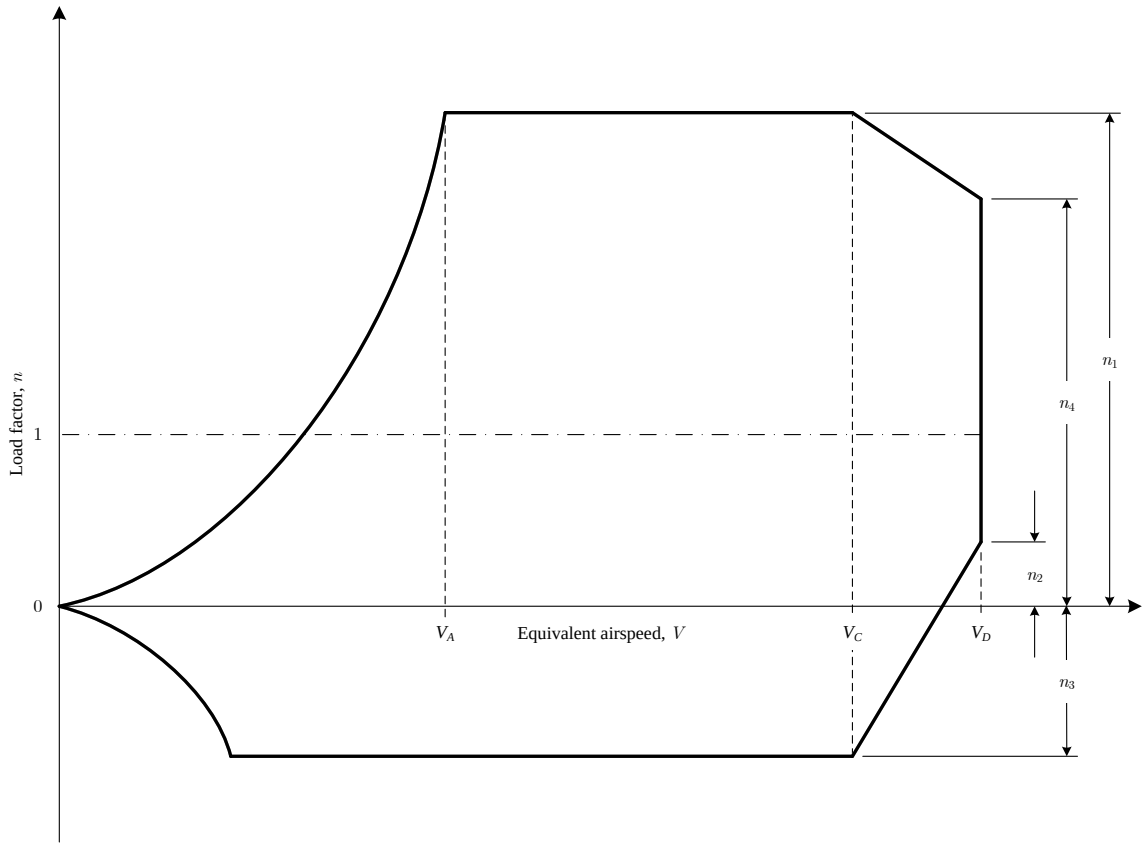

Figure A.2: Manoeuvre envelope

A.4.1.2 Gust Envelope

The gust envelope considers discrete gusting conditions encountered by the aircraft. A gust is approximated as a column of air moving at a known velocity in a vertical or lateral direction relative to the flight path. The gust profile of a one-minus type discrete gust is shown in Fig. A.3.

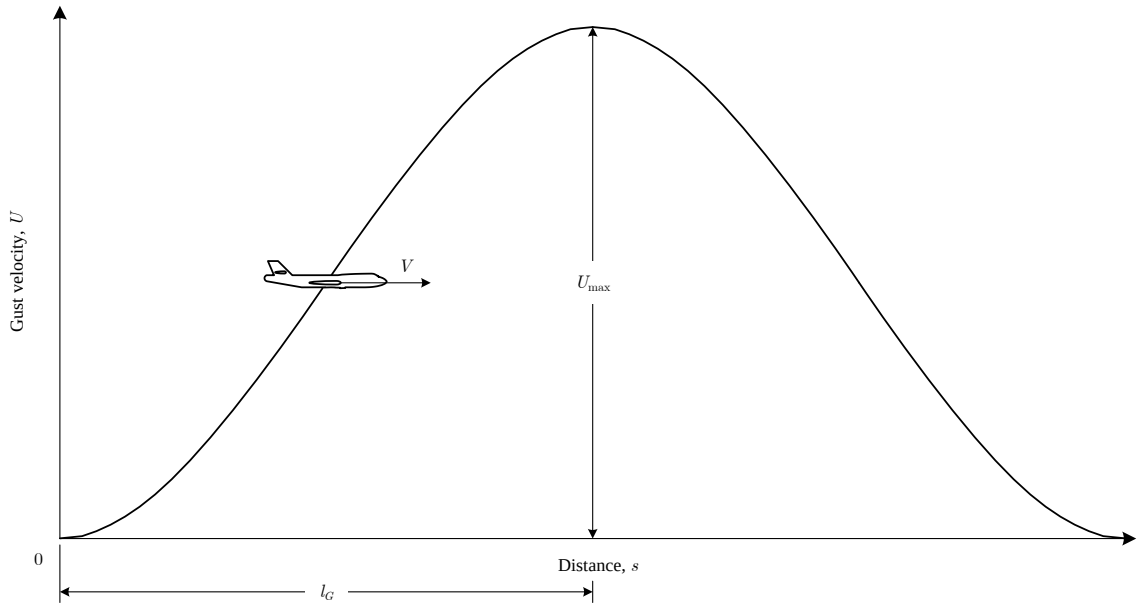

Figure A.3: One minus cosine type discrete gust

A gust possesses the following velocity at a distance s along the gust profile in Fig. A.3

$$U = \frac{U_{de}}{2}\left\{1 - \cos\left(\frac{\pi s}{l_G}\right)\right\} \text{ for } 0 > s > 2l_G \tag{A.41}$$

where U_{de} discrete gust design velocity, m/s
l_G gust gradient length, m

Table A.12 lists the design gust velocities defined by the airworthiness requirements (CS-23.333, CS-25.341, Def.Stan.00-970.3.5.8), where V_B denotes airspeed corresponding to the gust of greatest velocity.

Table A.12: Design gust velocity limits

Aircraft class	Airspeed, V	Design gust velocity, U_{de}
Civil light	V_B	20.12 m/s (66 ft/s) below 6,096 m (20,000 ft) *decreases linearly* 11.58 m/s (38 ft/s) above 15,240 m (50,000 ft)
	V_C	15.24 m/s (50 ft/s) below 6,096 m (20,000 ft) *decreases linearly* 7.62 m/s (25 ft/s) at 15,240 m (50,000 ft)
	V_D	0.5 times values for V_C
Civil large	V_B	17.07 m/s (56 ft/s) at sea level *decreases linearly* 13.41 m/s (44 ft/s) at 4,572 m (15,000 ft) *decreases linearly* 6.36 m/s (20.86 ft/s) at 18,288 m (60,000 ft)
	V_C	same as values for V_B
	V_D	0.5 times values for V_C
Military	V_B	20.0 m/s (66 ft/s) below 6,100 m (20,000 ft) *decreases linearly* 11.6 m/s (38 ft/s) above 15,200 m (50,000 ft)
	V_C	15.2 m/s (50 ft/s) below 6,100 m (20,000 ft) *decreases linearly* 7.6 m/s (25 ft/s) above 15,200 m (50,000 ft)
	V_D	7.6 m/s (25 ft/s) below 6,100 m (20,000 ft) *decreases linearly* 3.8 m/s (12.5 ft/s) above 15,200 m (50,000 ft)

The gradient length, empirically-defined as $12.5\bar{c}$, defines the gust boundary and midpoint position of maximum velocity. An alleviation factor is applied to account for variation from this empirical value

$$F_G = \frac{0.88\mu_G}{5.3 + \mu_G} \tag{A.42}$$

where $\mu_G = \begin{cases} \dfrac{2m}{\rho S_w \bar{c}_w a_{0,wb}} & \text{for vertical gust on wing} \\ \dfrac{2m\,(k_y/\Delta z_{vt})}{\rho S_{vt} \bar{c}_{vt} a_{0,vt}} & \text{for lateral gust on vertical tail} \end{cases}$

$a_{0,vt}$ lift curve slope for vertical tail fin, 1/rad
$a_{0,wb}$ lift curve slope for wing-body combination, 1/rad
k_y aircraft radius of gyration in yaw, m

The load factors applied to the aircraft at a given airspeed are subsequently calculated

$$n = 1 \pm \frac{F_G \rho_0 U_{de} V a_{0,wb}}{2(W/S)} \tag{A.43}$$

The gust envelope is consequently constructed as in Fig. A.4, which includes an overlay of gust velocity contours for a military aircraft at sea level to illustrate their effects on the shape of the envelope.

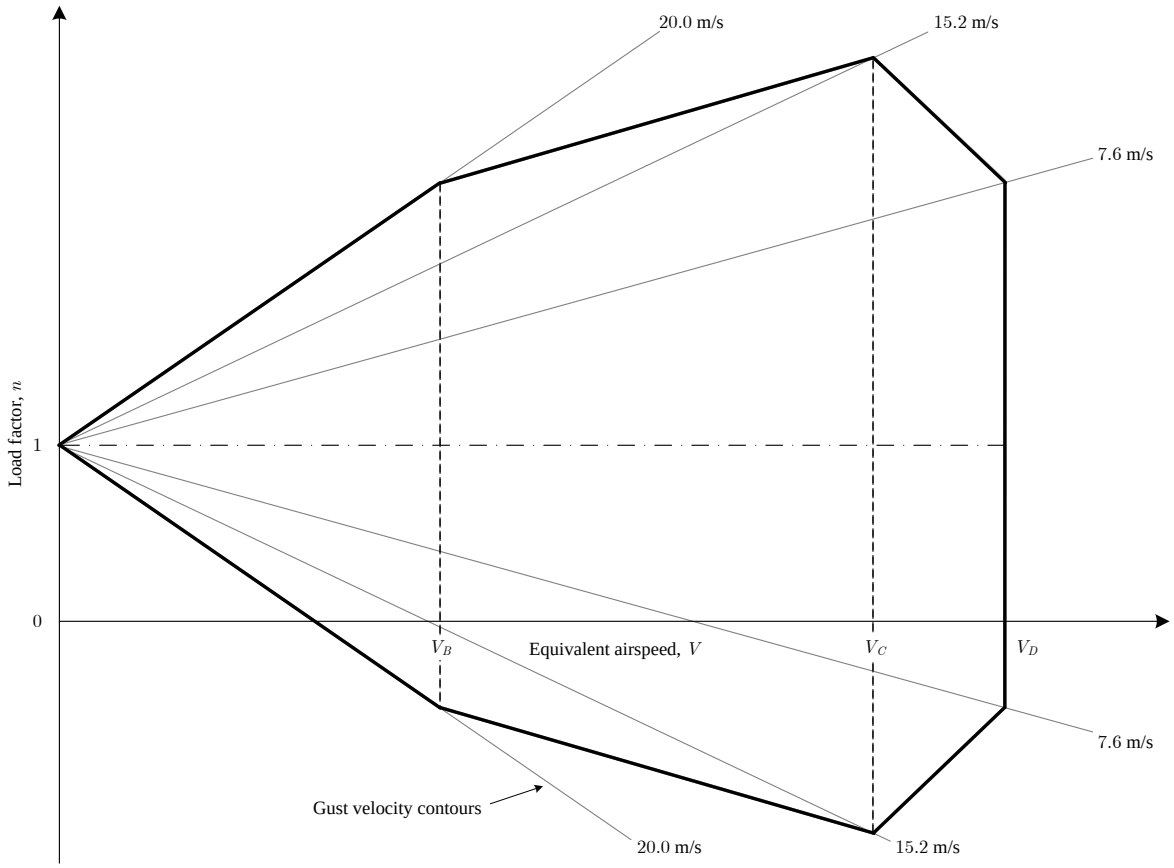

Figure A.4: Gust envelope

A.4.1.3 Flight Envelope

The flight envelope is generated through the superposition of the manoeuvre and gust envelopes to indicate the operating load requirements of the aircraft at various airspeeds. This is shown in Fig. 5.5, including the positions of the flight loads within Table A.3 on the envelope.

A.4.2 Ground Loads

Ground loads concern the conditions resulting from landing and ground manoeuvres. These loads ensure adequate design of the undercarriage supporting structure during touchdown and operation on the ground.

A.4.2.1 Landing Cases

Landing loads are determined by the vertical velocity upon touchdown, V_v. Table A.13 lists the vertical velocity as defined in the airworthiness requirements (CS-23.473, CS-25.473, Def.Stan.00-970.4.11.42).

Table A.13: Landing load vertical velocity limits

Aircraft class	Landing mass, m_L	Take-off mass, m_{TO}
Civil light	$4.4\sqrt[4]{W/S}$ ft/s (7 ft/s $< V_v <$ 10 ft/s with W/S in imperial units, lb/ft^2)	
Civil large	3.05 m/s (10 ft/s)	1.83 m/s (6 ft/s)
Military trainer	3.96 m/s (13 ft/s)	3.17 m/s (10.4 ft/s)
Military other	3.66 m/s (12 ft/s)	2.93 m/s (9.6 ft/s)

The landing loads consider two-point, i.e. main undercarriage only, and three-point, i.e. nose and main undercarriage, touchdowns. The resulting loads on the main and nose units are defined respectively as

$$R_{mu,2L} = \frac{m_L {V_v}^2}{4\eta_{mu}\delta_{mu}} \tag{A.44a}$$

$$R_{nu,2L} = \frac{2R_{mu}\left(\Delta z_{mu} + K_L \Delta y_{mu}\right)}{\sqrt{\left(\Delta z_{mu} + \Delta z_{nu}\right)\left(\Delta z_{nu} - K_L \Delta y_{nu}\right)}} \tag{A.44b}$$

$$R_{mu,3L} = \frac{m_L {V_v}^2 \left(\Delta z_{nu} - K_L \Delta y_{mu}\right)}{4\eta_{mu}\delta_{mu}\left(\Delta z_{mu} + \Delta z_{nu}\right)} \tag{A.45a}$$

$$R_{nu,3L} = \frac{m_L {V_v}^2 \left(\Delta z_{mu} + K_L \Delta y_{mu}\right)}{4\eta_{nu}\delta_{nu}\left(\Delta z_{mu} + \Delta z_{nu}\right)} \tag{A.45b}$$

where $K_L = \begin{cases} 0.25 & \text{for civil aircraft} \\ 0.4 & \text{for miliary aircraft} \end{cases}$

δ_{mu} vertical deflection of main undercarriage unit, m

δ_{nu} vertical deflection of nose undercarriage unit, m

η_{mu} nose undercarriage unit tyre and shock absorber efficiency

η_{nu} main undercarriage unit tyre and shock absorber efficiency

Table A.14 lists the loads applied in each direction for different landing cases stated in the airworthiness requirements (CS-23.485, CS-25.485, Def.Stan.00-970.4.11.38).

Table A.14: Landing load case components

Load case	Vertical load	Drag load	Inboard side load	Outboard side load
Drag load only	R	$0.25R$	0	0
Side load only:				
Civil light	$0.5R$	0	$0.5R$	$0.33R$
Civil large	$0.5R$	0	$0.8R$	$0.6R$
Military	$0.5R$	0	$0.4R$	$0.3R$
Combined drag and side load:				
Civil	$0.75R$	$0.4R$	$0.25R$	$0.25R$
Military	R	$0.4R$	$0.25R$	$0.25R$

The airworthiness requirements states that the combined drag and side load is the critical landing case (CS-25.479). Further, side loads are applied in opposing directions to the main undercarriage units.

A.4.2.2 Ground Manoeuvres

The vertical dynamic braking load on the nose undercarriage for civil large aircraft is calculated as

$$R_{nu,v} = \begin{cases} \dfrac{mg}{\Delta z_{mu} + \Delta z_{nu}} \left\{ \Delta z_{mu} + \dfrac{2\mu \Delta z_{nu} \Delta z_{mu}}{\Delta z_{mu} + \Delta z_{nu} + \mu_f \Delta y_{mu}} \right\} & \text{for civil large aircraft} \\ \dfrac{\Delta z_{mu} + 2\Delta y_{mu} \hat{R}}{\Delta z_{mu} + \Delta z_{nu}} & \text{for military aircraft} \end{cases} \tag{A.46}$$

where $\hat{R} = 0.8mg \left\{ \dfrac{\Delta z_{nu}}{\Delta z_{mu} + \Delta z_{nu}} \right\}$

For all other aircraft classes and load directions, Table A.15 lists the applied load factors as defined by the airworthiness requirements (CS-23.493, CS-23.499, CS-25.493, CS-25.507, Def.Stan.00-970. 4.13.1).

Table A.15: Undercarriage load factors under braking

	Main undercarriage		Nose undercarriage			
Aircraft class	Vertical	Drag	Vertical	Drag	Forward	Side
Civil light	1.33	1.064	2.25	1.8	0.9	1.575
Civil large	1.2 if $m = m_{TO}$ 1.0 if $m = m_L$	0.8	Eqn. (A.46)	0	0	0
Military	1.0	0.8	Eqn. (A.46)	0	0	0

Surface unevenness considers the loads on the undercarriage upon encountering a bump during ground operations. A load factor of $n = 2.0$ is applied to the undercarriage units for civil aircraft as stated in the airworthiness requirements (CS-23.473). Surface unevenness for military aircraft considers encountering a 30 cm high bump on a class A runway defined by the airworthiness requirements (Def.Stan.00-970.4.13.3). The size of the bump at a distance s along the bump profile of height h_b is

$$h_s = h_b \left\{ 1 - \cos\left(\frac{2\pi s}{l_b} \right) \right\} \tag{A.47}$$

The bump length is constrained between 0.25 m $< l_b <$ 1.25 m, whilst the bump factor is determined as follows, where $\delta_{ty,0}$ is the estimated initial tyre deflection

$$F_b = \left\{ 1 + \frac{h_s}{\delta_{ty,0}} \right\}^{1.1} \tag{A.48}$$

The resulting loads on the undercarriage units during taxi and take-off are respectively

$$R_{TAX} = F_b mg \left\{ \frac{\Delta z_{nu}}{\Delta z_{mu} + \Delta z_{nu}} - \frac{\Delta y_{mu}}{3\left(\Delta z_{mu} + \Delta z_{nu}\right)} \right\} \tag{A.49}$$

$$R_{mu,TO} = F_b mg \left\{ \frac{\Delta z_{nu}}{\Delta z_{mu} + \Delta z_{nu}} \right\} - L \tag{A.50a}$$

$$R_{nu,TO} = F_b mg + (L_{ht} - L_{\max}) \tag{A.50b}$$

where L lift force, N

L_{ht} horizontal tail lift at take-off rotation, N

Table A.16 lists the load components applied to the undercarriage units as a result of the surface uneven-

ness loads defined by Eqns. (A.49) and (A.50) (Def.Stan.00-970. 4.13.1).

Table A.16: Surface unevenness load components

	Main undercarriage			Nose undercarriage		
Ground operation	Vertical	Drag	Side	Vertical	Drag	Side
Taxi	R_{TAX}	$0.4R_{TAX}$	$0.25R_{TAX}$	R_{TAX}	$0.25R_{TAX}$	$0.25R_{TAX}$
Take-off	$R_{mu,TO}$	$0.25R_{mu,TO}$	$0.25R_{mu,TO}$	$R_{nu,TO}$	$0.25R_{nu,TO}$	$0.25R_{nu,TO}$

A.4.3 Miscellaneous Loads

Miscellaneous load cases that are not determined by flight or ground operations include:

- self-weight;
- powerplant thrust;
- cabin pressurisation.

The self-weight of the aircraft resulting from gravity is critical to ensure the aircraft can support its own mass. Powerplant thrust is also important to ensure the airframe can withstand the forces and moments created by the engines at their attachment points. Cabin pressurisation simulates the pressure of a lower altitude than the current flight level for passenger and crew comfort, causing a pressure differential between the inner and outer fuselage surfaces. Table A.17 lists the cabin altitudes at different flight levels as defined in the airworthiness requirements (CS-23.365, CS-25.365, Def.Stan.00-970.3.7.3, Def.Stan.00-970.3.7.5), where the following classifications apply for military aircraft:

- low differential pressure: short mission, fixed crew positions, using oxygen routinely;
- high differential pressure: long mission, free crew positions, not using oxygen routinely.

Table A.17: Cabin altitude

Aircraft class	Maximum simulated cabin altitude
Civil light	Flight altitude below 7,620 m (25,000 ft) 4,572 m (15,000 ft) above 7,620 m (25,000 ft)
Civil large	Flight altitude below 2,438 m (8,000 ft) 2,438 m (8,000 ft) from 2,438 m (8,000 ft) to 7,620 m (25,000 ft) 4,572 m (15,000 ft) above 7,620 m (25,000 ft)
Military	
Low differential pressure	Flight altitude at 1,500 m (4,900 ft) *increases linearly* 5,000 m (16,400 ft) at altitude of maximum pressure differential *increases linearly at constant pressure differential* 6,700 m (22,000 ft) at ceiling or maximum operational altitude
High differential pressure	1,850 m (6,060 ft) at maximum operational altitude 2,500 m (8,200 ft) at ceiling

A.4.4 Lifting Line Theory

The Kutta-Joukowski theorem states that the lift force per unit span on an aerofoil body is a function of the freestream fluid density, velocity and the circulation around the body

$$L(x) = \rho_\infty V_\infty \Gamma \tag{A.51}$$

where $L(x)$ lift force per unit span, N/m
V_∞ freestream air velocity, m/s
Γ lift circulation, m^2/s
ρ_∞ freestream air density, kg/m^3

The freestream represents a position in the fluid far upstream of the body that is not affected by the presence of the body in the fluid. Herein, the body and fluid concerned are the lifting surface and air respectively. Circulation describes a line integral of fluid velocity about a closed curve, C, in the flow

$$\Gamma = \oint_C V ds \tag{A.52}$$

A vortex is a singularity within the flow with streamlines of concentric circles about a point. Streamline vectors have constant velocity of increasing magnitude with the radial distance, r, from the point. Radial velocities are zero whilst the tangential velocities are given by considering Eqn. (A.52) as

$$V_\theta = -\frac{\Gamma}{2\pi r} \tag{A.53}$$

Similarly, the velocity potential of the vortex flow at a point at angle θ to the vortex centre is

$$\phi = -\frac{\Gamma}{2\pi}\theta \tag{A.54}$$

The circulation around the body is found by considering a vortex bound between the limits of the lifting surface span. This vortex is represented as a horseshoe vortex by assuming that it continues as a free vortex trailing to infinity at either end of the body. This is a requirement of Helmhotz's theorem that a vortex possesses constant strength along its length and either extends to the fluid boundaries or forms a closed path. The resulting substitution is illustrated in Fig. A.5(a), however does not accurately simulate the distribution of downwash, i.e. the downward vertical velocity component induced by the vortex, as downwash tends to infinity towards the tips. Hence, many horseshoe vortices are superimposed along the span such that they are coincident along the spanwise lifting line as shown in Fig. A.5(b).

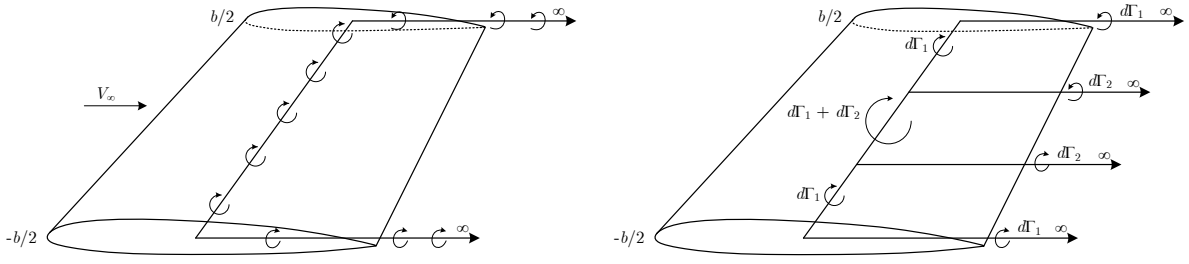

(a) Lifting surface as single horseshoe vortex (b) Lifting surface as multiple horseshoe vortices

Figure A.5: Finite lifting body with horseshoe vortices

The downwash induced at a spanwise position point is the sum of the velocities induced by infinitesimally small segments of the lifting line. These velocities are found using the Biot-Savart law which states that the velocity induced by a segment of a the vortex line $\vec{dl}$ at a point at radius r from the segment is

$$d\vec{V} = \frac{\Gamma}{4\pi}\frac{\vec{dl} \times \vec{r}}{|\vec{r}|^3} \tag{A.55}$$

This lead to the derivation of the downwash at a position x along the span

$$w(x_0) = -\frac{1}{4\pi}\int_{-b/2}^{b/2} \frac{d\Gamma/dx}{x_0 - x}\, dx \tag{A.56}$$

where w downwash velocity, m/s
x_0 lifting surface root spanwise position, m

The effects of downwash on the lifting surface in the freestream include induced drag and an induced angle-of-attack (AoA) of the aerofoil lifting body to the freestream, the latter of which is calculated as follows assuming the downwash to be much smaller than the freestream velocity, i.e. a small AoA

$$\alpha_i(x_0) = -\frac{w(x_0)}{V_\infty} \tag{A.57}$$

The induced AoA is expressed in terms of circulation through substitution of Eqn. (A.56) into (A.57)

$$\alpha_i(x_0) = \frac{1}{4\pi V_\infty}\int_{-b/2}^{b/2} \frac{d\Gamma/dx}{x_0 - x}\, dx \tag{A.58}$$

The effective AoA, $\alpha_e(x_0)$, representing the angle of the aerofoil relative to the freestream direction is calculated with consideration for the aerofoil lift coefficient

$$C_L(x) = a_0(x)\left\{\alpha_e(x_0) - \alpha_0\right\} \tag{A.59}$$

where a_0 aerofoil lift curve slope, 1/rad
α_0 zero-lift AoA, rad

Thin aerofoil theory replaces a_0 with 2π whilst α_0 is assumed to be known for a given lifting surface of chord length c. Further, the aerofoil lift per unit span is expressed as

$$L(x) = \frac{1}{2}C_L(x)\rho_\infty V_\infty^2 c(x_0) \tag{A.60}$$

Therefore, Eqn. (A.59) is rearranged using the Kutta-Joukowski theorem and Eqn. (A.60) as

$$\alpha_e(x_0) = \frac{\Gamma(x_0)}{\pi V_\infty c(x_0)} + \alpha_0 \tag{A.61}$$

This leads to the fundamental equation of lifting line theory, stating that the AoA of an aerofoil in a freestream is the sum of the effective and induced AoAs in terms of the circulation around the body

$$\alpha(x_0) = \frac{1}{4\pi V_\infty}\int_{-b/2}^{b/2} \frac{d\Gamma/dx}{x_0 - x}\, dx + \frac{\Gamma(x_0)}{\pi V_\infty c(x_0)} + \alpha_0 \tag{A.62}$$

By solving Eqn. (A.62) across the lifting surface span, key aerodynamic characteristics of finite wings are established including the lift coefficient and, through inspection, the induced drag coefficient respectively

$$C_L = \frac{2}{V_\infty S}\int_{-b/2}^{b/2} \Gamma(x)\, dx \tag{A.63a}$$

$$C_{D,i} = \frac{2}{V_\infty S}\int_{-b/2}^{b/2} \Gamma(x)\alpha_i(x)\, dx \tag{A.63b}$$

A.4.5 Schrenk Approximation

The elliptical load distribution over a lifting surface span, and therefore circulation distribution given the Kutta-Joukowski theorem of Eqn. (A.51), is calculated by considering the load at a spanwise position x

$$L(x) = \rho_\infty V_\infty \Gamma_0 \sqrt{1 - \frac{2x}{b}^2} \tag{A.64}$$

where Γ_0 denotes the root circulation. This distribution has constant downwash and induced AoA across the span and zero load at the tips using lifting line theory. Hence, the induced drag coefficient of the distribution is derived as

$$C_{D,i} = \frac{C_L^2}{\pi \delta \mathcal{AR}} \tag{A.65}$$

where δ expresses the summation of the coefficients of a Fourier sine series, $A_1, A_2, \ldots, A_n$, used to implement the lifting line theory for a general distribution

$$\delta = \sum_{i=2}^{n} i \left\{ \frac{A_i}{A_1} \right\}^2$$

An elliptical load distribution yields minimum induced drag because $\delta = 0$ and thus represents the ideal load distribution over a lifting surface. Lifting surfaces rarely possess such a planform due to the inherently high manufacturing costs, whereas rectangular planforms are cheaper to produce but generate a poor load distribution. Therefore, the lifting surface planform is traditionally trapezoidal to provide a compromise between cost and appropriate load distribution.

A common approximation of the load distribution, presented in Schrenk (1940), considers the distribution of an unswept non-elliptical surface of moderate to high aspect ratio as the mean of that for an elliptical planform and the actual lifting surface planform. For a trapezoidal planform, such a load distribution is calculated as follows

$$L(x)_a = \frac{1}{2} \left\{ L(x)_e + L(x)_t \right\} \tag{A.66}$$

where
$$L(x)_e = \frac{4L}{\pi b} \sqrt{1 - \frac{2x}{b}^2} \quad \text{for elliptical planform}$$
$$L(x)_t = \frac{2L}{b\,(1+\lambda)} \sqrt{1 - \frac{2x}{b}\,(1-\lambda)} \quad \text{for trapezoidal planform}$$

The load distribution represented by Eqn. (A.66) can be plotted over the semi-span of a lifting surface as shown in Fig. A.6. This approximation does not account for the effect of lifting surface twist on the spanwise load. A twisted surface generates zero net lift, therefore equilibrium is obtained with a positive load close to the root and a negative load outboard of this position. This effect is accounted for by

$$L(x)_b = \frac{1}{4} \left\{ \rho_\infty V_\infty^2 a_0(x) \left(\alpha_0 + \varepsilon(x) \right) \right\} \tag{A.67}$$

where ε represents the angle of twist of the section relative to section zero-lift line. The total load distribution is the sum of the distributions calculated in Eqns. (A.66) and (A.67) at each spanwise location along the lifting surface

$$L(x) = L(x)_a + L(x)_b \tag{A.68}$$

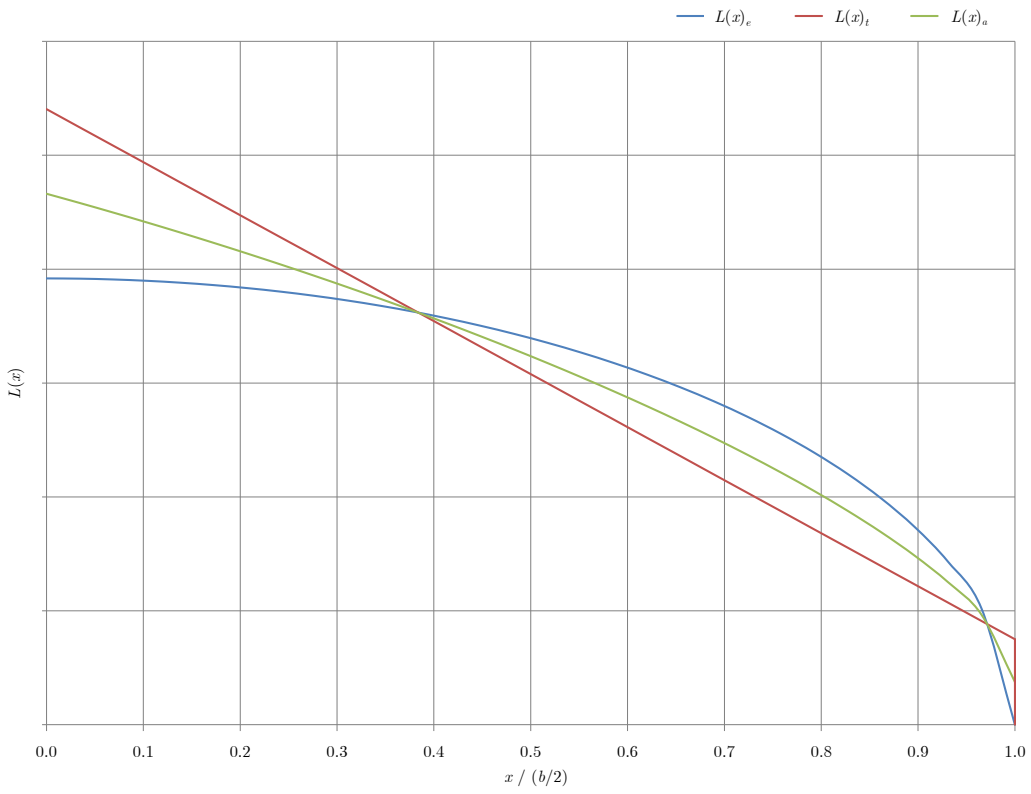

Figure A.6: Schrenk approximation of spanwise load distribution

A.4.6 Vortex Panel Method

The vortex panel method considers a body surface as a streamline of the flow by covering the surface with a sheet of vortices. This streamline is determined by discretising the surface into a series of panels of constant vortex strength per unit length. The vortex strengths are found by constructing a sheet of infinitesimally small vortices of strength γ over the surface, such that the circulation over the sheet is

$$\Gamma = \int_j \gamma_j \, ds_j \tag{A.69}$$

The strengths of vortices are evaluated by the change in the tangential flow velocity on crossing the sheet

$$\gamma = \frac{dV}{dn} \tag{A.70}$$

A vortex sheet of two-dimensional panels represents the flow over the surface as in Fig. A.7, with boundary points at the joints between panels and control points at the midpoint of each panel. The velocity potential induced at an arbitrary point, $P(z, y)$, within the flow at a known distance from the jth panel is derived using Eqns. (A.54) and (A.69)

$$\Delta\phi_j = -\frac{1}{2\pi} \int_j \theta_{pj} \gamma_j \, ds_j \tag{A.71}$$

where $\theta_{pj} = \tan^{-1} \dfrac{y - y_j}{z - z_j}$

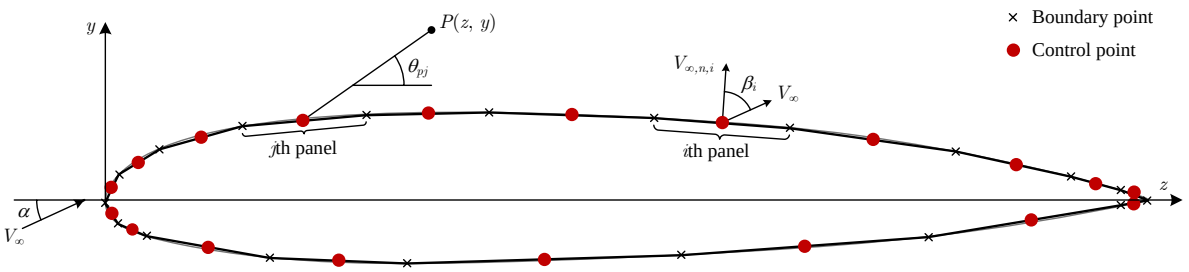

Figure A.7: Two-dimensional panel distribution

The total velocity potential induced at P is determined by applying Eqn. (A.71) to all n_p panels. Hence, the velocity potential induced by all panels at the ith panel control point is calculated as

$$\phi(z_i, y_i) = -\sum_{j=1}^{n_p} \frac{\gamma_j}{2\pi} \int_j \theta_{ij}\, ds_j \tag{A.72}$$

where (x_i, y_i) represents the coordinates of the ith panel control point. The normal component of velocity induced at the control point is

$$V_{n,i} = \frac{\partial}{\partial n_i} \phi(z_i, y_i) \tag{A.73}$$

Similarly, the normal component of the freestream velocity may be determined using Fig. A.7 as

$$V_{\infty,n,i} = V_\infty \cos \beta_i \tag{A.74}$$

where β_i is the angle between freestream velocity and vector normal to panel directed away from body. Boundary conditions dictate that the velocity normal to a control point must be zero, i.e. $V_n + V_{\infty,n} = 0$. This leads to the derivation of the principal equation of the vortex panel method

$$V_\infty \cos \beta_i - \sum_{j=1}^{n_p} \frac{\gamma_j}{2\pi} \int_j \frac{\partial \theta_{ij}}{\partial n}\, ds_j = 0 \tag{A.75}$$

Subsequently, a linear algebraic equation for the boundary condition of the flow at the ith panel control point is obtained containing n_p unknowns of γ. A system of n_p simultaneous linear equations with n_p unknowns is subsequently obtained by considering Eqn. (A.75) for all panels. However, an infinite number of potential flow solutions exist for an aerofoil at a given AoA leading to infinite theoretical circulations about the aerofoil. Prandtl and Tietjens (1934) showed that the flow over an aerofoil develops over a transient period, leading to the aftward movement of the stagnation point along the upper aerofoil surface. The flow then settles such that a smooth flow exists over both aerofoil surfaces at the trailing edge. The requirement for smooth flow over the trailing edge of the aerofoil is known as the Kutta condition and must be satisfied when calculating potential flow over an aerofoil

$$\begin{aligned} V_u = V_l = 0 \;\; &\text{for finite-angle trailing edge} \\ V_u = V_l \neq 0 \;\; &\text{for cusped trailing edge} \end{aligned} \tag{A.76}$$

where V_l flow velocity at trailing edge of lower aerofoil surface, m/s
V_u flow velocity at trailing edge of upper aerofoil surface, m/s

The strength of the vortex at the aerofoil trailing edge must, therefore, equal zero. To satisfy this

boundary condition, the strengths of the vortices on the panels closest to the trailing edge on the upper and lower aerofoil surfaces must be equal and opposite. However, the inclusion of this condition within the vortex panel problem results in an overdetermined system of $n_p + 1$ equations and n_p unknowns. Therefore, one control point is ignored to reduce the number of equations to n_p. The aerofoil leading and trailing edges are critical to the flow and are thus modelled by a large number of small panels, whilst panels of equal length are placed at the trailing edge for consideration of the Kutta condition. Hence, the control point of the panel midway along the lower aerofoil surface is the one neglected such that the solution to the series of equations is found by Gaussian elimination, the procedure for which is described in Appendix B.4.1 through its use during finite element analysis (FEA).

Having obtained the vortex strengths of each panel, the surface is considered as a streamline of the flow satisfying the Kutta condition. This first-order approach assumes constant vortex strength over each panel. The flow velocity tangential to the vortex sheet is then calculated using Eqn. (A.70). The pressure distribution around the section is subsequently found by recalling Eqn. (A.69), leading to the calculation of chordwise load distribution using the Kutta-Joukowski theorem, Eqn. (A.51).

A.5 Sectional Properties

The cross-sectional area defines the size of the surface enclosed by the member section

$$A = \int_S dS \tag{A.77}$$

The centroid represents the geometric centre of the section through which all loads are assumed to act for a section of uniform density, i.e. the centre of mass, formed of n partitions

$$\bar{y} = \frac{\sum_{i=1}^{n} \overline{y_i} A_i}{\sum_{i=1}^{n} A_i} \tag{A.78a}$$

$$\bar{z} = \frac{\sum_{i=1}^{n} \overline{z_i} A_i}{\sum_{i=1}^{n} A_i} \tag{A.78b}$$

where the local coordinate system herein defines the cross-section of the zy-plane with the x-axis denoting the out-of-plane axial direction. The second moments of area determine the resistance of the section to deflection and bending about the cross-sectional axes, with the product second moment of area defining such resistance in directions other than that of the applied load, which is of notable significance for asymmetric cross-sections

$$I_{zz} = \iint_A y^2 \, dz \, dy \tag{A.79a}$$

$$I_{yy} = \iint_A z^2 \, dy \, dz \tag{A.79b}$$

$$I_{zy} = \iint_A zy \, dz \, dy \tag{A.79c}$$

These expressions can be rewritten with knowledge of the cross-sectional shape, e.g. for a rectangular section of breadth b and depth d the above formulae become

$$A = bd \tag{A.80a}$$

$$\bar{y} = \frac{d}{2} \tag{A.80b}$$

$$\bar{z} = \frac{b}{2} \tag{A.80c}$$

$$I_{yy} = \frac{b^3 d}{12} \tag{A.80d}$$

$$I_{zz} = \frac{b d^3}{12} \tag{A.80e}$$

$$I_{zy} = \bar{z}\bar{y}A \tag{A.80f}$$

Equation (A.79) assumes that the axes about which the second moment of areas are defined pass through the centroid of the section. The parallel axis theorem is employed when this is not the case to calculate the moment about a datum axis given the section second moment of area about a parallel axis

$$I_{yy} = \frac{b^3 d}{12} + A(\Delta\bar{z})^2 \tag{A.81a}$$

$$I_{zz} = \frac{b d^3}{12} + A(\Delta\bar{y})^2 \tag{A.81b}$$

where $\Delta\bar{y}$ perpendicular distance between parallel axes in y-direction
$\Delta\bar{z}$ perpendicular distance between parallel axes in z-direction

The torsion constant defines the section resistance to torsion, e.g. for a rectangular section

$$J = \frac{1}{3}\left\{\min(b,d)^3 \cdot \max(b,d)\right\} \tag{A.82}$$

The torsion constant reduces to polar second moment of area for a square or cylindrical section

$$I_{xx} = I_{yy} + I_{zz} \tag{A.83}$$

Table A.18 lists the equations used to calculation the sectional properties of the aircraft member cross-sections. The product second moment of area and torsion constant are found by using Eqns. (A.79c) and (A.82) respectively to sum the values for the rectangular sub-sections, i.e. flanges and web, within the airframe member cross-sections.

For members rotated axially by an anticlockwise angle γ with respect to a given coordinate system, the second moments of areas are revised as

$$I_{yy}{}' = \frac{I_{yy} + I_{zz}}{2} - \frac{I_{zz} - I_{yy}}{2}\cos(2\gamma) + I_{zy}\sin(2\gamma) \tag{A.84a}$$

$$I_{zz}{}' = \frac{I_{yy} + I_{zz}}{2} + \frac{I_{zz} - I_{yy}}{2}\cos(2\gamma) - I_{zy}\sin(2\gamma) \tag{A.84b}$$

$$I_{zy}{}' = \frac{I_{zz} - I_{yy}}{2}\sin(2\gamma) + I_{zy}\cos(2\gamma) \tag{A.84c}$$

It should be noted that, for simplicity, the symbols I_{yy}, I_{zz} and I_{zy} are used throughout this document to denote the second moments of area whether or not the section is submitted to an axial rotation.

Table A.18: Properties of common member cross-sections

Cross-section	Formulae for sectional properties
C-section 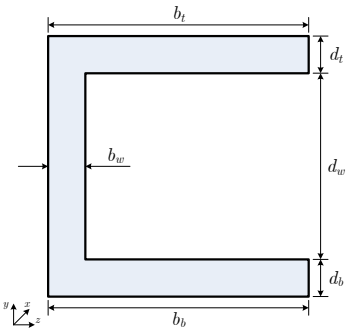	$A = b_b d_b + b_w d_w + b_t d_t$ $\bar{y} = \frac{1}{2A}\left\{b_b d_b^2 + b_w d_w\left[2d_b + d_w\right] + b_t d_t\left[2\left(d_b + d_w\right) + d_t\right]\right\}$ $\bar{z} = \frac{1}{2A}\left\{b_b^2 d_b + b_w^2 d_w + b_t^2 d_t\right\}$ $I_{yy} = \frac{1}{12}\left\{b_b^3 d_b + b_w^3 d_w + b_t^3 d_t\right\} + b_b d_b\left\{\frac{b_b}{2} - \bar{z}\right\}^2 + b_w d_w\left\{\frac{b_w}{2} - \bar{z}\right\}^2 + b_t d_t\left\{\frac{b_t}{2} - \bar{z}\right\}^2$ $I_{zz} = \frac{1}{12}\left\{b_b d_b^3 + b_w d_w^3 + b_t d_t^3\right\} + b_b d_b\left\{\frac{d_b}{2} - \bar{y}\right\}^2 + b_w d_w\left\{d_b + \frac{d_w}{2} - \bar{y}\right\}^2 + b_t d_t\left\{d_b + d_w + \frac{d_t}{2} - \bar{y}\right\}^2$
I-section 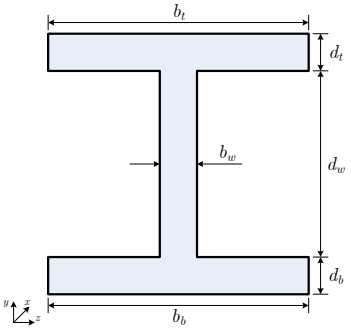	$A = b_b d_b + b_w d_w + b_t d_t$ $\bar{y} = \frac{1}{2A}\left\{b_b d_b^2 + b_w d_w\left[2d_b + d_w\right] + b_t d_t\left[2\left(d_b + d_w\right) + d_t\right]\right\}$ $\bar{z} = \frac{b_b}{2}$ $I_{yy} = \frac{1}{12}\left\{b_b^3 d_b + b_w^3 d_w + b_t^3 d_t\right\} + A\left\{\frac{b_b}{2} - \bar{z}\right\}^2$ $I_{zz} = \frac{1}{12}\left\{b_b d_b^3 + b_w d_w^3 + b_t d_t^3\right\} + b_b d_b\left\{\frac{d_b}{2} - \bar{y}\right\}^2 + b_w d_w\left\{d_b + \frac{d_w}{2} - \bar{y}\right\}^2 + b_t d_t\left\{d_b + d_w + \frac{d_t}{2} - \bar{y}\right\}^2$
T-section 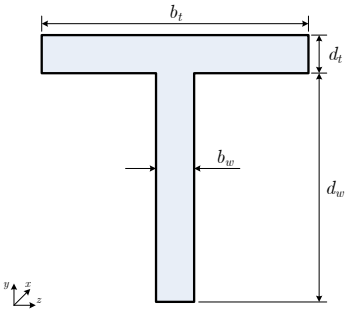	$A = b_w d_w + b_t d_t$ $\bar{y} = \frac{1}{2A}\left\{b_w d_w^2 + b_t d_t\left[2d_w + d_t\right]\right\}$ $\bar{z} = \frac{b_t}{2}$ $I_{yy} = \frac{1}{12}\left\{b_w^3 d_w + b_t^3 d_t\right\} + A\left\{\frac{b_t}{2} - \bar{z}\right\}^2$ $I_{zz} = \frac{1}{12}\left\{b_w d_w^3 + b_t d_t^3\right\} + b_w d_w\left\{\frac{d_w}{2} - \bar{y}\right\}^2 + b_t d_t\left\{d_w + \frac{d_t}{2} - \bar{y}\right\}^2$
Z-section 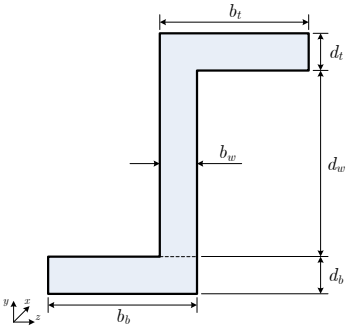	$A = b_b d_b + b_w d_w + b_t d_t$ $\bar{y} = \frac{1}{2A}\left\{b_b d_b^2 + b_w d_w\left[2d_b + d_w\right] + b_t d_t\left[2\left(d_b + d_w\right) + d_t\right]\right\}$ $\bar{z} = \frac{1}{2A}\left\{b_b^2 d_b + b_w d_w\left[2b_b + b_w\right] + b_t d_t\left[2\left(b_b + b_w\right) + b_t\right]\right\}$ $I_{yy} = \frac{1}{12}\left\{b_b^3 d_b + b_w^3 d_w + b_t^3 d_t\right\} + b_b d_b\left\{\frac{b_b}{2} - \bar{z}\right\}^2 + b_w d_w\left\{b_b - \frac{b_w}{2} - \bar{z}\right\}^2 + b_t d_t\left\{b_b - b_w + \frac{b_t}{2} - \bar{z}\right\}^2$ $I_{zz} = \frac{1}{12}\left\{b_b d_b^3 + b_w d_w^3 + b_t d_t^3\right\} + b_b d_b\left\{\frac{d_b}{2} - \bar{y}\right\}^2 + b_w d_w\left\{d_b + \frac{d_w}{2} - \bar{y}\right\}^2 + b_t d_t\left\{d_b + d_w + \frac{d_t}{2} - \bar{y}\right\}^2$

A.6 Stress Analysis

Stress analysis is performed given the forces and moments within a structural member. Analysis herein considers the stress within a member as calculated by the stress tenor as well as when subjected to compressive forces that could lead to buckling and the bending of simply-supported beams.

A.6.1 Stress Tensor

The stress field at locations within a member is calculated given the forces and moments within the member. This ia accomplished through consideration of the member direct, i.e. normal, and shear, i.e. tangential, stresses; as shown for an arbitrary parallelepiped in Fig. A.8.

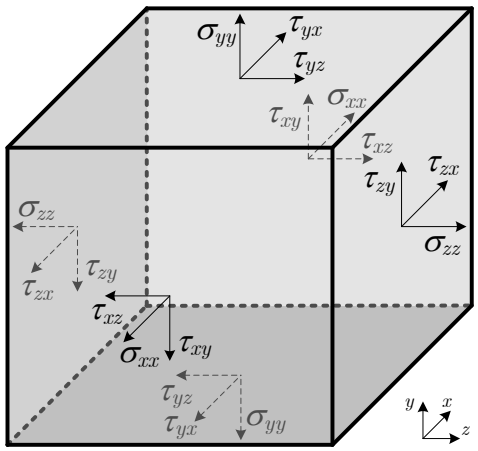

Figure A.8: Stress components of parallelepiped

Sign convention for normal stresses dictate tensile stresses as positive and compressive stresses as negative. The components of stress illustrated above may be presented in matrix form as the stress tensor

$$[\sigma] = \begin{bmatrix} \sigma_{xx} & \tau_{xy} & \tau_{xz} \\ \tau_{yx} & \sigma_{yy} & \tau_{yz} \\ \tau_{zx} & \tau_{zy} & \sigma_{zz} \end{bmatrix} \tag{A.85}$$

where σ normal stress, Pa
τ shear stress, Pa

Opposing shear stresses, e.g. τ_{xy} and τ_{yx}, are assumed to be of equal magnitude to satisfy equilibrium, i.e. complimentary shear stresses; therefore the stress tensor becomes symmetric and is expressed as

$$\{\sigma\} = \begin{Bmatrix} \sigma_{xx} & \sigma_{yy} & \sigma_{zz} & \tau_{xz} & \tau_{yz} & \tau_{zx} \end{Bmatrix}^T \tag{A.86}$$

The components of the stress tensor are calculated using well-established formulae for the stress within members of different cross-sections. The tensile or compressive stress, σ_{xx}, considers the force normal to the member cross-section. The fibre stresses, σ_{yy} and σ_{zz}, consider the bending moments at an evaluation point on the cross-section using bending theory. The transverse shear stresses, τ_{xy} and τ_{zx}, consider the shear flows within shear sections bounded between the evaluation point and the member cross-section. A shear section, A_j, represents the area between the evaluation point and the closest section boundary in the corresponding direction of shear. Torsional shear stress, τ_{yz}, is estimated at the evaluation point on the member cross-section using the torsion constant in Eqn. (A.82) and the minimum thickness in either direction at the point. Table A.19 gives the expressions used to calculate the stress components at an

arbitrary evaluation point i on the cross-section of an I-section member.

Table A.19: Stress tensor components at points on I-section

Axial stress	Torsional stress
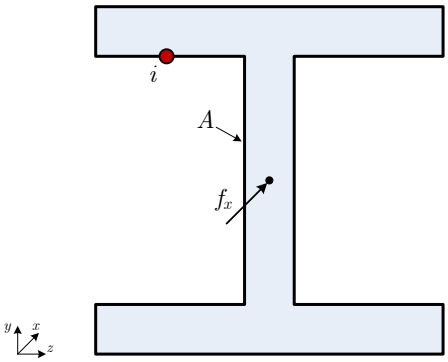	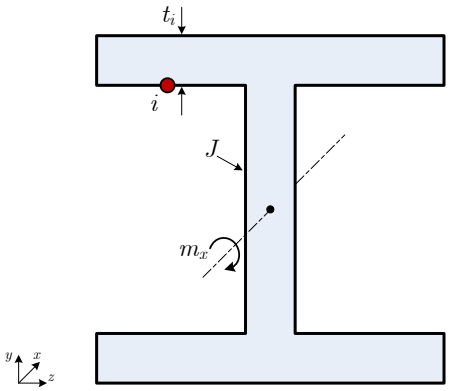
$\sigma_{xx} = \frac{f_x}{A}$	$\tau_{yz} = \frac{m_x t_i}{J}$ where $t_i = d_t$
Bending stress	**Shear stress**
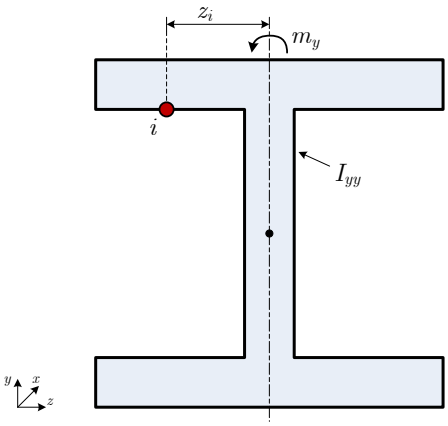	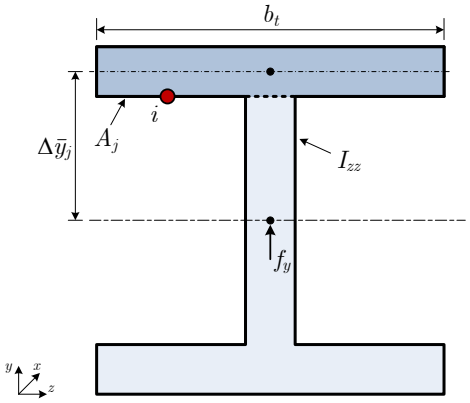
$\sigma_{yy} = \frac{m_y z_i}{I_{yy}}$	$\tau_{xy} = \frac{f_y}{t_i I_{zz}} \sum_{j=1}^{n} A_j \Delta\bar{y}_j$ where $t_i = b_t$
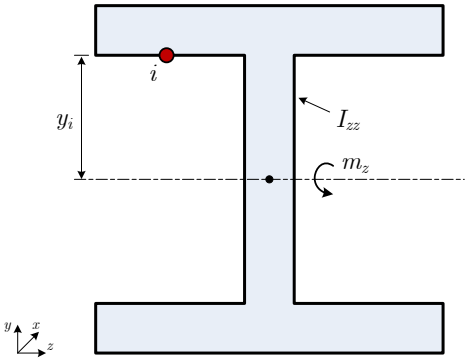	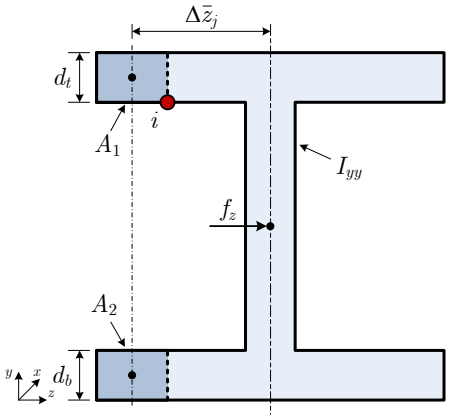
$\sigma_{zz} = \frac{m_z y_i}{I_{zz}}$	$\tau_{zx} = \frac{f_z}{t_i I_{yy}} \sum_{j=1}^{n} A_j \Delta\bar{z}_j$ where $t_i = d_b + d_t$

Similar expressions to those in Table A.19 are used for members with C, T and Z-sections. The principal stresses, σ_1, σ_2 and σ_3, at each point are calculated as the eigenvalues of the stress tensor, from which the factor of safety (FoS) under yield as defined by the von Mises criterion is calculated as

$$n_{VM} = \frac{\sigma_y}{\sqrt{\frac{1}{2}\left[(\sigma_1 - \sigma_2)^2 + (\sigma_2 - \sigma_3)^2 + (\sigma_3 - \sigma_1)^2\right]}} \tag{A.87}$$

A.6.2 Beam Buckling

The Euler buckling load of a pin-ended strut at the onset of the first buckling mode is given by

$$f_E = \frac{\pi^2 EI}{l^2} \tag{A.88}$$

The following assumptions are made when considering the Euler buckling load:

- perfectly straight strut of uniform cross-section throughout its length and linear elastic material;
- perfectly axial load, i.e. without any lateral eccentricity;
- lateral deflections small relative to strut length with no axial shortening during load application.

For situations where a strut is not pinned at both ends, the effective length of the member, kl, defines the required length of a pin-ended strut for it to buckle under the same load as the strut with its end conditions. Typical effective lengths determined by the strut end conditions include:

- both ends pinned: l;
- both ends fixed: $0.5l$;
- one end pinned, other end free: $0.7l$;
- one end fixed, other end free: $2l$.

This leads to the calculation of the critical buckling load as

$$f_{cr} = \frac{\pi^2 EI_{zz}}{(kl)^2} \tag{A.89}$$

The critical buckling stress as a result of this buckling load is given by

$$\sigma_{cr} = \frac{f_{cr}}{A} \tag{A.90}$$

The resulting FoS against an axial compressive stress is calculated as

$$n_E = \frac{\sigma_{cr}}{\sigma_{xx}} \tag{A.91}$$

A.6.3 Beam Bending

The maximum bending stress within a simply-supported beam under a vertical uniformly-distributed load is given as follows at the maximum fibre position in the minor axis, y

$$\sigma_b = \frac{\omega l y_{\max}}{8 I_{zz}} \tag{A.92}$$

where ω uniformly-distributed load, N/m

Therefore, the FoS against yield under this beam bending stress is

$$n_b = \frac{\sigma_y}{\sigma_b} \tag{A.93}$$

Nomenclature

The principal nomenclature used within this appendix is given below. Symbols i, j and k are employed as arbitrary counters within formulae. Subscripts w, ht, vt, f, mu, nu and e are used throughout, most notably in Appendix A.3.2, to associate a property with the wing, horizontal tail, vertical tail, fuselage, main undercarriage, nose undercarriage and engine respectively.

A	cross-sectional area, m^2
a_0	aerofoil lift curve slope, 1/rad
$a_{0,vt}$	lift curve slope for vertical tail fin, 1/rad
$a_{0,wb}$	lift curve slope for wing-body combination, 1/rad
b	breadth, m
b	span, m
b_b	base flange breadth, m
b_t	top flange breadth, m
b_w	web breadth, m
$C_{D,0}$	zero-lift drag coefficient
$C_{D,i}$	induced drag coefficient
C_j	jet engine specific fuel consumption, mg/Ns
C_L	lift coefficient
$C_{L,\alpha}$	lift coefficient per incidence
$C_{l,\alpha}$	lift curve slope
C_p	propeller engine specific fuel consumption, mg/J
c	chord length, m
$\bar{c}$	mean aerodynamic chord length, m
c_r	root chord length, m
c_t	tip chord length, m
d	depth, m
d_b	base flange depth, m
d_e	engine nacelle diameter, m
d_f	fuselage diameter, m
d_t	top flange depth, m
d_w	web depth, m
e	Oswald efficiency number
F	model fidelity level
F_b	bump factor
F_G	gust alleviation factor
f_{cr}	critical buckling load, N
f_E	Euler buckling load, N

f_x, f_y, f_z	force parallel to x, y, z-axis, N
h_b	bump height, m
h_s	bump size, m
h_{sc}	screen height, m
h_{tr}	transition height, m
I_{xx}	polar second moment of area about x-axis, m^4
I_{yy}, I_{zz}	second moment of area about minor y, major z-axis, m^4
I_{zy}	product moment of area in zy-plane, m^4
J	torsion constant, m^4
k	drag-due-to-lift factor
k_y	aircraft radius of gyration in yaw, m
L	lift force, N
L1,...,11	load case ID
$L(x)$	lift force per unit span, N/m
(L/D)	lift-to-drag ratio
l	length, m
l_b	bump length, m
l_c	cabin length, m
l_e	engine nacelle length, m
l_f	fuselage length, m
l_{fd}	flight deck length, m
l_G	gradient length of gust, m
l_{ht}, l_{vt}	horizontal, vertical tail arm, m
l_{mu}, l_{nu}	main, nose undercarriage unit length, m
(l/d)	fuselage fineness ratio
M	mass fraction
M_C	cruise Mach number
m	mass, kg
m_0	ramp mass, kg
m_D	disposable mass, kg
m_E	empty aircraft mass, kg
m_F	fuel mass, kg
m_L	landing mass, kg
m_{TFO}	trapped fuel and oil mass, kg
m_{TO}	take-off mass, kg
m_x, m_y, m_z	moment about x, y, z-axis, Nm
n	normal acceleration load factor
n_b	FoS against yield under beam bending stress
n_E	FoS against critical Euler buckling stress
n_e	number of engines
n_m	number of mission stages

n_p	number of panels
n_s	number of seats
n_{ss}	number of shock struts
$n_{s,r}$	number of seats per row
n_{VM}	FoS against yield with respect to von Mises criterion
n_w	number of wheels
$(\hat{P}/W)$	peak power-to-weight ratio
p_s	seat pitch, m
R	ground load, N
R	range of mission stage, m
r	radial distance, m
r_n	nose radius, m
S	reference surface area, m^2
S_f	fuselage wetted surface area, m^2
s	distance along profile, m
s_a	approach distance, m
s_{BFL}	balanced field length, m
s_c	climb distance, m
s_{fl}	flare distance, m
s_g	ground roll distance, m
s_{tr}	transition distance, m
T	loiter duration, s
T_e	engine thrust, N
T_{pr}	pilot reaction time, s
$(\hat{T}/W)$	peak thrust-to-weight ratio
$(\overline{T}/W)$	mean thrust-to-weight ratio
t	thickness, m
(t/c)	thickness-to-chord ratio
U	discrete gust velocity, m/s
U_{de}	discrete gust design velocity, m/s
V	airspeed, kts
V_1	decision speed, m/s
V_2	take-off safety speed, m/s
V_A	manoeuvre speed, kts
V_B	maximum gust velocity speed, kts
V_C	cruise speed, kts
V_{CO}	cut-off speed, m/s
V_D	design diving speed, kts
V_n	normal velocity, m/s
V_R	rotation speed, m/s
V_s	stall speed, m/s
V_v	vertical velocity, m/s

V_θ	tangential velocity, m/s
V_∞	freestream air velocity, m/s
v_f	fuselage volume, m^3
v_{ft}	fuel tank volume, m^3
(W/S)	wing loading coefficient, N/m^2
w	downwash velocity, m/s
$w_{f,ht}$	fuselage width at horizontal tail, ft
x	position in x-direction, m
y	position in y-direction, m
$\bar{y}$	centroid position in y-direction, m
z	position in z-direction, m
$\bar{z}$	centroid position in z-direction, m
z_{CoG}	aircraft CoG position in longitudinal z-direction, m
z_{NS}	aircraft neutral stability position in longitudinal z-direction, m
z_{θ_b}	fuselage tail base taper position in longitudinal z-direction, m
z_{θ_s}	fuselage tail side taper position in longitudinal z-direction, m
α	Newmark-β direct integration method constant
α_0	zero-lift AoA, rad
α_e	effective AoA, rad
α_i	induced AoA, rad
β	angle between freestream and vector normal to surface, rad
β	Newmark-β direct integration method constant
Γ	lift circulation, m^2/s
γ	rotation, rad
γ	vortex strength, m/s
γ_c	climb angle, rad
ΔP	cabin differential pressure, Pa
Δy, Δz	distance to CoG in y, z-direction, m
$\Delta\bar{y}$, $\Delta\bar{z}$	perpendicular distance between parallel axis in y, z-direction, m
δ_{mu}, δ_{nu}	vertical deflection of main, nose undercarriage unit, m
$\delta_{ty,0}$	initial tyre deflection from bump in runway, m
$\frac{\partial\varepsilon}{\partial\alpha}$	downwash derivative
ε	lifting surface twist, rad
η_{ht}	horizontal tail relative dynamic pressure
η_{mu}, η_{nu}	main, nose undercarriage unit tyre and shock absorber efficiency
η_p	propeller efficiency

θ	angle between vectors, rad
θ	Wilson-θ direct integration method constant
θ_b	fuselage tail base taper, rad
θ_s	fuselage tail side taper, rad
$\Lambda_{c/4}$	quarter-chord sweep, rad
Λ_{LE}	leading edge sweep, rad
λ	taper ratio
μ_f	rolling friction coefficient
ρ_0	sea level air density, kg/m^3
ρ_a	aerodrome altitude air density, kg/m^3
ρ_C	cruise altitude air density, kg/m^3
ρ_∞	freestream air density, kg/m^3
σ_1, σ_2, σ_3	first, second, third principal stress, Pa
σ_b	bending stress, Pa
σ_{cr}	critical buckling stress, Pa
σ_{xx}, σ_{yy}, σ_{zz}	normal stress parallel to x, y, z-axis, Pa
σ_y	yield stress, Pa
τ_{xy}, τ_{yz}, τ_{zx}	shear stress in xy, yz, zx-plane, Pa
ϕ	velocity potential, m/s
ω	uniformly-distributed load, N/m
$\mathcal{AR}$	aspect ratio

Appendix B

Finite Element Analysis

This appendix provides an overview of finite element analysis (FEA) as applied within the framework to perform structural analysis of an individual airframe design in order to establish its feasibility with respect to the design constraints. Principal resources supporting this theory include Benham et al. (1996), Coates et al. (1988), Cook (1995), Craig and Kurdila (2011), McGuire et al. (1999), Press et al. (2002), Rao (1989), Rao (2004), Süli and Mayer (2003) and Young et al. (2012). The nomenclature used to describe this theory is listed at the end of this appendix.

B.1 Problem Formulation

The response of a system, as represented by a finite element (FE) model, to a static or dynamic load is determined by satisfying the equation of motion (EoM) for equilibrium of the system. The system response to a static excitation load is found using the direct stiffness method to solve the following EoM of a linear system

$$\{f\} = [K]\{d\} \tag{B.1}$$

where $[K]$ stiffness matrix
$\{d\}$ displacement vector
$\{f\}$ excitation vector

Such linear static analysis assumes that the response does not affect the behaviour of the excitation and excludes any plastic behaviour within the system. The dynamic system response considers variation over time due to acceleration and velocity, i.e. inertial and damping effects. This leads to the following EoM

$$\{f\} = [M]\{\ddot{d}\} + [C]\{\dot{d}\} + [K]\{d\} \tag{B.2}$$

where $[C]$ damping matrix
$[M]$ mass matrix
$\{\dot{d}\}$ velocity vector
$\{\ddot{d}\}$ acceleration vector

Linear transient dynamic analysis measures the system response over a series of time steps, making the same assumptions as linear static analysis. Such dynamic analysis may be substituted with quasi-static analysis using pseudo-static loads to reduce the computational effort required to solve the EoM over numerous time steps.

The EoM is solved having formed the problem using the mechanical properties of the FE model to populate the global system matrices. These matrices represent the system stiffness, mass and damping properties, and are formed through the consideration of similar matrices for each model element as follows:

1. generation of element stiffness matrices, also mass and damping matrices for dynamic analysis;
2. transformation of local element matrices into global coordinate system;
3. positioning of transformed local element matrices into global system matrices.

B.1.1 Stiffness Matrix

The element stiffness matrix describes the stiffness of an element in each nodal degree of freedom (DoF) as derived from Hooke's law. The stiffness matrix is symmetric by assuming linear material behaviour within the element and is derived through the superposition of the direct stiffness method expressions for independent translations and rotations in each DoF. The resulting stiffness matrix of a pin-jointed truss element without any rotational DoFs is as follows, with labels indicating the corresponding DoFs

$$[k^e] = \frac{EA}{l} \begin{array}{c} \begin{array}{cccccc} d_{x_1} & d_{y_1} & d_{z_1} & d_{x_2} & d_{y_2} & d_{z_2} \end{array} \\ \begin{bmatrix} 1 & 0 & 0 & -1 & 0 & 0 \\ & 0 & 0 & 0 & 0 & 0 \\ & & 0 & 0 & 0 & 0 \\ & & & 1 & 0 & 0 \\ & \textit{sym.} & & & 0 & 0 \\ & & & & & 0 \end{bmatrix} \end{array} \begin{array}{c} d_{x_1} \\ d_{y_1} \\ d_{z_1} \\ d_{x_2} \\ d_{y_2} \\ d_{z_2} \end{array} \tag{B.3}$$

where A cross-sectional area, m^2
d_{i_j} translational DoF of jth element node in ith direction
E elastic modulus, Pa
l length, m

The stiffness matrix of a fix-ended space frame element with rotational DoFs is

$$[k^e] = \frac{EA}{l} \begin{array}{c} \begin{array}{cccccccccccc} d_{x_1} & d_{y_1} & d_{z_1} & \theta_{x_1} & \theta_{y_1} & \theta_{z_1} & d_{x_2} & d_{y_2} & d_{z_2} & \theta_{x_2} & \theta_{y_2} & \theta_{z_2} \end{array} \\ \begin{bmatrix} 1 & 0 & 0 & 0 & 0 & 0 & -1 & 0 & 0 & 0 & 0 & 0 \\ & \frac{12I_{zz}}{Al^2} & 0 & 0 & 0 & \frac{6I_{zz}}{Al} & 0 & \frac{-12I_{zz}}{Al^2} & 0 & 0 & 0 & \frac{6I_{zz}}{Al} \\ & & \frac{12I_{yy}}{Al^2} & 0 & \frac{-6I_{yy}}{Al} & 0 & 0 & 0 & \frac{-12I_{yy}}{Al^2} & 0 & \frac{-6I_{yy}}{Al} & 0 \\ & & & \frac{GJ}{AE} & 0 & 0 & 0 & 0 & 0 & \frac{-GJ}{AE} & 0 & 0 \\ & & & & \frac{4I_{yy}}{A} & 0 & 0 & 0 & \frac{6I_{yy}}{Al} & 0 & \frac{2I_{yy}}{A} & 0 \\ & & & & & \frac{4I_{zz}}{A} & 0 & \frac{-6I_{zz}}{Al} & 0 & 0 & 0 & \frac{2I_{zz}}{A} \\ & & & & & & 1 & 0 & 0 & 0 & 0 & 0 \\ & & & & & & & \frac{12I_{zz}}{Al^2} & 0 & 0 & 0 & \frac{-6I_{zz}}{Al} \\ & & & \textit{sym.} & & & & & \frac{12I_{yy}}{Al^2} & 0 & \frac{6I_{yy}}{Al} & 0 \\ & & & & & & & & & \frac{GJ}{AE} & 0 & 0 \\ & & & & & & & & & & \frac{4I_{yy}}{A} & 0 \\ & & & & & & & & & & & \frac{4I_{zz}}{A} \end{bmatrix} \end{array} \begin{array}{c} d_{x_1} \\ d_{y_1} \\ d_{z_1} \\ \theta_{x_1} \\ \theta_{y_1} \\ \theta_{z_1} \\ d_{x_2} \\ d_{y_2} \\ d_{z_2} \\ \theta_{x_2} \\ \theta_{y_2} \\ \theta_{z_2} \end{array} \tag{B.4}$$

where G shear modulus, Pa
I_{yy} second moment of area about minor y-axis, m^4
I_{zz} second moment of area about major z-axis, m^4
J torsion constant, m^4
θ_{i_j} rotational DoF of jth element node in ith direction

B.1.2 Mass Matrix

The mass matrix accounts for the effects of acceleration of an element under dynamic loading as required by Newton's second law. A lumped mass matrix assumes that the mass of the element is positioned solely at its nodes. This leads to the following lumped mass matrix for a pin-jointed truss element with no rotational DoFs

$$[m^e] = \rho A l \begin{array}{c} \begin{matrix} \ddot{d}_{x_1} & \ddot{d}_{y_1} & \ddot{d}_{z_1} & \ddot{d}_{x_2} & \ddot{d}_{y_2} & \ddot{d}_{z_2} \end{matrix} \\ \begin{bmatrix} \frac{1}{2} & 0 & 0 & 0 & 0 & 0 \\ & \frac{1}{2} & 0 & 0 & 0 & 0 \\ & & \frac{1}{2} & 0 & 0 & 0 \\ & & & \frac{1}{2} & 0 & 0 \\ & & \textit{sym.} & & \frac{1}{2} & 0 \\ & & & & & \frac{1}{2} \end{bmatrix} \end{array} \begin{matrix} \ddot{d}_{x_1} \\ \ddot{d}_{y_1} \\ \ddot{d}_{z_1} \\ \ddot{d}_{x_2} \\ \ddot{d}_{y_2} \\ \ddot{d}_{z_2} \end{matrix} \tag{B.5}$$

where ρ density, $\mathrm{kg/m}^3$

Each matrix column represents the nodal load vector to be applied to the element such that the acceleration field is maintained, where the corresponding nodal DoF has unit value in the second time derivative. The lumped mass matrix is most appropriate to models with large concentrations of mass positioned at the nodes; however, it is generally more appropriate to assume that mass is distributed throughout the element. Therefore, the consistent mass matrix more reasonably models the element mass and is derived in a manner consistent with that of the element stiffness matrix. Consequently, the consistent mass matrix of a pin-jointed truss element is as follows

$$[m^e] = \rho A l \begin{array}{c} \begin{matrix} \ddot{d}_{x_1} & \ddot{d}_{y_1} & \ddot{d}_{z_1} & \ddot{d}_{x_2} & \ddot{d}_{y_2} & \ddot{d}_{z_2} \end{matrix} \\ \begin{bmatrix} \frac{1}{3} & 0 & 0 & \frac{1}{6} & 0 & 0 \\ & \frac{1}{3} & 0 & 0 & \frac{1}{6} & 0 \\ & & \frac{1}{3} & 0 & 0 & \frac{1}{6} \\ & & & \frac{1}{3} & 0 & 0 \\ & & \textit{sym.} & & \frac{1}{3} & 0 \\ & & & & & \frac{1}{3} \end{bmatrix} \end{array} \begin{matrix} \ddot{d}_{x_1} \\ \ddot{d}_{y_1} \\ \ddot{d}_{z_1} \\ \ddot{d}_{x_2} \\ \ddot{d}_{y_2} \\ \ddot{d}_{z_2} \end{matrix} \tag{B.6}$$

The consistent mass matrix of a frame element is derived similarly to the stiffness matrix by considering the translation and rotation of the element in each DoF

$$
[m^e] = \rho A l \begin{array}{c}
\begin{array}{cccccccccccc}
\ddot{d}_{x_1} & \ddot{d}_{y_1} & \ddot{d}_{z_1} & \ddot{\theta}_{x_1} & \ddot{\theta}_{y_1} & \ddot{\theta}_{z_1} & \ddot{d}_{x_2} & \ddot{d}_{y_2} & \ddot{d}_{z_2} & \ddot{\theta}_{x_2} & \ddot{\theta}_{y_2} & \ddot{\theta}_{z_2}
\end{array} \\
\left[\begin{array}{cccccccccccc}
\frac{1}{3} & 0 & 0 & 0 & 0 & 0 & \frac{1}{6} & 0 & 0 & 0 & 0 & 0 \\
 & \frac{13}{35} & 0 & 0 & 0 & \frac{11l}{210} & 0 & \frac{9}{70} & 0 & 0 & 0 & \frac{-13l}{420} \\
 & & \frac{13}{35} & 0 & \frac{-11l}{210} & 0 & 0 & 0 & \frac{9}{70} & 0 & \frac{13l}{420} & 0 \\
 & & & \frac{J}{3A} & 0 & 0 & 0 & 0 & 0 & \frac{J}{6A} & 0 & 0 \\
 & & & & \frac{l^2}{105} & 0 & 0 & 0 & \frac{-13l}{420} & 0 & \frac{-l^2}{140} & 0 \\
 & & & & & \frac{l^2}{105} & 0 & \frac{13l}{420} & 0 & 0 & 0 & \frac{-l^2}{140} \\
 & & & & & & \frac{1}{3} & 0 & 0 & 0 & 0 & 0 \\
 & & & & & & & \frac{13}{35} & 0 & 0 & 0 & \frac{-11l}{210} \\
 & & & & \textit{sym.} & & & & \frac{13}{35} & 0 & \frac{11l}{210} & 0 \\
 & & & & & & & & & \frac{J}{3A} & 0 & 0 \\
 & & & & & & & & & & \frac{l^2}{105} & 0 \\
 & & & & & & & & & & & \frac{l^2}{105}
\end{array}\right]
\end{array}
\begin{array}{c}
\ddot{d}_{x_1} \\ \ddot{d}_{y_1} \\ \ddot{d}_{z_1} \\ \ddot{\theta}_{x_1} \\ \ddot{\theta}_{y_1} \\ \ddot{\theta}_{z_1} \\ \ddot{d}_{x_2} \\ \ddot{d}_{y_2} \\ \ddot{d}_{z_2} \\ \ddot{\theta}_{x_2} \\ \ddot{\theta}_{y_2} \\ \ddot{\theta}_{z_2}
\end{array}
\tag{B.7}
$$

B.1.3 Damping Matrix

Viscous damping is considered by assuming that the duration of the system response is significantly longer than the system natural periods. The damping matrix may be derived in a similar manner to the stiffness and mass matrices, however the viscous damping properties of the elements are rarely sufficiently defined. Furthermore, damping can result from non-structural elements and joints within the system. Hence, the global damping matrix is calculated rather than element damping matrices. Damping is approximated as Rayleigh damping, i.e. classical or proportional damping, by the idealising the damping matrix as a linear combination of the mass and stiffness matrices, where n_{DoF} denotes the number of DoFs

$$
[C] = [M] \sum_{k=0}^{n_{DoF}-1} a_k \big([M]^{-1}[K]\big)^k \tag{B.8}
$$

where a_k denotes the damping coefficient in the kth DoF. System damping is determined by finding the damping coefficients. This firstly requires solving the eigenvalue problem as described in Appendix B.1.3.1. As damping is approximated as a linear combination of mass and stiffness, the modes of vibration are orthogonal to the system matrices. Hence, the ith modal damping coefficient is expressed

in the form of Eqn. (B.19) which, through the substitution of Eqn. (B.8), gives

$$C_i = \{\phi\}_i^T [M] \sum_{k=0}^{n_{DoF}-1} a_k \big([M]^{-1}[K]\big)^k \{\phi\}_i \tag{B.9}$$

where $\{\phi\}_i$ represents the ith system mode shape. Respective substitution of Eqns. (B.19) and (B.20) for the mass and stiffness matrices gives

$$C_i = \sum_{k=0}^{n_{DoF}-1} a_k \omega_i^{2k} M_i \tag{B.10}$$

where ω_i denotes the ith natural frequency of vibration. The damping coefficient may be expressed using generalised coordinates as

$$C_i = 2\zeta_i \omega_i M_i \tag{B.11}$$

where ζ_i is the damping ratio of ith mode of vibration. The ith damping ratio is thus found for the case of normalised modal mass, i.e. $M_i = 1$, as

$$\zeta_i = \frac{1}{2\omega_i} \sum_{k=0}^{n_{DoF}-1} a_k \omega_i^{2k} \tag{B.12}$$

Rayleigh damping considers only the first two modes of vibration due to the impracticality of considering all modes

$$[C] = a_0[M] + a_1[K] \tag{B.13}$$

where $a_{0,1}$ are the Rayleigh damping coefficients. Therefore, the damping matrix is determined through consideration of the Rayleigh damping coefficients for the first two modes of vibration. These coefficients are calculated using the natural frequencies and damping ratios of modes of vibration i and j

$$\begin{Bmatrix} a_0 \\ a_1 \end{Bmatrix} = 2 \begin{bmatrix} \omega_i^{-1} & \omega_i \\ \omega_j^{-1} & \omega_j \end{bmatrix}^{-1} \begin{Bmatrix} \zeta_i \\ \zeta_j \end{Bmatrix} \tag{B.14}$$

Given the natural frequencies of vibration found by solving the eigenvalue problem, Eqn. (B.14) is reduced by considering only the first two modes of vibration, i.e. $\{i, j\} = \{1, 2\}$, and assuming negligible difference between the damping ratios of the first two successive modes

$$\begin{Bmatrix} a_0 \\ a_1 \end{Bmatrix} = \frac{2\zeta}{\omega_1 + \omega_2} \begin{Bmatrix} \omega_1\omega_2 \\ 1 \end{Bmatrix} \tag{B.15}$$

Each element damping matrix, $[c^e]$, is obtained by proportionally combining the element stiffness and mass matrices as defined by the Rayleigh damping coefficients. This is only an approximation as these coefficients consider the global system viscous properties rather than individual elements, however is an accepted method of obtaining the damping properties of an element.

B.1.3.1 Eigenvalue Problem

The vibration of a dynamic system is established by solving the eigenvalue problem. The governing equation of an undamped system under free vibration is

$$[M]\{\ddot{d}\} + [K]\{d\} = \{0\} \tag{B.16}$$

A solution is assumed to this expression using a function of time, $T(t)$

$$\{d\}(t) = \{\phi\}\, T(t) \tag{B.17}$$

The amplitude ratio of two displacements is subsequently assumed to be independent of time, thus the system configuration is constant throughout motion whilst amplitude may vary. This configuration is described by the system mode shapes, where mode shape orthogonality is important such that the two modes i and j may be described as

$$\{\phi\}_i^T [K] \{\phi\}_j = 0 \tag{B.18}$$

where $\quad i \neq j$

The generalised system mode coefficients are subsequently obtained, e.g. for the ith modal stiffness

$$K_i = \{\phi\}_i^T [K] \{\phi\}_i \tag{B.19}$$

Equations (B.18) and (B.19) may also be expressed in terms of mass through similar modal orthogonality. The mode shapes are then used to solve the eigenvalue problem as follows. Assuming harmonic response of the system, Eqn. (B.17) is substituted into Eqn. (B.16) to obtain

$$\left[[K] - \omega^2 [M]\right] \{\phi\} = \{0\} \tag{B.20}$$

The determinant of the matrix $\left[[K] - \omega^2 [M]\right]$ must be zero for a non-trivial solution to Eqn. (B.20), thus giving the characteristic equation of the eigenvalue problem as

$$\left|[K] - \omega^2 [M]\right| = 0 \tag{B.21}$$

Several approaches may be applied to solve the characteristic equation for ω, the ease of application of which is highly dependent on the size of the problem, i.e. the number of DoFs. The method employed herein considers the dynamical matrix, $[D]$, and system eigenvalues, λ, such that

$$[D] = [K]^{-1} [M] \tag{B.22}$$

$$\lambda = \frac{1}{\omega^2} \tag{B.23}$$

This representation leads to the standard eigenvalue problem, where $[I]$ is the identity matrix

$$[\lambda [I] - [D]]\, \{\phi\} = \{0\} \tag{B.24}$$

The system eigenvalues are found by solving the eigenvalue problem. The selection of solution method is dependent on the characteristics of the dynamical matrix, which can include:

- symmetric: equal to its transpose, $[D] = [D]^T$;
- orthogonal: transpose equal to its inverse, $[D]^T [D] = [D][D]^T = [I]$;
- tridiagonal: non-zero terms within main diagonal and first subdiagonal and superdiagonal,

$$[D] = \begin{bmatrix} a_{11} & a_{12} & 0 & 0 \\ a_{21} & a_{22} & a_{23} & 0 \\ 0 & a_{32} & a_{33} & a_{34} \\ 0 & 0 & a_{43} & a_{44} \end{bmatrix}$$

- triangular: zero terms below or above leading diagonal,

$$\text{upper-triangular } [D] = \begin{bmatrix} a_{11} & a_{12} & a_{13} & a_{14} \\ 0 & a_{22} & a_{23} & a_{24} \\ 0 & 0 & a_{33} & a_{34} \\ 0 & 0 & 0 & a_{44} \end{bmatrix} \quad \text{lower-triangular } [D] = \begin{bmatrix} a_{11} & 0 & 0 & 0 \\ a_{21} & a_{22} & 0 & 0 \\ a_{31} & a_{32} & a_{33} & 0 \\ a_{41} & a_{42} & a_{43} & a_{44} \end{bmatrix}$$

- Hessenberg: zero terms below first subdiagonal or above first superdiagonal,

$$\text{upper Hessenberg } [D] = \begin{bmatrix} a_{11} & a_{12} & a_{13} & a_{14} \\ a_{21} & a_{22} & a_{23} & a_{24} \\ 0 & a_{32} & a_{33} & a_{34} \\ 0 & 0 & a_{43} & a_{44} \end{bmatrix} \quad \text{lower Hessenberg } [D] = \begin{bmatrix} a_{11} & a_{12} & 0 & 0 \\ a_{21} & a_{22} & a_{23} & 0 \\ a_{31} & a_{32} & a_{33} & a_{34} \\ a_{41} & a_{42} & a_{43} & a_{44} \end{bmatrix}$$

  where a_{ij} denotes a non-zero term in the ith row and jth column of the matrix

The dynamical matrix is not always symmetric even when the stiffness and mass matrices are symmetric; therefore, the solution method must consider real nonsymmetric matrices. The dynamical matrix is firstly balanced to reduce the eigenvalue sensitivity to changes made to the matrix and thus the accumulated rounding errors. This is performed using similarity transformations such that the corresponding rows and columns have comparable Euclidean norms, i.e. the square roots of the sum of the square of indexes within the row or column. This reduces the norm of the overall matrix without affecting the eigenvalues. The matrix is then reduced into upper Hessenberg form using Gaussian elimination, which is described in Appendix B.4.1. The Givens rotation and Householder reduction methods are alternative approaches but are less efficient than Gaussian elimination for unsymmetrical matrices. The QL or QR method is then applied to obtain the matrix eigenvalues by assuming that a real matrix may be expressed as the product of an orthogonal matrix, $[Q]$, and lower or upper-triangular matrix, $[L]$ and $[R]$ respectively, e.g.

$$[D] = [Q][R] \tag{B.25}$$

The orthogonal transformation of $[D]$ is then obtained as

$$[D'] = [Q]^T[D][Q] \tag{B.26}$$

This leads to a series of transformations to diagonalise the dynamical matrix such that the eigenvalues remain on the leading diagonal. Implicit shifting increases the rate of convergence. Householder reduction followed by the QL method can be employed for symmetric matrices with improved efficiency. The solution of the eigenvalue problem gives the dynamical matrix eigenvalues and thus the natural frequencies of vibration of the system modes. The natural periods of oscillation are then calculated as

$$\{\tau\} = \frac{2\pi}{\{\omega\}} \tag{B.27}$$

Finally, the critical time step of the dynamic response for a stable solution is found as follows given the minimum natural period of oscillation, $\tau_{\min}$

$$\Delta t_{cr} = \frac{\tau_{\min}}{\pi} \tag{B.28}$$

B.1.4 Transformation Matrix

To account for the misalignment of the local and global coordinate systems, the element matrices are transformed to the equivalent matrices with respect to the global coordinate system. The rotation matrix

defines the required transformation of each DoF between coordinate systems

$$[R_0] = [T^\gamma][M^\gamma][R^\gamma] \tag{B.29}$$

where $[M^\gamma]$, $[R^\gamma]$ and $[T^\gamma]$ are the rotation matrix component matrices. The rotation matrix is formed by considering the required repositioning of an element to align itself with the global coordinate system at the origin. An element is initially of arbitrary axial rotation at an arbitrary position within the global system prior to transformation. The element is then transformed from this arbitrary configuration to the origin of the global system through the following operations:

1. axial rotation of the element;
2. rotation about an arbitrary global axis;
3. translation to a position relative to the global origin.

Euler angles are used to rotate the element such that the axial rotation of the element relative to the global coordinate system is eliminated. These angles describe the orientation of the element in the global system as anticlockwise rotations of γ relative to the local coordinate system of the element. Herein, the element axial rotation of γ_x is eliminated using the following Euler angles

$$[R^\gamma] = \begin{bmatrix} 1 & 0 & 0 & 0 \\ 0 & \cos\gamma_x & -\sin\gamma_x & 0 \\ 0 & \sin\gamma_x & \cos\gamma_x & 0 \\ 0 & 0 & 0 & 1 \end{bmatrix} \tag{B.30}$$

The element is then rotated about an arbitrary global system axis to be collinear with another axis

$$[M^\gamma] = \begin{bmatrix} u_x^\gamma & u_y^\gamma & u_z^\gamma & 0 \\ v_x^\gamma & v_y^\gamma & v_z^\gamma & 0 \\ w_x^\gamma & w_y^\gamma & w_z^\gamma & 0 \\ 0 & 0 & 0 & 1 \end{bmatrix} \tag{B.31}$$

where $\{u^\gamma\}$, $\{v^\gamma\}$ and $\{w^\gamma\}$ are orthonormal system vectors defined as

$$\{u^\gamma\} = \frac{\{e\}}{\|e\|} \tag{B.32a}$$

$$\{v^\gamma\} = \frac{\{p\}}{\|p\|} \tag{B.32b}$$

$$\{w^\gamma\} = \{u^\gamma\} \times \{v^\gamma\} \tag{B.32c}$$

where $\{e\} = \begin{Bmatrix} x_{N_2} - x_{N_1} & y_{N_2} - y_{N_1} & z_{N_2} - z_{N_1} \end{Bmatrix}^T$

$\{p\} = \{\hat{a}\} \times \{u^\gamma\}$

The vector $\{e\}$ represents the element as defined by its nodal coordinates, where the coordinates of the ith element node in the x, y and z-directions are given by x_{N_i}, y_{N_i} and z_{N_i} respectively. The vector $\{\hat{a}\}$

represents the unit vector of the global axis about which the element is rotated

$$\{\hat{a}\} = \begin{cases} \begin{Bmatrix} 1 & 0 & 0 \end{Bmatrix}^T & \text{for } x\text{-axis} \\ \begin{Bmatrix} 0 & 1 & 0 \end{Bmatrix}^T & \text{for } y\text{-axis} \\ \begin{Bmatrix} 0 & 0 & 1 \end{Bmatrix}^T & \text{for } z\text{-axis} \end{cases} \tag{B.33}$$

Finally, the element is translated to position its first node at the origin of the global coordinate system

$$[T^\gamma] = \begin{bmatrix} 1 & 0 & 0 & -x_{N_1} \\ 0 & 1 & 0 & -y_{N_1} \\ 0 & 0 & 1 & -z_{N_1} \\ 0 & 0 & 0 & 1 \end{bmatrix} \tag{B.34}$$

The rotation matrix is reduced to a 3x3 matrix through the elimination of the final row and column before being positioned within the transformation matrix

$$[T] = \begin{bmatrix} [R_0] & & & \\ & [R_0] & & \\ & & [R_0] & \\ & & & [R_0] \end{bmatrix} \tag{B.35}$$

The element matrices are transformed into the global coordinate system as

$$[K^e] = [T]^T [k^e][T] \tag{B.36}$$

Conversely, the element matrix in its local coordinate system is recovered as

$$[k^e] = [T][K^e][T]^T \tag{B.37}$$

Similar expressions are used for the mass and damping matrices through their substitution for the stiffness matrix. The transformation of vectors from their local coordinate system to the global system and the reverse is performed similarly, as shown here respectively for the displacement vector

$$\{D^e\} = [T]^T \{d^e\} \tag{B.38a}$$

$$\{d^e\} = [T]^T \{D^e\} \tag{B.38b}$$

where $\{d^e\}$ element displacement vector in local coordinate system
$\{D^e\}$ element displacement vector in global coordinate system

B.1.5 Sorting of Global Matrices

The element matrices are inserted into the global matrices once transformed into the global coordinate system. The element properties at each node are isolated through consideration of the element matrices as quadrants defined by the DoFs of the element nodes

$$[K^e] = \begin{bmatrix} [K^e_{N_1,N_1}] & [K^e_{N_1,N_2}] \\ [K^e_{N_2,N_1}] & [K^e_{N_2,N_2}] \end{bmatrix} \tag{B.39}$$

The subscripts of each quadrant denote the element nodes represented by the quadrant. The position of

each quadrant within the global matrix is determined by the global node number and size of the quadrant, i.e. number of DoFs per element node as defined by element type. Herein the global system contains six DoFs per node to allow translation and rotation of all nodes; conversely, the quadrants associated with pin-jointed elements extend along half as many rows and columns as those for fixed elements. The positioning of the quadrants of the stiffness matrix of a fixed element within the global stiffness matrix is as follows assuming a nodal numbering system from 1 to n_{DoF} and that $N_1 < N_2$

	$1 \dots 6(N_1-1)$	$6(N_1-1)+1 \dots 6N_1$	$6N_1+1 \dots 6(N_2-1)$	$6(N_2-1)+1 \dots 6N_2$	$6N_2+1 \dots n_{DoF}$
1 $\vdots$ $6(N_1-1)$	$\ddots$	$\vdots$	$\vdots$	$\vdots$	$\vdots$
$6(N_1-1)+1$ $\vdots$ $6N_1$	$\cdots$	$[K^e_{N_1,N_1}]$	$\cdots$	$[K^e_{N_1,N_2}]$	$\cdots$
$6N_1+1$ $\vdots$ $6(N_2-1)$	$\cdots$	$\vdots$	$\ddots$	$\vdots$	$\cdots$
$6(N_2-1)+1$ $\vdots$ $6N_2$	$\cdots$	$[K^e_{N_2,N_1}]$	$\cdots$	$[K^e_{N_2,N_2}]$	$\cdots$
$6N_2+1$ $\vdots$ n_{DoF}	$\vdots$	$\vdots$	$\vdots$	$\vdots$	$\ddots$

B.2 Boundary Conditions

Boundary conditions are applied as specific nodal translational or rotational displacements. If inadequate boundary conditions are applied then the system matrices become singular, resulting in an infinite number of solutions and, thus, an insolvable problem. Nodes are described, as indicated in Fig. B.1, as either:

- free: may displace without constraint in the DoF;
- fixed: constrained to a specified displacement in the DoF.

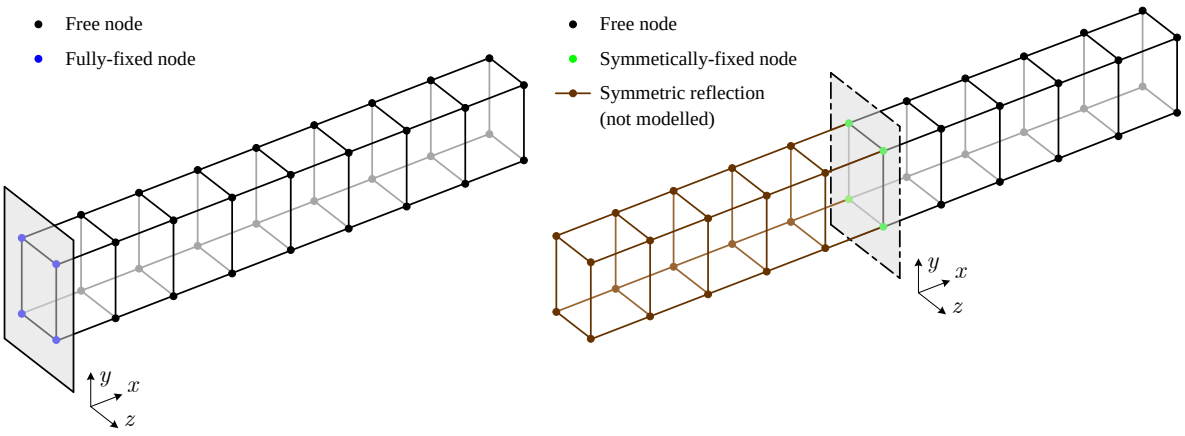

(a) Cantilever beam fully-fixed at root (b) Beam modelled symmetrically in yz-plane

Figure B.1: Examples of boundary conditions

Figure B.1(a) illustrates a cantilever beam with fully-fixed root nodes. These nodes are constrained in all DoFs whereas free nodes are not constrained in any DoFs. A symmetric problem introduces symmetrically-fixed nodes on the plane of symmetry to constrain translation normal to and rotation about the plane, as shown in Fig. B.1(b). A symmetric problem assumes a symmetric response of the system in the plane of symmetry, thus reducing the number of DoFs by eliminating the system behind the plane. The fixed and symmetric boundary conditions shown in Fig. B.1 are applied to the ith node on the boundary respectively as

$$\left\{d_{x_{N_i}} \quad d_{y_{N_i}} \quad d_{z_{N_i}} \quad \theta_{x_{N_i}} \quad \theta_{y_{N_i}} \quad \theta_{z_{N_i}}\right\}^T = \{0\} \tag{B.40a}$$

$$\left\{d_{x_{N_i}} \quad \theta_{y_{N_i}} \quad \theta_{z_{N_i}}\right\}^T = \{0\} \tag{B.40b}$$

Boundary conditions are applied by striking-out the rows and columns within the matrices and vectors associated with constrained DoFs. This reduces the sizes of the system matrices, leading to reduced bandwidth with fewer calculations required to solve the problem. Bandwidth reduction is critical in reducing the problem size and subsequent computational effort required to obtain a solution. The bandwidth of a matrix is defined as

$$B = B_L + B_U + 1 \tag{B.41}$$

where the lower and upper bandwidth, B_L and B_U respectively, denote the distance from the diagonal to the final non-zero term in the corresponding direction. A banded matrix possesses reasonably small bandwidth, e.g. $B = 1$ for a diagonal matrix and $B = 3$ for a tridiagonal matrix as described in Appendix B.1.3.1. The bandwidth of the global matrices is reduced by appropriate node numbering such that the nodes of connecting elements are numbered closely. This leads to the close proximity of these nodal DoFs within the global matrices as described in Appendix B.1.5.

B.3 System Excitation

Loads are applied to an FE model in order to excite the system and generate a response in terms of displacements and rotations. Loads take the form of concentrated forces and moments applied to system nodes. A node may be loaded in any DoF, resulting in up to six possible loads per node: a force and moment in each of the x, y, and z-directions. As a result, the system excitation vector takes the form of

$$\{f\} = \left\{f_{x_{N_1}} \quad f_{y_{N_1}} \quad f_{z_{N_1}} \quad m_{x_{N_1}} \quad m_{y_{N_1}} \quad m_{z_{N_1}} \quad f_{x_{N_2}} \quad f_{y_{N_2}} \quad \dots \quad m_{y_{N_{n_N}}} \quad m_{z_{N_{n_N}}}\right\}^T \tag{B.42}$$

where
- $f_{x_{N_i}}$ force parallel to x-axis applied to ith node, N
- $f_{y_{N_i}}$ force parallel to y-axis applied to ith node, N
- $f_{z_{N_i}}$ force parallel to z-axis applied to ith node, N
- $m_{x_{N_i}}$ moment about x-axis applied to ith node, Nm
- $m_{y_{N_i}}$ moment about y-axis applied to ith node, Nm
- $m_{z_{N_i}}$ moment about z-axis applied to ith node, Nm

Nodal force and moment components are defined by the load cases selected for application to the FE model, resulting in a series of point and pressure loads to be applied in the nodal DoFs. The response of the system to these applied nodal loads is subsequently calculated.

B.4 System Response

The system static or dynamic response is calculated by solving the respective EoM, i.e. Eqn. (B.1) or (B.2) respectively, given the formed problem, applied boundary conditions and applied excitation.

B.4.1 Static Response

The system response to a static or pseudo-static load is given by rearranging Eqn. (B.1) as

$$\{d\} = [K]^{-1}\{f\} \tag{B.43}$$

Equation (B.43) requires the inversion of the stiffness matrix, however this is often computationally expensive for large FEA problems. Therefore, Gaussian elimination with back-substitution is performed to reduce the stiffness matrix to upper-triangular form and subsequently solve, with greater efficiency, the series of simultaneous equations formed by considering each DoF of Eqn. (B.1) as an independent equation. This yields the exact solution of the response vector without excessive rounding or truncation errors. This procedure solves Eqn. (B.1) as the following series of n_{DoF} linear simultaneous equations with n_{DoF} unknowns in $\{d\}$

$$\begin{aligned} f_1 &= K_{11}d_1 + K_{12}d_2 + \cdots + K_{1n_{DoF}}d_{n_{DoF}} \\ f_2 &= K_{21}d_1 + K_{22}d_2 + \cdots + K_{2n_{DoF}}d_{n_{DoF}} \\ &\vdots \\ f_{n_{DoF}} &= K_{n_{DoF}1}d_1 + K_{n_{DoF}2}d_2 + \cdots + K_{n_{DoF}n_{DoF}}d_{n_{DoF}} \end{aligned} \tag{B.44}$$

The series of equations is solved in numerical order where for the kth expression of f

$$d_k = \frac{1}{K_{kk}^{k-1}}\left(f_k^{k-1} + \sum_{j=k+1}^{n_{DoF}} K_{kj}^{k-1}d_j\right) \tag{B.45}$$

where $K_{ij}^{k} = K_{ij}^{k-1} - \dfrac{K_{ik}^{k-1}}{K_{kk}^{k-1}}K_{kj}^{k-1}$ for $i, j = k+1, \ldots, n_{DoF}$

$$f_i^k = f_i^{k-1} - \frac{K_{ik}^{k-1}}{K_{kk}^{k-1}}f_k^{k-1}$$

Back-substitution is used to input the result of Eqn. (B.45) into (B.44). The process progresses iteratively $n_{DoF} - 1$ times until Eqn. (B.44) is reduced to

$$f_{n_{DoF}}^{n_{DoF}-1} = K_{n_{DoF}n_{DoF}}^{n_{DoF}-1}d_{n_{DoF}} \tag{B.46}$$

The expressions in Eqn. (B.45) are then solved for d_k in decrementing order of k. If the pivot term equals zero, i.e. $K_{kk}^{k-1} = 0$, the remaining rows require re-evaluation in order to obtain a non-zero denominator in Eqn. (B.45). If this is not possible the stiffness matrix is singular and a solution cannot be found.

B.4.2 Dynamic Response

The system response to a linear transient dynamic load is determined by solving Eqn. (B.2) by direct numerical integration. This involves the rearrangement of the EoM to find the displacement of the system whilst considering the system excitation, velocity and acceleration. Direct integration requires reduced computational effort to determine the closed-form solution to the problem than alternative methods, e.g. vibration analysis of the system natural frequencies or modal superposition. Direct integration of the EoM over the simulation length approximates the dynamic system response at specific time intervals. The size of time step, Δt, and set-up of the integration method determine the accuracy of this approximation. The time step must be sufficiently small for adequate sampling of the response whilst avoiding an excessive

number of evaluations. Integration methods vary in the approximations made of the system response between time intervals. The methods included herein are:

- central difference;
- Houbolt;
- Wilson-θ;
- Newmark-β.

The central difference method is explicit in that the calculation of displacement at each time step considers only the response at previous time steps. The remaining methods are implicit wherein the response at each time step is determined by considering the next time step as well as recent intervals. Explicit methods generally possess greater accuracy, however implicit methods can be configured for unconditional stability.

B.4.2.1 Central Difference Method

The central difference method performs a finite difference approximation of the EoM to express the system response as approximations of the first two system derivatives, i.e. velocity and acceleration. Evaluation is made at intervals in time determined by a finite number of points over the simulation length. Acceleration and velocity at the current time step are calculated respectively as

$$\{\ddot{d}\}_t = \frac{1}{(\Delta t)^2}\left\{\{d\}_{t+\Delta t} - 2\{d\}_t + \{d\}_{t-\Delta t}\right\} \tag{B.47}$$

$$\{\dot{d}\}_t = \frac{1}{2\Delta t}\left\{\{d\}_{t+\Delta t} - \{d\}_{t-\Delta t}\right\} \tag{B.48}$$

Substitution of the above expressions into the EoM and subsequent rearrangement generates the expression for the displacement of the system at the time step under investigation

$$\begin{aligned}\{d\}_{t+\Delta t} = \left[\frac{1}{(\Delta t)^2}[M] + \frac{1}{2\Delta t}[C]\right]^{-1}\Bigg[\{f\}_t - \left[[K] - \frac{2}{(\Delta t)^2}[M]\right]\{d\}_t \\ - \left[\frac{1}{(\Delta t)^2}[M] - \frac{1}{2\Delta t}[C]\right]\{d\}_{t-\Delta t}\Bigg]\end{aligned} \tag{B.49}$$

Acceleration and velocity are then updated in Eqns. (B.47) and (B.48) such that the response is obtained iteratively. The displacement at time step $-\Delta t$ is determined such that the displacement at $t = 0$ can be found by substituting Eqn. (B.48) into (B.47) and rearranging the expression as

$$\{d\}_{-\Delta t} = \{d\}_0 - \Delta t\{\dot{d}\}_0 + \frac{(\Delta t)^2}{2}\{\ddot{d}\}_0 \tag{B.50}$$

The system is assumed to be initially at rest with no displacement or velocity and an acceleration of

$$\{\ddot{d}\}_0 = [M]^{-1}\left[\{f\} - [C]\{\dot{d}\}_0 - [K]\{d\}_0\right] \tag{B.51}$$

Equations (B.50) and (B.51) are used to obtain the initial conditions of all integration methods herein. An appropriate time step is key to successful integration. Too large a time step reduces the number of response evaluations, thus diminishing precision, whilst too small a step requires an excessive number of evaluations. Moreover, explicit methods require a small enough step to prevent solution instability due to the accumulation of truncation errors from higher-order terms, i.e. $\Delta t \leq \Delta t_{cr}$ where Δt_{cr} denotes the critical time step defined in Eqn. (B.28). Hence, the time step is typically constrained as follows to ensure unconditional stability

$$\Delta t \leq \frac{\tau_{\min}}{10} \tag{B.52}$$

B.4.2.2 Houbolt Method

The Houbolt method also applies finite difference expansions to the derivatives of the EoM, leading to the following respective expressions for the acceleration and velocity within the system at each time step

$$\{\ddot{d}\}_{t+\Delta t} = \frac{1}{(\Delta t)^2}\left\{2\{d\}_{t+\Delta t} - 5\{d\}_t + 4\{d\}_{t-\Delta t} - \{d\}_{t-2\Delta t}\right\} \tag{B.53}$$

$$\{\dot{d}\}_{t+\Delta t} = \frac{1}{6\Delta t}\left\{11\{d\}_{t+\Delta t} - 18\{d\}_t + 9\{d\}_{t-\Delta t} - 2\{d\}_{t-2\Delta t}\right\} \tag{B.54}$$

Substitution of these expressions into the EoM generates the expression for displacement at the time step

$$\begin{aligned}\{d\}_{t+\Delta t} = \left[\frac{2}{(\Delta t)^2}[M] + \frac{11}{6\Delta t}[C] + [K]\right]^{-1}\Bigg[\{f\}_{t+\Delta t} + \left[\frac{5}{(\Delta t)^2}[M] + \frac{3}{\Delta t}[C]\right]\{d\}_t \\ - \left[\frac{4}{(\Delta t)^2}[M] + \frac{3}{2\Delta t}[C]\right]\{d\}_{t-\Delta t} + \left[\frac{1}{(\Delta t)^2}[M] + \frac{1}{3\Delta t}[C]\right]\{d\}_{t-2\Delta t}\Bigg]\end{aligned} \tag{B.55}$$

The Houbolt method is not self-starting due to the third-order interpolation within Eqn. (B.55) requiring knowledge of the displacement at the first three time steps before it can be used. Therefore, these values are obtained using the central difference method leading to similar stability considerations.

B.4.2.3 Wilson-θ Method

The Wilson-θ method assumes linear variation of acceleration between two points in time and also considers an additional point in time, $t + \theta\Delta t$, thus requiring evaluation of the system at the points $t, t + \theta\Delta t, t + \Delta t$. The effective force at this additional point is firstly determined as follows, where the coefficients are obtained by integrating acceleration over the interval $0 \leq \tau \leq \Delta t$

$$\begin{aligned}\{\tilde{f}\}_{t+\theta\Delta t} = \{f\}_t + \theta\left\{\{f\}_{t+\Delta t} - \{f\}_t\right\} + [M]\left\{\frac{6}{\theta^2(\Delta t)^2}\{d\}_t + \frac{6}{\theta\Delta t}\{\dot{d}\}_t + 2\{\ddot{d}\}_t\right\} \\ + [C]\left\{\frac{3}{\theta\Delta t}\{d\}_t + 2\{\dot{d}\}_t + \frac{\theta\Delta t}{2}\{\ddot{d}\}_t\right\}\end{aligned} \tag{B.56}$$

The rearranged EoM is then used to obtain the displacement at $t + \theta\Delta t$

$$\{d\}_{t+\theta\Delta t} = \left[\frac{6}{\theta^2(\Delta t)^2}[M] + \frac{3}{\theta\Delta t}[C] + [K]\right]^{-1}\{\tilde{f}\}_{t+\theta\Delta t} \tag{B.57}$$

Given the displacement at $t+\theta\Delta t$, the system acceleration and velocity are calculated by assuming linear acceleration variation between t and $t + \theta\Delta t$

$$\{\ddot{d}\}_{t+\Delta t} = \frac{6}{\theta^3(\Delta t)^2}\left\{\{d\}_{t+\theta\Delta t} - \{d\}_t\right\} - \frac{6}{\theta^2\Delta t}\{\dot{d}\}_t + \left(1 - \frac{3}{\theta}\right)\{\ddot{d}\}_t \tag{B.58}$$

$$\{\dot{d}\}_{t+\Delta t} = \{\dot{d}\}_t + \frac{\Delta t}{2}\left\{\{\ddot{d}\}_{t+\Delta t} + \{\ddot{d}\}_t\right\} \tag{B.59}$$

Finally, the displacement at $t + \Delta t$ is obtained by

$$\{d\}_{t+\Delta t} = \{d\}_t + \Delta t\{\dot{d}\}_t + \frac{(\Delta t)^2}{6}\left\{\{\ddot{d}\}_{t+\Delta t} + 2\{\ddot{d}\}_t\right\} \tag{B.60}$$

The constant θ is set such that $\theta \geq 1$, with the method reducing to a linear acceleration scheme if $\theta = 1$. The Wilson-θ method is unconditionally stable if $\theta \geq 1.37$, hence a common value is $\theta = 1.4$.

B.4.2.4 Newmark-β Method

The Newmark-β method also considers linear variation in acceleration between two points in time. Two constants, α and β, control the influence of this acceleration during the time interval on the resulting velocity and displacement. The expressions for acceleration and velocity are given respectively as

$$\{\ddot{d}\}_{t+\Delta t} = \frac{1}{\alpha(\Delta t)^2}\left\{\{d\}_{t+\Delta t} - \{d\}_t\right\} - \frac{1}{\alpha \Delta t}\{\dot{d}\}_t - \left(\frac{1}{2\alpha} - 1\right)\{\ddot{d}\}_t \tag{B.61}$$

$$\{\dot{d}\}_{t+\Delta t} = \{\dot{d}\}_t + \Delta t\left\{(1-\beta)\{\ddot{d}\}_t + \beta\{\ddot{d}\}_{t+\Delta t}\right\} \tag{B.62}$$

The displacement at the next step is then calculated by substituting the above formulae into the EoM

$$\begin{aligned}\{d\}_{t+\Delta t} = \left[\frac{1}{\alpha(\Delta t)^2}[M] + \frac{\beta}{\alpha \Delta t}[C] + [K]\right]^{-1} \Bigg[\{f\}_{t+\Delta t} + [M]\left\{\frac{1}{\alpha(\Delta t)^2}\{d\}_t + \frac{1}{\alpha \Delta t}\{\dot{d}\}_t + \left(\frac{1}{2\alpha} - 1\right)\{\ddot{d}\}_t\right\} \\ + [C]\left\{\frac{\beta}{\alpha \Delta t}\{d\}_t + \left(\frac{\beta}{\alpha} - 1\right)\{\dot{d}\}_t + \frac{\Delta t}{2}\left(\frac{\beta}{\alpha} - 2\right)\{\ddot{d}\}_t\right\}\Bigg]\end{aligned} \tag{B.63}$$

Constants α and β determine the accuracy and stability of the Newmark-β method. For example, a linear acceleration method exists when $\alpha = 1/6$ and $\beta = 1/2$. The value of β is critical as spurious damping of magnitude proportional to $(\beta - 1/2)$ is introduced if $\beta \neq 1/2$. Negative damping occurs when $\beta < 1/2$ and positive damping if $\beta > 1/2$. As a result, the Newmark-β method is unconditionally stable if $\beta \geq 1/2$ and $\alpha \geq {(\beta + 1/2)^2}/4$, leading to standard values of $\alpha = 1/4$ and $\beta = 1/2$.

Nomenclature

The principal nomenclature used within this appendix is given below. Symbols i, j and k are employed as arbitrary counters within formulae.

A	cross-sectional area, m^2
a	damping coefficient
B	matrix bandwidth
$[C]$	damping matrix; $[c^e]$, $[C^e]$ for element in local, global coordinate system
d_x, d_y, d_z	displacement parallel to x, y, z-axis, m
$[D]$	dynamical matrix
$\{d\}$	displacement vector; $\{d^e\}$, $\{D^e\}$ for element in local, global coordinate system
$\{\dot{d}\}$	velocity vector; $\{\dot{d}^e\}$, $\{\dot{D}^e\}$ for element in local, global coordinate system
$\{\ddot{d}\}$	acceleration vector; $\{\ddot{d}^e\}$, $\{\ddot{D}^e\}$ for element in local, global coordinate system
E	elastic modulus, Pa
f_x, f_y, f_z	force parallel to x, y, z-axis, N
$\{f\}$	excitation vector; $\{f^e\}$, $\{F^e\}$ for element in local, global coordinate system
$\{\tilde{f}\}$	effective excitation vector
G	shear modulus, Pa

I_{yy}, I_{zz}	second moment of area about minor y, major z-axis, m^4
J	torsion constant, m^4
$[K]$	stiffness matrix; $[k^e]$, $[K^e]$ for element in local, global coordinate system
l	length, m
m_x, m_y, m_z	moment about x, y, z-axis, Nm
$[M]$	mass matrix; $[m^e]$, $[M^e]$ for element in local, global coordinate system
N	node number
n_{DoF}	number of DoFs
n_N	number of nodes
$[R_0]$	rotation matrix
$T(t)$	time function
$[T]$	transformation matrix
x, y, z	nodal coordinates in x, y, z-directions
α, β	Newmark-β direct integration method constants
γ	rotation, rad
Δt	time step length, s
Δt_{cr}	critical time step length, s
ζ	damping ratio
θ	Wilson-θ direct integration method constant
θ_x, θ_y, θ_z	rotation about x, y, z-axis, rad
λ	system eigenvalues, $1/rad^2$
ρ	density, kg/m^3
τ	natural period of oscillation, s
ϕ	undamped mode shape
ω	natural frequency of vibration, rad

Appendix C

Benchmark Functions

This appendix describes the benchmark functions used during the preliminary investigation within §7.2. These functions are taken from those commonly used within the literature (Molga and Smutnicki, 2005; Özcan et al., 2008; Rafique et al., 2011; Yang, 2010). The descriptions include the limits on the solution space, i.e. on the design variables, used during the investigations in §7.2 as taken from the literature. The global minimum within these limits is also provided alongside a two-dimensional illustration of the solution space created by the function.

C.1 De Jong Sphere

The De Jong sphere function is a continuous, convex, unimodal function applied with a global minimum of $f(x) = 0$ at $\{x\} = \{0\}$. The function is applied herein within an n_v-dimensional hypercubic solution space with the common limits of $-5.12 \leq x_v \leq 5.12$ for $v = 1, 2, \ldots, n_v$ (De Jong, 1975)

$$f(x) = \sum_{v=1}^{n_v} x_v^2 \tag{C.1}$$

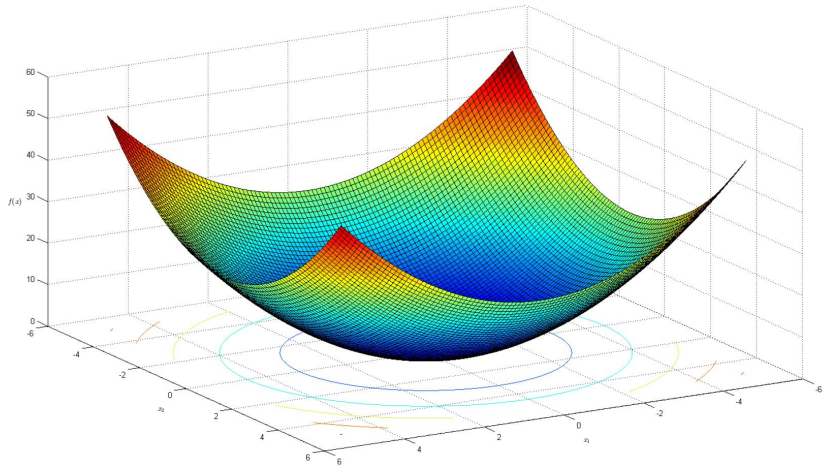

Figure C.1: De Jong sphere function

C.2 Axis-Parallel Hyper-Ellipsoid

The continuous, convex and unimodal axis-parallel hyper-ellipsoid function possesses the same global minimum and domain limits as the De Jong sphere (De Jong, 1975)

$$f(x) = \sum_{v=1}^{n_v} v x_v^2 \tag{C.2}$$

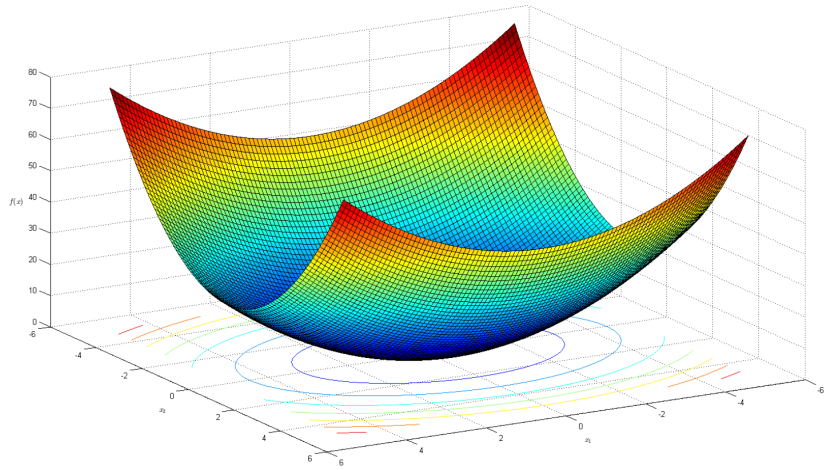

Figure C.2: Axis-parallel hyper-ellipsoid function

C.3 Schwefel Double Sum

Similarly continuous, convex and unimodal, the Schwefel double sum produces rotated hyper-ellipsoids with respect to the coordinate axis. The function has a global minimum of $f(x) = 0$ at $\{x\} = \{0\}$ and is restricted to the hypercube $-65.536 \leq x_v \leq 65.536$ for $v = 1, 2, \ldots, n_v$ with an additional counter w (Schwefel, 1981)

$$f(x) = \sum_{v=1}^{n_v} \sum_{w=1}^{v} x_w^2 \tag{C.3}$$

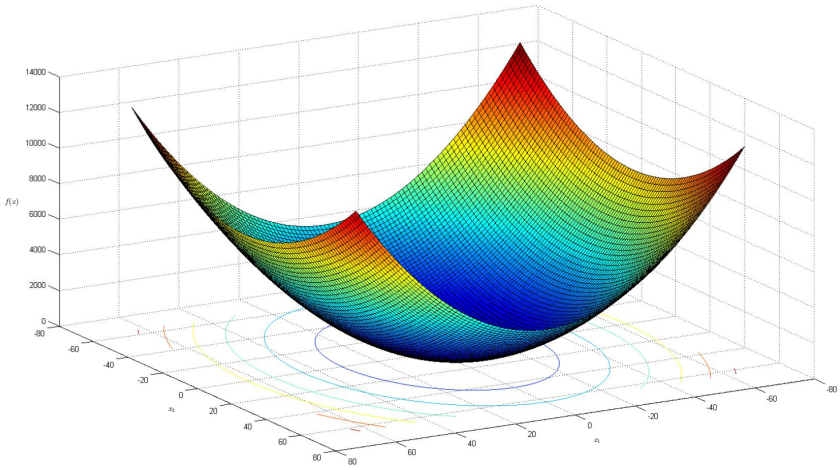

Figure C.3: Schwefel double sum function

C.4 Rastrigin

This continuous function uses cosine modulation to generate many regularly distributed local minima. The function is highly multimodal and non-convex, and is applied to the hypercube $-5.12 \leq x_v \leq 5.12$ for $v = 1, 2, \ldots, n_v$ and possesses a global minimum at $\{x\} = \{0\}$ of $f(x) = 0$ (Rastrigin, 1974)

$$f(x) = 10n_v + \sum_{v=1}^{n_v} x_v^2 - 10\cos(2\pi x_v) \tag{C.4}$$

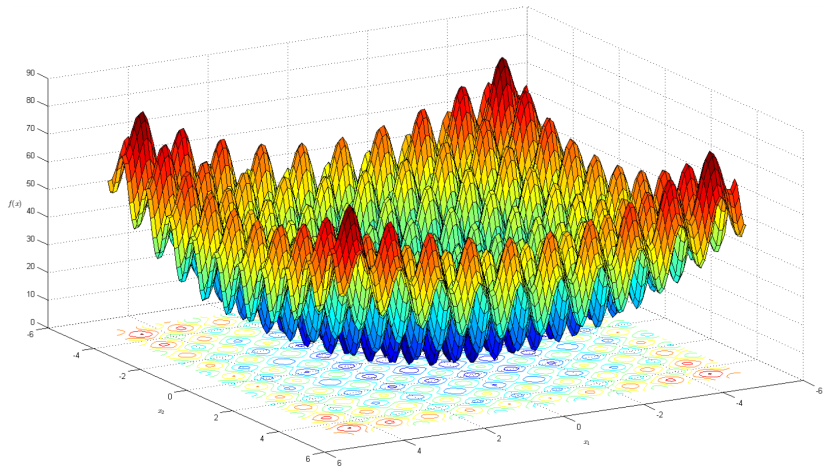

Figure C.4: Rastrigin function

C.5 Griewank

The continuous multimodal Griewank function has many local minima at widespread regular intervals, the quantity of which increases exponentially with the number of variables. The global minimum of $f(x) = 0$ is at $\{x\} = \{0\}$ within a domain of $-600 \leq x_v \leq 600$ for $v = 1, 2, \ldots, n_v$ (Griewank, 1981)

$$f(x) = \frac{1}{4000}\sum_{v=1}^{n_v} x_v^2 - \prod_{v=1}^{n_v} \cos\left(\frac{x_v}{\sqrt{v}}\right) + 1 \tag{C.5}$$

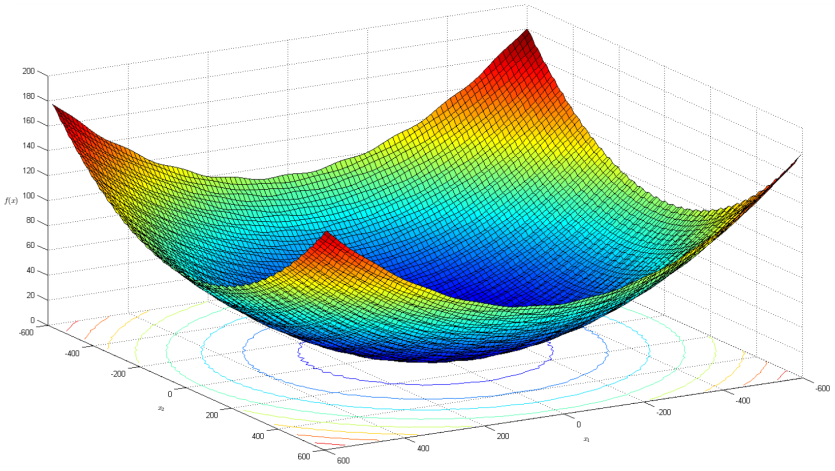

Figure C.5: Griewank function

C.6 Schwefel

This deceptive function is continuous and multimodal with great distances between local and global minima, thus rendering optimisation techniques vulnerable to convergence on local optima. A global minimum of $f(x) = -418.9829n_v$ is located at $\{x\} = \{420.9687\}$ for the range $-500 \leq x_v \leq 500$ for $v = 1, 2, \ldots, n_v$ (Schwefel, 1981)

$$f(x) = \sum_{v=1}^{n_v} -x_v \sin \sqrt{|x_v|} \tag{C.6}$$

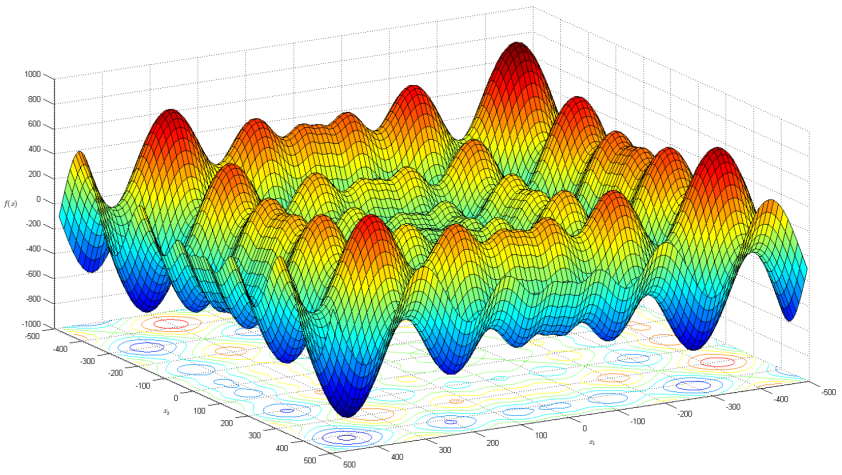

Figure C.6: Schwefel function

C.7 Six-Hump Camel Back

The six-hump camel function back is continuous and multimodal with four local minima and two global minima within a solution space bounded by $-3 \leq x_1 \leq 3$ and $-2 \leq x_2 \leq 2$. The global optima of $f(x) = -1.0316$ are at $\{x_1, x_2\} = \{-0.0898, 0.7126\}$, $\{0.0898, -0.7126\}$ (Dixon and Szego, 1978)

$$f(x) = \left\{4 - 2.1x_1^2 + \frac{x_1^4}{3}\right\} x_1^2 + x_1 x_2 + \left\{4x_2^2 - 4\right\} x_2^2 \tag{C.7}$$

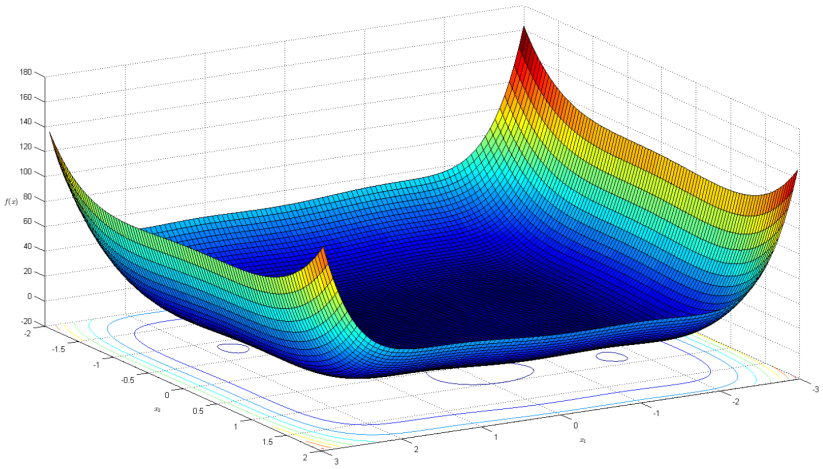

Figure C.7: Six-hump camel back function

C.8 Rosenbrock Valley

The continuous multimodal Rosenbrock valley contains a global minimum within a narrow parabolic valley. Discovery of the valley is trivial, however convergence towards the minimum of $f(x) = 0$ at $\{x\} = \{1\}$ is not. A solution space of $-2.048 \leq x_v \leq 2.048$ for $v = 1, 2, \ldots, n_v$ is used (Rosenbrock, 1960)

$$f(x) = \sum_{v=1}^{n_v - 1} 100 \left(x_{v+1} - x_v^2\right)^2 + (1 - x_v)^2 \tag{C.8}$$

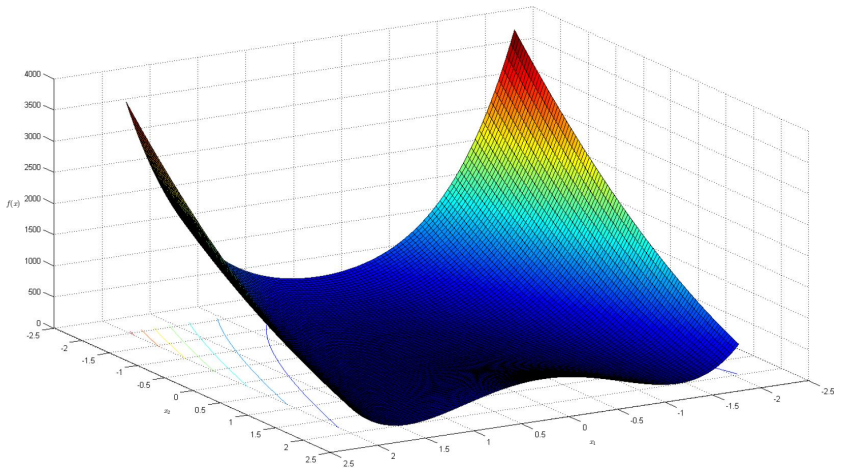

Figure C.8: Rosenbrock valley function

C.9 Branin

This continuous and multimodal function generates three equally-sized global minima of $f(x) = 0.397887$ at $\{x_1, x_2\} = \{-\pi, 12.275\}$, $\{\pi, 2.275\}$, $\{9.42478, 2.475\}$ in the domain of $-5 \leq x_v \leq 15$ for $v = 1, 2$ with constants $a = 1$, $b = {}^{5.1}/_{4\pi^2}$, $c = {}^{5}/_{\pi}$, $d = 6$, $e = 10$, $f = {}^{1}/_{8\pi}$ (Branin, 1972)

$$f(x) = a \left(x_2 - bx_1^2 + cx_1 - d\right)^2 + e\,(1 - f)\cos x_1 + e \tag{C.9}$$

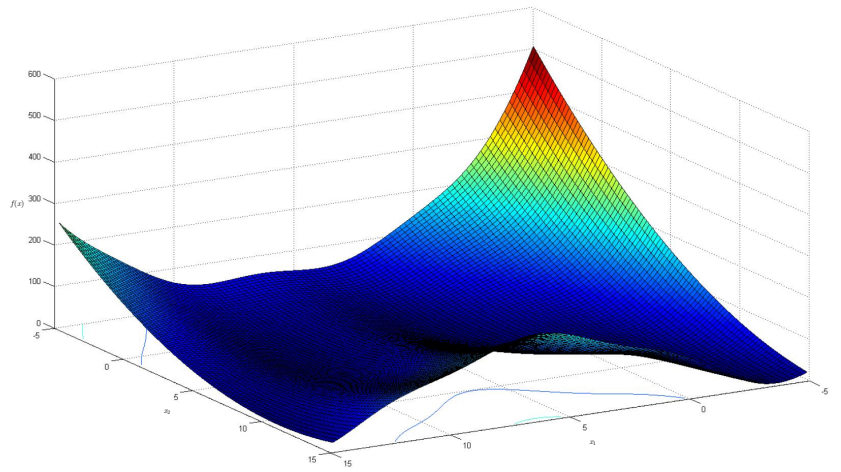

Figure C.9: Branin function

C.10 Easom

The Easom function global minimum is $f(x) = -1$ at $\{x\} = \{\pi\}$ and covers a relatively small area of the continuous unimodal solution space bounded by $-2\pi \leq x_v \leq 2\pi$ for $v = 1, 2, \ldots, n_v$ (Easom, 1990; Yang, 2010)

$$f(x) = -(-1)^{n_v} \left[\prod_{v=1}^{n_v} \cos^2 x_v \right] \exp \left[-\sum_{v=1}^{n_v} (x_v - \pi)^2 \right] \tag{C.10}$$

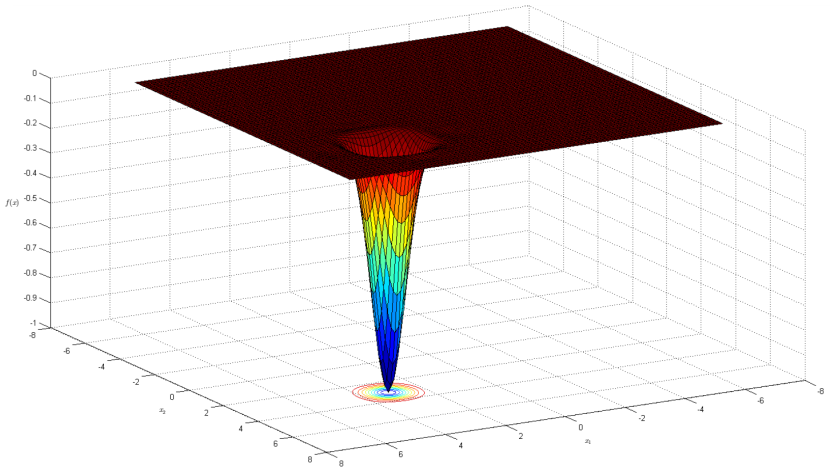

Figure C.10: Easom function

C.11 Ackley Path

The continuous and multimodal Ackley path is applied over a domain bounded by $-32.768 \leq x_v \leq 32.768$ for $v = 1, 2, \ldots, n_v$. The function contains several local minima and one global minimum of $f(x) = 0$ at $\{x\} = \{0\}$ with constants $a = 20$, $b = 0.2$, $c = 2\pi$ (Ackley, 1987)

$$f(x) = -a \exp \left\{ -b \sqrt{\frac{1}{n_v} \sum_{v=1}^{n_v} x_v^2} \right\} - \exp \left\{ \frac{1}{n_v} \sum_{v=1}^{n_v} \cos(c x_v) \right\} + a + \exp\{1\} \tag{C.11}$$

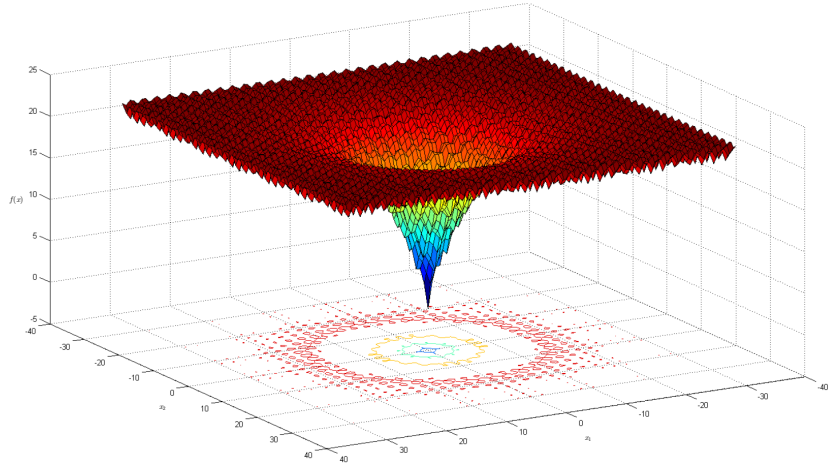

Figure C.11: Ackley path function

C.12 Drop Wave

The similarly continuous and multimodal drop wave function has a global minimum of $f(x) = -1$ at $\{x\} = \{0\}$ within the domain of $-5.12 \leq x_v \leq 5.12$ for $v = 1, 2$ (Molga and Smutnicki, 2005)

$$f(x) = -\frac{1 + \cos\left(12\sqrt{x_1^2 + x_2^2}\right)}{\frac{1}{2}\left(x_1^2 + x_2^2\right) + 2} \tag{C.12}$$

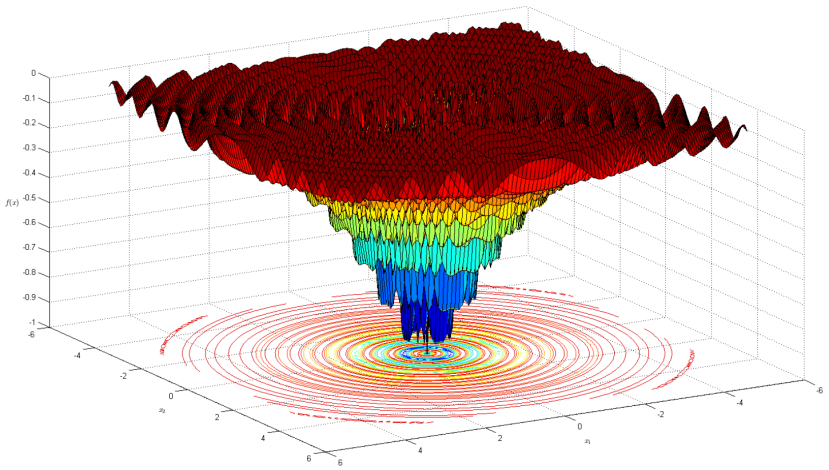

Figure C.12: Drop Wave function

C.13 Step

The continuous and unimodal step function possess a global minimum of $f(x) = 0$ at $\{x\} = \{-5.12\}$ and is applied to a solution space of $-5.12 \leq x_v \leq 5.12$ for $v = 1, 2, \ldots, n_v$ (De Jong, 1975)

$$f(x) = 6n_v + \sum_{v=1}^{n_v} \lfloor x_v \rfloor \tag{C.13}$$

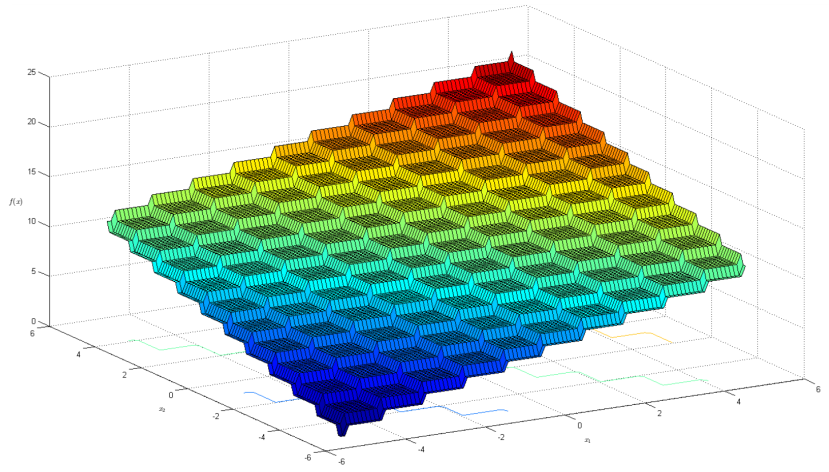

Figure C.13: Step function

C.14 Goldberg

The deceptive and discrete Goldberg function represents design variables as binary chromosomes, leading to its definition using Table C.1 (Goldberg, 1989a,b; Özcan et al., 2008).

$$f(x) = \sum_{v=1}^{n_v} f(x_v) \tag{C.14}$$

Table C.1: Goldberg function variable values

x_v	000	001	010	011	100	101	110	111
$f(x_v)$	1	3	3	8	5	8	8	0

C.15 Whitley

The similarly deceptive and discrete Whitley function extends the binary chromosome from 3 to 4-bits per variable, as such is defined by Table C.2 (Özcan et al., 2008; Whitley, 1991).

$$f(x) = \sum_{v=1}^{n_v} f(x_v) \tag{C.15}$$

Table C.2: Whitley function variable values

x_v	0000	0001	0010	0011	0100	0101	0110	0111
$f(x_v)$	2	4	6	12	8	14	16	30
x_v	1000	1001	1010	1011	1100	1101	1110	1111
$f(x_v)$	11	18	20	28	22	26	24	0

Appendix D

Experimental Results

This appendix contains tables of experimental data for the preliminary investigations in Chapter 7.

D.1 Optimisation Verification

Table D.1 presents the results of the preliminary investigation into verification of the optimisation process. The data include the mean and standard deviation of the final solution objective value found by each low-level heuristic (LLH) to each benchmark function, $\overline{\Phi_{\min}}$ and $\sigma(\Phi_{\min})$ respectively, and the success rate of the LLH in obtaining a solution within 4×10^{-4} of the known global minimum, η.

Table D.1: Optimisation verification preliminary investigation results

	De Jong sphere			Axis-parallel hyper-ellipsoid			Schwefel double sum		
LLH	$\overline{\Phi_{\min}}$	$\sigma(\Phi_{\min})$	η, %	$\overline{\Phi_{\min}}$	$\sigma(\Phi_{\min})$	η, %	$\overline{\Phi_{\min}}$	$\sigma(\Phi_{\min})$	η, %
MC	8.34×10^{-5}	6.83×10^{-2}	74	2.28×10^{-4}	5.28×10^{-2}	81	7.59×10^{-4}	8.55	84
RI	8.37×10^{-5}	6.74×10^{-2}	78	2.37×10^{-4}	5.28×10^{-2}	88	6.91×10^{-4}	8.60	86
KQ	1.20×10^{-7}	8.19×10^{-3}	99	3.05×10^{-7}	2.56×10^{-3}	99	4.58×10^{-5}	2.94×10^{-1}	94
DE	2.60×10^{-5}	4.11×10^{-2}	91	6.41×10^{-6}	3.42×10^{-3}	87	1.04×10^{-4}	5.74×10^{-1}	96
RW	7.50×10^{-6}	9.58×10^{-3}	97	3.34×10^{-7}	8.28×10^{-5}	100	5.58×10^{-5}	1.37×10^{-2}	97
TO	9.66×10^{-6}	1.28×10^{-2}	95	6.94×10^{-7}	1.85×10^{-4}	96	1.18×10^{-4}	3.10×10^{-2}	95
BP	2.14×10^{-7}	2.89×10^{-4}	89	2.21×10^{-7}	7.80×10^{-6}	100	3.63×10^{-5}	1.35×10^{-3}	98
RC	9.25×10^{-5}	7.67×10^{-2}	92	3.23×10^{-4}	7.59×10^{-2}	91	2.92×10^{-4}	13.17	96
PSO	2.87×10^{-6}	2.98×10^{-3}	100	5.51×10^{-6}	1.39×10^{-3}	90	3.63×10^{-5}	1.03×10^{-3}	94
HC	2.61×10^{-4}	4.44×10^{-1}	86	2.37×10^{-4}	1.51×10^{-2}	87	7.73×10^{-3}	2.42×10^{2}	79
SA	2.58×10^{-4}	4.46×10^{-1}	98	2.34×10^{-4}	1.53×10^{-2}	94	5.19×10^{-3}	2.38×10^{2}	82
TS	2.60×10^{-4}	4.52×10^{-1}	91	2.38×10^{-4}	1.56×10^{-2}	91	6.04×10^{-3}	2.47×10^{2}	80
	Rastrigin			Griewank			Schwefel		
LLH	$\overline{\Phi_{\min}}$	$\sigma(\Phi_{\min})$	η, %	$\overline{\Phi_{\min}}$	$\sigma(\Phi_{\min})$	η, %	$\overline{\Phi_{\min}}$	$\sigma(\Phi_{\min})$	η, %
MC	1.63×10^{-4}	8.79×10^{-2}	67	1.84×10^{-4}	3.93×10^{-2}	64	3.24×10^{-4}	1.24	65
RI	1.64×10^{-4}	9.17×10^{-2}	77	1.89×10^{-4}	4.00×10^{-2}	72	3.50×10^{-4}	1.32	79
KQ	1.15×10^{-5}	5.72×10^{-2}	88	1.02×10^{-5}	1.46×10^{-3}	91	2.58×10^{-4}	2.04	82
DE	6.88×10^{-5}	8.58×10^{-2}	84	1.49×10^{-5}	2.50×10^{-3}	89	1.73×10^{-4}	8.13×10^{-1}	85
RW	2.86×10^{-5}	3.38×10^{-2}	85	1.02×10^{-5}	3.49×10^{-4}	84	3.48×10^{-5}	1.00×10^{-1}	96
TO	3.39×10^{-5}	3.74×10^{-2}	87	1.05×10^{-5}	1.42×10^{-4}	87	6.40×10^{-5}	1.77×10^{-2}	95
BP	1.25×10^{-5}	4.74×10^{-2}	85	1.01×10^{-5}	3.50×10^{-4}	89	8.72×10^{-6}	9.95×10^{-2}	91
RC	1.75×10^{-4}	1.01×10^{-1}	76	4.99×10^{-5}	5.81×10^{-2}	71	1.56×10^{-2}	1.37	88
PSO	7.91×10^{-5}	7.46×10^{-2}	83	1.15×10^{-4}	2.47×10^{-1}	82	2.66×10^{-2}	2.57	96
HC	3.45×10^{-4}	4.39×10^{-1}	70	4.81×10^{-4}	8.34×10^{-1}	74	3.99×10^{-2}	6.06	71
SA	3.46×10^{-4}	4.63×10^{-1}	78	4.72×10^{-4}	8.47×10^{-1}	79	3.96×10^{-2}	5.97	86
TS	3.47×10^{-4}	4.53×10^{-1}	77	3.23×10^{-4}	8.40×10^{-1}	84	3.97×10^{-2}	6.07	77

Table D.1: Optimisation verification preliminary investigation results (cont.)

	Six-hump camel back			Rosenbrock valley			Branin		
LLH	$\overline{\Phi_{\min}}$	$\sigma(\Phi_{\min})$	η, %	$\overline{\Phi_{\min}}$	$\sigma(\Phi_{\min})$	η, %	$\overline{\Phi_{\min}}$	$\sigma(\Phi_{\min})$	η, %
MC	-1.032	1.42×10^{-5}	100	7.11×10^{-4}	1.19	74	3.98×10^{-1}	4.06×10^{-5}	100
RI	-1.032	1.17×10^{-5}	100	7.25×10^{-4}	1.14	82	3.98×10^{-1}	3.96×10^{-5}	100
KQ	-1.032	2.95×10^{-3}	100	7.05×10^{-5}	2.70	94	3.98×10^{-1}	3.63×10^{-4}	98
DE	-1.032	1.36×10^{-5}	100	1.51×10^{-4}	3.55×10^{-1}	90	3.98×10^{-1}	4.90×10^{-5}	100
RW	-1.032	8.25×10^{-3}	100	4.60×10^{-5}	5.24×10^{-2}	89	3.98×10^{-1}	8.95×10^{-5}	100
TO	-1.032	7.81×10^{-3}	100	6.27×10^{-5}	8.01×10^{-2}	85	3.98×10^{-1}	1.30×10^{-4}	100
BP	-1.031	1.06×10^{-2}	100	3.58×10^{-5}	2.96×10^{-1}	91	3.98×10^{-1}	1.28×10^{-4}	100
RC	-1.032	4.44×10^{-4}	100	4.61×10^{-4}	1.72	81	3.98×10^{-1}	1.13×10^{-5}	100
PSO	-1.032	1.46×10^{-5}	100	1.22×10^{-4}	1.57×10^{-1}	95	3.98×10^{-1}	1.32×10^{-5}	100
HC	-1.031	74.62	80	9.02×10^{-4}	31.26	63	4.07×10^{-1}	5.87×10^{-3}	49
SA	-1.031	78.90	90	6.04×10^{-4}	30.79	81	3.99×10^{-1}	5.89×10^{-3}	90
TS	-1.032	71.27	85	6.18×10^{-4}	31.41	80	4.00×10^{-1}	6.07×10^{-3}	60
	Easom			Ackley path			Drop wave		
LLH	$\overline{\Phi_{\min}}$	$\sigma(\Phi_{\min})$	η, %	$\overline{\Phi_{\min}}$	$\sigma(\Phi_{\min})$	η, %	$\overline{\Phi_{\min}}$	$\sigma(\Phi_{\min})$	η, %
MC	-2.21×10^{-1}	1.35×10^{-3}	22	1.35×10^{-4}	9.10×10^{-3}	68	-9.97×10^{-1}	1.18×10^{-5}	95
RI	-6.02×10^{-1}	1.27×10^{-3}	34	1.36×10^{-4}	9.40×10^{-3}	72	-9.97×10^{-1}	1.19×10^{-5}	100
KQ	-5.17×10^{-1}	1.46×10^{-4}	51	1.24×10^{-5}	2.41×10^{-3}	79	-9.97×10^{-1}	5.40×10^{-5}	100
DE	-9.99×10^{-1}	9.92×10^{-5}	98	4.22×10^{-5}	6.92×10^{-3}	79	-9.98×10^{-1}	1.32×10^{-5}	100
RW	-9.98×10^{-1}	2.88×10^{-5}	99	1.46×10^{-5}	2.33×10^{-3}	92	-9.99×10^{-1}	1.52×10^{-4}	99
TO	-1.00	2.99×10^{-5}	99	2.15×10^{-5}	2.51×10^{-3}	93	-9.98×10^{-1}	1.69×10^{-4}	99
BP	-9.97×10^{-1}	2.99×10^{-5}	94	1.23×10^{-5}	4.24×10^{-4}	86	-9.99×10^{-1}	1.62×10^{-4}	99
RC	-9.15×10^{-1}	8.83×10^{-4}	64	1.48×10^{-4}	9.85×10^{-3}	82	-1.00	6.80×10^{-5}	100
PSO	-9.97×10^{-1}	8.07×10^{-5}	98	1.23×10^{-5}	1.76×10^{-5}	88	-9.99×10^{-1}	1.14×10^{-5}	100
HC	-2.95×10^{-1}	2.89×10^{-8}	34	2.01×10^{-4}	6.32×10^{-3}	61	-3.50×10^{-1}	1.75×10^{-3}	12
SA	-4.28×10^{-1}	6.62×10^{-9}	52	2.01×10^{-4}	6.33×10^{-3}	80	-4.12×10^{-1}	1.81×10^{-3}	25
TS	-2.98×10^{-1}	1.01×10^{-11}	37	2.01×10^{-4}	6.41×10^{-3}	79	-4.96×10^{-1}	1.66×10^{-3}	31
	Step			Goldberg			Whitley		
LLH	$\overline{\Phi_{\min}}$	$\sigma(\Phi_{\min})$	η, %	$\overline{\Phi_{\min}}$	$\sigma(\Phi_{\min})$	η, %	$\overline{\Phi_{\min}}$	$\sigma(\Phi_{\min})$	η, %
MC	1.48×10^{-4}	1.30×10^{-2}	90	7.61×10^{-2}	3.80×10^{-1}	81	8.69×10^{-3}	2.28×10^{-1}	84
RI	1.48×10^{-4}	1.49×10^{-2}	92	7.67×10^{-2}	3.62×10^{-1}	85	8.93×10^{-3}	2.38×10^{-1}	86
KQ	3.19×10^{-4}	3.84×10^{-2}	95	2.86×10^{-2}	2.57	92	5.43×10^{-3}	8.00×10^{-1}	94
DE	5.16×10^{-5}	1.26×10^{-2}	98	4.94×10^{-2}	4.40×10^{-1}	91	5.20×10^{-3}	1.26×10^{-1}	90
RW	0.00	0.00	100	8.07×10^{-3}	1.59×10^{-1}	95	5.66×10^{-3}	2.38×10^{-1}	87
TO	0.00	0.00	100	1.16×10^{-2}	1.68×10^{-1}	97	6.18×10^{-3}	2.36×10^{-1}	86
BP	0.00	0.00	100	1.58×10^{-2}	2.72×10^{-1}	99	5.96×10^{-3}	2.41×10^{-1}	91
RC	1.77×10^{-4}	1.64×10^{-2}	97	8.10×10^{-2}	3.77×10^{-1}	90	1.33×10^{-2}	2.71×10^{-1}	92
PSO	0.00	0.00	100	2.02×10^{-2}	2.66×10^{-1}	98	1.50×10^{-2}	5.43×10^{-1}	84
HC	5.38×10^{-4}	9.19×10^{-2}	100	1.50×10^{-1}	1.59	84	9.04×10^{-2}	2.18	56
SA	5.44×10^{-4}	9.65×10^{-2}	100	1.49×10^{-1}	1.59	89	9.18×10^{-2}	2.20	70
TS	5.38×10^{-4}	9.31×10^{-2}	100	1.50×10^{-1}	1.58	90	9.08×10^{-2}	2.22	84

D.2 Parameter Evaluation

Table D.2 lists the different experimental set-ups of the parameter evaluation preliminary investigation. The notation used in this section is used for all subsequent tables within this appendix. The data in Table D.2 include the experiment identification (ID), LLH employed, solution representation, population size, μ, and LLH-specific parameters. For consistency, the same value of n_b, the number of strand bits, is used for real number representation as for the corresponding binary representation experiments when calculating the population size, e.g. $n_b = 8$ for PE6 and PE12, therefore this value is also used for PE18, PE24 and PE30 when performing the calculation $\mu = 4n_v n_b$.

Table D.2: Parameter evaluation preliminary investigation set-up

ID	LLH	Representation	μ	LLH set-up
PE1	MC	8-bit binary	50	
PE2			100	
PE3			200	
PE4			$20n_v$	
PE5			400	
PE6			$4n_v n_b$	
PE7	RW	8-bit binary	50	Uniform crossover; $p_{c,GA} = 0.9$
PE8			100	
PE9			200	
PE10			$20n_v$	
PE11			400	
PE12			$4n_v n_b$	
PE13		Real	50	
PE14			100	
PE15			200	
PE16			$20n_v$	
PE17			400	
PE18			$4n_v n_b$	
PE19	DE	Real	50	$p_{c,DE} = 0.5$; $F_{DE} = 0.9$
PE20			100	
PE21			200	
PE22			$20n_v$	
PE23			400	
PE24			$4n_v n_b$	
PE25	PSO	Real	50	$\omega_{PSO} = 0.65$; $c_{1,PSO} = 1.75$; $c_{2,PSO} = 1.35$; $\kappa_{PSO} = 0.5$
PE26			100	
PE27			200	
PE28			$20n_v$	
PE29			400	
PE30			$4n_v n_b$	
PE31	RW	8-bit binary	$20n_v$	1-point crossover; $p_{c,GA} = 0.9$
PE32				2-point crossover
PE33				Random crossover
PE34				Random parameterwise crossover
PE35		4-bit binary	$20n_v$	1-point crossover
PE36				2-point crossover
PE37				Uniform crossover
PE38				Random crossover
PE39				Random parameterwise crossover
PE40		16-bit binary	$20n_v$	1-point crossover
PE41				2-point crossover
PE42				Uniform crossover
PE43				Random crossover
PE44				Random parameterwise crossover
PE45		Real	$20n_v$	1-point crossover
PE46				2-point crossover
PE47				Uniform crossover
PE48				Random crossover
PE49				Blend crossover
PE50	RW	8-bit binary	$20n_v$	Uniform crossover; $p_{c,GA} = 1.0$
PE51				$p_{c,GA} = 0.75$
PE52				$p_{c,GA} = 0.6$
PE53				$p_{c,GA} = 0.4$
PE54	RW	Real	100	Uniform crossover; $p_{c,GA} = 0.9$; random mutation; $p_m = \frac{1}{\mu}$

Table D.2: Parameter evaluation preliminary investigation set-up (cont.)

ID	LLH	Representation	μ	LLH set-up
PE55				Non-uniform mutation
PE56				Gaussian mutation
PE57				Random mutation; $p_m = \frac{1+n_b}{2\mu n_b}$
PE58				Non-uniform mutation
PE59				Gaussian mutation
PE60	RW	8-bit binary	100	Uniform crossover; $p_{c,GA} = 0.9$; bit-flip mutation; $p_m = \frac{1}{\mu n_b}$
PE61				$p_m = \frac{1+n_b}{2\mu n_b}$
PE62		4-bit binary	$20n_v$	$p_m = \frac{1}{\mu n_b}$
PE63				$p_m = \frac{1+n_b}{2\mu n_b}$
PE64		16-bit binary	$20n_v$	$p_m = \frac{1}{\mu n_b}$
PE65				$p_m = \frac{1+n_b}{2\mu n_b}$
PE66	KQ	8-bit binary	$20n_v$	$p_m = 0.95$
PE67				$p_m = 0.75$
PE68				$p_m = 0.5$
PE69		Real	$20n_v$	$p_m = 0.95$
PE70				$p_m = 0.75$
PE71				$p_m = 0.5$
PE72	RI	8-bit binary	$20n_v$	$\alpha_{RI} = 0.1$
PE73				$\alpha_{RI} = 0.25$
PE74				$\alpha_{RI} = 0.5$
PE75		Real	$20n_v$	$\alpha_{RI} = 0.1$
PE76				$\alpha_{RI} = 0.25$
PE77				$\alpha_{RI} = 0.5$
PE78	BP	8-bit binary	$20n_v$	Uniform crossover; $p_{c,GA} = 0.9$; $\alpha_{BP} = 0.1$
PE79				$\alpha_{BP} = 0.25$
PE80				$\alpha_{BP} = 0.5$
PE81		Real	$20n_v$	Uniform crossover; $p_{c,GA} = 0.9$; $\alpha_{BP} = 0.1$
PE82				$\alpha_{BP} = 0.25$
PE83				$\alpha_{BP} = 0.5$
PE84	RC	8-bit binary	$20n_v$	Uniform crossover; $p_{c,GA} = 0.9$; $\alpha_{RC} = 0.1$
PE85				$\alpha_{RC} = 0.25$
PE86				$\alpha_{RC} = 0.5$
PE87		Real	$20n_v$	Uniform crossover; $p_{c,GA} = 0.9$; $\alpha_{RC} = 0.1$
PE88				$\alpha_{RC} = 0.25$
PE89				$\alpha_{RC} = 0.5$
PE90	DE	Real	$20n_v$	$p_{c,DE} = 0.5$; $F_{DE} = 1.2$
PE91				$F_{DE} = 0.95$
PE92				$F_{DE} = 0.6$
PE93				$p_{c,DE} = 1.0$; $F_{DE} = 0.9$
PE94				$p_{c,DE} = 0.65$
PE95				$p_{c,DE} = 0.4$
PE96	PSO	Real	$20n_v$	$\omega_{PSO} = 0.6$; $c_{1,PSO} = 1.7$; $c_{2,PSO} = 1.4$; $\kappa_{PSO} = 0.5$
PE97				$\omega_{PSO} = 0.8$
PE98				$\omega_{PSO} = 0.6$; $c_{1,PSO} = 1.4$
PE99				$c_{1,PSO} = 2.1$
PE100				$c_{1,PSO} = 1.7$; $c_{2,PSO} = 0.9$
PE101				$c_{2,PSO} = 1.8$

Table D.2: Parameter evaluation preliminary investigation set-up (cont.)

ID	LLH	Representation	μ	LLH set-up
PE102				$c_{2,PSO} = 1.4$; $\kappa_{PSO} = 0.0$
PE103				$\kappa_{PSO} = 1.0$
PE104	HC	Real	1	$\Delta x_v = 0.05\Delta \mathrm{V}_v$
PE105				$\Delta x_v = 0.1\Delta \mathrm{V}_v$
PE106				$\Delta x_v = 0.2\Delta \mathrm{V}_v$
PE107				$\Delta x_v = 0.5\Delta \mathrm{V}_v$
PE108				$\Delta x_v = \Delta \mathrm{V}_v$
PE109		8-bit binary	1	$\Delta x_v = 0.05\Delta \mathrm{V}_v$
PE110				$\Delta x_v = 0.1\Delta \mathrm{V}_v$
PE111				$\Delta x_v = 0.2\Delta \mathrm{V}_v$
PE112				$\Delta x_v = 0.5\Delta \mathrm{V}_v$
PE113				$\Delta x_v = \Delta \mathrm{V}_v$
PE114	SA	Real	1	$\Delta x_v = 0.1\Delta \mathrm{V}_v$; exponential cooling; $T^0_{SA} = 0.9$; $\alpha_{SA} = 0.95$
PE115				$\alpha_{SA} = 0.85$
PE116				$\alpha_{SA} = 0.75$
PE117				$T^0_{SA} = 1.0$; $\alpha_{SA} = 0.95$
PE118				$T^0_{SA} = 0.75$
PE119				$T^0_{SA} = 0.5$
PE120				Linear cooling; $\alpha_{SA} = \frac{1}{n_k}$; $T^0_{SA} = 1.0$
PE121				$T^0_{SA} = 0.9$
PE122				$T^0_{SA} = 0.75$
PE123				$T^0_{SA} = 0.5$
PE124	TS	Real	1	$\Delta x_v = 0.1\Delta \mathrm{V}_v$; $n_{TS} = 1,000$
PE125				$n_{TS} = 500$
PE126				$n_{TS} = 100$
PE127				$n_{TS} = 50$
PE128				$n_{TS} = 10$
PE129				$n_{TS} = 5$
PE130				$n_{TS} = 1$

Table D.3 presents the results of each experiment for the run that generated the best solution. Results include the best solution unpenalised and penalised objective values, $f_{\min}$ and $\Phi_{\min}$ respectively, corresponding worst values with respect to the design constraints, c_1 and c_2, and percentage of feasible members within the design, η. Final population feasibility, $\beta(\mathrm{X}^{n_k})$, and affinity, $A(\mathrm{X}^{n_k})$, are included as well as the generation of best solution discovery, N, and computation time taken, T.

Table D.3: Parameter evaluation preliminary investigation solution of minimal mass results

ID	$f_{\min}$	$\Phi_{\min}$	c_1	c_2, m	η, %	$\beta(\mathrm{X}^{n_k})$, %	$A(\mathrm{X}^{n_k})$, %	N	T, h
PE1	55,602	57,684	1.35	0.20	99.77	6.00	15.50	43	1.15
PE2	55,541	56,602	1.46	0.34	97.41	14.00	12.90	25	2.02
PE3	57,908	58,059	1.46	0.37	99.76	11.00	11.06	122	7.17
PE4	58,092	58,092	1.61	0.28	100.00	10.00	9.42	50	8.18
PE5	54,633	54,633	1.52	-0.08	100.00	10.25	8.97	163	13.01
PE6	54,467	54,467	1.52	0.24	100.00	10.11	8.65	147	17.02
PE7	53,088	53,088	1.65	0.22	100.00	50.00	34.18	140	1.03
PE8	52,288	52,356	1.47	-0.14	99.65	51.00	28.73	128	1.94
PE9	53,046	53,046	1.50	0.47	100.00	47.00	25.08	101	3.10
PE10	52,767	53,159	1.44	0.27	99.78	51.76	21.04	222	7.17
PE11	52,519	52,772	1.45	0.20	99.74	47.25	20.92	58	5.41

Table D.3: Parameter evaluation preliminary investigation solution of minimal mass results (cont.)

ID	$f_{\min}$	$\Phi_{\min}$	c_1	c_2, m	η, %	$\beta(\mathrm{X}^{n_k})$, %	$A(\mathrm{X}^{n_k})$, %	N	T, h
PE12	52,915	53,392	1.43	0.21	99.72	52.39	17.90	162	9.65
PE13	50,553	50,553	1.51	0.30	100.00	64.00	33.19	546	1.40
PE14	49,993	50,351	1.44	0.14	99.53	11.00	33.86	443	1.93
PE15	50,235	50,305	1.47	0.28	99.55	0.00	96.39	397	2.99
PE16	50,137	50,367	1.45	0.30	99.08	0.00	41.22	218	3.30
PE17	50,447	50,447	1.52	-0.23	100.00	0.00	39.68	159	3.58
PE18	50,032	50,199	1.46	0.32	99.53	0.00	38.10	155	4.23
PE19	59,619	59,619	1.61	0.05	100.00	12.00	76.17	2	0.83
PE20	56,058	56,060	1.50	-0.16	99.73	9.00	8.55	120	3.52
PE21	57,160	57,160	1.63	0.28	100.00	8.00	8.02	3	3.35
PE22	56,482	57,195	1.42	0.37	99.78	7.06	7.80	4	5.69
PE23	57,227	57,227	1.52	0.26	100.00	5.25	7.62	70	10.99
PE24	56,752	58,117	1.38	0.12	99.78	8.64	76.05	108	16.08
PE25	84,666	84,708	1.48	0.49	99.80	0.00	55.49	124	1.10
PE26	57,032	59,895	1.33	0.39	99.76	0.00	55.40	135	1.93
PE27	57,171	61,095	1.30	0.38	99.76	4.50	55.48	261	5.06
PE28	57,090	60,650	1.31	0.37	99.74	28.82	54.84	116	6.87
PE29	56,497	60,028	1.31	0.38	99.73	12.00	55.07	207	8.77
PE30	57,310	59,121	1.37	0.14	99.76	31.62	99.45	146	9.53
PE31	52,411	53,370	1.40	0.16	99.76	48.53	22.40	80	4.84
PE32	52,084	52,154	1.47	0.28	99.75	47.65	21.38	51	3.83
PE33	52,864	52,938	1.47	-0.14	99.67	43.82	22.81	37	3.88
PE34	51,751	51,900	1.46	0.16	99.75	52.35	20.85	174	6.54
PE35	51,303	51,342	1.48	0.15	99.69	45.29	27.65	60	4.46
PE36	51,237	51,303	1.47	0.42	99.77	41.47	27.82	38	3.81
PE37	51,366	51,399	1.48	0.34	99.73	48.82	28.17	94	5.90
PE38	52,048	52,217	1.46	0.41	99.72	45.59	28.03	22	3.33
PE39	51,615	51,786	1.46	-0.38	99.69	46.76	25.84	155	6.97
PE40	52,266	52,266	1.52	0.20	100.00	47.65	19.27	172	10.24
PE41	52,046	52,854	1.41	0.12	99.66	45.00	18.88	109	7.48
PE42	53,173	53,393	1.49	0.49	97.17	52.06	18.14	72	6.94
PE43	53,398	53,398	1.63	0.13	100.00	41.47	18.79	42	5.43
PE44	52,732	52,732	1.55	0.34	100.00	49.41	18.94	63	6.10
PE45	49,818	49,868	1.48	0.38	99.54	0.00	96.63	278	3.14
PE46	49,806	49,869	1.47	0.38	99.54	0.00	47.68	286	3.25
PE47	49,964	50,127	1.46	0.35	99.57	0.00	93.12	201	3.20
PE48	49,814	49,866	1.48	0.38	99.54	0.00	50.02	292	2.56
PE49	50,468	50,704	1.46	0.37	99.15	10.00	37.63	288	3.98
PE50	52,649	52,649	1.53	0.26	100.00	47.94	21.42	139	6.10
PE51	53,068	53,068	1.69	0.21	100.00	51.18	20.60	27	4.08
PE52	53,390	54,326	1.40	0.56	99.76	39.41	18.70	217	10.12
PE53	53,704	55,268	1.37	0.31	99.71	42.06	17.61	86	6.51
PE54	50,109	50,279	1.46	0.23	99.54	1.18	34.86	219	2.78
PE55	50,333	50,401	1.47	0.29	99.52	0.00	53.92	248	1.76
PE56	50,220	50,220	1.51	0.34	100.00	0.59	40.39	128	1.87
PE57	50,242	50,557	1.44	0.30	99.59	49.12	17.22	180	4.65
PE58	50,202	50,578	1.44	0.26	99.61	0.00	54.53	31	1.73
PE59	49,970	50,024	1.48	0.30	96.59	6.76	33.14	222	2.48
PE60	51,239	51,268	1.48	0.36	99.58	88.00	85.49	55	0.23
PE61	50,155	50,212	1.47	0.32	99.53	9.00	85.19	139	0.48
PE62	51,243	51,243	1.58	0.26	100.00	96.00	85.91	46	0.20
PE63	50,840	50,883	1.48	0.28	99.06	95.00	85.56	71	0.31
PE64	51,360	51,360	1.52	0.39	100.00	93.00	85.17	63	0.46
PE65	50,667	50,674	1.49	0.27	99.53	3.00	85.12	68	0.43
PE66	87,723	87,723	2.00	0.29	100.00	0.00	90.60	1	0.14
PE67	55,097	56,575	1.38	0.03	99.78	1.76	52.47	44	9.41

Table D.3: Parameter evaluation preliminary investigation solution of minimal mass results (cont.)

ID	$f_{\min}$	$\Phi_{\min}$	c_1	c_2, m	η, %	$\beta(\mathrm{X}^{n_k})$, %	$A(\mathrm{X}^{n_k})$, %	N	T, h
PE68	54,997	55,562	1.42	-0.17	99.77	12.65	9.13	39	7.74
PE69	49,917	49,994	1.47	0.38	99.58	0.00	55.55	280	8.45
PE70	50,091	50,145	1.48	0.40	99.10	0.00	55.55	291	7.25
PE71	49,814	49,865	1.48	0.38	99.54	0.00	55.55	293	5.91
PE72	56,520	56,520	1.58	0.14	100.00	12.35	10.07	111	11.13
PE73	53,712	54,364	1.42	-0.06	99.73	17.35	11.03	34	6.68
PE74	56,209	56,236	1.48	0.24	99.77	30.00	11.82	130	10.02
PE75	55,774	55,926	1.46	0.20	99.76	15.00	3.71	77	8.73
PE76	57,039	57,039	1.54	0.35	100.00	19.41	3.85	59	7.87
PE77	57,170	57,170	1.58	0.37	100.00	29.71	4.17	59	6.60
PE78	49,934	50,057	1.46	0.34	99.57	26.76	54.47	102	3.29
PE79	51,134	51,197	1.47	0.25	99.69	39.12	34.96	220	5.07
PE80	51,984	51,984	1.53	0.08	100.00	42.65	24.19	65	4.23
PE81	49,845	49,897	1.48	0.35	95.77	0.00	55.12	277	2.38
PE82	49,931	49,955	1.48	0.39	99.55	4.12	41.92	128	2.05
PE83	50,209	50,243	1.48	0.22	99.56	1.18	35.46	104	2.00
PE84	54,035	54,035	1.57	0.17	100.00	10.00	15.12	200	14.65
PE85	53,535	56,570	1.32	0.14	99.78	10.59	16.43	64	8.95
PE86	54,138	56,174	1.35	0.05	99.80	7.35	17.45	109	11.43
PE87	57,135	58,250	1.40	0.24	99.71	6.47	9.53	64	9.02
PE88	56,430	56,892	1.43	0.24	99.76	8.53	7.69	33	5.78
PE89	55,785	56,484	1.42	0.46	99.78	18.24	16.86	137	12.83
PE90	57,895	57,895	1.52	0.30	100.00	12.35	5.82	83	4.85
PE91	57,573	57,573	1.51	-0.12	100.00	10.59	7.71	4	2.42
PE92	54,310	54,310	1.59	0.07	100.00	8.24	10.33	14	3.67
PE93	55,046	59,602	1.38	0.29	99.49	9.41	8.00	58	4.38
PE94	55,265	55,822	1.42	0.39	99.80	5.88	8.18	27	3.51
PE95	52,797	52,800	1.49	0.23	99.68	12.94	7.75	411	13.64
PE96	56,534	60,241	1.31	0.37	99.47	0.00	55.30	272	7.88
PE97	56,840	60,410	1.31	0.39	99.74	5.59	55.17	295	7.28
PE98	56,730	60,286	1.31	0.39	99.73	2.65	54.75	290	9.33
PE99	56,380	61,884	1.31	0.35	99.48	0.00	55.45	233	7.86
PE100	56,411	61,124	1.31	0.37	99.47	0.00	53.56	54	5.71
PE101	56,628	60,086	1.31	0.35	99.73	0.59	55.00	295	7.42
PE102	87,723	87,723	2.00	0.29	100.00	8.24	3.30	1	5.57
PE103	51,230	52,224	1.40	0.39	99.72	0.00	45.37	291	4.57
PE104	55,591	55,658	1.47	0.40	99.74	-	-	4,911	1.27
PE105	52,602	52,875	1.45	0.38	99.73	-	-	6,654	1.25
PE106	52,981	52,991	1.49	0.19	99.70	-	-	2,674	0.61
PE107	51,009	51,077	1.48	0.18	99.30	-	-	2,664	0.75
PE108	50,439	50,694	1.45	0.28	99.61	-	-	933	0.63
PE109	186,595	186,595	2.27	0.80	100.00	-	-	768	1.37
PE110	185,971	185,971	2.23	0.77	100.00	-	-	206	0.84
PE111	185,628	185,628	2.15	0.77	100.00	-	-	446	1.17
PE112	175,214	175,214	2.06	0.73	100.00	-	-	3,113	2.75
PE113	53,538	53,538	1.50	0.40	99.73	-	-	70	0.61
PE114	53,567	53,627	1.48	0.37	99.72	-	-	5,397	1.35
PE115	52,743	53,036	1.44	0.16	99.70	-	-	6,568	1.09
PE116	53,953	54,200	1.45	0.22	99.75	-	-	4,946	0.83
PE117	53,720	53,943	1.45	0.21	99.77	-	-	3,629	0.87
PE118	54,898	54,900	1.50	0.31	99.75	-	-	2,517	0.56
PE119	53,059	53,188	1.46	0.34	99.73	-	-	6,876	1.85
PE120	53,849	53,941	1.47	0.17	99.74	-	-	4,065	0.68
PE121	52,861	53,255	1.44	0.38	99.73	-	-	5,789	0.99
PE122	53,644	53,753	1.47	0.37	99.74	-	-	5,347	1.11
PE123	53,722	53,993	1.45	0.15	99.75	-	-	5,644	0.89

Table D.3: Parameter evaluation preliminary investigation solution of minimal mass results (cont.)

ID	$f_{\min}$	$\Phi_{\min}$	c_1	c_2, m	η, %	$\beta(\mathrm{X}^{n_k})$, %	$A(\mathrm{X}^{n_k})$, %	N	T, h
PE124	53,794	53,851	1.48	0.19	99.71	-	-	4,951	0.93
PE125	53,350	53,418	1.47	0.30	99.71	-	-	8,295	1.30
PE126	53,026	53,072	1.48	0.17	99.72	-	-	4,617	0.93
PE127	53,344	53,611	1.45	0.16	99.74	-	-	5,828	1.00
PE128	53,487	53,662	1.46	0.31	99.72	-	-	7,883	1.47
PE129	52,900	53,188	1.44	0.32	99.69	-	-	8,116	1.25
PE130	53,218	53,473	1.45	0.27	99.73	-	-	4,383	0.82

Table D.4 presents similar data to Table D.3 to indicate the mean values of the best solutions found by all five runs of each experiment as well as the standard deviation in the final solution objective value, $\sigma(\Phi_{\min})$. Mean values with respect to the design constraints are not appropriate, thus not included.

Table D.4: Parameter evaluation preliminary investigation average results

ID	$\overline{f_{\min}}$	$\overline{\Phi_{\min}}$	$\overline{\sigma(\Phi_{\min})}$	$\overline{\beta(\mathrm{X}^{n_k})}$, %	$\overline{A(\mathrm{X}^{n_k})}$, %	$\overline{N}$	$\overline{T}$, h
PE1	59,137	63,507	3,529	12.00	15.99	22.6	0.99
PE2	58,208	58,570	1,114	10.20	12.87	44.2	2.21
PE3	57,589	62,102	3,425	10.40	10.80	48.8	4.76
PE4	57,399	61,064	4,042	10.59	9.61	32.4	7.36
PE5	55,790	57,600	2,631	9.45	9.12	79.2	10.09
PE6	54,667	56,750	2,215	10.29	8.73	77.6	13.64
PE7	54,183	54,210	1,058	50.80	34.40	101.0	0.86
PE8	53,749	54,314	1,501	50.80	28.22	94.6	1.67
PE9	53,254	53,753	701	50.80	24.44	67.8	2.78
PE10	53,489	53,672	539	50.47	21.47	84.2	4.87
PE11	53,098	54,023	1,590	49.50	20.35	53.2	4.77
PE12	53,224	53,713	335	51.51	18.85	96.4	8.03
PE13	50,663	51,071	554	34.00	38.35	320.0	0.94
PE14	50,478	50,603	275	22.60	39.12	260.8	1.40
PE15	50,408	50,524	198	3.90	53.32	355.0	2.89
PE16	50,465	50,927	818	6.06	48.59	158.2	2.92
PE17	50,604	51,062	1,016	5.60	47.24	174.0	3.08
PE18	50,473	50,568	216	0.00	47.45	168.6	3.72
PE19	62,791	64,769	4,153	8.40	21.67	75.6	1.40
PE20	57,873	62,013	7,003	8.20	21.57	70.6	2.65
PE21	60,238	65,112	7,954	8.30	21.42	12.4	3.67
PE22	57,496	59,133	2,705	8.29	21.36	42.2	7.66
PE23	57,210	58,764	1,633	7.45	21.41	41.8	8.92
PE24	57,852	59,831	1,160	7.76	21.42	60.8	13.09
PE25	84,903	86,162	1,442	0.00	64.02	90.2	0.94
PE26	61,718	71,698	9,665	0.00	62.03	32.4	1.42
PE27	66,150	69,133	4,698	0.90	63.66	121.2	3.73
PE28	56,330	64,598	3,118	5.76	62.90	77.0	6.20
PE29	56,557	61,884	3,074	5.00	63.63	138.4	7.90
PE30	56,908	61,874	1,848	6.40	63.33	126.4	9.29
PE31	52,828	53,820	519	46.59	22.67	58.8	4.26
PE32	52,738	54,160	2,682	44.24	21.36	69.4	4.62
PE33	53,163	54,319	1,388	47.41	21.60	58.4	4.38
PE34	52,132	53,141	917	50.12	20.83	99.4	5.44
PE35	51,677	53,198	1,249	42.18	28.76	39.6	3.77
PE36	51,652	51,690	327	41.23	27.55	81.2	5.16

Table D.4: Parameter evaluation preliminary investigation average results (cont.)

ID	$\overline{f_{\min}}$	$\overline{\Phi_{\min}}$	$\overline{\sigma(\Phi_{\min})}$	$\overline{\beta(\mathrm{X}^{n_k})}$, %	$\overline{A(\mathrm{X}^{n_k})}$, %	$\overline{N}$	$\overline{T}$, h
PE37	52,227	52,248	811	46.12	27.99	85.0	5.27
PE38	52,387	52,585	314	43.65	28.30	46.8	3.87
PE39	51,960	52,256	365	47.41	72.14	101.0	5.45
PE40	52,588	53,397	767	45.00	18.13	121.0	8.04
PE41	52,524	55,483	4,980	44.82	18.43	83.2	6.71
PE42	52,920	53,968	496	50.88	17.57	91.0	7.62
PE43	52,516	53,670	327	45.88	19.27	64.2	6.00
PE44	53,390	53,719	869	50.00	17.73	62.8	7.16
PE45	49,831	49,899	31	0.00	57.79	269.8	3.06
PE46	50,011	50,196	373	0.71	55.51	240.6	3.10
PE47	50,430	50,684	454	4.35	47.52	184.0	2.96
PE48	49,883	49,950	119	0.00	59.36	262.2	2.94
PE49	50,932	51,065	209	11.47	47.75	290.0	3.66
PE50	52,684	53,227	509	51.06	21.84	94.0	5.07
PE51	54,052	54,355	914	50.70	20.23	56.4	5.00
PE52	53,679	55,857	1,478	48.24	19.15	82.6	6.45
PE53	54,688	56,903	2,685	40.00	16.74	50.2	5.92
PE54	50,548	50,647	208	0.53	34.49	158.8	2.58
PE55	49,999	50,853	431	0.00	51.79	80.8	2.06
PE56	50,582	50,625	247	0.53	40.91	167.2	2.20
PE57	50,611	50,697	121	33.00	18.56	220.8	4.28
PE58	49,938	50,778	149	0.00	54.27	36.6	1.79
PE59	50,195	50,228	284	5.82	33.12	181.0	2.38
PE60	51,463	51,539	393	39.80	85.28	52.4	0.23
PE61	50,578	50,854	637	23.80	84.68	140.2	0.53
PE62	51,772	51,873	623	82.40	85.81	38.6	0.22
PE63	51,085	51,217	406	73.40	85.50	58.2	0.29
PE64	51,367	51,653	238	56.60	85.41	60.6	0.40
PE65	50,799	51,079	331	39.40	84.56	113.0	0.49
PE66	87,723	87,723	0	0.00	90.62	22.0	0.14
PE67	59,908	61,862	3,150	2.64	52.74	29.0	8.48
PE68	56,158	57,675	1,910	10.18	9.44	44.8	7.87
PE69	50,343	50,400	453	0.00	64.44	288.6	8.29
PE70	51,575	52,179	2,085	11.29	48.79	141.4	5.60
PE71	49,841	50,157	577	1.76	62.58	233.8	5.44
PE72	55,929	57,920	1,032	13.41	9.77	63.6	8.50
PE73	57,077	59,310	3,635	17.53	10.98	36.8	6.76
PE74	57,112	58,699	3,311	30.35	12.05	94.8	8.12
PE75	56,836	57,026	839	14.00	17.67	58.4	8.22
PE76	55,947	60,338	4,822	19.65	17.98	57.6	7.73
PE77	57,856	59,764	2,355	30.94	18.44	78.4	7.44
PE78	50,664	50,864	535	24.06	52.33	61.4	2.59
PE79	51,357	51,406	231	41.59	35.79	109.8	3.53
PE80	52,257	52,638	465	45.35	24.56	77.6	3.93
PE81	49,860	49,945	59	1.12	61.33	179.8	2.26
PE82	49,936	50,181	205	2.65	49.65	100.0	1.94
PE83	50,592	50,630	229	1.59	49.32	159.8	2.56
PE84	56,681	57,490	2,057	11.53	15.33	109.4	11.32
PE85	57,015	57,862	1,435	14.71	15.97	26.8	6.95
PE86	56,444	59,537	4,838	12.47	18.52	69.6	9.24
PE87	57,531	63,439	8,294	9.82	23.10	33.8	7.41
PE88	56,969	60,046	2,935	13.94	23.14	39.6	7.01
PE89	56,523	59,107	2,560	13.76	26.84	74.8	8.85
PE90	56,538	63,459	8,235	9.29	6.14	77.2	5.00
PE91	58,234	60,989	4,739	10.00	7.35	108.4	5.59
PE92	58,329	61,581	7,140	5.77	10.25	23.6	3.71

Table D.4: Parameter evaluation preliminary investigation average results (cont.)

ID	$\overline{f_{\min}}$	$\overline{\Phi_{\min}}$	$\overline{\sigma(\Phi_{\min})}$	$\overline{\beta(\mathrm{X}^{n_k})}$, %	$\overline{A(\mathrm{X}^{n_k})}$, %	$\overline{N}$	$\overline{T}$, h
PE93	58,059	63,777	4,467	8.23	7.54	74.2	4.81
PE94	58,668	60,925	6,479	6.82	7.76	13.8	2.99
PE95	60,962	63,308	6,982	9.53	7.60	277.6	9.70
PE96	56,549	63,416	4,586	0.06	63.07	114.4	6.64
PE97	56,257	63,327	2,762	1.12	63.33	126.8	6.38
PE98	56,810	62,400	2,850	1.71	63.52	203.8	7.41
PE99	56,360	65,554	3,026	0.00	62.89	89.0	6.04
PE100	56,505	65,827	4,578	0.00	61.32	32.2	5.21
PE101	56,629	62,114	1,440	0.12	63.65	141.8	6.72
PE102	87,723	87,723	0	8.24	17.41	1.0	5.64
PE103	53,070	54,547	1,423	0.00	55.62	277.4	4.51
PE104	62,034	62,282	7,712	-	-	3,251.8	0.84
PE105	54,100	54,342	1,625	-	-	4,839.0	1.21
PE106	53,287	53,806	1,148	-	-	1,974.6	0.80
PE107	52,298	52,809	1,571	-	-	1,090.8	0.54
PE108	51,597	52,901	2,516	-	-	857.2	0.82
PE109	186,630	186,630	31	-	-	304.4	0.87
PE110	186,048	186,048	71	-	-	85.8	0.91
PE111	185,755	185,755	99	-	-	527.0	1.11
PE112	176,237	176,237	858	-	-	1,979.4	1.95
PE113	57,058	58,307	4,038	-	-	936.6	1.14
PE114	55,284	55,534	1,728	-	-	2,916.6	0.74
PE115	53,244	53,468	407	-	-	4,699.8	1.03
PE116	55,461	55,675	994	-	-	3,033.8	0.82
PE117	55,103	55,304	1,299	-	-	2,559.2	0.64
PE118	55,392	55,508	604	-	-	2,028.4	0.54
PE119	54,363	54,443	1,304	-	-	4,420.4	1.08
PE120	55,326	55,570	1,283	-	-	2,871.6	0.56
PE121	57,759	58,078	6,520	-	-	2,277.6	0.59
PE122	55,178	55,335	1,396	-	-	3,670.4	0.78
PE123	55,001	55,232	898	-	-	3,263.8	0.70
PE124	54,666	54,801	984	-	-	3,077.8	0.74
PE125	54,769	55,011	1,016	-	-	3,659.8	0.82
PE126	55,617	55,864	1,787	-	-	2,251.2	0.67
PE127	54,220	54,516	921	-	-	3,364.8	0.68
PE128	55,191	55,552	1,281	-	-	3,658.4	0.79
PE129	53,789	54,045	725	-	-	4,479.2	0.82
PE130	54,799	55,096	1,614	-	-	3,760.6	0.69

D.3 Penalty Function

The set-ups of the penalty function preliminary investigation are listed in Table D.5. The set-ups vary in the penalty function employed, value of penalty parameter, λ, population size and adaptation interval.

Table D.5: Penalty function preliminary investigation set-up

ID	Penalty function	λ	μ	$n_{k,\lambda}$
PF1	None	N/A	100	N/A
PF2			$20n_v$	
PF3			$4n_v n_b$	
PF4	Death	N/A	100	N/A
PF5			$20n_v$	

Table D.5: Penalty function preliminary investigation set-up (cont.)

ID	Penalty function	λ	μ	$n_{k,\lambda}$
PF6			$4n_v n_b$	
PF7	Interior	1.0	100	N/A
PF8			$20n_v$	
PF9			$4n_v n_b$	
PF10		2.0	100	N/A
PF11			$20n_v$	
PF12			$4n_v n_b$	
PF13	Interior barrier	1.0	100	N/A
PF14			$20n_v$	
PF15			$4n_v n_b$	
PF16		2.0	100	N/A
PF17			$20n_v$	
PF18			$4n_v n_b$	
PF19	Static exterior	1.0	100	N/A
PF20			$20n_v$	
PF21			$4n_v n_b$	
PF22		2.0	100	N/A
PF23			$20n_v$	
PF24			$4n_v n_b$	
PF25	Scaled static exterior	1.0	100	N/A
PF26			$20n_v$	
PF27			$4n_v n_b$	
PF28		2.0	100	N/A
PF29			$20n_v$	
PF30			$4n_v n_b$	
PF31	Dynamic exterior	1.0	100	N/A
PF32			$20n_v$	
PF33			$4n_v n_b$	
PF34		2.0	100	N/A
PF35			$20n_v$	
PF36			$4n_v n_b$	
PF37	Static adaptive exterior	1.0-2.0	100	1
PF38				5
PF39				10
PF40				20
PF41				50
PF42		1.0-5.0	100	1
PF43				5
PF44				10
PF45				20
PF46				50
PF47	Dynamic adaptive exterior	1.0-2.0	100	1
PF48				5
PF49				10
PF50				20
PF51				50
PF52		1.0-5.0	100	1
PF53				5
PF54				10
PF55				20
PF56				50

The results of the run that generated the best solution for each experiment are presented in Table D.6 and the average results of all runs in Table D.7.

Table D.6: Penalty function preliminary investigation solution of minimal mass results

ID	$f_{\min}$	$\Phi_{\min}$	c_1	c_2, m	η, %	$\beta(\mathrm{X}^{n_k})$, %	$A(\mathrm{X}^{n_k})$, %	N	T, h
PF1	30,166	30,166	0.39	0.30	45.19	0.00	100.00	57	2.78
PF2	30,147	30,147	0.20	0.46	49.76	0.00	99.74	56	4.95
PF3	30,147	30,147	0.27	0.46	43.96	0.00	99.08	48	4.75
PF4	82,096	82,096	1.65	0.43	100.00	100.00	100.00	2	3.73
PF5	60,901	60,901	1.51	0.29	100.00	100.00	99.77	2	3.57
PF6	61,648	61,648	1.50	0.39	100.00	100.00	99.10	3	4.30
PF7	31,179	63,192	0.46	0.00	56.91	0.00	100.00	63	3.43
PF8	30,642	62,423	0.45	-0.01	53.17	0.00	99.51	88	5.80
PF9	30,648	62,371	0.45	-0.01	61.17	0.00	99.69	69	4.77
PF10	31,415	96,041	0.04	0.00	60.08	0.00	100.00	69	2.60
PF11	30,850	94,199	0.45	0.00	60.18	0.00	99.83	75	6.18
PF12	30,887	94,468	0.49	0.00	52.88	0.00	99.47	93	4.20
PF13	72,125	72,125	1.78	0.40	100.00	100.00	100.00	53	3.73
PF14	69,478	69,478	1.52	0.40	100.00	100.00	99.40	54	4.37
PF15	69,242	69,242	1.68	0.46	100.00	100.00	99.61	49	6.97
PF16	68,046	68,046	1.58	0.29	100.00	100.00	100.00	50	4.69
PF17	62,046	62,046	1.60	0.18	100.00	100.00	99.61	56	4.27
PF18	62,145	62,145	1.59	0.50	100.00	100.00	99.26	52	4.72
PF19	55,859	55,859	1.54	0.53	100.00	100.00	100.00	77	16.74
PF20	55,310	55,310	1.54	0.20	100.00	0.00	99.95	73	23.28
PF21	55,153	55,191	1.46	0.33	99.84	0.00	99.85	100	15.92
PF22	56,357	56,377	1.48	0.42	99.86	0.00	100.00	61	15.22
PF23	55,401	55,401	1.59	0.36	100.00	100.00	99.94	85	18.61
PF24	55,224	55,239	1.48	0.37	99.84	0.00	99.90	101	20.56
PF25	32,788	49,182	0.45	0.47	90.71	0.00	100.00	78	4.94
PF26	32,415	48,622	0.44	0.43	90.91	0.00	99.69	80	3.78
PF27	31,754	47,631	0.43	-0.13	84.86	0.00	99.49	91	4.12
PF28	32,651	48,977	0.43	0.06	84.80	0.00	100.00	70	3.47
PF29	32,135	47,187	0.41	-0.11	88.66	0.00	99.21	48	3.11
PF30	31,851	47,557	0.44	-0.92	92.38	0.00	99.11	12	4.88
PF31	59,497	59,497	1.51	0.29	100.00	100.00	100.00	73	25.04
PF32	56,249	56,249	1.59	0.40	100.00	100.00	99.91	93	19.49
PF33	56,678	56,678	1.56	0.39	100.00	100.00	99.93	50	23.91
PF34	57,416	57,416	1.63	0.44	100.00	100.00	100.00	71	18.75
PF35	55,649	55,649	1.54	0.44	100.00	100.00	99.94	91	20.50
PF36	56,887	56,887	1.51	0.36	100.00	100.00	99.89	70	21.15
PF37	63,476	65,663	1.43	0.30	99.66	0.00	99.95	28	6.79
PF38	63,944	65,822	1.49	0.58	97.60	0.00	99.86	26	7.03
PF39	61,031	61,128	1.46	0.40	99.90	0.00	99.83	34	7.86
PF40	66,086	66,451	1.43	0.25	99.68	0.00	99.97	79	9.65
PF41	62,330	62,471	1.45	0.42	99.89	0.00	99.98	31	22.13
PF42	68,418	68,427	1.49	0.27	99.89	0.00	100.00	10	7.30
PF43	60,460	60,460	1.52	0.59	100.00	0.00	99.94	21	7.34
PF44	65,582	66,944	1.40	0.15	99.87	0.00	100.00	33	13.12
PF45	69,138	69,169	1.49	0.34	99.81	0.00	100.00	41	7.39
PF46	62,352	62,398	1.48	0.47	99.88	0.00	99.73	53	7.63
PF47	63,466	63,466	1.51	0.29	100.00	0.00	99.97	48	14.11
PF48	63,245	63,245	1.50	0.32	100.00	0.00	100.00	24	12.95
PF49	66,344	66,344	1.52	0.40	100.00	0.00	99.94	3	9.05
PF50	59,973	59,973	1.54	0.40	100.00	0.00	99.93	78	13.63
PF51	59,019	59,019	1.57	0.46	100.00	0.00	99.99	23	10.54
PF52	63,863	69,333	1.47	0.35	99.65	0.00	98.45	844	22.93
PF53	64,828	64,828	1.52	0.24	100.00	0.00	99.99	149	10.55
PF54	62,719	62,719	1.50	0.37	100.00	0.00	99.99	49	17.91
PF55	65,515	65,515	1.53	0.31	100.00	0.00	99.96	24	8.04
PF56	62,072	62,072	1.52	0.46	100.00	0.00	99.93	11	9.77

Table D.7: Penalty function preliminary investigation average results

ID	$\overline{f_{\min}}$	$\overline{\Phi_{\min}}$	$\overline{\sigma(\Phi_{\min})}$	$\overline{\beta(\mathrm{X}^{n_k})}$, %	$\overline{A(\mathrm{X}^{n_k})}$, %	$\overline{N}$	$\overline{T}$, h
PF1	30,183	30,183	12	0.00	100.00	55.0	3.19
PF2	30,147	30,147	0	0.00	99.50	53.0	4.46
PF3	30,147	30,147	0	0.00	99.27	50.6	4.83
PF4	89,526	89,526	4,153	100.00	100.00	1.2	4.03
PF5	66,544	66,544	4,074	100.00	99.60	3.8	4.30
PF6	65,931	65,931	2,940	100.00	99.33	2.6	4.96
PF7	31,284	64,123	956	0.00	100.00	62.2	3.96
PF8	30,645	62,882	360	0.00	99.67	73.4	4.49
PF9	30,636	62,656	326	0.00	99.53	72.8	4.69
PF10	31,586	97,263	1,109	0.00	100.00	62.6	4.28
PF11	30,935	94,962	643	0.00	99.76	72.8	5.12
PF12	30,893	94,965	638	0.00	99.50	76.4	4.03
PF13	78,913	78,913	5,387	100.00	100.00	52.4	3.42
PF14	75,306	75,306	3,920	100.00	99.46	56.2	4.49
PF15	72,533	72,533	2,278	100.00	99.27	52.0	5.04
PF16	71,446	71,446	3,383	100.00	100.00	54.4	4.48
PF17	70,566	70,566	5,728	100.00	99.64	57.4	4.79
PF18	70,440	70,440	5,172	100.00	99.41	52.8	4.19
PF19	56,939	56,989	1,104	20.00	100.00	73.0	25.00
PF20	55,802	55,814	585	20.00	99.93	84.6	19.26
PF21	55,821	55,828	500	80.00	99.87	84.2	19.24
PF22	57,004	57,036	669	20.00	100.00	72.6	22.93
PF23	55,969	55,987	567	60.00	99.94	83.8	21.27
PF24	55,848	55,851	498	80.00	99.87	86.2	22.36
PF25	33,201	49,673	485	0.00	100.00	65.8	4.47
PF26	32,732	49,063	378	0.00	99.74	75.4	4.34
PF27	32,253	48,428	704	0.00	99.44	78.8	4.15
PF28	33,222	49,833	862	0.00	100.00	67.6	3.91
PF29	32,845	49,064	1,447	0.00	99.46	83.2	4.04
PF30	32,304	48,452	854	0.00	99.17	67.6	4.40
PF31	61,006	61,006	1,484	100.00	100.00	54.6	22.95
PF32	58,805	58,805	1,604	100.00	99.96	67.8	24.92
PF33	57,673	57,673	569	100.00	99.88	36.6	27.06
PF34	58,177	58,178	925	80.00	100.00	55.2	24.70
PF35	56,902	56,902	1,196	100.00	99.95	83.0	24.21
PF36	57,617	57,617	773	100.00	99.86	59.4	24.47
PF37	66,917	67,930	1,627	0.00	99.96	14.0	13.82
PF38	66,422	68,051	1,495	0.00	99.92	10.6	7.95
PF39	65,850	66,383	3,506	0.00	99.90	23.8	9.39
PF40	68,000	68,559	1,179	0.00	99.98	16.6	8.91
PF41	65,701	65,871	2,629	0.00	99.97	41.8	14.88
PF42	68,466	69,683	702	0.00	99.94	2.8	9.24
PF43	64,798	65,503	4,339	0.00	99.89	15.8	7.73
PF44	68,085	69,016	1,364	0.00	99.95	30.0	8.95
PF45	67,386	71,830	4,577	0.00	99.83	11.2	7.87
PF46	64,565	67,075	4,005	0.00	99.89	31.0	10.84
PF47	73,902	1.53×10^{7}	3.39×10^{7}	0.00	99.99	27.8	11.86
PF48	71,749	71,749	9,393	0.00	99.96	18.4	10.31
PF49	66,696	364,716	6.60×10^{5}	0.00	99.98	18.4	10.45
PF50	74,293	74,293	11,620	0.00	99.93	21.4	12.48
PF51	65,286	5.88×10^{6}	1.30×10^{7}	0.00	100.00	23.0	10.06
PF52	70,030	84,573	9,565	0.80	91.94	318.0	22.90
PF53	66,678	67,288	2,198	0.00	98.06	35.4	12.57
PF54	72,432	72,433	10,706	0.00	99.98	29.2	16.51
PF55	74,599	74,599	8,762	0.00	99.97	20.2	9.79
PF56	70,336	70,336	7,139	0.00	99.97	11.8	10.61

D.4 Technique Evaluation

Table D.8 lists the different problem set-ups of the technique evaluation preliminary investigation.

Table D.8: Technique evaluation preliminary investigation set-up

ID	LLH	Representation	LLH set-up
TE1	MC	Real	
TE2		4-bit binary	
TE3		8-bit binary	
TE4		16-bit binary	
TE5	RI	Real	$\alpha_{RI} = 0.1$
TE6			$\alpha_{RI} = 0.2$
TE7			$\alpha_{RI} = 0.3$
TE8		8-bit binary	$\alpha_{RI} = 0.1$
TE9			$\alpha_{RI} = 0.2$
TE10			$\alpha_{RI} = 0.3$
TE11	KQ	Real	$p_m = 0.95$
TE12			$p_m = 0.5$
TE13			$p_m = 0.25$
TE14		8-bit binary	$p_m = 0.95$
TE15			$p_m = 0.5$
TE16			$p_m = 0.25$
TE17	RW	Real	1-point crossover; $p_{c,GA} = 0.9$
TE18			2-point crossover
TE19			Uniform crossover
TE20			Random crossover
TE21			Blend crossover
TE22		8-bit binary	1-point crossover
TE23			2-point crossover
TE24			Uniform crossover
TE25			Random crossover
TE26			Random parameterwise crossover
TE27	TO	Real	1-point crossover; $p_{c,GA} = 0.9$
TE28			2-point crossover
TE29			Uniform crossover
TE30			Random crossover
TE31			Blend crossover
TE32		8-bit binary	1-point crossover
TE33			2-point crossover
TE34			Uniform crossover
TE35			Random crossover
TE36			Random parameterwise crossover
TE37	BP	Real	1-point crossover; $p_{c,GA} = 0.9$; $\alpha_{BP} = 0.1$
TE38			2-point crossover
TE39			Uniform crossover
TE40			Random crossover
TE41			Blend crossover
TE42		8-bit binary	1-point crossover
TE43			2-point crossover
TE44			Uniform crossover
TE45			Random crossover
TE46			Random parameterwise crossover
TE47		Real	1-point crossover; $p_{c,GA} = 0.9$; $\alpha_{BP} = 0.2$
TE48			2-point crossover

Table D.8: Technique evaluation preliminary investigation set-up (cont.)

ID	LLH	Representation	LLH set-up
TE49			Uniform crossover
TE50			Random crossover
TE51			Blend crossover
TE52		8-bit binary	1-point crossover
TE53			2-point crossover
TE54			Uniform crossover
TE55			Random crossover
TE56			Random parameterwise crossover
TE57	RC	Real	1-point crossover; $p_{c,GA} = 0.9$; $\alpha_{RC} = 0.1$
TE58			2-point crossover
TE59			Uniform crossover
TE60			Random crossover
TE61			Blend crossover
TE62		8-bit binary	1-point crossover
TE63			2-point crossover
TE64			Uniform crossover
TE65			Random crossover
TE66			Random parameterwise crossover
TE67		Real	1-point crossover; $p_{c,GA} = 0.9$; $\alpha_{RC} = 0.2$
TE68			2-point crossover
TE69			Uniform crossover
TE70			Random crossover
TE71			Blend crossover
TE72		8-bit binary	1-point crossover
TE73			2-point crossover
TE74			Uniform crossover
TE75			Random crossover
TE76			Random parameterwise crossover
TE77	DE	Real	$p_{c,DE} = 0.5$; $F_{DE} = 0.9$
TE78			$p_{c,DE} = 0.9$; $F_{DE} = 0.75$
TE79			$p_{c,DE} = 0.8803$; $F_{DE} = 0.4717$
TE80			$p_{c,DE} = 0.9455$; $F_{DE} = 0.6497$
TE81			$p_{c,DE} = 0.4147$; $F_{DE} = 0.5983$
TE82	PSO	Real	$\omega_{PSO} = 0.729$; $c_{1,PSO} = 1.8$; $c_{2,PSO} = 1.3$; $\kappa_{PSO} = 1.0$
TE83			$\kappa_{PSO} = 0.75$
TE84			$\kappa_{PSO} = 0.5$
TE85			$\kappa_{PSO} = 0.25$
TE86			$c_{1,PSO} = 2.8\omega_{PSO}$; $c_{2,PSO} = 1.3\omega_{PSO}$; $\kappa_{PSO} = 1.0$
TE87			$\kappa_{PSO} = 0.5$
TE88			$c_{1,PSO} = c_{2,PSO} = 2.05$; $\kappa_{PSO} = 1.0$
TE89			$\kappa_{PSO} = 0.5$
TE90			$c_{1,PSO} = c_{2,PSO} = 1.49$; $\kappa_{PSO} = 1.0$
TE91			$\kappa_{PSO} = 0.5$
TE92			$\omega_{PSO} = 0.6$; $c_{1,PSO} = c_{2,PSO} = 1.7$; $\kappa_{PSO} = 1.0$
TE93			$\kappa_{PSO} = 0.5$
TE94	HC	Real	$\Delta x_v = 0.1\Delta \mathrm{V}_v$
TE95			$\Delta x_v = 0.2\Delta \mathrm{V}_v$
TE96			$\Delta x_v = 0.3\Delta \mathrm{V}_v$
TE97			$\Delta x_v = 0.4\Delta \mathrm{V}_v$
TE98			$\Delta x_v = 0.5\Delta \mathrm{V}_v$
TE99	SA	Real	$\Delta x_v = 0.1\Delta \mathrm{V}_v$; exponential cooling; $\alpha_{SA} = 0.95$
TE100			$\Delta x_v = 0.25\Delta \mathrm{V}_v$
TE101			$\Delta x_v = 0.5\Delta \mathrm{V}_v$
TE102			$\Delta x_v = 0.1\Delta \mathrm{V}_v$; exponential cooling; $\alpha_{SA} = 0.85$
TE103			$\Delta x_v = 0.25\Delta \mathrm{V}_v$

Table D.8: Technique evaluation preliminary investigation set-up (cont.)

ID	LLH	Representation	LLH set-up
TE104			$\Delta x_v = 0.5\Delta \mathrm{V}_v$
TE105			$\Delta x_v = 0.1\Delta \mathrm{V}_v$; linear cooling; $\alpha_{SA} = \frac{1}{n_k}$
TE106			$\Delta x_v = 0.25\Delta \mathrm{V}_v$
TE107			$\Delta x_v = 0.5\Delta \mathrm{V}_v$
TE108	TS	Real	$\Delta x_v = 0.1\Delta \mathrm{V}_v$; $n_{TS} = 100$
TE109			$\Delta x_v = 0.25\Delta \mathrm{V}_v$
TE110			$\Delta x_v = 0.5\Delta \mathrm{V}_v$
TE111			$\Delta x_v = 0.1\Delta \mathrm{V}_v$; $n_{TS} = 50$
TE112			$\Delta x_v = 0.25\Delta \mathrm{V}_v$
TE113			$\Delta x_v = 0.5\Delta \mathrm{V}_v$
TE114			$\Delta x_v = 0.1\Delta \mathrm{V}_v$; $n_{TS} = 10$
TE115			$\Delta x_v = 0.25\Delta \mathrm{V}_v$
TE116			$\Delta x_v = 0.5\Delta \mathrm{V}_v$

Table D.9 presents the results corresponding to the best solutions generated in all experiment runs during the technique evaluation preliminary investigation.

Table D.9: Technique evaluation preliminary investigation solution of minimal mass results

ID	$f_{\min}$	$\Phi_{\min}$	c_1	c_2, m	η, %	$\beta(\mathrm{X}^{n_k})$, %	$A(\mathrm{X}^{n_k})$, %	N	T, h
TE1	52,798	52,798	1.60	0.07	100.00	41.00	90.20	80	22.02
TE2	52,592	52,592	1.61	-0.03	100.00	38.00	89.58	132	23.82
TE3	54,041	54,041	1.58	0.45	100.00	37.00	90.16	111	21.75
TE4	53,740	53,779	1.47	0.22	99.73	32.00	90.26	150	22.79
TE5	53,828	53,853	1.48	0.38	99.78	34.00	90.05	278	22.30
TE6	53,653	53,653	1.64	0.14	100.00	46.00	89.97	768	19.98
TE7	54,225	54,258	1.47	0.10	99.80	45.00	90.08	513	22.28
TE8	52,610	52,610	1.53	0.38	100.00	46.00	90.17	350	20.44
TE9	53,203	53,203	1.58	0.19	100.00	39.00	90.06	317	21.39
TE10	54,588	54,588	1.60	0.26	100.00	50.00	90.21	346	21.00
TE11	48,779	48,782	1.49	0.30	99.56	22.00	96.86	523	3.49
TE12	48,749	48,755	1.49	0.40	99.54	28.00	97.73	329	4.83
TE13	48,744	48,754	1.48	0.40	99.54	8.00	98.33	192	4.28
TE14	64,160	64,312	1.45	0.28	99.38	12.00	95.53	1	36.15
TE15	53,251	53,312	1.46	0.02	99.79	42.00	90.37	631	22.31
TE16	50,141	50,141	1.50	0.20	100.00	36.00	91.70	847	9.01
TE17	48,750	48,755	1.49	0.40	99.54	0.00	99.35	893	3.78
TE18	48,742	48,755	1.48	0.40	99.54	1.00	99.54	982	3.75
TE19	49,082	49,083	1.50	0.42	99.53	1.00	99.59	452	2.28
TE20	48,739	48,755	1.48	0.40	99.54	0.00	99.32	339	3.80
TE21	48,745	48,754	1.49	0.40	99.54	2.00	99.81	915	3.67
TE22	48,806	48,812	1.49	0.37	99.56	72.00	95.68	452	3.91
TE23	48,826	48,828	1.49	0.37	99.55	35.00	95.97	437	4.62
TE24	48,807	48,821	1.48	0.14	99.55	49.00	95.50	434	4.70
TE25	48,791	48,794	1.49	0.24	99.56	35.00	95.56	260	4.60
TE26	48,803	48,821	1.48	0.30	99.56	33.00	96.43	340	4.06
TE27	48,759	48,760	1.50	0.40	99.54	1.00	99.44	361	3.40
TE28	48,742	48,755	1.48	0.40	99.54	1.00	99.16	373	3.36
TE29	49,067	49,074	1.49	0.42	99.53	0.00	99.53	135	3.76
TE30	48,751	48,755	1.49	0.40	99.54	1.00	99.59	567	3.82

Table D.9: Technique evaluation preliminary investigation solution of minimal mass results (cont.)

ID	$f_{\min}$	$\Phi_{\min}$	c_1	c_2, m	η, %	$\beta(\mathrm{X}^{n_k})$, %	$A(\mathrm{X}^{n_k})$, %	N	T, h
TE31	48,745	48,754	1.49	0.40	99.54	3.00	99.48	711	3.30
TE32	48,824	48,869	1.47	0.32	99.55	67.00	95.92	684	4.07
TE33	48,864	48,876	1.48	0.36	99.55	44.00	96.21	861	4.72
TE34	49,085	49,085	1.66	0.24	100.00	47.00	95.97	823	4.11
TE35	48,767	48,813	1.47	0.30	99.56	59.00	96.49	731	4.54
TE36	48,863	48,878	1.48	0.17	99.55	76.00	96.26	875	4.25
TE37	48,726	48,765	1.47	0.40	99.54	0.00	99.62	922	3.66
TE38	49,098	49,115	1.48	0.44	99.52	0.00	99.77	465	3.62
TE39	49,070	49,082	1.48	0.42	99.53	1.00	99.49	153	3.41
TE40	49,065	49,089	1.48	0.43	99.53	0.00	99.68	716	3.20
TE41	48,745	48,754	1.49	0.40	99.54	1.00	99.50	956	3.93
TE42	48,753	48,757	1.49	0.40	99.55	14.00	98.31	360	3.82
TE43	48,769	48,769	1.50	0.39	100.00	80.00	98.16	71	4.35
TE44	48,767	48,767	1.50	0.39	100.00	84.00	98.29	105	3.86
TE45	48,769	48,769	1.50	0.39	100.00	77.00	97.89	207	4.17
TE46	48,751	48,755	1.49	0.40	99.54	11.00	97.91	300	4.00
TE47	48,733	48,758	1.48	0.40	99.54	1.00	99.73	606	3.43
TE48	49,060	49,074	1.48	0.42	99.53	0.00	99.71	548	2.80
TE49	48,749	48,755	1.49	0.40	99.54	98.00	99.55	588	3.66
TE50	48,754	48,756	1.49	0.40	99.54	0.00	99.62	498	3.44
TE51	48,745	48,754	1.49	0.40	99.54	1.00	99.34	228	3.54
TE52	48,753	48,757	1.49	0.40	99.55	11.00	98.12	397	4.31
TE53	48,753	48,757	1.49	0.40	99.55	13.00	98.05	115	4.70
TE54	48,751	48,755	1.49	0.40	99.54	10.00	97.91	53	4.49
TE55	48,753	48,757	1.49	0.40	99.55	8.00	97.65	742	4.24
TE56	48,753	48,757	1.49	0.40	99.55	6.00	98.06	331	4.51
TE57	58,358	58,358	1.55	0.09	100.00	0.00	96.66	30	18.33
TE58	59,444	59,444	1.92	0.24	100.00	0.00	96.79	27	30.46
TE59	60,406	60,406	1.61	0.23	100.00	72.00	97.19	3	32.69
TE60	58,926	58,926	1.59	0.19	100.00	98.00	96.75	12	45.07
TE61	48,750	48,755	1.49	0.40	99.54	50.00	98.48	675	3.87
TE62	54,757	54,757	1.59	0.54	100.00	36.00	91.28	654	20.92
TE63	56,626	56,643	1.48	0.58	99.78	26.00	91.97	989	22.28
TE64	54,953	54,953	1.53	0.38	100.00	58.00	91.63	883	24.66
TE65	55,870	55,870	1.63	0.14	100.00	48.00	91.66	297	14.84
TE66	55,584	55,584	1.54	0.28	100.00	64.00	91.44	799	18.09
TE67	59,464	59,464	1.70	0.02	100.00	11.00	96.68	13	16.00
TE68	60,183	60,183	1.57	0.11	100.00	100.00	97.31	47	12.50
TE69	61,514	61,514	1.52	0.18	100.00	0.00	97.07	18	17.42
TE70	57,896	57,896	1.60	0.35	100.00	23.00	96.38	18	45.02
TE71	48,752	48,757	1.49	0.40	99.55	55.00	98.21	493	3.50
TE72	54,973	54,973	1.54	0.52	100.00	63.00	91.69	415	20.58
TE73	54,096	54,096	1.64	0.39	100.00	35.00	91.24	429	20.83
TE74	55,188	55,188	1.54	0.44	100.00	85.00	92.02	920	21.31
TE75	56,856	56,856	1.68	0.24	100.00	37.00	90.48	924	21.68
TE76	55,421	55,421	1.55	0.21	100.00	68.00	92.11	111	17.96
TE77	50,986	50,986	1.54	0.08	100.00	45.00	91.00	999	21.10
TE78	54,009	54,009	1.54	0.30	100.00	49.00	91.48	577	19.92
TE79	54,073	54,174	1.45	0.27	99.77	38.00	91.83	505	22.29
TE80	53,978	54,227	1.43	0.28	99.75	32.00	91.40	686	21.91
TE81	50,589	50,631	1.47	0.56	99.75	37.00	91.23	999	18.83
TE82	48,746	48,754	1.49	0.40	99.54	64.00	99.61	813	4.64
TE83	53,575	53,580	1.49	0.22	99.72	0.00	99.01	937	6.11
TE84	59,242	59,242	1.53	0.28	100.00	89.00	99.13	978	7.39
TE85	61,341	61,341	1.70	0.37	100.00	70.00	98.20	687	10.29
TE86	48,744	48,755	1.48	0.40	99.54	15.00	97.23	986	5.88

Table D.9: Technique evaluation preliminary investigation solution of minimal mass results (cont.)

ID	$f_{\min}$	$\Phi_{\min}$	c_1	c_2, m	η, %	$\beta(\mathrm{X}^{n_k})$, %	$A(\mathrm{X}^{n_k})$, %	N	T, h
TE87	58,863	58,863	1.66	0.24	100.00	31.00	98.60	557	8.69
TE88	48,868	48,872	1.49	0.39	99.63	65.00	99.29	953	4.36
TE89	58,346	58,346	1.67	0.21	100.00	84.00	99.02	826	8.62
TE90	48,745	48,754	1.49	0.40	99.54	80.00	99.65	971	4.00
TE91	58,942	58,942	1.65	0.36	100.00	44.00	98.80	413	6.29
TE92	48,747	48,755	1.49	0.40	99.54	37.00	99.53	969	4.46
TE93	57,626	57,626	1.50	0.36	97.72	0.00	99.12	949	8.03
TE94	50,475	50,485	1.48	0.30	99.67	-	-	50,617	11.89
TE95	49,464	49,475	1.48	0.23	99.68	-	-	36,601	10.50
TE96	49,318	49,318	1.50	0.28	99.62	-	-	48,440	11.73
TE97	49,373	49,373	1.54	0.21	100.00	-	-	33,965	11.58
TE98	49,577	49,592	1.48	0.26	99.63	-	-	13,238	5.36
TE99	50,143	50,225	1.46	-0.03	99.70	-	-	26,482	6.75
TE100	49,317	49,317	1.50	-0.04	99.63	-	-	52,573	11.57
TE101	49,149	49,180	1.47	0.19	99.67	-	-	26,069	7.85
TE102	50,383	50,395	1.48	0.30	99.62	-	-	64,234	12.34
TE103	49,354	49,379	1.48	0.22	99.66	-	-	26,843	8.27
TE104	49,249	49,311	1.46	0.31	99.60	-	-	7,807	4.25
TE105	50,156	50,168	1.48	0.27	99.59	-	-	92,422	16.71
TE106	49,200	49,235	1.47	0.13	99.63	-	-	26,967	6.77
TE107	49,241	49,241	1.50	0.25	100.00	-	-	16,289	5.85
TE108	50,047	50,056	1.49	0.32	99.70	-	-	28,719	7.79
TE109	49,335	49,396	1.46	-0.07	99.37	-	-	65,418	14.31
TE110	49,441	49,459	1.48	0.26	99.64	-	-	25,655	8.40
TE111	49,351	49,356	1.49	0.31	99.63	-	-	98,027	16.96
TE112	49,330	49,351	1.48	0.37	99.62	-	-	52,518	16.04
TE113	49,087	49,093	1.49	0.21	99.65	-	-	17,418	6.60
TE114	49,667	49,678	1.48	-0.05	99.66	-	-	63,269	15.28
TE115	49,361	49,496	1.46	0.24	99.21	-	-	40,472	9.66
TE116	49,559	49,559	1.53	0.35	100.00	-	-	9,725	4.57

The average results upon termination of each technique evaluation preliminary investigation experiment are listed in Table D.10.

Table D.10: Technique evaluation preliminary investigation average results

ID	$\overline{f_{\min}}$	$\overline{\Phi_{\min}}$	$\overline{\sigma(\Phi_{\min})}$	$\overline{\beta(\mathrm{X}^{n_k})}$, %	$\overline{A(\mathrm{X}^{n_k})}$, %	$\overline{N}$	$\overline{T}$, h
TE1	54,119	54,155	1,430	37.00	90.26	239.4	20.62
TE2	53,071	53,228	474	35.80	89.55	460.4	24.20
TE3	54,909	54,925	540	36.60	90.19	159.8	32.33
TE4	54,145	54,286	423	37.20	90.25	499.6	23.03
TE5	55,162	55,168	1,066	40.20	90.16	442.6	21.55
TE6	55,002	55,002	831	44.20	90.07	608.6	18.78
TE7	55,517	55,523	766	48.80	90.18	432.2	19.49
TE8	54,374	54,374	1,266	41.20	90.10	328.4	22.86
TE9	54,897	54,946	1,396	44.20	90.10	687.2	20.24
TE10	55,223	55,223	463	52.40	90.18	537.6	19.27
TE11	49,168	49,179	428	33.00	96.64	744.4	4.41
TE12	48,736	48,759	6	19.40	97.62	403.2	4.00
TE13	48,746	48,755	0	13.00	98.31	373.2	3.89
TE14	64,160	64,312	0	12.00	95.37	1.0	35.47
TE15	54,275	54,290	854	38.40	90.30	534.2	22.09

Table D.10: Technique evaluation preliminary investigation average results (cont.)

ID	$\overline{f_{\min}}$	$\overline{\Phi_{\min}}$	$\overline{\sigma(\Phi_{\min})}$	$\overline{\beta(\mathrm{X}^{n_k})}$, %	$\overline{A(\mathrm{X}^{n_k})}$, %	$\overline{N}$	$\overline{T}$, h
TE16	50,270	50,305	181	38.80	91.55	670.8	11.80
TE17	48,816	48,832	165	18.80	99.36	435.8	3.74
TE18	48,963	48,973	195	20.20	99.57	471.6	3.73
TE19	49,279	49,288	376	0.60	99.36	285.2	3.42
TE20	49,142	49,154	332	0.20	99.43	526.0	3.55
TE21	48,969	48,982	208	0.60	99.69	542.0	3.72
TE22	49,031	49,043	142	50.60	95.75	621.6	4.50
TE23	49,058	49,080	145	39.00	96.11	658.4	4.60
TE24	49,009	49,018	175	56.40	95.81	591.6	4.18
TE25	48,975	48,992	233	42.00	95.95	606.2	4.68
TE26	49,042	49,058	144	36.00	96.13	495.2	4.33
TE27	49,199	49,217	449	0.60	99.41	626.2	3.70
TE28	48,923	48,942	176	1.00	99.39	448.2	3.63
TE29	49,104	49,123	29	20.20	99.48	435.2	3.77
TE30	48,888	48,910	204	1.20	99.50	779.6	3.73
TE31	48,895	48,906	208	1.20	99.62	561.2	3.53
TE32	49,099	49,112	166	58.60	96.04	627.6	4.52
TE33	49,064	49,072	194	51.00	95.79	845.0	4.39
TE34	49,234	49,238	146	62.20	95.81	655.2	4.40
TE35	48,890	48,914	90	41.60	96.08	470.4	4.35
TE36	49,017	49,050	143	50.40	96.39	738.4	4.63
TE37	49,218	49,240	500	0.80	99.61	507.6	3.53
TE38	49,296	49,307	403	0.60	99.69	455.0	3.68
TE39	49,081	49,110	19	0.80	99.64	347.8	3.49
TE40	49,298	49,323	477	0.20	99.62	346.4	3.23
TE41	48,816	48,826	159	0.60	99.59	748.4	3.74
TE42	49,048	49,058	171	22.20	97.98	224.2	3.98
TE43	49,043	49,054	163	34.80	98.02	300.4	4.26
TE44	48,965	48,998	207	52.40	98.18	243.0	3.96
TE45	48,989	48,994	155	39.20	98.06	233.0	4.27
TE46	48,956	48,967	193	6.20	98.29	370.0	4.07
TE47	48,947	48,972	194	0.80	99.57	322.2	3.69
TE48	49,096	49,113	24	0.40	99.74	470.8	3.25
TE49	49,003	49,015	156	20.40	99.64	604.8	3.49
TE50	49,261	49,274	537	20.20	99.65	408.8	3.33
TE51	48,746	48,754	0	1.54	99.94	699.0	3.59
TE52	49,022	49,036	156	7.60	97.98	277.8	4.42
TE53	48,934	48,937	148	40.20	97.98	310.8	4.29
TE54	48,924	48,935	249	34.40	98.00	129.8	4.26
TE55	48,981	48,990	157	21.20	97.85	225.2	4.22
TE56	48,923	48,927	179	22.60	97.92	337.2	4.08
TE57	61,483	61,517	2,315	44.40	96.80	30.2	15.20
TE58	63,116	63,216	2,113	20.00	96.83	7.0	23.92
TE59	62,851	62,918	1,650	33.40	96.93	7.4	27.31
TE60	61,478	61,545	2,525	22.80	97.29	88.8	25.70
TE61	48,833	48,836	125	61.60	97.22	462.6	3.66
TE62	57,055	57,329	2,261	51.60	91.40	665.8	22.51
TE63	58,512	58,520	1,149	37.60	91.60	631.4	21.82
TE64	56,642	56,642	1,141	41.40	91.58	398.8	23.31
TE65	56,815	56,857	891	49.40	91.75	475.0	20.87
TE66	57,718	57,737	1,373	39.00	91.56	413.4	19.26
TE67	63,027	63,094	2,057	41.00	97.10	4.6	17.24
TE68	61,764	62,715	1,688	80.00	97.31	30.6	23.49
TE69	63,067	63,196	1,209	38.20	97.06	6.2	22.27
TE70	61,247	61,476	2,870	37.60	96.97	131.2	22.45

Table D.10: Technique evaluation preliminary investigation average results (cont.)

ID	$\overline{f_{\min}}$	$\overline{\Phi_{\min}}$	$\overline{\sigma(\Phi_{\min})}$	$\overline{\beta(\mathrm{X}^{n_k})}$, %	$\overline{A(\mathrm{X}^{n_k})}$, %	$\overline{N}$	$\overline{T}$, h
TE71	48,825	48,835	167	54.80	97.88	672.8	3.57
TE72	56,951	56,951	2,094	48.60	91.74	423.2	22.10
TE73	57,173	57,241	2,241	42.80	91.74	527.8	20.71
TE74	57,454	57,460	1,680	52.40	91.96	715.2	22.69
TE75	57,759	57,759	1,091	42.20	91.44	533.0	21.13
TE76	58,120	58,120	1,650	56.00	91.89	268.8	19.74
TE77	51,873	51,883	885	45.20	90.91	976.8	20.73
TE78	55,169	55,457	1,201	39.60	91.20	623.0	20.85
TE79	56,015	56,139	1,549	33.80	91.93	488.8	23.21
TE80	55,152	55,210	647	36.60	91.32	689.6	21.42
TE81	51,315	51,323	780	40.60	91.38	875.0	19.04
TE82	49,100	49,111	493	36.00	99.46	864.4	4.41
TE83	54,516	54,526	908	0.00	99.49	897.4	7.09
TE84	60,284	60,290	971	74.40	99.29	718.4	7.85
TE85	61,786	61,786	468	64.60	98.46	669.8	10.16
TE86	49,066	49,078	292	9.60	98.87	919.8	5.20
TE87	59,824	59,824	975	37.60	98.32	809.6	10.44
TE88	49,281	49,287	305	35.20	99.21	974.8	4.60
TE89	59,335	59,335	1,017	62.00	99.25	866.6	7.89
TE90	49,008	49,015	366	43.40	99.53	977.6	3.76
TE91	59,814	59,824	936	37.60	98.98	817.6	7.52
TE92	49,072	49,083	663	34.60	99.23	989.8	4.62
TE93	59,695	59,699	1,410	59.00	99.48	965.0	7.38
TE94	50,775	50,785	300	-	-	36,824.2	8.75
TE95	50,009	50,044	450	-	-	26,250.8	7.22
TE96	49,868	49,894	523	-	-	24,056.8	7.00
TE97	49,759	49,761	497	-	-	18,301.0	7.41
TE98	49,967	50,010	406	-	-	11,201.6	5.13
TE99	50,448	50,481	255	-	-	53,822.4	11.42
TE100	50,082	50,107	742	-	-	30,488.6	7.86
TE101	49,486	49,500	245	-	-	15,986.4	6.12
TE102	51,151	51,171	635	-	-	49,220.8	11.45
TE103	49,978	49,998	467	-	-	30,207.2	7.90
TE104	49,448	49,521	227	-	-	11,503.4	5.45
TE105	50,618	50,629	495	-	-	66,745.6	13.00
TE106	49,710	49,813	438	-	-	23,978.8	6.61
TE107	49,494	49,562	318	-	-	15,541.0	5.91
TE108	51,032	51,040	754	-	-	52,305.4	10.84
TE109	49,890	49,913	727	-	-	35,079.6	8.55
TE110	49,731	49,752	374	-	-	17,116.8	6.54
TE111	50,568	50,588	837	-	-	56,573.6	11.03
TE112	49,550	49,564	130	-	-	29,210.6	8.17
TE113	49,605	49,646	422	-	-	14,464.8	5.96
TE114	50,658	50,677	709	-	-	51,589.8	11.67
TE115	50,247	50,286	524	-	-	30,318.4	7.36
TE116	50,054	50,078	508	-	-	10,380.4	5.31

D.5 Heuristic Selection

The heuristic selection preliminary investigation is set up as listed in Table D.11. Variations in process set-up include the hyper-heuristic employed to select an LLH as well as the measure of improvement (MoI) criterion and move acceptance rules employed. The MoI may be either the problem domain objective value, Eqn. (4.1), choice function, Eqn. (3.6), or hyper-heuristic domain objective function, Eqn. (4.3).

Table D.11: Heuristic selection preliminary investigation set-up

ID	Hyper-heuristic	MoI criterion	Move acceptance
HS1	SR	None	AM
HS2			IE
HS3			EMCQ
HS4			SA
HS5	RD	None	AM
HS6			IE
HS7			EMCQ
HS8			SA
HS9	PE	None	AM
HS10			IE
HS11			EMCQ
HS12			SA
HS13		Objective value	AM
HS14			IE
HS15			EMCQ
HS16			SA
HS17		Choice function	AM
HS18			IE
HS19			EMCQ
HS20			SA
HS21		Hyper-heuristic objective function	AM
HS22			IE
HS23			EMCQ
HS24			SA
HS25	PD	None	AM
HS26			IE
HS27			EMCQ
HS28			SA
HS29		Objective value	AM
HS30			IE
HS31			EMCQ
HS32			SA
HS33		Choice function	AM
HS34			IE
HS35			EMCQ
HS36			SA
HS37		Hyper-heuristic objective function	AM
HS38			IE
HS39			EMCQ
HS40			SA
HS41	GR	Objective value	AM
HS42			IE
HS43			EMCQ
HS44			SA
HS45		Choice function	AM
HS46			IE
HS47			EMCQ
HS48			SA
HS49		Hyper-heuristic objective function	AM
HS50			IE
HS51			EMCQ
HS52			SA
HS53	PK	Objective value	AM
HS54			IE
HS55			EMCQ

Table D.11: Heuristic selection preliminary investigation set-up (cont.)

ID	Hyper-heuristic	MoI criterion	Move acceptance
HS56			SA
HS57		Choice function	AM
HS58			IE
HS59			EMCQ
HS60			SA
HS61		Hyper-heuristic objective function	AM
HS62			IE
HS63			EMCQ
HS64			SA
HS65	RW	Objective value	AM
HS66			IE
HS67			EMCQ
HS68			SA
HS69		Choice function	AM
HS70			IE
HS71			EMCQ
HS72			SA
HS73		Hyper-heuristic objective function	AM
HS74			IE
HS75			EMCQ
HS76			SA
HS77	TO	Objective value	AM
HS78			IE
HS79			EMCQ
HS80			SA
HS81		Choice function	AM
HS82			IE
HS83			EMCQ
HS84			SA
HS85		Hyper-heuristic objective function	AM
HS86			IE
HS87			EMCQ
HS88			SA
HS89	TS	Objective value	AM
HS90			IE
HS91			EMCQ
HS92			SA
HS93		Choice function	AM
HS94			IE
HS95			EMCQ
HS96			SA
HS97		Hyper-heuristic objective function	AM
HS98			IE
HS99			EMCQ
HS100			SA
HS101	Tabu-assisted GR	Choice function	IE
HS102		Choice function	EMCQ
HS103		Hyper-heuristic objective function	IE
HS104		Objective value	IE
HS105	MoI-penalised GR	Choice function	IE
HS106		Choice function	EMCQ
HS107		Hyper-heuristic objective function	IE
HS108		Objective value	IE
HS109	Tabu-assisted PK	Choice function	AM
HS110		Hyper-heuristic objective function	IE
HS111		Hyper-heuristic objective function	EMCQ

Table D.11: Heuristic selection preliminary investigation set-up (cont.)

ID	Hyper-heuristic	MoI criterion	Move acceptance
HS112		Choice function	EMCQ
HS113	MoI-penalised PK	Choice function	AM
HS114		Hyper-heuristic objective function	IE
HS115		Hyper-heuristic objective function	EMCQ
HS116		Choice function	EMCQ
HS117	Tabu-assisted RW	Choice function	SA
HS118		Choice function	EMCQ
HS119		Objective value	AM
HS120		Objective value	EMCQ
HS121	MoI-penalised RW	Choice function	SA
HS122		Choice function	EMCQ
HS123		Objective value	AM
HS124		Objective value	EMCQ
HS125	Tabu-assisted TO	Choice function	AM
HS126		Choice function	EMCQ
HS127		Objective value	SA
HS128		Hyper-heuristic objective function	AM
HS129	MoI-penalised TO	Choice function	AM
HS130		Choice function	EMCQ
HS131		Objective value	SA
HS132		Hyper-heuristic objective function	AM

Table D.12 lists the best solutions and corresponding final population for each experiment of the investigation. These results also include the LLH that generated each best solution listed.

Table D.12: Heuristic selection preliminary investigation solution of minimal mass results

ID	$f_{\min}$	$\Phi_{\min}$	c_1	c_2, m	η, %	LLH	$\beta(\mathrm{X}^{n_k})$, %	$A(\mathrm{X}^{n_k})$, %	N	T, h
HS1	54,867	54,867	1.51	0.49	100.00	KQ	1.00	92.36	436	16.18
HS2	54,673	54,673	1.50	0.42	99.00	BP	19.00	95.04	10	6.41
HS3	54,269	54,378	1.48	0.39	98.00	BP	4.00	90.34	102	8.10
HS4	54,126	54,273	1.47	0.10	98.00	KQ	4.00	90.72	277	12.34
HS5	54,423	54,427	1.50	0.31	98.00	RW	9.00	95.57	277	10.71
HS6	54,598	54,598	1.50	0.37	98.00	TS	2.00	95.61	255	10.50
HS7	55,112	55,173	1.48	0.45	98.00	BP	5.00	95.91	254	11.80
HS8	54,635	54,638	1.50	-0.03	98.00	KQ	32.00	96.79	191	9.95
HS9	55,851	55,895	1.49	0.40	98.00	DE	2.00	90.74	145	8.39
HS10	54,807	54,825	1.48	0.49	99.00	RW	1.00	99.66	638	15.95
HS11	54,169	54,169	1.50	0.37	100.00	RW	1.00	99.63	315	9.92
HS12	54,132	54,146	1.49	0.36	97.00	BP	0.00	99.67	421	11.36
HS13	53,954	54,042	1.48	0.49	98.00	TO	4.00	91.19	248	11.50
HS14	54,334	54,334	1.50	0.20	98.00	TS	19.00	95.05	60	7.09
HS15	53,906	54,566	1.45	0.44	97.00	PSO	8.00	95.66	213	10.86
HS16	53,625	53,625	1.51	0.51	100.00	BP	15.00	95.94	380	13.82
HS17	54,247	54,708	1.45	0.34	98.00	DE	4.00	91.26	50	5.95
HS18	54,770	54,831	1.48	0.13	98.00	PSO	1.00	99.06	482	15.14
HS19	52,340	52,391	1.48	0.49	97.00	RW	0.00	99.63	911	18.74
HS20	54,545	54,804	1.46	0.14	98.00	HC	8.00	97.75	141	7.22
HS21	54,885	54,885	1.52	0.19	100.00	KQ	31.00	96.43	19	5.34
HS22	54,766	54,815	1.48	0.35	98.00	BP	7.00	94.01	500	15.56
HS23	54,578	54,626	1.49	0.41	96.00	RW	4.00	93.50	136	8.80
HS24	53,342	54,393	1.43	0.31	98.00	KQ	4.00	90.45	129	9.20

Table D.12: Heuristic selection preliminary investigation solution of minimal mass results (cont.)

ID	$f_{\min}$	$\Phi_{\min}$	c_1	c_2, m	η, %	LLH	$\beta(\mathrm{X}^{n_k})$, %	$A(\mathrm{X}^{n_k})$, %	N	T, h
HS25	54,731	54,766	1.48	0.42	97.00	RW	0.00	99.59	117	6.84
HS26	54,485	54,565	1.48	0.46	97.00	PSO	0.00	97.45	915	16.65
HS27	54,297	54,297	1.50	0.42	100.00	TO	0.00	99.70	136	6.99
HS28	54,746	54,779	1.47	0.47	99.00	RW	0.00	99.86	442	12.81
HS29	53,032	53,043	1.49	0.34	99.00	RW	0.00	90.04	168	9.37
HS30	53,847	53,896	1.48	0.66	97.00	SA	22.00	95.67	210	10.26
HS31	53,996	53,996	1.51	0.45	100.00	BP	0.00	95.50	77	7.69
HS32	53,869	53,869	1.51	0.21	100.00	PSO	2.00	91.36	126	8.93
HS33	55,337	55,364	1.49	0.34	98.00	KQ	1.00	90.09	109	9.47
HS34	53,823	54,096	1.46	0.17	98.00	TS	18.00	97.87	86	7.02
HS35	54,184	54,285	1.48	0.26	98.00	BP	0.00	96.76	500	14.79
HS36	53,359	53,359	1.51	0.47	100.00	RW	1.00	90.15	36	6.34
HS37	54,141	54,390	1.46	0.43	98.00	RW	0.00	90.66	557	18.72
HS38	53,227	53,230	1.50	0.44	98.00	HC	0.00	91.01	187	10.66
HS39	53,658	53,713	1.48	0.46	98.00	BP	1.00	91.76	552	18.23
HS40	53,429	53,525	1.46	0.68	99.00	BP	2.00	90.08	72	6.41
HS41	55,807	55,807	1.50	0.34	100.00	RW	7.00	90.17	11	5.87
HS42	52,163	52,226	1.47	0.16	97.00	BP	0.00	99.70	920	17.21
HS43	55,201	55,215	1.49	0.43	98.00	BP	5.00	90.29	29	6.23
HS44	54,879	54,884	1.50	0.33	98.00	DE	0.00	90.28	214	10.30
HS45	55,691	55,917	1.47	0.28	98.00	RC	4.00	90.18	59	6.75
HS46	51,358	51,443	1.48	0.21	98.00	DE	0.00	97.36	976	13.89
HS47	51,958	51,974	1.49	0.47	97.00	PSO	0.00	98.02	944	18.08
HS48	54,474	54,474	1.51	0.49	100.00	BP	4.00	90.11	12	5.94
HS49	54,800	54,895	1.48	0.50	98.00	HC	5.00	90.19	18	6.02
HS50	52,163	52,178	1.49	0.49	98.00	BP	1.00	99.62	861	16.51
HS51	55,525	55,645	1.48	0.27	98.00	RI	0.00	90.27	232	10.94
HS52	55,422	55,422	1.50	0.46	98.00	RI	2.00	90.15	177	9.55
HS53	53,028	53,312	1.46	0.24	98.00	DE	4.00	96.13	342	13.01
HS54	55,177	55,553	1.46	0.43	98.00	SA	2.00	90.02	61	5.50
HS55	54,710	54,795	1.48	0.27	98.00	BP	7.00	90.31	22	5.85
HS56	55,431	55,818	1.46	0.40	98.00	PSO	2.00	91.20	273	11.46
HS57	51,251	51,312	1.48	0.14	98.00	PSO	11.00	98.81	951	10.07
HS58	55,596	55,696	1.48	0.26	98.00	SA	0.00	90.57	791	22.33
HS59	55,517	55,636	1.48	0.41	98.00	SA	2.00	90.71	70	7.78
HS60	51,724	52,095	1.46	0.31	98.00	TO	20.00	97.65	141	7.28
HS61	55,766	56,008	1.47	0.41	97.00	RW	2.00	90.27	29	6.03
HS62	54,917	55,115	1.47	0.46	98.00	MC	3.00	90.26	47	6.62
HS63	55,635	55,801	1.47	0.37	98.00	KQ	1.00	90.78	151	9.16
HS64	56,437	56,944	1.45	0.41	98.00	MC	0.00	90.09	21	6.01
HS65	56,393	56,393	1.50	0.38	100.00	PSO	1.00	90.21	217	10.31
HS66	54,703	54,809	1.48	0.33	98.00	RC	2.00	90.78	283	12.15
HS67	52,943	53,581	1.44	0.15	98.00	PSO	13.00	96.13	96	5.61
HS68	54,994	55,175	1.47	0.17	98.00	RW	2.00	90.20	202	8.62
HS69	54,356	54,356	1.52	0.24	100.00	KQ	0.00	91.08	395	14.42
HS70	54,608	54,697	1.48	0.43	96.00	KQ	9.00	90.99	511	16.95
HS71	53,796	53,840	1.48	0.52	97.00	BP	0.00	90.27	148	9.05
HS72	53,316	54,210	1.38	0.53	97.00	PSO	1.00	90.21	246	11.20
HS73	53,929	54,475	1.45	0.39	98.00	BP	6.00	90.92	69	7.58
HS74	53,860	54,653	1.44	0.44	96.00	KQ	4.00	90.97	399	14.83
HS75	53,110	53,170	1.48	0.15	98.00	RC	4.00	90.18	332	12.12
HS76	55,452	55,452	1.55	0.19	100.00	TS	7.00	92.15	208	8.16
HS77	53,873	54,223	1.46	0.43	98.00	TS	2.00	90.08	117	8.34
HS78	55,057	55,057	1.51	0.32	100.00	KQ	1.00	90.49	190	10.24
HS79	54,919	55,123	1.47	0.45	98.00	KQ	3.00	95.79	159	9.77
HS80	54,000	54,000	1.50	0.13	100.00	TO	2.00	90.63	76	7.43

Table D.12: Heuristic selection preliminary investigation solution of minimal mass results (cont.)

ID	$f_{\min}$	$\Phi_{\min}$	c_1	c_2, m	η, %	LLH	$\beta(\mathrm{X}^{n_k})$, %	$A(\mathrm{X}^{n_k})$, %	N	T, h
HS81	51,238	51,242	1.50	0.12	98.00	SA	30.00	91.61	450	15.88
HS82	54,287	54,287	1.51	0.53	100.00	BP	1.00	91.31	302	12.54
HS83	51,197	52,206	1.43	0.49	98.00	KQ	10.00	95.79	235	11.21
HS84	53,101	53,481	1.46	0.45	97.00	TS	4.00	96.79	245	9.59
HS85	54,074	54,074	1.51	0.07	100.00	RC	0.00	91.58	42	6.32
HS86	54,084	54,619	1.45	0.09	98.00	RW	12.00	95.58	365	14.01
HS87	54,330	54,704	1.46	0.49	96.00	PSO	1.00	90.72	380	15.15
HS88	53,928	54,986	1.45	0.14	96.00	RC	9.00	94.57	389	14.21
HS89	55,146	55,146	1.52	0.22	100.00	RW	4.00	90.37	117	8.15
HS90	53,665	55,155	1.44	0.58	97.00	DE	2.00	90.23	251	10.84
HS91	54,904	56,812	1.43	0.46	96.00	DE	2.00	90.88	42	6.50
HS92	56,770	56,770	1.51	0.51	100.00	BP	7.00	90.12	51	6.79
HS93	52,455	52,464	1.49	0.50	99.00	BP	2.00	99.77	566	14.08
HS94	52,147	52,150	1.49	0.45	99.00	PSO	24.00	98.61	968	18.55
HS95	52,215	52,273	1.48	0.48	97.00	PSO	9.00	98.68	335	10.74
HS96	55,058	55,476	1.47	0.40	95.00	RC	22.00	96.29	77	12.53
HS97	55,767	55,791	1.49	0.21	98.00	RI	3.00	90.21	85	7.71
HS98	53,636	53,711	1.48	0.34	98.00	KQ	3.00	90.30	37	6.58
HS99	56,213	56,895	1.45	0.39	97.00	MC	3.00	90.21	126	8.64
HS100	54,849	55,053	1.47	-0.03	98.00	KQ	0.00	90.12	439	14.18
HS101	54,667	54,667	1.51	0.21	100.00	DE	4.00	90.81	902	24.41
HS102	52,482	52,482	1.50	0.36	100.00	RW	0.00	99.79	197	8.55
HS103	56,028	56,703	1.45	0.35	97.00	KQ	1.00	90.16	26	7.22
HS104	52,019	52,130	1.48	0.37	98.00	RW	0.00	99.56	457	10.61
HS105	52,872	52,902	1.47	0.50	99.00	TO	0.00	99.80	923	22.62
HS106	52,662	52,672	1.49	0.50	99.00	RW	0.00	99.71	245	8.59
HS107	56,553	56,787	1.47	0.45	97.00	TO	0.00	90.15	24	6.23
HS108	51,104	51,104	1.50	0.43	100.00	BP	0.00	99.72	429	10.72
HS109	54,091	54,108	1.49	0.38	98.00	KQ	1.00	90.19	123	8.92
HS110	54,867	54,929	1.47	0.49	97.00	RI	0.00	90.88	242	10.85
HS111	55,877	56,142	1.47	0.43	97.00	DE	5.00	90.38	13	5.93
HS112	52,353	52,406	1.47	0.28	99.00	RW	15.00	95.67	686	19.26
HS113	54,034	54,091	1.47	0.48	99.00	PSO	15.00	97.36	892	17.85
HS114	51,270	51,306	1.45	0.21	96.00	BP	1.00	90.53	24	6.23
HS115	55,674	55,946	1.46	0.37	98.00	KQ	2.00	90.40	22	6.55
HS116	51,457	51,687	1.46	0.04	98.00	BP	19.00	96.45	339	12.65
HS117	54,317	54,317	1.51	0.25	100.00	RW	6.00	91.36	85	8.87
HS118	53,867	54,000	1.47	0.53	98.00	SA	1.00	91.06	15	6.17
HS119	55,075	55,075	1.51	0.47	100.00	RW	1.00	90.55	465	17.32
HS120	53,968	53,968	1.52	0.35	100.00	TO	3.00	91.90	446	17.62
HS121	53,719	53,719	1.51	0.35	100.00	BP	7.00	92.50	164	11.06
HS122	53,495	54,033	1.46	0.16	97.00	RW	3.00	90.40	407	14.86
HS123	51,161	51,161	1.51	0.31	100.00	KQ	1.00	91.72	286	14.72
HS124	53,185	53,429	1.46	0.13	97.00	TS	14.00	92.72	322	13.11
HS125	52,511	52,870	1.46	0.26	98.00	KQ	14.00	93.83	205	11.04
HS126	53,415	53,621	1.47	0.46	98.00	TO	16.00	92.75	212	10.87
HS127	52,270	53,594	1.42	0.20	98.00	DE	8.00	92.71	187	10.08
HS128	55,107	55,107	1.52	0.22	100.00	TO	3.00	90.58	398	14.64
HS129	53,169	53,665	1.47	0.51	96.00	RW	2.00	92.57	393	15.83
HS130	53,809	53,831	1.49	0.54	97.00	TO	7.00	90.78	707	17.97
HS131	53,427	53,484	1.48	0.27	98.00	KQ	2.00	90.77	516	18.91
HS132	54,272	54,388	1.48	0.36	98.00	RW	2.00	90.65	722	18.45

The average results of the heuristic selection preliminary investigation are presented in Table D.13.

Table D.13: Heuristic selection preliminary investigation average results

ID	$\overline{f_{\min}}$	$\overline{\Phi_{\min}}$	$\overline{\sigma(\Phi_{\min})}$	$\overline{\beta(\mathrm{X}^{n_k})}$, %	$\overline{A(\mathrm{X}^{n_k})}$, %	$\overline{N}$	$\overline{T}$, h
HS1	55,411	55,648	653	7.20	92.16	148.2	9.32
HS2	55,646	55,650	918	7.00	91.71	111.0	8.40
HS3	54,465	55,040	562	11.40	91.73	229.8	10.82
HS4	55,131	55,223	561	3.40	92.18	229.2	11.32
HS5	54,842	54,937	381	12.00	94.76	167.4	9.45
HS6	54,797	55,128	513	6.80	93.23	159.6	9.38
HS7	55,350	55,679	582	4.20	92.47	200.6	10.58
HS8	55,305	55,754	1,187	10.40	93.49	95.6	7.94
HS9	56,610	56,681	791	28.00	95.13	443.8	13.08
HS10	57,887	57,995	1,866	0.40	97.39	717.6	14.89
HS11	55,773	55,777	1,501	1.20	95.45	471.0	12.81
HS12	55,934	57,250	3,477	0.40	97.92	550.0	13.22
HS13	54,506	54,657	583	2.80	90.51	233.8	11.43
HS14	54,997	55,177	911	6.20	93.67	192.6	10.16
HS15	55,019	55,277	674	11.40	92.60	131.8	8.84
HS16	54,527	54,631	650	6.00	91.67	368.0	13.46
HS17	55,531	56,005	1,697	6.40	95.01	385.6	13.84
HS18	55,589	55,634	872	2.40	95.47	397.0	11.94
HS19	54,941	55,049	2,416	7.20	97.63	376.4	11.35
HS20	56,373	56,653	1,594	2.60	94.08	263.0	9.32
HS21	55,709	56,071	1,546	7.60	92.01	134.6	8.83
HS22	55,522	55,591	813	10.20	93.43	258.6	11.68
HS23	55,086	55,216	573	7.80	93.53	191.4	10.83
HS24	54,601	55,096	511	6.20	91.98	161.6	9.63
HS25	58,130	58,261	5,346	0.20	98.57	338.2	9.03
HS26	58,712	59,326	5,186	1.00	96.32	439.2	10.04
HS27	57,150	57,567	2,311	0.60	95.90	404.4	12.22
HS28	56,711	56,727	2,283	0.60	95.31	345.2	11.29
HS29	54,571	54,606	1,618	10.00	92.20	172.6	10.44
HS30	53,911	54,256	410	16.40	93.76	298.0	12.38
HS31	54,935	55,064	835	2.40	91.86	111.4	7.73
HS32	54,002	54,615	496	3.80	92.14	100.2	8.09
HS33	55,706	56,361	1,147	1.00	93.15	72.6	6.71
HS34	55,971	56,200	1,809	5.00	96.10	104.0	6.93
HS35	55,075	55,181	750	5.00	94.20	376.2	12.43
HS36	54,397	54,795	1,535	2.80	92.75	56.0	6.53
HS37	54,583	54,945	383	1.60	92.62	196.8	10.42
HS38	55,081	55,114	1,079	5.80	91.37	183.4	10.23
HS39	54,924	55,132	908	6.20	93.07	197.2	10.65
HS40	54,665	54,916	1,305	3.00	90.43	87.4	7.49
HS41	57,561	57,850	1,588	3.20	91.32	75.8	7.10
HS42	55,047	55,287	2,554	0.20	96.82	238.6	8.25
HS43	56,490	56,941	1,118	2.00	90.50	74.6	7.28
HS44	56,401	56,459	1,085	1.40	90.18	176.4	9.05
HS45	56,483	56,531	840	2.20	90.93	29.2	6.14
HS46	55,157	55,210	3,129	2.20	94.74	449.2	10.86
HS47	54,687	54,990	3,369	9.60	98.30	329.2	10.93
HS48	55,684	55,994	1,465	2.80	90.25	105.0	7.99
HS49	56,578	56,946	1,606	2.60	90.25	131.4	8.67
HS50	54,393	54,459	2,973	1.20	97.19	349.4	8.95
HS51	56,889	56,944	1,210	1.20	90.16	70.8	7.35
HS52	56,401	56,417	917	1.20	90.38	198.4	9.64
HS53	56,208	56,489	3,334	4.00	95.27	150.8	8.59
HS54	56,812	57,173	1,633	1.40	90.57	57.4	6.65
HS55	56,267	56,711	1,231	2.20	90.85	145.8	7.99

Table D.13: Heuristic selection preliminary investigation average results (cont.)

ID	$\overline{f_{\min}}$	$\overline{\Phi_{\min}}$	$\overline{\sigma(\Phi_{\min})}$	$\overline{\beta(\mathrm{X}^{n_k})}$, %	$\overline{A(\mathrm{X}^{n_k})}$, %	$\overline{N}$	$\overline{T}$, h
HS56	56,853	57,350	1,341	0.80	90.40	162.6	9.34
HS57	53,780	53,837	1,766	22.00	94.40	383.6	10.45
HS58	57,117	57,234	1,114	1.00	90.84	207.2	10.11
HS59	56,641	57,072	1,604	10.00	93.62	180.2	9.71
HS60	55,415	55,591	2,610	7.60	94.47	188.2	9.43
HS61	57,231	57,446	1,336	2.00	90.47	72.4	7.39
HS62	56,772	56,881	1,195	3.40	91.12	100.0	7.64
HS63	56,705	57,028	1,337	2.20	90.84	200.6	10.10
HS64	56,426	57,437	312	1.80	90.27	49.2	6.73
HS65	56,351	56,850	385	6.00	90.74	104.8	7.99
HS66	55,550	55,768	933	3.40	90.83	202.0	10.29
HS67	55,086	55,249	1,026	4.80	93.87	166.8	8.78
HS68	55,214	55,939	703	1.40	90.74	189.6	10.04
HS69	54,362	54,520	177	14.40	92.09	291.4	12.31
HS70	54,591	55,405	529	3.20	91.06	203.2	10.18
HS71	53,751	54,088	268	8.20	93.77	359.8	13.34
HS72	54,149	54,708	411	4.40	92.25	180.2	10.45
HS73	55,896	56,118	1,406	5.40	91.78	115.0	8.48
HS74	55,852	56,481	1,182	4.80	92.24	99.8	7.82
HS75	55,415	55,873	1,740	6.00	91.22	184.8	9.86
HS76	56,072	56,410	929	6.40	91.70	107.8	7.93
HS77	56,046	56,268	1,219	4.80	91.46	79.2	7.18
HS78	55,991	56,740	1,099	2.00	90.46	125.0	8.40
HS79	55,906	56,129	746	1.80	91.84	55.6	7.18
HS80	56,291	56,296	1,323	6.40	91.37	127.6	8.56
HS81	52,626	52,748	1,218	23.60	93.65	338.4	13.26
HS82	55,261	55,692	1,361	9.80	93.30	304.8	12.32
HS83	54,135	54,418	1,336	28.80	94.77	175.2	9.58
HS84	54,555	54,814	921	7.60	93.99	184.2	9.86
HS85	55,604	55,701	1,092	0.80	91.01	173.6	9.14
HS86	56,006	56,297	1,105	7.40	93.47	190.2	9.94
HS87	56,104	56,312	1,172	2.40	92.47	229.0	11.01
HS88	55,222	55,578	434	6.20	92.75	143.4	8.66
HS89	56,193	56,251	952	1.40	90.25	57.8	6.94
HS90	56,376	57,069	1,462	1.40	90.38	142.0	8.67
HS91	56,881	57,672	758	1.60	90.36	100.8	8.02
HS92	56,655	57,243	559	4.00	90.20	173.2	9.13
HS93	53,424	54,113	2,358	1.20	95.58	481.8	13.65
HS94	54,057	54,331	1,730	7.20	93.94	298.0	9.91
HS95	54,398	54,463	2,874	3.00	96.70	429.6	12.03
HS96	56,757	56,967	959	5.80	92.95	73.0	8.76
HS97	56,497	56,538	828	2.40	90.18	194.4	10.34
HS98	55,133	55,761	1,371	2.80	90.39	44.6	6.45
HS99	57,294	57,540	562	2.20	90.97	75.6	7.26
HS100	55,636	56,460	1,103	2.20	90.13	249.6	10.79
HS101	57,179	57,262	1,560	1.00	94.28	202.6	9.65
HS102	54,070	54,123	1,880	0.20	98.00	329.4	9.58
HS103	57,271	57,835	1,235	2.60	90.17	45.2	7.39
HS104	53,492	53,548	2,033	1.20	96.78	431.2	11.57
HS105	57,642	57,782	4,114	0.00	97.36	216.6	9.98
HS106	55,989	56,202	3,047	2.60	94.58	184.2	8.70
HS107	57,204	57,738	914	3.00	90.25	235.8	11.05
HS108	52,032	52,129	579	0.80	98.09	405.2	10.16
HS109	54,341	54,650	488	16.40	92.49	240.0	12.15
HS110	55,751	56,262	1,159	2.20	90.34	198.6	10.29
HS111	57,216	57,278	900	2.00	90.38	133.8	9.42

Table D.13: Heuristic selection preliminary investigation average results (cont.)

ID	$\overline{f_{\min}}$	$\overline{\Phi_{\min}}$	$\overline{\sigma(\Phi_{\min})}$	$\overline{\beta(\mathrm{X}^{n_k})}$, %	$\overline{A(\mathrm{X}^{n_k})}$, %	$\overline{N}$	$\overline{T}$, h
HS112	53,184	53,821	1,328	10.40	94.87	376.0	12.62
HS113	54,975	55,355	1,061	9.60	94.04	438.2	14.93
HS114	51,831	51,919	396	3.20	90.39	225.8	10.91
HS115	56,560	57,253	1,112	1.80	90.32	153.8	9.25
HS116	52,676	52,819	1,014	16.80	96.43	315.4	12.24
HS117	54,509	54,593	340	10.00	91.86	303.6	13.47
HS118	54,055	54,591	599	6.80	93.65	115.8	8.16
HS119	55,995	56,413	1,356	3.20	91.11	196.4	10.79
HS120	54,427	54,719	635	4.20	93.92	227.2	11.60
HS121	54,112	54,371	435	3.00	91.34	210.0	11.73
HS122	54,819	55,052	958	9.80	92.91	375.0	13.45
HS123	51,560	51,682	406	3.20	90.81	191.0	11.13
HS124	53,983	54,074	720	8.60	93.52	364.2	14.38
HS125	53,544	54,553	1,046	22.00	94.84	405.8	15.96
HS126	54,738	54,881	1,366	8.80	92.51	175.4	9.83
HS127	53,700	54,111	524	4.60	93.01	365.0	14.38
HS128	56,063	56,482	1,469	1.40	90.93	162.6	9.14
HS129	54,604	54,855	1,672	9.40	92.90	280.8	12.47
HS130	54,283	54,738	980	2.80	92.35	294.4	11.89
HS131	53,614	53,700	190	2.00	94.18	300.4	13.53
HS132	55,917	56,316	1,307	2.20	91.53	230.6	10.08

D.6 Population Distribution

The set-ups of the population distribution preliminary investigation are presented in Table D.14. Set-up variations include the distribution method, i.e. even distribution or by heuristic selection using a hyper-heuristic, MoI criterion from those listed in Appendix D.5, move acceptance rules, the number of LLHs in the heuristic set, n_{LLH}, population size and population distribution interval.

Table D.14: Population distribution preliminary investigation set-up

ID	Distribution	MoI criterion	Move acceptance	n_{LLH}	μ	Δk
PD1	Even	None	None	12	1,200	1
PD2					800	
PD3					600	
PD4					300	
PD5					100	
PD6				6	1,200	
PD7					800	
PD8					600	
PD9					300	
PD10					100	
PD11				4	1,200	
PD12					800	
PD13					600	
PD14					300	
PD15					100	
PD16				3	1,200	
PD17					800	
PD18					600	
PD19					300	

Table D.14: Population distribution preliminary investigation set-up (cont.)

ID	Distribution	MoI criterion	Move acceptance	n_{LLH}	μ	Δk
PD20					100	
PD21	SR	None	AM	12	1,200	1
PD22					600	
PD23					300	
PD24					100	
PD25				6	1,200	
PD26					600	
PD27					300	
PD28					100	
PD29				3	1,200	
PD30					600	
PD31					300	
PD32					100	
PD33	MoI-penalised GR	Objective value	IE	12	100	1
PD34				4	600	
PD35				4	100	
PD36				3	300	
PD37				6	300	
PD38				6	1,200	
PD39	MoI-penalised RW	Hyper-heuristic objective function	EMCQ	12	100	1
PD40				4	600	
PD41				4	100	
PD42				3	300	
PD43				6	300	
PD44				6	1,200	
PD45	TO	Choice function	AM	12	100	1
PD46				4	600	
PD47				4	100	
PD48				3	300	
PD49				6	300	
PD50				6	1,200	
PD51	MoI-penalised PK	Choice function	SA	12	100	1
PD52				4	600	
PD53				4	100	
PD54				3	300	
PD55				6	300	
PD56				6	1,200	
PD57	MoI-penalised RW	Hyper-heuristic objective function	EMCQ	4	100	1
PD58						5
PD59						10
PD60						20
PD61						40
PD62						60
PD63						80
PD64						100
PD65	TO	Choice function	AM	6	1,200	1
PD66						5
PD67						10
PD68						20
PD69						40
PD70						60
PD71						80
PD72						100

Table D.14: Population distribution preliminary investigation set-up (cont.)

ID	Distribution	MoI criterion	Move acceptance	n_{LLH}	μ	Δk
PD73	MoI-penalised RW	Hyper-heuristic objective function	EMCQ	3	300	1
PD74						5
PD75						10
PD76						20
PD77						40
PD78						60
PD79						80
PD80						100
PD81	MoI-penalised GR	Objective value	IE	12	100	1
PD82						5
PD83						10
PD84						20
PD85						40
PD86						60
PD87						80
PD88						100
PD89	SR	None	IE	12	100	1
PD90						5
PD91						10
PD92						20
PD93						40
PD94						60
PD95						80
PD96						100

The best solutions from each experiment of the investigation are presented in Table D.15.

Table D.15: Population distribution preliminary investigation solution of minimal mass results

ID	$f_{\min}$	$\Phi_{\min}$	c_1	c_2, m	η, %	LLH	$\beta(\mathrm{X}^{n_k})$, %	$A(\mathrm{X}^{n_k})$, %	N	T, h
PD1	53,211	53,212	1.50	-0.04	98.00	PSO	7.33	91.65	78	25.49
PD2	51,917	52,339	1.45	0.60	97.00	PSO	11.00	91.49	98	22.80
PD3	51,372	51,482	1.48	0.35	98.00	PSO	7.83	91.51	156	19.22
PD4	50,842	51,978	1.43	0.36	97.00	PSO	10.67	91.47	264	23.93
PD5	51,921	51,985	1.48	0.39	97.00	PSO	4.00	91.46	971	19.94
PD6	50,822	51,152	1.46	0.11	97.00	PSO	12.00	96.16	82	21.17
PD7	52,608	52,836	1.48	0.40	97.00	PSO	4.38	96.21	112	16.73
PD8	52,101	52,245	1.47	0.19	98.00	PSO	8.00	96.03	159	20.76
PD9	51,570	51,855	1.46	0.41	98.00	PSO	4.00	96.28	334	19.49
PD10	51,597	51,892	1.46	0.17	98.00	PSO	10.00	96.44	763	17.23
PD11	49,414	51,307	1.40	0.06	97.00	PSO	5.92	96.21	65	19.26
PD12	52,176	52,409	1.48	0.31	96.00	PSO	2.50	96.23	118	19.81
PD13	49,507	50,665	1.42	-0.16	97.00	KQ	6.33	96.22	139	14.94
PD14	51,641	51,714	1.48	0.20	98.00	PSO	4.67	96.32	314	18.40
PD15	51,008	51,315	1.46	0.20	98.00	PSO	4.00	96.61	968	20.30
PD16	53,710	53,756	1.48	0.39	98.00	RW	21.67	97.72	81	21.56
PD17	52,685	52,778	1.48	0.41	98.00	PSO	14.00	97.92	118	16.32
PD18	53,089	53,170	1.48	0.40	97.00	RW	5.67	97.73	161	19.47
PD19	52,604	52,674	1.48	0.42	97.00	RW	14.33	97.90	304	18.60
PD20	52,435	52,444	1.49	0.43	97.00	PSO	8.00	98.16	744	18.41
PD21	52,268	52,419	1.48	0.40	96.00	KQ	12.92	91.70	62	23.03

Table D.15: Population distribution preliminary investigation solution of minimal mass results (cont.)

ID	$f_{\min}$	$\Phi_{\min}$	c_1	c_2, m	η, %	LLH	$\beta(\mathrm{X}^{n_k})$, %	$A(\mathrm{X}^{n_k})$, %	N	T, h
PD22	52,751	52,751	1.50	0.32	98.00	PSO	8.17	91.73	166	23.50
PD23	51,923	52,365	1.46	0.13	97.00	RW	7.67	91.73	299	19.12
PD24	51,130	51,443	1.46	0.33	98.00	BP	5.00	92.27	981	19.46
PD25	50,852	51,065	1.47	0.20	97.00	TO	13.75	96.17	82	21.19
PD26	51,771	51,832	1.48	-0.04	98.00	PSO	5.83	96.18	142	19.45
PD27	51,718	51,944	1.46	0.42	98.00	PSO	8.00	96.35	330	19.48
PD28	51,589	51,744	1.47	0.17	98.00	PSO	1.00	96.55	938	15.93
PD29	53,041	53,257	1.47	0.43	98.00	RW	19.00	97.80	83	21.47
PD30	52,624	52,644	1.49	0.42	97.00	RW	19.50	98.01	151	19.05
PD31	52,305	52,505	1.47	0.31	98.00	PSO	16.00	97.98	327	18.46
PD32	52,108	52,165	1.48	0.48	98.00	PSO	12.00	98.24	834	18.00
PD33	51,050	51,063	1.49	0.25	98.00	BP	1.00	92.27	995	19.27
PD34	51,805	51,860	1.48	0.21	98.00	KQ	2.33	96.21	129	18.06
PD35	51,874	52,225	1.46	0.58	98.00	KQ	0.00	96.54	405	13.40
PD36	51,650	51,779	1.47	0.42	98.00	KQ	3.00	96.26	332	17.76
PD37	51,268	51,399	1.47	0.27	98.00	KQ	2.00	96.33	123	18.66
PD38	50,370	51,579	1.43	0.13	97.00	KQ	1.08	96.05	4	17.42
PD39	49,242	51,091	1.40	0.07	97.00	BP	5.00	96.07	722	15.79
PD40	51,102	52,037	1.43	0.22	98.00	PSO	1.50	96.46	128	18.46
PD41	50,445	50,445	1.50	0.22	100.00	TO	8.00	96.81	990	17.32
PD42	50,901	50,901	1.50	0.06	100.00	PSO	5.00	97.02	325	19.15
PD43	51,698	51,797	1.48	0.08	98.00	PSO	1.00	96.50	312	17.40
PD44	50,676	50,922	1.47	0.30	97.00	PSO	15.75	96.62	84	19.14
PD45	51,878	52,092	1.47	0.35	98.00	BP	4.00	91.45	274	10.76
PD46	50,250	51,338	1.42	0.27	98.00	RW	17.83	96.52	164	19.76
PD47	51,220	51,504	1.46	0.45	97.00	PSO	9.00	97.86	960	20.93
PD48	51,604	51,642	1.47	0.13	99.00	PSO	1.67	96.77	321	18.62
PD49	51,930	51,944	1.49	0.30	98.00	RW	6.00	96.51	334	19.07
PD50	50,747	50,763	1.49	0.04	98.00	KQ	21.08	96.80	51	25.18
PD51	52,122	52,133	1.48	0.28	99.00	PSO	2.00	91.48	597	16.91
PD52	51,775	51,828	1.48	0.23	98.00	PSO	11.50	96.81	145	19.40
PD53	51,825	51,888	1.48	0.43	98.00	PSO	1.00	96.08	724	18.12
PD54	51,272	51,346	1.48	0.45	97.00	PSO	4.67	96.81	300	18.85
PD55	52,135	52,225	1.48	0.28	98.00	PSO	4.00	96.53	240	18.69
PD56	52,189	52,312	1.48	0.29	96.00	PSO	7.50	96.80	60	20.21
PD57	51,288	51,403	1.48	0.45	97.00	BP	3.00	94.09	944	21.75
PD58	51,253	51,319	1.48	0.49	98.00	BP	7.00	91.26	988	14.91
PD59	51,095	51,195	1.48	0.42	98.00	BP	3.00	90.70	996	20.63
PD60	51,219	51,300	1.48	0.40	98.00	PSO	1.00	91.00	694	15.39
PD61	49,940	49,940	1.50	0.15	98.00	RW	30.00	96.46	971	22.32
PD62	50,351	50,386	1.47	0.58	99.00	DE	2.00	91.72	917	18.26
PD63	51,303	51,417	1.48	0.11	97.00	BP	1.00	91.83	1,000	20.34
PD64	51,179	51,181	1.49	0.16	99.00	PSO	3.00	96.92	961	17.84
PD65	49,868	49,924	1.48	-0.13	97.00	TO	18.50	96.76	70	24.35
PD66	50,610	51,777	1.42	0.09	98.00	PSO	9.67	96.37	81	18.82
PD67	51,438	51,885	1.45	0.30	98.00	RW	5.25	95.60	81	19.77
PD68	50,095	51,178	1.42	0.03	98.00	PSO	7.83	96.40	69	19.58
PD69	50,220	50,544	1.46	-0.07	97.00	PSO	9.75	96.37	57	21.55
PD70	50,630	50,747	1.47	0.25	98.00	KQ	9.42	95.72	66	18.93
PD71	50,086	51,418	1.43	0.21	96.00	PSO	9.33	96.51	80	21.76
PD72	51,805	51,989	1.47	0.10	98.00	KQ	19.42	96.01	71	19.23
PD73	48,754	50,602	1.40	0.31	98.00	PSO	5.67	96.39	314	17.08
PD74	51,047	51,141	1.48	0.14	98.00	PSO	0.67	96.84	246	16.80
PD75	51,482	51,551	1.48	-0.04	97.00	RW	4.67	96.37	332	21.43
PD76	51,520	51,576	1.48	0.13	98.00	PSO	3.00	96.88	304	18.99

Table D.15: Population distribution preliminary investigation solution of minimal mass results (cont.)

ID	$f_{\min}$	$\Phi_{\min}$	c_1	c_2, m	η, %	LLH	$\beta(\mathrm{X}^{n_k})$, %	$A(\mathrm{X}^{n_k})$, %	N	T, h
PD77	51,941	51,992	1.47	0.43	97.00	PSO	1.00	97.04	315	20.14
PD78	51,652	51,711	1.48	0.10	98.00	PSO	2.67	96.32	321	18.26
PD79	51,291	51,567	1.46	0.26	98.00	PSO	3.33	97.04	321	17.62
PD80	52,485	52,485	1.50	0.34	100.00	PSO	4.33	96.19	326	19.88
PD81	51,757	51,846	1.48	0.24	97.00	PSO	4.00	96.86	316	18.52
PD82	49,251	51,063	1.40	0.24	97.00	PSO	5.00	96.51	333	20.76
PD83	51,470	51,521	1.48	0.31	98.00	PSO	4.33	96.46	299	21.23
PD84	51,879	51,901	1.49	0.04	97.00	PSO	5.00	96.48	262	19.00
PD85	51,749	51,810	1.48	0.23	98.00	PSO	4.67	96.43	331	21.25
PD86	52,092	52,092	1.50	0.11	100.00	RW	3.33	96.73	271	16.07
PD87	51,892	51,953	1.48	-0.10	98.00	RW	10.00	96.83	275	18.29
PD88	51,592	51,893	1.46	0.40	98.00	PSO	2.00	96.41	323	23.59
PD89	51,450	52,047	1.45	0.27	97.00	KQ	0.00	95.97	289	10.75
PD90	51,774	51,776	1.50	0.22	98.00	BP	0.00	99.75	305	7.38
PD91	51,713	51,900	1.47	0.37	98.00	KQ	2.00	96.13	215	9.50
PD92	50,523	51,518	1.43	0.14	98.00	KQ	2.00	95.97	746	20.08
PD93	51,917	51,987	1.48	0.25	98.00	KQ	0.00	96.39	929	21.66
PD94	51,767	51,942	1.48	0.23	96.00	KQ	1.00	96.39	412	11.65
PD95	52,397	52,401	1.50	0.14	98.00	KQ	1.00	95.97	839	19.65
PD96	52,085	52,167	1.48	0.40	97.00	KQ	2.00	96.56	511	16.53

Table D.16 presents the average results of the population distribution investigation.

Table D.16: Population distribution preliminary investigation average results

ID	$\overline{f_{\min}}$	$\overline{\Phi_{\min}}$	$\overline{\sigma(\Phi_{\min})}$	$\overline{\beta(\mathrm{X}^{n_k})}$, %	$\overline{A(\mathrm{X}^{n_k})}$, %	$\overline{N}$	$\overline{T}$, h
PD1	53,620	53,715	529	7.52	91.75	67.2	25.33
PD2	53,038	53,248	548	8.02	91.64	112.4	23.21
PD3	52,698	52,889	800	6.83	91.66	154.8	22.63
PD4	52,058	52,415	471	7.94	91.63	270.6	23.49
PD5	52,065	52,107	139	4.20	91.42	915.6	19.91
PD6	51,304	52,057	810	9.22	96.19	66.2	20.58
PD7	52,866	53,110	258	5.70	96.12	108.4	20.66
PD8	52,721	52,907	385	7.77	96.22	140.6	20.77
PD9	51,941	52,237	225	5.33	96.32	311.4	19.33
PD10	51,919	52,108	200	6.60	96.48	898.4	17.17
PD11	52,285	52,698	797	5.77	96.24	61.2	20.55
PD12	53,013	53,084	485	5.68	96.19	109.8	20.49
PD13	51,636	51,950	841	4.30	96.18	144.2	19.97
PD14	51,949	52,029	308	5.27	96.32	304.8	17.69
PD15	52,077	52,250	750	3.40	96.49	947.8	20.51
PD16	54,135	54,278	517	13.33	97.79	75.8	19.94
PD17	53,182	53,316	519	12.55	97.80	119.0	20.15
PD18	53,758	53,896	511	10.83	97.77	148.0	19.84
PD19	53,084	53,194	493	10.47	97.98	294.2	19.50
PD20	52,529	52,585	218	8.20	98.12	719.4	17.09
PD21	52,828	53,165	472	8.43	91.67	75.2	24.73
PD22	53,001	53,529	765	7.04	91.80	143.2	22.01
PD23	52,659	52,853	447	7.67	91.86	295.6	21.63
PD24	51,559	51,737	222	5.20	92.20	987.6	19.09
PD25	51,850	52,456	805	10.77	96.18	78.0	20.80
PD26	52,885	53,100	1,044	8.43	96.26	148.2	21.94

Table D.16: Population distribution preliminary investigation average results (cont.)

ID	$\overline{f_{\min}}$	$\overline{\Phi_{\min}}$	$\overline{\sigma(\Phi_{\min})}$	$\overline{\beta(\mathrm{X}^{n_k})}$, %	$\overline{A(\mathrm{X}^{n_k})}$, %	$\overline{N}$	$\overline{T}$, h
PD27	52,157	52,449	376	5.13	96.38	320.8	18.48
PD28	51,976	52,088	234	6.20	96.53	939.6	18.27
PD29	53,428	53,645	482	13.28	97.71	78.8	22.25
PD30	53,443	53,498	772	15.47	97.91	158.8	23.04
PD31	52,846	52,962	402	15.47	97.97	315.2	19.23
PD32	52,515	52,624	419	8.60	98.14	815.2	17.67
PD33	51,680	51,728	405	8.80	92.10	931.6	19.24
PD34	52,140	52,315	414	1.80	96.09	130.8	18.98
PD35	53,018	53,372	1,024	2.00	96.11	361.4	12.72
PD36	52,530	52,592	736	1.73	97.45	280.8	19.16
PD37	52,087	52,345	708	1.20	96.04	214.4	19.38
PD38	51,693	52,439	621	1.43	95.99	55.2	19.30
PD39	50,978	51,389	299	2.80	94.44	880.6	18.28
PD40	52,093	52,371	258	5.77	96.47	154.0	18.98
PD41	51,995	52,114	1,044	12.00	96.48	792.2	16.24
PD42	52,142	52,171	739	4.67	96.68	293.2	18.42
PD43	52,025	52,369	327	7.53	96.10	288.6	18.60
PD44	51,067	51,581	580	14.36	96.38	74.0	19.81
PD45	52,390	52,589	609	8.00	92.38	386.6	14.00
PD46	52,029	52,319	583	7.30	96.56	141.4	20.64
PD47	52,030	52,275	635	7.00	96.99	691.0	16.78
PD48	51,894	51,962	293	3.00	96.72	322.4	19.12
PD49	52,375	52,423	382	9.87	96.48	317.4	19.27
PD50	52,127	52,244	888	12.95	96.83	68.8	21.48
PD51	52,076	52,273	121	2.60	92.22	504.4	15.82
PD52	52,173	52,275	416	8.70	96.76	137.8	19.47
PD53	52,008	52,185	216	2.00	96.63	787.2	17.11
PD54	51,690	51,970	568	4.60	96.53	310.0	18.55
PD55	52,584	52,644	339	7.80	96.38	295.8	19.17
PD56	52,053	52,736	418	12.77	96.50	70.0	20.66
PD57	51,513	51,627	303	3.00	95.97	954.8	19.36
PD58	51,608	51,650	437	4.40	93.51	811.4	16.90
PD59	51,470	51,532	372	2.40	92.52	766.4	18.81
PD60	51,702	51,804	607	1.00	93.33	738.6	15.64
PD61	50,980	51,079	685	9.00	94.50	699.6	17.53
PD62	51,464	51,524	710	8.00	95.60	742.2	15.90
PD63	51,583	51,680	256	2.40	92.24	879.4	21.28
PD64	51,718	51,824	459	2.60	95.23	577.2	15.11
PD65	51,553	51,739	1,020	12.37	96.61	72.8	21.43
PD66	51,741	52,157	337	6.79	96.49	74.6	19.51
PD67	52,196	52,298	286	8.18	96.04	68.6	20.10
PD68	51,940	52,228	741	7.93	96.37	79.4	19.47
PD69	51,652	51,809	841	8.47	96.32	75.0	21.11
PD70	51,437	51,877	998	8.53	96.23	75.0	19.44
PD71	51,819	52,374	581	9.60	96.16	76.6	20.91
PD72	52,262	52,372	347	12.05	96.15	77.4	19.52
PD73	51,058	51,524	517	3.13	96.59	321.2	20.40
PD74	51,696	51,759	446	4.20	96.97	309.8	18.83
PD75	51,759	51,882	484	4.13	96.89	318.2	19.45
PD76	51,901	51,993	397	1.33	96.66	305.2	21.32
PD77	52,220	52,496	305	3.07	96.33	310.4	21.90
PD78	52,023	52,138	451	2.20	96.50	310.0	18.28
PD79	51,896	52,015	433	5.07	96.46	310.6	19.66
PD80	52,524	52,666	136	2.00	96.22	307.0	20.03
PD81	51,974	52,124	284	5.87	96.54	301.2	20.16

Table D.16: Population distribution preliminary investigation average results (cont.)

ID	$\overline{f_{\min}}$	$\overline{\Phi_{\min}}$	$\overline{\sigma(\Phi_{\min})}$	$\overline{\beta(\mathrm{X}^{n_k})}$, %	$\overline{A(\mathrm{X}^{n_k})}$, %	$\overline{N}$	$\overline{T}$, h
PD82	51,508	52,009	797	4.33	96.62	312.2	19.70
PD83	52,026	52,200	652	3.93	96.55	300.2	20.45
PD84	52,188	52,263	272	7.20	96.61	282.8	19.22
PD85	52,324	52,413	373	3.87	96.61	317.4	20.47
PD86	52,591	52,750	687	6.00	96.55	312.4	20.84
PD87	52,302	52,333	322	7.93	96.80	304.2	20.18
PD88	51,934	52,364	324	6.13	96.46	325.4	21.21
PD89	52,175	52,441	399	1.40	96.84	470.4	15.01
PD90	52,000	52,170	344	0.00	98.25	502.2	14.03
PD91	53,117	53,428	971	1.60	95.93	320.6	13.43
PD92	51,957	52,517	580	1.20	96.13	377.8	12.31
PD93	53,810	53,902	2,659	1.80	96.10	442.6	14.14
PD94	52,844	53,140	842	3.00	96.86	292.6	10.97
PD95	54,439	54,473	2,852	2.40	95.51	386.2	12.92
PD96	52,755	52,953	671	2.20	96.16	355.4	12.18

D.7 Perturbation Analysis

Table D.17 lists the perturbation analysis set-ups during the preliminary investigation. Variations include the hyper-heuristic employed for perturbation analysis as well as the evolutionary principle, method of population sampling, i.e. best or random individuals, perturbed population sample size, μ_{PA}, and perturbation scale, $\Delta x_{v,PA}$.

Table D.17: Perturbation analysis preliminary investigation set-up

ID	Hyper-heuristic	Evolution	Sample	μ_{PA}	$\Delta x_{v,PA}$
PA1	HC	Lamarckian	Best	1	$0.1\Delta \mathrm{V}_v$
PA2				0.1μ	
PA3				0.25μ	
PA4				0.5μ	
PA5			Random	1	
PA6				0.1μ	
PA7				0.25μ	
PA8				0.5μ	
PA9				μ	
PA10		Baldwinian	Best	1	
PA11				0.1μ	
PA12				0.25μ	
PA13				0.5μ	
PA14			Random	1	
PA15				0.1μ	
PA16				0.25μ	
PA17				0.5μ	
PA18				μ	
PA19	SA	Lamarckian	Best	1	$0.1\Delta \mathrm{V}_v$
PA20				0.1μ	
PA21				0.25μ	
PA22				0.5μ	
PA23			Random	1	
PA24				0.1μ	

Table D.17: Perturbation analysis preliminary investigation set-up (cont.)

ID	Hyper-heuristic	Evolution	Sample	μ_{PA}	$\Delta x_{v,PA}$
PA25				0.25μ	
PA26				0.5μ	
PA27				μ	
PA28		Baldwinian	Best	1	
PA29				0.1μ	
PA30				0.25μ	
PA31				0.5μ	
PA32			Random	1	
PA33				0.1μ	
PA34				0.25μ	
PA35				0.5μ	
PA36				μ	
PA37	TS	Lamarckian	Best	1	$0.1\Delta \mathrm{V}_v$
PA38				0.1μ	
PA39				0.25μ	
PA40				0.5μ	
PA41			Random	1	
PA42				0.1μ	
PA43				0.25μ	
PA44				0.5μ	
PA45				μ	
PA46		Baldwinian	Best	1	
PA47				0.1μ	
PA48				0.25μ	
PA49				0.5μ	
PA50			Random	1	
PA51				0.1μ	
PA52				0.25μ	
PA53				0.5μ	
PA54				μ	
PA55	TS	Lamarckian	Best	1	$0.05\Delta \mathrm{V}_v$
PA56					$0.025\Delta \mathrm{V}_v$
PA57					$0.01\Delta \mathrm{V}_v$
PA58					$0.005\Delta \mathrm{V}_v$
PA59	TS	Baldwinian	Random	1	$0.05\Delta \mathrm{V}_v$
PA60					$0.025\Delta \mathrm{V}_v$
PA61					$0.01\Delta \mathrm{V}_v$
PA62					$0.005\Delta \mathrm{V}_v$
PA63	SA	Lamarckian	Best	0.1μ	$0.05\Delta \mathrm{V}_v$
PA64					$0.025\Delta \mathrm{V}_v$
PA65					$0.01\Delta \mathrm{V}_v$
PA66					$0.005\Delta \mathrm{V}_v$
PA67	SA	Lamarckian	Best	0.25μ	$0.05\Delta \mathrm{V}_v$
PA68					$0.025\Delta \mathrm{V}_v$
PA69					$0.01\Delta \mathrm{V}_v$
PA70					$0.005\Delta \mathrm{V}_v$
PA71	SA	Lamarckian	Best	1	$0.05\Delta \mathrm{V}_v$
PA72					$0.025\Delta \mathrm{V}_v$
PA73					$0.01\Delta \mathrm{V}_v$
PA74					$0.005\Delta \mathrm{V}_v$

Table D.18 lists the results corresponding to the runs that generated the solutions of minimal mass for each experiment of this investigation.

Table D.18: Perturbation analysis preliminary investigation solution of minimal mass results

ID	$f_{\min}$	$\Phi_{\min}$	c_1	c_2, m	η, %	$\beta(\mathrm{X}^{n_k})$, %	$A(\mathrm{X}^{n_k})$, %	N	T, h
PA1	52,252	52,269	1.49	0.49	98.00	0.00	99.56	183	6.71
PA2	52,188	52,168	1.49	0.47	95.00	1.00	99.71	918	16.41
PA3	52,227	52,315	1.46	0.49	99.00	1.00	99.57	625	19.47
PA4	52,186	52,244	1.48	0.35	98.00	0.00	99.70	429	12.46
PA5	52,248	52,253	1.50	0.37	91.00	0.00	99.53	445	13.13
PA6	52,236	52,258	1.49	0.51	98.00	91.00	99.67	382	13.52
PA7	52,293	52,321	1.49	0.50	97.00	0.00	99.64	530	13.87
PA8	52,184	52,214	1.49	0.48	97.00	0.00	99.54	449	12.55
PA9	50,061	51,048	1.43	0.46	98.00	0.00	99.69	275	9.42
PA10	52,375	52,388	1.48	0.50	99.00	0.00	99.74	519	13.96
PA11	50,924	51,047	1.48	0.47	97.00	0.00	99.60	205	9.41
PA12	52,536	52,546	1.49	0.33	97.00	0.00	99.67	95	6.88
PA13	52,240	52,257	1.49	0.26	97.00	0.00	99.61	153	8.53
PA14	52,010	52,041	1.47	0.32	99.00	0.00	99.59	492	12.41
PA15	52,176	52,203	1.48	0.37	97.00	0.00	99.58	893	16.28
PA16	52,369	52,399	1.49	0.48	95.00	0.00	99.83	346	15.47
PA17	52,354	52,385	1.47	0.50	99.00	1.00	99.64	163	10.03
PA18	52,306	52,338	1.48	0.38	95.00	0.00	99.71	309	11.01
PA19	51,930	51,952	1.48	0.37	97.00	0.00	99.68	686	10.16
PA20	51,835	51,835	1.50	0.36	100.00	0.00	99.65	361	9.04
PA21	51,903	51,928	1.48	0.30	97.00	0.00	99.56	431	8.93
PA22	52,382	52,415	1.48	0.37	97.00	0.00	99.55	316	11.77
PA23	52,043	52,091	1.48	0.47	95.00	0.00	99.59	336	9.87
PA24	52,388	52,388	1.50	0.47	100.00	0.00	99.58	174	7.46
PA25	52,105	52,167	1.48	0.31	98.00	0.00	99.67	390	11.11
PA26	51,904	52,027	1.48	0.33	97.00	0.00	99.46	226	8.32
PA27	52,378	52,382	1.49	0.30	97.00	0.00	99.69	268	10.62
PA28	52,041	52,073	1.48	0.45	97.00	0.00	99.53	220	7.49
PA29	52,155	52,170	1.49	0.49	98.00	0.00	99.55	324	9.61
PA30	52,469	52,501	1.49	0.44	98.00	0.00	99.68	429	12.81
PA31	52,310	52,312	1.50	0.41	98.00	1.00	99.74	148	9.22
PA32	52,597	52,598	1.50	0.45	98.00	1.00	99.60	141	7.32
PA33	52,030	52,050	1.49	0.45	96.00	0.00	99.55	296	9.41
PA34	52,338	52,353	1.49	0.47	98.00	1.00	99.66	338	11.04
PA35	51,234	51,314	1.48	0.38	98.00	0.00	99.54	209	8.22
PA36	52,119	52,146	1.49	0.44	97.00	0.00	99.75	570	15.61
PA37	50,858	50,981	1.48	0.41	97.00	0.00	99.62	601	15.24
PA38	52,217	52,218	1.50	0.42	98.00	0.00	99.55	663	14.12
PA39	51,812	51,814	1.50	0.31	97.00	0.00	99.54	307	8.33
PA40	52,050	52,099	1.48	0.49	97.00	0.00	99.66	464	12.99
PA41	52,170	52,196	1.49	0.25	97.00	0.00	99.62	321	9.90
PA42	52,229	52,291	1.48	0.30	98.00	0.00	99.53	361	10.53
PA43	52,151	52,226	1.48	0.37	97.00	1.00	99.52	176	8.08
PA44	52,046	52,056	1.49	0.37	98.00	2.00	99.65	125	7.24
PA45	51,874	51,936	1.48	0.31	95.00	1.00	99.59	787	19.53
PA46	52,222	52,269	1.48	0.33	97.00	0.00	99.78	913	22.71
PA47	52,015	52,077	1.48	0.37	98.00	0.00	99.51	268	8.27
PA48	52,105	52,135	1.49	0.41	96.00	0.00	99.72	941	24.38
PA49	52,202	52,213	1.49	0.32	97.00	0.00	99.65	305	10.52
PA50	50,983	51,479	1.43	0.37	97.00	0.00	99.66	54	5.75
PA51	52,053	52,061	1.49	0.44	99.00	1.00	99.72	670	19.92
PA52	52,012	52,080	1.48	0.38	97.00	0.00	99.72	312	10.80
PA53	52,356	52,419	1.49	0.51	95.00	0.00	99.75	253	10.98
PA54	52,158	52,173	1.49	0.49	98.00	0.00	99.61	363	10.52
PA55	52,300	52,303	1.50	0.47	95.00	0.00	99.64	440	12.33

Table D.18: Perturbation analysis preliminary investigation solution of minimal mass results (cont.)

ID	$f_{\min}$	$\Phi_{\min}$	c_1	c_2, m	η, %	$\beta(\mathrm{X}^{n_k})$, %	$A(\mathrm{X}^{n_k})$, %	N	T, h
PA56	52,086	52,101	1.49	0.46	98.00	0.00	99.58	525	13.30
PA57	52,201	52,222	1.48	0.47	95.00	0.00	99.52	488	14.87
PA58	50,794	51,321	1.46	0.24	96.00	1.00	99.66	60	6.47
PA59	51,927	51,941	1.49	0.43	98.00	0.00	99.59	211	8.96
PA60	52,198	52,201	1.50	0.38	95.00	0.00	99.79	157	7.22
PA61	52,270	52,332	1.48	0.26	98.00	0.00	99.70	368	12.18
PA62	52,337	52,341	1.49	0.21	98.00	0.00	99.69	542	14.88
PA63	52,135	52,160	1.48	0.34	99.00	0.00	99.76	680	15.79
PA64	52,303	52,317	1.49	0.25	97.00	1.00	99.70	135	7.97
PA65	52,030	52,032	1.49	0.44	99.00	1.00	99.64	267	10.17
PA66	51,968	51,970	1.50	0.32	97.00	0.00	99.69	571	13.37
PA67	52,324	52,333	1.49	0.33	97.00	0.00	99.77	199	10.41
PA68	52,473	52,493	1.48	0.52	99.00	0.00	99.64	342	11.46
PA69	52,131	52,173	1.49	0.49	97.00	0.00	99.57	171	8.52
PA70	52,250	52,262	1.48	0.51	99.00	3.00	99.49	148	7.18
PA71	52,172	52,196	1.49	0.42	97.00	0.00	99.69	313	10.03
PA72	52,608	52,624	1.48	0.35	99.00	0.00	99.69	565	14.69
PA73	52,369	52,420	1.47	0.40	99.00	1.00	99.73	331	13.92
PA74	52,354	52,363	1.49	0.44	98.00	1.00	99.69	126	6.69

The mean results of the perturbation analysis preliminary investigation are presented in Table D.19.

Table D.19: Perturbation analysis preliminary investigation average results

ID	$\overline{f_{\min}}$	$\overline{\Phi_{\min}}$	$\overline{\sigma(\Phi_{\min})}$	$\overline{\beta(\mathrm{X}^{n_k})}$, %	$\overline{A(\mathrm{X}^{n_k})}$, %	$\overline{N}$	$\overline{T}$, h
PA1	52,709	52,730	420	0.20	99.66	396.0	14.14
PA2	52,424	52,445	225	18.20	99.72	422.0	11.61
PA3	52,451	52,472	166	1.40	99.63	365.2	13.94
PA4	52,429	52,447	266	4.20	99.66	259.4	10.07
PA5	52,696	52,709	358	0.40	99.62	658.0	16.96
PA6	52,691	52,716	282	18.80	99.59	369.2	12.84
PA7	52,591	52,615	585	18.20	99.65	341.6	10.79
PA8	52,328	52,372	143	0.20	99.65	438.4	12.75
PA9	51,998	52,331	748	18.40	99.66	323.8	11.53
PA10	52,626	52,658	252	19.60	99.70	341.6	11.03
PA11	55,266	55,306	4,614	18.60	99.66	420.4	12.96
PA12	52,764	52,771	225	0.40	99.69	367.0	11.68
PA13	52,607	52,623	273	1.00	99.61	369.6	13.19
PA14	52,454	52,470	320	18.80	99.64	522.4	13.42
PA15	52,397	52,435	137	0.20	99.70	419.8	11.90
PA16	52,860	52,883	446	18.60	99.69	346.8	12.27
PA17	52,622	52,645	236	0.20	99.66	399.4	14.91
PA18	52,449	52,950	802	18.20	99.66	158.2	8.25
PA19	52,649	52,658	539	18.20	99.63	418.6	12.57
PA20	52,348	52,369	359	0.60	99.65	402.2	12.71
PA21	52,252	52,275	223	0.00	99.62	336.8	9.69
PA22	52,598	52,630	203	18.40	99.59	342.6	12.41
PA23	52,559	52,610	346	0.20	99.65	337.4	11.09
PA24	52,513	52,517	147	0.80	99.58	305.0	10.72
PA25	52,459	52,543	311	0.00	99.68	336.0	9.78
PA26	52,216	52,309	186	0.20	99.62	387.8	11.44
PA27	52,603	52,673	237	0.80	99.69	400.8	12.35

Table D.19: Perturbation analysis preliminary investigation average results (cont.)

ID	$\overline{f_{\min}}$	$\overline{\Phi_{\min}}$	$\overline{\sigma(\Phi_{\min})}$	$\overline{\beta(\mathrm{X}^{n_k})}$, %	$\overline{A(\mathrm{X}^{n_k})}$, %	$\overline{N}$	$\overline{T}$, h
PA28	52,493	52,513	341	0.00	99.59	505.8	14.08
PA29	52,298	52,322	130	18.40	99.61	285.4	9.70
PA30	52,758	52,776	164	20.20	99.67	487.2	13.38
PA31	52,594	52,728	393	0.60	99.73	428.8	14.88
PA32	52,789	52,817	263	1.80	99.60	390.2	11.74
PA33	52,615	52,639	440	0.40	99.64	408.4	13.61
PA34	52,622	52,667	210	0.80	99.60	256.4	9.19
PA35	52,058	52,089	476	18.20	99.64	316.8	10.99
PA36	52,564	52,591	368	0.20	99.57	339.8	11.41
PA37	52,296	52,336	838	19.00	99.66	584.2	16.18
PA38	52,719	52,724	396	18.20	99.64	562.4	14.62
PA39	53,866	53,877	3,565	20.00	99.70	292.0	11.24
PA40	53,782	53,833	3,439	0.00	99.63	327.2	11.20
PA41	52,541	52,592	341	0.60	99.58	265.6	9.38
PA42	52,500	52,523	201	19.20	99.63	258.4	9.86
PA43	52,675	52,696	411	19.00	99.66	234.8	9.23
PA44	52,703	52,786	830	0.80	99.66	285.0	11.89
PA45	52,464	52,495	492	1.00	99.58	344.0	11.33
PA46	52,779	52,793	428	18.40	99.68	413.8	13.75
PA47	52,548	52,567	309	0.60	99.66	450.4	12.53
PA48	52,368	52,380	185	35.60	99.64	484.0	15.02
PA49	52,410	52,436	214	0.60	99.61	397.8	11.46
PA50	52,327	52,434	568	18.20	99.70	375.2	11.41
PA51	52,389	52,394	345	18.60	99.66	388.0	12.29
PA52	52,342	52,360	321	0.60	99.67	410.2	12.38
PA53	52,503	52,528	173	0.60	99.66	430.4	15.16
PA54	52,379	52,399	228	0.00	99.67	326.2	10.48
PA55	52,552	52,608	223	0.20	99.71	427.0	13.87
PA56	52,694	52,709	565	0.20	99.62	403.6	12.43
PA57	52,361	52,390	256	0.00	99.57	408.8	13.27
PA58	53,714	53,853	3,358	18.60	99.71	185.6	9.66
PA59	52,557	52,651	590	19.40	99.63	365.8	12.32
PA60	52,521	52,574	329	0.40	99.66	537.2	14.57
PA61	52,537	52,559	240	0.20	99.67	448.0	14.48
PA62	52,756	52,809	341	0.00	99.69	370.8	13.80
PA63	52,327	52,343	165	1.60	99.67	400.2	12.36
PA64	52,559	52,578	382	1.00	99.66	262.8	9.90
PA65	52,366	52,433	231	1.00	99.67	290.8	11.66
PA66	52,350	52,361	348	18.20	99.70	384.8	11.30
PA67	53,811	53,863	2,524	53.80	99.64	168.2	8.50
PA68	52,588	52,608	103	0.20	99.69	419.4	11.87
PA69	52,698	52,717	460	18.40	99.61	377.4	11.23
PA70	54,114	54,132	3,381	1.20	99.65	367.2	10.60
PA71	52,512	52,535	354	18.20	99.66	406.8	13.13
PA72	54,451	54,468	3,190	0.60	99.71	567.2	14.17
PA73	52,612	52,632	227	0.60	99.69	460.6	14.67
PA74	52,578	52,596	280	1.00	99.69	279.8	9.85

D.8 Parameter Control

The parameter control preliminary investigation is set up as stated in Table D.20. Variations are made in the parameter controlled and its range, the LLH employed, the hyper-heuristic in control and the hyper-heuristic objective function measurement period.

Table D.20: Parameter control preliminary investigation set-up

ID	Parameter	Range	LLH	Hyper-heuristic	Δk
PC1	P1	$0.1 \leq F \leq 0.4$	RW	HC	1
PC2					10
PC3					50
PC4				SA	1
PC5					10
PC6					50
PC7				TS	1
PC8					10
PC9					50
PC10	P2	$1 \leq \lambda \leq 5$	RW	HC	1
PC11					10
PC12					50
PC13				SA	1
PC14					10
PC15					50
PC16				TS	1
PC17					10
PC18					50
PC19	P4	$0.1 \leq \alpha_{RI} \leq 0.5$	RI	HC	1
PC20					10
PC21					50
PC22				SA	1
PC23					10
PC24					50
PC25				TS	1
PC26					10
PC27					50
PC28	P5	$0.5 \leq p_{c,DE} \leq 1.0$	DE	HC	1
	P6	$0.4 \leq F_{DE} \leq 1.2$			
PC29					10
PC30					50
PC31				SA	1
PC32					10
PC33					50
PC34				TS	1
PC35					10
PC36					50
PC37	P3	4-bits $\leq n_b \leq$ 16-bits	RW	HC	1
	P7	$1 \leq n_c \leq$ random			
	P8	$0.5 \leq p_{c,GA} \leq 1.0$			
	P9	$0.005 \leq p_m \leq 0.05$			
PC38					10
PC39					50
PC40				SA	1
PC41					10
PC42					50
PC43				TS	1
PC44					10
PC45					50
PC46	P10	$0.1 \leq \alpha_{BP} \leq 0.5$	BP	HC	1
PC47					10
PC48					50
PC49				SA	1
PC50					10
PC51					50

Table D.20: Parameter control preliminary investigation set-up (cont.)

ID	Parameter	Range	LLH	Hyper-heuristic	Δk
PC52				TS	1
PC53					10
PC54					50
PC55	P11	$0.1 \leq \alpha_{RC} \leq 0.5$	RC	HC	1
PC56					10
PC57					50
PC58				SA	1
PC59					10
PC60					50
PC61				TS	1
PC62					10
PC63					50
PC64	P12	$0.6 \leq \omega_{PSO} \leq 0.8$	PSO	HC	1
	P13	$1.4 \leq c_{1,PSO} \leq 2.1$			
	P14	$1.3 \leq c_{2,PSO} \leq 1.7$			
	P15	$0.8 \leq \kappa_{PSO} \leq 1.0$			
PC65					10
PC66					50
PC67				SA	1
PC68					10
PC69					50
PC70				TS	1
PC71					10
PC72					50
PC73	P16	$0.01\Delta \mathrm{V}_v \leq \Delta x_v \leq 0.1\Delta \mathrm{V}_v$	HC	HC	1
PC74					10
PC75					50
PC76				SA	1
PC77					10
PC78					50
PC79				TS	1
PC80					10
PC81					50
PC82	P17	$0.0 \leq \alpha_{SA} \leq 0.9$	HC	HC	1
PC83					10
PC84					50
PC85				SA	1
PC86					10
PC87					50
PC88				TS	1
PC89					10
PC90					50
PC91	P18	$1 \leq n_{TS} \leq 1000$	HC	HC	1
PC92					10
PC93					50
PC94				SA	1
PC95					10
PC96					50
PC97				TS	1
PC98					10
PC99					50

Table D.21 presents the results of the run of each experiment that generated the best solution.

Table D.21: Parameter control preliminary investigation solution of minimal mass results

ID	$f_{\min}$	$\Phi_{\min}$	c_1	c_2, m	η, %	$\beta(\mathrm{X}^{n_k})$, %	$A(\mathrm{X}^{n_k})$, %	N	T, h
PC1	42,766	42,811	1.48	0.29	98.00	0.00	99.69	677	51.23
PC2	41,475	41,953	1.39	0.22	99.00	0.00	99.65	705	31.27
PC3	42,334	42,375	1.47	0.26	98.00	12.00	99.30	594	23.41
PC4	41,722	42,677	1.37	0.22	97.00	0.00	99.41	720	23.23
PC5	42,963	43,544	1.38	0.32	99.00	0.00	99.63	802	37.72
PC6	42,093	42,336	1.42	0.24	98.00	0.00	99.45	751	48.12
PC7	42,640	42,766	1.44	0.29	99.00	0.00	99.14	587	22.58
PC8	43,060	43,547	1.48	0.26	95.00	0.00	99.60	595	19.52
PC9	42,292	42,450	1.45	0.27	98.00	0.00	99.45	678	21.96
PC10	50,006	50,078	1.48	0.11	98.00	2.00	99.66	153	6.59
PC11	50,442	51,316	1.41	0.23	97.00	0.00	99.60	64	6.12
PC12	52,474	52,474	1.50	0.49	98.00	0.00	99.75	440	12.62
PC13	52,128	52,184	1.48	0.65	95.00	0.00	99.56	400	11.14
PC14	52,500	52,500	1.51	0.18	100.00	89.00	99.63	125	7.22
PC15	52,088	52,155	1.49	0.36	95.00	0.00	99.72	656	19.94
PC16	52,360	52,386	1.48	0.37	99.00	1.00	99.60	950	18.53
PC17	52,078	52,123	1.47	0.39	99.00	0.00	99.61	400	10.04
PC18	52,348	52,416	1.48	0.47	99.00	0.00	99.63	588	20.33
PC19	57,543	57,543	1.50	0.37	100.00	19.00	90.77	479	18.73
PC20	51,563	55,017	1.43	0.20	96.00	4.00	90.22	271	11.46
PC21	55,868	55,922	1.48	0.44	98.00	2.00	90.29	127	8.61
PC22	55,449	56,339	1.44	0.26	96.00	7.00	90.19	62	6.98
PC23	55,515	55,760	1.47	0.38	95.00	19.00	90.47	429	17.07
PC24	56,474	56,474	1.57	0.27	100.00	4.00	90.37	74	7.27
PC25	55,550	55,550	1.51	0.33	100.00	4.00	90.00	248	14.47
PC26	54,578	54,958	1.45	0.37	97.00	9.00	90.39	370	13.95
PC27	53,855	53,856	1.50	0.21	98.00	5.00	90.22	259	11.10
PC28	54,833	55,552	1.44	0.24	98.00	1.00	90.86	170	8.76
PC29	56,260	56,437	1.47	0.39	98.00	1.00	90.79	136	8.23
PC30	55,762	55,762	1.56	0.37	100.00	2.00	90.63	191	9.38
PC31	54,376	54,803	1.47	0.39	95.00	3.00	90.61	114	7.96
PC32	55,080	55,146	1.48	0.41	98.00	1.00	90.58	212	9.91
PC33	56,039	56,039	1.51	0.43	100.00	0.00	90.74	231	10.84
PC34	54,940	55,658	1.45	0.39	96.00	0.00	90.40	203	9.59
PC35	53,556	53,991	1.40	0.12	99.00	0.00	90.48	298	11.93
PC36	55,380	55,395	1.48	0.26	99.00	3.00	90.43	409	13.89
PC37	51,099	51,754	1.45	0.48	95.00	0.00	99.81	308	9.13
PC38	51,199	51,728	1.45	0.42	98.00	0.00	99.66	418	11.34
PC39	51,243	52,042	1.44	0.49	97.00	0.00	99.88	488	10.47
PC40	52,299	52,347	1.47	0.52	99.00	1.00	99.72	308	9.83
PC41	52,121	52,163	1.49	0.30	96.00	0.00	99.52	281	9.64
PC42	52,156	52,171	1.49	0.49	98.00	0.00	99.75	568	13.64
PC43	50,292	50,292	1.50	0.53	100.00	90.00	99.60	631	14.37
PC44	52,391	52,402	1.49	0.37	98.00	91.00	99.77	239	9.98
PC45	52,161	52,196	1.49	0.48	97.00	0.00	99.83	375	15.13
PC46	52,252	52,283	1.49	0.38	96.00	0.00	99.75	658	16.41
PC47	52,237	52,238	1.50	0.35	98.00	0.00	99.77	244	10.61
PC48	52,469	52,492	1.48	0.39	99.00	0.00	99.76	385	11.69
PC49	52,362	52,362	1.50	0.46	100.00	0.00	99.56	578	14.32
PC50	52,418	52,428	1.49	0.34	97.00	0.00	99.68	297	10.20
PC51	52,465	52,465	1.51	0.34	100.00	94.00	99.75	120	6.83
PC52	52,402	52,417	1.48	0.52	99.00	0.00	99.64	414	11.90
PC53	52,578	52,578	1.50	0.30	100.00	92.00	99.68	57	5.33
PC54	52,366	52,388	1.48	0.34	99.00	0.00	99.66	402	12.03
PC55	62,053	62,053	1.55	0.35	100.00	0.00	97.56	161	9.24

Table D.21: Parameter control preliminary investigation solution of minimal mass results (cont.)

ID	$f_{\min}$	$\Phi_{\min}$	c_1	c_2, m	η, %	$\beta(\mathrm{X}^{n_k})$, %	$A(\mathrm{X}^{n_k})$, %	N	T, h
PC56	63,029	63,029	1.50	0.33	98.00	0.00	97.52	41	5.61
PC57	60,931	60,932	1.49	0.31	99.00	0.00	97.33	22	3.99
PC58	60,847	60,847	1.55	0.55	100.00	0.00	97.93	66	5.67
PC59	56,666	59,287	1.43	0.29	95.00	0.00	97.18	77	3.72
PC60	60,146	60,147	1.50	0.34	50.00	0.00	97.68	24	2.81
PC61	56,594	56,594	1.52	0.28	100.00	0.00	96.77	26	4.88
PC62	58,495	59,998	1.33	0.33	99.00	0.00	97.60	3	3.41
PC63	60,296	61,624	1.46	0.11	96.00	0.00	97.73	53	3.57
PC64	51,157	51,248	1.48	0.44	74.00	0.00	97.17	747	16.37
PC65	51,769	51,830	1.48	0.48	96.00	0.00	97.94	602	15.03
PC66	51,832	51,848	1.49	0.47	97.00	0.00	97.03	576	18.52
PC67	51,844	51,905	1.48	0.45	96.00	0.00	97.35	749	22.70
PC68	51,777	51,784	1.50	0.41	97.00	0.00	98.43	552	15.10
PC69	51,427	51,500	1.48	0.43	98.00	0.00	97.01	834	21.63
PC70	51,803	51,859	1.48	0.43	98.00	0.00	98.14	629	15.51
PC71	51,804	51,856	1.48	0.46	98.00	0.00	97.27	985	16.93
PC72	51,315	51,407	1.48	0.49	88.00	0.00	98.14	773	15.75
PC73	55,661	55,769	1.48	0.45	98.00	-	-	1,068	0.99
PC74	57,316	58,096	1.44	0.38	97.00	-	-	587	0.56
PC75	55,896	56,001	1.48	0.44	98.00	-	-	1,660	1.43
PC76	57,103	57,104	1.50	0.49	98.00	-	-	1,197	0.98
PC77	57,398	57,585	1.47	0.41	98.00	-	-	981	0.98
PC78	55,362	55,454	1.48	0.45	98.00	-	-	1,345	1.19
PC79	56,905	57,157	1.46	0.40	98.00	-	-	1,003	0.98
PC80	55,882	56,482	1.45	0.42	98.00	-	-	1,635	2.18
PC81	56,780	57,042	1.46	0.41	98.00	-	-	1,279	1.16
PC82	56,412	56,822	1.45	0.40	98.00	-	-	1,532	1.29
PC83	55,004	55,559	1.45	0.47	98.00	-	-	2,355	2.18
PC84	55,660	55,755	1.48	0.41	98.00	-	-	1,775	1.44
PC85	56,630	56,728	1.48	0.41	98.00	-	-	1,075	0.94
PC86	56,336	56,433	1.48	0.40	98.00	-	-	1,823	1.58
PC87	55,888	56,506	1.44	0.41	98.00	-	-	680	0.72
PC88	57,159	57,255	1.48	0.38	98.00	-	-	685	0.75
PC89	56,679	56,834	1.47	0.41	98.00	-	-	1,068	1.75
PC90	55,939	56,327	1.46	0.39	98.00	-	-	990	1.27
PC91	57,276	57,373	1.48	0.38	98.00	-	-	1,318	1.12
PC92	56,249	56,704	1.45	0.40	96.00	-	-	1,414	1.16
PC93	56,348	56,614	1.46	0.37	98.00	-	-	859	0.79
PC94	57,194	57,410	1.47	0.49	97.00	-	-	820	0.94
PC95	57,109	57,209	1.48	0.36	98.00	-	-	1,061	1.03
PC96	55,621	56,141	1.45	0.47	98.00	-	-	1,038	1.02
PC97	56,693	57,027	1.47	0.50	97.00	-	-	688	0.72
PC98	56,150	56,617	1.46	0.41	96.00	-	-	1,107	1.23
PC99	56,764	57,031	1.46	0.46	98.00	-	-	904	0.85

The mean results of the parameter control preliminary investigation are listed in Table D.22.

Table D.22: Parameter control preliminary investigation average results

ID	$\overline{f_{\min}}$	$\overline{\Phi_{\min}}$	$\overline{\sigma(\Phi_{\min})}$	$\overline{\beta(\mathrm{X}^{n_k})}$, %	$\overline{A(\mathrm{X}^{n_k})}$, %	$\overline{N}$	$\overline{T}$, h
PC1	43,865	44,072	1,058	0.00	99.57	661.4	44.18
PC2	44,835	44,991	2,068	17.20	99.63	429.6	24.34

Table D.22: Parameter control preliminary investigation average results (cont.)

ID	$\overline{f_{\min}}$	$\overline{\Phi_{\min}}$	$\overline{\sigma(\Phi_{\min})}$	$\overline{\beta(\mathrm{X}^{n_k})}$, %	$\overline{A(\mathrm{X}^{n_k})}$, %	$\overline{N}$	$\overline{T}$, h
PC3	43,210	43,493	1,421	36.00	99.38	541.0	27.35
PC4	43,322	44,106	1,849	0.00	99.52	512.2	30.87
PC5	46,289	46,436	1,695	10.80	99.53	296.6	14.82
PC6	43,840	44,299	1,730	12.00	99.41	532.8	23.04
PC7	44,666	44,723	1,965	19.00	99.44	450.0	22.63
PC8	45,044	45,207	1,381	0.20	99.56	481.4	18.18
PC9	43,597	43,905	1,926	0.40	99.48	587.2	21.57
PC10	53,294	53,326	3,715	0.40	99.68	480.0	10.60
PC11	52,185	52,362	617	0.40	99.65	362.2	11.31
PC12	52,660	52,665	221	0.40	99.65	581.8	14.80
PC13	53,570	53,589	3,067	18.40	99.62	455.0	12.33
PC14	52,882	52,898	302	55.60	99.65	269.8	10.54
PC15	52,642	52,674	347	37.40	99.66	336.0	11.49
PC16	52,633	52,652	224	0.40	99.68	558.8	14.19
PC17	52,585	52,600	486	18.80	99.70	304.8	9.56
PC18	52,502	52,554	140	18.20	99.60	295.2	10.97
PC19	58,144	58,392	985	7.20	90.31	207.4	10.47
PC20	56,164	57,081	1,300	6.40	90.20	298.8	12.55
PC21	57,325	57,367	960	3.60	90.23	155.4	9.48
PC22	58,010	58,313	1,311	6.00	90.17	74.2	7.41
PC23	56,948	57,205	953	12.60	90.33	223.0	10.90
PC24	56,905	57,077	537	7.80	90.31	154.2	8.98
PC25	57,756	57,800	1,366	4.60	90.15	163.6	10.11
PC26	57,415	57,491	1,480	5.80	90.28	171.8	9.16
PC27	55,895	56,024	1,849	7.60	90.23	204.2	10.64
PC28	57,457	57,838	1,896	1.20	90.56	202.4	9.79
PC29	57,377	57,617	704	0.80	90.67	198.2	9.87
PC30	56,070	56,218	323	1.20	90.60	410.0	14.62
PC31	56,247	56,431	1,200	1.40	90.61	244.8	10.82
PC32	56,502	56,517	1,463	0.60	90.60	197.4	9.73
PC33	56,916	57,178	795	0.40	90.72	278.6	11.59
PC34	56,336	56,600	1,087	1.60	90.60	216.4	11.46
PC35	56,146	56,393	1,441	1.20	90.57	361.8	12.09
PC36	56,932	56,971	1,426	2.60	90.56	247.4	12.14
PC37	52,250	52,437	394	36.00	99.68	236.6	9.66
PC38	52,259	52,374	399	0.20	99.78	363.0	12.23
PC39	51,937	52,319	207	18.80	99.56	345.2	10.97
PC40	52,326	52,488	238	0.40	99.62	269.4	8.78
PC41	52,357	52,408	302	0.40	99.77	361.0	12.86
PC42	52,333	52,408	135	0.20	99.80	412.2	12.98
PC43	52,138	52,149	1,052	18.20	99.66	391.8	13.21
PC44	52,627	52,644	227	18.80	99.64	290.8	10.68
PC45	52,406	52,432	277	0.00	99.83	363.6	13.01
PC46	52,559	52,575	204	18.60	99.71	319.4	10.85
PC47	52,423	52,495	232	0.20	99.73	301.0	12.31
PC48	52,691	52,741	187	18.20	99.72	403.8	12.01
PC49	52,611	52,619	203	19.00	99.66	404.6	12.52
PC50	52,722	52,749	305	18.60	99.65	247.0	9.33
PC51	52,703	52,734	191	37.80	99.77	189.4	8.34
PC52	52,698	52,721	245	38.60	99.72	287.2	10.67
PC53	53,970	53,975	2,977	18.60	99.67	151.6	7.37
PC54	52,646	52,670	199	55.80	99.72	212.0	8.86
PC55	66,384	66,537	2,921	0.00	97.58	53.0	5.31
PC56	64,065	64,759	1,642	0.00	97.27	25.2	4.40
PC57	64,050	64,879	2,623	0.00	97.34	20.0	6.21

Table D.22: Parameter control preliminary investigation average results (cont.)

ID	$\overline{f_{\min}}$	$\overline{\Phi_{\min}}$	$\overline{\sigma(\Phi_{\min})}$	$\overline{\beta(\mathrm{X}^{n_k})}$, %	$\overline{A(\mathrm{X}^{n_k})}$, %	$\overline{N}$	$\overline{T}$, h
PC58	63,412	63,819	2,214	0.00	97.42	25.4	5.25
PC59	63,484	64,452	3,588	0.00	97.37	19.2	4.33
PC60	64,822	64,960	3,280	0.00	97.29	9.6	4.47
PC61	62,232	62,624	4,246	0.00	97.16	16.8	4.84
PC62	64,569	65,294	3,900	0.00	97.62	7.8	3.72
PC63	63,307	64,239	2,401	0.00	97.53	27.6	6.08
PC64	51,921	51,962	493	0.40	97.54	797.8	17.33
PC65	51,991	52,139	268	0.20	97.35	709.4	16.96
PC66	52,694	52,731	816	0.00	96.99	678.2	15.96
PC67	52,404	52,463	331	0.00	97.56	805.8	20.62
PC68	52,086	52,110	388	1.00	98.04	790.4	16.18
PC69	52,152	52,190	583	0.60	97.47	872.8	19.58
PC70	52,307	52,354	372	1.40	97.56	767.4	17.54
PC71	52,665	52,706	577	3.40	96.93	878.6	16.97
PC72	52,205	52,305	608	0.00	97.62	813.6	16.48
PC73	56,859	57,183	935	-	-	1,012.2	1.14
PC74	59,290	59,546	1,250	-	-	431.6	0.56
PC75	57,609	57,691	2,039	-	-	919.2	0.90
PC76	58,353	58,577	1,330	-	-	814.2	0.88
PC77	58,728	58,973	1,348	-	-	589.6	0.68
PC78	57,532	57,694	1,838	-	-	825.0	0.89
PC79	58,090	58,279	1,062	-	-	776.8	0.80
PC80	58,915	59,218	2,306	-	-	746.2	0.93
PC81	59,260	59,438	1,480	-	-	700.4	0.80
PC82	58,003	58,319	1,444	-	-	926.8	0.91
PC83	57,264	57,451	2,012	-	-	1,060.6	1.02
PC84	56,622	57,022	1,251	-	-	1,234.0	1.11
PC85	57,692	57,901	915	-	-	737.6	0.93
PC86	57,527	57,848	1,104	-	-	948.2	0.95
PC87	56,831	57,036	531	-	-	864.8	0.92
PC88	58,998	59,292	3,906	-	-	724.8	0.79
PC89	58,958	59,254	2,066	-	-	584.4	0.83
PC90	57,417	57,753	1,572	-	-	1,109.6	1.11
PC91	59,954	60,106	3,321	-	-	458.0	0.62
PC92	57,901	58,079	1,104	-	-	928.4	0.92
PC93	58,027	58,478	2,319	-	-	649.0	0.68
PC94	58,856	59,325	2,291	-	-	666.6	0.87
PC95	57,677	57,967	654	-	-	766.6	0.79
PC96	57,123	57,368	1,270	-	-	1,018.0	1.16
PC97	57,272	57,506	494	-	-	701.8	0.79
PC98	58,277	58,566	2,730	-	-	744.4	0.87
PC99	58,147	58,331	1,416	-	-	689.0	0.74